THE APPLICATION OF FINITE ELEMENTS TO PROBLEMS OF SOIL

MICHAEL DEREK CUNNELL

A THESIS SUBMITTED FOR THE DEGREE OF DOCTOR OF PHILOSOPHY

Department of Civil Engineering
The University of Aston in Birmingham

May 1974

SUMMARY.

The finite element method is now well established as an extremely useful tool for the displacement and stress analysis of problems with complicated boundary conditions. One aim of this thesis is to investigate the suitability of the method in the solution of the range of Civil Engineering problems usually associated with Soil and Rock Mechanics. A further aim has been to extend the method into the analysis of complete structures integral with the foundation material.

A suite of programs has been written to carry out finite element analysis in two or three dimensions using the new families of Isoparametric elements. The accuracy and efficiency of these elements has been assessed in relation to a typical foundation problem which can be analysed using more conventional methods.

Two important non-linear two dimensional problems have been investigated namely the analysis of the plane strain compression test, involving the idealisation of smooth interfaces, and, crack propagation. In the former an iterative process has been followed to analyse the test and compare results with experimental conclusions. The process of crack propagation has been followed using an incremental method which involves changing compatibility conditions to introduce separations at element boundaries.

The major part of this thesis is concerned with a method for analysing complete three dimensional structures together with their foundation materials. With this method it is possible to include the complex interactions of structure and foundation as well as the non-linear stress-strain response of the soil. In order to assess the accuracy of the method it was necessary to construct a model testing apparatus and conduct a series of experiments.

ACKNOWLEDGEMENTS.

The Author would like to express his deepest gratitude to his Tutor, Professor K.I.Majid for his invaluable advice and encouragement throughout the last three years. His sincere thanks are also given to Dr.K.Al-Hashimi and Dr.K.H.M.Bray for their many helpful discussions. Thanks are also due to the Chief Technician, Mr.W.Parsons and his team of technicians, particularly Mr.J.Hollins and Mr.M.Lyons without whom it would not have been possible to complete the experimental work.

In the preparation of this thesis the Author would like to thank Mrs.M.Hasleton for typing the script, Miss P.Sage for preparing the diagrams and his wife for her encouragement and patience in checking the script.

The Author would also like to thank the Staff of the Atlas Computer Laboratory and the Aston Computer Centre for their prompt service and technical advice. Finally, thanks are due to the Science Research Council for their financial support.

C O N T E N T S.

C O N T E N T S (contd)

C O N T E N T S (contd)

C O N T E N T S (contd)

C O N T E N T S (contd)

NOTATION.

$\{f\}$	Components of Displacement
$[N]$	Shape function matrix
$\{\delta\}_e$	Vector of nodal displacements
$\{\epsilon\}_e$	Vector of Elastic strains
$\underline{B}$	Strain matrix
$\{\sigma\}_e$	Vector of elastic stresses
$\underline{D}$	Elasticity matrix
$\{\epsilon\}_o$	Initial strain vector
$\{\sigma\}_o$	Initial stress vector
$\{F\}_e$	Vector of nodal forces
$\{f_i\}$	Components of nodal force
$\{P\}$	Distributed loads vector
$d\{a\}$	Increment of vector $\{a\}$
$\{a\}^T$	Transpose of vector $\{a\}$
$\underline{k}$	Overall stiffness matrix
$\{F\}_p$	Nodal forces due to distributed loads
$\{F\}_{\sigma_o}$	Nodal forces due to initial stresses
$\{F\}_{\epsilon_o}$	Nodal forces due to initial strains
σ_x	Normal stress in direction x
τ_{xy}	Shear stress in plane xy
σ_y	Normal stress in direction y
u	Displacement in x direction
v	Displacement in y direction
E	Young's modulus
$\epsilon_x \epsilon_y \gamma_{xy}$	Components of strain
ν	Poisson's ratio
χ	Airey's stress function
∇_1^2	Laplace operator

NOTATION (contd)

e^{xry}	Exponential function of power xry
U,i,N G	Arbitrary constants
A,B,C and D	Arbitrary constants
P_1,P_2,P	Applied pressures
a,b and c	Dimensions of thick plate
p and q	Non-dimensional co-ordinates
s and t	Approximation functions
I_1,I_2 and I_3	Integrals
f,g and h	Arbitrary constants
ϵ_z	Strain in direction z
τ_{oct}	Octahedral shear stress
G	Shear modulus
γ_{oct}	Octahedral shear strain
σ_1, σ_2 and σ_3	Principal stresses
τ_j, τ_{j-1}, γ_j and γ_{j-1}	Points on curve
A	Tolerance
L	Length
D	Diameter
dL_j	j^{th} increment of load
$d\sigma^i_{xj}$, $d\sigma^i_{yj}$ and $d\tau^i_{xyj}$	Increments of stress after the j^{th} increment at joint i.
θ_i	Slope of radial line at joint i
λ^i_j	Cracking load after j^{th} increment of load, joint i.
ϕ^i_j	Slope of stress/load curve after j^{th} increment of load at joint i.
D_{10} and D_{60}	Percentage particle sizes
μ	Uniformity coefficient
G_s	Specific gravity
n_{max} and n_{min}	Maximum and minimum porosity
n_r	Relative porosity

NOTATION (contd)

y_d, $y_{(4)}$	Apperture coefficients
M	Extension modulus of Latex
σ_{cm}	Correction for Latex strength
ϵ_1 ϵ_2 ϵ_3	Principal Strains
σ_1 σ_2 σ_3	Principal Stresses
D_o	Original sample diameter
σ_{cw}	Correction for platten mass
W_{TP} and W_{LT}	Weights of platten and transducer.
σ_c and σ_c'	Cell pressure
a_p	Area of load piston
σ_{cc}	Correction for height of sample
γ_w	Density of water
H_s	Height to mid-height of sample
ϵ_V	Volumetric strain
V_o	Original volume of sample
S_c	Volume Change calibration factor
L_c	Load transducer calibration factor
γ_m	Density of Mercury
H	Head of cell water
ϕ'	Coloumb angle of internal friction
C'	Cohesion
ϵ_{oct} and γ_{oct}	Octahedral Strain Components
k, k_o	Bulk Modulus
G, G_o, G_i	Shear Modulus
J_2	Second invariant of stress
σ_{oct} and τ_{oct}	Octahedral stress components
a, b	Hyperbolic parameters
x_i and y_i	Experimental values
$\bar{x}$ and $\bar{y}$	Mean values

NOTATION (contd)

μ_1, S_x and S_y	Statistical parameter
r	Regression coefficient
ν	Poisson's ratio
$\delta\{X\}$ and $\delta\{L\}$	Incremental displacement and load vectors
$\delta\{\varepsilon\}$ and $\delta\{\sigma\}$	Incremental strain and stress vectors
A_c	Accuracy of fit
e	Eccentricity
δ_L and δ_R	Vertical pad displacements
δ_{DF}	Differential settlement
δ_{SW}	Sway
H_i, V_i and M_i	Applied loads and moment
u_i, v_i and θ_i	Displacements and rotation
A B C F T e f	Terms in the stiffness
	Matrix of a Member Element
I	Moment of Inertia
L_p, M_p, L_q and M_q	Direction cosines
k_{ij}	Element of stiffness matrix
p and q	Local Cartesian coordinates
α_1, α_2 and α_3	Terms of Elasticity Matrix
x y	Global Cartesian coordinates
a_1, a_2 etc.	Polynomial constants
N_1, N_2 etc.	Shape functions
$\underline{C}$	Geometric matrix
L_i^n	Lagrangian polynomial
p and q	Non-dimensional curvilinear coordinates
[J]	Jacobian matrix
E(1), E(2), E(3) and E(4)	Terms in Elasticity Matrix
$\underline{B}^*$	Revised strain matrix
H_j	Gaussian quadrature weight coefficient
a_j	Gaussian quadrature specific point

NOTATION (contd)

$f_{(aj)}$	Function value at a_j
r	Third non-dimensional curvilinear coordinate
W	Displacement component
Z	Third Cartesian coordinate
A,B,D,E,F,G,K and L	Terms in Jacobian Matrix
ϵ_z, γ_{xz} and γ_{yz}	Strain components
B_{ij}	Element of strain matrix

CHAPTER 1

INTRODUCTION.

1.1) Introduction.

Except for a few very simple problems the inherent non-linearity of soil deformations cannot be analysed by normal techniques. It is the usual practice in soil mechanics to differentiate clearly between two different classes of computations of the state of stress and deformations in a soil mass. Terzaghi[83] referred to the two groups as the "elasticity problem" and the "stability problem".

The stability problem is solved using limit analysis, which is performed by invoking a particular failure criteria, using a corresponding value of ultimate strength characteristic derived from a laboratory test. By this method, problems involving slopes, retaining walls and foundations have more or less successfully been treated. This method is considered adequate to check overall stability but it cannot, by definition, give any indication of the state of stress and deformation up to failure. Deformations are assumed to be zero up to failure, which is then sudden and catastrophic. The method provides at best an upper or kinematic bound to the problem.

Stability analysis is useful in giving a first check to a design but the governing criterion is more likely to be one of working load deformations. Well before failure, as indicated by limit analysis, the interior panels and structure of most buildings would have suffered extensive damage, making the structure unstable. At present, common practice is to predict deformations on the assumption of linear elastic theory. A typical example of this is the design of footings on sand. Plate loading tests are carried out from which a representative value of Young's modulus is calculated. This modulus is then used in one of the classical

1.1) contd.

solutions to calculate the deformations, which are invariably severely underestimated.

There is obviously an urgent need for more realistic deformation analysis, particularly under general conditions. This need becomes even more urgent in the light of the pressures design Engineers are under, not only to create cheaper structures, but to build in areas formerly considered unsuitable. Engineers need rational scientific methods of analysis and as classical mathematics is capable of solving only very idealised field problems, it becomes necessary to turn to the field of numerical analysis for the answer.

1.2.1) The Finite Element Method.

The field of numerical analysis offers two main methods of solution. One, to solve the governing differential equations defining the displacements or stresses and then solve them numerically by methods such as the finite difference, or, the two matrix methods. The latter methods have proved more powerful and adaptable than the finite difference methods in the field of structural and continuum analysis particularly because complex boundary conditions and shapes present easier solution. The matrix methods have evolved in the field of structural analysis where it is assumed that any structure consists of elements, each with a defined stiffness, which, when assembled into a structure behave as nearly as the actual structure. The matrix displacement method has proved the most popular. This expresses the internal member forces in terms of displacements at the nodes, and then proceeds to solve a set of joint equilibrium equations to determine the unknown displacements.

1.2.1) contd.

The matrix displacement method has been extended to include the analysis of two and three dimensional continua. Conventional engineering structures can readily be idealised to an assemblage of elements interconnected at a discrete number of nodes. In a continua the true number of interconnections is infinite so the application of the method is not immediately obvious. The concept of Finite Elements, introduced by Turner, Clough, Martin and Topp[88] attempts to surmount this problem by assuming the real continuum to be divided into elements interconnected at a finite number of points, at which, fictitious forces representing the loading are assumed to act. This reduces the problem to that of a conventional structural type on which matrix methods can be used.

In a text by Zienkiewicz[98] five points are listed on how the approximation is made;

(a) The continuum is separated by imaginary lines or surfaces into a number of finite elements.

(b) The elements are assumed to be interconnected at a discrete number of nodal points situated on their boundaries. These nodal displacements are the basic unknown parameters.

(c) A function (or functions) is chosen to define uniquely the state of displacement within each element in terms of the nodal displacements.

(d) This function now defines the state of strain within an element in terms of the nodal displacements. These strains together with any initial strains and the elastic properties are used to calculate the stress throughout the element.

(e) A system of forces concentrated at the nodes and equilibrating

1.2.1) contd.

(e) contd.

the boundary stresses and any distributed loads is determined resulting in the characteristic stiffness relationship.

A finite element analysis is carried out by the use of relevant computer programs. The logical steps carried out in such a process are described briefly below;

(1) Idealisation of the structural system. This requires the selection of the type and size of finite elements to generate the mesh to describe the system geometrically. It also requires a definition of the elastic properties, boundary and loading conditions.

(2) Generation of the stiffness matrix quantities for the elements.

(3) Superposition of the element stiffness matrices to develop the overall stiffness matrix of the total structural system.

(4) Determination of the unknown nodal displacements of the problem by the solution of the system of linear simultaneous equations obtained using the equilibrium conditions at the nodes.

(5) Computations of all other required values such as stresses and strains associated with the problem.

Usually the accuracy and effectiveness of the finite element method will depend on the type and number of elements used in the mesh generation. Indeed, it may be noted that the finite element method provides an exact mathematical solution to a simplified structural idealisation of a given problem, so the idealisation is all important. By comparison, the finite difference technique provides an approximate Mathematical solution to equations which 'exactly" represent the physical system.

1.2.2) Finite Element Formulation.

For a typical element the components of displacement $\{f\}$ are defined in terms of the nodal displacements $\{\delta\}_e$ by;

$$\{f\} = [N]\ \{\delta\}_e \qquad (1.1)$$

where [N] is a shape function matrix and is defined in such a way that the convergence criteria (discussed later) are obeyed. The strain at a point in the element can be determined from the differentiation of $\{f\}$ to give a relationship of the form;

$$\{\epsilon\}_e = \underline{B}\ \{\delta\}_e \qquad (1.2)$$

Following usual elastic theory the stress $\{\sigma\}_e$ can be obtained from;

$$\{\sigma\}_e = \underline{D}[\{\epsilon\}_e - \{\epsilon\}_o] + \{\sigma\}_o \qquad (1.3)$$

where $\underline{D}$ is the elasticity matrix containing material properties, and $\{\epsilon\}_o$ and $\{\sigma\}_o$ are initial strain and stress vectors developed independently.

The nodal forces, which are statically equivalent to the boundary stresses and distributed loads on the element, are defined as;

$$\{F\}_e = \{\underline{F}_1\ \underline{F}_2 \cdots \underline{F}_i \cdots \underline{F}_n\} \qquad (1.4)$$

where each of the forces $\{\underline{F}_i\}$ contains the same number of components as the corresponding nodal displacements $\{\delta_i\}_e$. The distributed loads $\{P\}$ are defined as those acting on a unit volume of material within the element corresponding to the components of $\{\epsilon\}$ at that point.

To satisfy equilibrium the nodal forces must be statically equivalent to the actual boundary stresses and distributed loads. The simplest procedure, Zienkiewicz[98] is to impose an arbitrary nodal displacement and to equate

1.2.2) contd.

the external and internal work done by the various forces and stresses during the virtual displacement.

If the virtual displacement at the nodes is $d\{\delta\}_e$, then from equations (1.1) and (1.2) the resulting displacements and strains are;

$$d\{f\} = \underline{N}\, d\{\delta\}_e \tag{1.5}$$

and

$$d\{\epsilon\}_e = \underline{B}\, d\{\delta\}_e \tag{1.6}$$

The work done by each of the nodal forces is equal to the sum of the products of the individual force and corresponding displacement components;

$$d\{\delta\}_e^T \{F\}_e \tag{1.7}$$

and, similarly the work done per unit volume by the stresses and distributed forces is;

$$d\{\epsilon\}^T \{\sigma\} - d\{f\}^T \{p\} \tag{1.8}$$

which using equations (1.5) and (1.6) become;

$$d\{\partial\}_e^T (\underline{B}^T \{\sigma\} - \underline{N}^T \{p\}) \tag{1.9}$$

Equating the external work with the total internal work, obtained by integrating over the volume of the element, the following expression is obtained;

$$d\{\delta\}_e^T \{F\}_e = d\{\delta\}_e^T \left(\int \underline{B}^T \{\sigma\}\, d(\text{vol}) - \int \underline{N}^T \{p\} (\text{vol}) \right) \tag{1.10}$$

It can readily be seen that the above expression is independent of the value of the virtual displacement. Substitution of equations (1.2) and (1.3) into (1.10) yields

$$\{F\}_e = \left(\int \underline{B}^T \underline{D}\, \underline{B}\, d(\text{vol})\, \{\delta\}^e - \int \underline{B}^T \underline{D}\, \{\epsilon_o\}\, d(\text{vol}) \right.$$
$$\left. + \int B^T \{\sigma_o\}\, d(\text{vol}) - \int \underline{N}^T \{p\}\, d(\text{vol}) \right. \tag{1.11}$$

This equation is the characteristic stiffness relation which is usually written as;

1.2.2) contd.

$$\{F\} = \underline{k}\{\delta\} + \{F\}_{\epsilon_o} + \{F\}_{\sigma_o} + \{F\}_p \qquad (1.12)$$

where the stiffness matrix is;

$$\underline{k} = \int \underline{B}^T \underline{D} \underline{B} \, d(vol) \qquad (1.13)$$

and the nodal forces due to distributed loads are;

$$\{F\}_p = - \int \underline{N}^T \{p\} \, d(vol) \qquad (1.14)$$

those due to initial strain are;

$$\{F\}_{\epsilon_o} = - \int \underline{B}^T \underline{D} \{\epsilon_o\} \, d(vol) \qquad (1.15)$$

and those due to initial stress are;

$$\{F\}_{\sigma_o} = \int \underline{B}^T \{\sigma_o\} \, d(vol) \qquad (1.16)$$

1.2.3) Requirements for Convergence.

The division of a continuum into elements with prescribed displacements introduces the approximation of reducing the number of degrees of freedom of the system to a finite number. All the elements described in this thesis are displacement models and the stiffnesses are obtained from the minimisation of their total energy. Veubeke[35], showed that this leads to a lower bound of the strain energy, so that in general the structure will be too stiff and hence displacements are underestimated. To ensure convergence to the correct solution by finer mesh sub-division there are certain requirements that the assumed displacement function must satisfy.[46,66,98]

The displacement function should be able to represent the true displacement distribution as closely as possible, which gives rise to the following requirements;

1.2.3) contd.

(a) Internal and interface compatability of displacements, between adjacent elements should be kept.

(b) Rigid body motions should be possible without straining.

(c) Any required constant strain could be reproduced.

1.3) Historical Review of the Finite Element Method.

Technological advancements have created a need for fast and accurate analysis of large and complex structural systems which present great difficulties to obtaining rigorous mathematical solutions. The development of high speed electronic digital computers has generated great interest in numerical methods related to the solution of engineering problems. Parallel development has occurred in matrix concepts and operations which have proved very adaptable to the logical operations of the digital computer. It is against this background that the Finite Element method, together with the displacement model, has developed to become one of the most powerful and adaptable tools available to the Engineer for analysis, relieving him from long hours of tedious mathematical computation.

It was as long ago as 1872 that Navier first suggested a method of analysis based on taking the deflections as the unknowns. The method received little attention at the time because of the amount of computation involved. Livesley[60,61] was one of the first to adopt the matrix displacement method for the computational analysis of bare frameworks. At about the same time Argyris[3] comprehensively formulated the matrix force and displacement methods. It was shown that the two methods stemmed from the concepts of complementary virtual work and virtual work respectively. Argyris also derived a

1.3) contd.

stiffness matrix for a two dimensional rectangular plate by assuming linear distribution of displacements, imposing unit displacements at each corner and adding the stiffnesses for each imposed deflection to build up the stiffness matrix of the plate.

It was really Turner et al.[88] two years later who laid the foundation of the Finite Element technique by deriving the stiffness matrices for various spar, rib and cover plate elements. The 'in plane' stiffness matrix of a triangular element was derived by assuming constant strain over the element. This was shown to lead to a linear distribution of displacements. To equilibrate the nodal forces to the stresses, the basic stress patterns, that could be expected, were considered and the forces obtained by direct equilibrium. It was pointed out that the same result could have been obtained using Castigliano's energy theorem. The stiffness of a quadrilateral element was also found by splitting the area up into triangles and summing the contributing stiffnesses.

Clough[15] extended the idea of assumed stress to derive the stiffness matrices of triangular and rectangular plate elements. The valuable contribution was the introduction of the principle of virtual work which was used to obtain the overall equilibrium of the element.

The next development was provided by Melosh[65] when the finite element method was extended to 'out of plane' or bending action. The stiffness matrix of a rectangular plate, whose nodes were allowed one translation normal to the plate and two rotations, was derived.

By this time definite methods of derivation of the stiffness matrix were being formulated and these were reviewed

1.3) contd.

by Gallagher[37] to be;

(1) Inversion of a flexibility matrix[34]

(2) Direct formulation[38]

(3) From virtual work or, unit displacement theorem[3].

Formulation by Castigliano's theorem might well have been included as the fourth. Although the interrelation of some derivations was noticed and, in fact, that they would give the same results of stiffness for particular elements, the actual implications of the basic assumptions were not yet realised.

The majority of elements thus formed were known to converge to a good value for solutions as their sub-division was refined but the extent of the accuracy that could be expected was not defined. It was Melosh[66] who first tackled this problem. Errors were classified as those involved in the structural idealisation, the computation, or the finite element itself. In the investigation of the latter it was shown that solutions obtained using extremum variational theorems of elasticity could be bounded between upper and lower limits. It was shown that using a displacement function 'minimised' the potential energy of the system and hence formed a lower bound. It was concluded that, as long as the structural idealisation was not redefined on subdivision, monotonic convergence would exist but not necessarily to the correct solution. It was stated that for this to be so, the function must satisfy certain requirements, namely;

1) Strains should be continuous over the elements.

2) Inter-element displacement continuity must exist, i.e. conform.

3) Functions must be expressible in the form of equation (1.1).

And optional requirements were;

4) They should exhibit monotonic convergence as previously described.

1.3) contd.

5) Rigid body movements should not cause straining.

The last option, in fact, should not be violated, as extra energy not existing in a structure, would be introduced into the idealisation.

Fraeijs de Veubeke[34,35] proved upper and lower limits for 'equilibrium and displacement models' but, while agreeing with Melosh's requirements, thought that different element patterns might cause convergence to an erroneous answer. The difficulty in forming a stiffness matrix from an equilibrium model (that is by inverting a flexibility matrix) that would include all possible rigid body deformations was pointed out. It was de Veubeke who first derived the quadratic triangle. This was an important contribution as it was the first high order element to be developed. To achieve this a special set of area coordinates was used. It was pointed out that this triangular element had a number of nodes such that a complete polynomial expansion was ensured.

Irons and Draper[46] relaxed Melosh's requirements for convergence and accuracy by proposing that;

(1) They must be able to exhibit all rigid body movements.

(2) They must have a continuous displacement within and across interfaces.

These reiterated Melosh's proposals but, in addition;

(3) They must be able to represent constant stress.

This last fact was substantiated by the fact that an infinite sub-division implies constant stress in the limit. These three criteria are now generally accepted and have been stated earlier.

The finite element technique developed along these

1.3) contd.

lines with the improvement of existing concepts and applications until 1966 when Irons[47] published a paper on the use of high order elements. It was proposed that the use of numerical integration in finding the various matrices needed for stress, stability and dynamic calculations would enable a greatly increased number of different problems to be solved for a given programming effort, but at the sacrifice of some computer time. It was further proposed that engineers were restricting themselves to trivial problems by using analytical integration, and that the finite element technique would only reveal its full potential when research workers were liberated from the time wasting effort of deducing matrices afresh for each new problem. The exposition took the form of a series of examples such as plane elements with curved edges, solid elements with curved edges and faces, with applications to plane stress, torsion and solid elasticity. It was thought that the economic value of decisive checking and numerical reliability would justify the extra computer time.

Irons explained that elements were too simple and that it was worthwhile to try more complicated elements, but it was not possible to forecast at what stage in the elaboration the economic optimum would be. It was pointed out that shape functions (usually known as displacement functions) were merely multipliers in a more or less complicated interpolation formula. The procedure recommended in numerical integration was to write a sub-routine to calculate the values of the shape functions at given points which could be easily checked numerically by calculating the known values at the nodes.

In the derivation of the stiffness matrices of the various elements the important assumption that the unknown

1.3) contd.

displacements and the coordinates should obey the same interpolation formulae was made. Irons went on to show that with simple modification individual nodes could be included or omitted at will. This introduced mixed elements whereby regions where the stresses were important, or where curved boundaries were needed, midside nodes could be included and elsewhere omitted. Irons proposed that the Gauss rule for numerical integration should be used. It was also shown that the elements all obeyed the convergence criteria.

In another paper the same year Irons[48] recognised that the pioneer work on stiffnesses was done by I.C.Taig but was not published and Irons recognised Taig's quadrilateral as the first of a powerful series of elements. The concept of elements having special 'osculatory' nodes was introduced to provide extra degrees of freedom and thus increase the nodal valency.

The term 'isoparametric', to describe these quadrilateral elements, was introduced by Ergatoudis, Irons and Zienkiewicz[31]. It was pointed out that such elements were able to follow prescribed boundaries and allow a good degree of approximation to curved shapes. Some examples were presented to illustrate the extreme accuracy of the higher order members of the family, and the disadvantage of the simple constant strain-triangle was highlighted. The case for the use of these isoparametric elements was further advanced by a series of papers[49] and [97] where further examples were presented. The development of isoparametric membrane and thick shell elements was presented by Ahmad, Irons and Zienkiewicz[1]. In these elements the thickness was allowed to vary according to the same function controlling the coordinates

1.3) contd.

and displacements.

The use of the finite element method up until the mid-sixties was restricted to various conditions. Some of these were that the analysis should remain in the linear elastic range and that deflections should be small. It was therefore a logical step to extend the analysis into the non-linear range. In order to analyse such problems it was assumed that the non-linear behaviour could be represented by a series of linear steps.

Elastic-plastic material properties were used in the finite element analysis by Pope[71] and Marcal[63]. In their approach the elastic properties were adjusted according to the stress level, as the load was applied in a series of increments. Each time the elastic properties were altered this changed the terms in the stiffness matrix and so this became known as the modified stiffness method. Argyris[5] and Gallagher[36] adopted a different approach to non-linear analysis. The load was still applied in a series of increments, in this case the elastic properties were not altered but the initial stress or strain vectors, as in equation (1.3), were adjusted. As the stiffness matrix did not alter, this method became known as the constant stiffness one.

Problems involving geometric non-linearities due to large displacements were investigated by Martin[64] and Argyris[4]. As the displacements become large the small strain approximation is in error, and to overcome this a new stiffness matrix was introduced to represent the additional terms in the strain-displacement equations. This matrix was then superimposed on the conventional stiffness matrix to furnish the complete stiffness matrix. The extension of the finite element

1.3) contd.

method to problems involving time, such as the dynamic behaviour of structures, was carried out by Zienkiewicz, Irons and Nath[93] and Clough and Chopra[16].

It was shown by Zienkiewicz[98] in his text that the finite element technique was not limited to structural problems, but was applicable to many other physical problems, such as, heat conduction, seepage, wave transmission and the distribution of electrical potential whether in a steady or transient stage. From the development up to this time, the finite element technique has become a major analytical, and, hence design, tool with applications to an extremely wide range of problems in engineering.

1.4) The Application of the Finite Element Method to Soil and Rock Mechanics.

It was in 1965 that Cheung and Zienkiewicz[13] determined the stress distribution and settlement beneath a foundation slab represented by rectangular plates. The foundation material was idealised as a Winkler foundation or a Boussinesq half space. Severn[76] carried out a similar analysis except that a spring coupling action was included to simulate shear resistance. Cheung and Nag[14] followed a similar approach using the Flamant half plane to represent the foundation material. A non-linearity was introduced in that separation between the footing and soil was allowed at points with negative contact pressures. Smith[77] further extended this approach and analysed axi-symmetric footings allowing the elastic modulus to vary linearly with depth. All the above methods added the stiffness of the idealised foundation material to that of the slab in the vertical direction. The results gave reasonable

1.4) contd.

comparison with closed form solutions, but the method was restricted to cases of assuming isotropy, homogeneity and linearity.

It was Clough and Woodward[17] who first demonstrated the power of the finite element method in soil mechanics, when a large earth dam was analysed. The embankment itself was idealised as a number of triangular elements, undergoing plane strain. Several important problems were investigated including, the effect of incremental loading, as compared to a single step load, and the effect of the flexibility of the base. In the incremental loading the dam was assumed to be constructed in a series of layers, each imposing a body force. It was shown that while this had little effect on the stresses, the displacements were much larger than those predicted from a single step loading. These investigators then went on to make the important step of introducing a non-linear material model. Triaxial tests were carried out over a range of confining pressures from which a series of values of the shear modulus were calculated. An incremental analysis was then carried out, and at the end of each load (construction) increment the elastic properties were adjusted according to the stress level. The result of this analysis was compared to field measurements and good agreement was found.

Girijavallabhan and Reese[38] analysed model tests carried out on an axi-symmetric footing on clay and a retaining wall pushed into a bed of sand by using rectangular finite elements. In this analysis another non-linear material model was used which involved deriving a unique relation, over a small range of initial stresses, between the octahedral components of shear stress and strain. The shear modulus could then be

1.4) contd.

calculated using an iterative procedure. The experimental and analytical results were in close agreement. Desai and Reese[22] followed a similar approach but here a degree of non-homogeniety was introduced, in that the clay beneath a circular footing was made up of two distinct layers. As before close agreement was found between the theoretical and experimental results.

In all the preceding investigations it was assumed that excess pore pressures were not developed and that all stresses were effective. Christian and Boehmer[18] developed a finite element technique to solve problems of consolidation of a linearly elastic material in plane strain. It was pointed out that the finite element method was not directly applicable to incompressible solids because the material is infinitely stiff with respect to volumetric stress. This difficulty was overcome by carrying out the usual type of analysis and then applying pore pressures to prevent change of volume, thus, the pore pressures became unknowns along with the displacements. The number of equations was balanced since the change in volume was considered to be zero. The extension to consolidation was made by realising that some change of volume, other than zero, could be specified in each element. The procedure gave displacements, pore pressures and effective stresses for any known distribution of volumetric strain. Hence, an incremental procedure could be followed starting from the known stress and volumetric strain distribution, and proceed to the zero pore pressure state using D'Arcy's law to calculate the increments of volume change from the pore pressures. The method was compared to various analytical solutions and some improvement was found.

1.4) contd.

Dunlop and Duncan[29] investigated the development of failure around clay slopes as excavation took place. In an approach similar to that of Clough[17] it was assumed that the excavation was made in a series of layers or increments. A bi-linear relation was used to represent the behaviour as that of a linear elastic perfectly plastic material. Various important field effects were included, like a variation of strength with depth, and initial stress conditions for normally and pre-consolidated clays. The development of plastic zones was shown and compared with stability analysis with which excellent correlation was found.

Duncan and Chang[25] analysed model tests, using a non-linear material model. In this model the non-linear stress strain curve was represented by a particularly simple function, namely the hyperbola developed by Kondner[56]. This curve is described by two constants, the initial slope and the asymptote. These two constants correspond to physically important properties namely the initial modulus and the ultimate strength. It was therefore possible to carry out a series of laboratory tests to establish relations between these parameters, and the porosity and confining pressure. This meant the relation could cover almost any range of conditions. This relation was then used in an incremental finite element method to analyse a model footing buried in sand at maximum or minimum porosity states. Good agreement was found between the theoretical and experimental results.

Duncan and Clough[26] used this method of analysis in a field problem when they investigated the earth pressure distribution on a concrete navigation lock, as construction progressed, to clarify the design needs and to help field

1.4) contd.

instrumentation. The interface between the concrete and back fill was represented by one dimensional line elements to allow relative displacements to occur. Good agreement was found between this analysis and field measurements for pressure and deflection at several positions. The idealisation of the incremental construction procedure as a series of layers became known as 'gravity turn on, or off' loading.

All the previously discussed non-linear analyses were carried out in the United States where there was easy access to large and fast digital computers. Because of this there was no great need for sophistication and all the investigations used simple triangular or rectangular elements, and simple, easy to establish constitutive relationships, with the modified stiffness method. Despite the over-simplifying assumptions made, the analyses all gave good agreement with measured results. Most important of all the finite element method was used, and proved, in real situations where comparison could be made with field measurements.

Elsewhere, the concentration was centred more on further sophistication of the constitutive relations and the use of better elements. Zeinkiewicz, Valliapan and King[94,96] completely formulated the constant stiffness, initial stress and strain, methods using elasto-plastic theory in the form of Von Mises yield criterion and Hills plastic potential hypothesis. From these it was possible to derive a relationship between the incremental stresses and strains which could represent a perfectly plastic or work hardening material. A number of examples were solved involving plastic and creep behaviour including a lined tunnel and a strip footing. Some problems with convergence were encountered but in general the

1.4) contd.

methods worked well although no comparison with experimental results were made.

It was noticed that a hypothetical material capable of sustaining only compressive stresses, without resistance to tension was similar in behaviour to an ideal plastic material. The stress transfer method could be applied to this problem by yielding a solution where all principal tensile stresses had been eliminated. In the examples solved a large difference was shown to exist between the elastic stress distribution and that of a material in a 'cracked' (no tension) state.

Naylor and Zienkiewicz[67,95] showed that the methods developed above were applicable to any theory provided it could be formulated in a similar way. Thus, it was possible to include a constitutive relation which had been specifically developed for a soil rather than one 'borrowed' from material mechanics, namely the Critical State Model developed at Cambridge[75,72]. This critical state concept had led to the formulation of the Cam Clay and Modified Cam Clay theories to represent the behaviour of clay under two dimensional conditions. A further departure was made from usual practice when eight noded isoparametric quadrilateral elementswere used, instead of the familiar triangles, to make up the mesh. Two hypothetical problems were solved namely the restrained sample in a triaxial test and an infinite strip footing. The results from the latter analysis were compared to a theoretical result based on the standard oedometer test and reasonable agreement was found.

Smith[78] and Smith and Kay[80] also used the critical state theories in conjunction with the finite element technique. A second approach to the formulation of a stress strain relationship for soil was made using the concept of stress dilatancy

1.4) contd.

developed by Rowe[73], which gives a particularly simple relation for the behaviour of drained sand. These relations were used to analyse the classical plane strain problem of a thick walled hollow cylinder subjected to a steadily increasing bore pressure. Comparisons were made between these results and experimental results carried out on hollow cylinders of sand and clay. Good correlation was found despite the fact that simple triangular elements made up the mesh.

Hoeg[44] used a simplified version of the cam clay theories in the finite element analysis of strain softening clays. It was pointed out that it was impossible to apply the usual non-linear elastic theories to this problem because of the necessity to introduce negative slopes. Results from computations with or without strain softening were compared and the model was applied to analyse the undrained behaviour of a soft clay under a large, instrumented, circular test fill. Good agreement was found and quite dramatic increases in deformations were found for only relatively modest amounts of strain softening.

Smith[79] used the finite element method to investigate the lateral pressure developed as a rigid retaining wall was rotated about its toe. It was pointed out that in any computed solution of a non-linear boundary value problem there are two major aspects;

(a) Adequate and general constitutive relationship for the material under consideration.

(b) Efficient and accurate techniques of computation.

Majid and Craig[99] used an incremental method to

1.4) contd.

carry out non-linear analysis using a material model similar to that of Girijavallabhan[38]. The method was used to analyse a model strip footing resting on a bed of sand. A mixture of triangular and rectangular elements was used to form the mesh allowing for large variations of stress near the footing to be adequately represented, but in regions of small stress changes triangular elements could be used to minimise computer time and effort. Good agreement was found between the theoretical and experimental results, and the importance of choosing an adequate number of load increments was highlighted.

Penman, Burland and Charles[68] reported one of the few cases outside America, when the finite element technique was used on an actual field problem. The method was used to predicts movements at a number of points in Scammonden Dam, a large earth embankment, during construction. Detailed measurements of the movements inside the dam were made enabling a comparison. In an approach similar to that of Clough[17] the incremental form of 'gravity turn on' loading was followed, but as the dam fill was not always placed in horizontal layers, the construction sequence was modelled as closely as possible. For the sake of simplicity, instead of adopting a non-linear material model, a constant value of Young's modulus was calculated from an equivalent value of compression modulus for a number of layers. It was emphasised that this kind of approach applied only during construction. This simplified analysis gave results which were in reasonable agreement with observations, and it was suggested that the method was sufficiently accurate for design purposes.

1.5) Scope of the Work.

The power of the finite element method as a tool for displacement and stress analysis has been highlighted in the previous sections. The basis of any finite element method is obviously an efficiently programmed library of elements and the various ancillary operations necessary to complete the method. The many advantages of the new families of Isoparametric elements have also been pointed out, and hence a large part of the project was taken up in programming these families of two and three dimensional elements.

Appendix (2) presents the development of the stiffness matrices of the various elements. In a novel approach the element stiffness matrix has been treated as the summation of a number of contributions from the combinations of pairs of joints to which the element nodes are connected. It was possible to derive a general expression for the contribution of one pair of nodes to cover all combinations and all elements. This meant that any element could be inserted into the library once its shape functions had been established. The programming of the elements, and ancillary routines, and the development of the finite element package for two and three dimensional analysis is given in Appendix (3).

It is obviously necessary to check the results of any finite element program carefully. As there are also quite a number of elements available, it was desirable to carry out an assessment of the performance of the various elements under some typical conditions, and hence, to select an element giving the best return for the effort.

An assessment and comparison of the various two dimensional elements is made in Chapter (2). The boundary conditions in a finite element mesh are most easily displacement

1.5) contd.

defined, whereas, the opposite is the case for mathematical solutions where boundaries are most easily defined by stresses. It was therefore necessary to use the principle of super-imposition on a classical solution to obtain the case of a flexible strip footing, loaded uniformly and resting on a block of material restrained by perfectly smooth rigid boundaries.

Despite the large number of publications concerning the finite element method, several important boundary value problems have not yet been satisfactorily resolved. Amongst them is the problem of representing smooth interfaces in a finite element mesh. A typical example of this arises when trying to analyse a compression test carried out under so called 'free end' or frictionless end conditions. While numerous investigations have examined the axially loaded cylinder with restrained ends, no comparison has been made to an analysis of the desired non-restrained case. Problems of this nature arise in many important field problem including footings and retaining walls where the interface condition has an important effect on the stress distribution.

Chapter (3) uses a particularly simple method of representing a smooth interface, or indeed any degree of roughness between that and full friction. These elements are used in a non-linear iterative finite element procedure to analyse the plane strain compression test under fixed and free end conditions. A comparison of the results is also made with an experimental one.

Another important problem that has been investigated is the development and propogation of cracks in materials of low tensile strength. The occurrence of cracks, considerably changes the distribution of stress from that predicted by

1.5) contd.

elastic theory, and the stiffness of the mass is reduced, thus reducing the load bearing capacity.

Chapter (4) suggests a method of analysis using the finite element method, whereby the compatability conditions are changed at boundaries where cracks occur. That is to say, that unlike most previous methods, a physical crack is allowed to occur in the mathematical model, rather than attempting to represent it as a zone of weak material, by allowing separation at joints along element boundaries. An incremental finite element procedure was designed as an interaction process of selection of crack position and then change of topology. The method was applied to the problem of an underground opening for which some experimental results were available, enabling a comparison to be made.

A good deal of interest has been shown in the use of the finite element technique in two dimensional conditions of plane strain and axial symmetry, but a large number of problems encountered in Geotechnical Engineering are three dimensional, particularly when concerned with foundations. Sophisticated methods of analysis are used as an aid to the design of structures, but in general, these analyses all make the assumption that the bases are rigidly fixed. The effect of settlement, particularly when it is not uniform across the structure, considerably changes the stress pattern. With the pressure on structural designers to make buildings cheaper they are necessarily becoming more flexible and it is therefore of the utmost importance to have an accurate picture of the settlement pattern and to include these efforts in the structural design. The extra design costs should be more than met by the savings in materials from a more accurate analysis.

1.5) contd.

It seemed logical to include the foundation material in the structural analysis and to analyse the whole structure - soil interaction process together, and the rest of the thesis is devoted to this end. The structure can be idealised as an assemblage of beam and plate elements resting on a foundation material which can be idealised as an assemblage of isoparametric hexahedral elements.

In proposing a method of analysis for space structures and their foundations it was necessary to have a number of test cases to analyse. In Chapter (5) an apparatus is described for performing such tests. The models were prototype space frame structures founded onto a bed of sand. To carry out these tests it was necessary to first design and construct the apparatus. These included a method of depositing a homogeneous bed of sand at known porosity into a test bed. It also involved making a loading frame, a measurement frame and evolving an efficient and reliable testing technique. These were then used to carry out tests on a variety of model structures loaded incrementally at a number of points.

Chapter (6) describes the measurement of the mechanical properties necessary to describe the non-linear response of the sand in the test bed. This involved the Author in design and construction of a triaxial test apparatus capable of imposing a known uniform state of stress on any specimens at the relatively low confining pressures which could be expected to be present in the test bed, and to be able to measure the various deformations. The results from these triaxial tests were used to define the stress-strain relation of the sand over the expected range of initial confining

1.5) contd.

pressures using the simple but effective hyperbolic response.

A non-linear method of analysis was developed to analyse the model tests. Some problems were encountered with the convergence of the iterative technique and so finally an incremental method of solution was adopted. The finite element program developed in this way is described in Chapter (7). The experimental model test results are also discussed in some detail in Chapter (8). A comparison between the theoretical and experimental results is made for one of the model tests and particular emphasis is laid on the effect of the settlement on the structure rather than on the behaviour of the sand.

CHAPTER 2

A CRITICAL ASSESSMENT OF ELEMENT PERFORMANCE.

2.1) Introduction.

Having written a series of programs to carry out stress analysis using the Finite Element Method it was clearly necessary to be able to check their accuracy. For a meaningful check, the solution that is compared with, must be one in which the assumptions inherent in the finite element method are applicable. The most obvious assumption about the method is that the boundary conditions are displacement defined.

Six elements are discussed for the analysis of two dimensional problems in Appendix (2) and programmed in Appendix (3). Faced with the limitless number of isoparametric elements that could be defined the Engineer has to make a choice of which one to use to obtain reasonable results at reasonable cost. In the finite element method, the cost will be made up from the computing costs and the data preparation costs. A great deal has been published about the choice of elements but the Author could find no quantitative comparison, from which a subjective evaluation of element performance could be made.

The three dimensional hexahedral elements, also discussed in Appendices (2) and (3) can be tested under two dimensional conditions. Hence, results could be checked against the two dimensional elements whose reliability had already been established.

2.2) Two Dimensional Equations of Elasticity.

To determine the distribution of stress in a perfectly elastic isotropic material under plane strain conditions, and in the absence of body force, it is necessary to solve the equations of equilibrium of force:

2.2) contd.

$$\frac{\partial \sigma_x}{\partial x} + \frac{\partial \tau_{xy}}{\partial y} = 0$$

$$\frac{\partial \sigma_y}{\partial y} + \frac{\partial \tau_{xy}}{\partial x} = 0 \qquad (2.1)$$

together with the geometric equations

$$\epsilon_x = \frac{\partial u}{\partial x} \quad \epsilon_y = \frac{\partial v}{\partial y} \quad \gamma_{xy} = \frac{\partial u}{\partial y} + \frac{\partial v}{\partial x} \qquad (2.2)$$

and the stress strain relation

$$\epsilon_y = \frac{1}{E}\left\{\sigma_x(1-\nu^2) - \sigma_y \nu(1+\nu)\right\}$$

$$\epsilon_x = \frac{1}{E}\left\{\sigma_y(1-\nu^2) - \sigma_x \nu(1+\nu)\right\} \qquad (2.3)$$

$$\gamma_{xy} = \frac{1}{E}\tau_{xy}\, 2(1+\nu)$$

differentiation of equation (2.2) gives the compatability relation for strains:

$$\frac{\partial^2 \epsilon_x}{\partial y^2} + \frac{\partial^2 \epsilon_y}{\partial x^2} = \frac{\partial^2 \gamma_{xy}}{\partial x \partial y} \qquad (2.4)$$

expressing the strains in terms of stresses from equation (2.3) gives the compatability relation for stresses, thus

$$\frac{\partial^2}{\partial y^2}\left\{\sigma_x - \nu(\sigma_x + \sigma_y)\right\} + \frac{\partial^2}{\partial x^2}\left\{\sigma_y - \nu(\sigma_x + \sigma_y)\right\} = 2\frac{\partial^2 \tau_{xy}}{\partial x \partial y} \qquad (2.5)$$

By supposing that there is a function χ such that

$$\tau_{xy} = -\frac{\partial^2 \chi}{\partial x \partial y} \qquad (2.6)$$

and substituting it into the equilibrium equations (2.1)

$$\frac{\partial}{\partial x}\left\{\sigma_x - \frac{\partial^2 \chi}{\partial y^2}\right\} = 0 \text{ and } \frac{\partial}{\partial y}\left\{\sigma_y - \frac{\partial^2 \chi}{\partial x^2}\right\} = 0 \qquad (2.7)$$

it follows that,

$$\sigma_x = \frac{\partial^2 \chi}{\partial y^2} \text{ and } \sigma_y = \frac{\partial^2 \chi}{\partial x^2}\ , \qquad (2.8)$$

and that the compatability relation (2.5) is satisfied if

2.2) contd.

$$\frac{\partial^4 \chi}{\partial y^4} + \frac{2\ \partial^4 \chi}{\partial^2 x\ \partial^2 y} + \frac{\partial^4 \chi}{\partial y^4} = 0 \qquad (2.9)$$

This is known as the biharmonic equation and is written in shorthand form as

$$\nabla_1{}^4\ \chi = 0 \qquad (2.10)$$

where $\nabla_1{}^2$ is the Laplacian operator and χ is the Airy stress function.

2.2.1) Stress Distribution in a Thick Plate.

Consider the case in Figure (2.1) of a two dimensional elastic media bounded by two parallel planes ($x = \pm b$) to form a thick plate. The plate is deformed by the application of normal pressure to infinitely long strips on the two surfaces. It can be seen that the plane $x = 0$ is a plane of symmetry, and hence on this plane vertical displacements (component u) and shear stresses will be zero. Thus, this plane represents a smooth rigid boundary, a condition easily imposed on a finite element mesh.

Sneddon[82] obtained a solution for this case. The steps to the solution are given in detail in his text so that only a brief outline is presented here. By applying the theory of Fourier transforms to the Laplace operator;

$$\int_{-\infty}^{\infty} \nabla_1{}^4\ f(y) e^{iry}\ dy = \left(\frac{d^2}{dx^2} - r^2\right)^2 \int_{-\infty}^{\infty} f(y)\ e^{iry} \qquad (2.11)$$

and defining

$$G = \int_{-\infty}^{\infty} \chi\ e^{iry} \qquad (2.12)$$

It follows from equation (2.12) that if χ is a

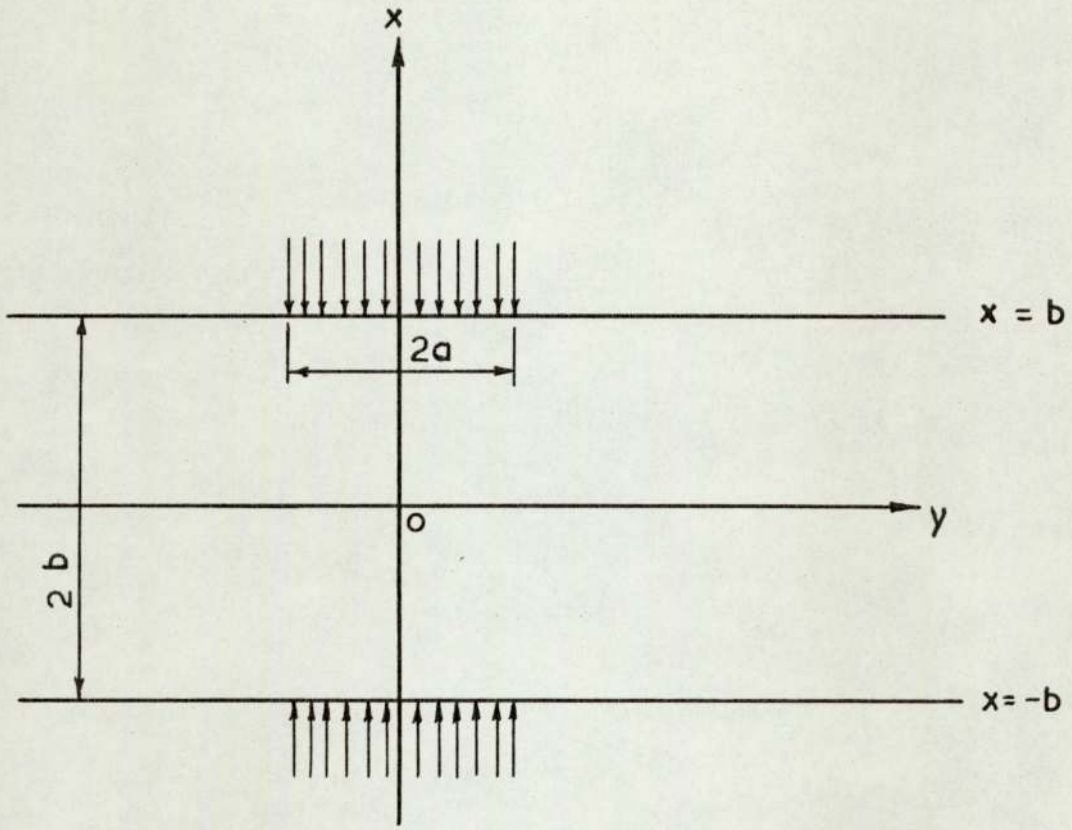

Figure 2.1 Symmetrical loading of a thick plate

2.2.1) contd.

solution of equation (2.10) then G is a solution of

$$\left(\frac{d^2}{dx^2} - r^2\right)^2 G = 0 \qquad (2.13)$$

whose general solution is

$$G = (A+Brx)\, e^{-|r|x} + (C+Drx)\, e^{+|r|x} \qquad (2.14)$$

Fourier inversion of equation (2.12) yields

$$\chi_{(x,y)} = \frac{1}{2\pi}\int_{-\infty}^{\infty} G(x,r)\, e^{-iry}\, dr \qquad (2.15)$$

The Airy stress function for this case can be derived from equations (2.14) and (2.15) when the arbitrary constants A,B,C,D are known. The constants depend upon the boundary conditions under consideration. To determine these constants the stresses are required in terms of the function G(x,r) and its derivatives with respect to x. Multiplying the first of equation (2.8) by e^{iry} and integrating the result gives;

$$\int_{-\infty}^{\infty} \sigma_x\, e^{iry}\, dy = \int_{-\infty}^{\infty} \frac{\partial^2 \chi}{\partial x^2}\, e^{iry}\, dy = -r^2 G \qquad (2.16)$$

Similar expressions can be obtained for the other stress components. Fourier inversion of these will yield,

$$\begin{aligned}
\sigma_x &= -\frac{1}{2\pi}\int_{-\infty}^{\infty} r^2 G\, e^{-iry}\, dr \\
\sigma_y &= -\frac{1}{2\pi}\int_{-\infty}^{\infty} \frac{d^2G}{dx^2}\, e^{-iry}\, dr \qquad (2.17) \\
\tau_{xy} &= -\frac{1}{2\pi}\int_{-\infty}^{\infty} ir\frac{dG}{dx}\, e^{-iry}\, dr
\end{aligned}$$

Now consider the case of a thick plate with the

2.2.1) contd.

following boundary conditions

(i) $\sigma_x = - p_1(y)$ & $\tau_{xy} = 0$ at $x = b$

(ii) $\sigma_x = - p_2(y)$ & $\tau_{xy} = 0$ at $x = -b$

From vertical equilibrium

$$\int_{-\infty}^{\infty} p_1(y)dy = \int_{-\infty}^{\infty} p_2(y)dy \qquad (2.18)$$

Since $p_1(y)$ and $p_2(y)$ are even functions then the odd parts of equation (2.17) can be ignored and only half the integral need be evaluated, thus

$$\sigma_x = - \frac{2}{\pi} \int_0^{\infty} r\, G\, \mathrm{Cos}(ry)dr$$

$$\tau_{xy} = - \frac{2}{\pi} \int_0^{\infty} r \frac{dG}{dx} \mathrm{Sin}(ry)\, dr \qquad (2.19)$$

$$\sigma_y = - \frac{2}{\pi} \int_0^{\infty} \frac{d^2G}{dx^2} \mathrm{Cos}(ry)\, dr$$

Similarly equation (2.14) can be simplified to

$$G = (A+Brx)\, \mathrm{Cosh}(rx) + (C+Drx)\, \mathrm{Sinh}(rx) \qquad (2.20)$$

The applied pressure can be expressed in terms of a Fourier cosine transform. In the particular case of $p_1(y) = p_2(y) = p$ over the region $-a \leqslant y \leqslant a$ on the plane $x = \pm b$, further simplification is possible:

$$\overline{p}_1(y) = \overline{p}_2(y) = p \frac{\mathrm{Sin}(ra)}{r} \qquad (2.21)$$

Inserting equation (2.20) into the first two parts of equation (2.19) and inserting the known boundary conditions yields four equations containing the four unknowns A,B,C and D.

2.2.1) contd.

Solving these equations and substituting their values back into equation (2.20) gives an expression for the function G(x,r) which can then be back substituted into equation (2.19) to obtain the solutions:

$$\sigma_x = -\frac{4p}{\pi}\int_0^\infty \left[\frac{(\sinh r + r\cosh r)\cosh(rq) - rq\,\sinh r\,\sinh(rq)}{2r + \sinh(2r)}\right] \times \frac{\sin(cr)}{r}\cos(rp)\,dr \qquad (2.22.1)$$

$$\tau_{xy} = -\frac{4p}{\pi}\int_0^\infty \left[\frac{rq\,\sinh r\,\cosh(rq) - r\,\cosh r\,\sinh(rq)}{2r + \sinh(2r)}\right] \frac{\sin(cr)}{r} \times \sin(rp)\,dr \qquad (2.22.2)$$

$$\sigma_y = -\frac{4p}{\pi}\int_0^\infty \left[\frac{(\sinh r - r\cosh r)\cosh(rq) + rq\,\sinh r\,\sinh(rq)}{2r + \sinh(2r)}\right] \times \frac{\sin(cr)}{r}\cos(pr)\,dr \qquad (2.22.3)$$

where $c = a/b \quad q = x/b \quad p = y/b$.

Sneddon[82] pointed out that the evaluation of these integrals would be troublesome, and suggested that it would be easiest to determine values by a series of numerical integrations.

Before the application of numerical techniques it is advisable to inspect the shape of the integrand. Consider equation (2.22.1), for a value of r = 0 the integrand is indeterminate, however taking limits:

$$\lim_{r \to 0} f(r) = \frac{c}{2} \quad , \quad \lim_{r \to \infty} f(r) = 0$$

Figures (2.2a) and (2.2b) show the shape of the integrand for two values of q on the plane y = 0 (or p = o),

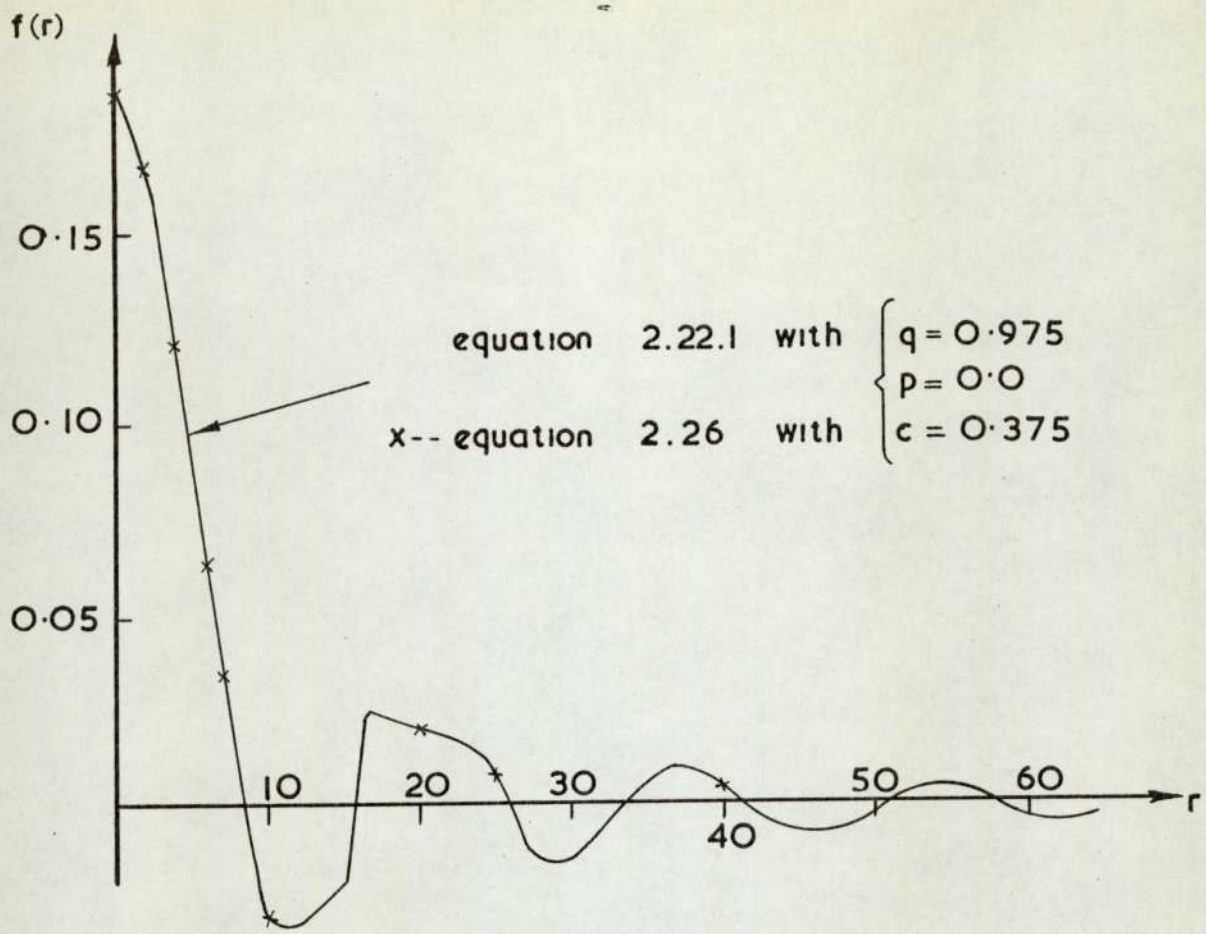

Figure 2. 2a

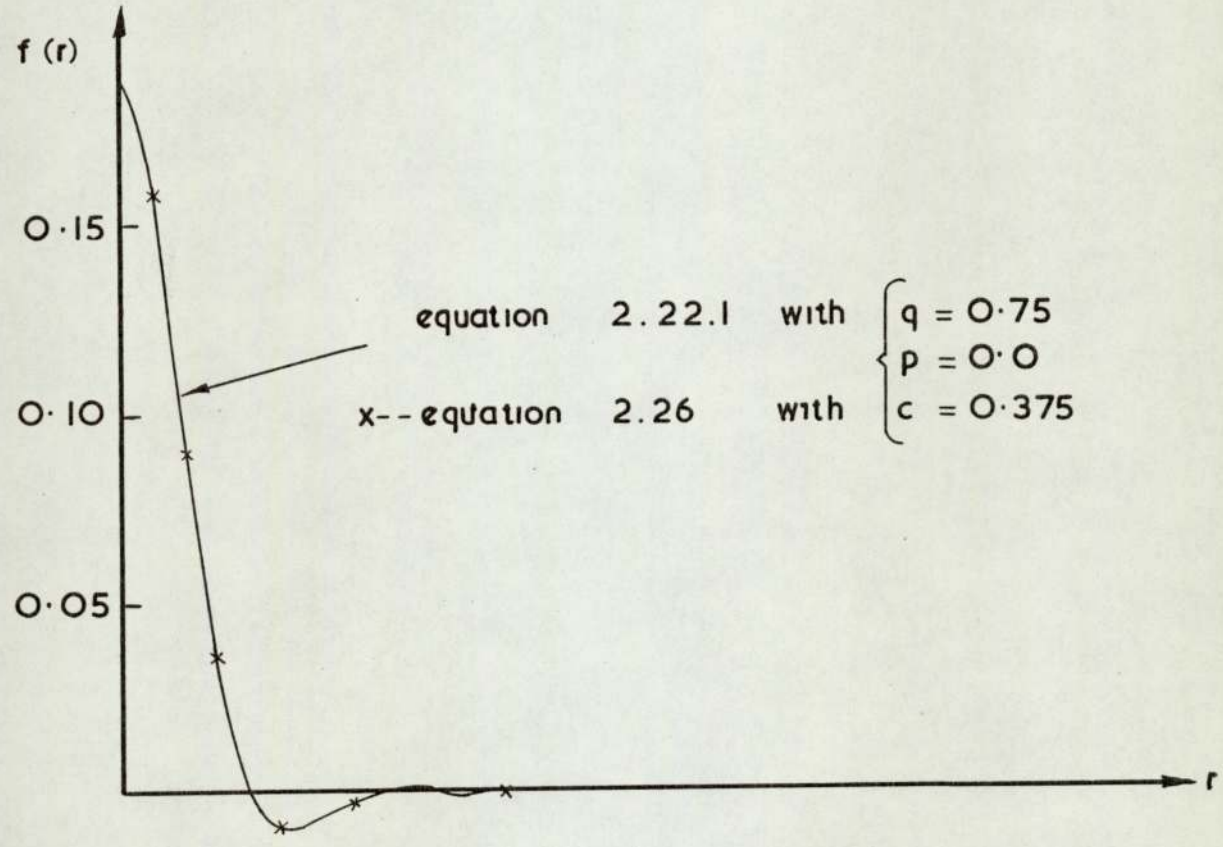

Figure 2.2 b

2.2.1) contd.

the first close to the applied pressure and the other some distance inside. The shape of the former reveals that decay is taking place very slowly. It must also be realised that at relatively large values of r the hyperbolic functions Sinh(r) and Cosh(r) diverge, which leads to numerical rounding errors in their evaluation. It is clear that numerical integration cannot be applied successfully to points relatively close to the loaded area. However, Figure (2.2b) shows that away from this zone the value of the integrand decays rapidly to zero and here numerical integration would give an accurate solution. It is in the zone near to the applied pressure that the largest stress changes occur, and so it is necessary to have accurate values. It was therefore necessary to look at other techniques.

Sneddon[81] pointed out that it is the appearance of the function $(2r + \mathrm{Sinh}(2r))$ in the denominator which makes analytical integration troublesome. This difficulty can be overcome by employing an approximate expression of the form;

$$f_1(u) = (su+\tfrac{1}{2})e^{-tu} + 2u\, e^{-u} \qquad (2.23)$$

to represent the function,

$$f(u) = \frac{u}{u+ \mathrm{Sinh}(u)} \qquad (2.24)$$

over the entire range of integration.

From equation (2.23) it can be seen that $f_1(u) \to \frac{1}{2}$ as $u \to o$ and that $f_1(u) \simeq 2ue^{-u}$ as $u \to \infty$. The arbitrary constants s and t are chosen to ensure that the fit is close for large values of u, because the function appears in the integrand as a product with an exponential factor. Any variation near the origin may be compensated for by keeping

2.2.1) contd.

the area under the curve $(f_1(u) - f(u))$ as small as possible. These conditions are satisfied by choosing

$$s = -1.55 \text{ and } t = 1.40 \qquad (2.25)$$

Substituting this approximation into equation (2.22.1) gives:

$$\sigma_x = -\frac{4p}{\pi}\int_0^\infty \left[(\text{Sinh}hr+r\text{Cosh}hr)\text{Cosh}(rq)-rq\text{Sinh}hr\text{Sinh}hrq\right]\frac{\text{Sin}(cr)}{2r^2}\text{Cos}(pr)$$

$$\times\left[(2sr+\tfrac{1}{2})e^{-2tr} + 4r\,e^{-2r}\right]dr \qquad (2.26)$$

Some values of the new integrand in equation (2.26) for a few values of r are indicated by small crosses in Figure (2.2a) and (2.2b). It can be seen that the approximation gives an excellent fit over the entire range of integration and throughout the plate.

The analytical integration of equation (2.26) can now proceed, rearranging the hyperbolic and trigonometric function products as sums gives:-

$$\sigma_x = -\frac{4p}{\pi}\int_0^\infty \left[\text{Sinh}(1+q)r+\text{Sinh}(1-q)r+r(1-q)\text{Cosh}(1+q)r+r(1+q)\text{Cosh}(1-q)r\right]$$

$$\times\left[\text{Sin}(c+p)r+\text{Sin}(c-p)r\right]\left[\frac{s}{4r}e^{-2tr} + \frac{1}{16r^2}e^{-2tr} + \frac{1}{2r}e^{-2r}\right]dr \qquad (2.27)$$

Expanding the hyperbolic functions in terms of exponentials

$$\sigma_x = -\frac{4p}{\pi}\int_0^\infty \left[e^{(1+q)r} - e^{-(1+q)r} + e^{(1-q)r} - e^{-(1-q)r} + r(1-q)e^{(1+q)r} + \right.$$

$$\left. + r(1-q)e^{-(1+q)r} + r(1+q)e^{(1-q)r} + r(1+q)e^{-(1-q)r}\right]$$

$$\times\left[\text{Sin}(c+p)r+\text{Sin}(c-p)r\right]\left[\frac{s}{8r}e^{-2tr} + \frac{1}{32r^2}e^{-2tr} + \frac{1}{4r}e^{2r}\right]dr \qquad (2.28)$$

2.2.1) contd.

Multiplying out equation (2.28)

$$\sigma_x = -\frac{4p}{\pi}\int_0^\infty \Bigg\{ \left[\frac{s}{8}(1-q)+\frac{(4s+1-q)}{32r}+\frac{1}{32r^2}\right]e^{-(-1-q+2t)r} + \left[\frac{s}{8}(1-q)+\frac{(-4s+1-q)}{32r}-\frac{1}{32r^2}\right]e^{-(1+q+2t)r}$$

$$+\left[\frac{s}{8}(1+q)+\frac{(4s+1+q)}{32r}+\frac{1}{32r^2}\right]e^{-(-1+q+2t)r} + \left[\frac{s}{8}(1+q)+\frac{(-4s+1+q)}{32r}-\frac{1}{32r^2}\right]e^{-(1-q+2t)r}$$

$$+\left[\frac{1}{4r}+\frac{(1-q)}{4}\right]e^{-(-1-q+2)r}+\left[-\frac{1}{4r}+\frac{(1-q)}{4}\right]e^{-(1+q+2)r} + \left[\frac{1}{4r}+\frac{(1+q)}{4}\right]e^{-(-1+q+2)r}$$

$$+\left[-\frac{1}{4r}+\frac{(1+q)}{4}\right]e^{-(-1+q+2)r}\Bigg\}(\mathrm{Sin}(c+p)r+\mathrm{Sin}(c-p)r)\,dr \qquad (2.29)$$

Multiplying out equation (2.29) will yield forty products, each of these products require integration. They will all be combinations of trigonometric functions, exponentials and powers and fall into one of the following three classes:-

(a) $I_1 = \int_0^\infty \mathrm{Sin}\, fx\, e^{-gx}\, dx$

(b) $I_2 = \int_0^\infty \mathrm{Sin}\, fx\, e^{-gx}\, \frac{dx}{x}$

(c) $I_3 = \int_0^\infty \frac{e^{-gx}-e^{-hx}}{x^2}\, \mathrm{Sin}\, fx\, dx$

The values of these integrals are (Gradshteyn and Ryzhik[40];

2.2.1) contd.

(a) $I_1 = \dfrac{f}{f^2+g^2}$ $\qquad g > 0$

(b) $I_2 = \tan^{-1}\left(\dfrac{g}{f}\right)$ $\qquad g > 0$

(c) $I_3 = \dfrac{f}{2}\log_n\left(\dfrac{f^2+h^2}{f^2+g^2}\right) + h\tan^{-1}\left(\dfrac{f}{h}\right) - g\tan^{-1}\left(\dfrac{f}{g}\right)$ $\quad g > 0$, $h > 0$

Each of the exponential powers has to be positive and since, $-1 \leqslant q \leqslant 1$ and $t \geqslant 1$ the condition is satisfied so the integration proceeds to yield

$$\sigma_x = -\frac{4p}{\pi}\left\{\frac{(4s+2-2t)}{32}\left[\tan^{-1}\left(\frac{c+p}{-1-q+2t}\right) + \tan^{-1}\left(\frac{c+p}{-1+q+2t}\right) + \right.\right.$$

$$\left. + \tan^{-1}\left(\frac{c-p}{-1-q+2t}\right) + \tan^{-1}\left(\frac{c-p}{-1+q+2t}\right)\right]$$

$$+ \frac{(-4s+2+2t)}{32}\left[\tan^{-1}\left(\frac{c+p}{1+q+2t}\right) + \tan^{-1}\left(\frac{c+p}{1-q+2t}\right) + \tan^{-1}\left(\frac{c-p}{1+q+2t}\right) + \tan^{-1}\left(\frac{c-p}{1-q+2t}\right)\right]$$

$$+ \frac{s}{8}(1-q)\left[\frac{(c+p)}{(c+p)^2+(-1-q+2t)^2} + \frac{(c+p)}{(c+p)^2+(1+q+2t)^2} + \frac{(c-p)}{(c-p)^2+(-1-q+2t)^2}\right.$$

$$\left. + \frac{(c-p)}{(c-p)^2+(1+q+2t)^2}\right] + \frac{s}{8}(1+q)\left[\frac{(c+p)}{(c+p)^2+(-1+q+2t)^2} + \frac{(c+p)}{(c+p)^2+(1-q+2t)^2}\right.$$

$$\left. + \frac{(c-p)}{(c-p)^2+(-1+q+2t)^2} + \frac{(c-p)}{(c-p)^2+(1-q+qt)^2}\right] + \frac{(c+p)}{64}\left[\log_n\left(\frac{(c+p)^2+(1+q+2t)^2}{(c+p)^2+(-1-q+2t)^2}\right)\right.$$

$$\left. + \log_n\left(\frac{(c+p)^2+(1-q+2t)^2}{(c+p)^2+(-1+q+2t)^2}\right)\right] + \frac{(c-p)}{64}\left[\log_n\left(\frac{(c-p)^2+(1+q+2t)^2}{(c-p)^2+(-1-q+2t)^2}\right)\right.$$

$$\left. + \log_n\left(\frac{(c-p)^2+(1-q+2t)^2}{(c-p)^2+(-1+q+2t)^2}\right)\right] + \frac{1}{4}\left[\tan^{-1}\left(\frac{c+p}{-1-q+2}\right) + \tan^{-1}\left(\frac{c+p}{-1+q+2}\right)\right.$$

$$\tan^{-1}\left(\frac{c-p}{-1-q+2}\right) + \tan^{-1}\left(\frac{c-p}{-1+q+2}\right) - \tan^{-1}\left(\frac{c+p}{1+q+2}\right) - \tan^{-1}\left(\frac{c+p}{1-q+2}\right) - \tan^{-1}\left(\frac{c-p}{1+q+2}\right)$$

$$\left. - \tan^{-1}\left(\frac{c-p}{1-q+2}\right)\right] + \frac{(1-q)}{4}\left[\frac{(c+p)}{(c+p)^2+(-1-q+2)^2} + \frac{(c+p)}{(c+p)^2+(1+q+2)^2} + \right.$$

$$\left. + \frac{(c-p)}{(c-p)^2+(-1-q+2)^2}\right.$$

2.2.1) contd.

$$+\frac{(c-p)}{(c-p)^2+(1+q+2)^2}\Bigg]+\frac{(1+q)}{4}\Bigg[\frac{(c+p)}{(c+p)^2+(-1+q+2)^2}+\frac{(c+p)}{(c+p)^2+(1-q+2)^2}$$

$$+\frac{(c-p)}{(c-p)^2+(-1+q+2)^2}+\frac{(c-p)}{(c-p)^2+(1-q+2)^2}\Bigg]\Bigg\} \quad (2.30)$$

In an identical manner a solution can be obtained from equation (2.22.3) for the horizontal stress.

$$\sigma_y = -\frac{4p}{\pi}\Bigg\{\frac{(-4s+2q-2t)}{32}\Bigg[\tan^{-1}\left(\frac{c+p}{-1-q+2t}\right)-\tan^{-1}\left(\frac{c+p}{1-q+2t}\right)$$

$$+\tan^{-1}\left(\frac{c-p}{-1-q+2t}\right)-\tan^{-1}\left(\frac{c-p}{1-q+2t}\right)\Bigg]$$

$$+\frac{(4s+2q+2t}{32}\Bigg[-\tan^{-1}\left(\frac{c+p}{-1+q+2t}\right)+\tan^{-1}\left(\frac{c+p}{1+q+2t}\right)-\tan^{-1}\left(\frac{c-p}{-1+q+2t}\right)+\tan^{-1}\left(\frac{c-p}{1+q+2t}\right)$$

$$+\frac{s}{8}(-1+q)\Bigg[\frac{(c+p)}{(c+p)^2+(-1-q+2t)^2}+\frac{(c+p)}{(c+p)^2+(1+q+2t)^2}+$$

$$+\frac{(c-p)}{(c-p)^2+(-1-q+2t)^2}+\frac{(c-p)}{(c-p)^2+(1+q+2t)^2}\Bigg]$$

$$+\frac{s}{8}(-1-q)\Bigg[\frac{(c+p)}{(c+p)^2+(-1+q+2t)^2}+\frac{(c+p)}{(c+p)^2+(1-q+2t)^2}+$$

$$+\frac{(c-p)}{(c-p)^2+(-1+q+2t)^2}+\frac{(c-p)}{(c-p)^2(1-q+2t)^2}\Bigg]$$

$$+\frac{(c+p)}{64}\Bigg[\log_n\left(\frac{(c+p)^2+(1+q+2t)^2}{(c+p)^2+(-1-q+2t)^2}\right)+\log_n\left(\frac{(c+p)^2+(1-q+2t)^2}{(c+p)^2+(-1+q+2t)^2}\right)\Bigg]$$

$$+\frac{(c-p)}{64}\Bigg[\log_n\left(\frac{(c-p)^2+(1+q+2t)^2}{(c-p)^2+(-1-q+2t)^2}\right)+\log_n\left(\frac{(c-p)^2+(1-q+2t)^2}{(c-p)^2+(-1+q+2t)^2}\right)\Bigg]$$

$$+\frac{1}{4}\Bigg[\tan^{-1}\left(\frac{c+p}{-1-q+2}\right)+\tan^{-1}\left(\frac{c+p}{-1+q+2}\right)+\tan^{-1}\left(\frac{c-p}{-1-q+2}\right)+\tan^{-1}\left(\frac{c-p}{-1+q+2}\right)$$

$$-\tan^{-1}\left(\frac{c+p}{1+q+2}\right)-\tan^{-1}\left(\frac{c+p}{1-q+2}\right)-\tan^{-1}\left(\frac{c-p}{1+q+2}\right)-\tan^{-1}\left(\frac{c-p}{1-q+2}\right)\Bigg]$$

2.2.1) contd.

$$+\frac{(-1+q)}{4}\left[\frac{(c+p)}{(c+p)^2+(-1-q+2)^2}+\frac{(c+p)}{(c+p)^2+(1+q+2)^2}+\right.$$

$$\left.+\frac{(c-p)}{(c-p)^2+(-1-q+2)^2}+\frac{(c-p)}{(c-p)^2+(1+q+2)^2}\right]$$

$$+\frac{(-1-q)}{4}\left[\frac{(c+p)}{(c+p)^2+(-1+q+2)^2}+\frac{(c+p)}{(c+p)^2+(1-q+2)^2}+\right.$$

$$\left.\left.+\frac{(c-p)}{(c-p)^2+(-1+q+2)^2}+\frac{(c-p)}{(c-p)^2+(1-q+2)^2}\right]\right\} \quad (2.31$$

A solution can also be obtained for equation (2.22.2) the shear stress, but the product Sin(cr) Sin(pr) cannot be treated in the same way because of the integral

$$\int_0^\infty e^{-cx}\,\mathrm{Cos}\,bx\,\frac{dx}{x} = \infty$$

By following similar steps, as before, equation (2.22.2) becomes

$$\tau_{xy} = -\frac{4p}{\pi}\int_0^\infty\left\{\left[\frac{s}{8}(q-1)e^{-(-1-q+2t)r}+\frac{(q-1)}{4}e^{-(-1-q+2)r}-\right.\right.$$

$$-\frac{\alpha}{8}(q+1)e^{-(1+q+2t)r}$$

$$-\frac{(q-1)}{4}e^{-(1+q+2)}+\frac{s}{8}(q+1)e^{-(1+q+2t)r}+\frac{(q+1)}{4}e^{-(-1+q+2)r}-$$

$$-\frac{s}{8}(q+1)e^{-(1-q+2t)r}$$

$$\left.-\frac{(q+1)}{4}e^{-(1-q+2)r}\right]\left[-\cos(c+p)r+\mathrm{Cos}(c-p)r\right]+$$

$$\left[\frac{(q-1)}{16r}e^{-(-1-q+2t)r}-\frac{(q-1)}{16r}e^{-(1+q+2t)r}\right.$$

$$\left.\left.+\frac{(q+1)}{16r}e^{-(-1+q+2t)r}-\frac{(q+1)}{16r}e^{-(1-q+2t)r}\right]\left[\mathrm{Sin}(cr)\mathrm{Sin}(pr)\right]\right\}dr \quad (2.32)$$

2.2.1) contd.

In this case the products fall into only two classes with values as shown (Gradshteyn and Rhyhik[40].

$$(a)\quad \int_0^\infty e^{-gx}\,\mathrm{Cos}\,fx\,dx = \frac{g}{g^2+f^2}$$

$$(b)\quad \int_0^\infty e^{-gx}\,\mathrm{Sin}\,fx\,\mathrm{Sin}\,hx\,\frac{dx}{x} = \frac{1}{4}\log_n\left[\frac{g^2+(f+n)^2}{g^2+(f-h)^2}\right]$$

The integration proceeds to yield

$$\tau_{xy} = \frac{4p}{\pi}\left\{\frac{q-1}{64}\left[\left\{\log_n\left(\frac{(-1-q+2t)^2+(c+p)^2}{(-1-q+2t)^2+(c-p)^2}\right) - \log_n\left(\frac{(1+q+2t)^2+(c+p)^2}{(1+q+2t)^2+(c-p)^2}\right)\right]\right.\right.$$

$$+\frac{(q+1)}{64}\left[\log_n\left(\frac{(-1+q+2t)^2+(c+p)^2}{(-1+q+2t)^2+(c-p)^2}\right) - \log_n\left(\frac{(1-q+2t)^2+(c+p)^2}{(1-q+2t)^2+(c-p)^2}\right)\right]$$

$$+\frac{s}{8}(q-1)\left[-\frac{(-1-q+2t)}{(-1-q+2t)^2+(c+p)^2} + \frac{(1+q+2t)}{(1+q+2t)^2+(c+p)^2} + \right.$$

$$\left.+\frac{(-1-q+2t)}{(-1-q+2t)^2+(c-p)^2} - \frac{(1+q+2t)}{(1+q+2t)^2+(c-p)^2}\right]$$

$$+\frac{s}{8}(q+1)\left[-\frac{(-1+q+2t)}{(-1+q+2t)^2+(c+p)^2} + \frac{(1-q+2t)}{(1-q+2t)^2+(c+p)^2} + \right.$$

$$\left.+\frac{(-1+q+2t)}{(-1+q+2t)^2+(c-p)^2} - \frac{(1-q+2t)}{(1-q+2t)^2+(c-p)^2}\right]$$

$$+\frac{(q-1)}{4}\left[-\frac{(-1-q+2)}{(-1-q+2)^2+(c+p)^2} + \frac{(1+q+2)}{(1+q+2)^2+(c+p)^2} + \right.$$

$$\left.\left.+\frac{(-1-q+2)}{(-1-q+2)^2+(c-p)^2} - \frac{(1+q+2)}{(1+q+2)^2+(c+p)^2}\right]\right.$$

2.2.1) contd.

$$+\frac{(q+1)}{4}\left[-\frac{(-1+q+2)}{(-1+q+2)^2(c+p)^2}+\frac{(1-q+2)}{(1-q+2)^2+(c+p)^2}+\right.$$

$$\left.+\frac{(-1+q+2)}{(-1+q+2)^2+(c-p)^2}-\frac{(1-q+2)}{(1-q+2)^2+(c-p)^2}\right]\Bigg\}$$

It has already been noticed that at points away from the loaded area numerical analysis would give an accurate solution. It is therefore possible to check values obtained from equations (2.30), (2.31) and (2.33) against those obtained from the numerical integration of equations (2.22).

To do this, the Author wrote a program incorporating an I.C.L. scientific subroutine[45] called F4INTGSS. This routine carries out numerical integration at a point using Gauss 4 and 6 point rules with a self adjusting step length. The routine shortens the step length until both rules agree to a specified accuracy (here 0.00005). Table (2.1) shows how the answers compared.

POSITION		σ_x		σ_y		τ_{xy}	
p	q	A.S.	N.I.S.	A.S.	N.I.S.	A.S.	N.I.S.
0.25	0.75	-0.7779	-0.7752	-0.3492	-0.3455	-0.1830	-0.1867
0.25	0.25	-0.5741	-0.5667	-0.1069	-0.1074	-0.0609	-0.0622

TABLE (2.1)

AS - Author's Solution

NIS - Numerical Int.Solutio

2.2.2) Periodic Loading of a Thick Plate.

Having obtained a solution to the problem in Figure (2.1) it is possible to use the principle of superimposition to obtain a solution for the case in Figure (2.3). This figure shows an

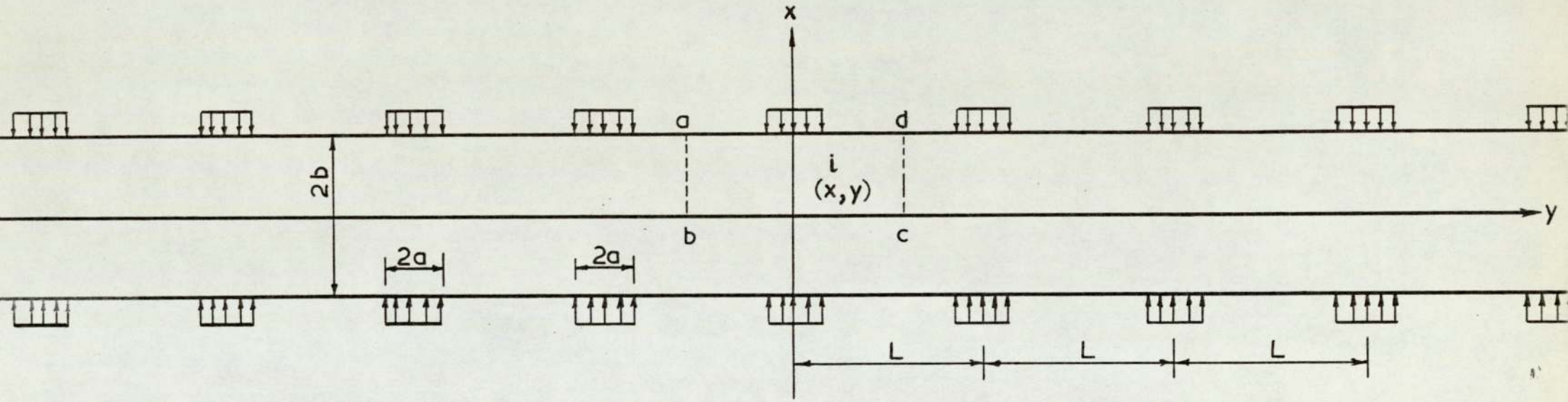

Figure. 2.3

2.2.2) contd.

infinite number of loaded strips at a period of ℓ. Thus the planes $y = \pm \ell/2$ now are both planes of horizontal symmetry and by the same reasoning as before they can be considered as smooth rigid boundaries. The region a,b,c,d in Figure (2.3) then represents an elastic material bounded on three sides by smooth rigid boundaries, and loaded by a region of applied pressure on the free surface.

To obtain the values of the three stress components at the point i in Figure (2.3) it is necessary to sum the contributions from a number of loaded strips each having a different y-coordinate. These coordinates will be (X,Y), (X,L-Y), (X,L+Y), (X,2L-Y), (X,2L+Y) etc, or in general terms (X,nL$\pm$Y) where n = 0,1,2 etc. In practice it was found only necessary to add in three strips on either side of the central one, for beyond this the contributions became insignificant. (St.Venants Principle).

2.3) Finite Element Analysis.

The chosen test problem is illustrated in Figure (2.4). In the finite element idealisation the smooth rigid boundaries will be represented by joints on rollers. The programs described in Appendix (3) did not include a facility to allow for the application of general surface pressures so these were converted into equivalent nodal forces, using the distribution coefficients quoted by Zienkiewicz[98] in his text and illustrated in Figure (2.5).

The Finite Element meshes used to analyse the problem in Figure (2.4) were all designed as a regular grid of joints so that all the elements were rectangular. This was done to

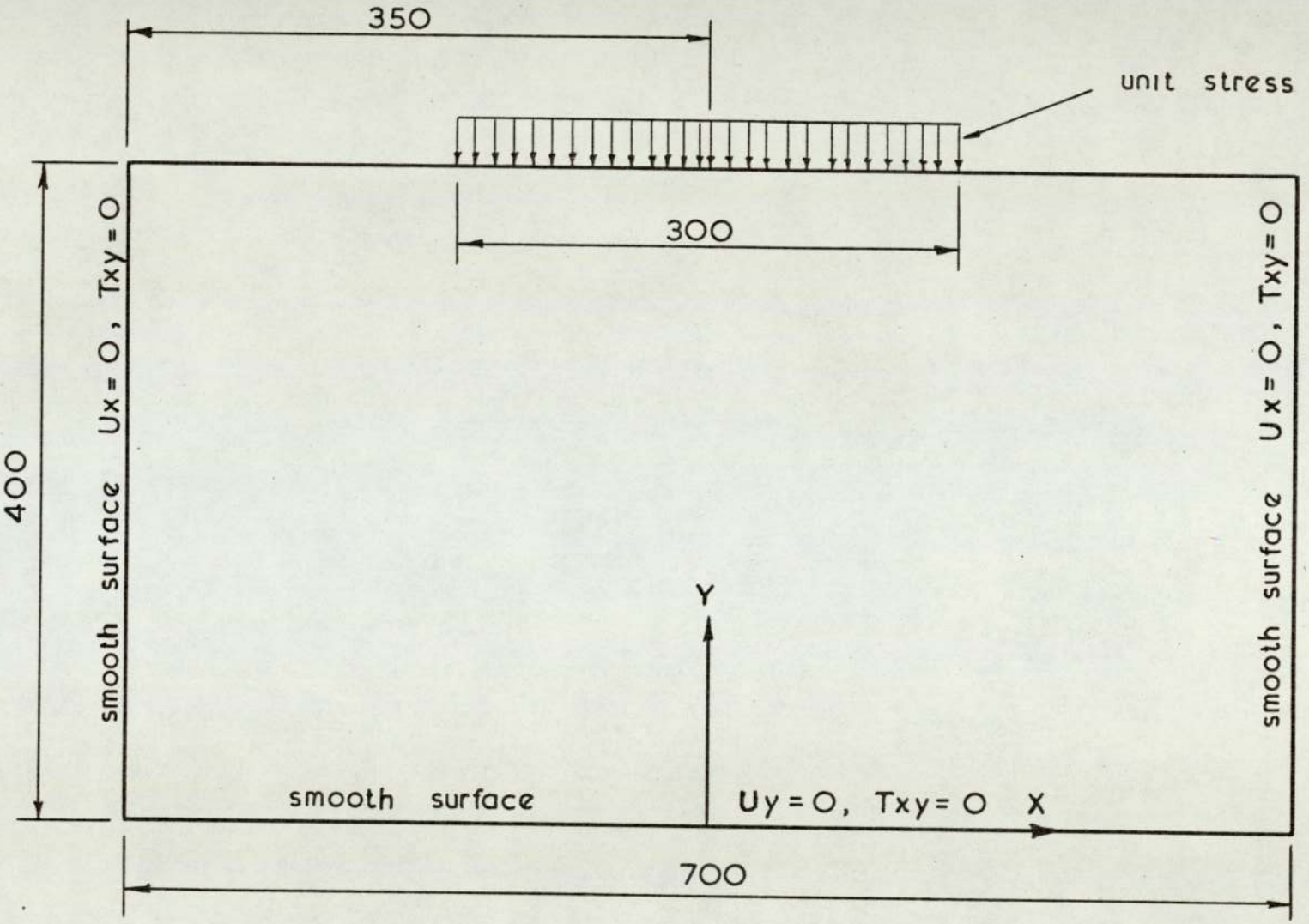

Figure 2.4. Definition of test problem

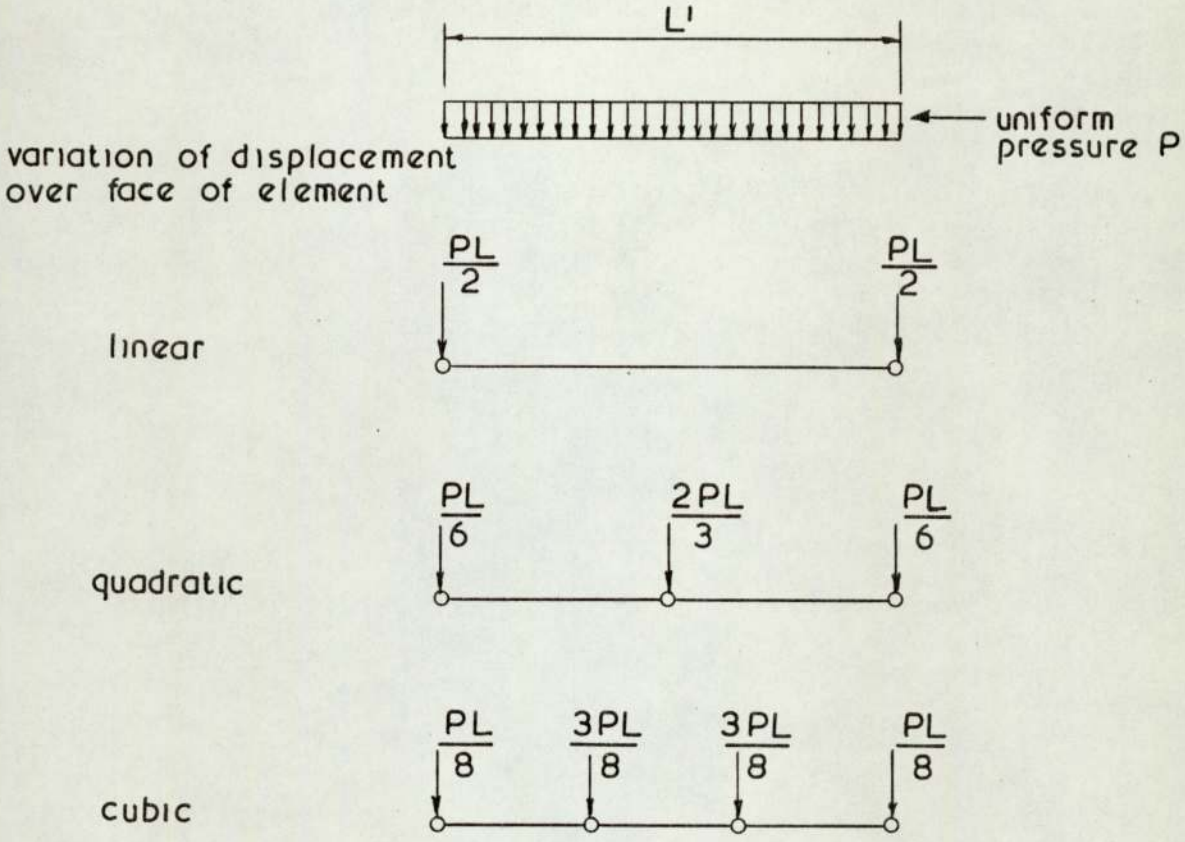

Figure. 2.5 Representation of a uniform pressure as equivalent nodal forces

2.3) contd.

facilitate the process of refinement of the mesh without changing the idealisation. Each of the six two dimensional elements was used to analyse the problem with three meshes. Each of these meshes was a definite sub-division of its predecessor. The eighteen Finite Element meshes are shownin Figures (2.6a)-(2.6f). In the analysis using Isoparametric elements, the number of Gauss points was varied to find the least number which each element required.

2.3.1) Results.

The normal stress components σ_x and σ_y, on the plane X = 0.0 of Figure (2.4), resulting from Finite Element analysis of each of the meshes in Figures (2.6a)-(2.6f), are plotted against depth in Figures (2.7a)-(2.7f). Also plotted in these figures is the result of the explicit solution obtained in the manner described in Section (2.2.2). The shear stress in the plane X = 0.0 is theoretically zero, due to symmetry, and all the finite element solutions yielded $\tau_{xy} < 10^{10}$. The minimum number of Gauss points that could be used in the numerical integration of the stiffness matrix for the isoparametric elements without any significant loss of accuracy in the calculation of the stress components is given in Table (2.2) below.

Quadrilateral Element name	Number of nodes	Minimum Number of Gauss Points.
Linear	4	2
Quadratic Serendipity	8	2
Cubic Serendipity	12	3
Quadratic Lagrangian	9	3
Cubic Lagrangian	16	4

TABLE (2.2)

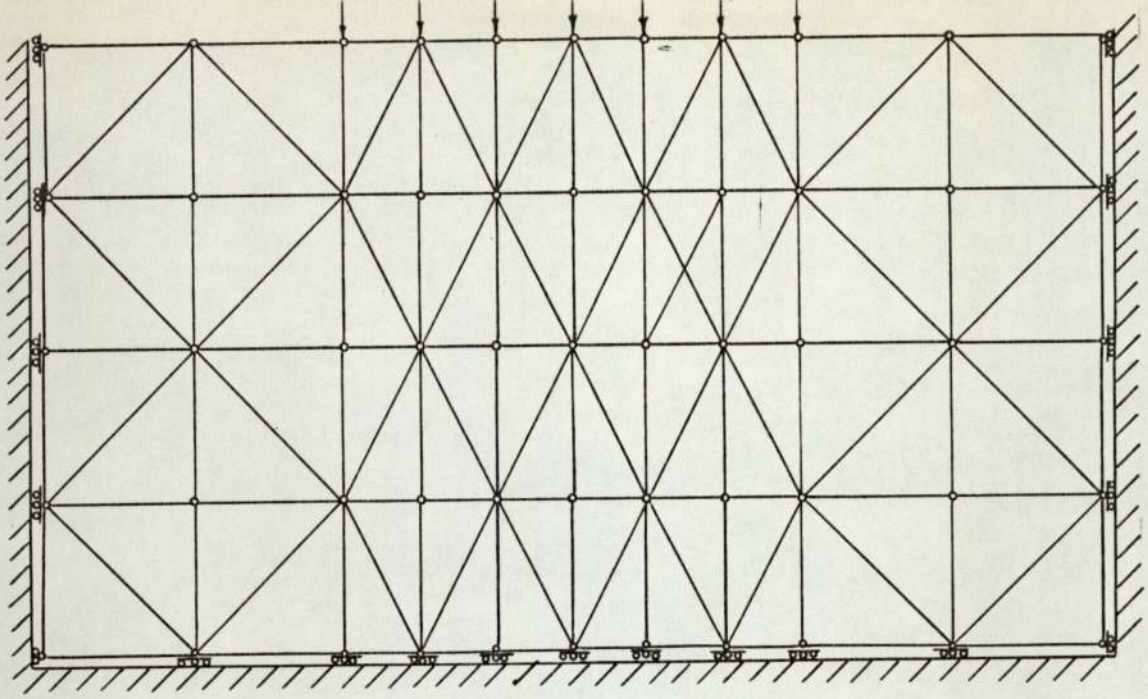

TRI 80
80 element
55 joints

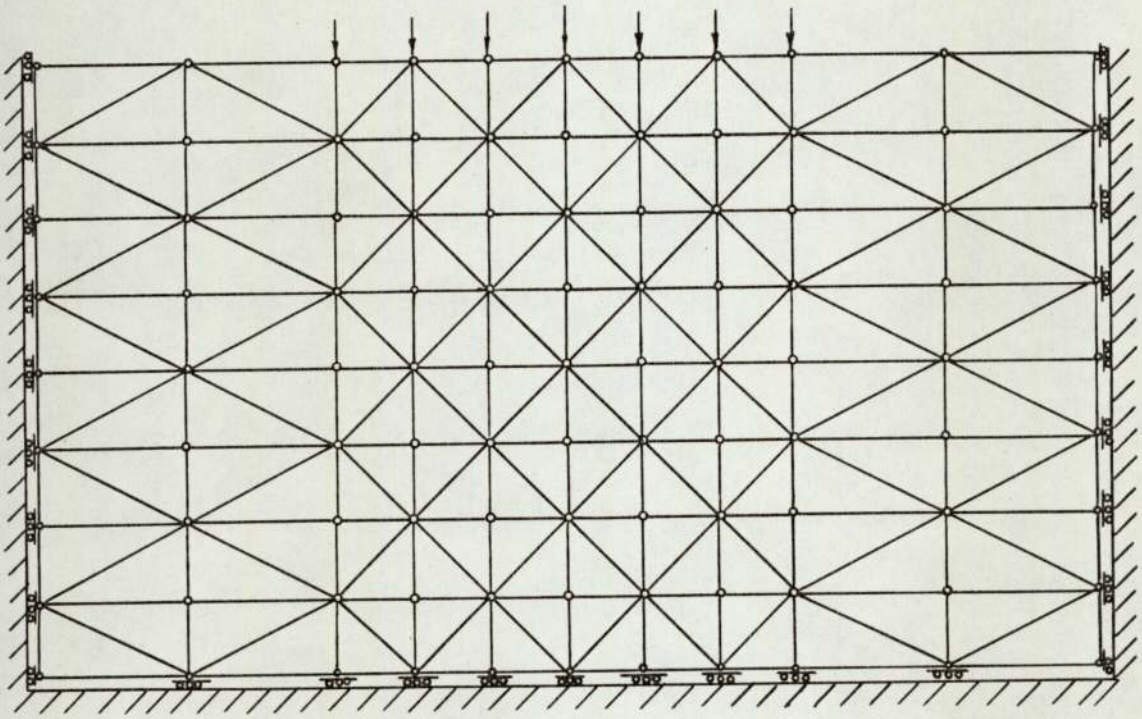

TRI 160
160 element
99 joints

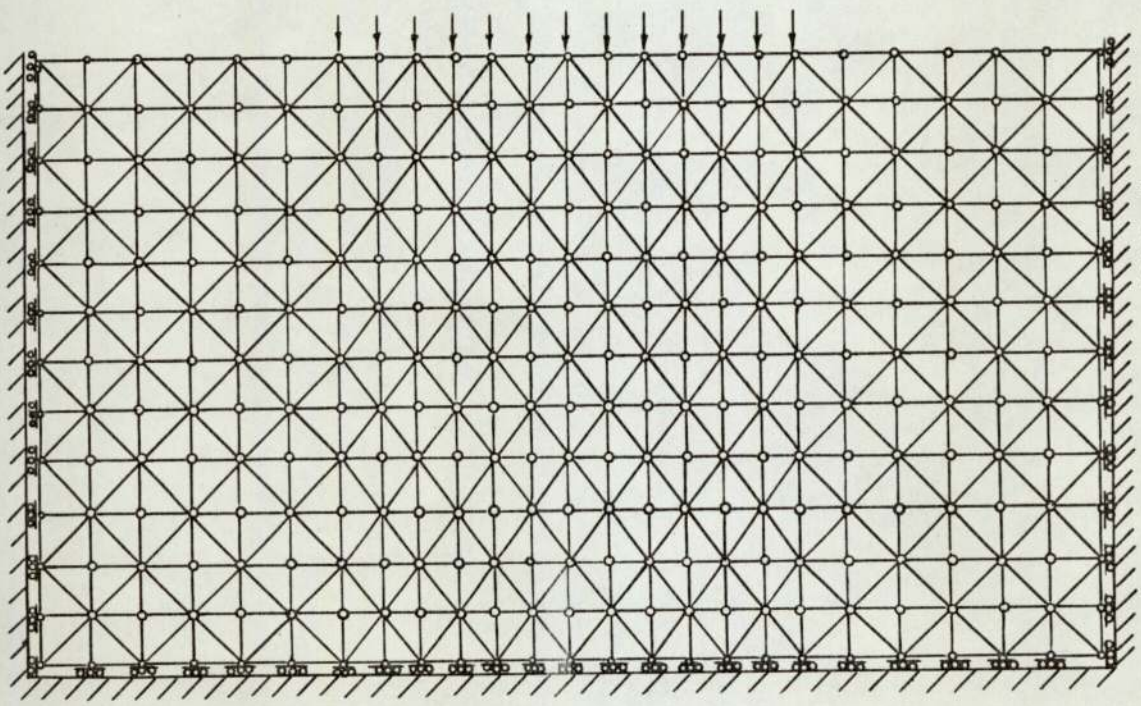

TRI 576
576 element
325 joints

Figure 2.6a

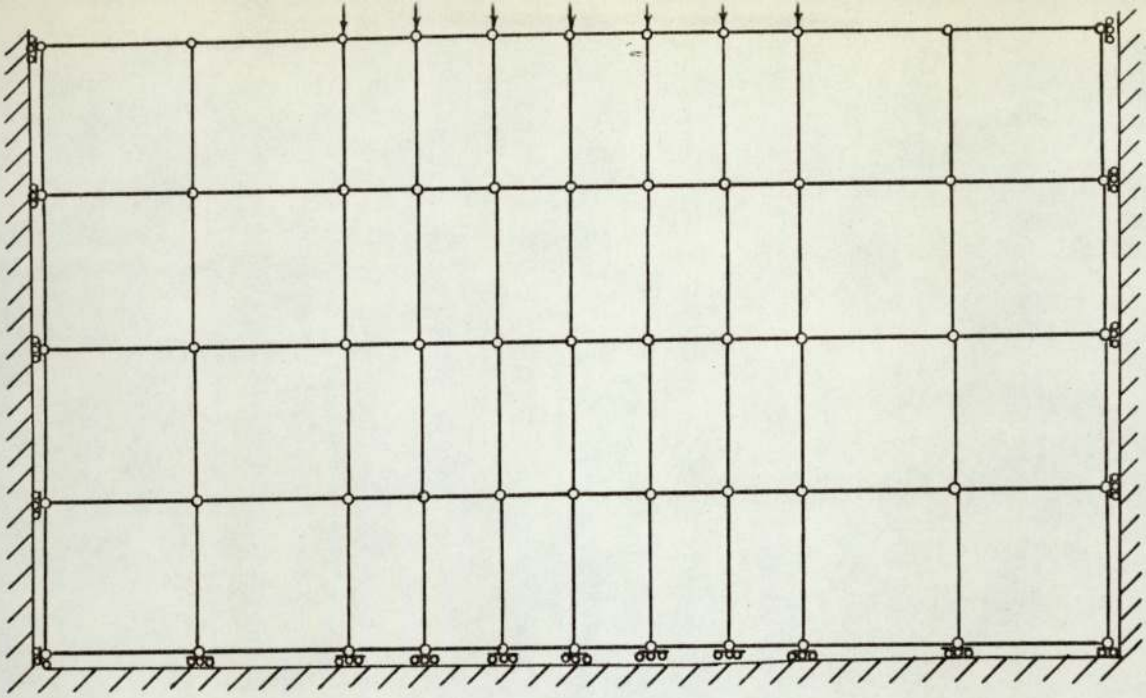
ISQ4Q40
40 elemen
55 joints

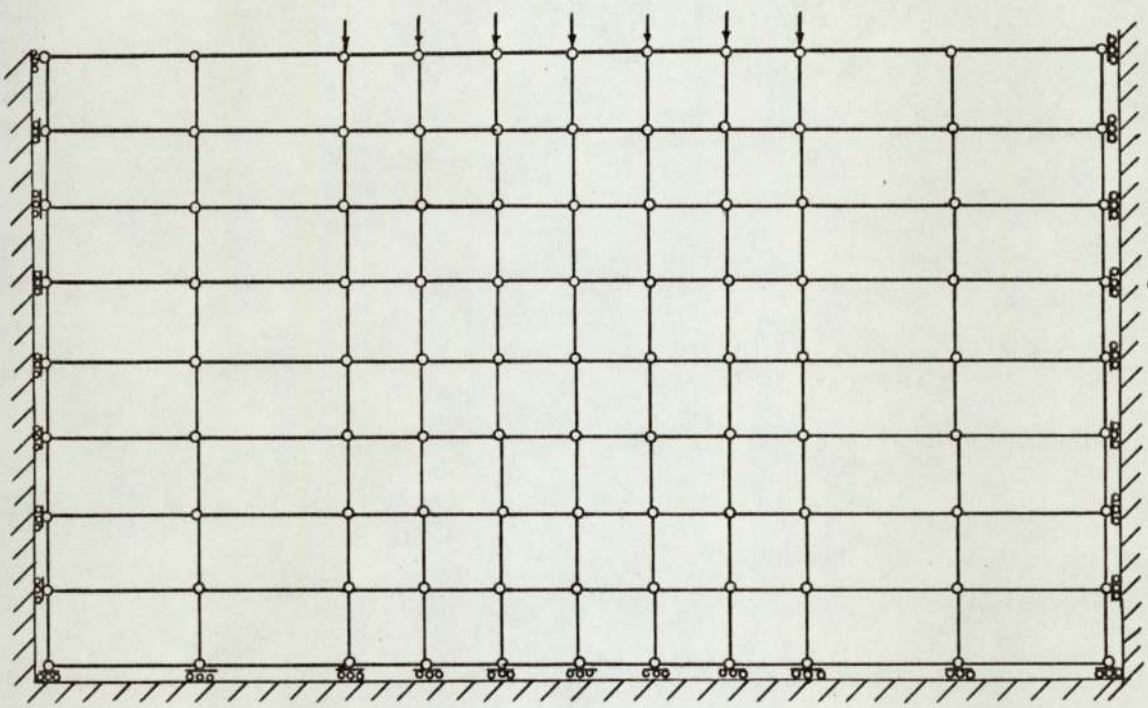
ISQ4Q80
80 elemen
99 joints

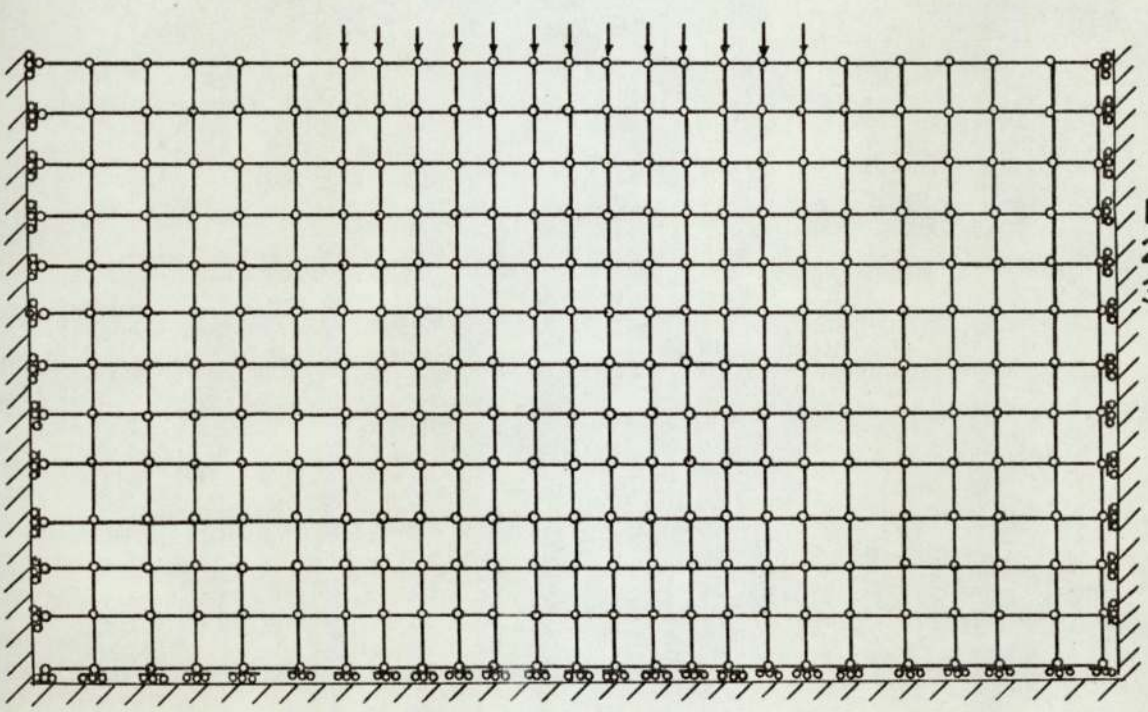
ISQ 4Q 28
288elemen
325 joints

Figure 2.6.b

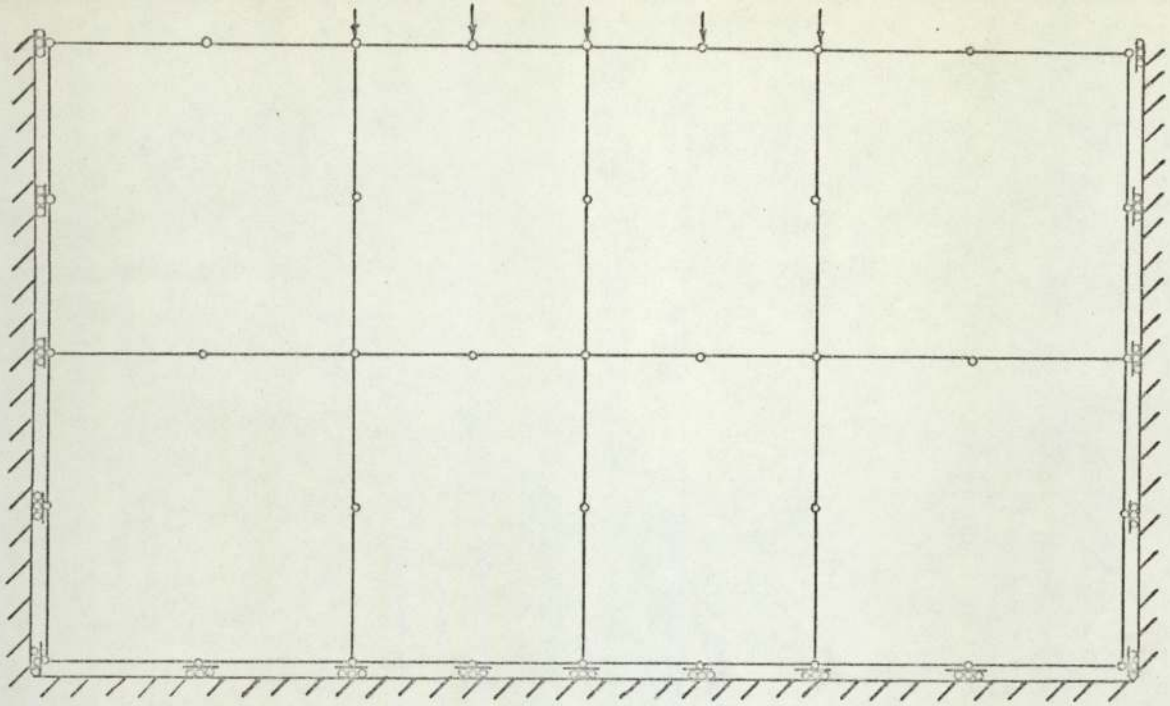
ISQ8Q8
8 element
37 joints

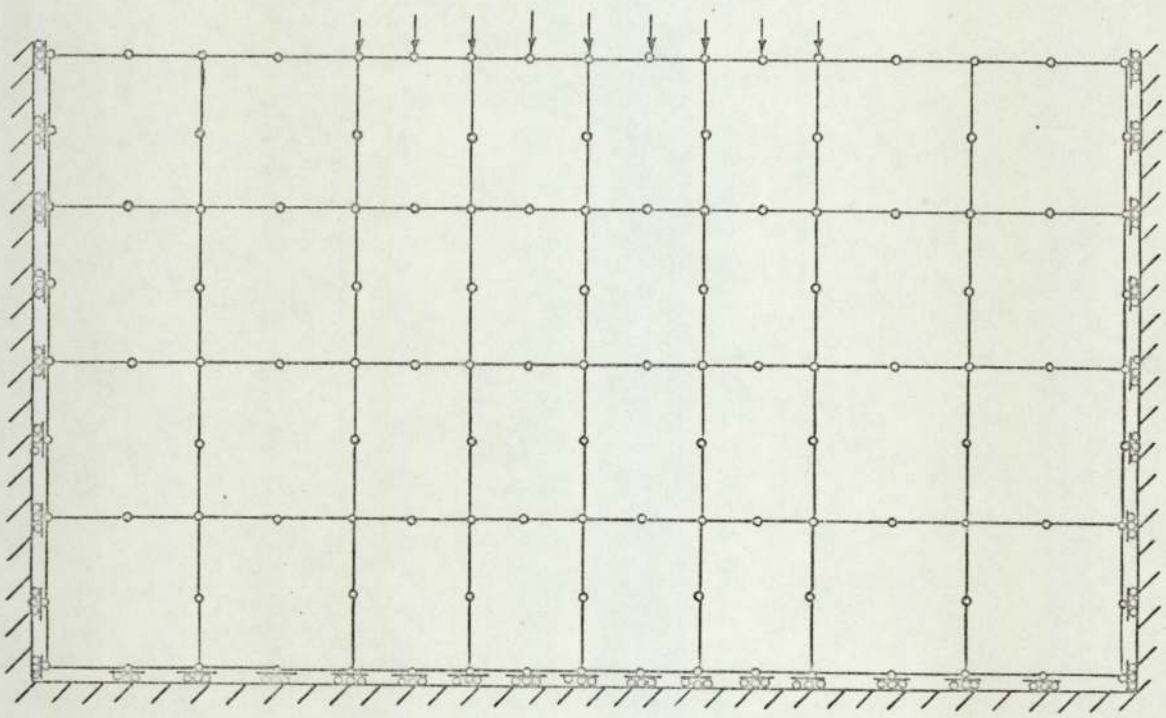
ISQ8Q32
32 elemen
121 joints

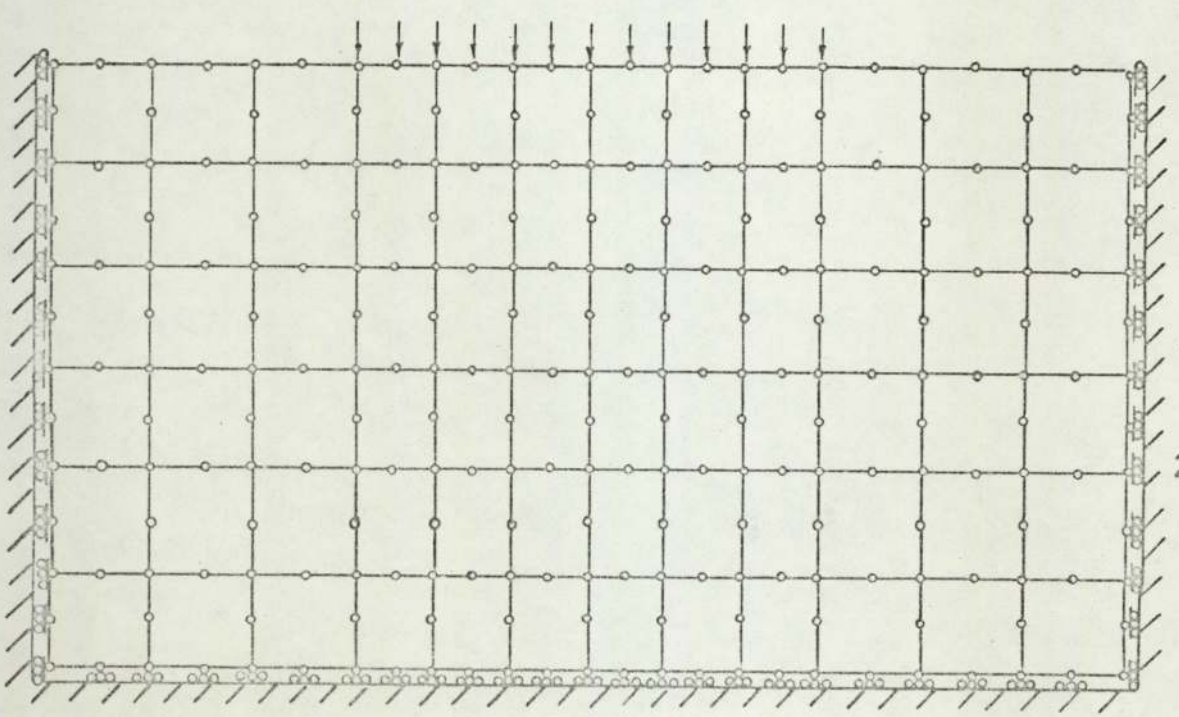
ISQ8Q72
72 element
253 joints

Figure 2.6.c

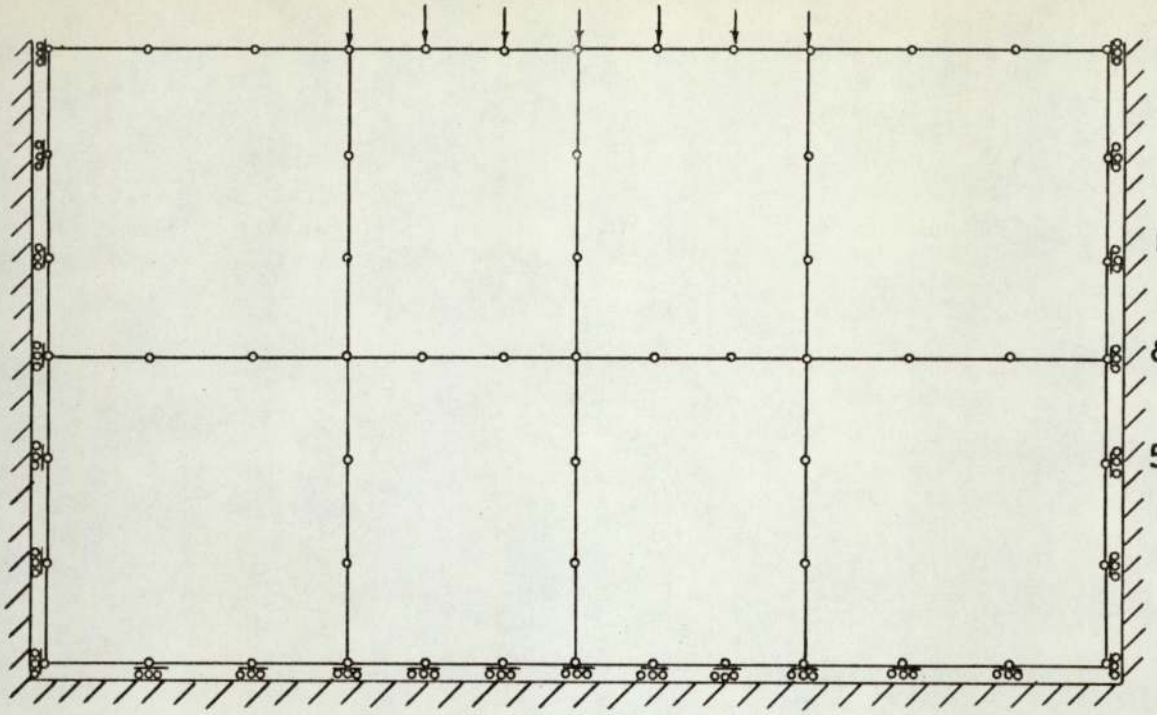
ISQ 12 Q8
8 elements
59 joints

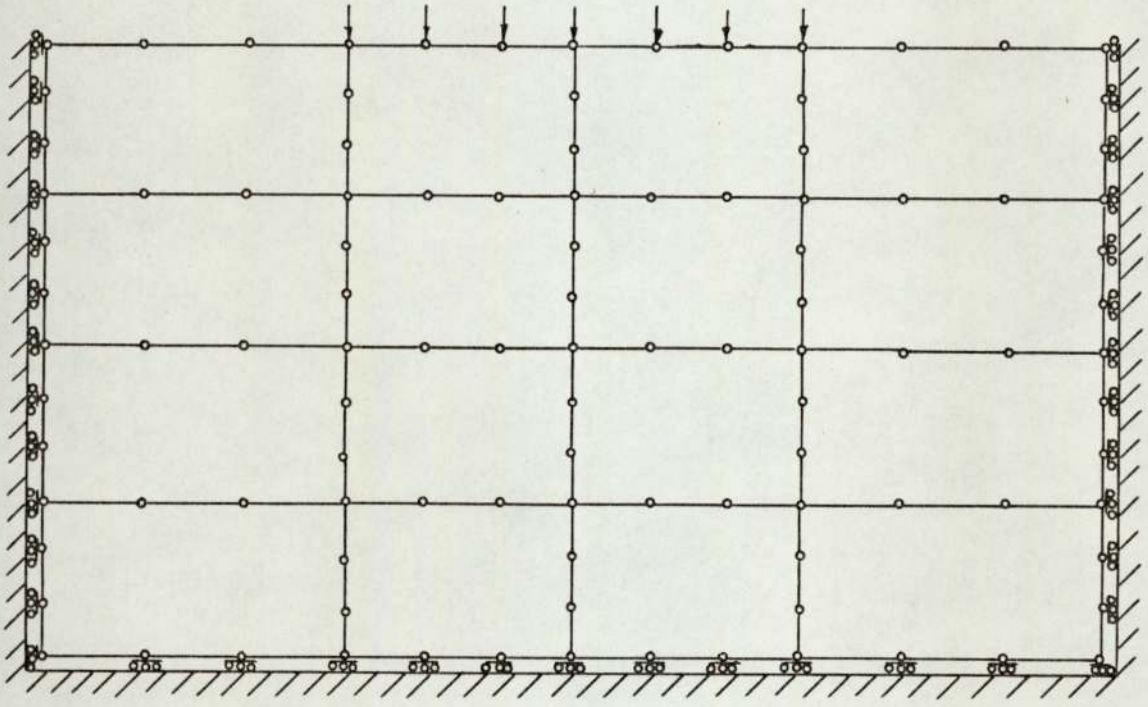
ISQ 12 Q16
16 elements
105 joints

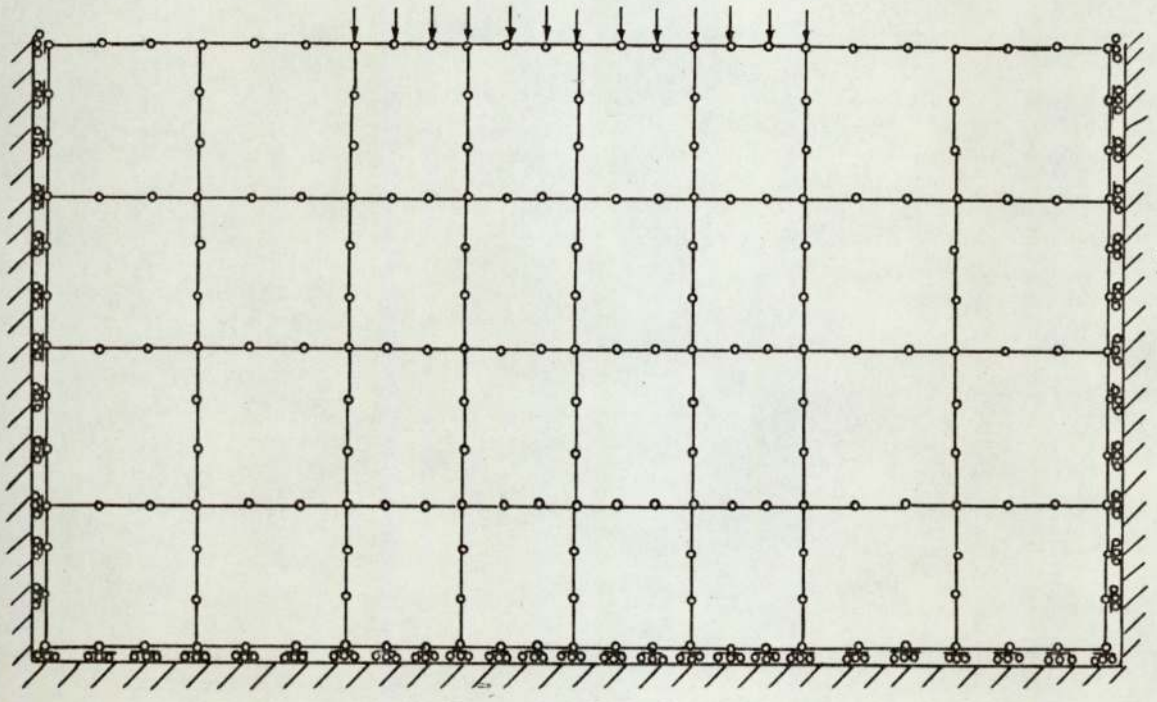
ISQ 12 Q32
32 elements
197 joints

Figure 2.6.d

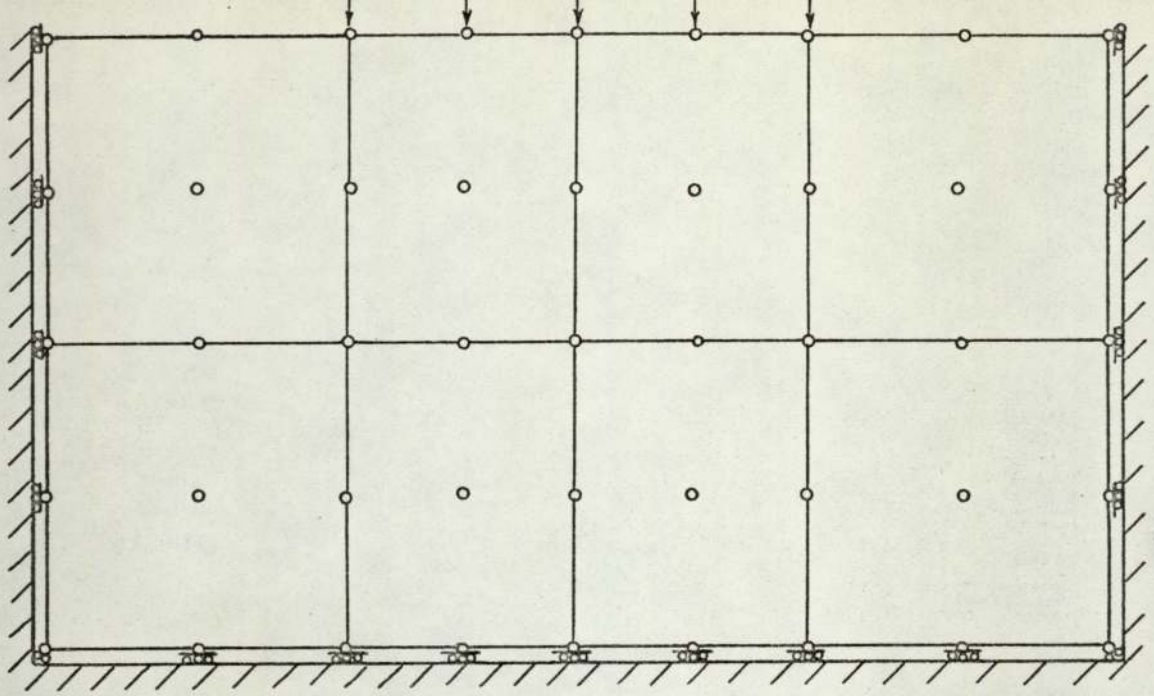
ISQ 9Q8
8 elements
45 joints

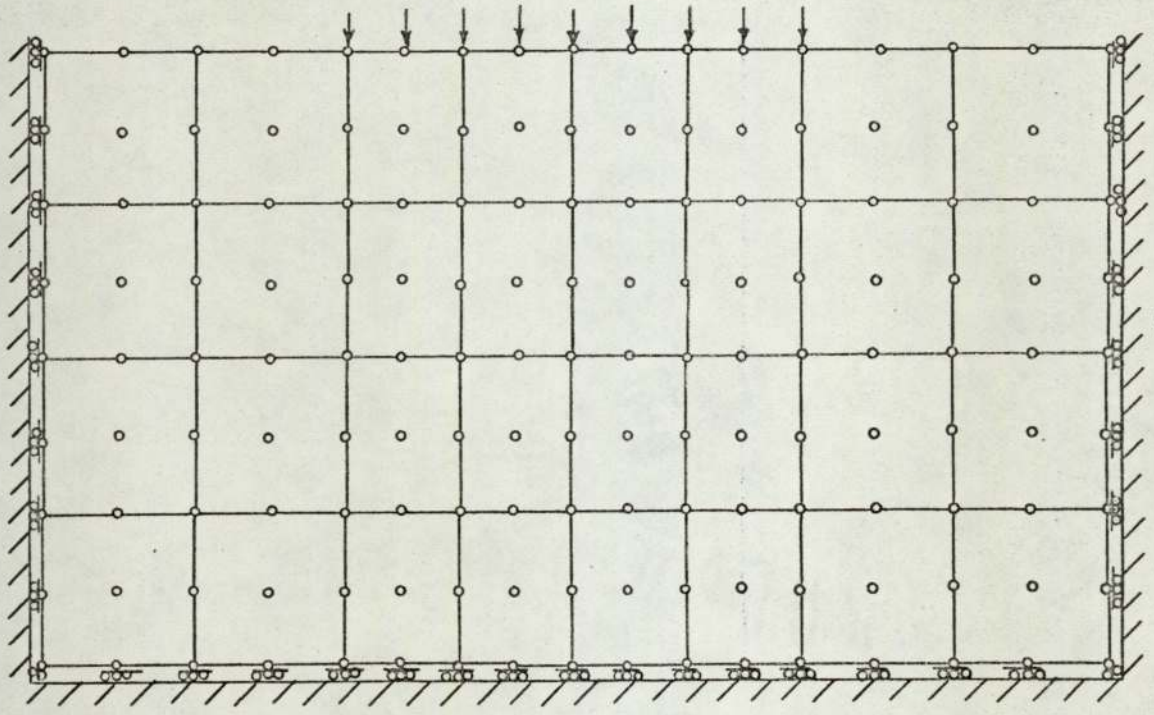
ISQ 9Q32
32 elements
153 joints

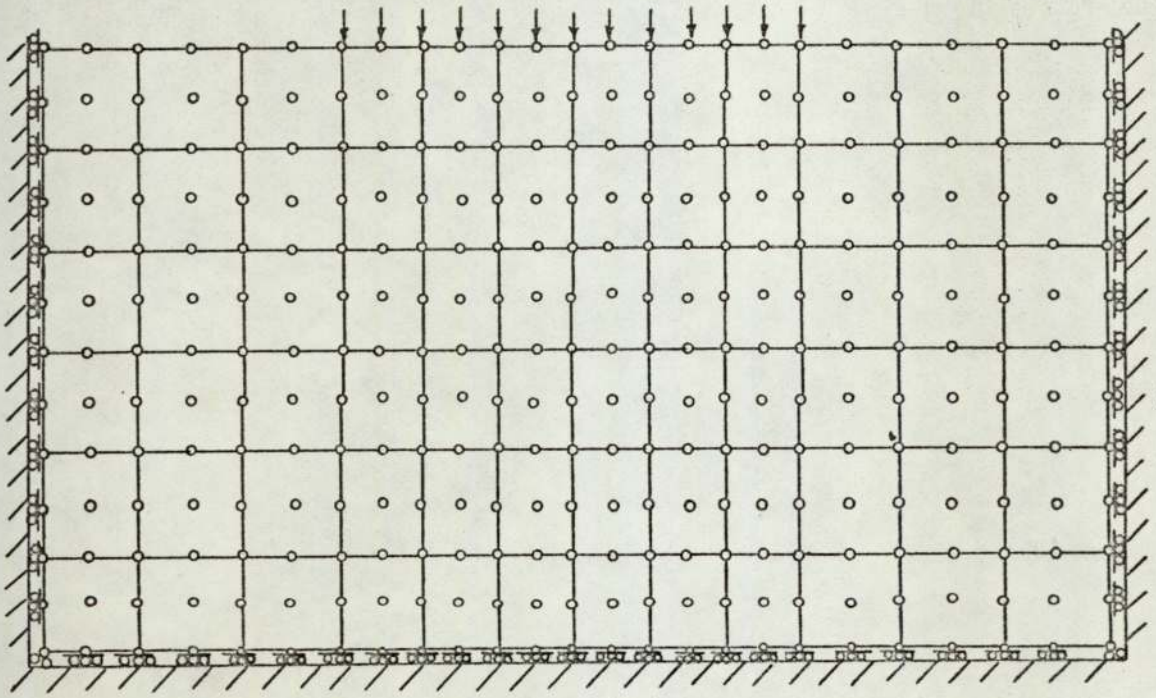
ISQ 9Q72
72 elements
325 joints

Figure 2.6.e.

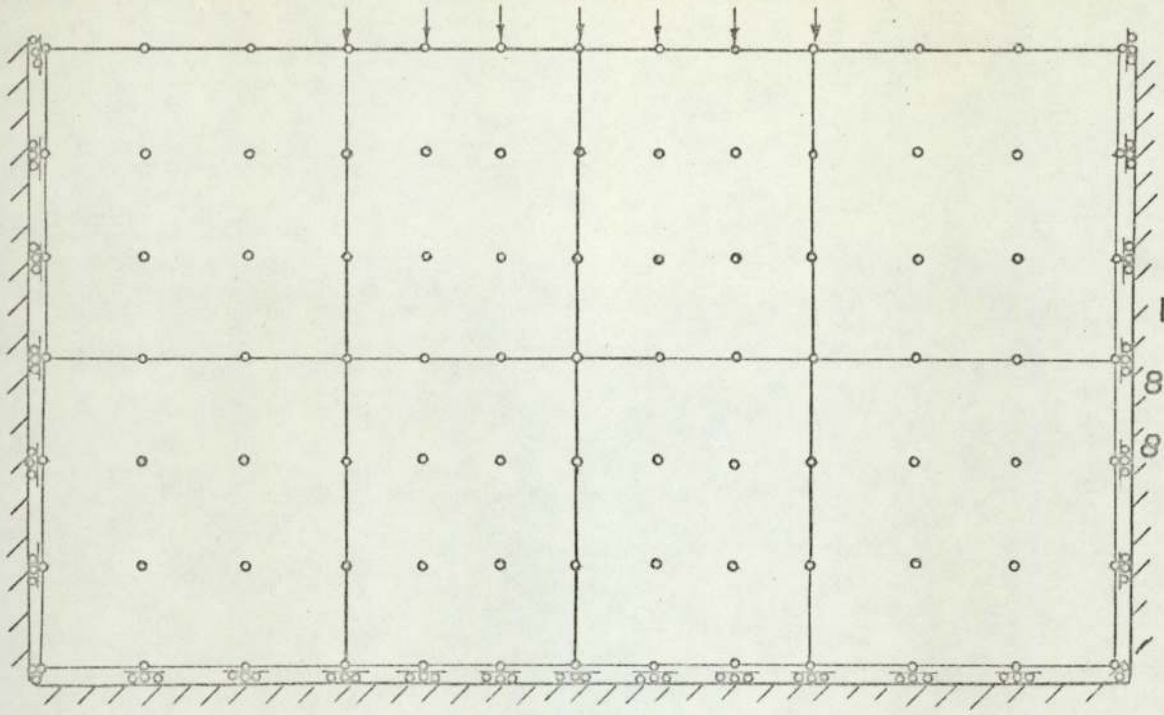
ISQ 16 Q
8elements
81 joints

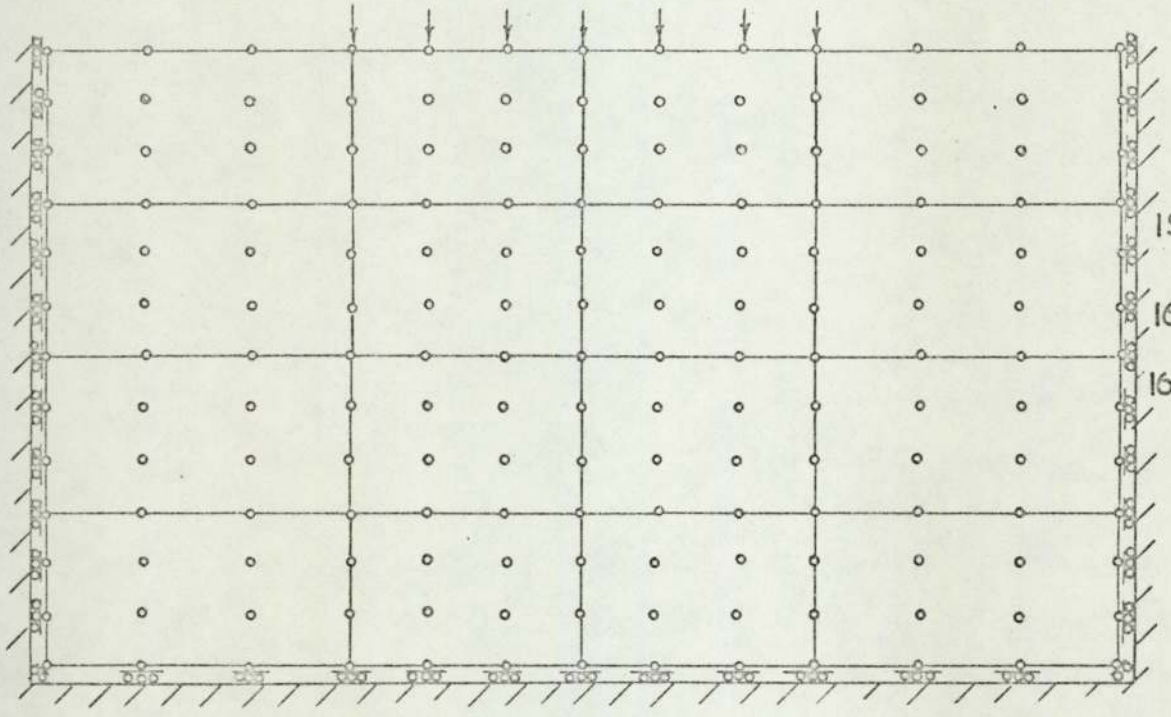
ISQ 16Q
16 element
169 joints

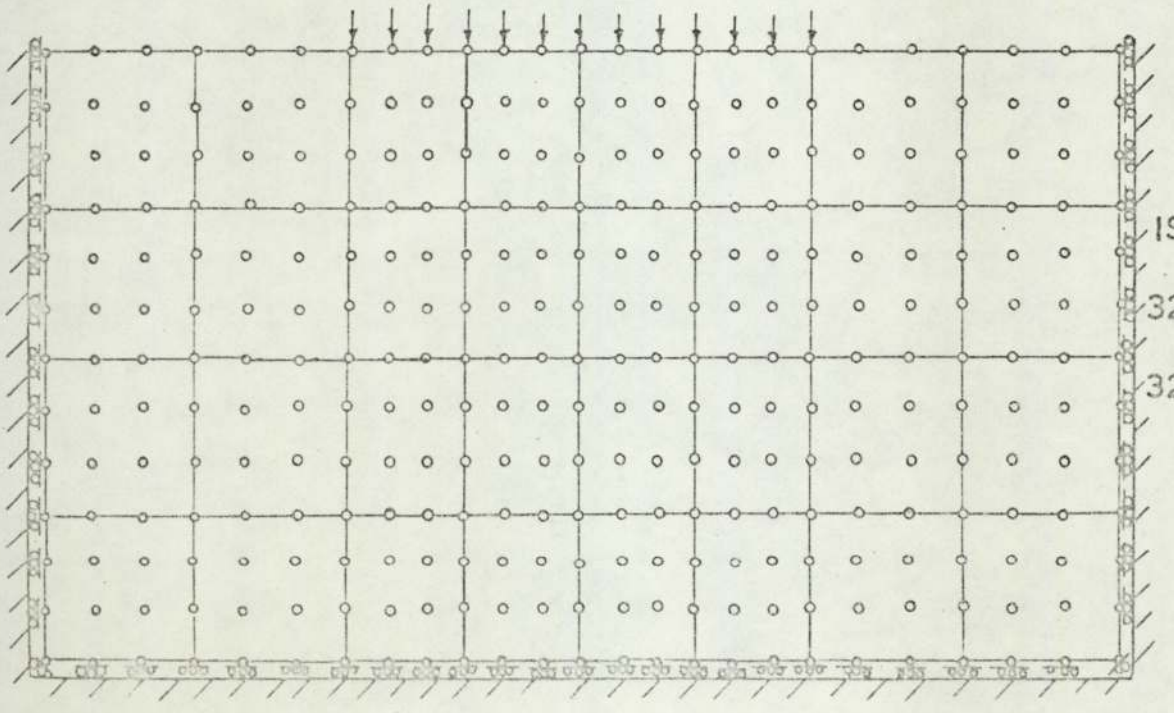
ISQ 16Q 3
32 element
325 joints

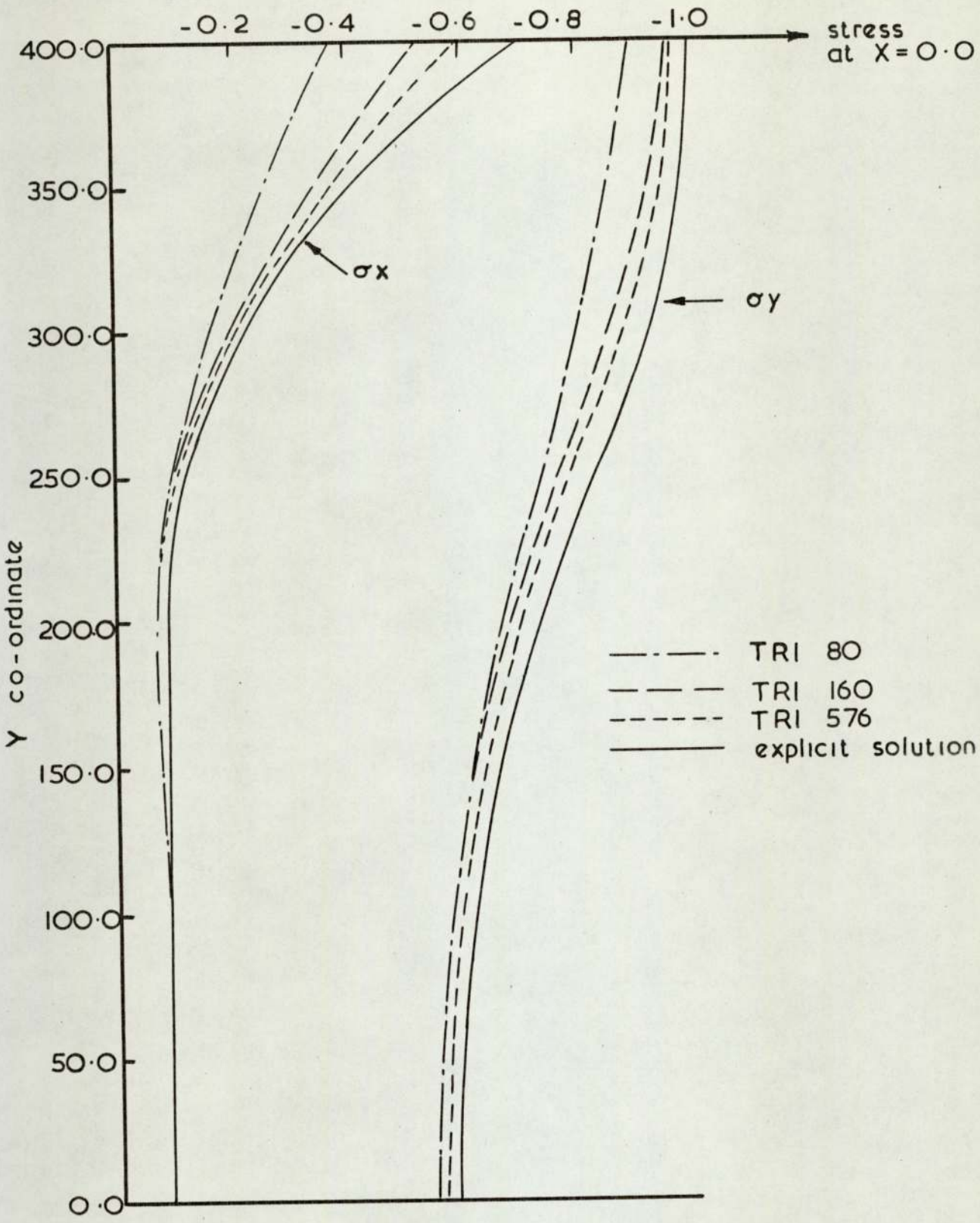

Figure 2.7 a. Comparison of the finit element method, using triangular elements, with the explicit solution

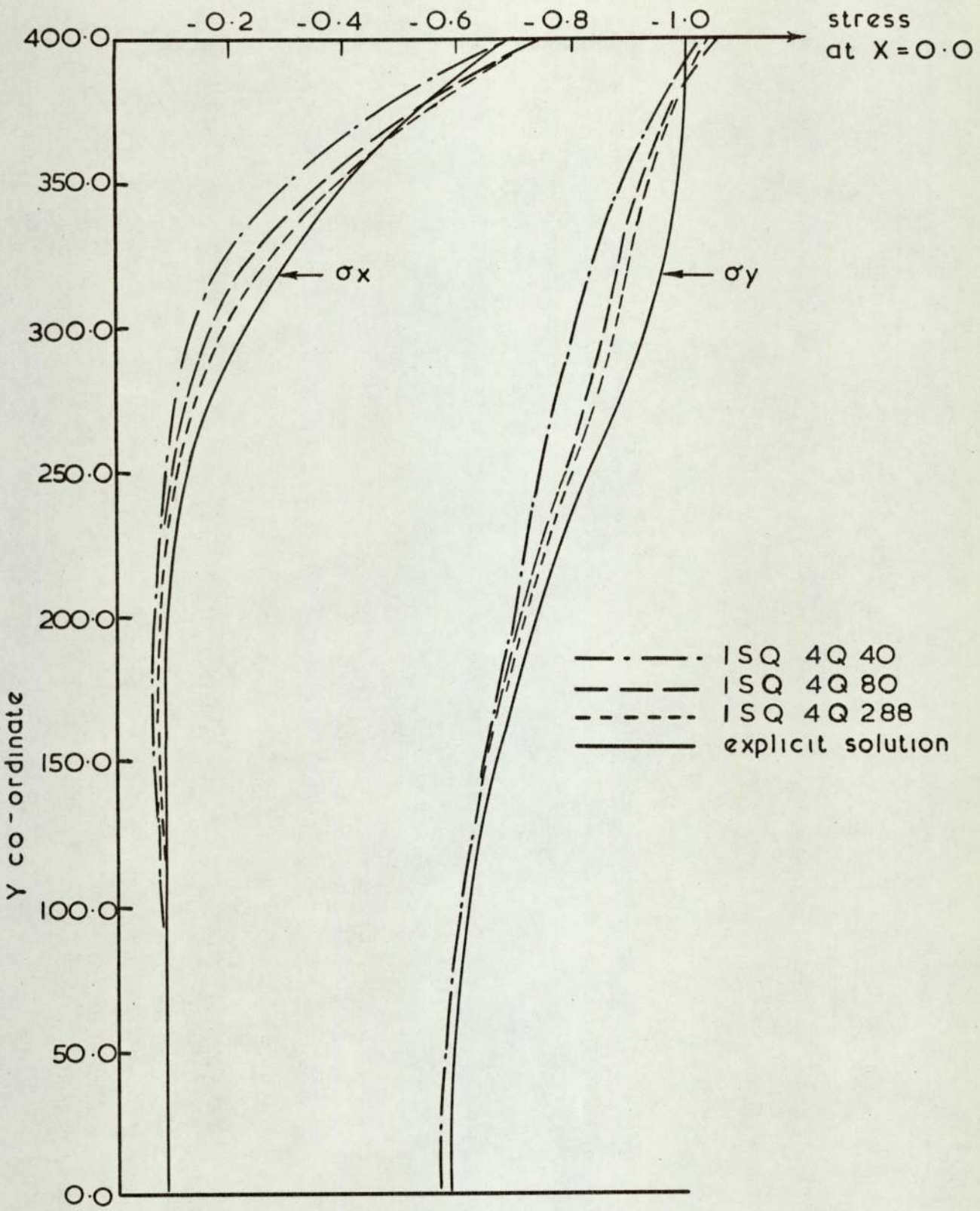

Figure 2.7.b Comparison of the finite element method, using isoparametric linear quadrilateral elements with the explicit solution

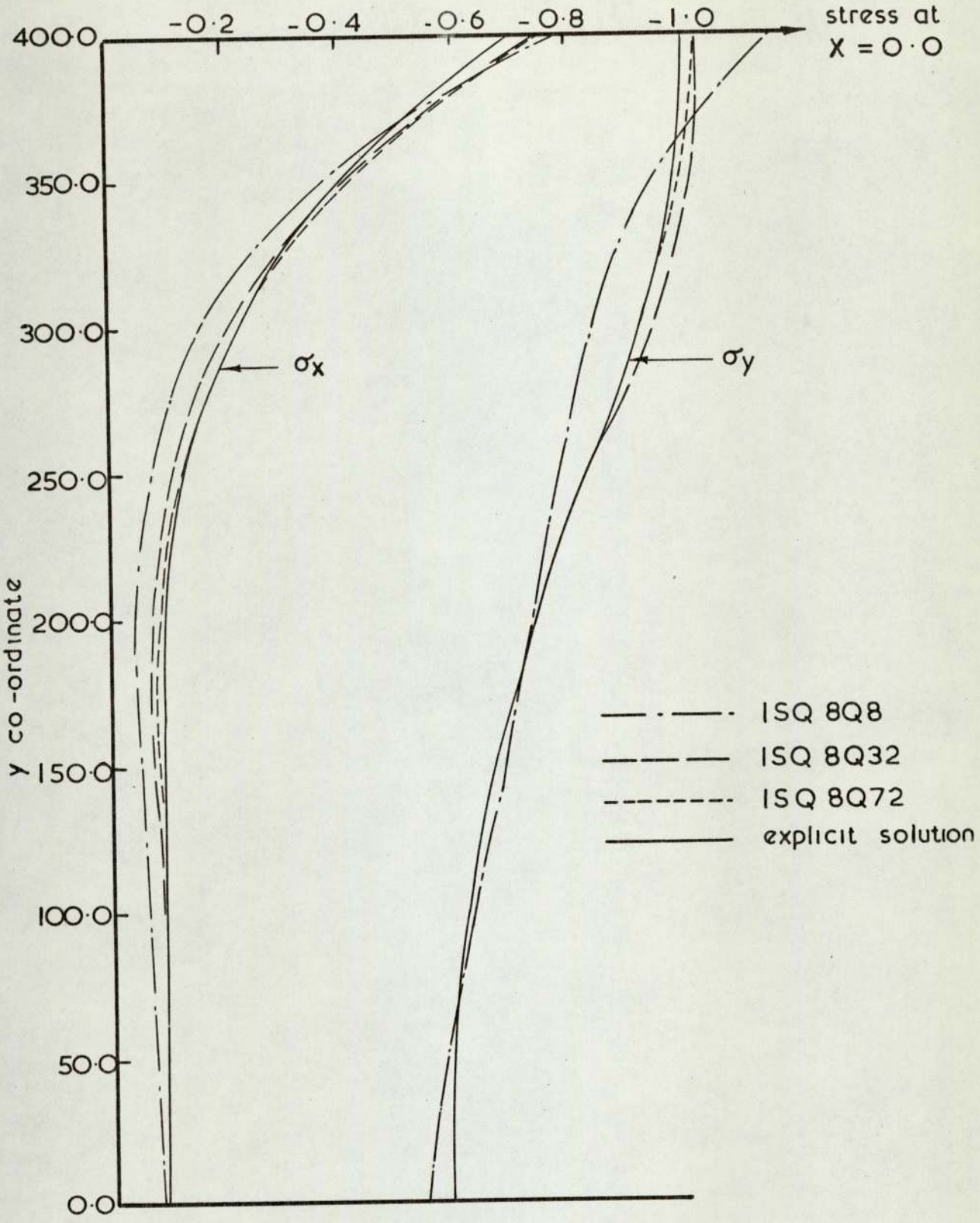

Figure 2.7c Comparison of the finite element method, using isoparametric serendipity quadratic quadrilateral elements, with the explicit solution

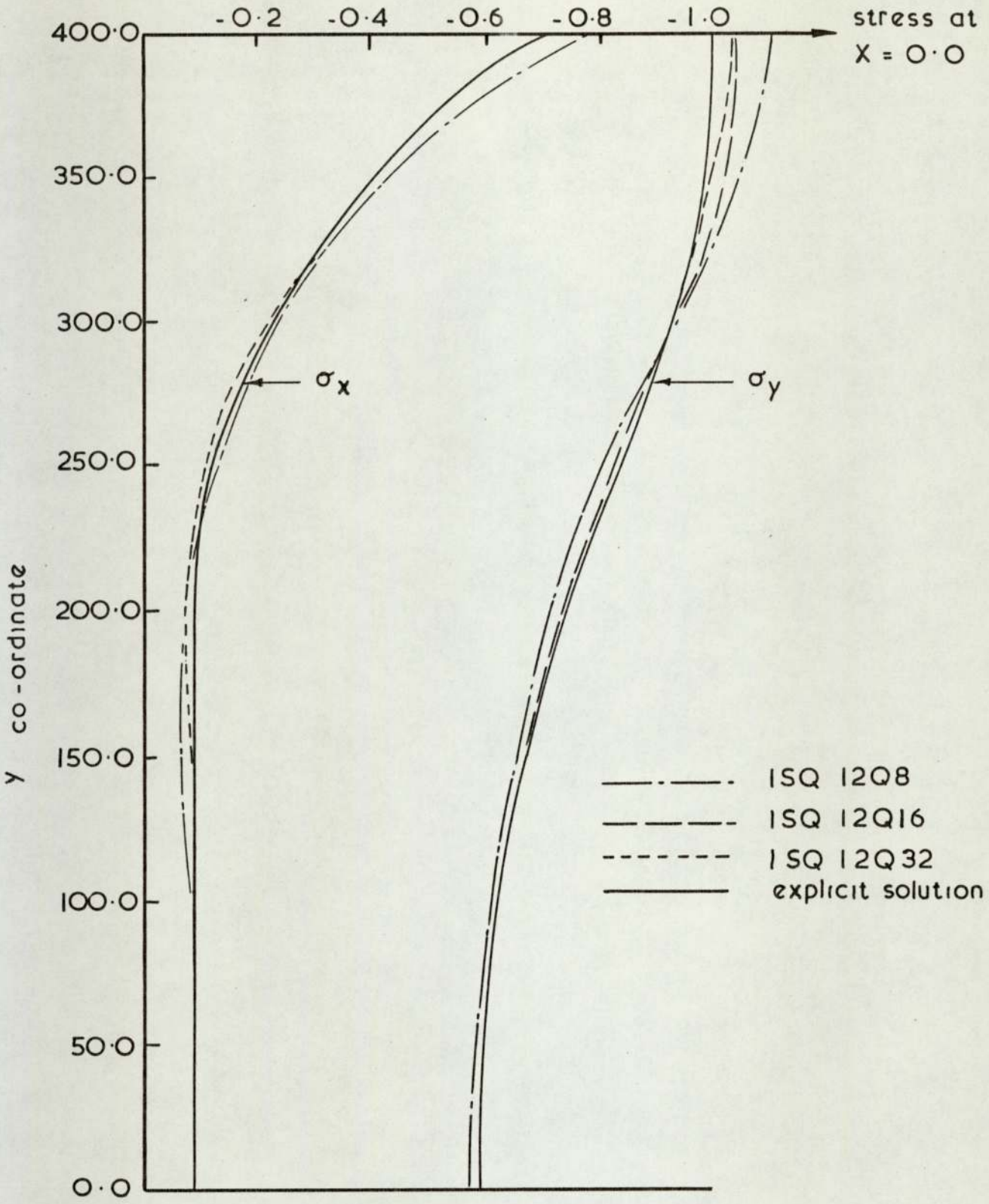

Figure 2.7 d. Comparison of the finite element method, using isoparametric serendipity cubic quadrilateral elements with the explicit solution

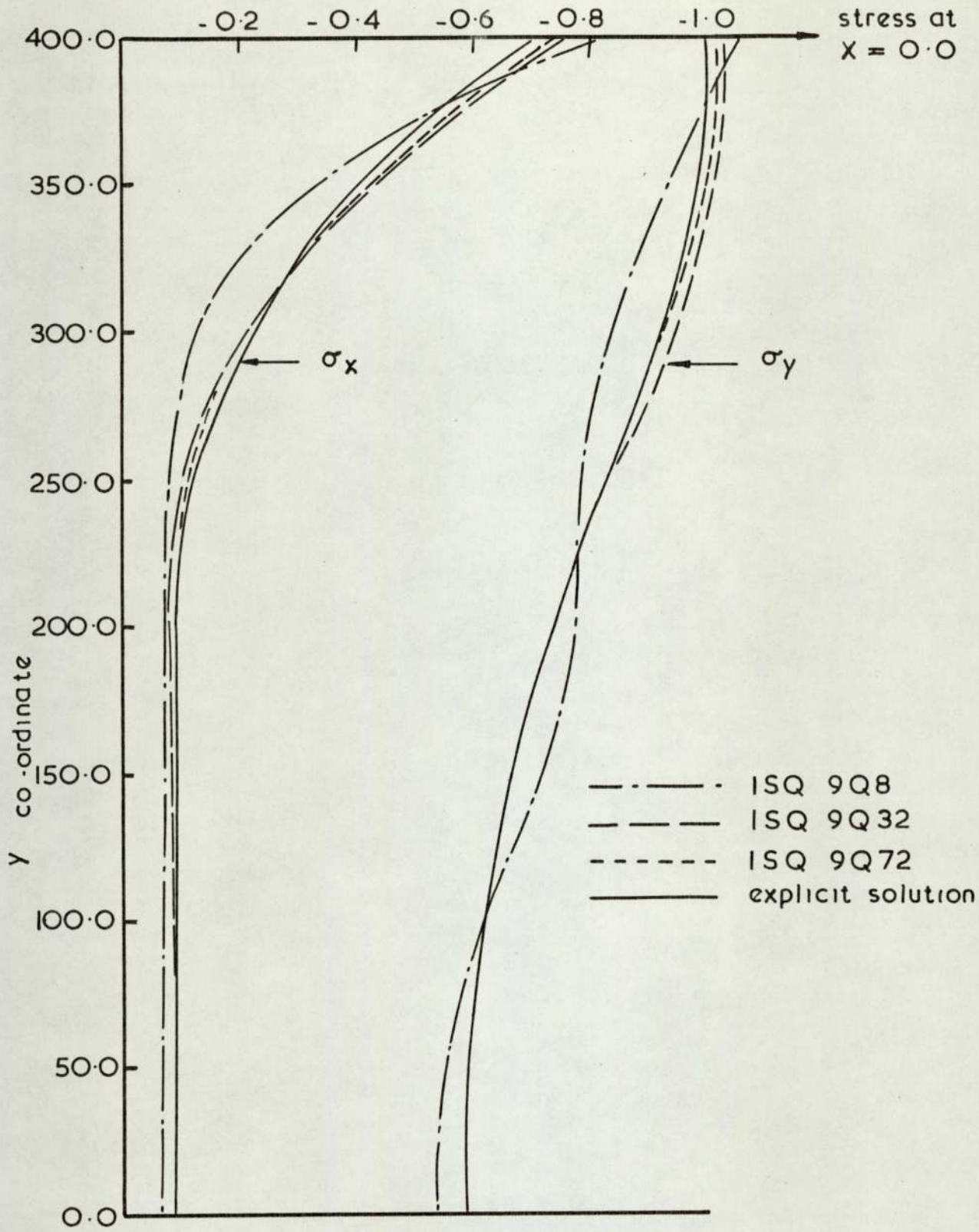

Figure 2.7 e Comparison of the finite element method, using lagrangian quadratic quadulateral elements, with the explicit solution

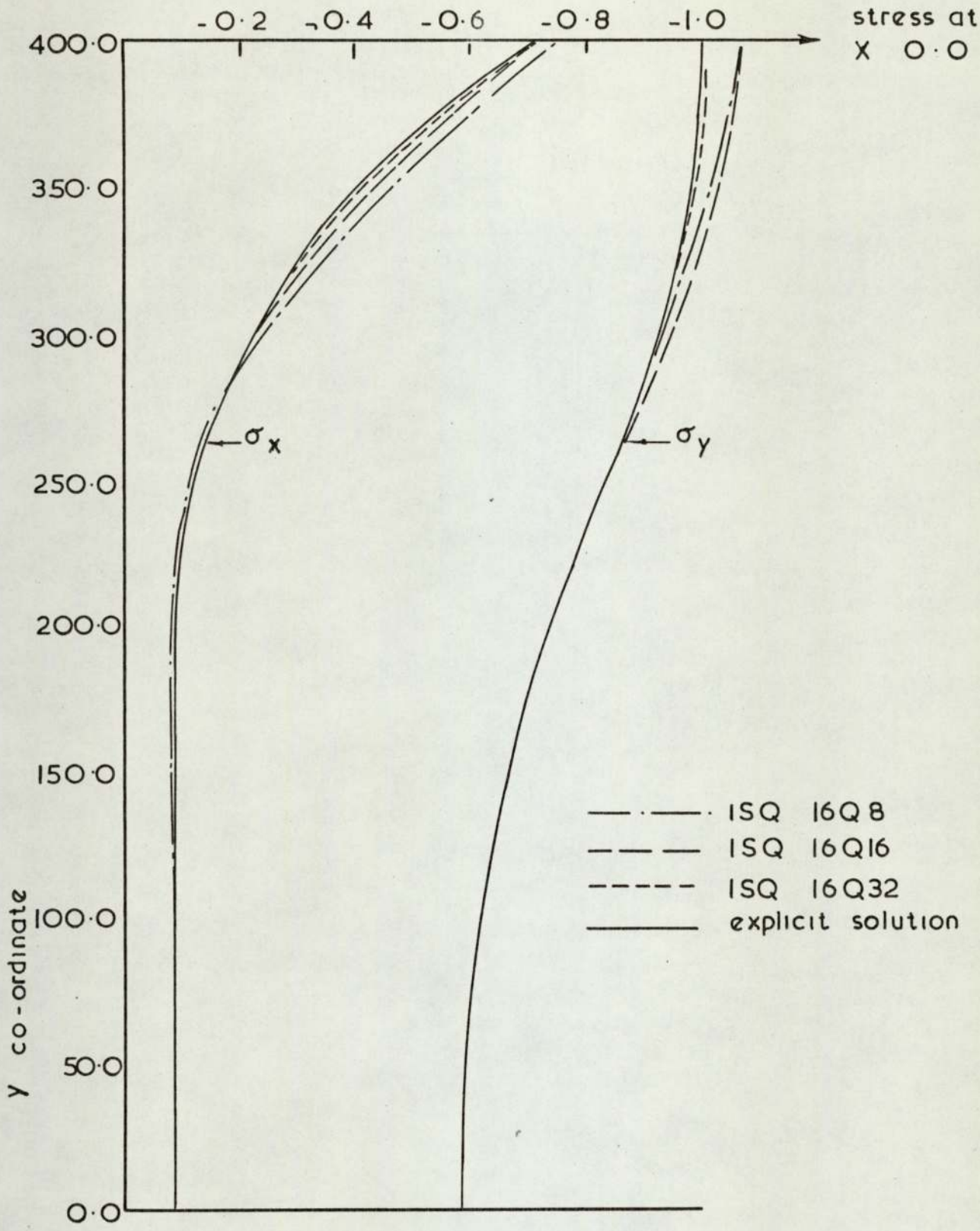

Figure 2.7 f Comparison of the finite element method using isoparametric lagrangian cubic quadrilateral elements with the explicit solution

2.3.2) Discussion of Results.

It can be seen from the results in Figures (2.7a)-(2.7f) that all the Finite Element analysis results were reasonable. The triangle and linear quadrilateral elements clearly converged towards the explicit solution as the meshes were refined. The higher order elements, while showing some convergence, did not exhibit this clear trend because the results were quite accurate for all the meshes. The Isoparametric quadrilaterals all overestimated the value of the supplied surface pressure, and the stresses generally close to the applied load. For the higher order elements, the refined idealisation of the load associated with mesh refinement had a greater effect than the actual number of elements. The results from the Isoparametric elements showed that the stress was overestimated for a region of one element depth beneath the applied load. Thus, as the mesh is refined, the elements become smaller, the equivalent nodal forces also become smaller and so the area of overestimation of stress becomes less.

To compare the cost of running each of the analyses in Figures (2.7), the stress component σ_y at X = 0.0, Y = 200.0 is plotted against computer store, mill time and number of input records, in Figures (2.8a)-(2.8c). The value of σ_y at the mid-depth point should be free of any distortion due to the loading idealisation, and only dependent on the element properties. Assuming the explicit solution is exact, the lines of stress level corresponding to $\pm$ 1%, 5% and 10% error are shown in Figures (2.8). The results obtained from the stress at this point, using the meshes in Figures (2.6), are plotted in the Figures (2.8), against the corresponding number of core units, mill units or input records.

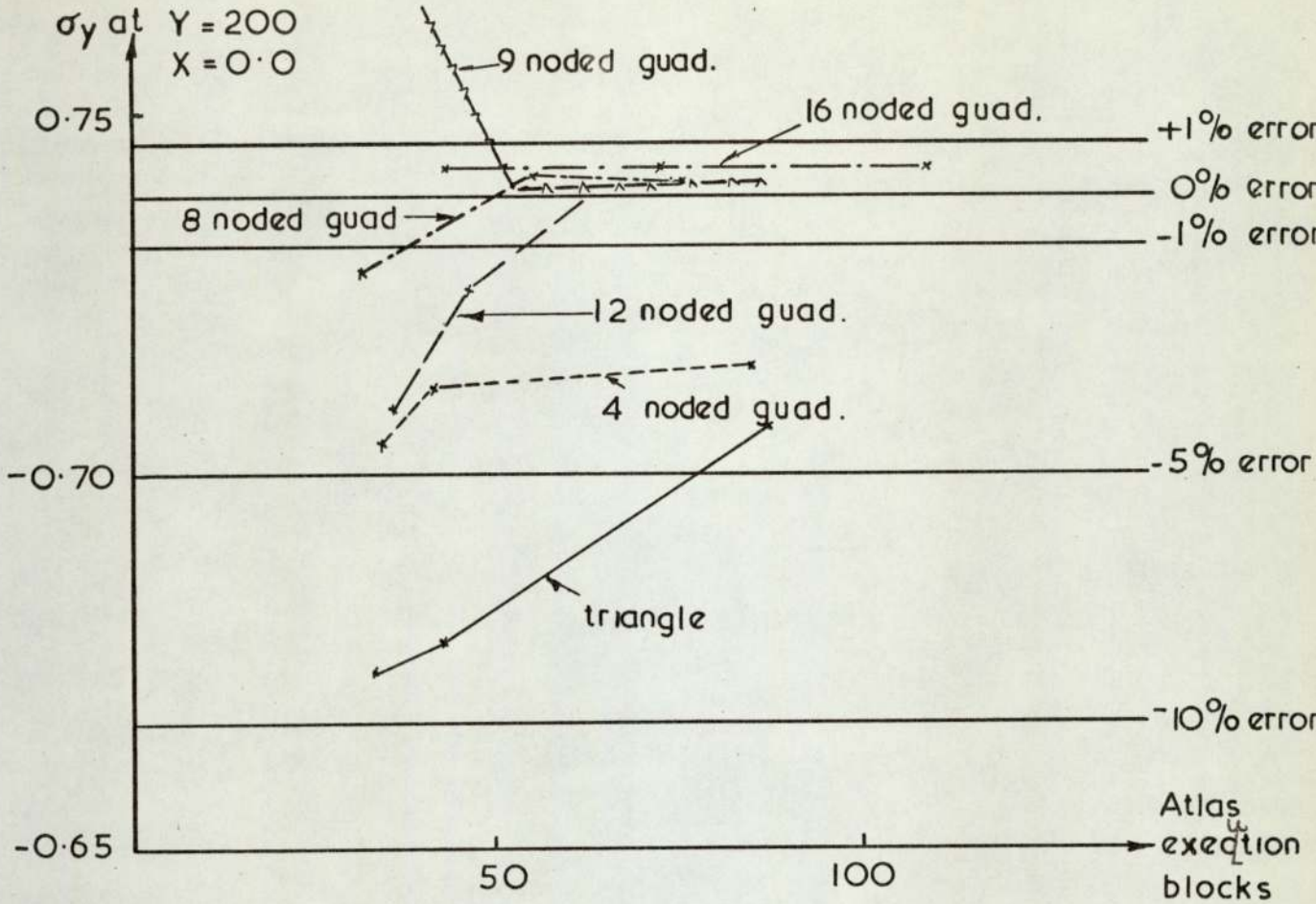

Figure 2.8 a

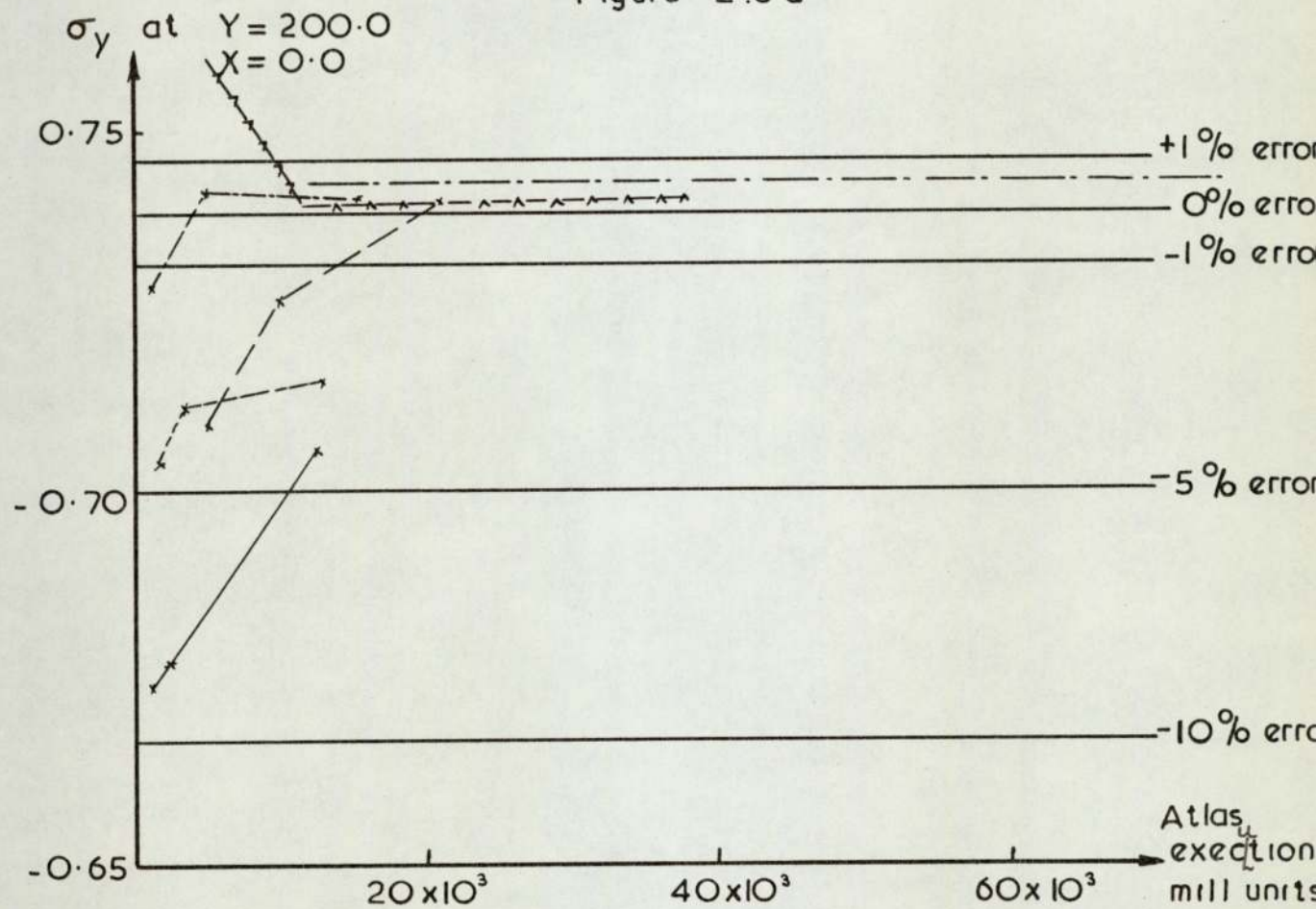

Figure 2.8 b

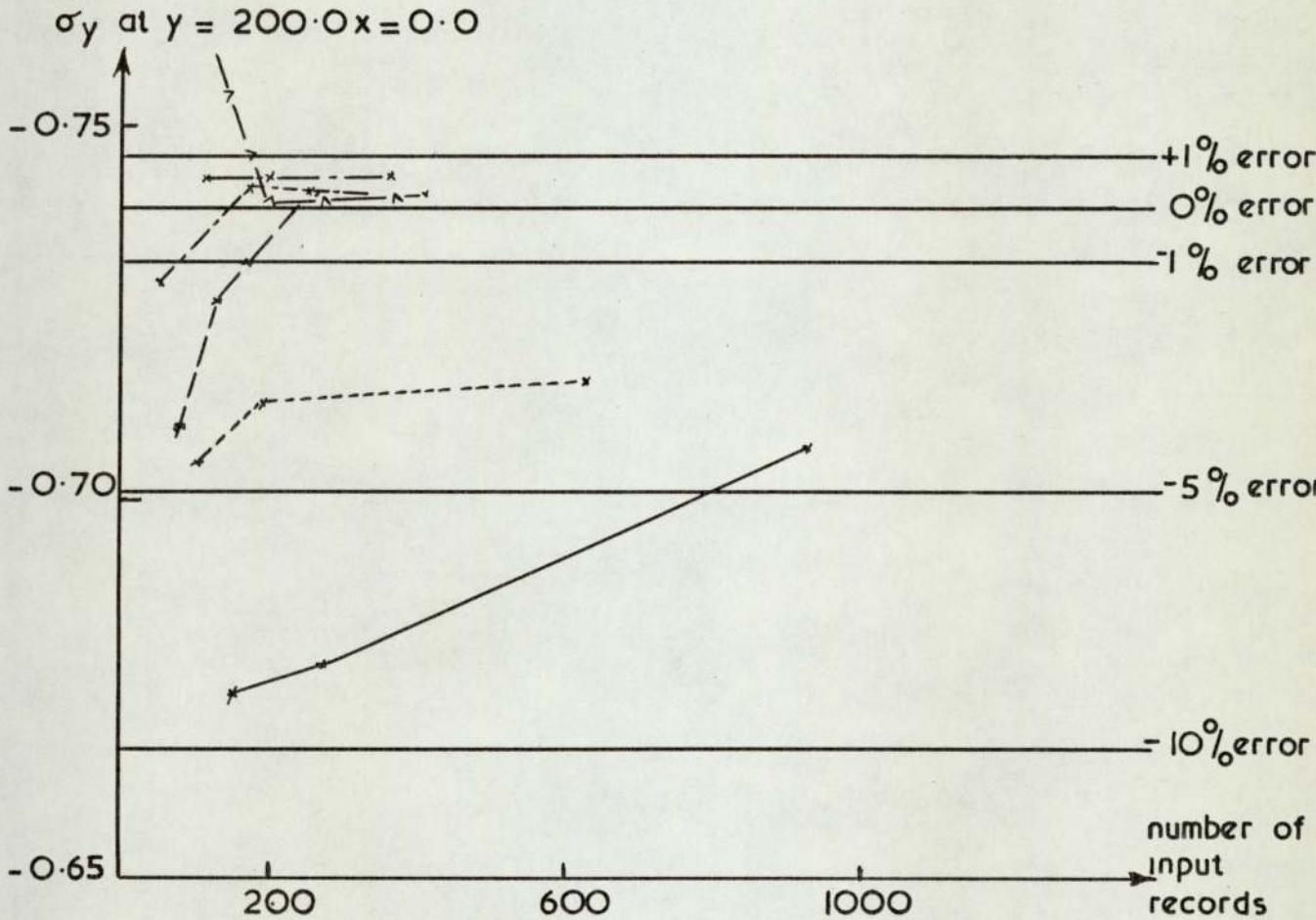
σy at y = 200·0 x = 0·0
-0·75
-0·70
-0·65
+1% error
0% error
-1% error
-5% error
-10% error
200
600
1000
number of input records

Figure 2.8.c

2.3.2) contd.

It can be seen from Figure (2.8a) that all the results lie within 10% of the explicit solution, all the isoparametric elements lie within 5% and a lot of these within 1%. The weakness of the constant strain triangular element is clearly seen in all three figures. This element gave very poor results as compared to the isoparametric elements using the same number of core and mill units, and is most expensive in data preparation.

The highest order element, the cubic Lagrangian quadrilateral gives consistently the best results but is clearly very expensive in computer mill time, because it requires four Gauss points for the integration. The cubic serendipity element can also be seen to be very efficient from the cost point of view, but both these elements suffer from overestimating the stress near to the applied load. This effect is more serious for the cubic elements where to be efficient in cost, only a relatively few large elements are used. The quadratic Lagrangian element is again fairly expensive in mill time and it can be seen from the figures that the results are erratic when only a few elements are used. The serendipity quadratic element, for which only two Gauss points are required, seems efficient, relative to the other elements, on all grounds. The linear quadratic element gives relatively poor results compared to the higher order elements, for the same order of cost, but is clearly much better than the triangle.

2.4) Hexahedral Element Testing.

Having established the reliability of the quadrilateral elements against an explicit solution it should

2.4) contd.

be adequate to check the hexahedral element results against theirs under two dimensional conditions.

Consider the test problem shown in Figure (2.9). This is a linearly elastic isotropic homogeneous block of material surrounded on all sides and the base by smooth rigid boundaries. The material is loaded by a uniformly distributed surface load on the centre line. Because of symmetry only half the block need be analysed. The smooth rigid boundaries and the symmetry of loading prevent deformation in the Z direction so the problem can be considered as a two dimensional plane strain one.

The problem in Figure (2.9) was analysed by the hexahedral elements described in Appendix (2) using almost identical mesh designs. The quadrilateral elements corresponding to these hexahedral elements were used to analyse the plane strain problem in Section B-B of Figure (2.9) using corresponding mesh arrangements.

2.4.1) Results.

The results for the two normal stress components σ_x and σ_y, obtained in the way described, are shown in Figure (2.10). The various results obtained from the meshes using the hexahedral elements compared exactly with those obtained from the corresponding quadrilateral elements. The erratic behaviour of the Lagrangian quadratic element is again illustrated by the results. As a further check the orientation of the global axis was changed twice, the problem reanalysed, and the results compared.

It was not thought necessary to carry out a rigorous

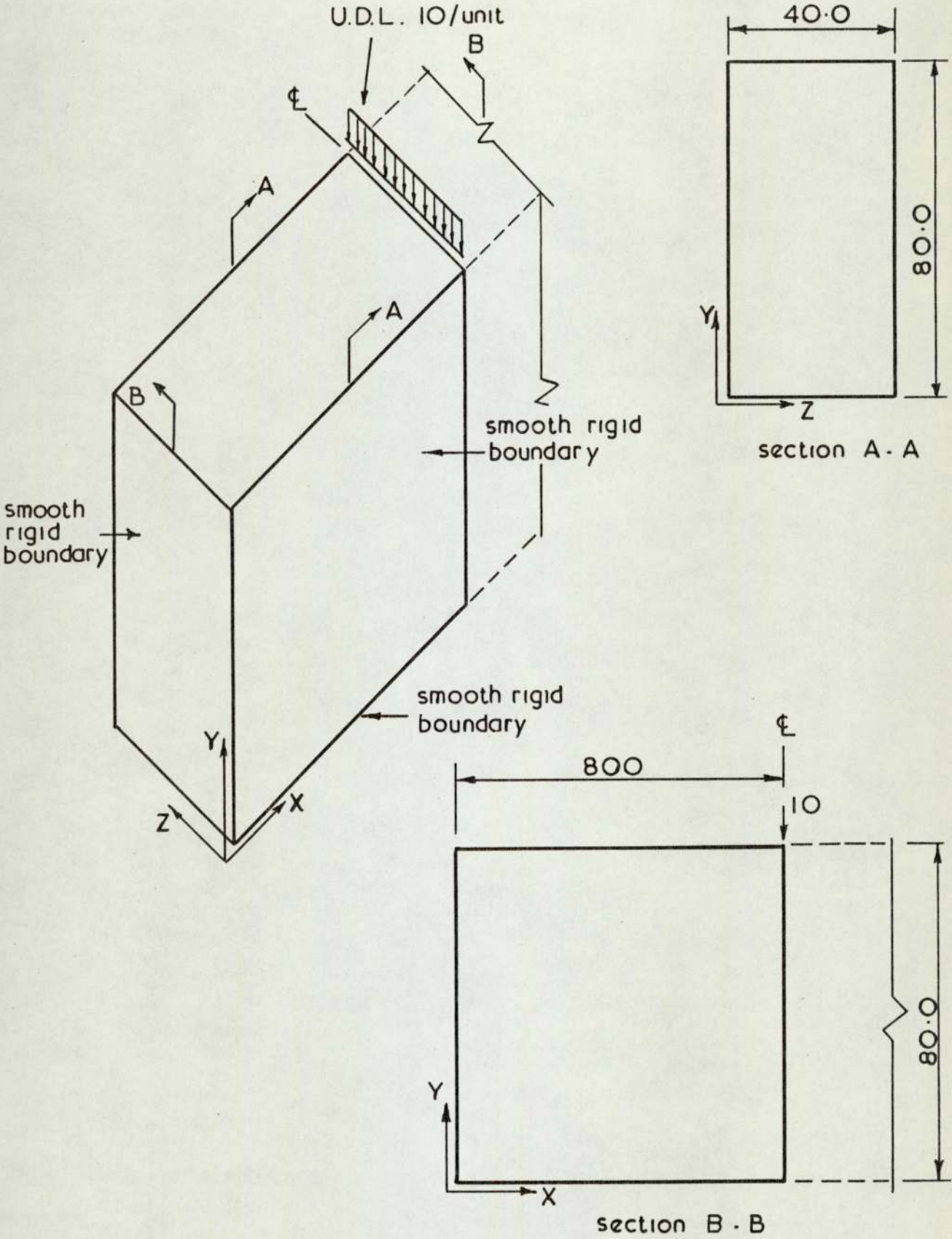

Figure 2.9 Test problem for hexahedral elements

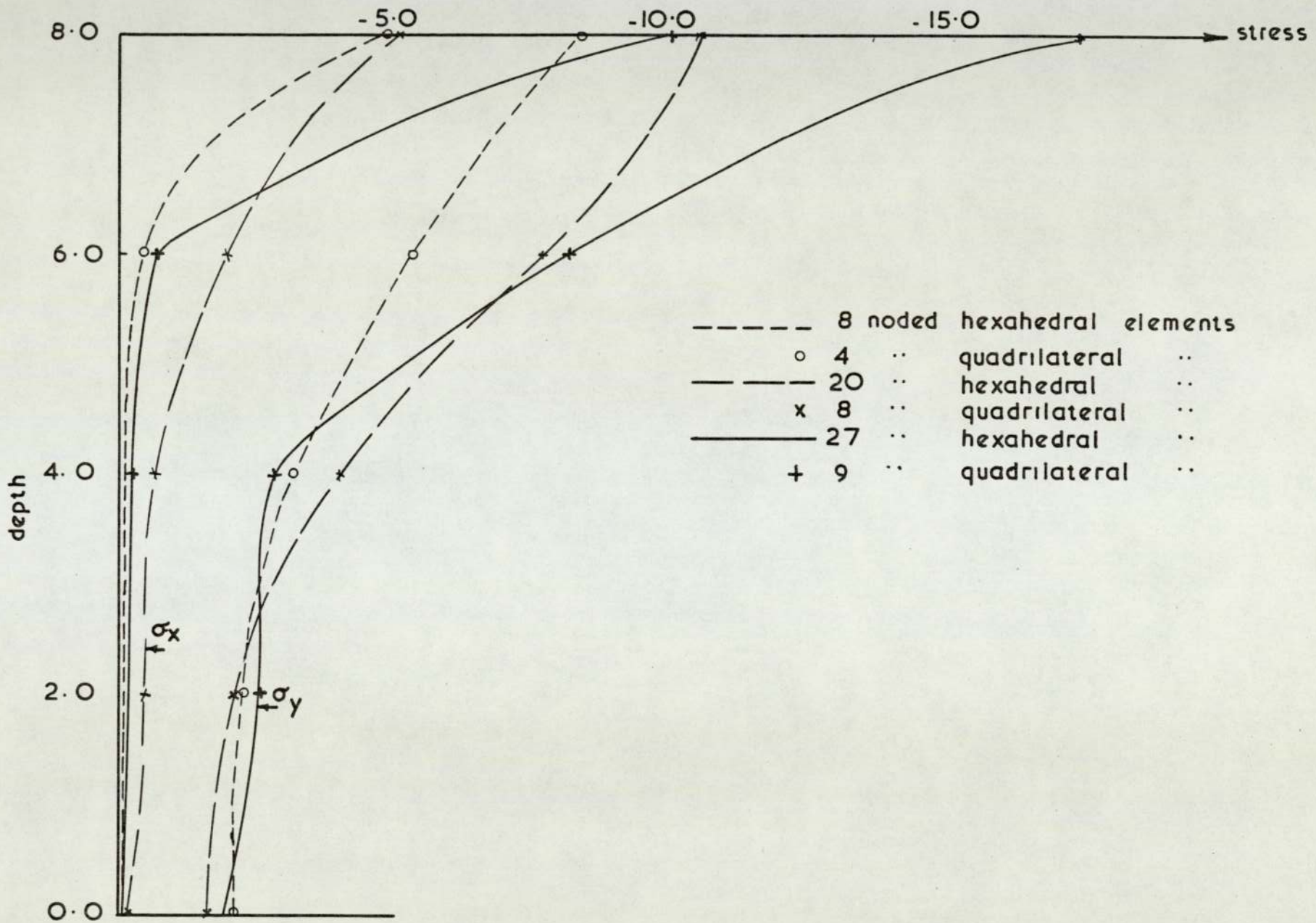
8·0
6·0
4·0
2·0
0·0
depth
-5·0
-10·0
-15·0
stress
8 noded hexahedral elements
4 .. quadrilateral ..
20 .. hexahedral ..
8 .. quadrilateral ..
27 .. hexahedral ..
9 .. quadrilateral ..
σx
σy

Figure 2·10

2.4.1) contd.

comparison of costs for the hexahedral elements because the properties discovered in the quadrilateral elements should also apply here.

2.4.2) Discussion of Results.

In Section (2.3.2) it was pointed out that the quadratic serendipity elements appeared to be the most efficient providing that two Gauss points were used and it seems that the same can be said for the hexahedral element. The choice of two or three Gauss points is even more important for hexahedral elements because the operations in forming the overall stiffness matrix have to be repeated n^3 times as opposed to n^2 times for two dimensional elements. This means that the relative time taken to form the overall stiffness matrix is 9:4 using two or three Gauss points for the quadrilaterals, but, the ratio is 27:8 for hexahedral elements, which is a considerable difference.

The same effect can be seen on the core required as the higher order hexahedral elements have 20 or 27 nodes which leads to a bandwidth of some considerable size.

2.5) Conclusions.

The two and three dimensional elements described in Appendix (2) that were programmed in Appendix (3) all give reliable results.

The quadratic serendipity elements seem to be the most efficient provided only two Gauss points are used in the numerical integration of the element stiffness matrix. It is reasonable to use two Gauss points except on the coarsest

2.5) contd.

of mesh divisions where the stresses could be overestimated by up to 10%.

CHAPTER 3

ANALYSIS OF THE PLANE STRAIN COMPRESSION TEST.

3.1) Solution of Non-Linear Problems.

In this chapter, non-linearity is taken to mean that the basic stress-strain law is non-linear rather than geometric effects. A number of investigations have been carried out into the use of Finite Element Method for the analysis of structures and materials exhibiting a non-linear load deformation response. These investigations have in general idealised the material as either non-linear elastic or as work hardening plastic which both have been treated in a similar manner. The work has always been based on the assumption that a non-linear problem can be reduced to a linear one, over some increment of load, and at certain points in the mass.

In general the procedure consists of representing each element as a homogeneous, linear isotropic material defined by two pseudo-elastic constants. It is assumed that these pseudo-elastic parameters are constant within the boundaries of the element. The solution of a load deformation problem for a given set of boundary conditions can be achieved by Finite Element analysis using pseudo-elastic parameters if each of the elements satisfies the true relation between the state of stress and the state of strain in the soil. Using this procedure two methods have emerged called the modified and constant stiffness methods.

In the modified stiffness method, as the name suggests, the terms of the elasticity matrix in:

$$\{\sigma\} = \underline{D}\ \{\varepsilon\} \qquad (3.1)$$

are varied, and each variation creates a new stiffness for the element. The method is used in an incremental or an iterative process. In the incremental process the change in loading is analysed in a series of steps as shown in Figure (3.1a). At the

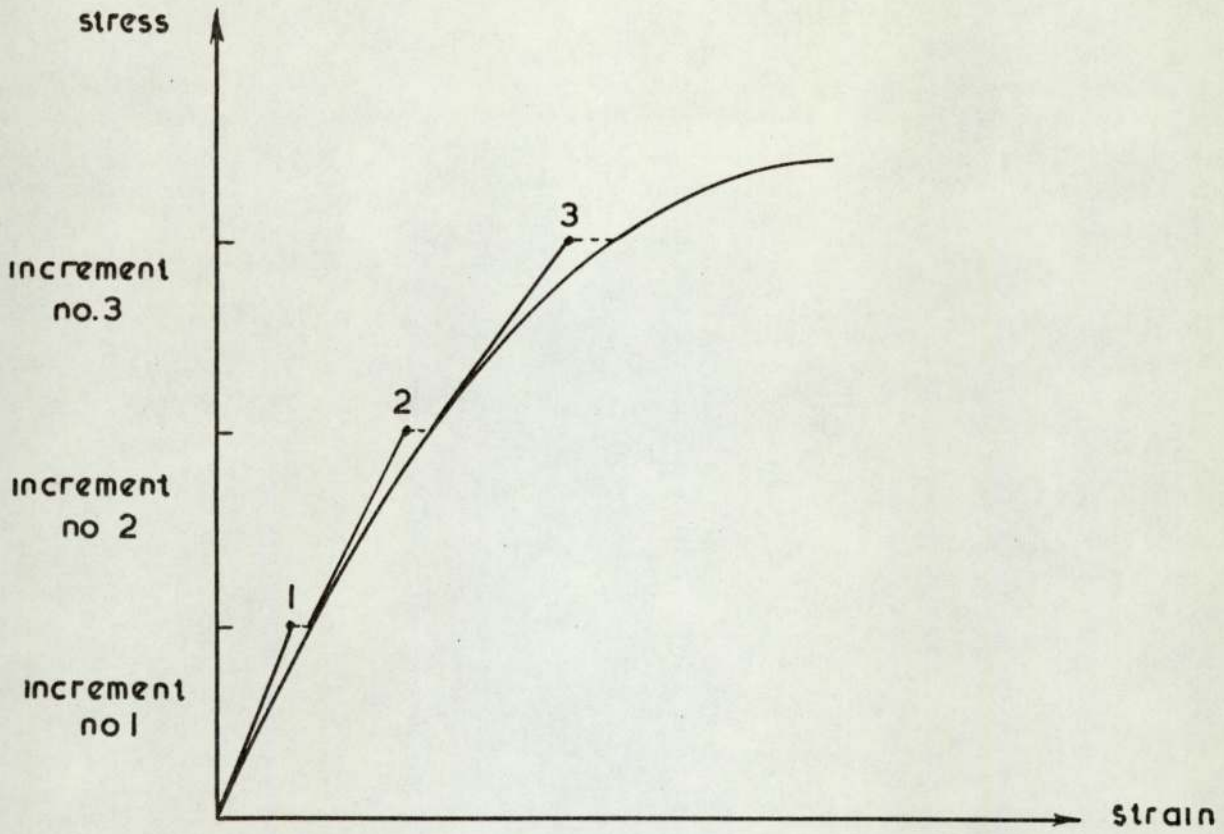

Figure 3.1.a Incremental process

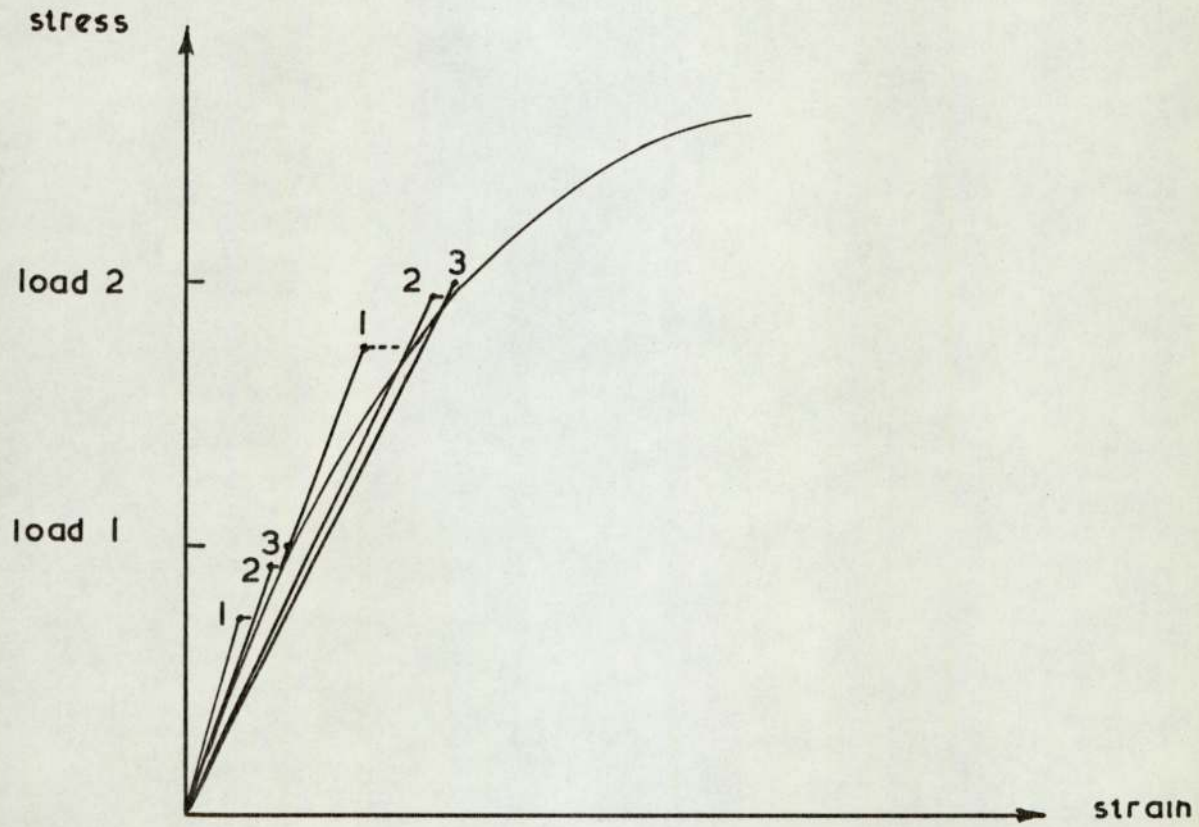

Figure 3.1.b Iterative process

3.1) contd.

beginning of each new increment an appropriate tangent modulus ($d\sigma/d\epsilon$) is selected for each element on the basis of the stress or strain in that element after the application of the last increment of the load. This method has been used by Clough and Woodward[17], Dunlop and Duncan[29] and Craig[20]. By the iterative procedure shown in Figure (3.1b) the same load is analysed repeatedly until the values of stress and strain within each element satisfy the appropriate non-linear relation. Thus, after the application of a load the analysis is carried out using some initial values of the pseudo-elastic constants, if after this iteration the stresses and strains are not within some tolerance of the non-linear relation, then the process is repeated using new values of the constants calculated from the secant modulus (σ/ε) at the end of the last iteration. Thus a process similar to the Newton-Raephson method is used to converge to the solution. This type of process was used by Girijavallabhan and Reese[38] and Duncan et al.[28].

The constant stiffness methods, on the other hand do not alter the terms in the elasticity matrix. The element is assumed to be always linearly elastic, and the stress or strain by which the element exceeds the linear case, due to non-linearity, is converted into fictitious nodal forces. Thus if the constitutive law can be written in the form:-

$$\{\sigma\} = f\{\varepsilon\}) \qquad (3.2)$$

then the basic equation;

$$\{\sigma\} = D(\{\varepsilon\} - \{\varepsilon_0\}) + \{\sigma_0\} \qquad (3.3)$$

where $\{\varepsilon_0\}$ and $\{\sigma_0\}$ are initial strain and stress vectors, can be made to coincide with equation (3.2) by adjusting the initial strain or stress vectors as shown in Figure (3.2a). The corresponding equivalent nodal forces are calculated from;

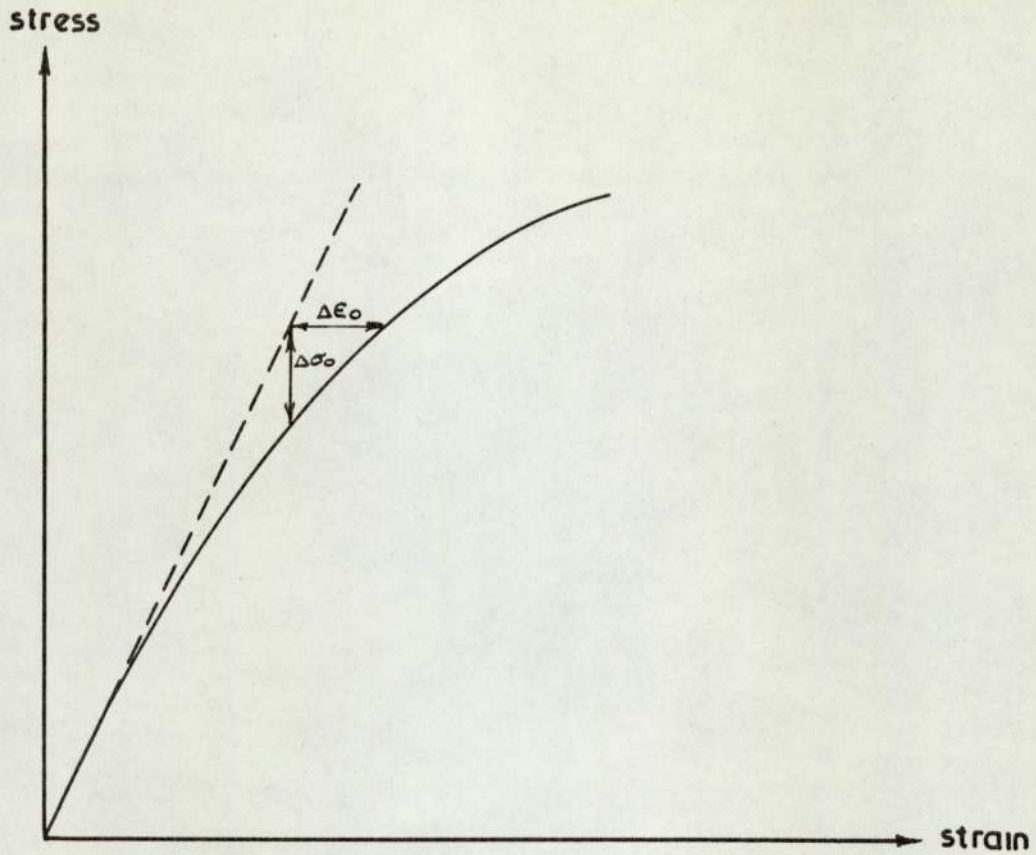

Figure 3.2.a Constant stiffness method

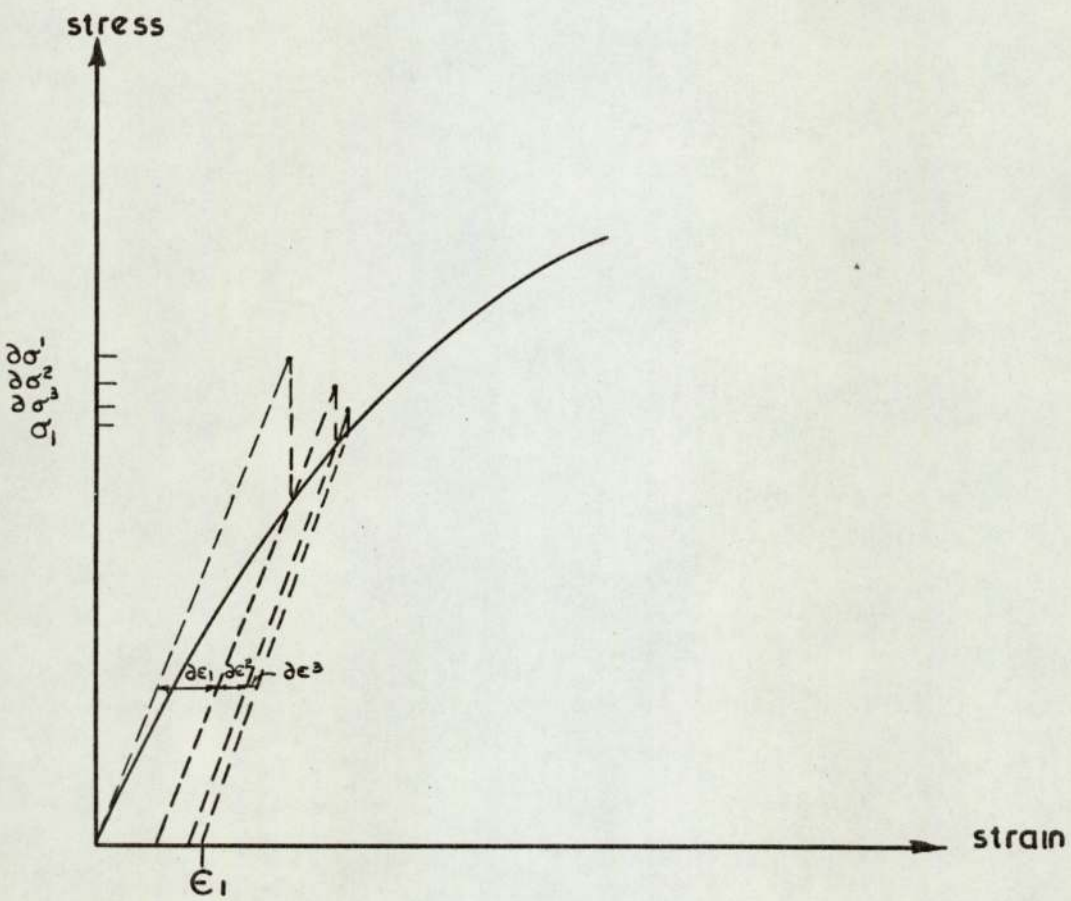

Figure 3.2.b Iterative process in the initial strain method

3.1) contd.

$$\{F\}_{\epsilon_o} = \int \underline{B}^T \underline{D} \{\epsilon_o\} \, d(vol) \qquad (3.4)$$

or $$\{F\}_{\sigma_o} = \int \underline{B}^T \{\sigma_o\} \, d(vol) \qquad (3.5)$$

and added to the load vector. Thus, an iterative process is followed until convergence is achieved, as shown in Figure (3.2b). The initial stress method has become more popular because the constitutive law can usually be expressed like equation (3.2). However, if it is only possible to determine strains in terms of stress, then the initial strain method would be used. This method has been used by Ualliapan[89], Naylor and Zienkiewicz[67] and Kay[51].

The incremental method of non-linear analysis is the easiest to program, but it requires extra store to hold the accumulating values of the stress and strain components. Because this method uses the tangent modulus, calculated after the last increment of load, to represent the pseudo-elastic constants over the next increment, it is clear that the accuracy of the solution will depend upon the size of the load increment. The accuracy of the method could be improved if some iterative process were used during each load increment. Initial stresses and strains can be readily accounted for but it is not possible to simulate post peak or peak conditions when the tangent modulus becomes negative or zero.

The other variable stiffness method of the iterative type can represent peak and post peak conditions but it is extremely complicated to account for non-zero initial stress or strain conditions. The method has the advantages that a specified accuracy to the stress-strain relation can be followed and minimum store is required because the total load is applied each time.

3.1) contd.

It is advantageous to use the secant modulus if the stress-strain law is approximated by some function. It is often true to say, that while the function is close to the real curve the slopes can be quite different. If a great number of points are required on the load deformation curve then this method is extremely expensive.

In the constant stiffness methods, if the elasticity matrix is kept constant the overall stiffness matrix can be kept in its inverted form and obviously will not need reassembling. Valliapan[89] found significant savings over the variable stiffness methods in a non-linear analysis using triangular elements. Equation (3.5) can be integrated analytically for triangular elements but requires numerical integration for the higher order elements. When the elasticity matrix is held constant the number of iterations required to converge to the true solution diverges. For this reason, Zienkiewicz[98] suggested altering the $\underline{D}$ matrix after each increment to accelerate the process. Thus, it seems that there can be little computational advantage in this method over the variable stiffness method when higher order elements are used. The great advantage of the method is that constitutive laws which are not formulated in terms of all the cartesian components of stress and strain can be used. This means that Rowe's Stress-Dilatancy theory or the Cambridge Critical State model, which are formulated in terms of principal and octahedral stress components could be used.

3.2) The Interpretation of Laboratory Tests.

A great deal of research has been involved in improving the methods of testing currently in use in Soil Mechanics. One of the most significant developments has been the introduction

3.2) contd.

of the so called 'free end' loading plattens for the triaxial test. These free ends have meant that the ends of the sample, hitherto held by friction, could expand over the plattens allowing uniform radial strains throughout the sample and ensuring that the major principal stress was vertical. Laboratory investigations[74],[52],[8],[7],[27] have shown that the end restraints have caused dead zones adjacent to the loading plattens causing internal pore pressure gradients and non-uniform volume changes. It was also shown that the relative size of the sample could be reduced if free ends were used and that a sample of height: diameter ratio of 2:1 with fixed ends gave the same strength as a free ends sample with a ratio of 1:1, but peak was reached at lower strain levels in the former case.

While the research into the need to improve the triaxial test has been mainly experimental several analytical investigations have been carried out. Balla[6] analysed the triaxial compressions test assuming elastic theory allowing for any degree of roughness and length to diameter ratio. Haythornwaite[43] carried out a similar analysis but assumed the material in the sample to be ideally plastic. The Finite Element method has been used to analyse the triaxial test by Perloff and Pembo[69] and Kraft and Krishnamwthy[59] using non-linear methods and triangular elements.

Perloff and Pembo[69] said very little about their Finite Element idealisation but Kraft and Krishnamwthy[59] suppressed the horizontal degrees of freedom of the joints at the top and bottom of the sample and applied a surface loading, which is not a true representation of the loading condition. However, both these Authors showed how useful the Finite Element method can be in interpreting test conditions. Now that the

3.2) contd.

technology of triaxial testing is being extended to plane strain conditions it was decided to use the Finite Element method to analyse the plane strain compression test using "better" elements and a more realistic idealisation, and to compare fixed and free ends analytically.

There is one important problem that arises when the Finite Element method is used to analyse conditions involving smooth interfaces. Consider the plane strain sample in Figure (3.3a) and the rather crude Finite Element idealisation below it in Figure (3.3b). When fixed end conditions are idealised the joints number 1 to 5 would be given no degree of freedom and joints 18 to 22 would be prevented from moving out sideways by the stiffness of the beam elements to which they are connected. For the other condition when free ends are assumed, joints 1 to 5 would be given a sideways degree of freedom, equivalent to a roller, but joints 18 to 22 must still be connected to, and hence restrained by the beam elements. Indeed, this same problem would arise in the finite element idealisation of smooth foundations and retaining walls or when conditions are neither perfectly rough nor smooth.

3.3) Representation of Non-Restrained Interfaces.

There seemed to be a direct analogy between the problem here and that faced by investigators trying to achieve free ends experimentally. Free ends were achieved experimentally by inserting a thin latex membrane between the sample and the polished loading platten. Because the membrane has relatively small stiffness compared to the sample, it provides little restraint and expands with the sample over the platten. The Author proposed to improve the finite element idealisation using the same kind of approach by inserting a thin sandwich element between the elements

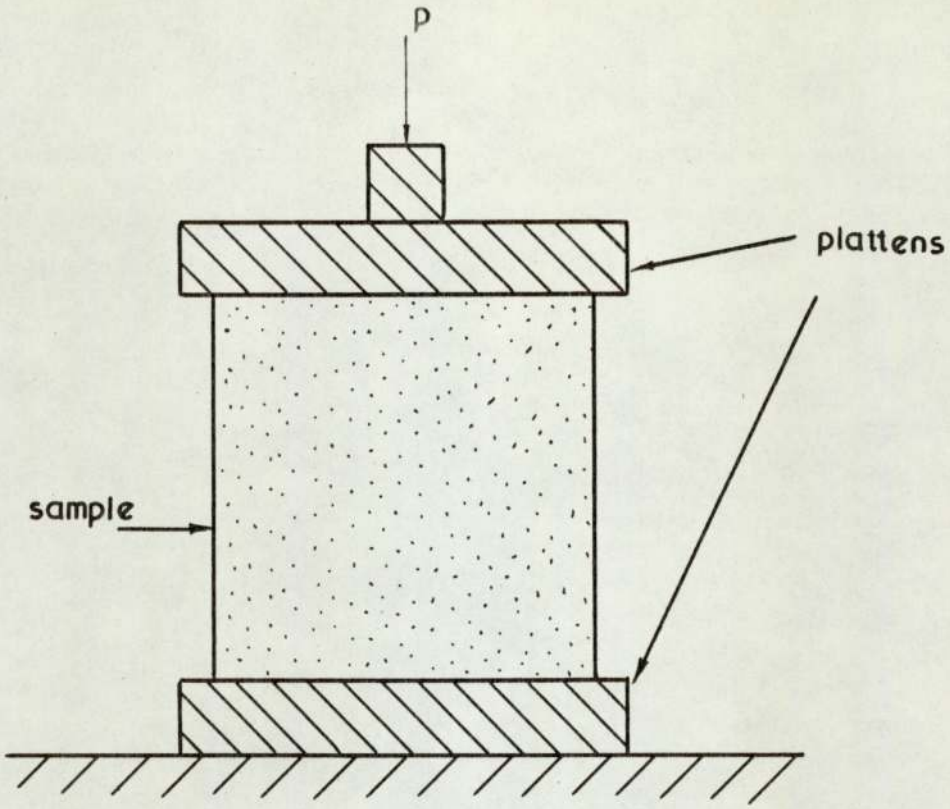

Figure 3.3 a The plane strain compression test

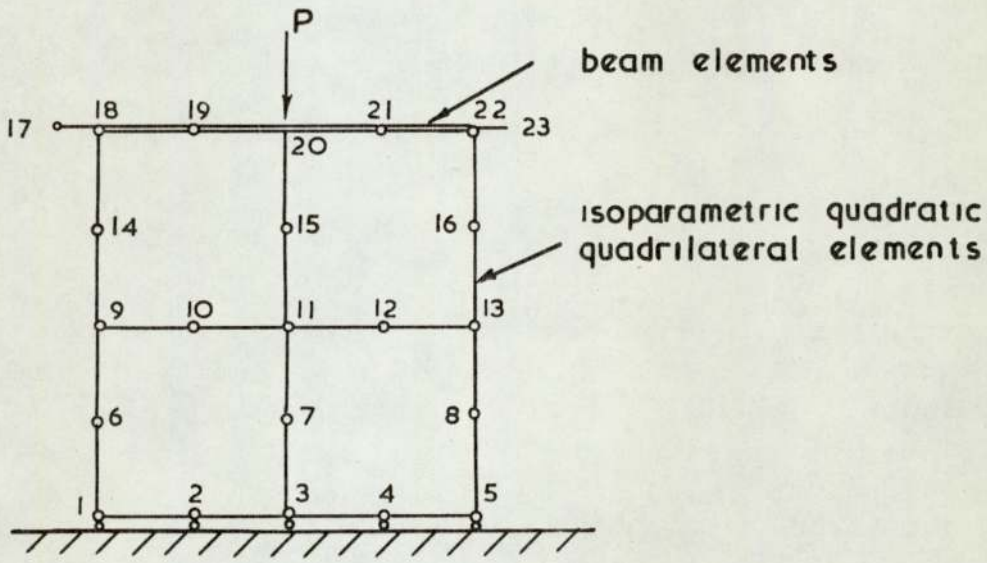

Figure 3.3.b Finite element representation of the plane strain compression test

3.3) contd.

representing the sample and those representing the loading platten, as shown in Figure (3.4). For fixed end conditions the two elements numbered 5 and 6 in the figure would be given the same properties as the other sample elements. Free end conditions can be approximated to by reducing the stiffness of the sandwich elements relative to the other elements representing the sample. Any condition of roughness or restraint could then be imposed on the joints numbered 17-21 by varying the stiffness of the sandwich elements between the two previous limits.

3.4) Test Problem.

The plane strain compression test is not common, particularly tests in which the value of the intermediate principal stress has been measured. Among tests reported are a series by Green[41] on samples of Ham River sand. Of these tests the one named ISC/3 was selected and its dimensions are shown in Figure (3.5).

In this test the cuboidal sample was isotropically consolidated under an ambient pressure of 30 psi, then the cell pressure (σ_3) was kept constant, the vertical stress (σ_1) was increased while deformation in the other direction (σ_2) was prevented by rigid plattens. The intermediate principal stress was measured. The results of the test ISC/3 as reported by Green[41] are shown in Figure (3.6).

3.5) Analytical Model.

The simple isotropic model is described by two pseudo-elastic constants. This model has been used by numerous investigators who have all obtained good results for little

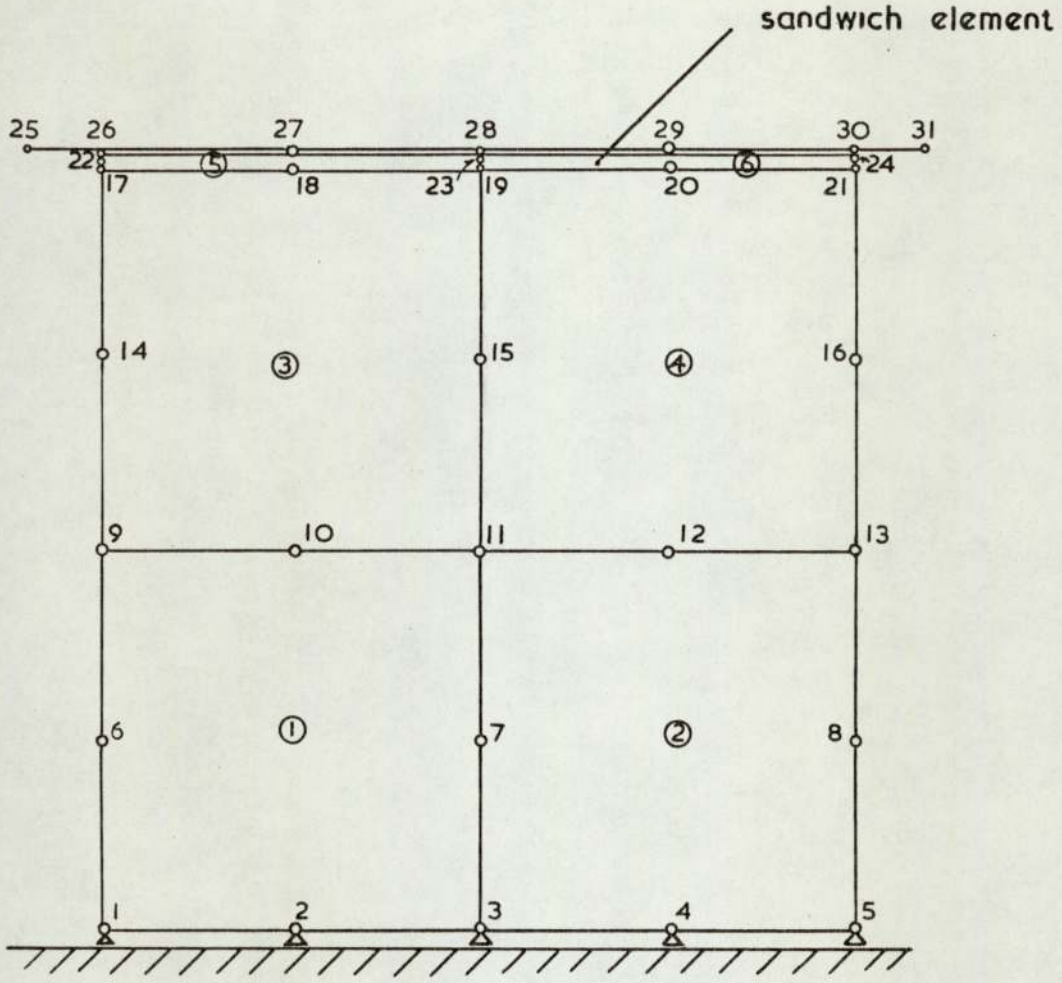

Figure 3.4. Improved finite element representation of the plane strain compression test

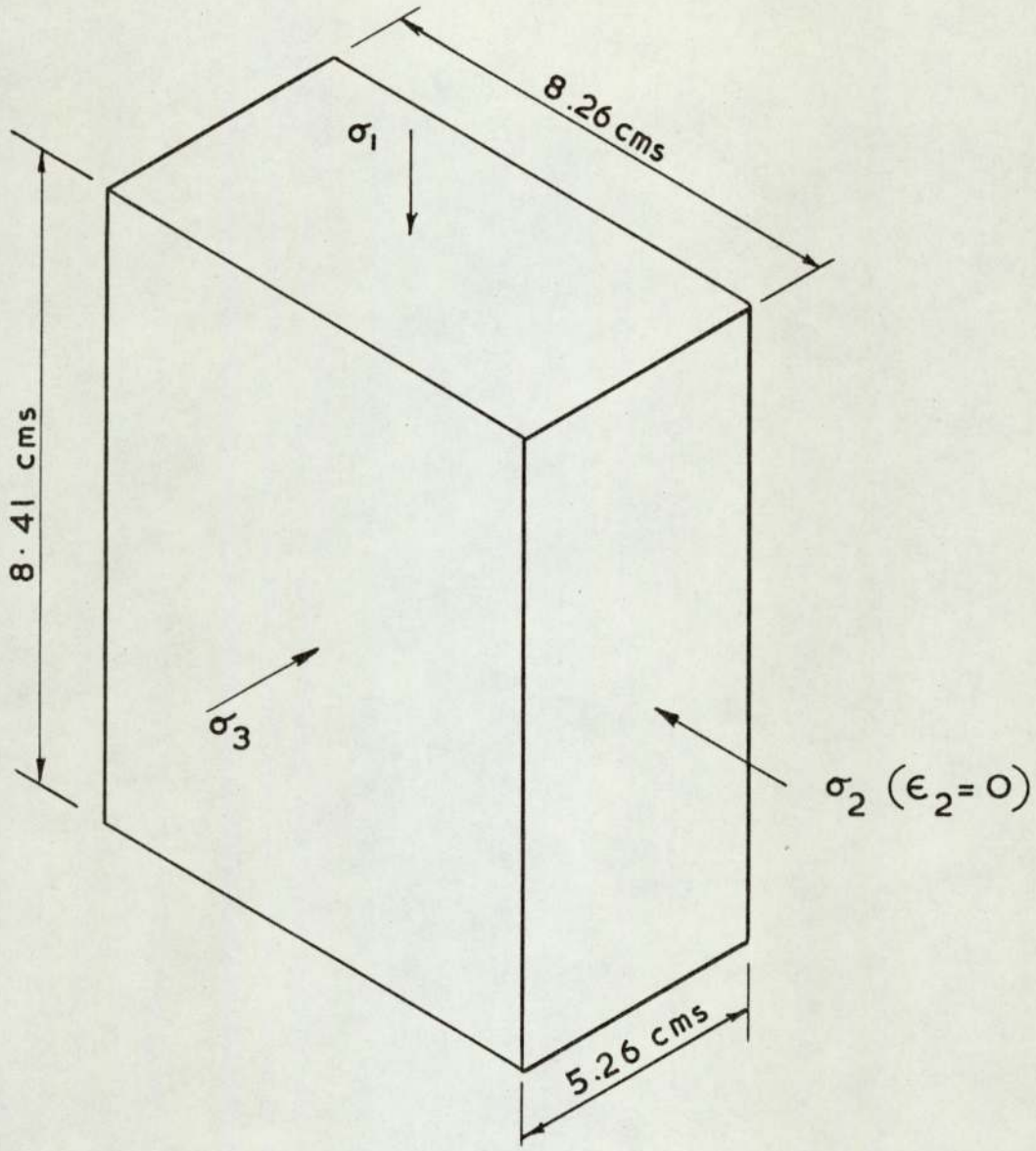

Figure 3.5 Test problem
Greens (41) Plane strain ISC/3

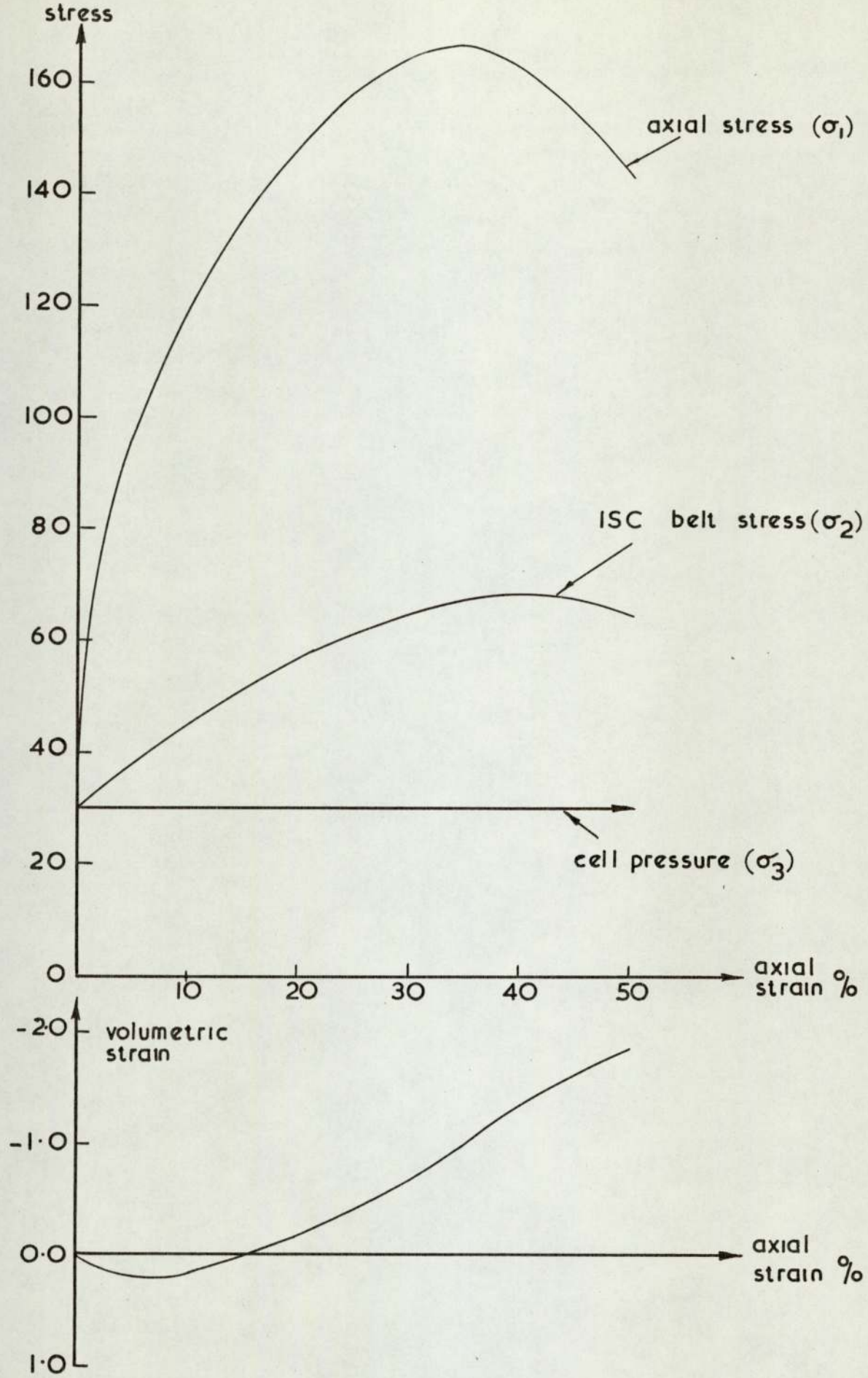

Figure 3.6 Test ISC/3 (PS) Ref green (41) fig. 4.11.3

3.5) contd.

effort in establishing the constitutive relation. This relation cannot be used to predict deformation in conditions when the load is decreasing, but this is not a serious drawback because Engineers are almost always interested in settlements that occur with the application of a load. The pseudo-elastic theory does not allow volume change to occur under shear, a condition which is inherent with sand. However, the volumetric strains are usually relatively small compared to the shear strains which should minimise any effects due to this error.

The majority of investigators using the isotropic model have used the two pseudo-elastic constants E, the Young's modulus and ν, the Poisson's ratio to describe the material properties. Under the conditions that exist in the plane strain compression test the deformation is likely to be mainly due to the shearing action of the deviatoric stress which makes it seem more logical to choose G, the shear modulus as one of the constants. Indeed, the stress can be divided into two components, a hydrostatic stress accounting for volume change and a deviatoric stress accounting for the change in shape. This is in line with the work done at Manchester[73] which suggests that the deformation of particulate materials can be divided into the elastic deformation of the sand grains due to mean normal stress and the irrecoverable deformation due to a change in geometry produced by interparticle shear forces resulting from deviatoric stress. The octahedral components of shear and normal stress and strain are often used to represent these two components. The octahedral shear stress and strain under plane strain conditions ($\epsilon_z = 0$) are calculated from:

3.5) contd.

$$\tau_{oct} = \frac{1}{3}\sqrt{\{(\sigma_x-\sigma_y)^2+(\sigma_x-\sigma_z)^2+(\sigma_y-\sigma_z)^2+6\ \tau_{xy}^2\}} \qquad (3.6)$$

$$\gamma_{oct} = \frac{2\sqrt{2}}{3}\sqrt{\{\epsilon_x^2 + \epsilon_y^2 - \epsilon_x\epsilon_y + \tfrac{3}{4}\gamma_{xy}^2\}} \qquad (3.7)$$

and they are linked by the relation;

$$\tau_{oct} = G\ \gamma_{oct}.$$

Figure (3.7a) shows a graph of τ_{oct} plotted against γ_{oct} calculated from the test result in Figure (3.6).

The natural choice for the other pseudo-elastic constant would be the bulk modulus. However, the relationship between the octahedral normal stress and strain, from which the bulk modulus would be calculated, is also non-linear. It is very difficult and expensive computationally to iterate along two non-linear curves. This is why many investigators have used constant values of bulk modulus or Poisson's ratio to complete the isotropic relation.

From the equations of elasticity under plane strain conditons, Poisson's ratio can be calculated from;

$$\nu = \left(\frac{\sigma_2}{\sigma_1+\sigma_3}\right) \qquad (3.8)$$

Figure (3.7b) shows a graph of the above ratio plotted against octahendral shear strain. It can be seen from Figure (3.7b) that the value of Poisson's ratio is roughly constant or more accurately a linear function of octahedral shear strain. Similar results to these have been obtained by Comforth[19]. It therefore seemed reasonable to choose Poisson's ratio as the second constant and to make it a function of shear strain level. A linear regression analysis was carried out on the points in Figure (3.7b) to obtain a least squares fit which gave the relation;

$$V = 0.296 + 0.56\ \gamma_{oct} \qquad (3.9)$$

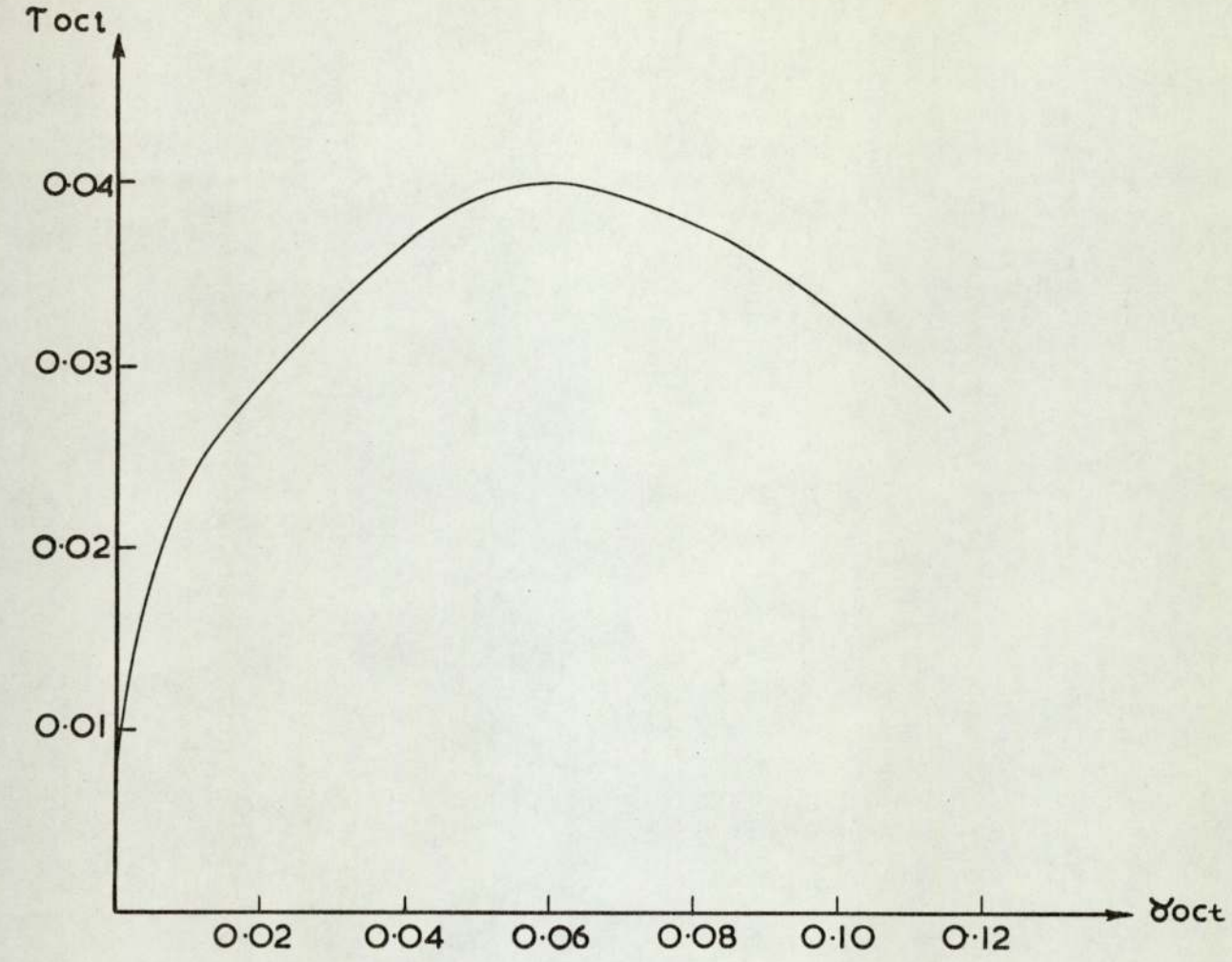

Figure 3.7.a

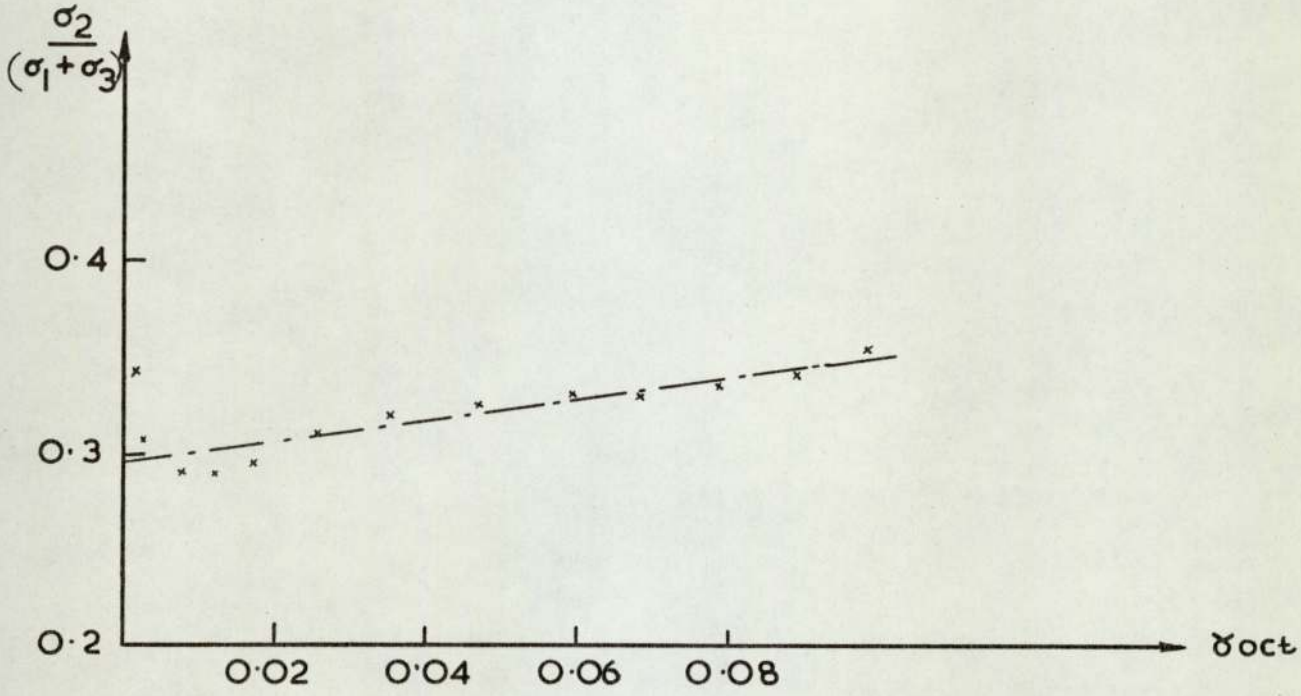

Figure 3.7.b

3.5) contd.

The adoption of the constants G and ν to describe the material properties meant that the elasticity matrix became;

$$\underline{D} = \begin{bmatrix} 2G\frac{(1-\nu)}{1-2\nu} & \frac{2G\nu}{1-2\nu} & 0 \\ \frac{2\nu G}{1-2\nu} & 2G\frac{(1-\nu)}{1-2\nu} & 0 \\ 0 & 0 & G \end{bmatrix} \qquad (3.10)$$

It would have been possible to represent the non-linear relation between τ_{oct} and γ_{oct} as a function but to obtain better accuracy it was decided to use the actual points on the curve in Figure (3.7a) as the relation, in a similar way to Craig[20]. Intermediate points can be easily interpolated. This procedure is possible because the sample is prepared to be homogeneous and it is not large enough to be affected by body forces, thus the properties of each element obey the same two functions.

3.6) Finite Element Analysis.

3.6.1) Representation.

The Finite Element mesh used to represent the plane strain compression test described in Figure (3.5) is shown in Figure (3.8). The mesh consisted of 48 eight noded isoparametric quadrilaterals, 6 sandwich elements and 12 beam elements. The member elements are shown separately from the sandwich elements for clarity in Figure (3.8), in reality they share common joints. The quadrilateral elements were all assumed to obey the two functions shown in Figures (3.7a) and (3.7b), and all the other elements were assumed to be linear.

As described in Section (3.3), the joints at the base were free to move in the x-direction for the free ends analysis, when the sandwich elements were also given a low stiffness. Several analyses were carried out to find which

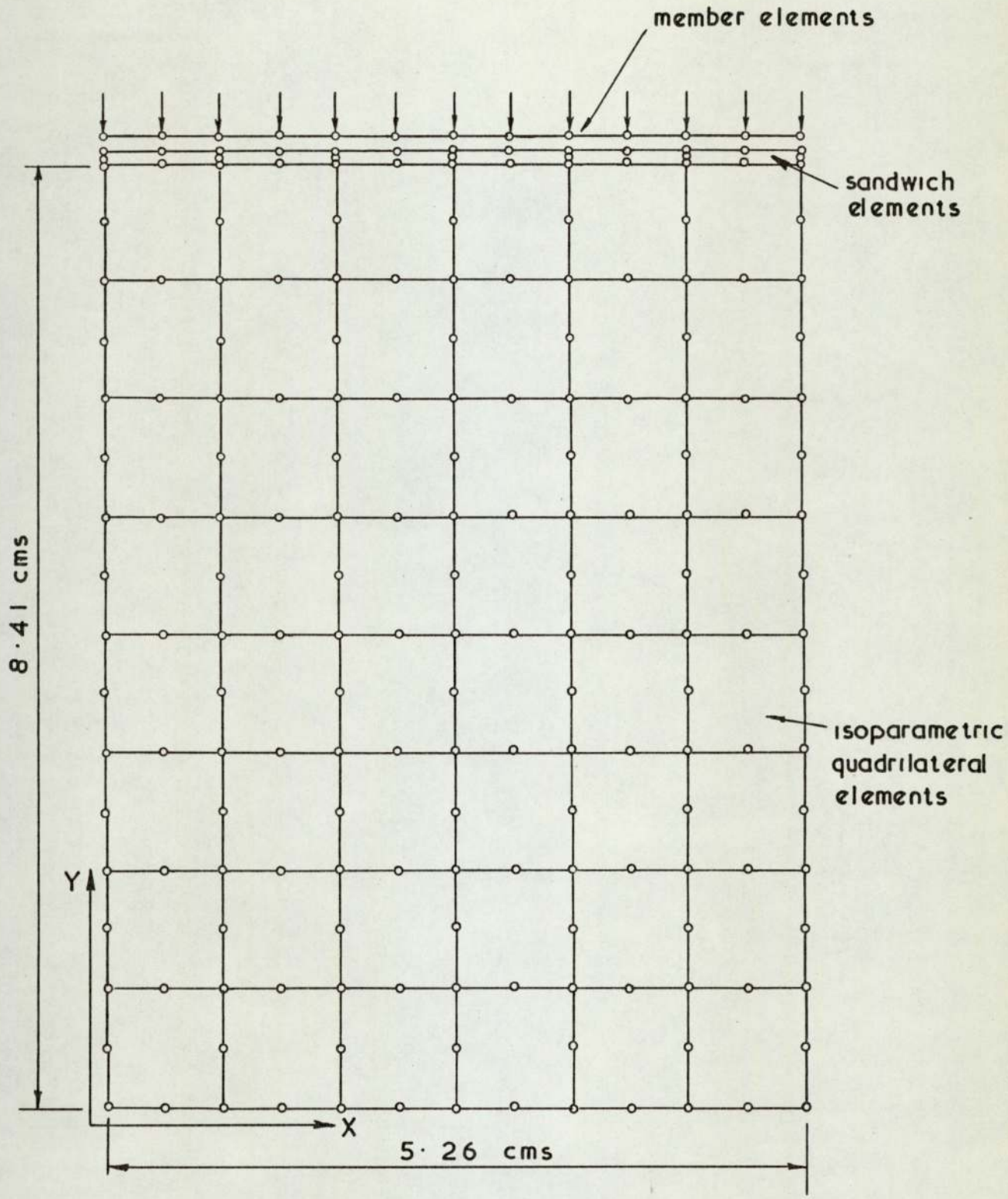

Figure 3.8 Finite element mesh

3.6.1) contd.

values of the elastic constants gave the sandwich elements a stiffness low enough to prevent any barrelling effect in the deformed shape of the loaded sample. For the analyses assuming fixed ends the joints at the base were rigidly fixed and the sandwich elements were given the same properties as the beam element. The sandwich elements were only 0.2 cms. thick and this had an insignificant effect on the overall vertical displacements.

3.6.2) The Program.

The subroutines describing the eight noded quadrilateral were joined with those of the member element and the standard library routines as described in Appendix (3) to form the basis of the program. To complete the program it was necessary to write a master segment and one other subroutine called CONTROL to control the non-linear interative procedure. The general procedure followed by this program is shown in flowchart (3.1). It can be seen from the flowchart that the operations labelled 5, 6 and 7 are the familiar operation carried out in a linear finite element analysis and all the other operations are concerned with the iterative procedure.

3.6.3) The Iterative Procedure.

The iterative procedure is designed to make the stresses and strains within each element representing the sample follow the curve in Figure (3.9) which represents the non-linear behaviour of sand. A load is applied, and then the Newton-Raephson method of solution and resolution followed, until the stresses and strains in each element fall on or near the curve. When all the elements have achieved this fit the correct

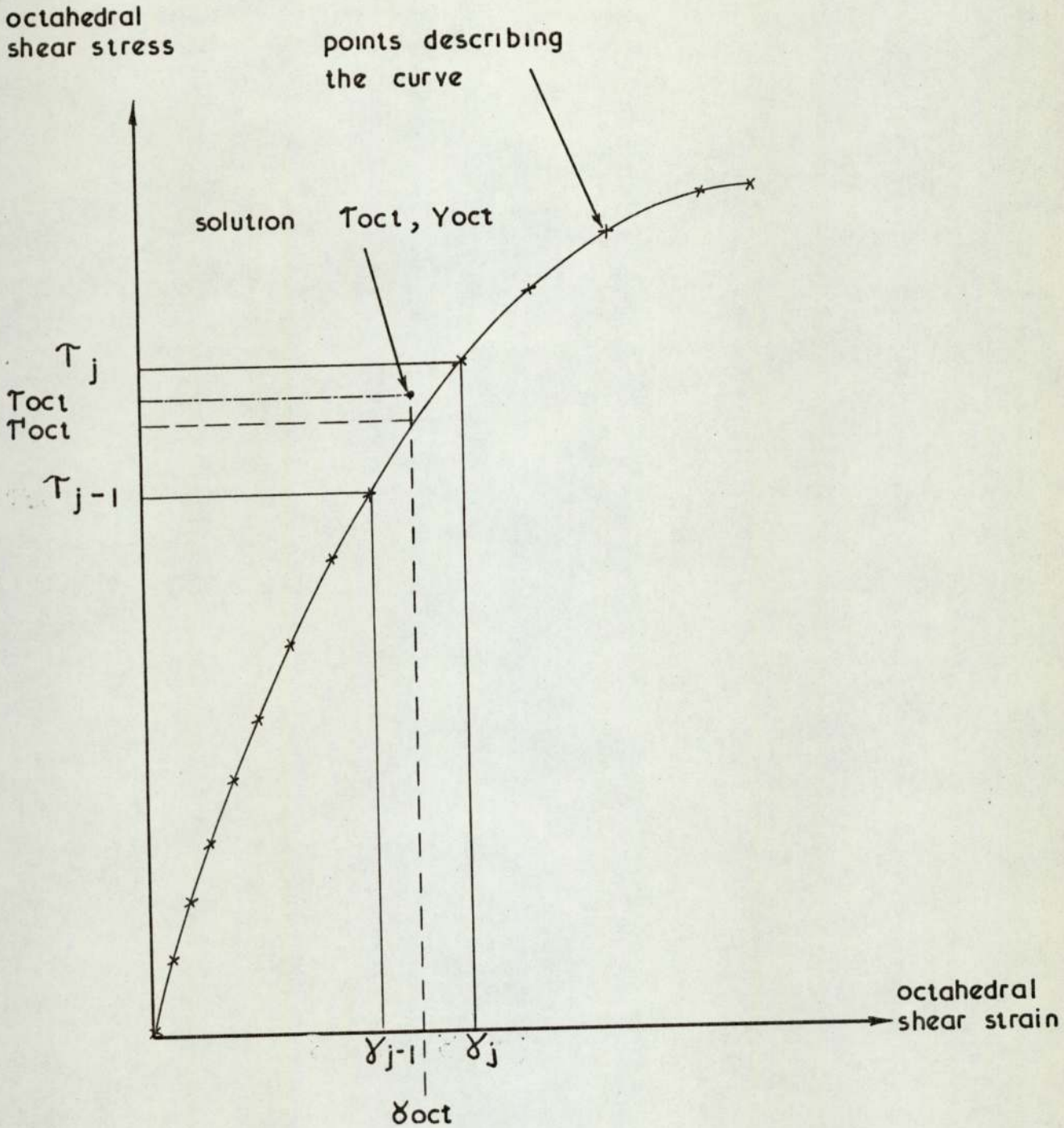

Figure 3.9 Idealised curve

Flowchart (3.1)

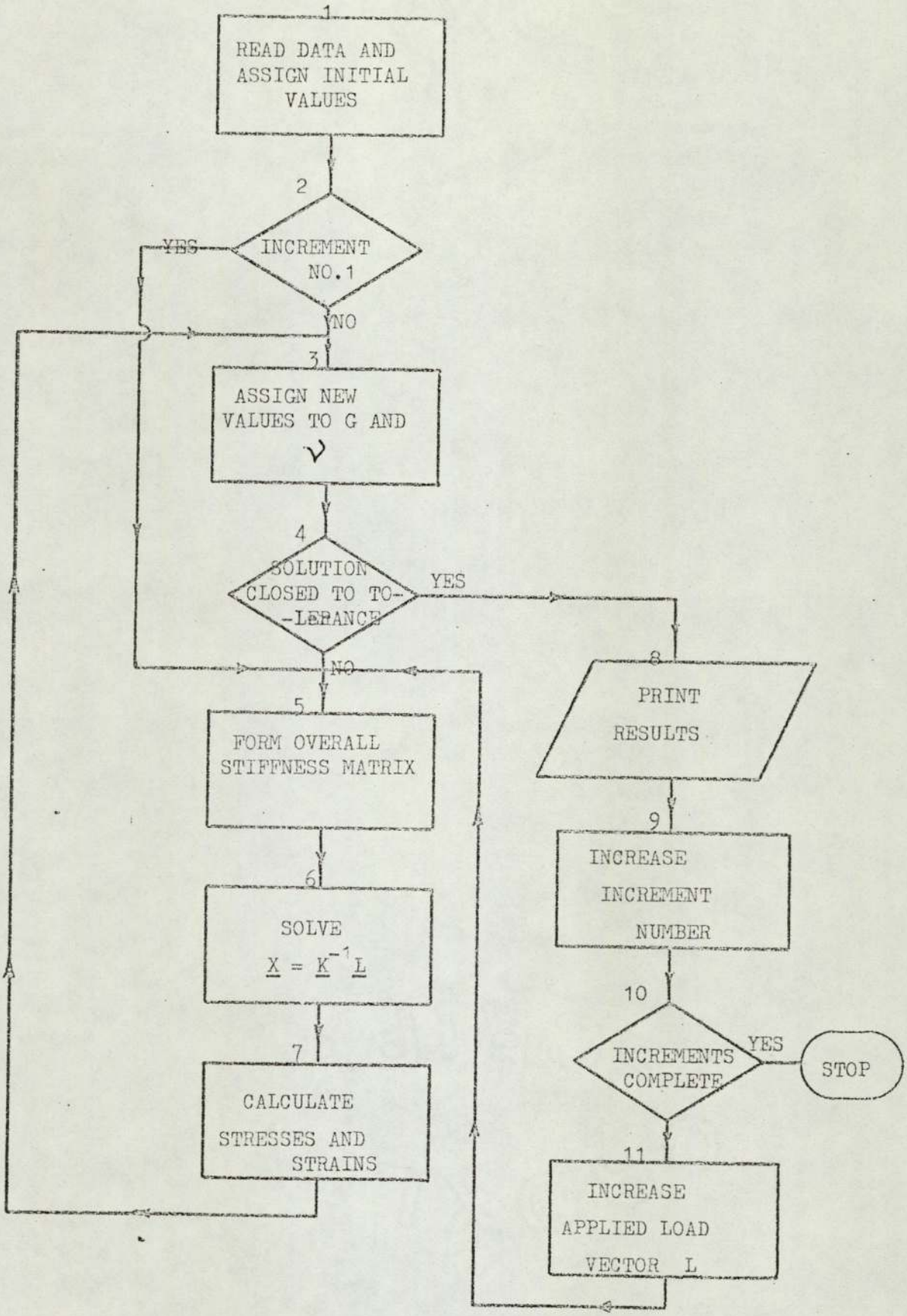

3.6.3) contd.

solution will have been found for this load.

To obtain a first approximation, initial values are assigned to the two pseudo-elastic parameters G, the shear modulus and ν, Poisson's ratio. The initial value for the latter is taken as the ordinate corresponding the zero octahedral shear strain level in figure (3.7b), while the value of G is arbitrary provided it is relatively high.

A finite element analysis was then carried out which resulted in cartesian stress and strain components at each joint in Figure (3.8). From these values, the octahedral shear stress and strain components were calculated at the centre of each quadrilateral element and then used to compute the new values of G and ν for each element. For any element having octahedral shear components τ_{oct} and γ_{ovt} the next value of the shear modulus could be calculated from the curve in Figure (3.9). The value τ'_{oct} is the value of octahedral shear stress corresponding exactly to γ_{oct} on the curve and was interpolated from;

$$\tau'_{oct} = \tau_j \left\{ (\gamma_j - \gamma_{oct})(\tau_j - \tau_{j-1})/(\gamma_j - \gamma_{j-1}) \right\} \qquad (3.11)$$

where γ_j and γ_{j-1} are points describing the curve between whose values γ_{oct} has been found to lie, and τ_j and τ_{j-1} are their corresponding stress ordinates from the curve.

The new value for G is the secant modulus of the curve at the strain level γ_{oct} which is calculated from;

$$G = \frac{\tau'_{oct}}{\gamma_{oct}} \qquad (3.12)$$

The new value for Poisson's ratio was calculated directly from the linear relation;

$$\nu = a + b\,\gamma_{oct} \qquad (3.13)$$

3.6.3) contd.

as in Figure (3.7b).

On the first run the problem would then be reanalysed using the improved approximation repeating the above process. On all subsequent runs the closeness of the stress-strain state in each element to the required behaviour would be measured using the quantity;

$$A = |(\tau'_{oct} - \tau_{oct})/\tau'_{oct}| \qquad (3.14)$$

It would have taken a great number of operations to make the quantity A become zero in every element. To overcome this it was assumed that the element had converged to the curve if the measure A was inside a specified tolerance, usually 0.05. When all the elements fell within the tolerance then the process was finished for this value of applied load and a complete solution had been found. Otherwise, the problem would be reanalysed and the process repeated until they were. Once a complete solution had been found the load was increased and the process repeated to find the next solution. The load was increased until the last increment had been processed when a complete non-linear load-deformation response would have been found.

The process described above is shown in more detail in flowchart (3.2).

3.7) Results.

It was found that when the sandwich elements were given approximately the same Poisson's ratio as that given to the elements representing the sample, and, a constant value of shear modulus of approximately $^1/1000$ of the initial values assigned to the non-linear elements, then no

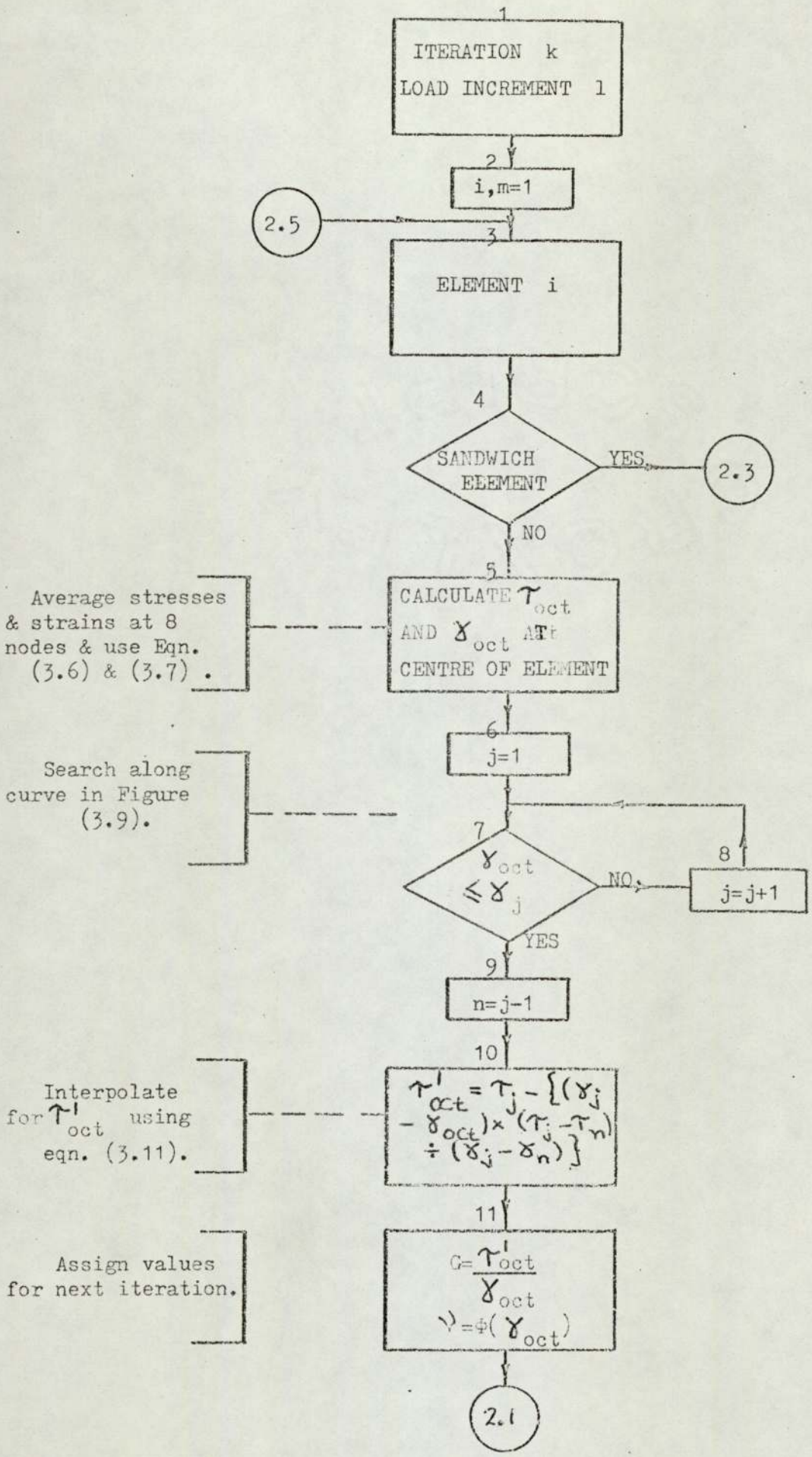
1
ITERATION k
LOAD INCREMENT 1
2
i,m=1
2.5
3
ELEMENT i
4
SANDWICH ELEMENT
YES
2.3
NO
5
CALCULATE τ_{oct} AND γ_{oct} AT CENTRE OF ELEMENT
Average stresses & strains at 8 nodes & use Eqn. (3.6) & (3.7).
6
j=1
Search along curve in Figure (3.9).
7
$\gamma_{oct} \leq \gamma_j$
NO
8
j=j+1
YES
9
n=j-1
10
$\tau'_{oct} = \tau_j - \{(\gamma_j - \gamma_{oct}) \times (\tau_j - \tau_n) \div (\gamma_j - \gamma_n)\}$
Interpolate for τ'_{oct} using eqn. (3.11).
11
$G = \frac{\tau'_{oct}}{\gamma_{oct}}$
$\nu = \Phi(\gamma_{oct})$
Assign values for next iteration.
2.1

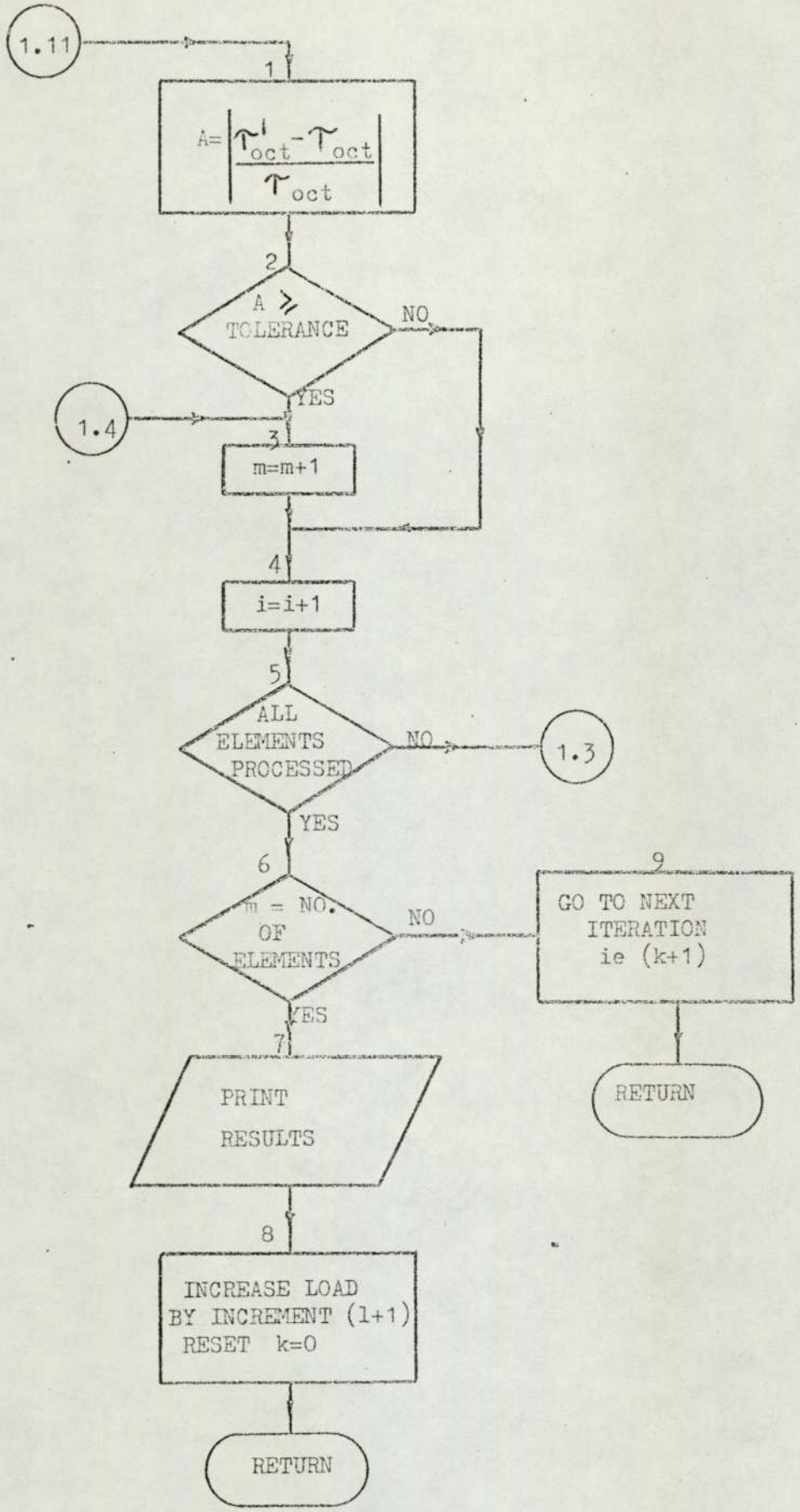
1.11
1
$A=\left|\frac{\tau'_{oct}-\tau_{oct}}{\tau_{oct}}\right|$
2
A ≥ TOLERANCE
NO
YES
1.4
3
m=m+1
4
i=i+1
5
ALL ELEMENTS PROCESSED
NO
1.3
YES
6
m = NO. OF ELEMENTS
NO
9
GO TO NEXT ITERATION ie (k+1)
RETURN
YES
7
PRINT RESULTS
8
INCREASE LOAD BY INCREMENT (l+1) RESET k=0
RETURN

3.7) contd.

significant barrelling resulted in the sample shape.

Figure (3.10) shows the comparison between the three load-deformation curves, from the fixed and free-end analyses and the experimental result. Both theoretical analyses failed under the application of a load of 0.54KN in the sense that no solution could be found. Figure (3.11a) shows the distribution of the stress component σ_y across the width of the sample, immediately adjacent to the loading platten (Y = 8.41) and at the mid-height of the sample (Y = 4.20) for both analyses at an applied load of 0.48 KN. The distribution of the vertical stress in the free ends analysis was completely homogeneous, and, no distortion under the applied load was encountered as the homogeneous stress level corresponded exactly to the value computed from load over area, and hence there is only one line in Figure (3.11a) for the free ends case. Figure (3.11b) shows the distribution of stress in the bottom half of the restrained sample expressed as a percentage of the homogeneous stress level in the other free ends case. In the fixed ends analysis the direction of the major principal stress varied from 25° to the vertical on the edge of the top platten to zero at the centre and the principal stress was approximately vertical between $y = 2.1$ and $Y = 6.3$ and no further rotation occurred with increase in applied load.

The distribution of horizontal displacement, together with the deformed shape of the sample for both of the analyses are compared in Figure (3.12). The distribution of horizontal displacement is also shown in Figure (3.13) as a function of increasing applied load. It was found that the vertical strain was constant throughout

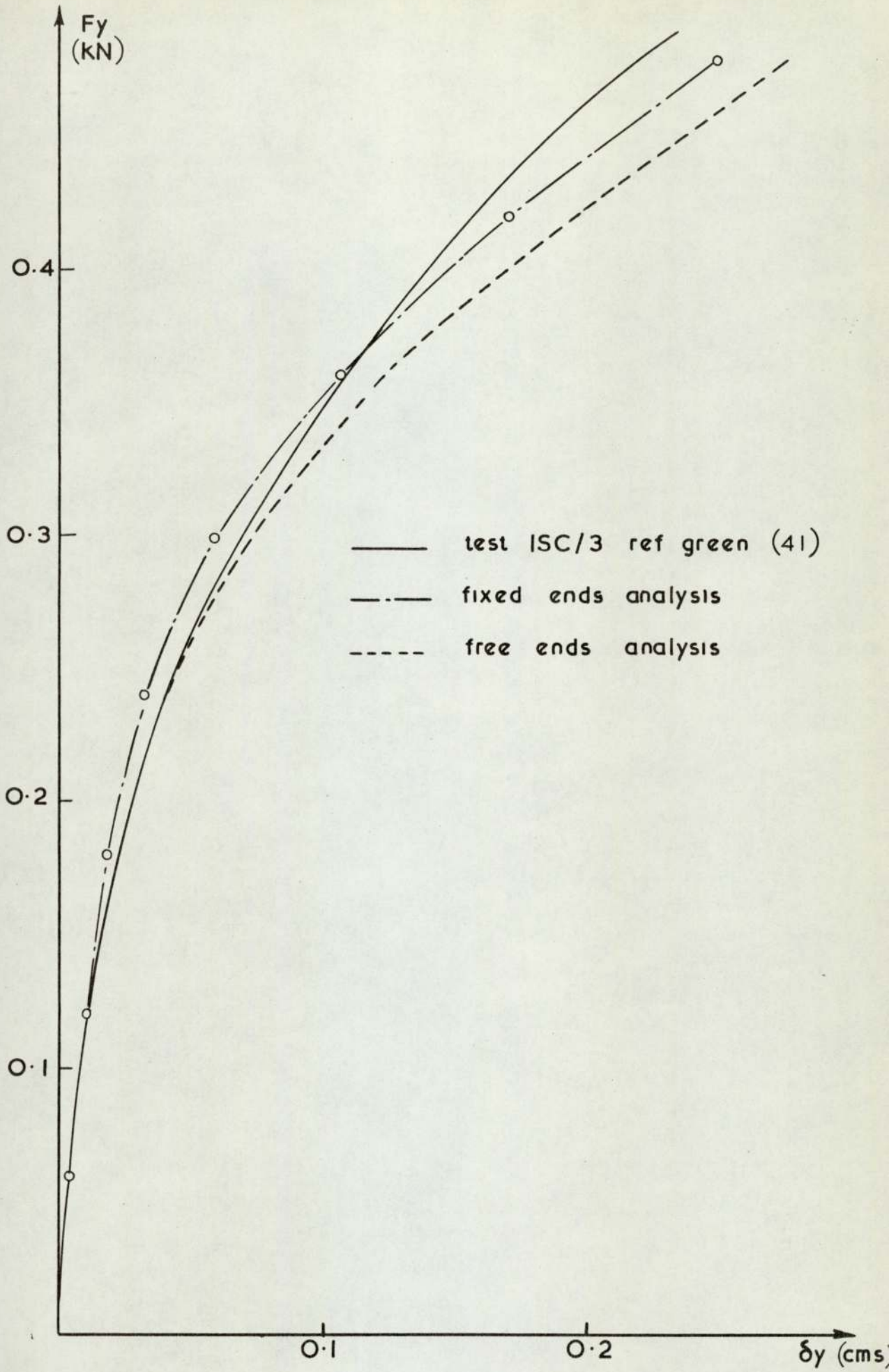

Figure 3.10. Axial load – deformation curve

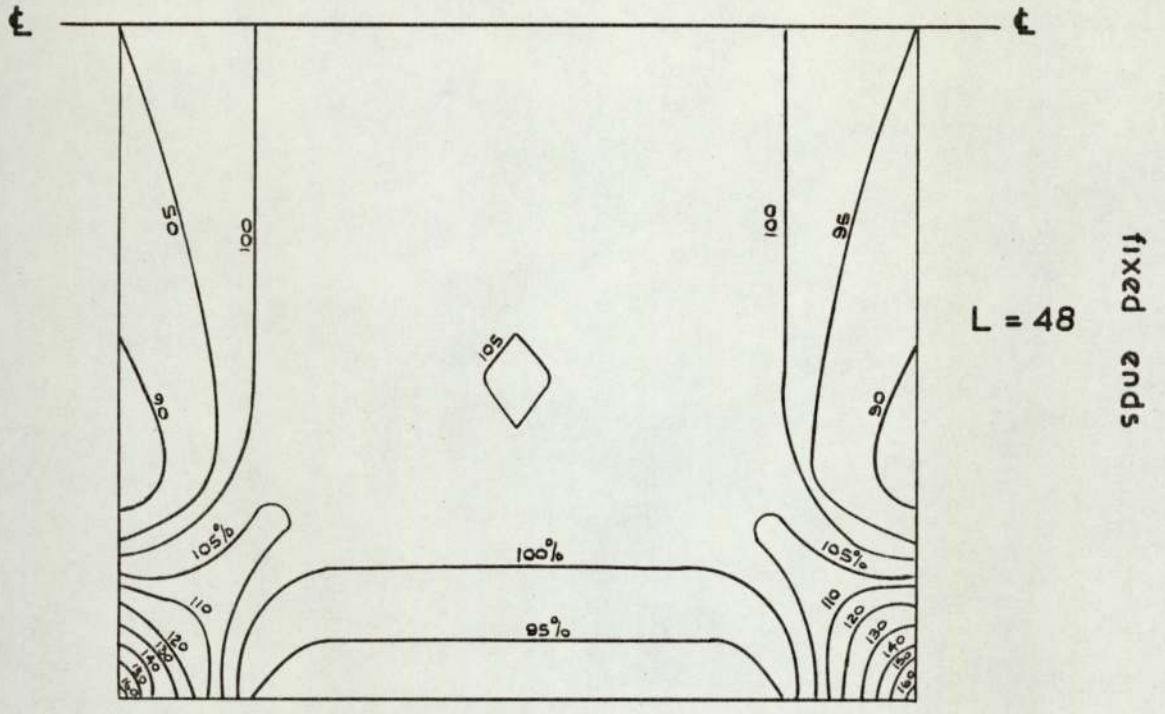

Figure 3.11 b Contour of σy, from fixed ends analysis load = 0·4 KN expressed as %age of homogenous stress level in free ends

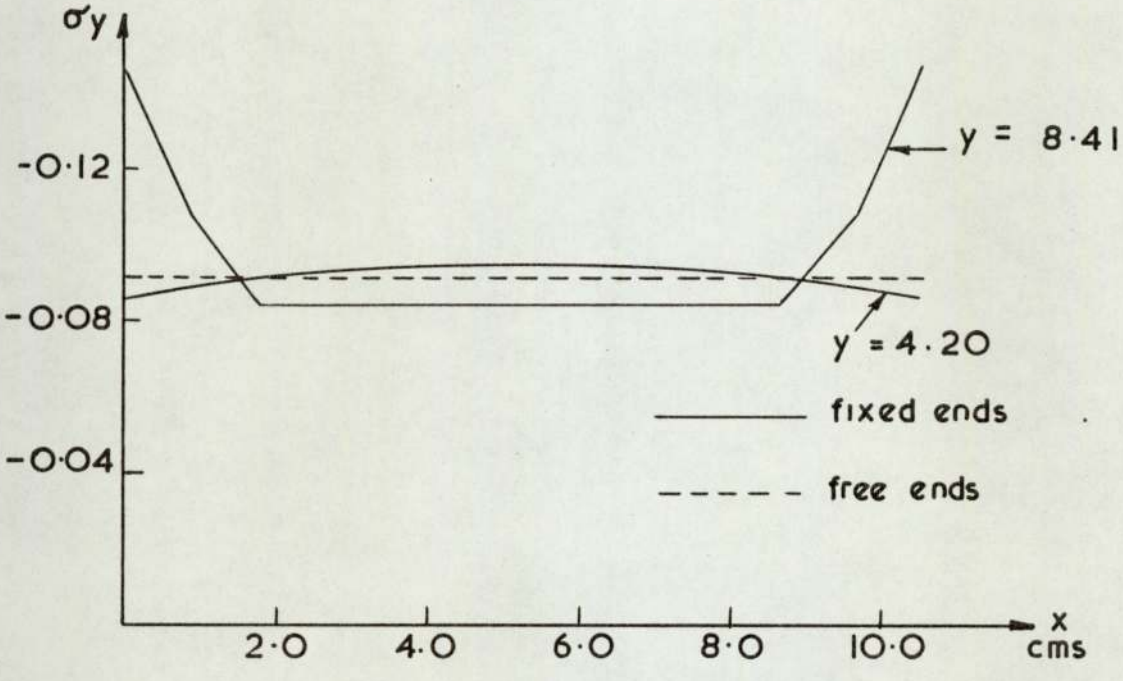

Figure 3.11a Distribution of σy

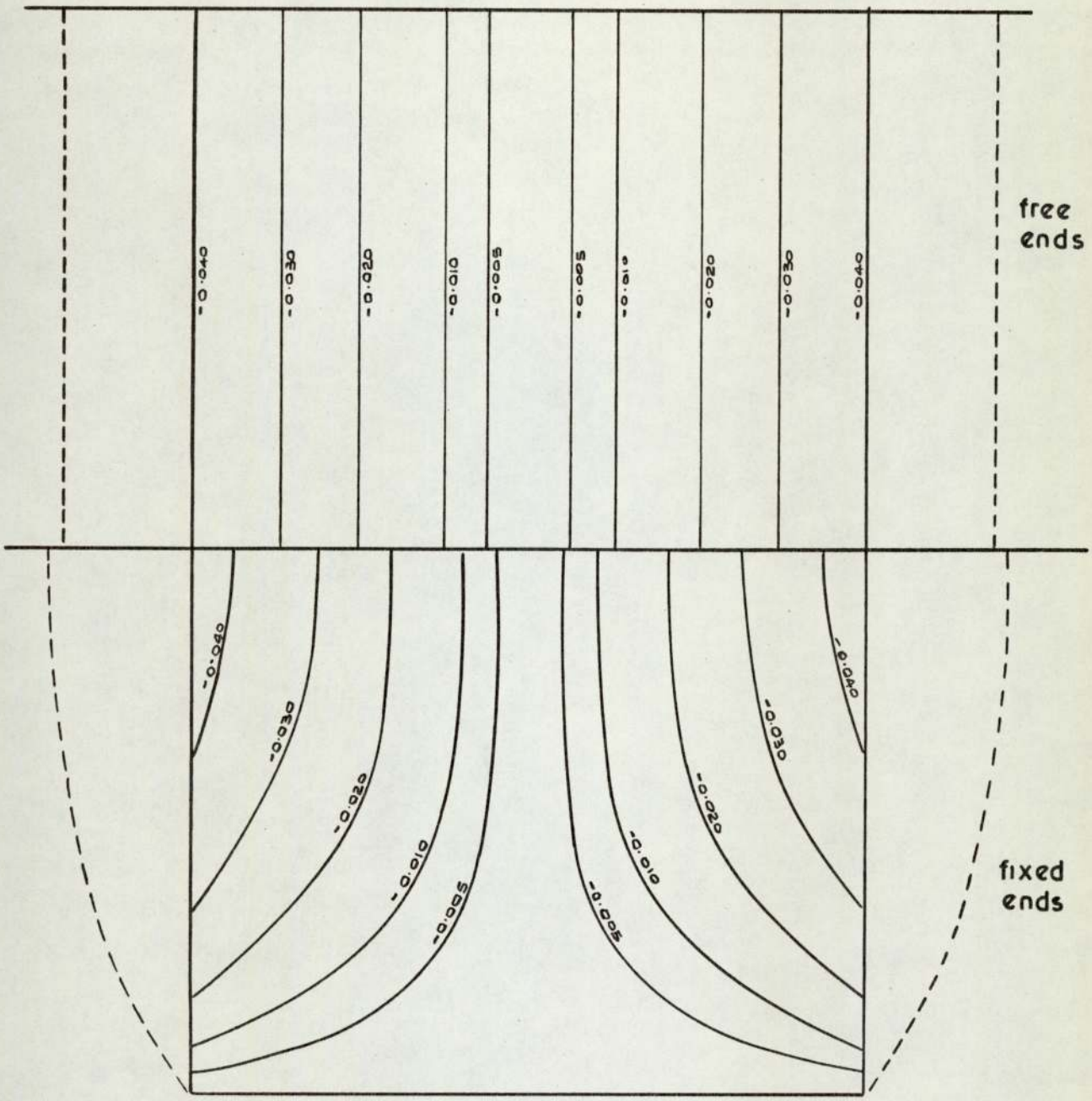

Figure 3.12 Contours of horizontal displacement at load = 0·48 K.N.

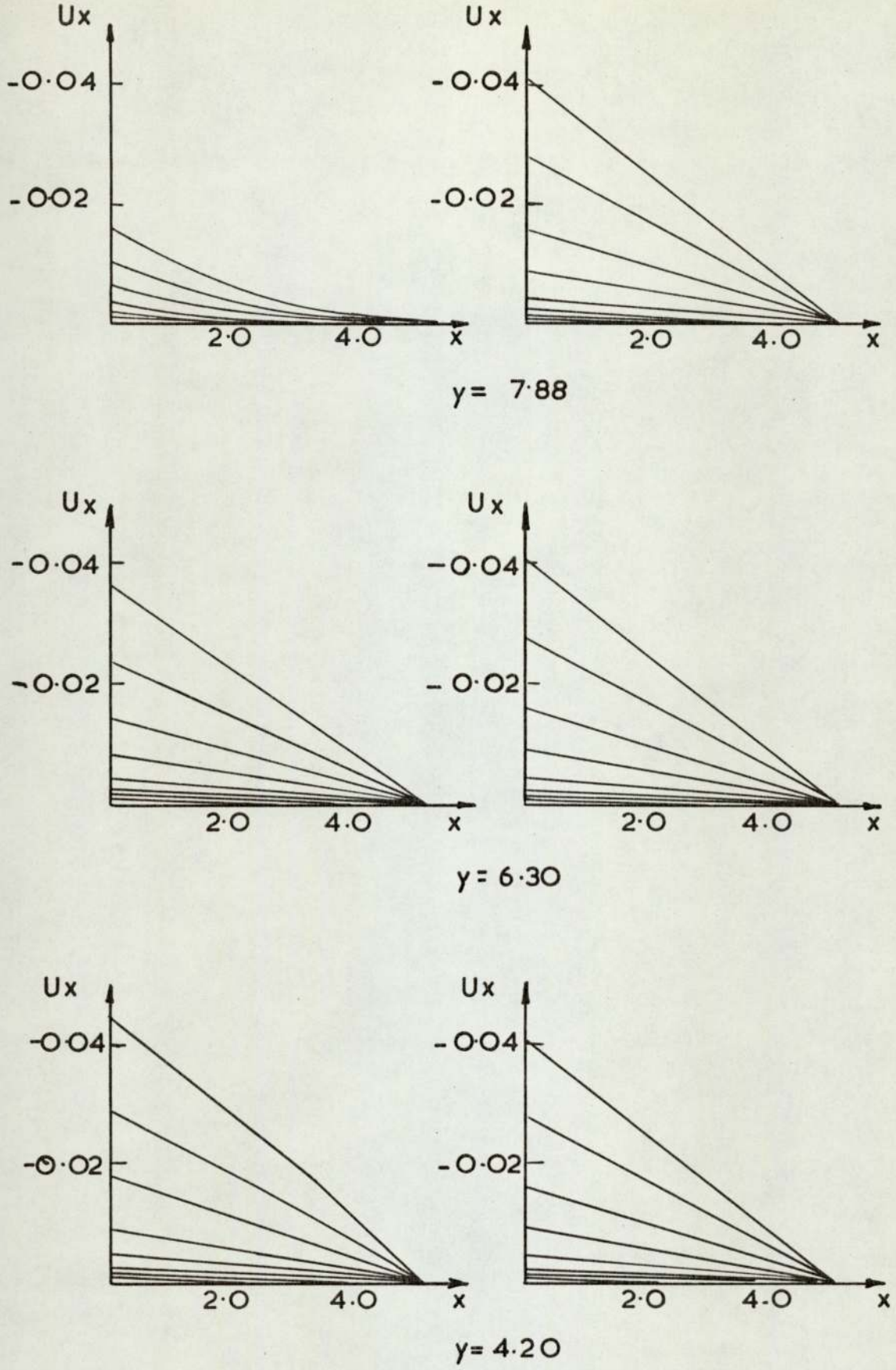

Figure 3. 13 Horizontal displacements

3.7) contd.

the sample in both cases.

3.8) Discussion of Results.

Bishop and Green[8] showed that under triaxial test conditions a sample with an L/D ratio of 2:1 (Length to diameter) with restrained ends gave the same strength (re.peak) as that of a free ends sample with L/D = 1:1 but at a lower strain level, and this effect can be seen in Figure (3.10) where the axial deformation from the fixed ends analysis is significantly less than that in the free ends case. The length to width ratio in this case is just over 3:2 and hence under plane strain conditions the samples could be expected to reach approximately the same peak. It can also be seen from Figure (3.10) that there is a reasonable agreement between the theoretical and experimental results. The theoretical free ends curve is in exact agreement with the experimental result up till a load of 0.24 kN but thereafter both theoretical results overestimate the axial deformations. This could be due to interpretation of the experimental results which were read off a graph and then recalculated backwards. Excellent agreement was found between all three peak values of load.

The non-uniform distribution of vertical stress due to the restrained ends is shown clearly in Figures (3.11). The stress concentrations under the corner of the platten which have been found are in agreement with the findings of other theoretical investigators. It can also be seen from these figures that the middle of the fixed end sample has a relatively homogeneous distribution of stress which supports the presumption of the experimental investigators that in the

3.8) contd.

taller samples the end effects are reduced.

It is extremely interesting to note that the stresses throughout the free ends sample were completely homogeneous. Quite severe overestimations had been found under the load in Chapter (2) but these had all been damped out by the beam and sandwich elements. It was noted in Chapter (2) that the overestimation occurred for a one element depth and this is amply supported here.

The dead end zones measured experimentally by Kirkpatrick and Belsahaw[52] are shown up in the contours in Figure (3.12) from which it can also be seen that the middle half of the restrained sample undergoes relatively uniform horizontal strain, but at generally smaller levels than those in the free ends case as can be seen from Figure (3.13). The exception to this is at the sample mid-height where the horizontal displacements of the restrained sample exceeds those of the free ends case. The mode of displacement at y = 7.88, Figure (3.13) corresponds well in shape to that measured under triaxial conditions by Kirkpatrick and Belshaw[52]

It can be seen from all the graphs of the free ends case that the sandwich elements successfully eliminated the effects of end restraint on the sample elements.

3.9) Conclusions.

Sandwich elements given relatively small stiffness can be used to represent smooth interfaces when inserted between the bulk of the elements and the loaded boundary. Best results are achieved when the sandwich elements are

3.9) contd.

given the same Poisson's ratio as the other elements but a reduced elastic modulus.

When the load is applied through a smooth rigid boundary, such as the loading platten in the free ends example, none of the severe over-estimations of stress, encountered in Chapter (2), occur.

The complicated boundary and loading conditions that occur in the plane strain compression test can be handled with ease by the Finite Element method. The simple isotropic analytical model assumed to govern the behaviour of the sand elements led to a good agreement with the experimental results.

The restraint imposed by fixed end loading plattens in the plane strain compression test leads to non-homogeneous distribution of stress and strain and reduces the vertical displacements. It is quite impossible to make a quantitative comparison with other investigators because they have all been interested in axi-symmetric conditions but as expected there are a great number of similarities in the results.

CHAPTER 4

CRACK PROPOGATION

4.1) Introduction.

An important cause of non-linearity is that due to material cracking. A mass of fissured material or material of relatively low tensile strength is incapable of sustaining a tensile stress which leads to the development of cracks, which in general reduces the stiffness of the mass. If subject to compressive stress, these same materials will transmit forces and exhibit approximately linear load-deformation behaviour. This type of effect is important in rock mechanics, and structural concrete because the occurrence of cracks considerably changes the distribution of stress from that assumed by linear elastic theory, and, of course reduces the load bearing capacity.

4.2) The Use of Finite Elements in Crack Propogation.

Blake[10] used triangular finite elements to analyse the problem of a circular underground opening and compared results with a classical solution of the Kirsch problem. Blake went on to analyse the same problem with a fault above the opening, similar in principle to a crack. The fault was simulated by a number of elements having only small stiffness,

Watson[91] used a similar approach to analyse material with no tensile strength. The problem was first analysed as an isotropicmaterial, and, then where elements developed tensile principal stress, they were assumed to be anisotropic with a very small elastic modulus normal to the tensile stress. The problem was then reanalysed and so the crack or weak zone developed.

Zienkiewicz, Valliapanand King[94] pointed out the

4.2) contd.

weakness in these methods and proposed a method called the 'stress-transfer' method. The problem is again analysed as an elastic one, but in this case the tensile stresses were eliminated by replacing them with temporary restraining forces, which are removed by equal but opposite nodal forces. The structure is then reanalysed and the process repeated. Further improvement in the solution was obtained by also reducing the modulus in the direction of the tensile stress.

Trikha and Edwards[85] used the stress-transfer method in conjunction with a non-linear material model to predict the crack pattern and mode of failure in concrete box girders. Analytical and experimental results were compared and found to be within normal engineering accuracy.

Other investigators including Watwood[92] applied the finite element method in conjunction with fracture mechanics. Watwood examined the state of stress around a sharp crack and calculated stress intensity factors. Recently, Al-Hashimi[2] used triangular elements in conjunction with fracture mechanics, and a method similar to that used by the Author to examine the behaviour of brittle stabilised soil.

Most of the previously discussed methods of predicting crack propogation have represented the crack as a zone of weakness. In a real mass of material however, the excess tensile stresses are relieved by a physical separation, the effects of which have been studied by those investigators using fracture mechanics. There has been little work done into incorporating the kind of physical separation, that occurs when a crack appears, into an automatic finite element analysis. Crack propogation can be studied[2] by allowing physical separations to occur in the element mesh.

4.2) contd.

The advantages of such a method are that cracks are allowed to start at any point and to change direction or branch off. It also caters for the possibility of cracks being arrested and others initiated. Over and above any other method, this approach means that crack widths can be calculated and the physical representation is clearly carried out in a more realistic manner.

The disadvantages of such a method are likely to be mainly on grounds of cost. The physical introduction of a crack will mean joint separation, which in turn means that the mesh will be redefined and, therefore some data changes will be necessary. Cracks will only be able to occur along element boundaries, so to some extent, the crack pattern will have been decided by the mesh design.

All the previous investigators used the simple triangular element which, as shown in Chapter (2), seriously underestimates the stress, so some improvement can be made by using higher order elements.

4.3) Theory.

Consider a point 'i' in the finite element mesh shown in Figure (4.1). For a crack to appear at this point, the principal stress must be tensile and exceed the tensile strength of the material. Cracks occur in a direction normal to the principal tensile stress, but it is clear from the figure that cracks can only occur along the element boundaries, which means that it is the stress normal to the element boundary which in this case will cause cracks. If it should happen that the principal tensile stress direction is not in reasonable agreement with the direction of the normal stresses then the

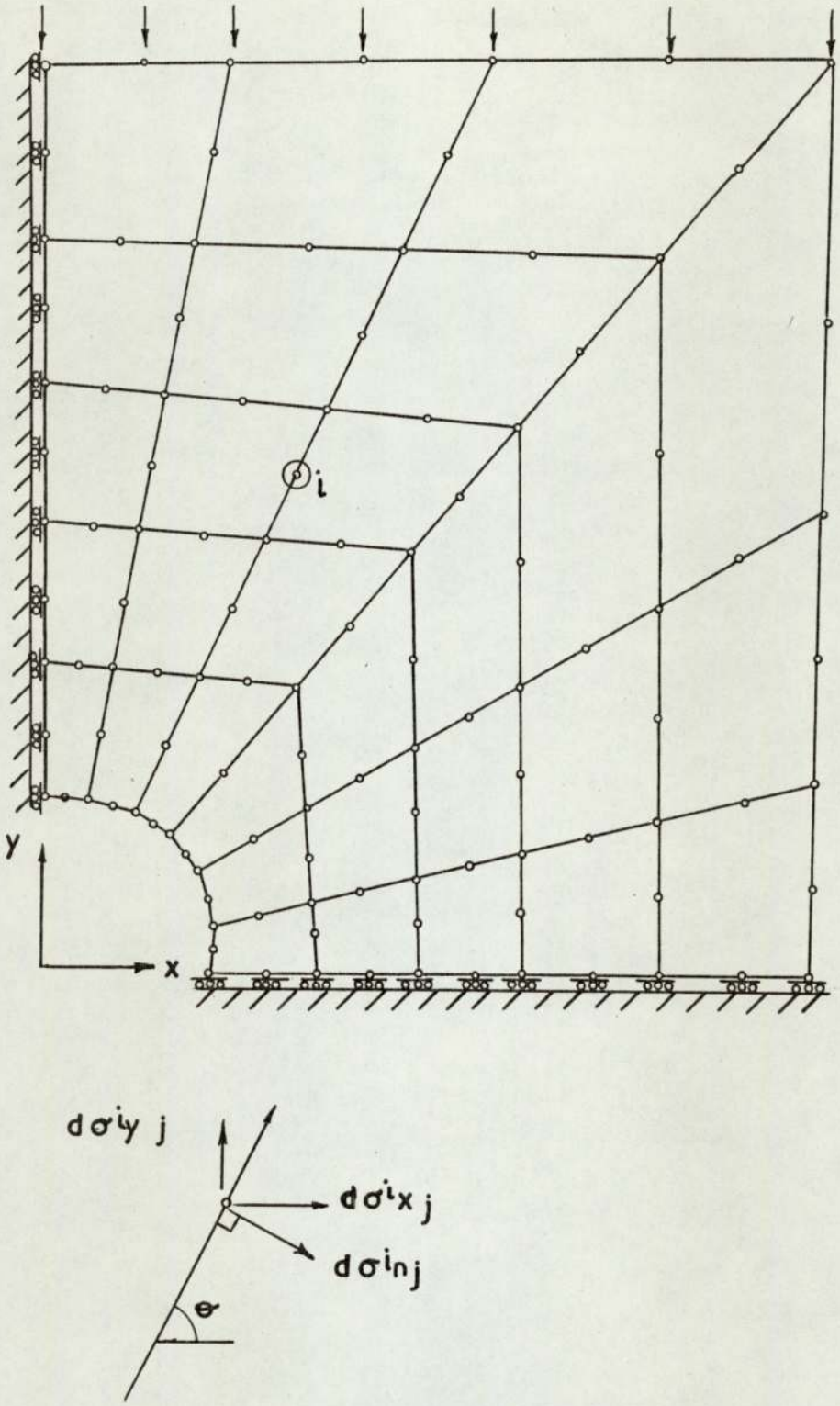

Figure 4.1 A finite element mesh

4.3) contd.

finite element mesh would have to be redesigned to avoid errors. Indeed, the best practice is to first analyse a very coarse mesh to get an idea of what the crack pattern and principal tensile stress direction would be, and then to design the refined mesh using these first results as a guide.

Assuming this exercise has been carried out, if an increment of load dL_j is then applied to the mesh this will produce increments of stress $d\sigma^i_{yj}$, $d\sigma^i_{xj}$ and $d\tau^i_{xyj}$ at point i. The increment of stress normal to the element boundary can be calculated from;

$$d\sigma^i_{nj} = \frac{1}{2}\left\{ d\sigma^i_{xj} + d\sigma^i_{yj} \right\} - \frac{1}{2}\left\{ d\sigma^i_{xj} - d\sigma^i_{yj} \right\} \mathrm{Cos}(2\theta^i) + d\tau^i_{xyj}\ \mathrm{Sin}(2\theta^i) \qquad (4.1)$$

$$\text{where,}\quad \theta^i = \tan^{-1}\left\{ \frac{y^i}{x^i} \right\} \qquad (4.2)$$

The increment of normal stress at point 'i' is plotted against the applied load increment that caused it in Figure (4.2a). To calculate the total load which would cause a crack to appear at point 'i' it was necessary to take into account the previous stress history, as shown in Figure (4.2b). λ_{j-1} is the total load that caused a crack, somewhere in the mesh, after the last increment of load. λ^i_j is the total load that would cause the normal stress at point i to reach the tensile strength of the material, and hence cause a crack to occur, during the application of the j^{th} load increment. Its value can be interpolated from;

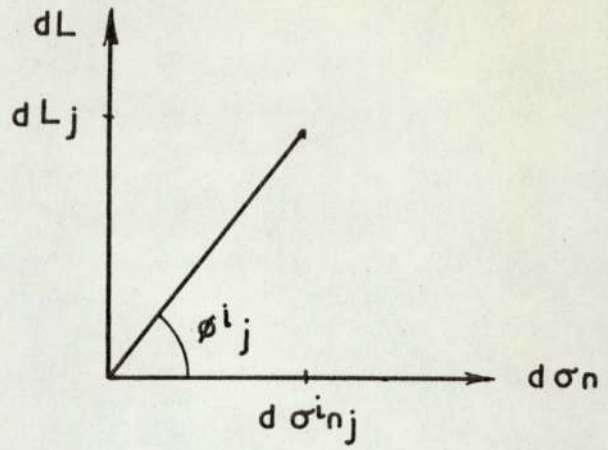

Figure 4.2 a

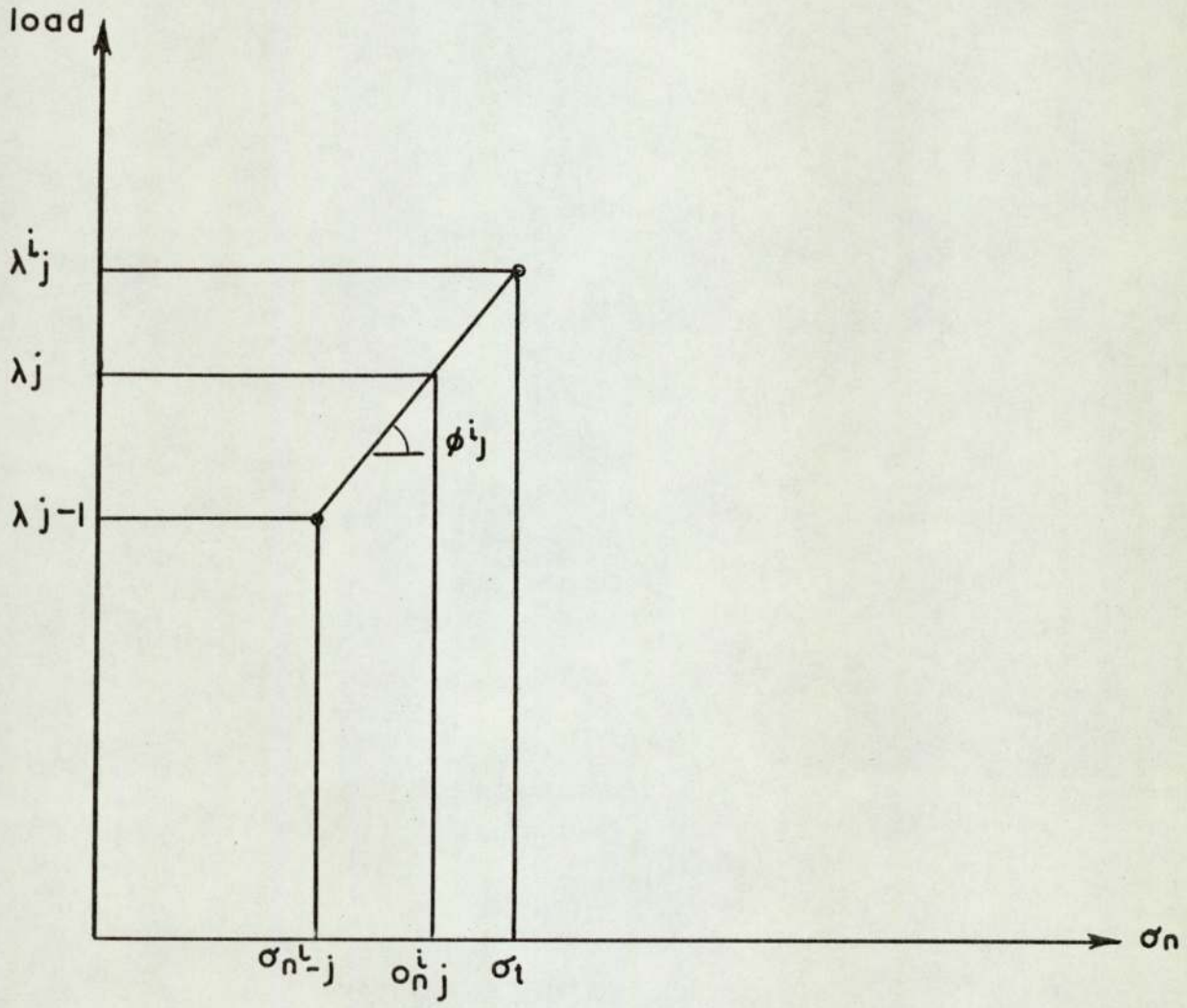

Figure 4.2.b

4.3) contd.

$$\lambda_j^i = \lambda_{j-1} + \tan \phi_j^i \left\{ \sigma_t - \sigma_{nj-1}^i \right\} \qquad (4.3)$$

where, $$\tan \phi_j^i = \frac{dL_j}{d\sigma_{nj}^i} , \qquad (4.4)$$

σ_{nj-1}^i is the accumulated normal stress up to the last increment, and σ_t is the tensile strength.

Equations (4.3) and (4.4) are applied to all joints in the mesh and hence a whole series of values of λ_j^i are obtained. It is the joint with the smallest positive value of λ_j^i at which the next crack should appear, because this joint requires the smallest increment of load to crack. This chosen least value then becomes λ_j. Hence, the total normal stress, due to the action of λ_j, can be calculated for each joint, using;

$$\sigma_{nj}^i = \sigma_{nj-1}^i + \left\{ \frac{\lambda_j - \lambda_{j-1}}{\tan \phi_j^i} \right\} \qquad (4.5)$$

A radial crack could then be introduced into the mesh, at the joint which had had the smallest value of λ_j^i, by allowing the element boundaries to separate.

This effect was achieved by having two joints at each point that a crack might be expected to occur one of which is a dummy joint with no degress of freedom and not defined in the element topology. Effectively this dummy joint takes no part in the analysis until a crack appears at its position. In the small part of a mesh shown in Figure (4.3a) the dummy joints are the numbers in a small box. The element numbers are encircled. It can be seen from this figure that cracks have not been allowed to develop everywhere, because in some cases

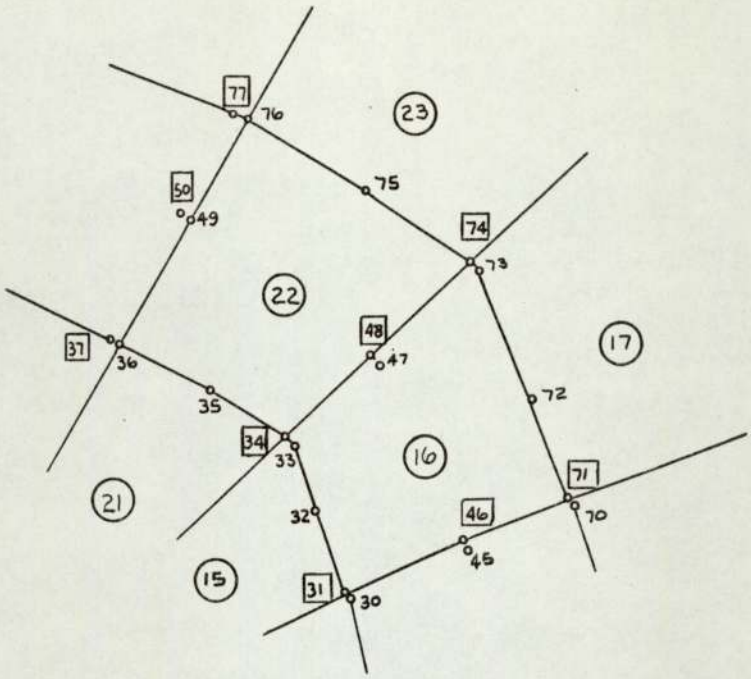

Figure 4.3.a

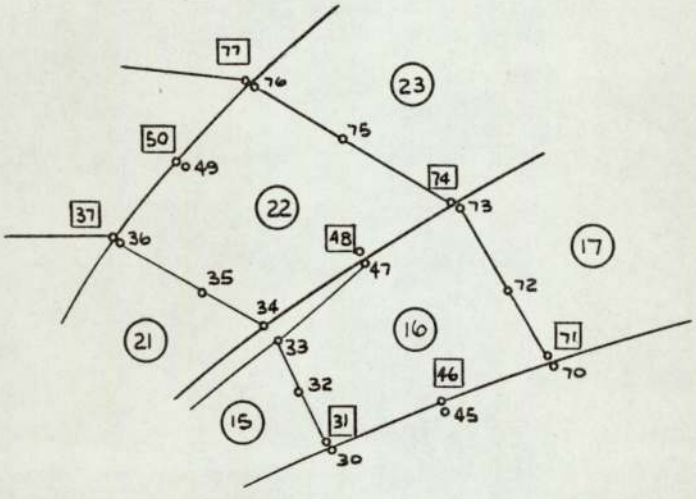

Figure 4.3.b

4.3) contd.

this would entail dividing an element. If active joint 33 was the point at which the crack was next due to appear, then the mesh would be modified to that shown in Figure (4.3b). Joint 34 is no longer a dummy and would be activated by giving it two degrees of freedom. The data describing elements 21 and 22 would also be amended to include the new active joint. That is to say that joint 33 would be replaced by joint 34 at the two corner nodes. The next increment of load would then be applied to the new mesh and the whole process repeated.

It can be seen from the meshes in Figures (4.3) that dummy joints were only provided at places that cracks could appear without dividing elements. If cracks consistently wanted to appear across element boundaries this would require redesigning the finite element mesh. The method could be extended allowing for tangential, as well as radial cracking, the meshes would have to be designed with one dummy joint at each element mid-side node position and three dummy joints at each corner node. Thus allowing for two way separation. It is only the equation (4.2) that requires any alteration for the method to apply to cracking in either direction.

4.4) Crack Propogation Program.

The isoparametric quadratic quadrilateral finite element was again used. The program for analysing the path of crack development used the sub-routines that described this element (see Appendix (3)) and one other subroutine. The sub-routine named CRACKPROP carried out the procedure described in the previous section.

It was noted in the previous section that cracks

4.4) contd.

cannot occur everywhere in the mesh, so, a variable IN_i was introduced for each joint. This variable could be specified as 1 or 0. A zero allowed a radial crack, and a 1 did not. Crack suppression was achieved by not allowing any joint with IN = 1 to be selected as the one having the minimum value of λ_j^i, that is the next crack position. It can be seen from equations (4.3) and (4.5) that the accumulated normal stress after the last increment must be known for each analysis. The accumulated stress, the array IN and the data describing the geometry and loading of the mesh, was stored on disc data files.

The general crack analysis system to trace the path of a crack is shown in flowchart (4.1) where two complete runs of the program are illustrated. It can be seen from this flowchart that three files constitute the input for the program. The file AFDAT2, assigned to card reader 1, contained λ_{j-1} (i.e. minimum(total load) after last run) and the accumulated normal stress for each joint after the last increment. AFDAT1, assigned to card reader 0, held the data describing the finite element mesh as it was after the last increment. AFDAT3 contained the array IN and was assigned to card reader 2.

In the j^{th} increment, the program calculates from these three input files the next joint to crack and writes the load that caused this crack, together with the new accumulated stress, to the next generation of the disc file AFDAT2. The program prints the result of the analysis and the crack calculations on the line printer for visual interpretation

The user then interprets these results and modifies the mesh to allow the crack to develop at the correct point by separation of the element boundaries. This changes the data

FLOWCHART (4.1)

SHEET 1

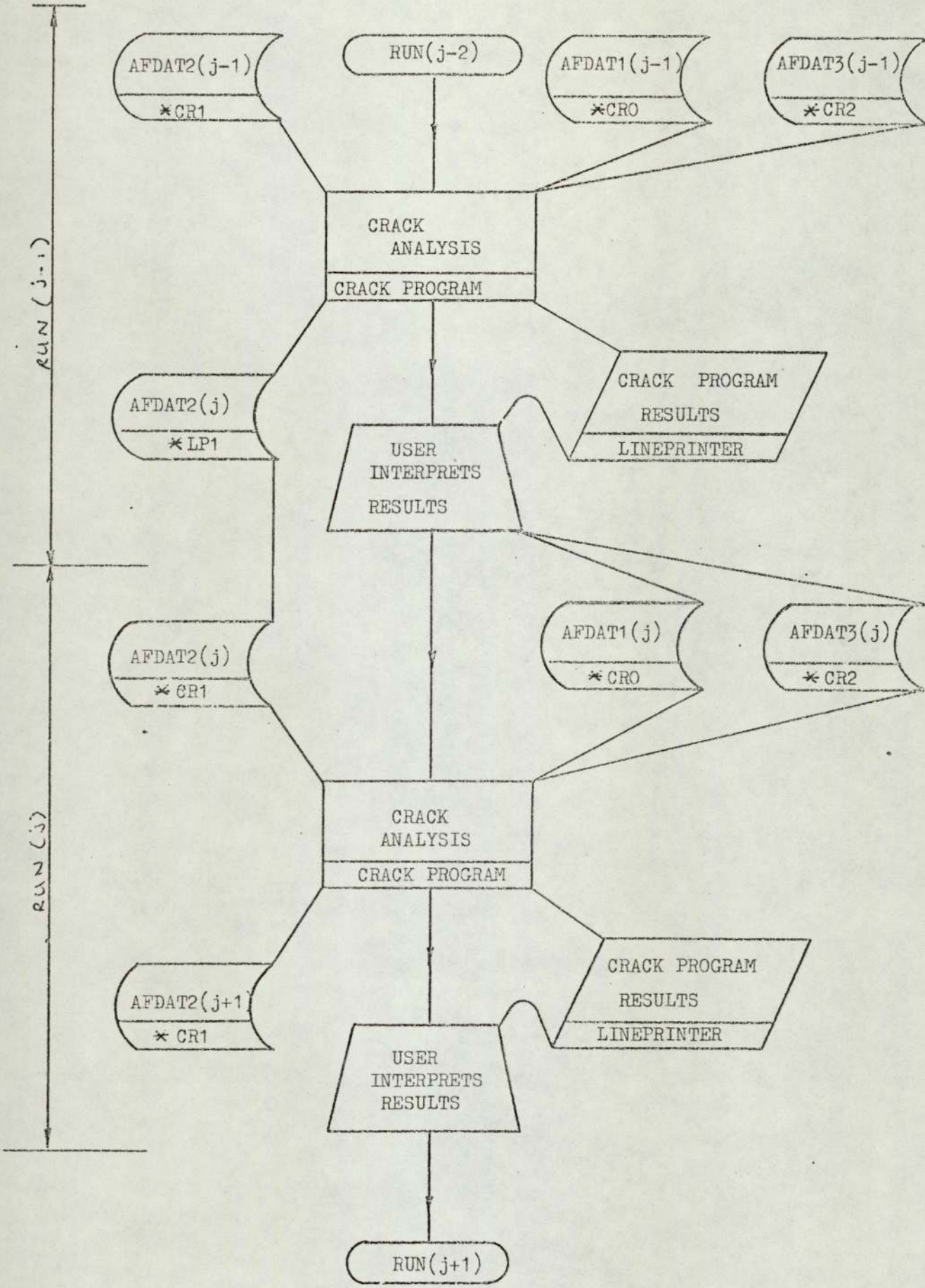

4.4) contd.

describing the topology of the mesh and hence a new version of AFDAT1 is created. The new finite element data is created by the user editting the old data file to activate the appropriate dummy joint. A new version of AFDAT3 was usually created so that the last joint to crack could not possibly crack again.

The stress components from the finite element analysis were used as the main input to the routine CRACKPROP, which carried out the cracking analysis calculations described in the previous section. The procedure followed by this routine is shown in flowchart (4.2). It is possible for cracks to occur at more than one joint. It is very important that no points at which cracks wanted to appear should be overlooked. If any points were overlooked, and subsequently cracks not inserted into the mesh, then the stress distribution after the next increment would not be correct, and if the overlooked point did not now want to crack, the whole pattern of crack development would have been distorted. To allow for this, a check was made after the accumulated normal stresses had been calculated to see if any of the stresses were within 0.1% of the tensile strength. This meant that if a crack wanted to appear in the middle of an element, it would not be overlooked either, and the mesh could be redesigned, if thought necessary.

When interpreting the results from an analysis it was necessary to check that no cracks had been closed. Displacement compatability is, of course, no longer held when element boundaries are separated by a crack. It was possible for joints, previously under tension and cracked, to become

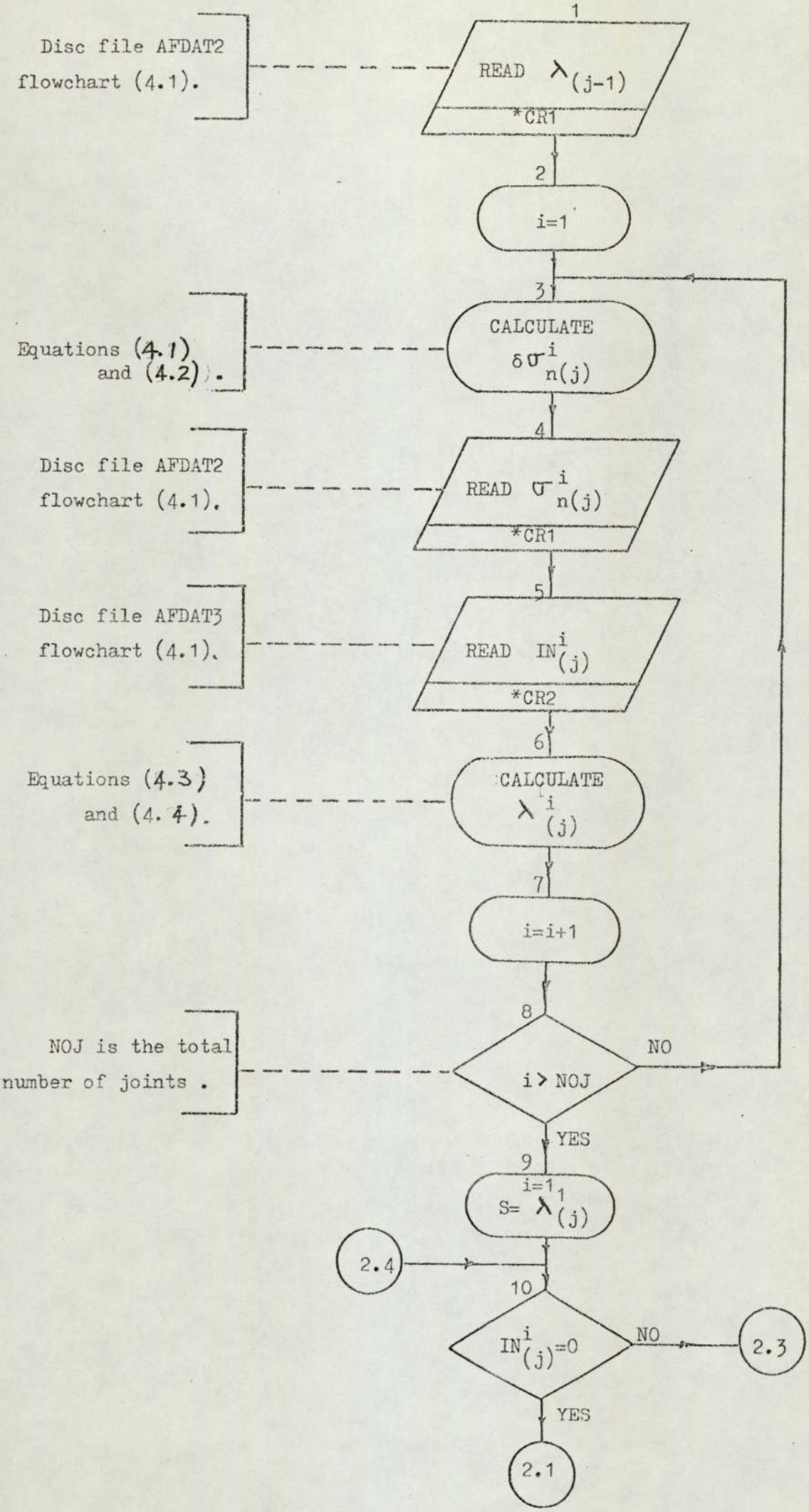
Disc file AFDAT2 flowchart (4.1).
1
READ $\lambda_{(j-1)}$
*CR1
2
i=1
3
Equations (4.1) and (4.2).
CALCULATE $\delta\sigma^{i}_{n(j)}$
Disc file AFDAT2 flowchart (4.1).
4
READ $\sigma^{i}_{n(j)}$
*CR1
Disc file AFDAT3 flowchart (4.1).
5
READ $IN^{i}_{(j)}$
*CR2
Equations (4.3) and (4.4).
6
CALCULATE $\lambda^{i}_{(j)}$
7
i=i+1
NOJ is the total number of joints .
8
i > NOJ
NO
YES
9
$S=\lambda^{i=1}_{1(j)}$
2.4
10
$IN^{i}_{(j)}=0$
NO
2.3
YES
2.1

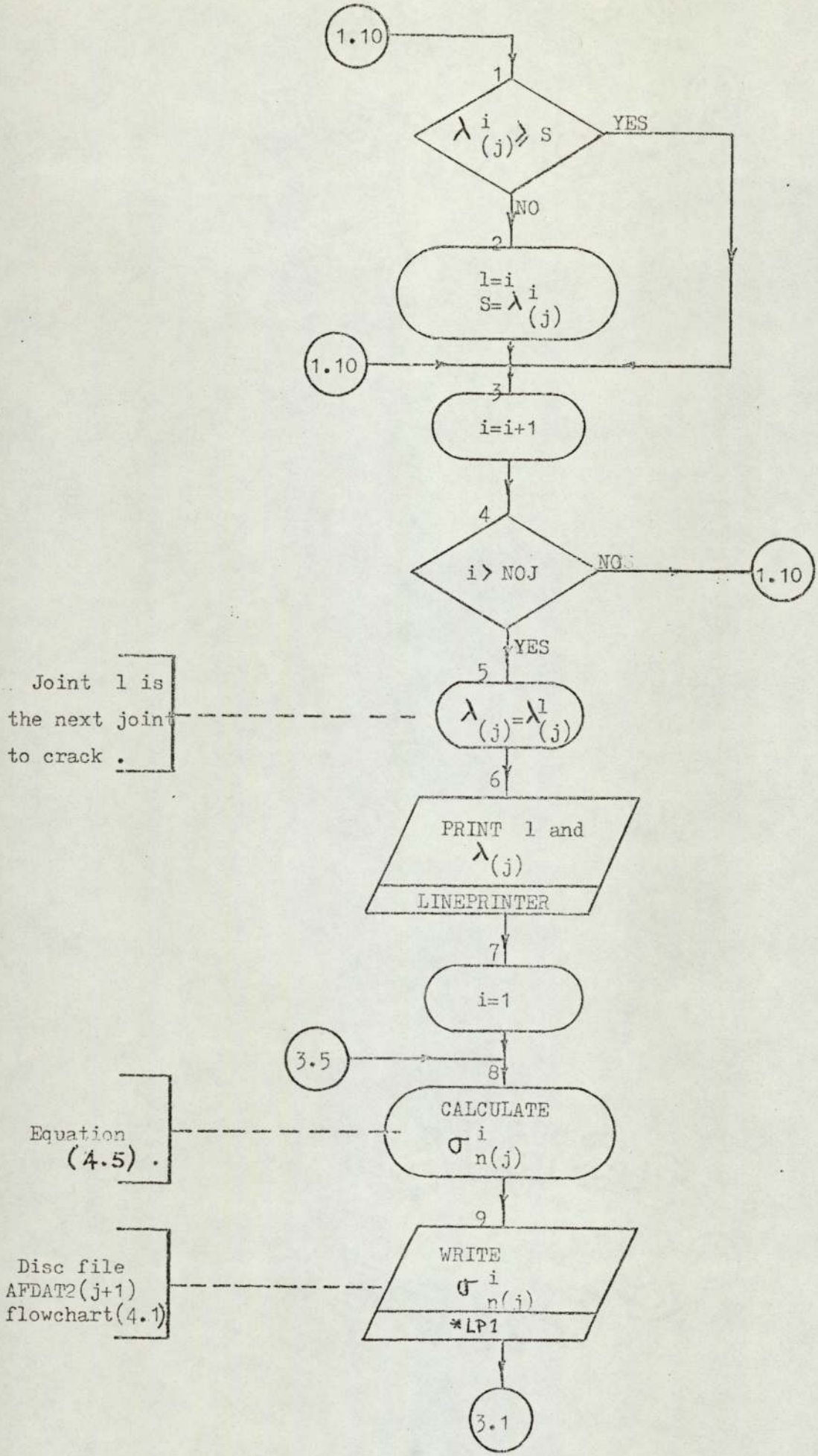
1.10
1
$\lambda^{i}_{(j)} \geq S$
YES
NO
2
l=i
$S=\lambda^{i}_{(j)}$
1.10
3
i=i+1
4
i > NOJ
NO
1.10
YES
5
$\lambda_{(j)}=\lambda^{l}_{(j)}$
Joint l is the next joint to crack .
6
PRINT l and $\lambda_{(j)}$
LINEPRINTER
7
i=1
3.5
8
CALCULATE $\sigma^{i}_{n(j)}$
Equation (4.5) .
9
WRITE $\sigma^{i}_{n(j)}$
*LP1
Disc file AFDAT2(j+1) flowchart(4.1)
3.1

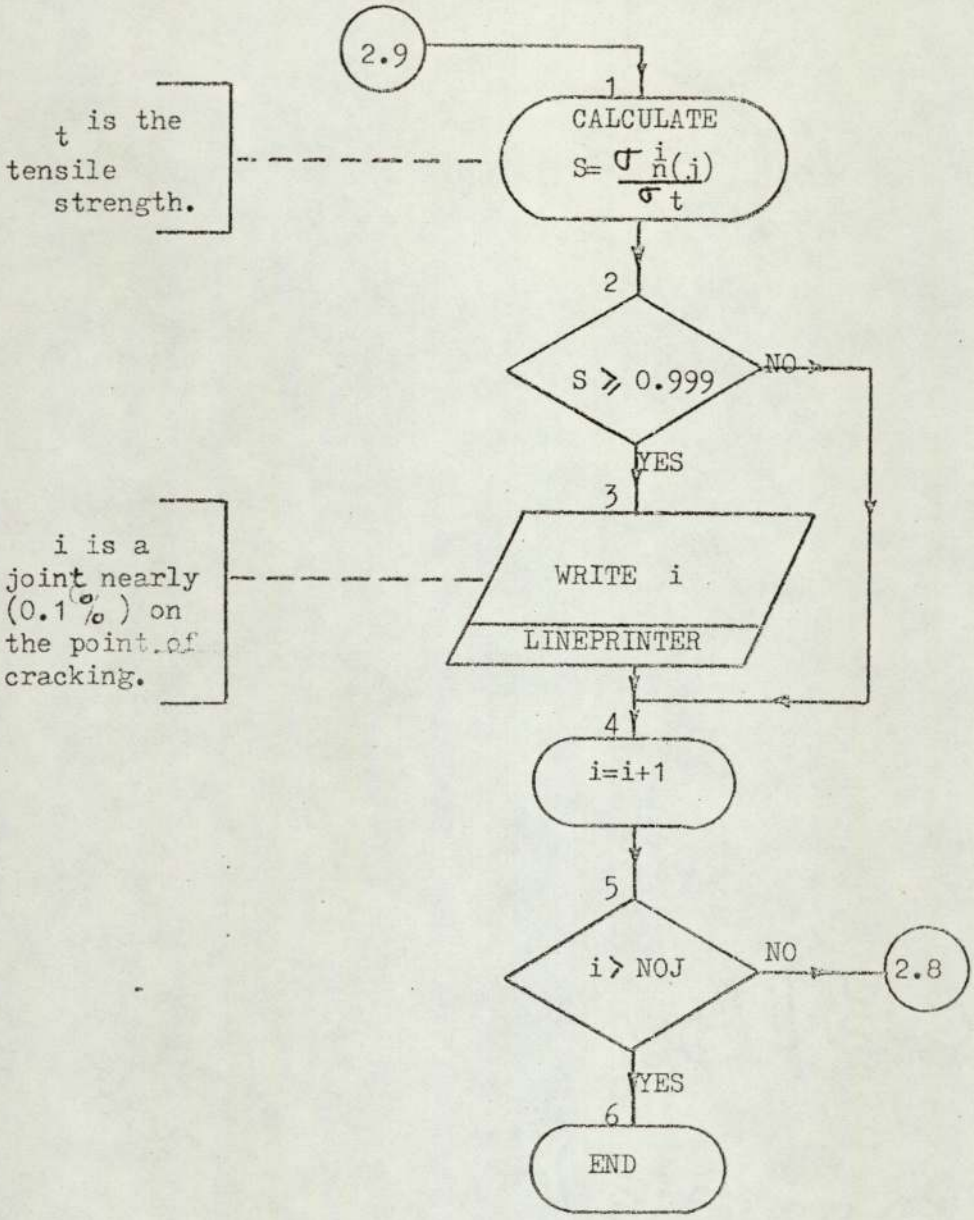
2.9
1
CALCULATE
S= σ i n(j) / σ t
σ t is the tensile strength.
2
S ⩾ 0.999
NO
YES
3
WRITE i
LINEPRINTER
i is a joint nearly (0.1 %) on the point of cracking.
4
i=i+1
5
i > NOJ
NO
2.8
YES
6
END

4.4) contd.

compressive as other cracks develop. If this were not noticed a negative crack width could occur, when an element moved over its neighbour. To facilitate data preparation and checking, on what should be a well used program, another small program was written to check, and if necessary amend the data input.

4.5) Analysis Problem.

It was decided to test the proposed method against an experimental result in order that the accuracy could be gauged. An experimental study of the behaviour of stabilised soil had been carried out by Al-Hashimi[2] and seemed ideal for the analysis. The soil-cement mix consisted of blue ball clay, packington sand and blended cement. The test specimens were rectangular prisms with a preformed cylindrical opening across the centre, and were prepared in an initial homogeneous, unstressed and uncracked state and then subjected to a uniaxial compressive uniformly distributed load up to failure.

The specimen details follow. The 300 × 100 × 100 mm prisms contained a 25 mmϕ flaw across the centre and they were made from a mix of sand:clay, 90:10 with 10% cement. The elastic parameters were measured at ν = 0.065 and E = 33.4 × 10^4 kN/m^2. The tensile strength was taken as 46 kN/m^2 and a total failure load of 5600 kN had been measured experimentally for the particular test sample.

4.6) Finite Element Analysis.

Three analyses were carried out, for ease of identification they were referred to as runs A, B and C. In all these analyses, radial cracks only were allowed to occur. By use of the IN array, described previously, cracks were not allowed to occur

4.6) contd.

which would cause element division. In runs B and C the IN array was also used to ensure that specific modes of crack formation were followed, by only allowing cracks to develop along specific radial lines.

The finite element mesh used for these three analyses is illustrated in Figure (4.4). The mesh consisted of 30 quadratic quadrilateral elements giving 147 joints of which 34 were dummies. The uniformly distributed load was applied as fictitious nodal forces in the manner described in Figure (2.5). It can be seen that the mesh was designed not to inhibit the formation of radial cracks. Because of symmetry only a quarter of the test specimen was analysed. A constant load of increment of 500 kN was used, and this figure is purely arbitrary as can be seen from Figure (4.2a).

4.7) Results.

4.7.1) Run A.

The sequence and positions of the crack formations resulting from this analysis are shown in Figure (4.5). It can be seen from this figure that cracks appeared in a zone at the top of the circular flaw and that cracks arrested and restarted several times. Figure (4.6) compares the load versus vertical deflection curves resulting from Run A and experiment. Figures (4.7) and (4.8) show the crack widths against increasing load for the vertical crack (at joint 147) and the crack along the first inclined radial line (i.e. the difference between joints 144 and 145). Run A was halted after the 12^{th} increment of load because application of the next increment caused about 10 joints to want to crack, it can also be seen that from Figures (4.7) and (4.8) that the specimen had become unstable.

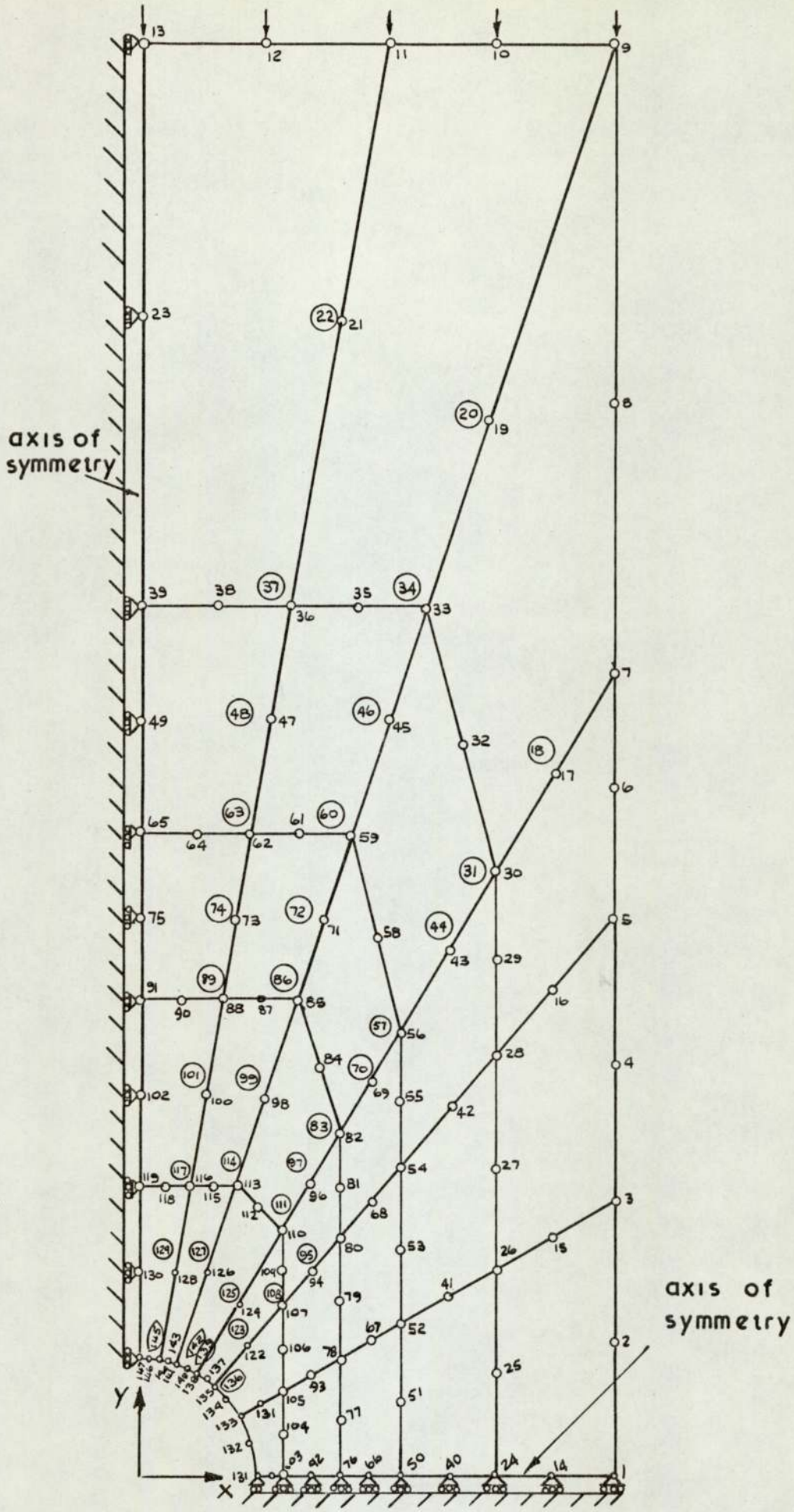

Figure 4.4 Finite element mesh

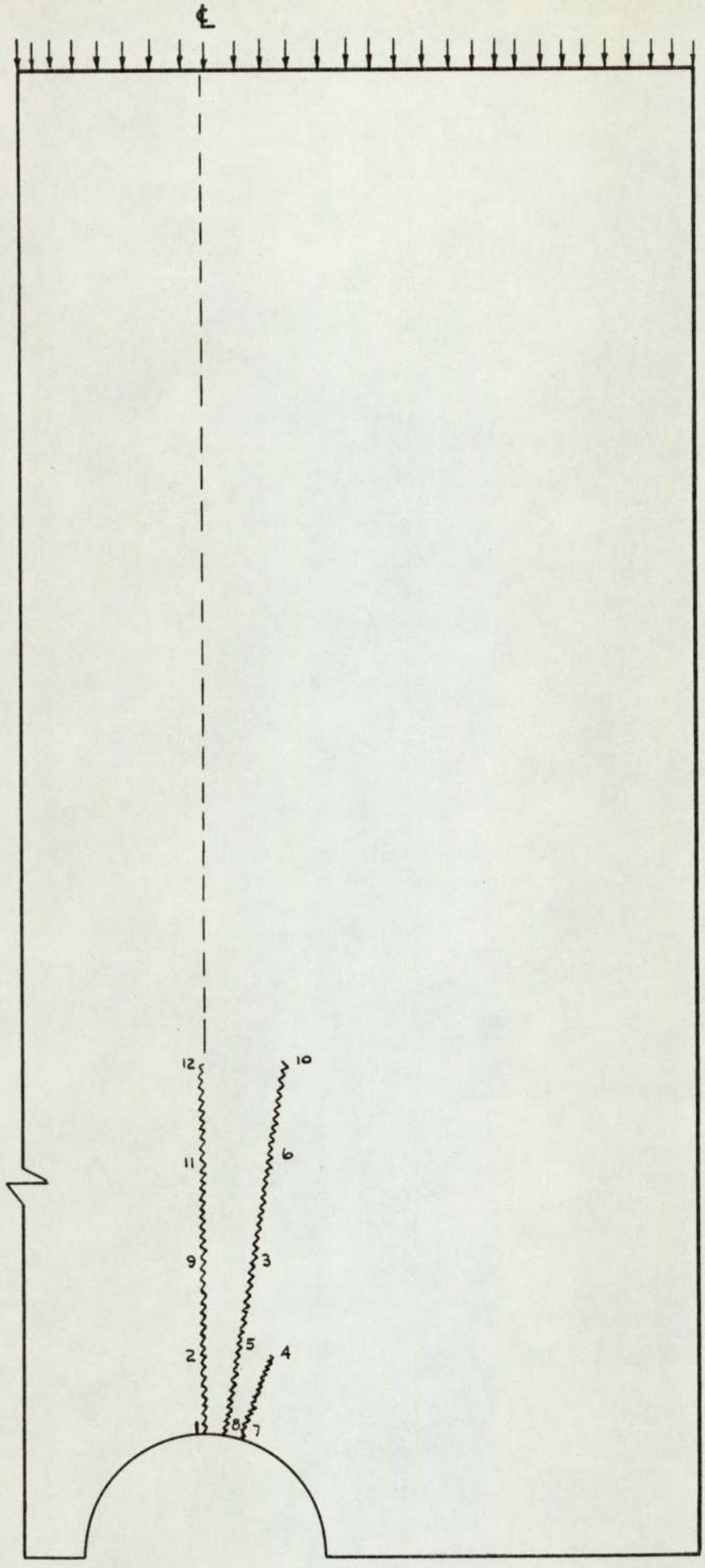

Figure 4.5 Sequence of crack formation, run A

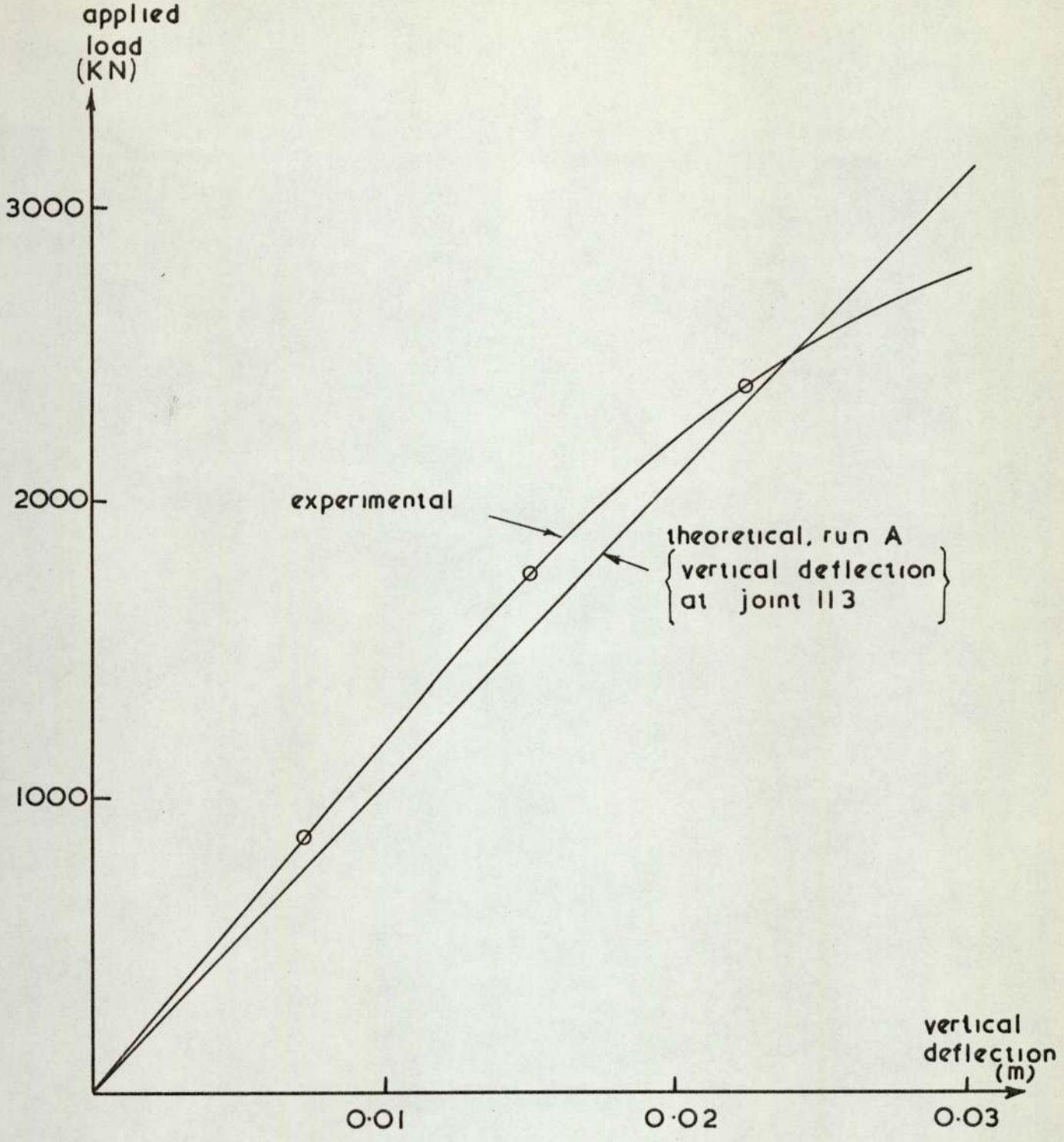

Figure 4.6. Comparison of theoretical and experimental load / deflection curves

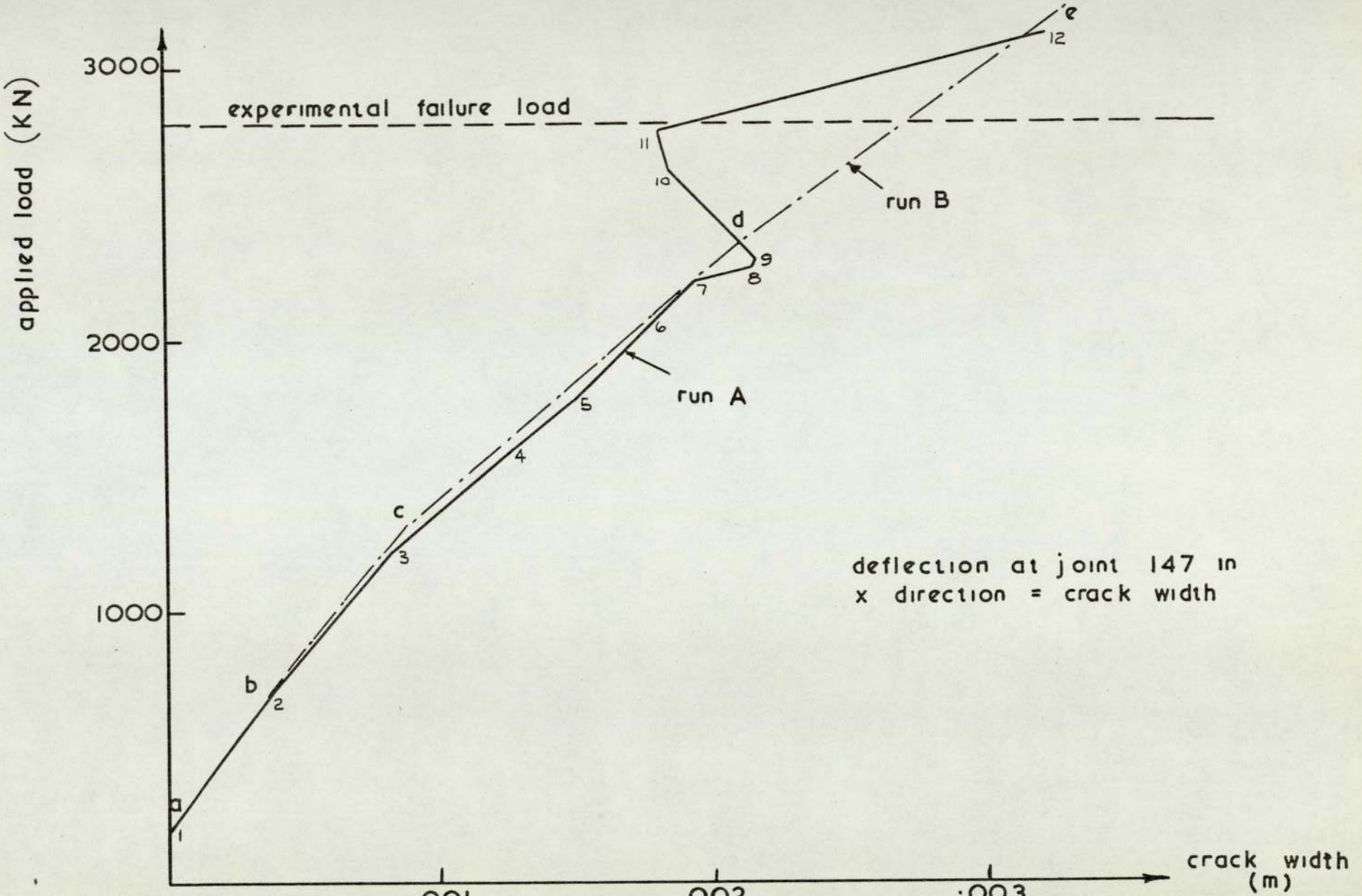
applied load (KN)
3000
2000
1000
experimental failure load
run A
run B
deflection at joint 147 in
x direction = crack width
·001
·002
·003
crack width
(m)
a
b
c
d
e
1
2
3
4
5
6
7
8
9
10
11
12

Figure 4.7

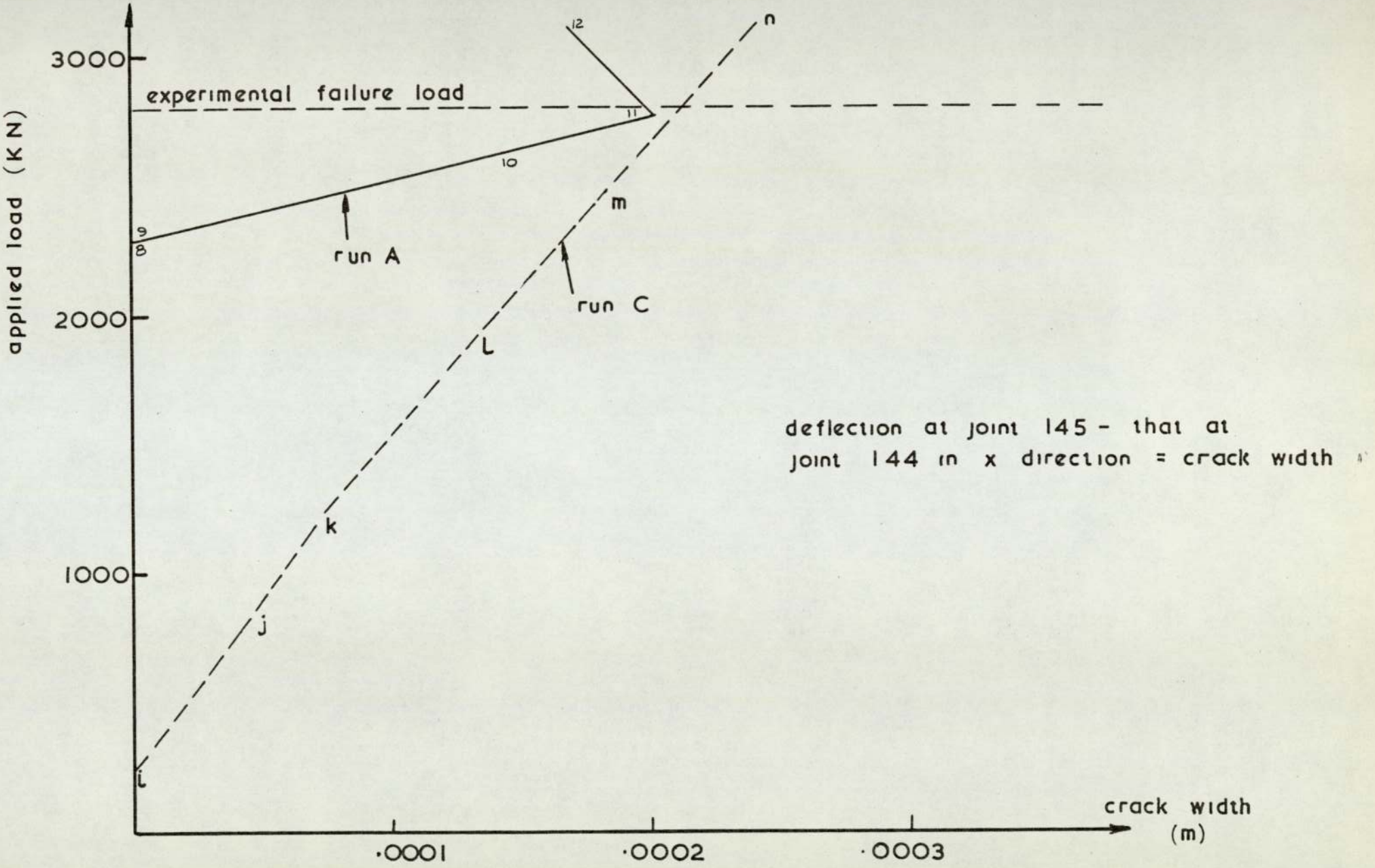
applied load (KN)
3000
2000
1000
experimental failure load
12
11
10
9
8
run A
run C
n
m
L
k
j
i
deflection at joint 145 - that at joint 144 in x direction = crack width
crack width (m)
·0001
·0002
·0003

Figure 4.8.

4.7.2) Run B.

In this run, cracks were only allowed to occur along the vertical axis of symmetry of the specimen (i.e. starting from joint 147). The sequence of crack formation is illustrated in Figure (4.9). The crack width obtained in this manner is compared with that obtained from Run A in Figure (4.7). The run was halted when the experimental failure load had been exceeded by about 20% without apparently reaching failure.

4.7.3) Run C.

For this run, cracks were only allowed to occur along the inclined radial line next to the axis of symmetry, (i.e. starting at 144, 145). The sequence of crack formation is shown in Figure (4.9). The crack width obtained in this run is compared with that obtained in Run A in Figure (4.8). Like Run B this run was halted without apparently reaching failure.

4.8) Discussion of Results.

The results obtained in Run A agreed well with the experimental results. The load-deflection curves were in good agreement although the experimental plot was more non-linear. This is probably the result of using a linear analysis, and an average value for the elastic constants, when the real response is only very approximately linear. The instability of the specimen around failure is well illustrated in Figure (4.7). The failure load is close to the experimental value. The reversal of displacement can be taken as a sign of failure, Majid[5] and the mode of failure agreed with the experimental observations of Al-Hashimi[4] that the cracks appeared in a general zone rather than in a specific plane. It is worth noting that failure

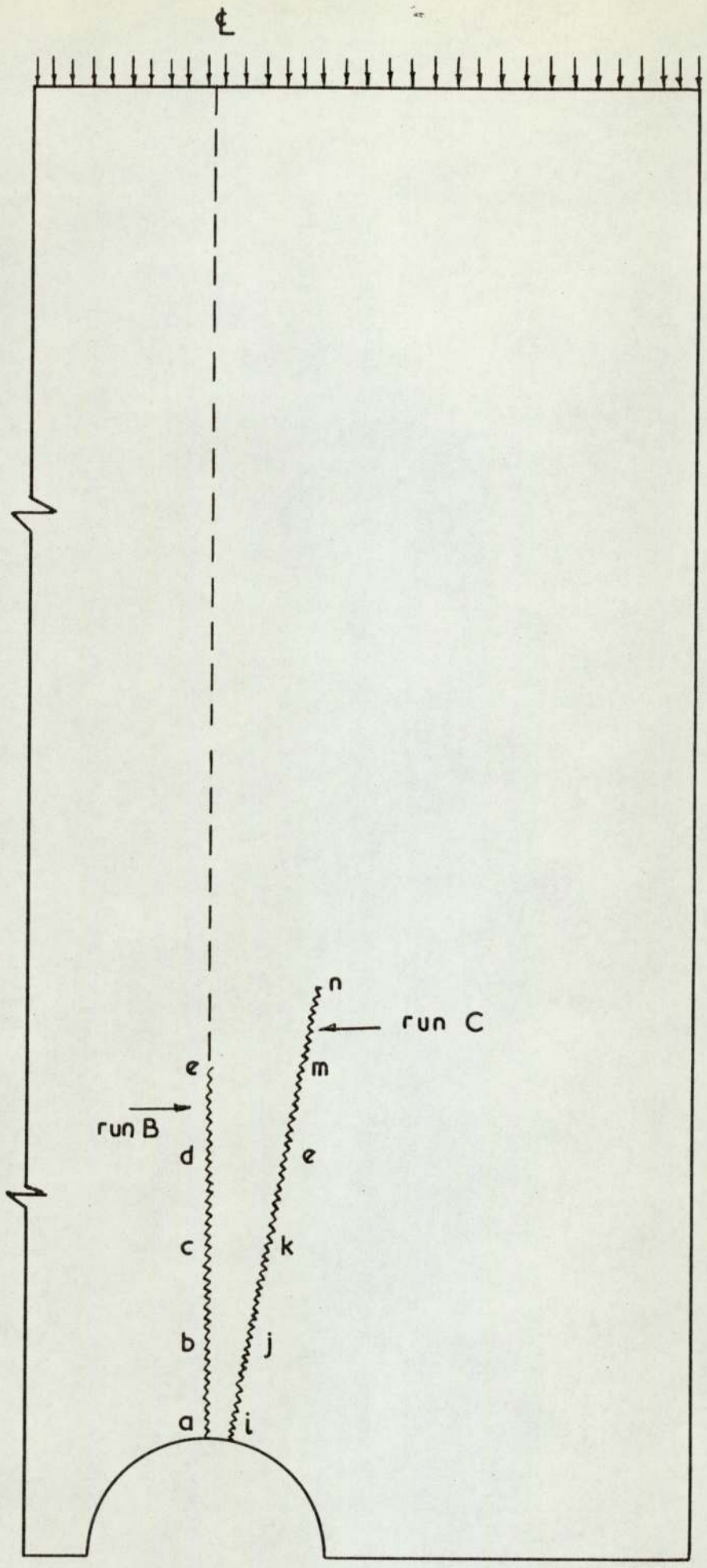

Figure 4.9 Sequence of crack formation, runs B & C

4.8) contd.

is not apparent in Figure (4.6) in either the experimental or theoretical curves. The brittle behaviour of the material allowed it to have a large stiffness right up to the point of failure. In the experiment, failure was then sudden and catastrophic which could not be predicted theoretically but was indicated by the number of joints that wanted to crack on the application of the 13^{th} load increment in Run A.

Runs B and C were carried out to see if the occurrence of either of the two major cracks, that occurred in Run A, could cause failure alone. This was not the case and indeed it can be seen from Figures (4.5) and (4.7) that instability did not start until increments 7 and 8 when the two inclined radial cracks were opened into the circular flaw.

4.9) Conclusions.

The method and program give good results for the analysis of this particular case. It cannot be concluded from this that the method is wholly justified but it is clearly worth more attention and further examples. Some improvements can be made, the most obvious of which is to include tangential cracking. Further improvement might follow from making the elastic parameters stress level dependent.

The program was not very expensive, each run costing about £1.00, but quite lengthy since user intervention was required between each run to change the data. This kind of operation could be best carried out on an 'on line' terminal rather than using batch processing. It would speed up the process if the data modification could be automated, but this would seem to be a very complicated project.

CHAPTER 5

MODEL TEST DESCRIPTION.

5.1) Introduction.

In this Chapter a series of model tests are described. These model tests were designed so that the stress conditions in the underlying foundation material were three dimensional, but also represented a realistic situation. The purpose of the tests was to provide a controlled set of experimental load-deformation curves with which theoretical analyses by the finite element method could be compared. These tests were necessitated by the fact that the Author could find no suitable experimental results reported, contrary to the situations which arose in Chapters (3) and (4).

The type of model test carried out was that of a small prototype structure. For the results to be useful it was important that the model should conform with the assumptions inherent in the proposed method of analysis. From the tests and their comparison with theory, it should be possible to assess the accuracy of the method of analysis and also to confirm the relevance of the stress/strain theory, established from some testing apparatus, in predicting the performance of the model.

Numerous investigators have carried out model tests under two dimensional conditions of plane strain or axial symmetry. In almost all these tests the aim has been to obtain a better understanding of the behaviour of the foundation material. The aim of the tests described in this chapter and the analysis in Chapter (7), apart from those already stated, was to investigate the iteraction, that not only occurs in the foundation material, but also between the various structural members as differential settlement and sway occur.

The philosophy has been that while the behaviour

5.1) contd.

of soil is an interesting and challenging subject, when concerned with foundations, it is important only in so far as the behaviour of the soil affects the structure founded upon it. Following this philosophy only the displacements at various points in the structure under test were measured. No attempt was made to measure contact stress or the stress components in the test bed.

The model tests were designed so that body force effects could not be ignored. The prototype structures were made of steel and about $^1/_5$ real size. A granular material was adopted for the foundation material because of its ease to place and lack of problems arising from pore pressure or time effects.

5.2) Test Series.

The model tests were all carried out on framed steel structures founded onto a bed of sand. The prototype structures were made up of steel beams and columns, the columns all rested on steel square pad footings. The three framed structures used in the test are illustrated in photographs (5.1a), (5.1b) and (5.1c), and detailed in Figure (5.1). Sand paper was glued to the underside of the pad footing to try and prevent lateral movement of the sand immediately under the footing. This problem was discussed in Chapter (3).

Four tests were carried out on each frame. For each frame the applied load acted at four different positions of eccentricity. The four loading points are shown in Figure (5.1). It was practically impossible to apply a load directly over the column,so in this case the load was applied as close to the column as was possible.

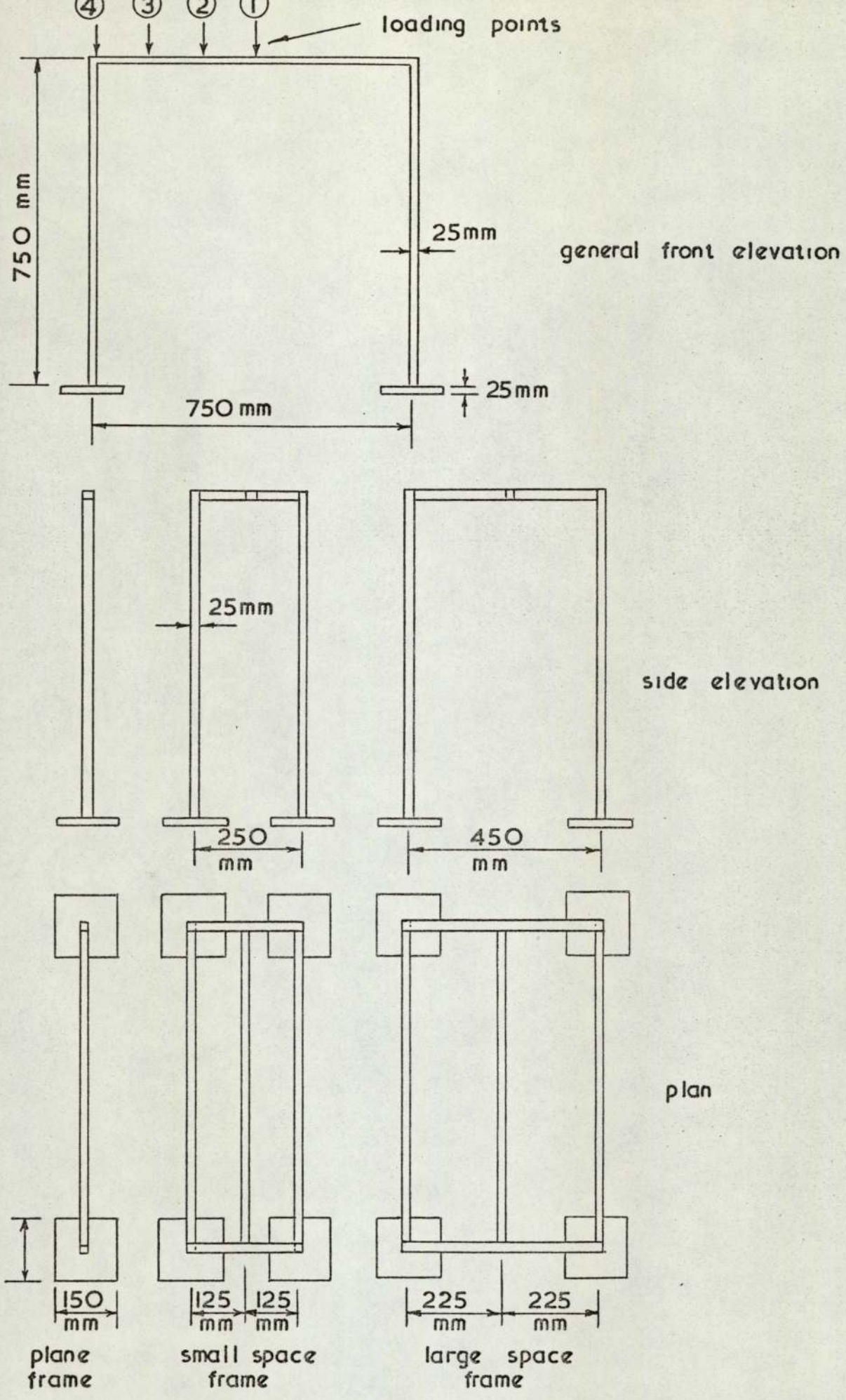

Figure 5.1. Model structure details

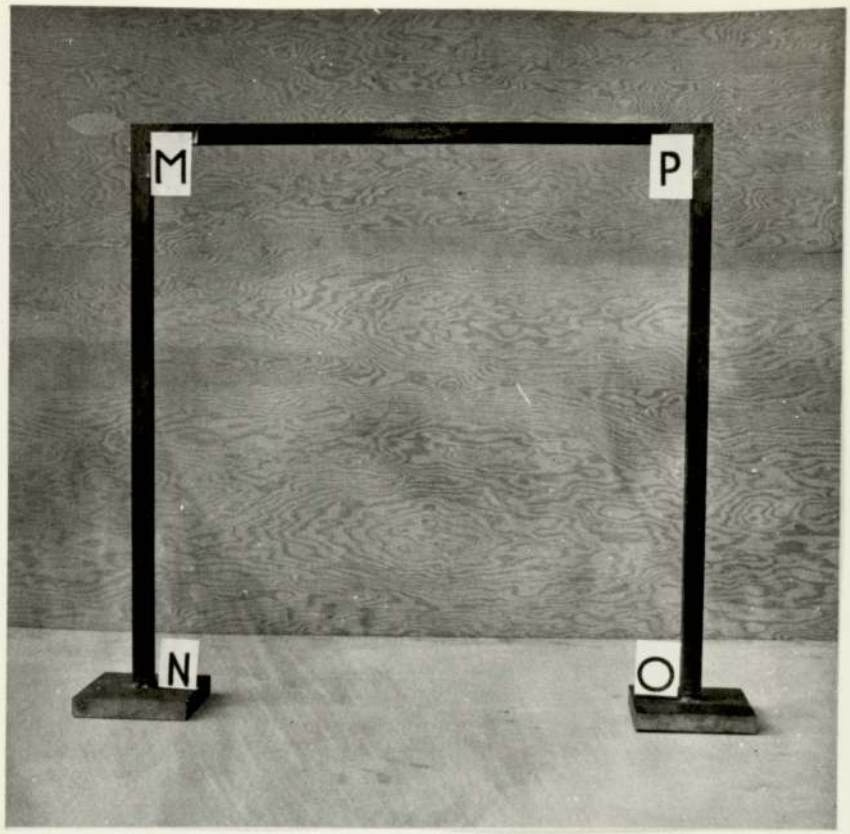

PLATE (5.1a) THE MODEL PLANE FRAME

PLATE(5.1b) THE SMALLER MODEL SPACE FRAME

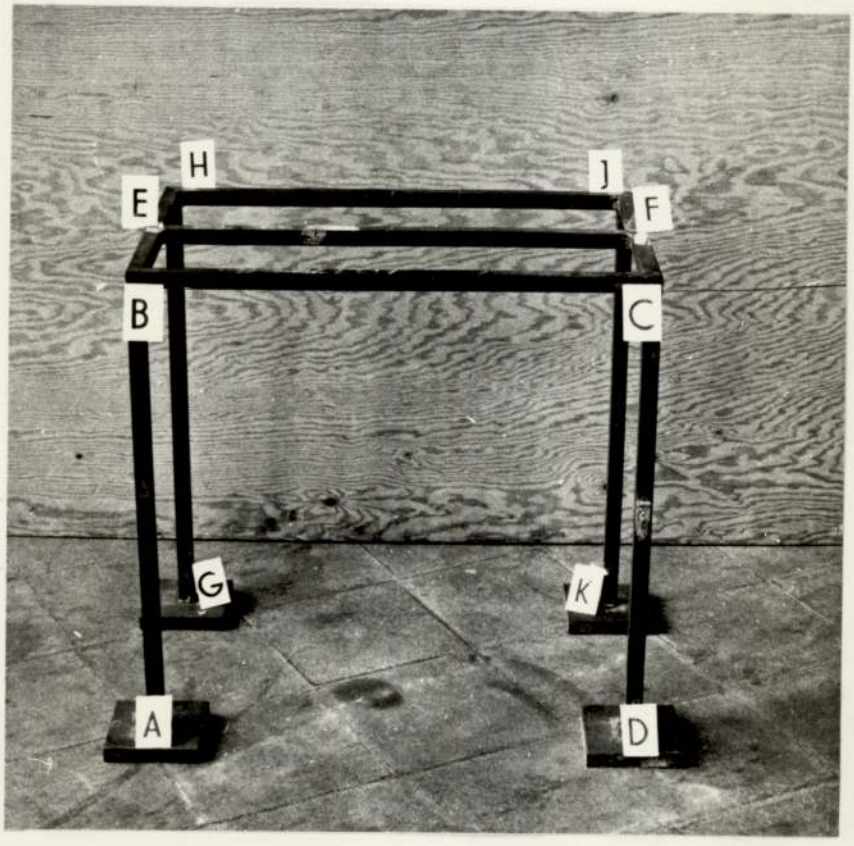

PLATE (5.1c) THE LARGER MODEL SPACE FRAME

5.3) Materials Used in the Model.

5.3.1) The Sand.

It was estimated that at minimum porosity the proposed test bed would require about five tons of sand to fill it. In order to enable comparisons to be carried out it was decided to use a Leighton Buzzard sand which has been popular with many other investigators. The sand, classified as grade 21, arrived washed, graded and dried in 100 fifty kilogram bags. These bags proved a convenient size for handling and storing the sand.

A standard sieve analysis was carried out on the sand and the particle size distribution obtained is shown in Figure (5.2). The analysis gave $D_{10} = 0.34$, $D_{60} = 0.48$ and the uniformity coefficient $\mu = 1.40$. It can be seen from these results that the sand was medium size and fairly uniform, largely falling between the 25 and 36 sieve sizes.

The specific gravity of the sand grains was measured in accordance with the procedure laid down in BS 1377. The value obtained was $G_s = 2.66$. This value was rather higher than expected but the test was repeated six times and consistent values were obtained. There was a fine black mineral mixed in with the quartz and it was presumed that this had led to a slightly higher specific gravity than that recorded by other investigators.

The maximum porosity of the sand was measured experimentally using the so called tilting method of Kolbuszewski[100]. This gave a consistent value of n_{max} of 43.9%. The minimum porosity of the sand was determined experimentally using a vibrating table. The mechanical vibrating table (usually used for concrete cubes) had a fixed amplitude

PARTICLE SIZE DISTRIBUTION

British Standard Sieve Sizes

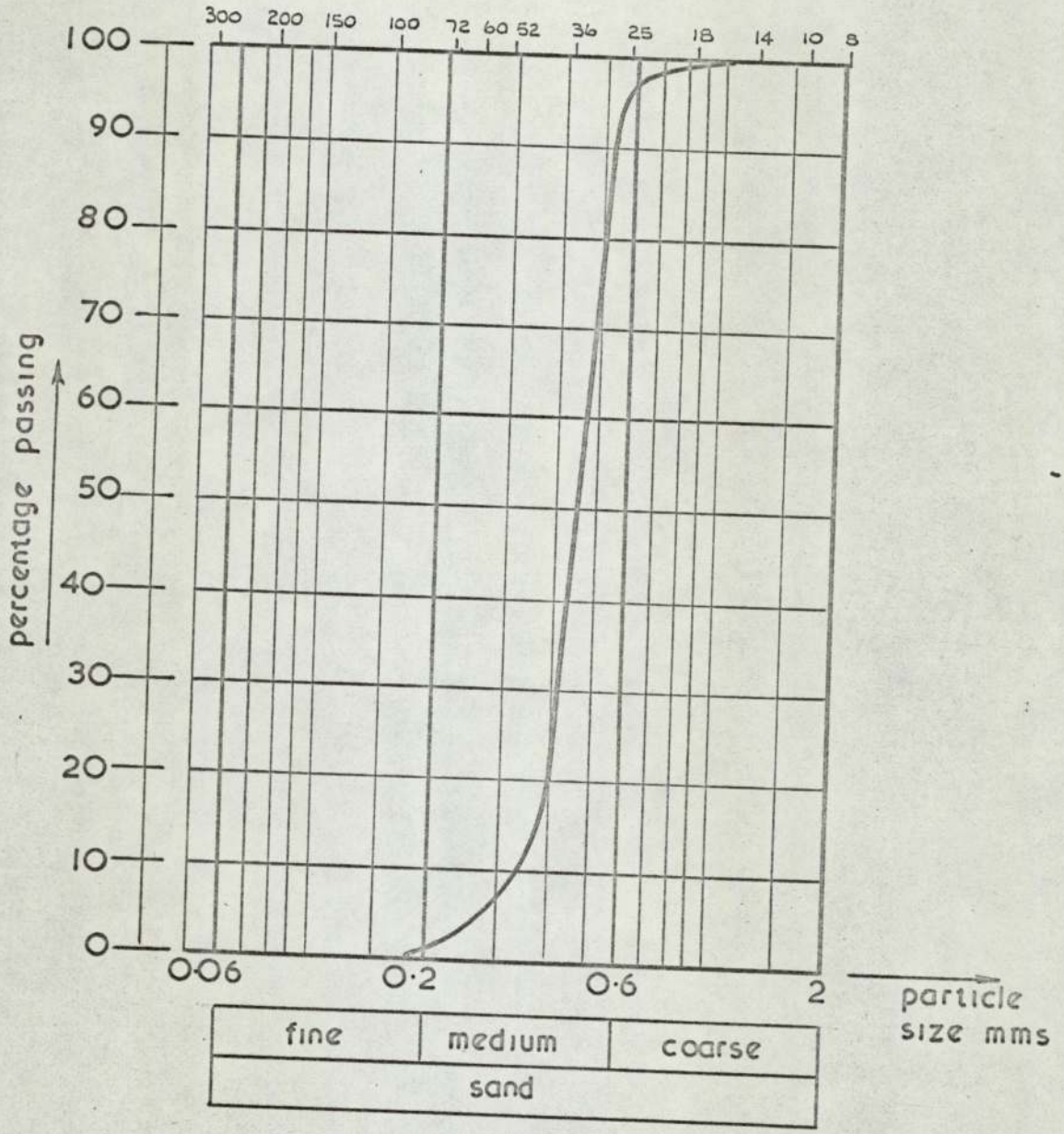

Figure 5.2

5.3.1) contd.

and variable frequency. The table was not calibrated in any way so it was not possible to record the frequency giving minimum porosity. The result obtained was n_{min} = 33.7%.

All these results were similar to those obtained by other investigators[53] using a similar size Leighton Buzzard Sand. The mechanical properties of the sand are discussed later in Chapter (6).

5.3.2) The Steel.

The same square black mild steel bar was used to make all the columns and beams for the three model structures. Its properties were measured in accordance with BS 18. An average value of Young's Modulus of 2.11×10^6 kg/cm^2 was obtained.

The pad footings were all made from the same strip of 6" × 1" section mild steel plate. Specimens were again prepared and tested in accordance with BS 18. An average value of Young's Modulus of 1.74×10^6 was obtained. The lateral strain was measured during the tensile test to enable the calculation of Poisson's Ratio, and an average value of 0.28 was thus obtained.

5.4) Sand Deposition Apparatus.

When carrying out laboratory scale experiments involving granular materials it is essential to have a method for preparing the test beds of sand at known uniform porosities at will, over and over again. This has involved the use of one of two major methods.

The first method is where the sand is deposited

5.4) contd.

and then its porosity adjusted using some mechanical method such as tamping or vibration. This method has not remained popular because the beds are left with locked in stresses due to compaction and it has been shown by Feda[32] that it is very difficult to control the variation of porosity throughout a sand mass.

The second, and currently most popular method, is where the porosity is controlled during deposition by varying the intensity and velocity of a rain of falling particles. This method has followed from the pioneer work of Kolbuszewski[100] who achieved variation of porosity by varying independently the height of fall of the grains and the rate of deposition.

Kolbuszewski and Jones[54] used these principles to design an apparatus capable of preparing homogeneous samples over a wide range of porosities. The intensity of the rain of sand grains was controlled by means of a 'variable aperture hopper'. The hopper was a rectangular box and had in its base a plate perforated with a regular pattern of holes. There were two other plates with the same pattern of holes above and below the base plate. By displacing these two plates relative to the base plate the effective aperture and hence the flow of sand out of the hopper could be varied. The sand then fell into a receiver which had the same plan dimensions as the hopper. The rain of sand was dispersed by a mesh underneath the hopper, but this seemed to have little effect. Kolbuszewski and Jones[54] found that the height of fall had practically little effect on the resulting porosity. Gisbourne[39] used a similar apparatus and obtained good results. The main problems occurring with this kind of apparatus centres around the turbulence caused by the displaced

5.4) contd.

air. Gisbourne provided a suction at the base of the receiver to remove the air, but some turbulence was still encountered.

A different approach, but using the same principles, was adopted by Walker and Whittaker[90]. In this method the bed was formed in a series of thin layers by a rain of sand falling from a hopper which passed backwards and forwards across the receiver. An electric driven cylindrical roller was positioned below the open base of the hopper. The intensity of the sand rain was varied by altering the speed of rotation of the roller. Whittaker and Walker[90] meet some trouble with air turbulence in their relatively small cylindrical receiver.

More recently Butterfield and Andrawes[12] described another apparatus similar in principle to Walker and Whittaker. This apparatus again used the moving sand curtain technique by discharging from an 'air activated spreader'. The sand was discharged from the hopper, through a horizontal slot, under air pressure. The intensity of the sand rain could be adjusted by altering the air pressure. Butterfield and Andrawes pointed out that the main defect associated with the moving sand spreader was that the sand was deposited in distinct layers which were detectable on X-ray photographs.

5.4.1) Design Considerations.

The size of the model test bed (8' × 4' in plan) precluded the use of a hopper the same size as the receiver and, anyway disturbance due to air currents seems less when using a travelling hopper because the displaced air can move away in front of the sand curtain. The methods described in

5.4.1) contd.

the last section which used a travelling hopper seem relatively complicated and gave only slightly better results than the simpler variable apperture apparatus. The Author therefore decided to adopt a variable apperture hopper in conjunction with a moving trolley.

A bed of sand about 3 to 4 feet deep was required. It was therefore necessary to have the hopper high enough to ensure that the decrease in the height of fall of the sand grains would have little effect on the porosity. This meant putting the hopper as high as possible. Because of the size of the container there should be little problem with displaced air except at the extreme edges. However, the disturbance at the edge should have little effect on the model tests which would take place in the centre of the container.

When the test bed was full it would contain 4-5 tons of sand. The hopper could not have this kind of capacity, so a method of filling the hopper after each pour had to be devised.

5.4.2) Description of Apparatus.

The travelling hopper is shown in plate (5.2a). The hopper consisted of a steel frame chassis and wooden body panels to give a capacity of 0.28 m^3. In the base of the hopper there were two plates, shown in some detail in plate (5.2b). Both these plates were drilled with a regular pattern of holes $^7/_{16}$" in diameter at 1" centre. It was found practically impossible to use $\frac{1}{2}$" diameter holes because of the leakage that occurred. The inner plate was welded to the hopper chassis and the outer plate was allowed to move

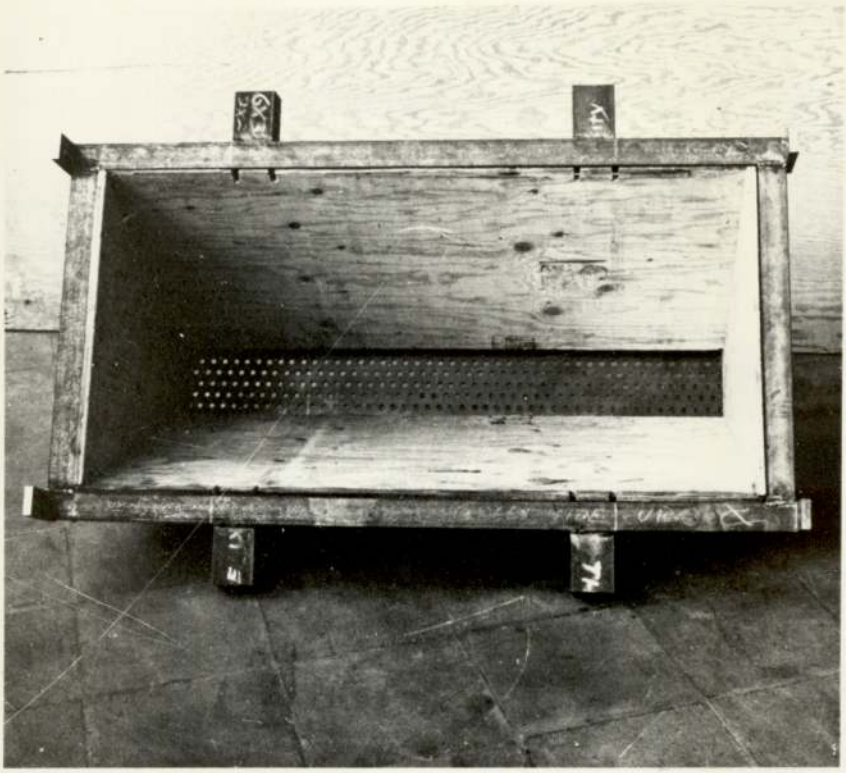

PLATE (5.2a) THE HOPPER

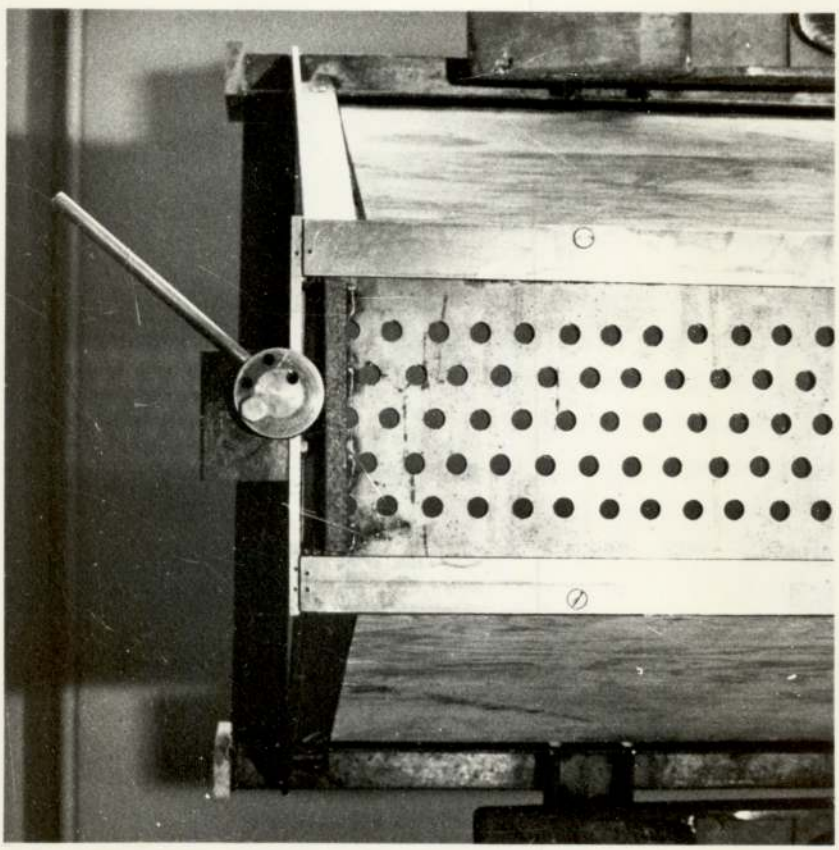

PLATE(5.2b) THE BASE PLATE AND ADJUSTING CAM

5.4.2) contd.

in a groove. In the zero position the holes in the inner plate coincided with the solid spaces in the outer plate, as shown as position 0 in Figure (5.3). The outer plate could be displaced by rotating the cam, shown on the left of the plate (5.2b), thus the holes in the outer plate could gradually be brought into full coincidence with those in the inner plate. A second cam was provided on the other side of the base of the hopper to return the outer plate to the zero position.

The adjusting cam was calibrated for three positions between the zero position and full coincidences of the holes. These positions corresponded to nominal displacements of the outer plate of $\frac{1}{8}$", $\frac{1}{4}$" and $\frac{3}{8}$", as shown in Figure (5.3), where the shaded areas represent the apperture. The position could be created by bringing the first, second or third hole drilled in the cam into coincidence with its corresponding hole on the retaining plate above it and then secured by a tapered steel pin.

The hopper could be attached to a trolley, shown in plate (5.2c), which ran along the top flange of the cross beam on top of the test rig, Figure (5.4). The hopper was connected to the trolley by means of four locating points, one at each corner of the hopper and trolley. These points which can be seen in the plates consisted of steel plates welded to the chassis and drilled with a 1" diameter hole. The plates in the trolley/hopper were lined up and then secured by bolts.

The trolley, which can be seen in plate (5.2c), consisted of four wheels, two axle and a steel frame.

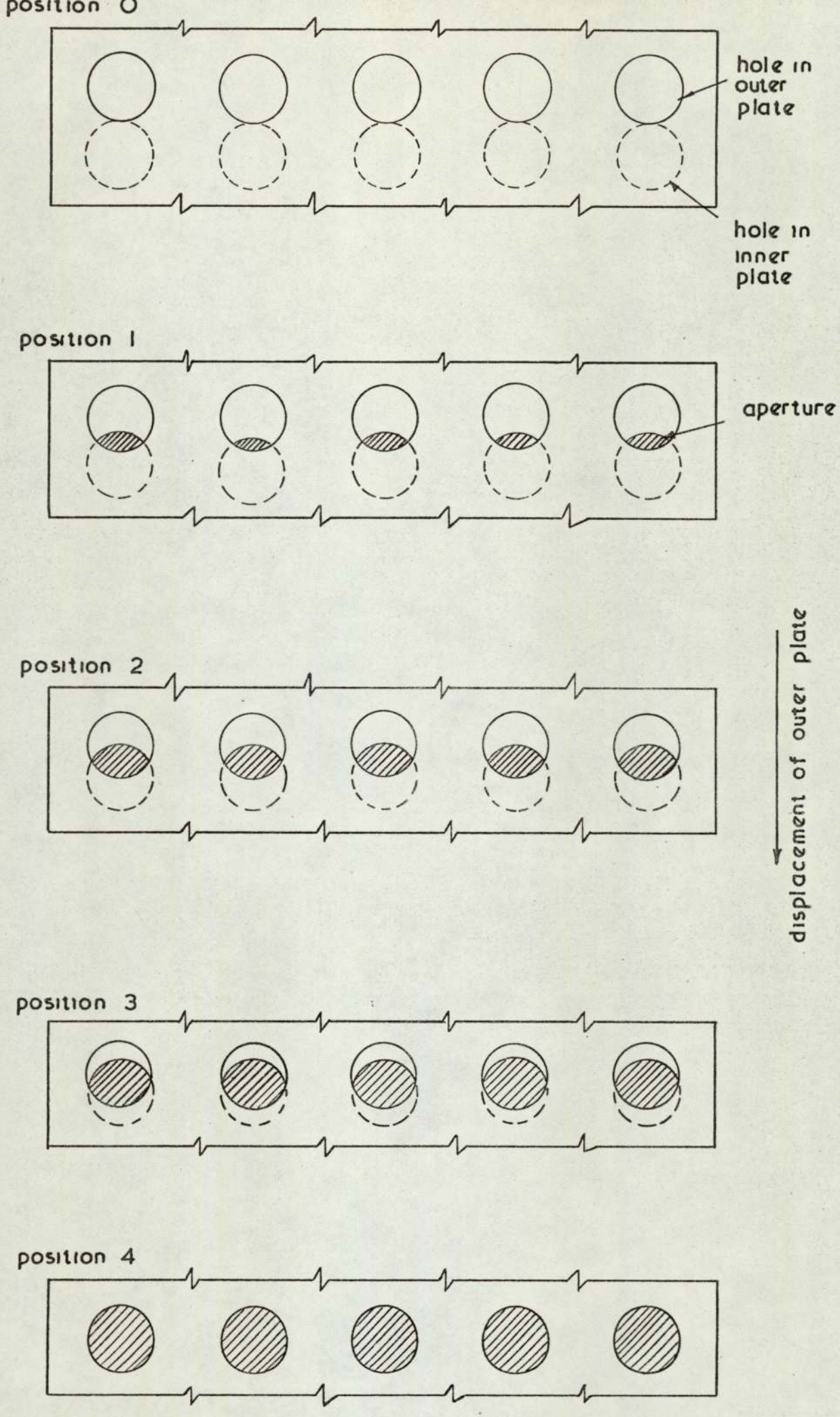
position 0
hole in outer plate
hole in inner plate
position 1
aperture
position 2
displacement of outer plate
position 3
position 4

Figure 5.3

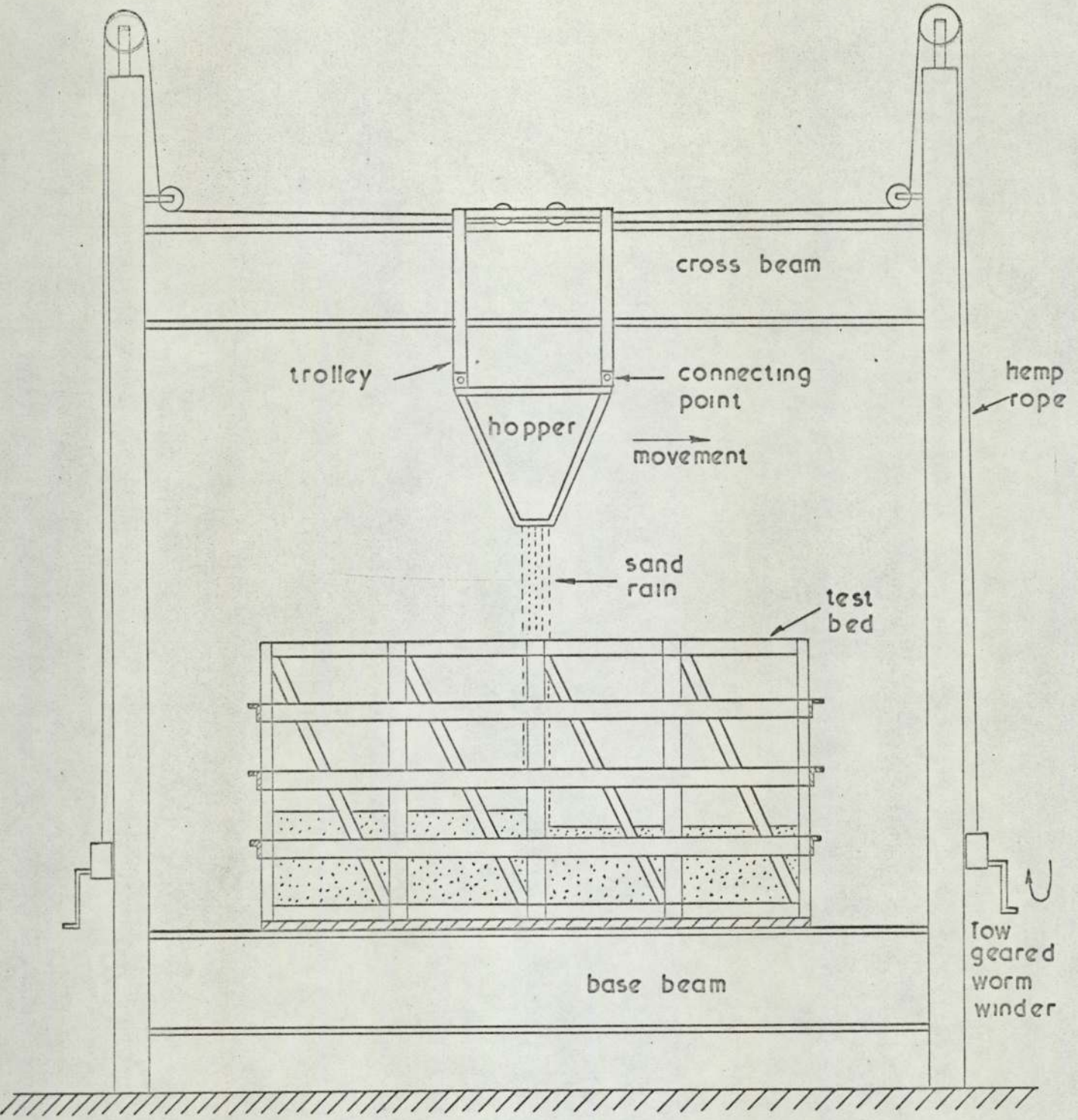

Figure 5.4 General layout of apparatus

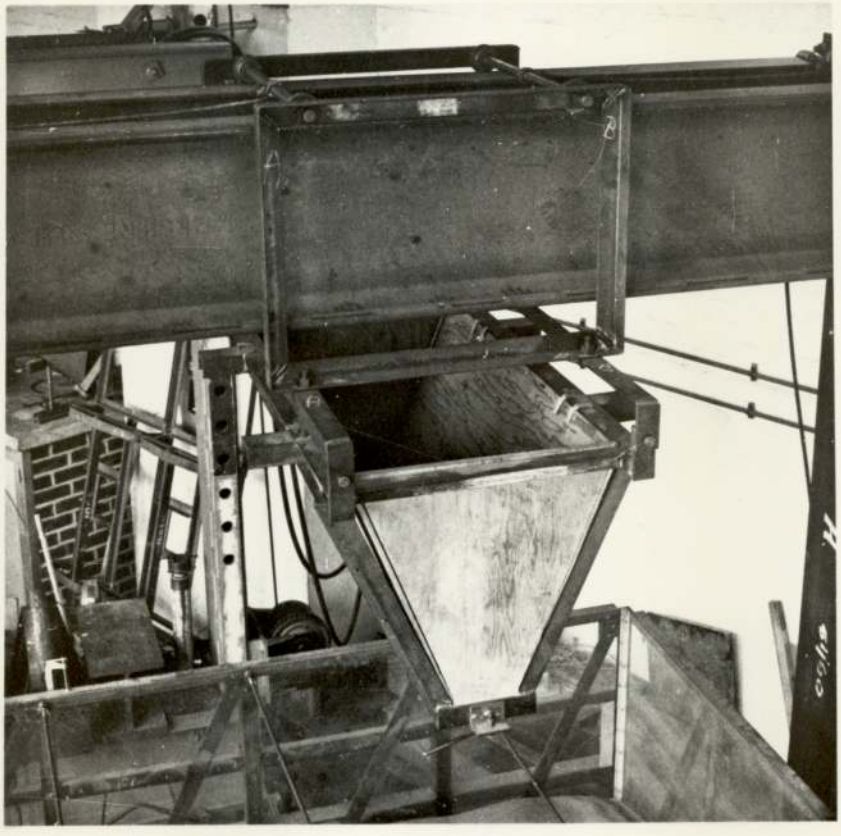

PLATE (5.2c) THE HOPPER MOUNTED ON THE TROLLEY

5.4.2) contd.

The wheels were supported, and guided by the top flange of the cross beam.

The trolley and its attached hopper could be moved over the length of the test bed by the manner shown in Figure (5.4). A hemp rope was attached to the centre of the axle and passed through and over two pulleys on the main support column and down to a worm geared winder. It was found necessary to use a fairly rigid hemp rope to avoid jerking. Less rigid materials stretched until the tension was high enough to move the hopper against the friction, at which time, the tension was relaxed as the hopper jerked forward, and then the process would be repeated This led to a considerable during effect on the surface of the sand. The winder was a standard fitting to the test ring and was normally used to adjust the height of the cross beam. Its low gearing made it ideal for its new job because turning the crank handle at moderate effort (~ 1.5 revs/sec) gave a reasonable speed (~ 30 cm/sec) to the trolley. The trolley would have been more evenly propelled by a motor but as a suitable one was not available for these tests, hand winding was used. Experience showed that it was quite easy to maintain an even speed.

The hopper was designed so that it could be filled at ground level and then lifted up to the trolley. To do this four struts made from steel channel section were welded to the hopper chassis, two on either side sand can be seen in plate (5.2a). These were provided so that the forks of the fork lift truck would fit underneath them and hence lift the hopper up to the trolley on the cross beam.

5.4.3) Measurement of Porosity.

The porosity of the sand was obtained by placing calibrated measuring cylinders, known as density tins, at different points in the receiver and weighing the sand deposited in each. The measuring cylinders were nominally 2" in diameter and $1\frac{1}{2}$" high made from brass tubing. Density tins usually have a gauze base to allow air to be displaced, but the bases soon sag due to the small stiffness of the gauze which introduces errors. The Author had density tins made with bases of brass plate perforated by a number of $\frac{1}{8}$" diameter holes and then the gauze was stuck to the inside face. Each of the twenty cylinders could be identified by a number stamped on it.

5.4.4) Calibration.

To calibrate the variable apperture hopper the porosity was measured for each of the apperture settings in Figure (5.3). It was also necessary to investigate what effect the decrease in height of fall, and, the decrease in head of sand in the hopper had on the porosity variation.

Ten density tins were placed close together in the bed at the mid-depth point of the receiver. The hopper, with the apperture set at position 1, Figure (5.3), was then passed over the tins. The full tins were screeded level, weighed and the porosity calculated. This test was repeated for the other three aperture positions.

Next, ten density tins were placed along the length of the bed at the mid-depths. A pass of the hopper was made to fill the tins and the porosities along the bed were calculated. No more than random variation was found. This meant the decrease of head of sand could be presumed

5.4.4) contd.

to have little or no effect.

Lastly, the density tins were placed together at the bottom of the bed and filled from the hopper, and the porosities then calculated. These tins were then replaced at the height of the proposed surface level of the bed and refilled. The difference between the average porosities calculated at this height and the bottom of the bed was again not higher than the random variation. The height of fall was reduced from 1.75 m. to 0.8 m. but this had very little effect on the porosity.

As a final check two full size pours were carried out in the test bed with the apperture set at position 4. Four density tins were placed in the bed after each pass of the hopper. When the bed was full the surface was screeded level and the dimensions measured. The bed was then emptied and the sand weighed as it was removed. The density tins were carefully retrieved. The bulk porosity, calculated from the volume of the bed and the total weight of sand removed, differed by only $\frac{1}{2}\%$ from the average porosity given by the density tins. This result was confirmed by both trial pours.

5.4.5) Variation of Porosity.

The porosity obtained from pouring with the apperture set at each of the positions in Figure (5.3) is plotted in Figure (5.5a). The varying intensity of the sand rain at positions 1 and 4 is shown clearly in plates (5.3a) and (5.3b). The variation of porosity at a given apperture setting was never more than $\pm$ 2% and the bulk porosities obtained in the two trial pours were the same.

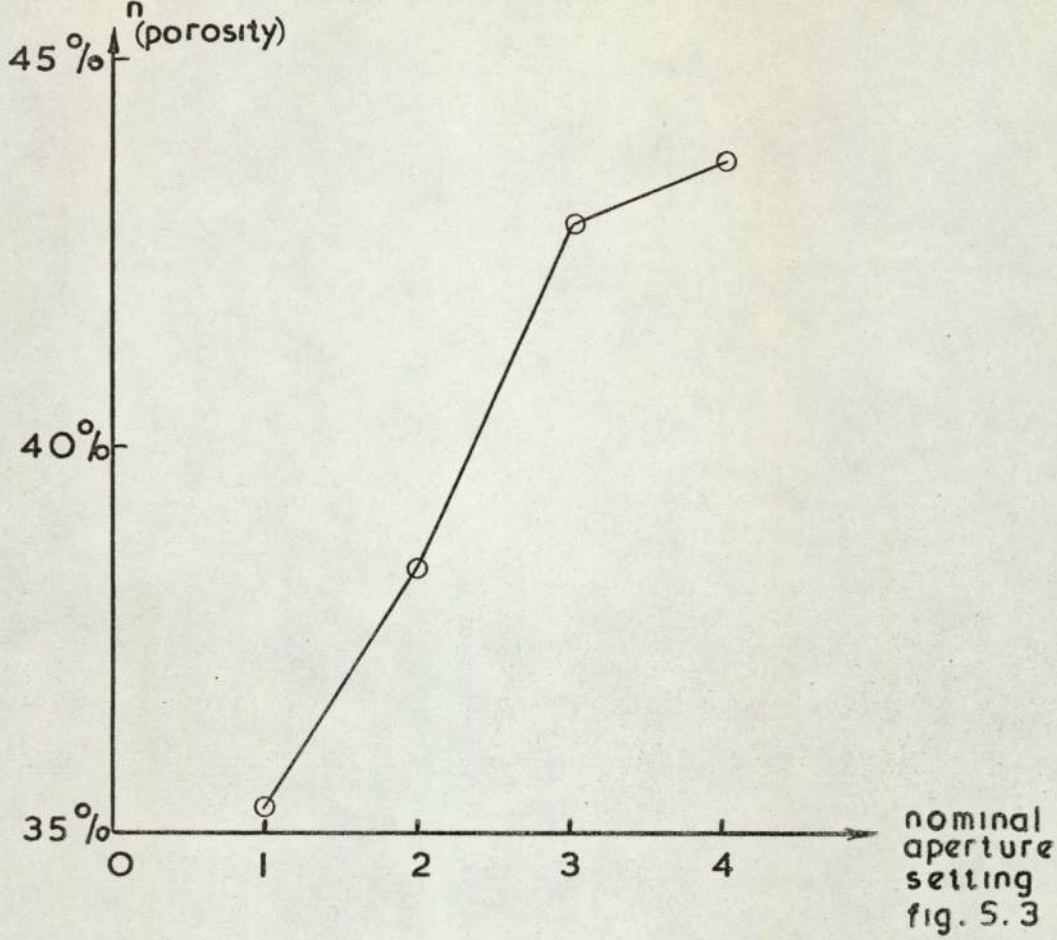

Figure 5.5.a.

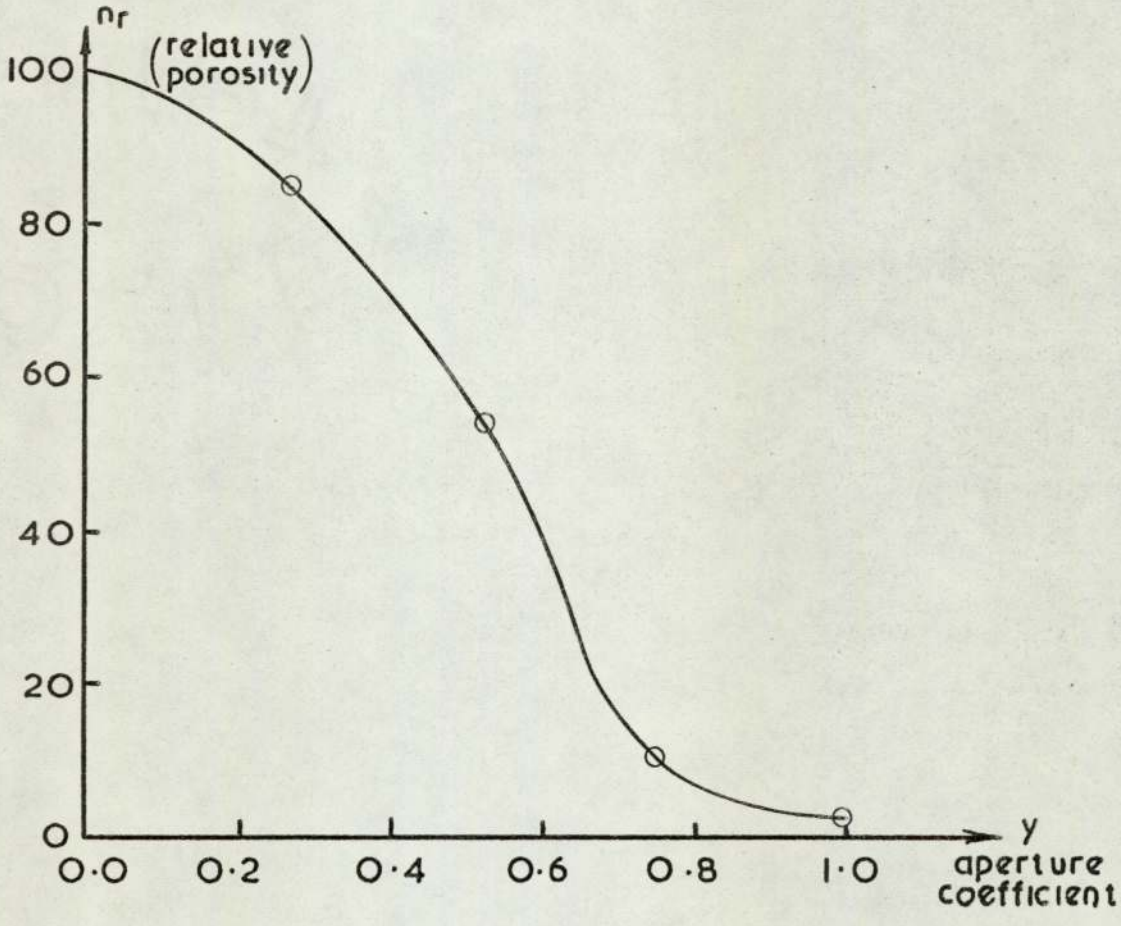

Figure 5.5 b

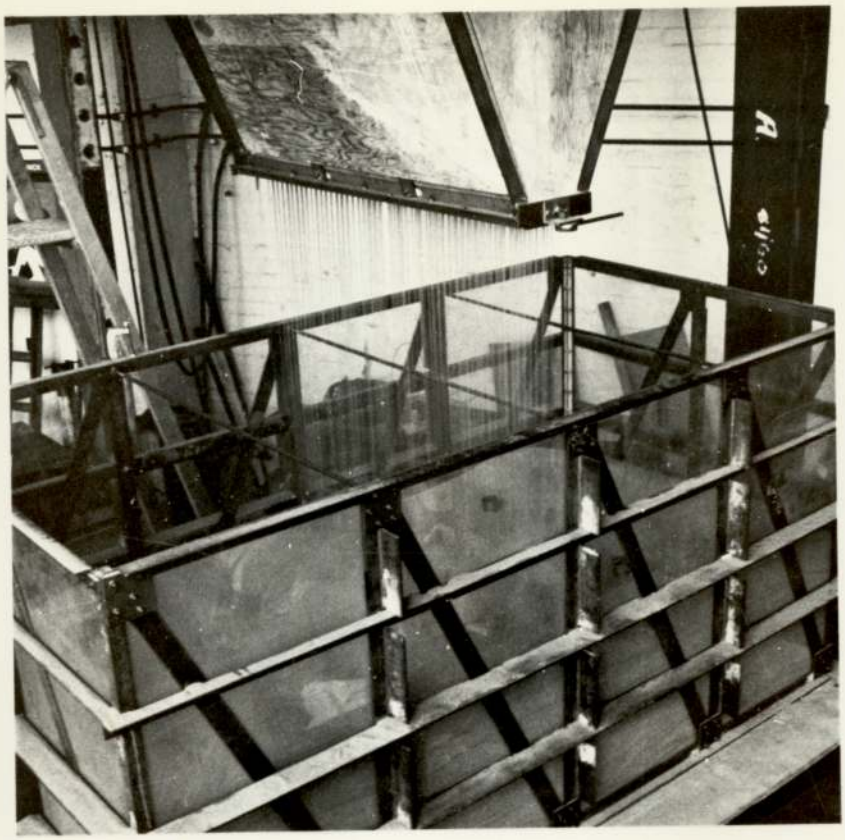

PLATE (5.3a) POURING AT APERTURE POSITION 1

PLATE (5.3b) POURING AT APERTURE POSITION 4

5.4.5) contd.

It can be seen from the Figure (5.5a) that using these four fairly arbitrary settings a good range of porosities was achieved.

Figure (5.5b) shows the relative porosity of sand plotted against, what Kolbuszewski and Jones[54] called, the apperture coefficient. The relative porosity n_r is calculated from:

$$n_r = \frac{n_{max} - n}{n_{max} - n_{min}} \qquad (5.1)$$

where n_{max} and n_{min} were measured in Section (5.3.1). The apperture coefficient y is the ratio $y_d/y_{(4)}$ where y_d is the actual maximum width of the apperature and $y_{(4)}$ is the apperture size at full coincidence. These dimensions were measured with a vernier gauge. The resulting shape of the curve in Figure (5.5b) is very similar to those obtained by the investigators mentioned in Section (5.4). It can also be seen that the curve has the correct form as it becomes asymptotic to the ordinates of 0% and 100% relative porosity.

5.5) The Test Bed.

The test bed, which can be seen in plate (5.3b) and Figure (5.4), consisted of a perspex box inside a steel frame. The steel frame was itself restrained in several places by bands of steel angle section which went round the perimeter. The top of the tank was restrained across the width by three reinforcing bars. These bars were circular and only $\frac{1}{2}$" in diameter and hence did not interfere with the sand rain. The box was made from $\frac{1}{4}$" perspex plate so that a visual check could be made on the result of the pours. The bed was designed large

5.5) contd.

enough so that the effect of the sides should be negligible.

The test bed was originally designed using standard engineering procedures but the maximum deflections were relatively large (~ 3mm), during the trial tests. The original $1\frac{1}{2} \times 1\frac{1}{2} \times \frac{1}{4}$ steel angle section in the frame and bands was replaced by $3 \times 1\frac{1}{2} \times \frac{3}{8}$ angle section and this reduced the maximum deflection to less than $\frac{1}{2}$ mm. The bed rested on a large piece of 1" thick plyboard which rested on the base beam of the rig. The bed overhung the sides of the base beam and the edges were supported on solid wooden blocks.

5.6) Loading System.

Initially it had been decided to use an hydraulic jack as the method of applying the load to the model structure. The base of the jack was bolted to a plate fixed to the underside of the cross beam. The load was applied, and thus measured, through a steel proving ring. It was not possible to use the self compensating hydraulic system installed in the laboratory because the vibration from the machinery visibly affected the sand, and so a hand pump was used. However, the system proved unstable. The pressure in the hand pump would decrease slightly with time, due presumably to a small leak. This decrease was found to be present in all the pumps tried. This effect was coupled with the fact that small settlements of the structure, which were largely irrecoverable, caused the load to decrease. The hydraulic pump had to be continually readjusted to maintain a constant reading on the proving ring. Each readjustment caused a further small settlement. It was therefore decided to change to a dead load system where none of these problems could arise.

5.6) contd.

The loading system that was made and used is shown in Figure (5.6) and plate (5.4). It consisted of four parts; the restraining strut, the lever arm, the loading arm and the hanger. The restraining strut could be fixed to the two flanges of the cross beam as shown in Figure (5.6). The strut had to be moveable, because the load would be applied at different points above the model, and removable, because otherwise it would obstruct the hopper. The knife edge at the bottom end of the strut located into the slot in the lever arm at K, in plate (5.4). In making the lever arm it was essential that the three loading points at K, H and L should all be on the centre line of the beam, as shown in the figure. To keep any errors due to friction to a minimum, the holes were all made 50% oversize and countersunk to a sharp edge so that the area of contact was a minimum.

The load was applied to the model structure by means of the loading arm. Connecting pins joined the loading arm to the lever arm and frame, by means of two 'u' brackets. These were connected through a universal joint to minimise any effects due to their not being aligned perfectly.

The load was applied to the lever arm by placing weights on the pan of the hanger which was connected at L, in plate (5.4).

The magnification of the lever arm was X3.9.

5.7) Experimental Procedure.

5.7.1) Preparation.

Sand was placed in the bottom of the test bed and banked round the edges. Experience showed that if this was not done, the edges would be lower than the centre of the

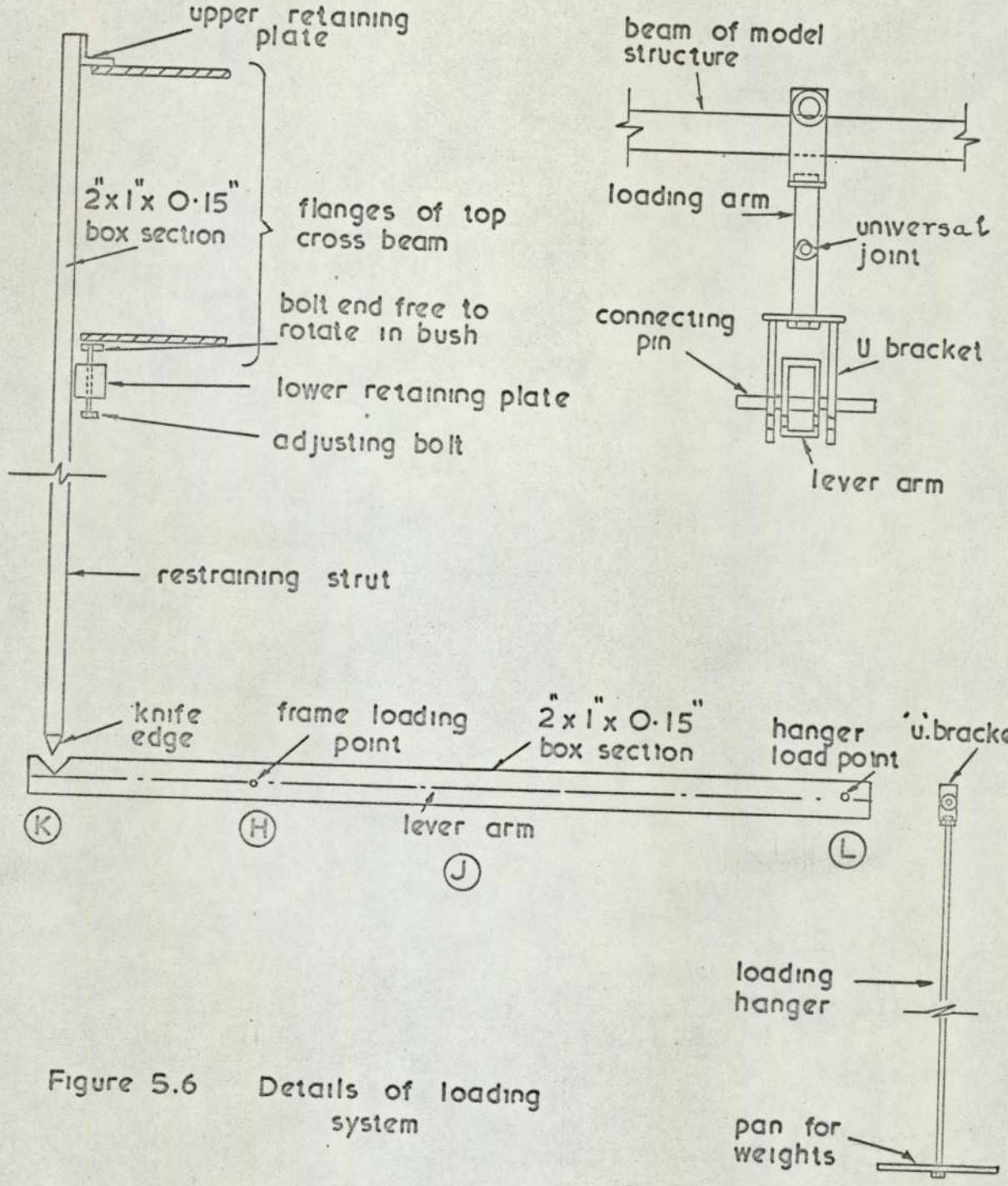

Figure 5.6 Details of loading system

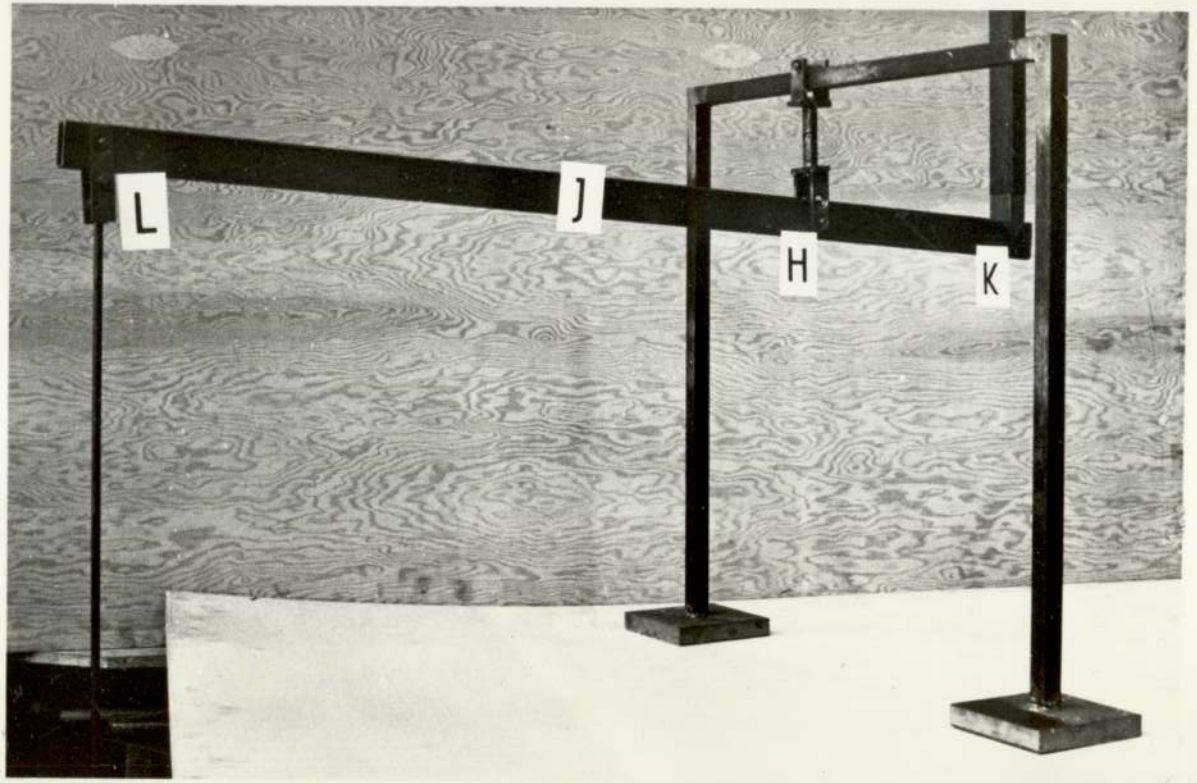

PLATE (5.4) THE DEAD LOADING SYSTEM

5.7.1) contd.

bed after the bed had been filled.

Four density tins were placed on the surface of the sand and their numbers and positions noted. The hopper, now at ground level and resting on a fork lift truck, was filled with sand from the bags, plate (5.5a). The fork lift truck, carrying the full hopper, was driven forward under the trolley and the hopper raised up and connected to the trolley; plate (5.5b). The truck was then removed. The hopper was moved to the starting position, marked on the cross beam, and the aperture set using the adjusting cam. By winding the crank of the worm gear the hopper was drawn gently across the length of the bed. When it reached the other end, the aperture was closed. For all the tests carried out by the Author the aperture was set at position 4, Figure (5.3). In this case the hopper was empty when it reached the end of the bed, and could be merely pulled back to the other end, after releasing the rope from the winding gear. When using other aperture settings the hopper would not be empty and so the aperture would have to be reset and wound back down the bed to deposit the next layer. In pulling the hopper across the bed it was found essential to keep a reasonable speed otherwise the motion was jerky leaving an undulating surface. When the hopper was empty it was lifted down from the trolley using the fork lift truck. This cycle of operations took about 15 mins. after practice, and the cycle had to be repeated until the bed was full.

When the sand bed was slightly deeper than required the surface was screeded level. This was achieved by gently scraping off the top few millimetres of sand using a board, the width of the bed, that fitted onto the top

PLATE (5.5a) THE FILLED HOPPER AT GROUND LEVEL

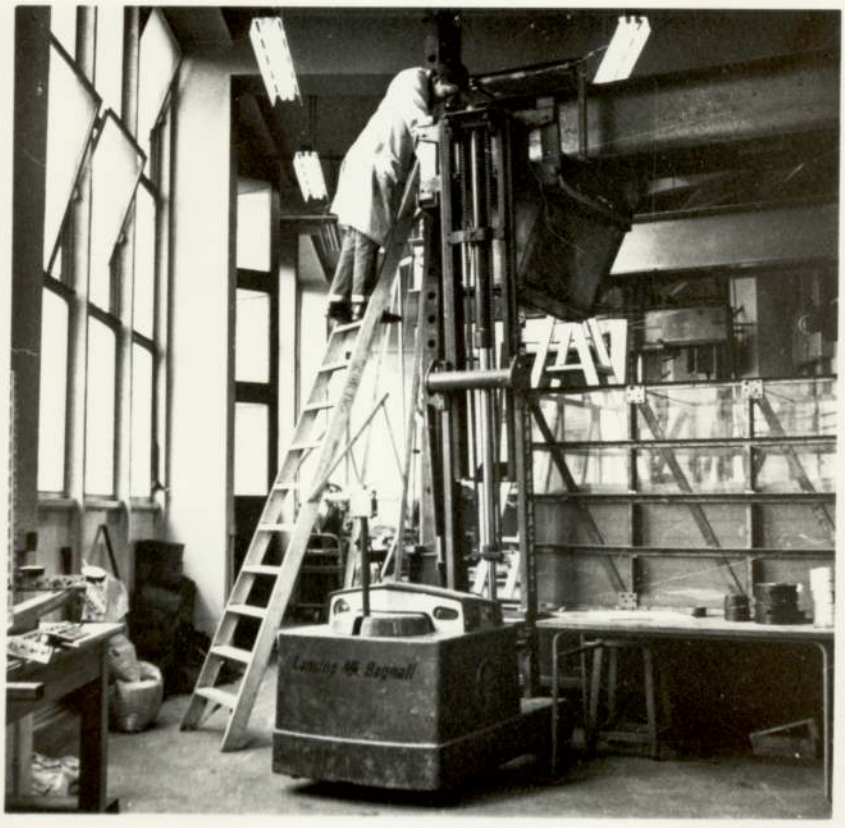

PLATE (5.5b) THE HOPPER BEING ATTACHED TO THE TROLLEY

5.7.1) contd.

channel of the frame of the bed. The model structure could then be placed centrally on the bed of sand. The largest space frame, plate (5.1c), weighed over 50 kg so lifting them on to the bed was aided by a rope over the cross beam to carry the weight, the frames could then be positioned with ease.

Once the model structure was in place, the frame to hold the dial gauges was built round it. This frame was bolted to the three top restraining bars and to the frame of the best bed. The dial gauge frame for the plane frame model structure, plate (5.1a), included two pairs of rollers which were placed against the columns of the model to prevent out of plane movement.

The loading device was then assembled and hung on the model at the desired loading point. Care was taken to ensure that the restraining strut was vertical so that the lever arm did not twist. It was also necessary to ensure that the strut was positioned so that the loading arm hung vertically.

The plane frame fully prepared for a test is shown in plate (5.5c). The plane frame itself is identified by the letters 'NMPO' in the plate and the loading device by the letters 'KJL'.

For this test there were only nine dial gauges, lettered 'A to I' in the plate. The dial gauges were all positioned to measure either settlement or sway. In the space frame models it was necessary to measure the deflections at twenty points. The preparation took about five hours per test.

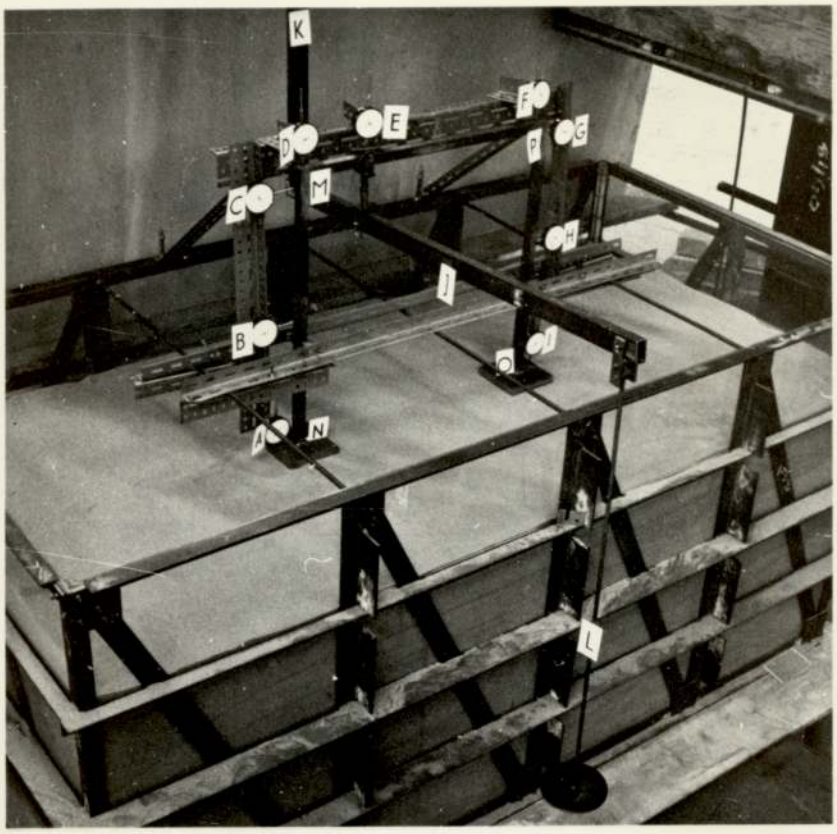

PLATE (5.5c) THE MODEL PLANE FRAME READY TO TEST

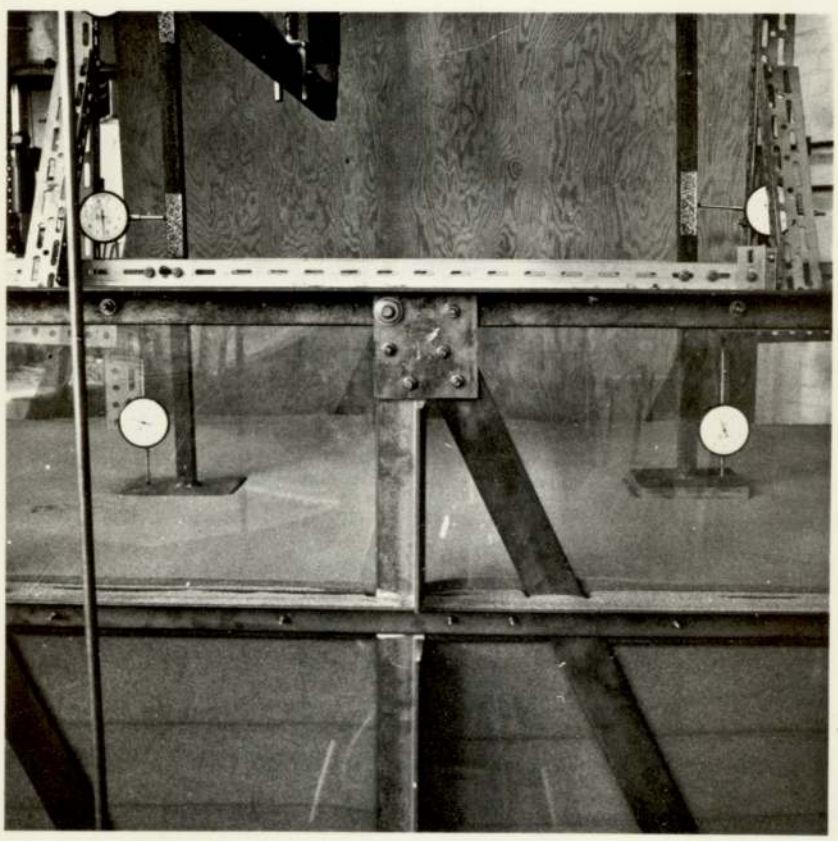

PLATE (5.5d) DIFFERENTIAL SETTLEMENT AT THE CONCLUSION OF A TEST

5.7.2) Testing.

The initial readings of the dial gauges were noted and the positions of the dial gauges relative to the initial position of the model were marked on the model structure. The first weight was then placed on the hanger. The size of this weight was chosen so that the largest deflection of any of the pad footings was less than 1 mm. Settlements took place very quickly and it was necessary to place the weights gently on the hanger to avoid dynamic loading. The weight was left on the pan until no increase in dial gauge reading was taking place, which usually took about 15 minutes. When the dial gauge readings had been taken the next increment of load was placed on the hanger and the procedure repeated until one of the pad footings had settled 25-30 mm. Plate (5.5d) shows the differential settlement at the conclusion of a test on the plane frame model structure. The dark bands which can be seen in plate (5.5d) illustrate quite clearly the layering effect discussed by Butterfield and Andrawes[12]. These dark bands were formed by the smaller dust particles which settled after the main stream. The test took about a day to complete.

5.7.3) Dismantling.

The dial gauge frame, loading device and model structure were removed from the bed. The sand was then emptied from the test bed through the two plug holes provided in the base of the bed. When the plug holes were opened the sand ran out into a plastic bag held underneath as shown in plate (5.5e). The density tins were retrieved as soon as they appeared and were weighed. About $\frac{2}{3}$ of the sand could be emptied without any interference, but the last $\frac{1}{3}$ had to be shovelled away from the centre of the bed into the

PLATE (5.5e) EMPTYING THE SAND FROM THE TEST BED

5.7.3) contd.

corners where the plug holes were situated. The dismantling operation took about half a day.

CHAPTER 6.

THE MEASUREMENT AND DERIVATION OF A CONSTITUTIVE RELATION FOR THE SAND.

6.1) Introduction.

In this Chapter the experimental apparatus and technique used to measure the mechanical properties of the sand filling the test bed are described in some detail. A simple constitutive relation is then derived, and developed into a comprehensive relation covering a range of confining pressures, from measured laboratory results.

6.2) The Experimental Determination of the Mechanical Properties of the Sand.

The parameters required for the non-linear analysis of a continuum should be measured under the particular stress or strain conditions expected to exist in the continuum itself. In the case of a general three dimensional continuum these conditions are mostly unknown, and even if they were known, it would be extremely difficult to design an experimental apparatus capable of imposing arbitrary stress and strain paths.

Laboratory axi-symmetric compression tests are the most common test in engineering practice, while tests under plane strain conditions are possible. In the model tests the confining stresses were small and from this point of view the shear box seemed ideal. However, the uncertain boundary conditions in this test make it unattractive, while the conditions in the test bed are likely to be nearer axi-symmetric than planestrain.

It was therefore decided to use the axi-symmetric compression test, commonly and inappropriately known as the triaxial test, to measure the sand properties. This apparatus has been the object of much improvement and by adopting these modern methods, the boundary conditions are accurately known.

6.2.1) Apparatus Requirements.

The triaxial apparatus had to be capable of achieving two main functions;

(a) to apply a known uniform stress at low values, and

(b) to be able to measure volume changes occurring in dry sand.

The function (a) above was necessary because the scale of the model tests meant that the confining pressures were low. To achieve uniform stress conditions at both ends of the sample it is necessary to create so called 'free end' conditions, when applied shear stresses are eliminated, ensuring that the major principal stress is vertical. At low stress levels it is important that the applied load is measured accurately. The effect of friction between the loading piston and sealing bush (in the top of the cell) could introduce large errors, which can only effectively be eliminated by measuring the load inside the cell. The apparatus will also have to be capable of applying and maintaining a low ambient pressure throughout the test.

Function (b) follows from the fact that the model tests were performed on dry sand and hence it is necessary to measure the mechanical properties under similar conditions. This meant that the apparatus had to be capable of measuring volume changes of air.

6.2.2) Description of Apparatus.

The general layout of the apparatus is shown in Figure (6.1). It consists of three main parts, a self compensating mercury manometer, the triaxial cell itself and a volume change measuring device.

The self compensating mercury manometer is

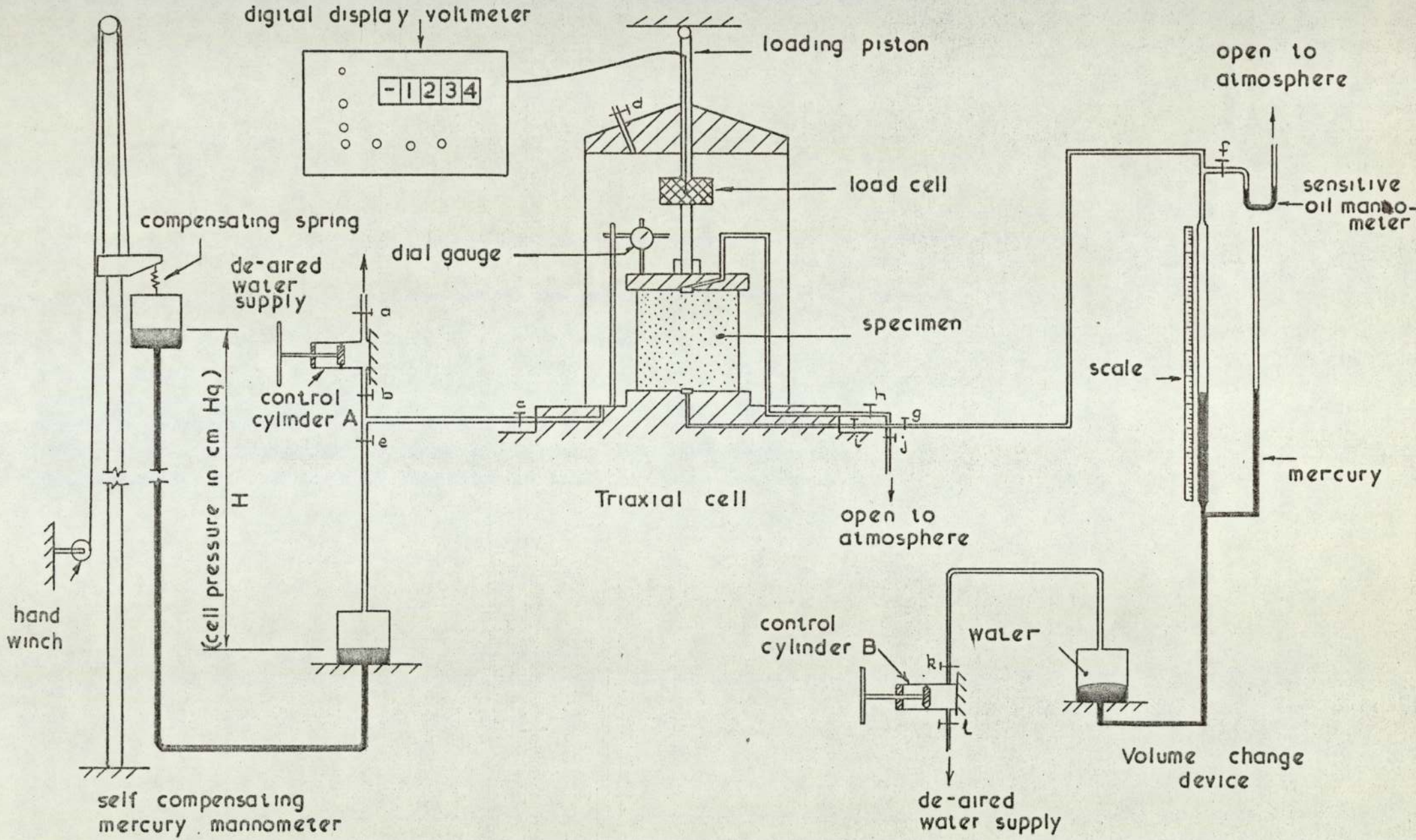

Figure 6.1 Triaxial compression apparatus for testing dry samples at low cell pressure

6.2.2) contd.

described in Bishop and Henkel[9], it is capable of maintaining low cell pressure throughout a test. It was very important, at these low pressures, to use a device like this, instead of say a control cylinder or fixed mannometer, because as the loading piston is pushed into the cell, and, the sample undergoes volume change, water must be able to leave the cell without changing the pressure, otherwise, large increases in cell pressure would occur. The hand winch was used to preset the head difference, H, of the two arms of the manometer, and the control cylinder A was used to adjust the initial levels of mercury.

At low cell pressures it is possible that friction in the tubing will have a significant effect on the cell pressure. To check for this effect, a mercury manometer was attached directly to the cell and the cell pressure varied. The dimension H, Figure (6.1), and the head difference in the manometer were compared, and no difference could be measured.

A conventional cell for testing 4" diameter specimens was modified to accommodate a load measurement transducer. This transducer had been designed for $1\frac{1}{2}$" diameter samples so a bush had to be machined to fit inside the collar already in the cap of the cell to accommodate the smaller diameter loading piston. The load transducer, manufactured by Wykeham Farance Ltd., type cone faced WF/17001, had a capacity of 1000 lb f. The transducer was energised by a constant supply of 10v dc. and set in a standard bridge, the output being measured on a digital display voltmeter. The transducer gave an output of 20 mv for a 1000 lb load. The digital voltmeter was reliable to 0.02 mv

6.2.2) contd.

which meant a sensitivity of 0.5 KN/m^2 in the measurement of vertical stress and this proved adequate.

The conventional 4" diameter end plattens were replaced by enlarged aluminium alloy plattens, 118 mm. in diameter, shown in Figure (6.2) and plate (6.1a), whose surfaces were ground flat and polished. Porous discs $12\frac{1}{2}$ mm. in diameter were used at both ends of the sample to permit drainage to take place. To eliminate end friction, and hence allow the sample to expand uniformly over the plattens, two thin discs of latex rubber were placed between the sand sample and the plattens. The interfaces between platten and latex, and latex and latex were coated with a thin smear of inert silicon grease. The bottom latex disc was slit radially around the circumference to remove any restraint that might be imposed by the latex disc at large strains.

The tip of the load piston of the load transducer located into a collar on the top of the loading platten, shown in Figure (6.2), so that no tilting could occur. The vertical deflection of the top cap was measured by a stainless steel dial gauge inside the cell. The gauge could be read to 0.02 mm. and had a full range extension of 13 mm.

Volume changes were measured in the device on the right hand side of Figure (6.1), it was taken from a design by Bishop and Henkel[9] and proved extremely effective. Any change of volume of the sample causes a small change in pressure which is registered on the sensitive oil manometer. The control cylinder B is then used to adjust the level in the mercury manometer so that the levels in the oil manometer are equalised. Thus, atmospheric pressure was maintained in the sample and any volume change was proportional to the change

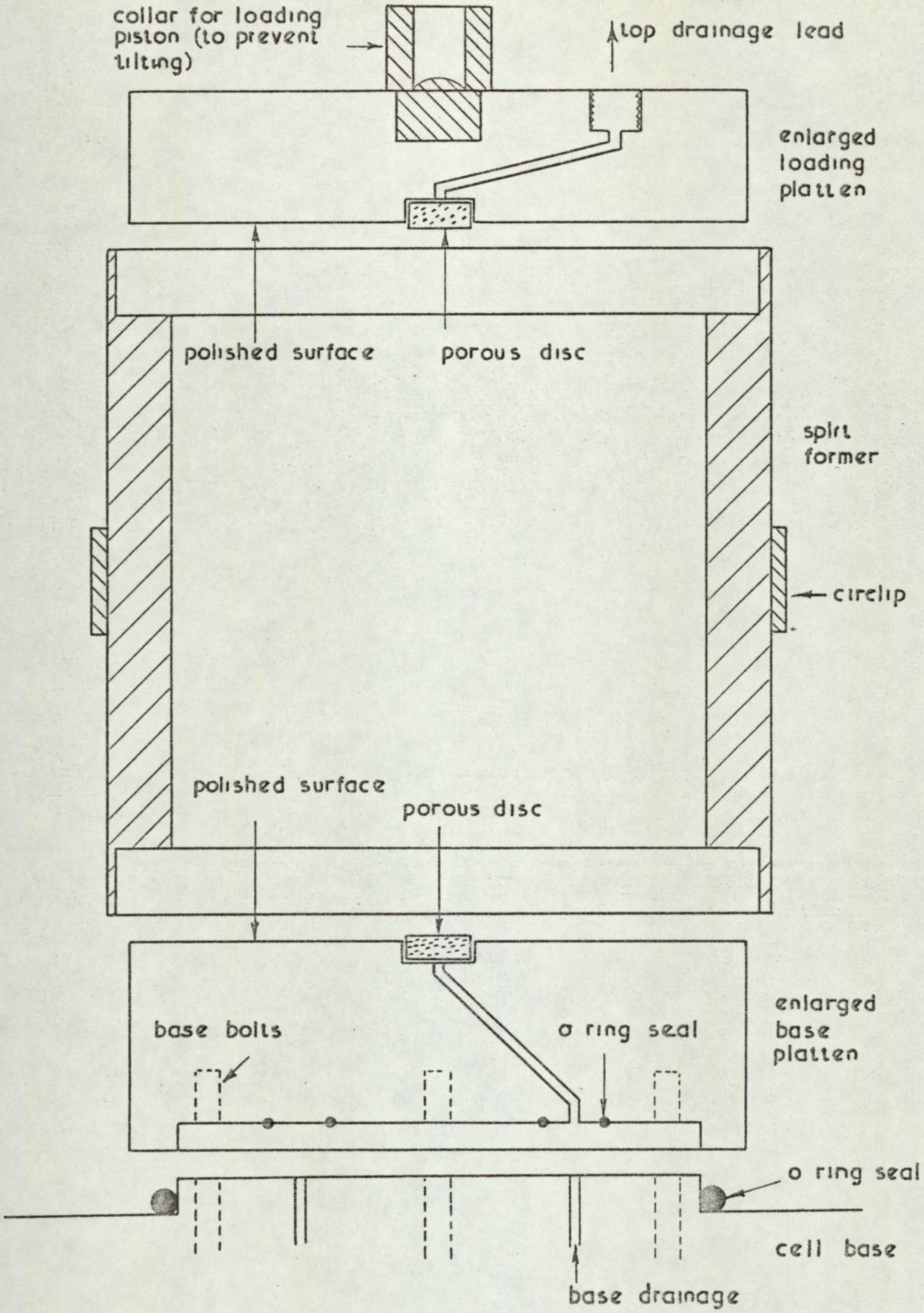

Figure 6.2 Apparatus details

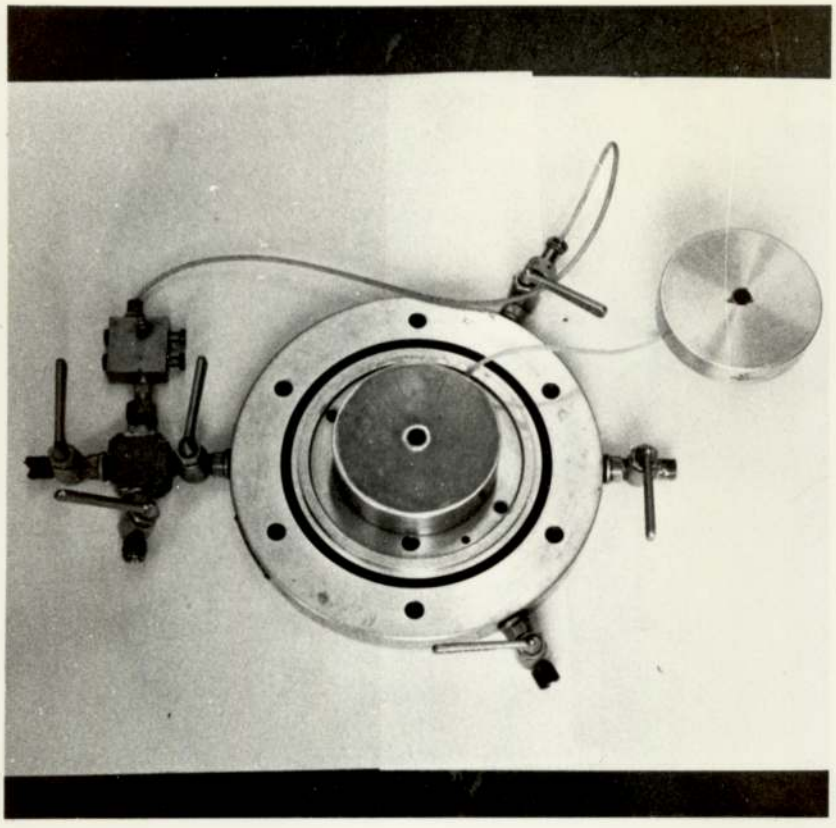

PLATE (6.1a) THE BASE AND TOP PLATTENS

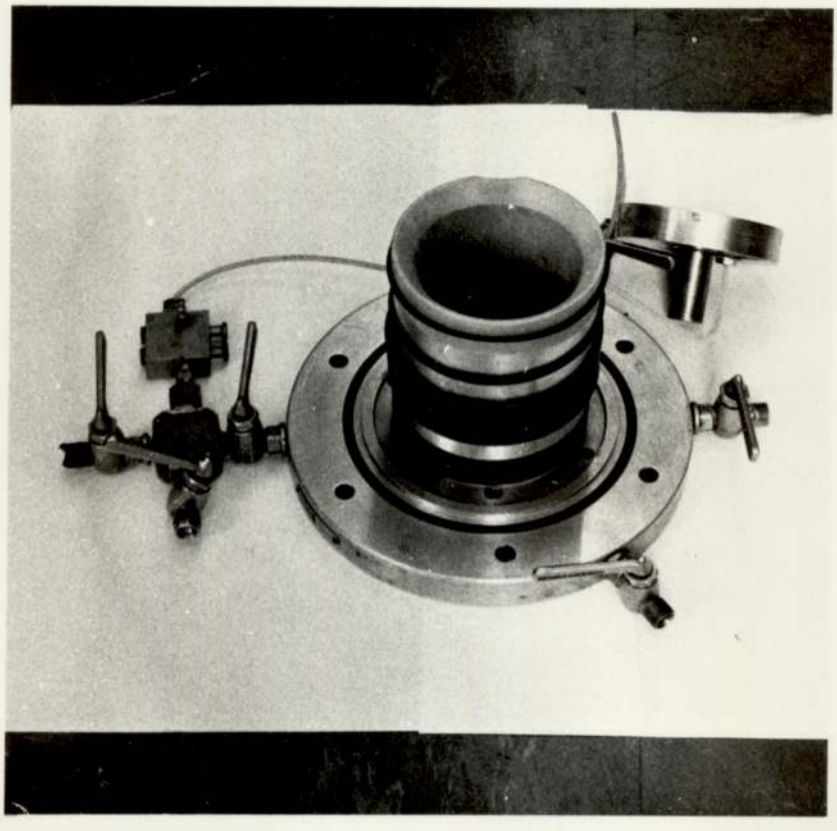

PLATE (6.1b) THE FORMER WITH THE MEMBRANE IN PLACE

6.2.2) contd.

in level of the mercury and could be read off the scale. Because of the extreme compressibility of air it was clearly important that atmospheric pressure was maintained in the sample. The volume change device was calibrated using a sensitive paraffin gauge and a factor of 0.193 cc/cm change in height was obtained.

6.2.3) Sample Preparation.

The sample size was chosen as approximately 100 mm. high and 100 mm. in diameter. To form the specimen a two piece split former was made and is shown in Figure (6.2). The former had to be designed to fit the bottom platten, produce a sample of the correct dimensions and allow the loading platten to be placed centrally without effort. The former was made in two pieces so that it could be removed once the enlarged top platten was in place. A gap was cut into the lip of the former to allow the air trapped under the top platten, as it was placed, to escape.

In an effort to faithfully reproduce the sand produced by the hopper, the samples were prepared in the test bed where they were filled from the hopper sand rain.

6.2.4) Experimental Procedure.

To remove any blockages or dirt the cell base and drainage leads were cleaned using compressed air. The surface of the bottom platten was lightly coated with silicone grease and a latex disc applied. This disc was then smoothed using a straight edge, itself greased, another latex disc applied and smoothed, see plate (6.1a). The excess grease from the smoothing operation was wiped around the side of the platten,

6.2.4) contd.

as experience showed this grease improved the seal between the platten and the sample membrane. The sample membrane was then placed on the bottom platten, adjusted to an upright position and secured by four rubber o-rings.

Silicone grease was also smeared on the outside of the membrane where it was stretched over the bottom platten, to ensure the membrane was not pinched and hence punctured when the sample former was placed round it. The two halves of the former were joined on the bottom platten, the top drainage lead passed through the circlip and the circlip placed round the former and tightened. The rubber membrane was gently stretched up and folded over the top lip of the former and held taut by 3 o-rings, see plate (6.1b). This operation had to be carried out with great care to avoid wrinkling the membrane.

The complete base was then carried down to the test bed and placed under the hopper. All the taps and various holes were covered to prevent sand entering, the hopper was opened to the required apperture and the former filled. The top few millimetres of sand could then be carefully spooned out to leave a level surface. Latex discs were placed on the top platten in the manner described earlier for the bottom platten. Extreme care was taken to ensure that the inner surface of the membrane which would be in contact with the side of the top platten was free of all particles. It was essential to have the two contact surfaces scrupulously clean to avoid the occurrence of leaks. The platten was then placed on top of the sand and gently pressed into contact with it, displaced air was let out through the gap in the former lip. It was found necessary to make

6.2.4) contd.

the sample somewhat tall, otherwise, if the top cap rested on the inner lip of the former it was impossible to remove the former without upsetting the top cap and spoiling the sample. The o-rings holding the membrane tight were rolled down and the membrane itself pulled up, while the top platten was held down, the o-rings were then rolled up on to the top platten to secure the membrane and seal the sample.

The complete base, now with a sample, was carried back to the testing laboratory and placed on the machine base. Excess sand was gently removed with compressed air. Particular care was taken to clean all taps and threads. The various leads were connected to the base and all taps closed. Tap k was then opened and control cylinder B used to induce a small suction (approximately 1.5 cms of Mercury) which could be measured on the volume change manometer, and was applied to the sample by opening taps, g, h and i. It was found necessary to adjust the control cylinder once or twice until the suction was maintained. The sample was left under suction for about ten minutes to check for leaks. If the suction were maintained throughout this period then the circlip was loosened, removed and the two halves of the former carefully separated and removed, see plate (6.2a).

The dimensions of the sample could then be measured. The overall height was measured using a vernier gauge and the diameter was measured several times using a micrometer, see plate (6.2b). Some difficulty was encountered using the micrometer because it was not easy to ensure that the diameter was actually being measured, and while doing so, it was easy to punch the sharp tips of the micrometer into the sample. To overcome this, some large brass feet (30 mm. in diameter)

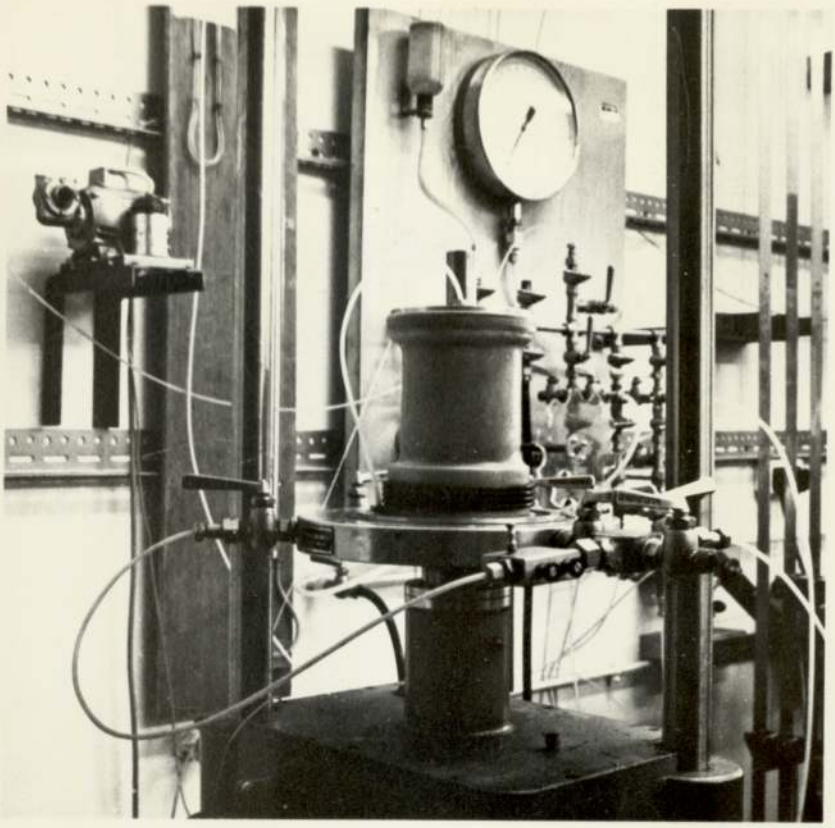

PLATE (6.2a) THE PREPARED SAMPLE UNDER SUCTION

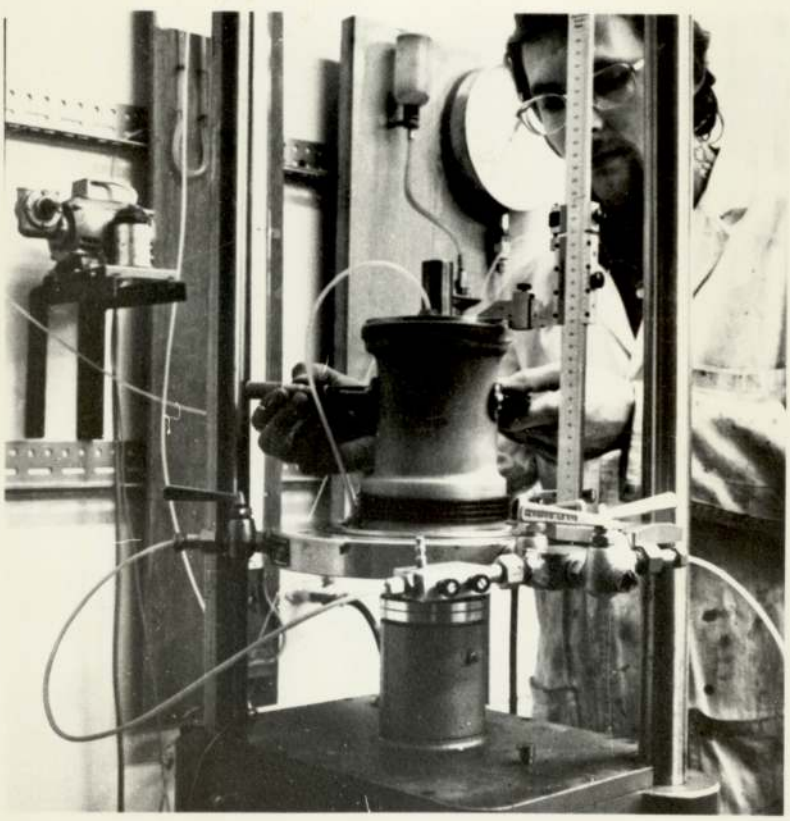

PLATE (6.2b) MEASURING UP THE SPECIMEN

6.2.4) contd.

were made to fit onto the micrometer jaws. These can be seen in plate (6.2b). The dial gauge stand was next screwed into the base, the dial gauge placed on it and fully compressed against the top platten. The dial gauge and volume change readings were noted and the sample was ready for testing.

The cell, complete with load transducer, was put on the base and secured. Taps a,b,c and d were opened and the cell filled with de-aired water. When water flowed out of tap d (cell full) tap a was closed and then taped. It was essential to close tap a before d otherwise the sample would have been subjected to a cell pressure equal to the natural head of the water system, in this case about 20 KN/m^2. The suction was then reduced to zero by readjusting control cylinder B and tap f was opened to bring the oil manometer into operation.

The next step was to check and adjust the levels in the mercury pots of the self compensating manometer to ensure they did not empty during a test. The cell pressure was then set to the desired value by adjusting the head difference H, and tap e opened. The sample was then allowed to consolidate under ambient pressure as shown in plate (6.3). Volume change and axial deformations were measured during consolidation.

When no further movement was detected, the loading piston was brought into contact with the top platten by adjusting the loading frame. The constant rate of strain motor was then started at a rate equal to about 2.5% compression per hour. Readings from the load transducer on the digital voltmeter, the dial gauge and volume change scale were read at

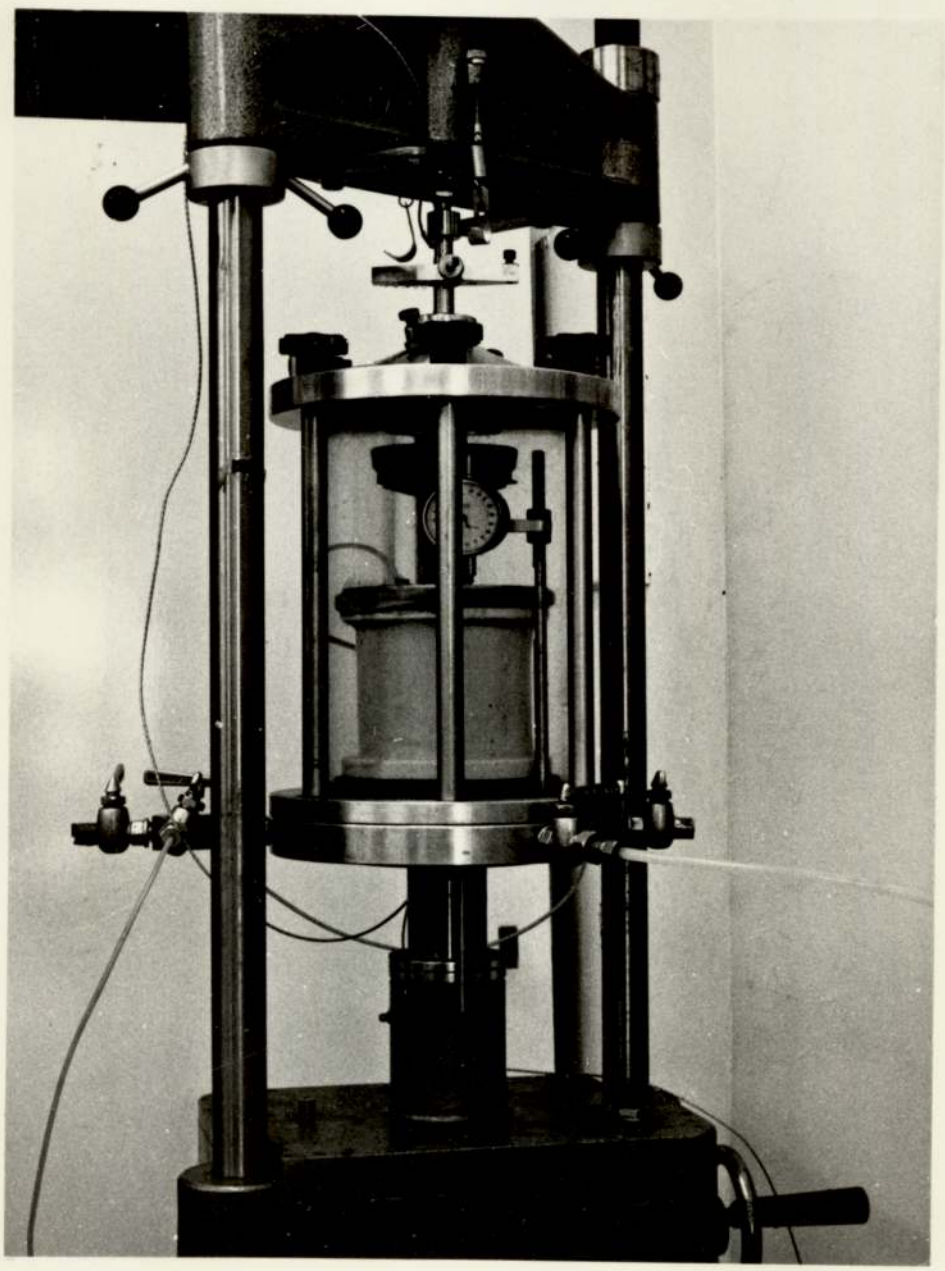

PLATE (6.3) THE ASSEMBLED CELL WITH THE SAMPLE UNDER AMBIENT PRESSURE

6.2.4) contd.

convenient intervals of strain. The test was stopped after the load transducer readings had dropped off or not increased for a long time. The load could then be removed, the cell water discharged to waste and the cell dismantled. The sand from the sample was carefully removed for weighing.

6.2.5) Corrections to Experimental Results.

The rubber membrane that encloses the sample in the cell contributes a small amount of strength that becomes significant when testing specimens at low pressures. The stiffness of the membrane was measured by the method suggested by Bishop and Henkel[9]. A circumferential strip of the membrane was hung between two glass rods which had been coated with French chalk to eliminate friction. The membrane was loaded by placing weights in a pan hung on the lower glass rod, and the extension measured with a vernier gauge. The compression modulus is assumed to be equal to the extension modulus in the correction factor and is calculated from,

$$M = \frac{\text{load per cm}}{\text{strain.}} \qquad (6.1)$$

The Author obtained an average value of 0.36 kg/cm. This was the value for membranes after they had been soaked in water. Fresh membrane had an average modulus 30% lower. The stiffness of the membrane meant that the vertical stress had to be increased by an amount σ_{cm} where;

$$\sigma_{cm} = \frac{4M\epsilon_1(1-\epsilon_1)}{Do} \quad , \qquad (6.2)$$

where Do is the original diameter of the sample, ϵ_1 is the major principal strain which is assumed to be vertical and M was defined in equation (6.1).

6.2.5) contd.

The weight of the top platten and load transducer were taken into account when calculating the vertical stress by a correction factor σ_{cw} in;

$$\sigma_{cw} = \frac{(W_{TP} + W_{LT})}{a} \quad , \qquad (6.3)$$

where W_{TP} is the weight of the top platten W_{LT} is the weight of the load transducer, and, a, the area of the sample.

The tip of the loading piston fitted neatly into the collar on top of the loading platten, so the cell pressure could not act over the whole top surface area. The full value of cell pressure was not used to calculate the vertical stress. The amount used was;

$$\sigma_c' = \left(1 - \frac{a_p}{a}\right) \sigma_c \qquad (6,4)$$

where a_p is the area of the loading piston and σ_c is the cell pressure.

The self compensating mercury manometer is connected to the base of the cell, therefore the cell pressure at the mid-height of the sample will be less than this. This correction becomes significant at very low pressure and is taken as;

$$\sigma_{cc} = - \gamma_w H_s \qquad (6.5)$$

where H_s is the height from the base to the mid-height of the sample.

No correction was made for the self weight of the sample and equation (6.4) was not modified in the manner described above, as the two different effects approximately cancel each other out.

6.2.6) Calculations.

The quantities recorded during the laboratory test were the axial deformation T, the scale readings of volume change S and the digital voltmeter reading L, which recorded the axial load. The major principal plane is assumed to be horizontal.

$$\epsilon_1 = \log_n(1 + T/H_o) \qquad (6.6)$$

where ϵ_1 is the major principal strain and H_o is the original height of the sample.

$$\epsilon_v = \log_n(1 + S.S_c/V_o) \qquad (6.7)$$

where ϵ_v is the volumetric strain, and S_c is the calibration factor for volume change and V_o is the original volume.

The minor principal strain can be calculated from;

$$\epsilon_3 = (\epsilon_v - \epsilon_1)/2 \qquad (6.8)$$

The major principal stress can be calculated from;

$$\sigma_1 = \frac{L.L_c}{a} + \sigma_3' + \sigma_{cw} + \sigma_{cm} \qquad (6.9)$$

where L_c is the calibration factor for the load transducer and a, the cross sectional area of the sample, is calculated from;

$$a = (V_o - S.S_c)/(H_o - T) \qquad (6.10)$$

The minor principal stress is calculated from;

$$\sigma_3 = \gamma_m H + \sigma_{cc} \qquad (6.11)$$

where γ_m is the density of mercury and H is the head difference.

A program was written to process the experimental data.

6.2.7) Results.

Five tests were carried out at different values of cell pressure to cover the expected range of initial stress conditions. The results are presented in Figure (6.3) as plots of major principal stress and, volumetric strain against the major principal strain. Some details about the tests are given in the table below.

TABLE (6.1)

Test No.	Cell Pressure KN/m^2	Stress Ratio at Failure	Porosity after Consolidation
1	5.23	5.0	40.5
2	9.99	4.4	39.9
3	14.74	3.5	40.2
4	19.74	3.5	40.5
5	25.68	3.3	39.9

Mohr's circle of stress is plotted in Figure (6.4) and this gave Coulombs $\phi' = 29°$ and an apparent cohesion $C' = 3\ KN/m^2$.

6.2.8) Discussion of Results.

The value of the principal stress ratio at failure at the higher cell pressures agrees with values quoted by other investigators testing at moderate pressures. The value of the angle of shearing resistance, also agrees with quoted values, and this seems little affected by the value of cell pressure. It can be seen from Table (6.1) that as the cell pressure decreases the value of R increases markedly. This can be explained by the apparent cohesion intercept giving an increased shear strength. The other departure from expected behaviour is shown in the volumetric strain. The samples all expanded almost from the start of shearing, whereas at moderate

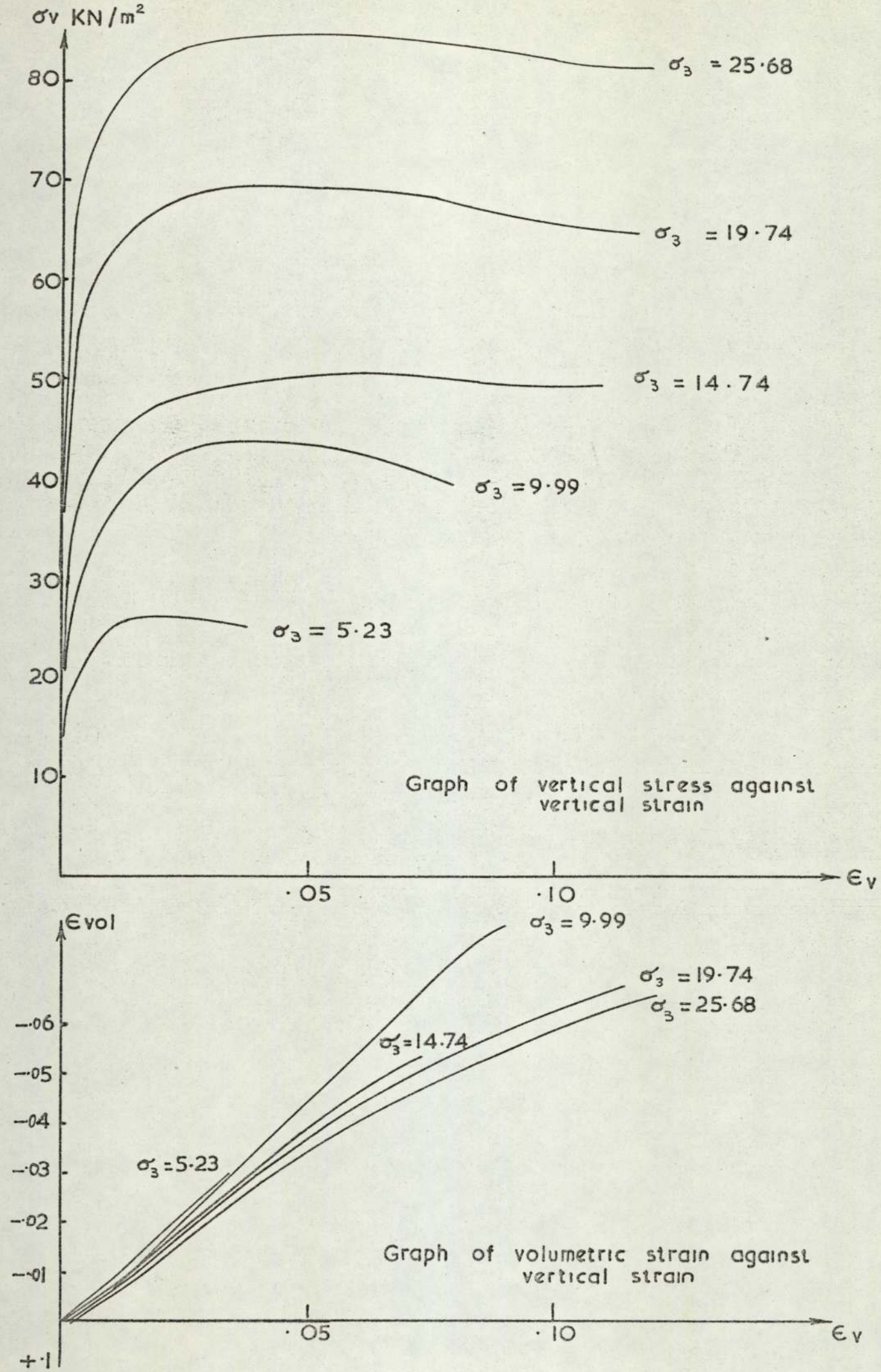
σv KN/m²
80
70
60
50
40
30
20
10
σ3 = 25·68
σ3 = 19·74
σ3 = 14·74
σ3 = 9·99
σ3 = 5·23
Graph of vertical stress against vertical strain
·05
·10
εv
εvol
σ3 = 9·99
σ3 = 19·74
σ3 = 25·68
σ3 = 14·74
σ3 = 5·23
-·06
-·05
-·04
-·03
-·02
-·01
+·1
Graph of volumetric strain against vertical strain
·05
·10
εv

Figure 6. 3

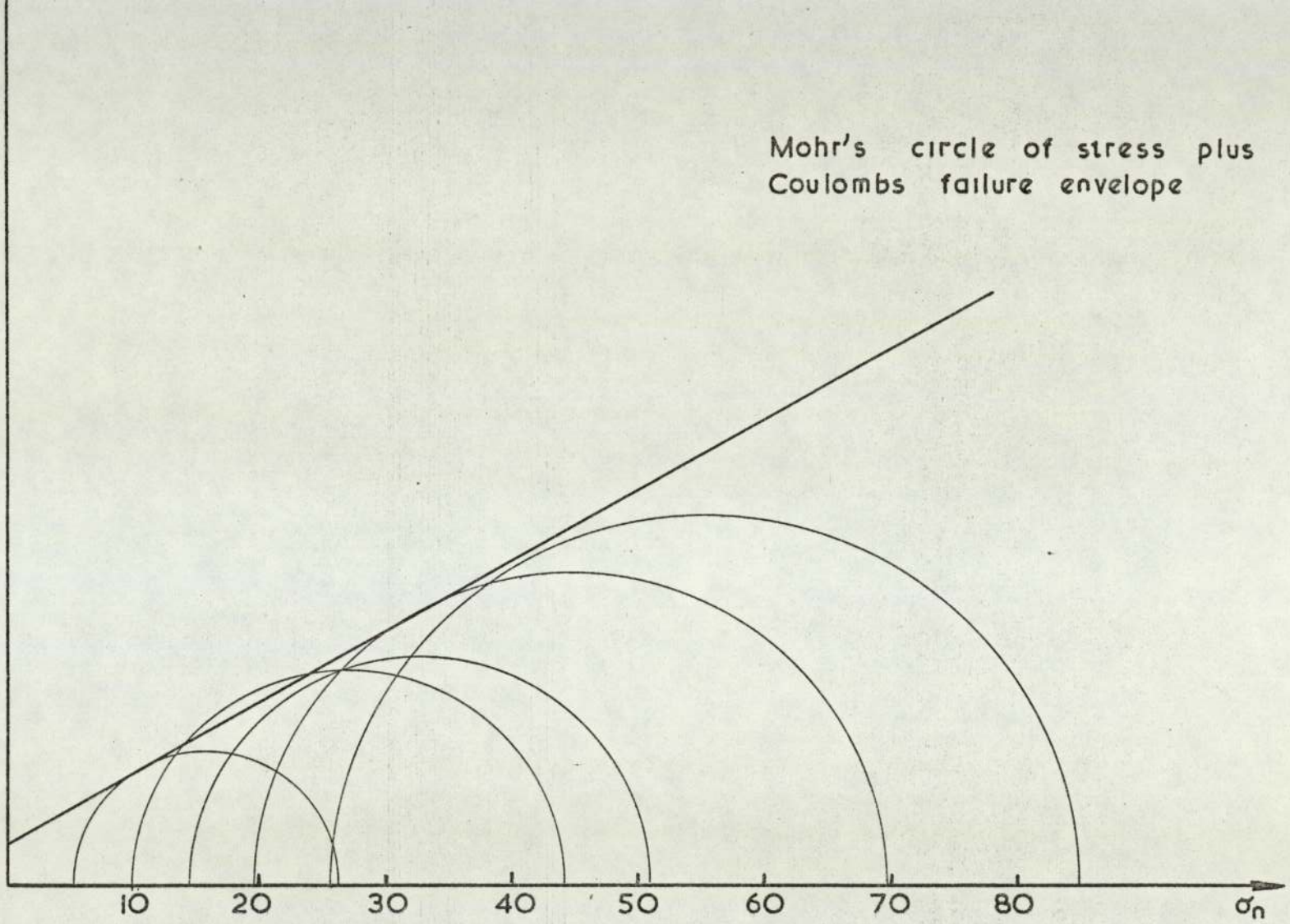
Mohr's circle of stress plus
Coulombs failure envelope
10
20
30
40
50
60
70
80
σ_n

Figure 6.4

6.2.8) contd.

pressures a loose sand would be expected to compress. Indeed, the volume change characteristics of loose sand at low pressure seem similar to those of a dense sand at moderate pressure. It can also be seen in Figure (6.3) that, as could be expected, increase in cell pressure decreases the volume change.

Ponce and Bell[70] who tested over a wide range of porosities and pressures obtained very similar results to those reported here. It was pointed out that the increase in strength at confining pressures below 5 psi was mainly due to the increased effect of the component of total strength associated with expansive volume change. The increase in dilatancy rate requires that more energy be spent during shear which causes a corresponding increase in the principal stress ratio at failure.

The result of the Mohr-Coulomb plot in Figure (6.4) was obtained by drawing the best straight tangent line through the circles, and this is why there is an apparent cohesion intercept. It is not plausible for a dry clean sand to have a cohesion, and so the Coulomb envelope is more likely in reality to pass through the origin. This agrees with the observations of other investigators and means in fact that the Coulomb envelope is curved near the origin, meaning that Coulomb's ϕ is much higher than stated, although the two quoted parameters provide a convenient way of expressing strength.

It is apparent from Figure (6.3) and the table in the previous Section, that Test 3 does not fit in with the pattern of the other tests. The Author would like to have repeated Test 3 and performed one more test at a lower pressure. Unfortunately the pressure on equipment in the

6.2.8) contd.

testing laboratory made this impossible. On reflection, it would have been better to have developed a method for preparing the samples in the testing laboratory, rather than removing the cell base. It can be seen from the table that the porosity varied and was slightly less than that measured in the test bed.

6.3) A Constitutive Relation.

Given the problem of analysing the model tests a constitutive relation is needed to govern the behaviour of the sand. There has been little research into the behaviour of sand under general three dimensional conditions and the choice of relations lies between the stress dilatancy laws or the assumptions of non-linear plasticity or elasticity.

The most scientifically appealing approach would be to use the stress dilatancy laws in conjunction with a Herzian elastic model[73] to predict the complete behaviour of slip and elastic strains under general conditions. The adaption of the model and the testing programme required to describe the model over a range of general conditions, is a project on its own.

The non-linear elasticity model has proved the most popular and was successfully used in Chapter (3) to analyse the plane strain compression test. In that analysis an actual experimental stress-strain curve was used to calculate the shear modulus and an almost constant value of Poisson's ratio was used. For the model tests described in Chapter (5) body forces will be important, so a relation is needed which can be described by differing initial stress levels. It must also be borne in mind that the relation should be able to be used in less ideal conditions than those that existed in the test bed,

6.3) contd.

such as, soils other than sand and non-homogeneous conditions.

Girijivallabhan and Reese[38] pointed out that the stress in a perfectly elastic material can be divided into two components, a hydrostatic stress accounting for volume change. and a deviatoric stress accounting for change in shape. The octahedral normal and shear stresses and strains are the best measure of these components. A soil composed of particles, however, experiences volume change during shear deformation. Both of these are dependent on normal and shear stress and could be found from a relation of the form;

$$\epsilon_{oct} = f_1(\sigma_{oct}, \tau_{oct}) \qquad (6.12)$$

$$\gamma_{oct} = f_2(\sigma_{oct}, \tau_{oct}) \qquad (6.13)$$

for a sand at a given porosity. This approach was then used to obtain a unique relation, over a small range of confining pressure, for τ_{oct}/σ_{oct} against γ_{oct}. The elastic modulus was obtained from this curve and a constant value of Poisson's ratio was assumed. A similar approach was used by Craig[20] and both he and Girijivallabhan[38] obtained good results. However, in the model tests here the scale is larger and a wider range of initial stress levels is expected.

Similar relations have been proposed by other investigators including Nelson and Baron[106] who proposed a relation of the form;

$$K = K_0 + K_1 \epsilon_{oct} + K_2 \epsilon_{oct}^2 \qquad (6.14)$$

$$G = G_0 + \gamma_1 \sigma_{oct} + \bar{\gamma}_1 \overline{J_2'} \qquad (6.15)$$

where J_2 is the second invariant of the stress deviator, similar to octahedral shear stress. To establish the constants required in the polynomial a relatively large number of tests are required. However, this relation is one of the very few

6.3) contd.

hypo-elastic relations which tries to take into account the fact that most soils dilate under shear.

The most popular and successful relationship has been that proposed by Kondner and Zelasko[56,57], when a hyperbola is used to represent the stress-strain curve. This approach has been studied by numerous investigators including Domaschuk and Wade[23] and used in conjunction with the finite element method by Kraft[59], Duncan[25], Clough[26] and Kulhawy[103]. It was also used by Smith and Kay[80] in conjunction with the stress dilatancy model. Apart from the simplicity of the curve, the great attraction is that few tests are needed to establish the parameters, and, that these parameters are of physical significance, namely the initial slope and the ultimate strength. These parameters can be related to initial stress conditions and porosity, enabling a complete description of behaviour to be formulated.

Kondner[55] showed that the hyperbola could also be applied to cohesive soils. Amendments to this relation have been proposed by Hansen[42] for use with cohesive soils, when the initial part of the curve is non-linear and strain softening occurs after peak.

In a recent paper by Desai[21] it was pointed out that despite its simplicity a hyperbola or one polynomial might not give a satisfactory representation over the entire stress range. It was shown , that the use of a spline function, which is made up of a number of polynomials, gave a better fit. For future improvements this type of relation looks rewarding but there is a considerable amount of testing and processing involved in obtaining the polynomials to cover a wide range.

6.3.1) Proposed Relation.

The soil response to an imposed stress system is best characterised by the use of a bulk and shear modulus each of which is associated with a separate physical component of behaviour. In terms of octahedral stress;

$$\tau_{oct} = G \ \gamma_{oct} \tag{6.16}$$

and

$$\sigma_{oct} = K \ \epsilon_{oct} \tag{6.17}$$

Under triaxial test conditions the octahedral stress and strain components can be obtained from;

$$\tau_{oct} = \sqrt{2}/3 \ (\sigma_1-\sigma_3) \tag{6.18}$$

$$\gamma_{oct} = 2\sqrt{2}/3 \ (\epsilon_1-\epsilon_3) \tag{6.19}$$

$$\sigma_{oct} = (\sigma_1+ 2\sigma_3)/3 \tag{6.20}$$

$$\epsilon_{oct} = \epsilon_v/3 \tag{6.21}$$

Equations (6.18) and (6.19) were used to calculate the experimental results and a plot of these is shown in Figure (6.5). It is clear from this figure that the resulting octahedral shear stress-strain response is highly non-linear and dependent on the initial stress level.

Kondner and Zelasko[56,57] proposed a hyperbolic response of the form

$$\sigma = \frac{\epsilon}{a+b\epsilon} \tag{6.22}$$

which is shown in Figure (6.6a). Differentiating equation (6.22) yields;

$$\frac{d\sigma}{d\epsilon} = \frac{a}{(a+ b\epsilon)^2} \tag{6.23}$$

and therefore at $\epsilon = 0$, $\frac{d\sigma}{d\epsilon} = \frac{1}{a}$ and hence, a is the reciprocal of the initial tangent modulus. Equation (6.22) can be rearranged into the form;

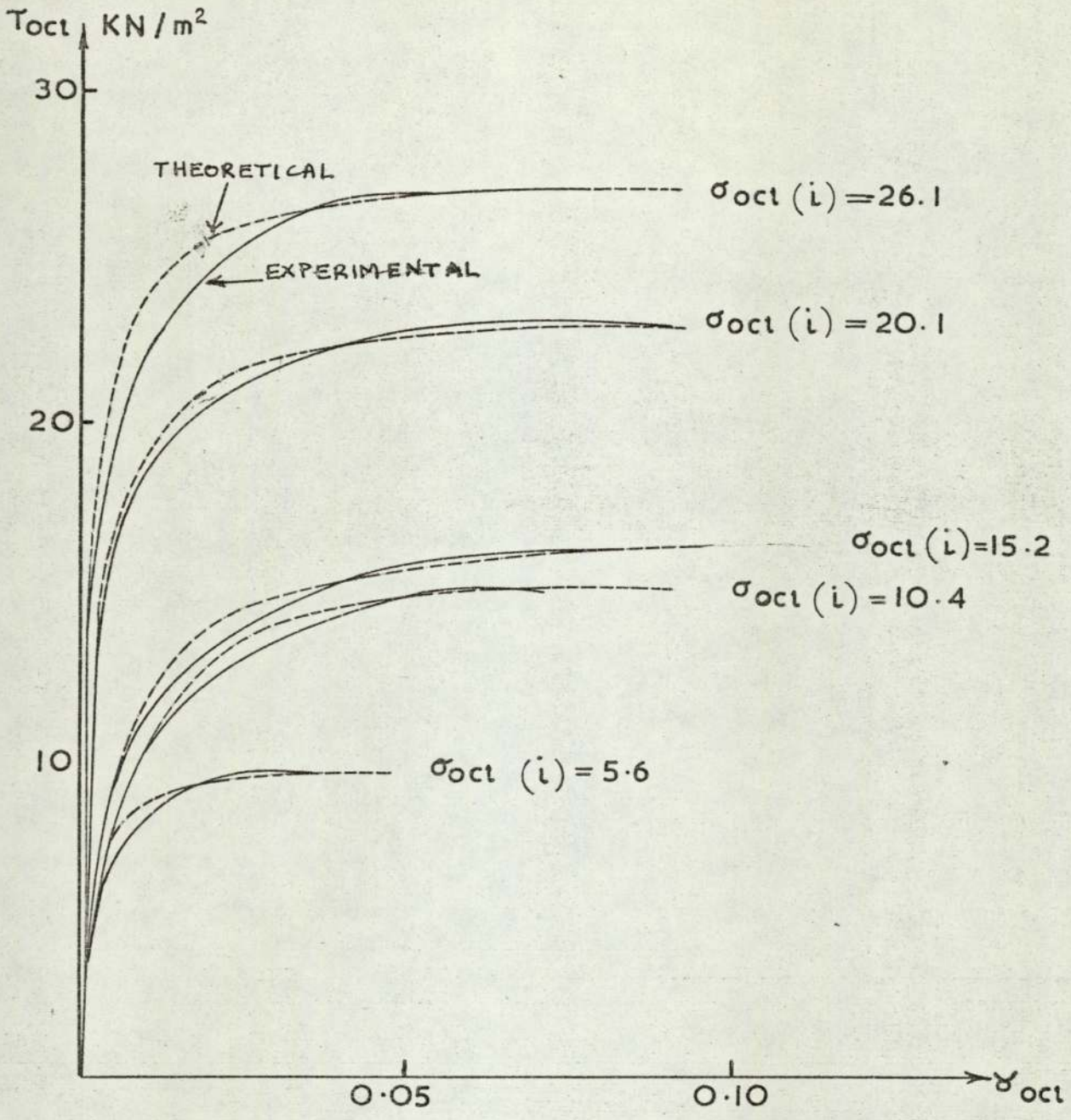

Figure 6.5 Graph of Toct against γoct showing theoretical and experimental curves

6.3.1) contd.

$$\sigma = \frac{1}{\frac{a}{\epsilon} + b} \tag{6.24}$$

Therefore $\lim_{\epsilon \to \infty}$, $\sigma = \frac{1}{b}$ and hence, b is the reciprocal of the ultimate value of stress reached.

The hyperbola in equation (6.22) can also be rearranged into the form;

$$\frac{\epsilon}{\sigma} = a + b\epsilon \tag{6.25}$$

which is the equation of a straight line,

$$y = c + mx \tag{6.26}$$

and this is shown in Figure (6.6b). The parameter a is the intercept on the $\frac{\epsilon}{\sigma}$ axis and b is the slope. As equation (6.22) can be transformed to a straight line statistical methods can be used to select the parameters a and b to give a 'best' fit over the entire range of experimental data.

It was pointed out by Kondner and Zelasko that theoretically the hyperbola will only reach the ultimate stress at infinity, so the relation must be rewritten as;

$$\sigma = \frac{\epsilon}{\frac{1}{E_i} + \frac{\epsilon}{K\sigma_f}} \tag{6.27}$$

where K is a factor, usually about 0.95, necessary to push the curve up to the asymptote at finite strain. If b is calculated from a transformed plot, as in Figure (6.6b), then this effect is already included. Kondner and Zelasko went on to propose that the parameters could be linked to initial conditions by linear equations of the form;

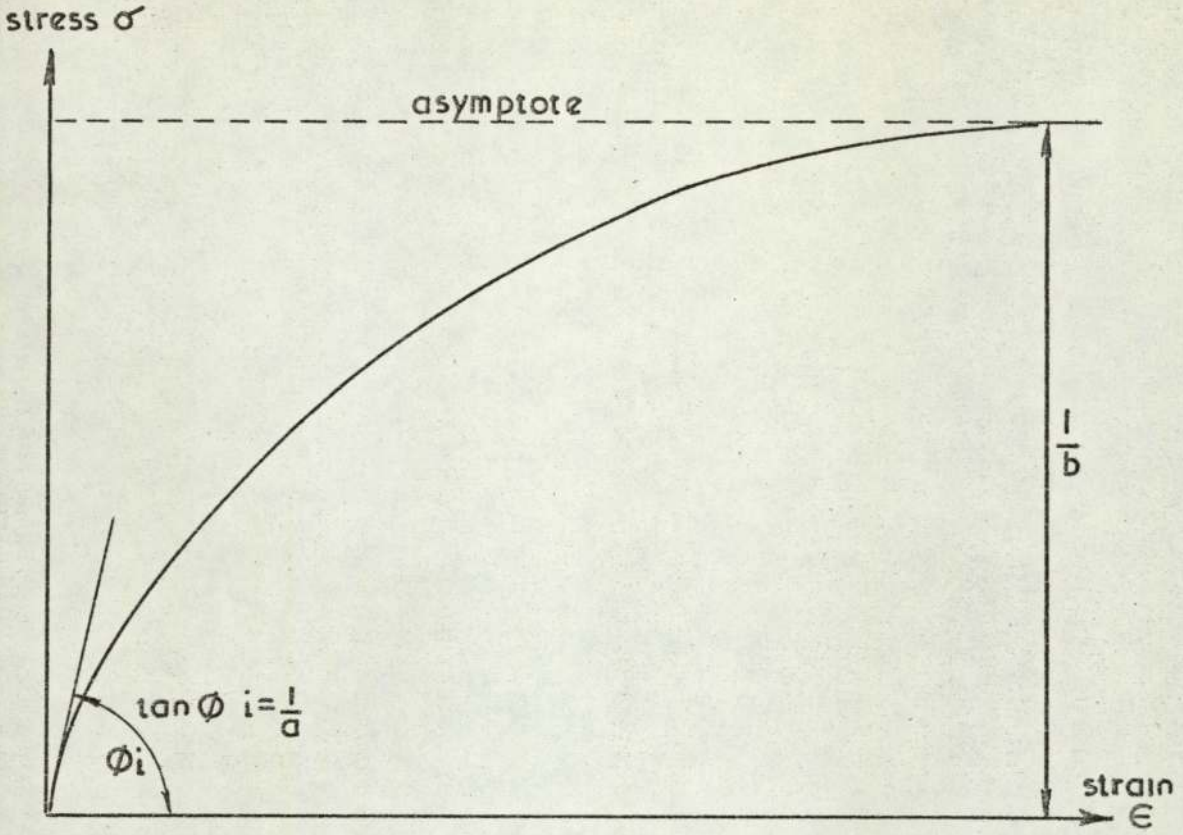

Figure 6.6 a. Rectangular hyperbolic representation of stress-strain

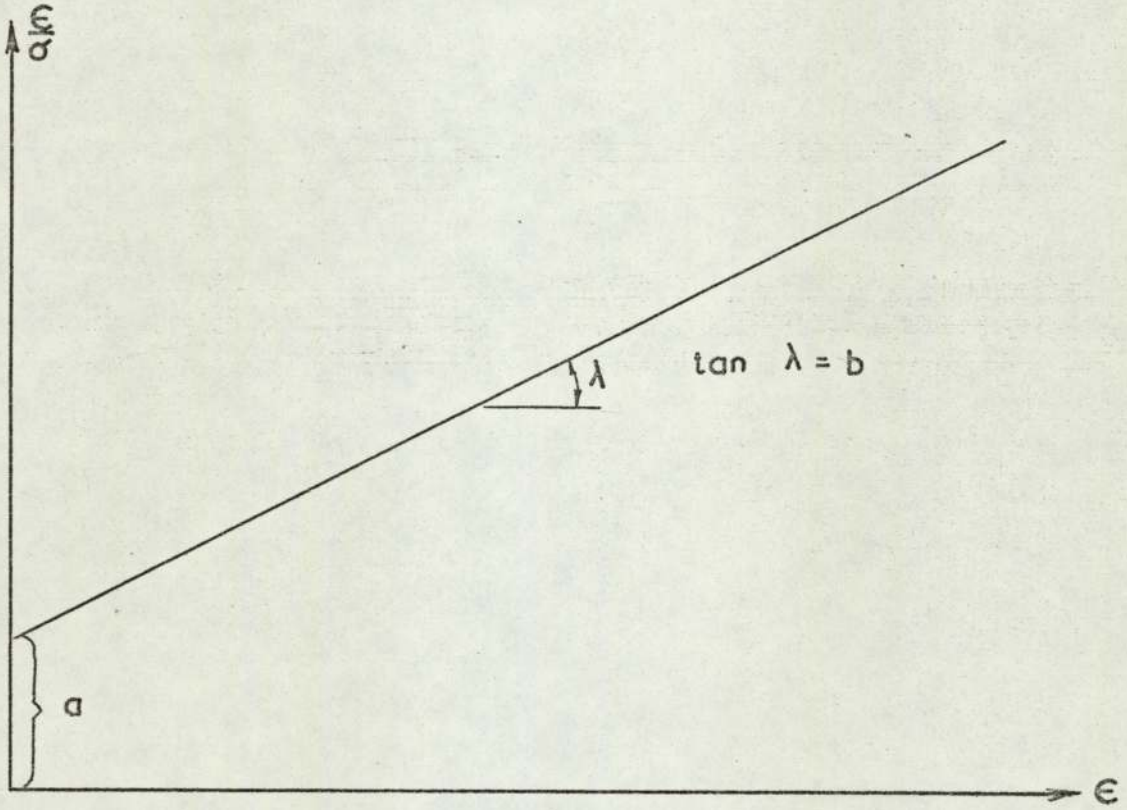

Figure 6.6. b. Transformed hyperbola

6.3.1) contd.

$$\frac{1}{a} = f_1(\sigma_{oct}, n) \tag{6.28}$$

and $$\frac{1}{b} = f_2(\sigma_{oct}, n) \tag{6.29}$$

where n is the initial porosity.

Domaschuk and Wade[23] rewrote equation (6.22) in the form

$$\tau_{oct} = \frac{\gamma_{oct}}{a + b\,\gamma_{oct}} \tag{6.30}$$

and this is the form required here. This equation can also be transformed to a straight line in the form

$$\frac{\gamma_{oct}}{\tau_{oct}} = a + b\,\gamma_{oct} \tag{6.31}$$

Using equation (6.31) a Gaussian least squares fit to the experimental data can be obtained from the equation;

$$y - \bar{y} = \frac{\mu_{11}}{Sx^2}(x - \bar{x}) \tag{6.32}$$

or, $$y = \frac{\mu_{11}}{Sx^2}x + \left(\bar{y} - \frac{\mu_{11}}{Sx^2}\bar{x}\right) \tag{6.33}$$

Hence $$a = \bar{y} - \frac{\mu_{11}}{Sx^2}\bar{x} \tag{6.34}$$

and $$b = \frac{\mu_{11}}{Sx^2} \tag{6.35}$$

where $$\mu_{11} = \frac{\sum_{i=1}^{n} x_i y_i - n\bar{x}\bar{y}}{n-1} \tag{6.36}$$

and $$Sx^2 = \frac{\sum_{i=1}^{n} x_i^2 - n\bar{x}^2}{n-1} \tag{6.37}$$

where $\bar{x}$ and $\bar{y}$ are the mean values of the n experimental points x_i and y_i. Equation (6.31) is a regression analysis of y on x and should only be used to estimate y from x. As

6.3.1) contd.

a check on the closeness of the fit, the correlation coefficient can be calculated from;

$$r = \frac{\mu_{11}}{Sx\ Sy} \tag{6.38}$$

where $$Sy^2 = \frac{\sum_{r=1}^{n} y_i^2 - n\bar{y}}{n - 1} \tag{6.39}$$

when, r = 1 this is perfect positive correlation, that is to say all points lie on a straight line of positive slope.

A program was written to carry out the analysis described above and applied to the experimental data in Figure (6.5), when the following parameters were obtained.

Test No.	a cm^2/kg	b cm^2/kg	r
1	0.04041	10.000	0.9976
2	0.02223	6.173	0.9991
3	0.01818	5.814	0.9995
4	0.00952	4.167	0.9997
5	0.00585	3.546	0.9996

TABLE (6.2)

From the above table it can be seen that very good correlation was obtained. The parameters in the table were used to predict the shape of stress-strain curve and compared with the experimental result in Figure (6.5). This figure shows that reasonable agreement was obtained, the maximum difference being about 7.5%. The experimental result is tending to curve more gently than the hyperbola, and this is probably the result of assuming the first part of the curve to be linear.

The parameters $^1/a$ and $^1/b$ are plotted against the initial octahedral stress in Figures (6.7a) and (6.7b)

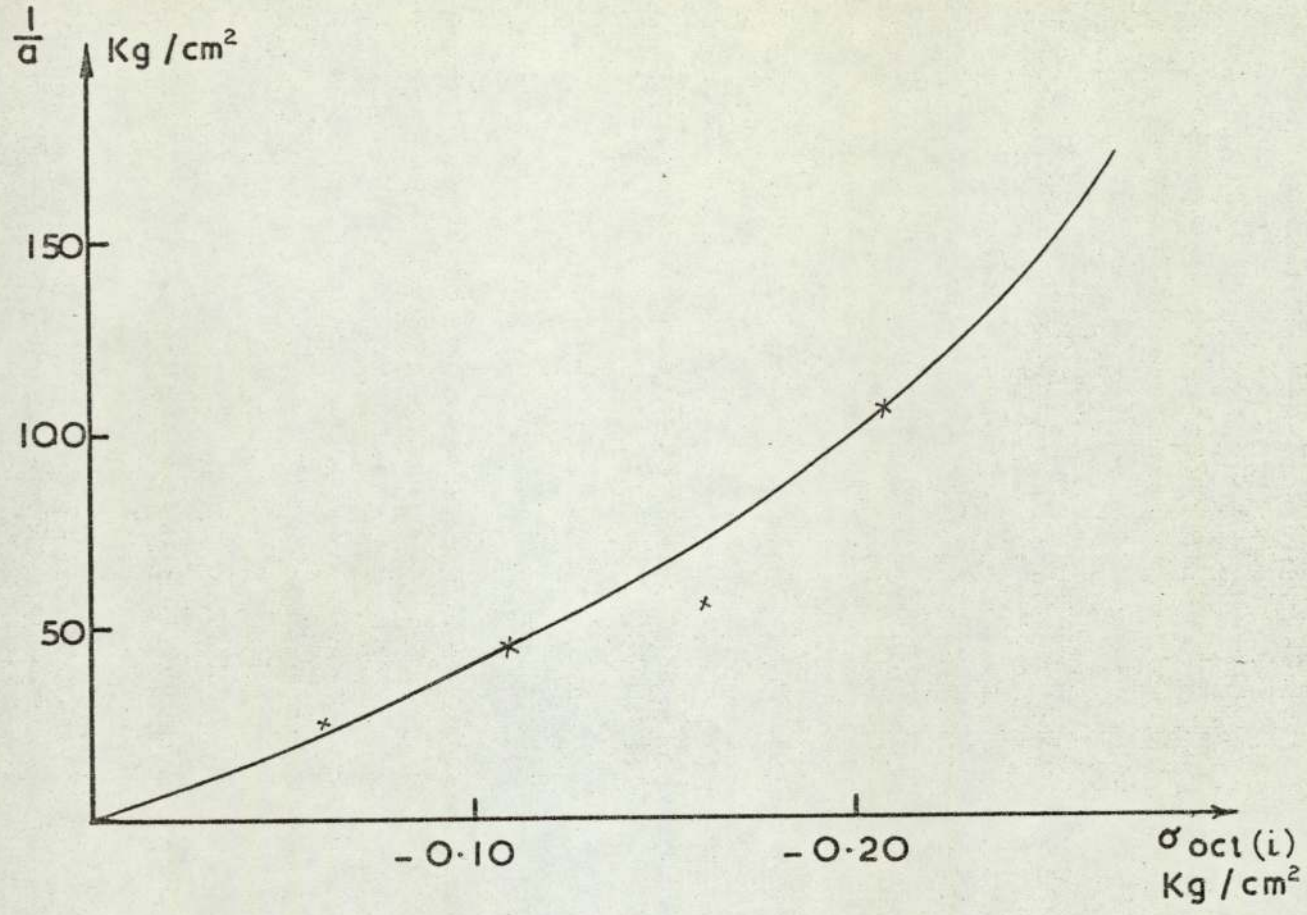

Figure 6.7 a

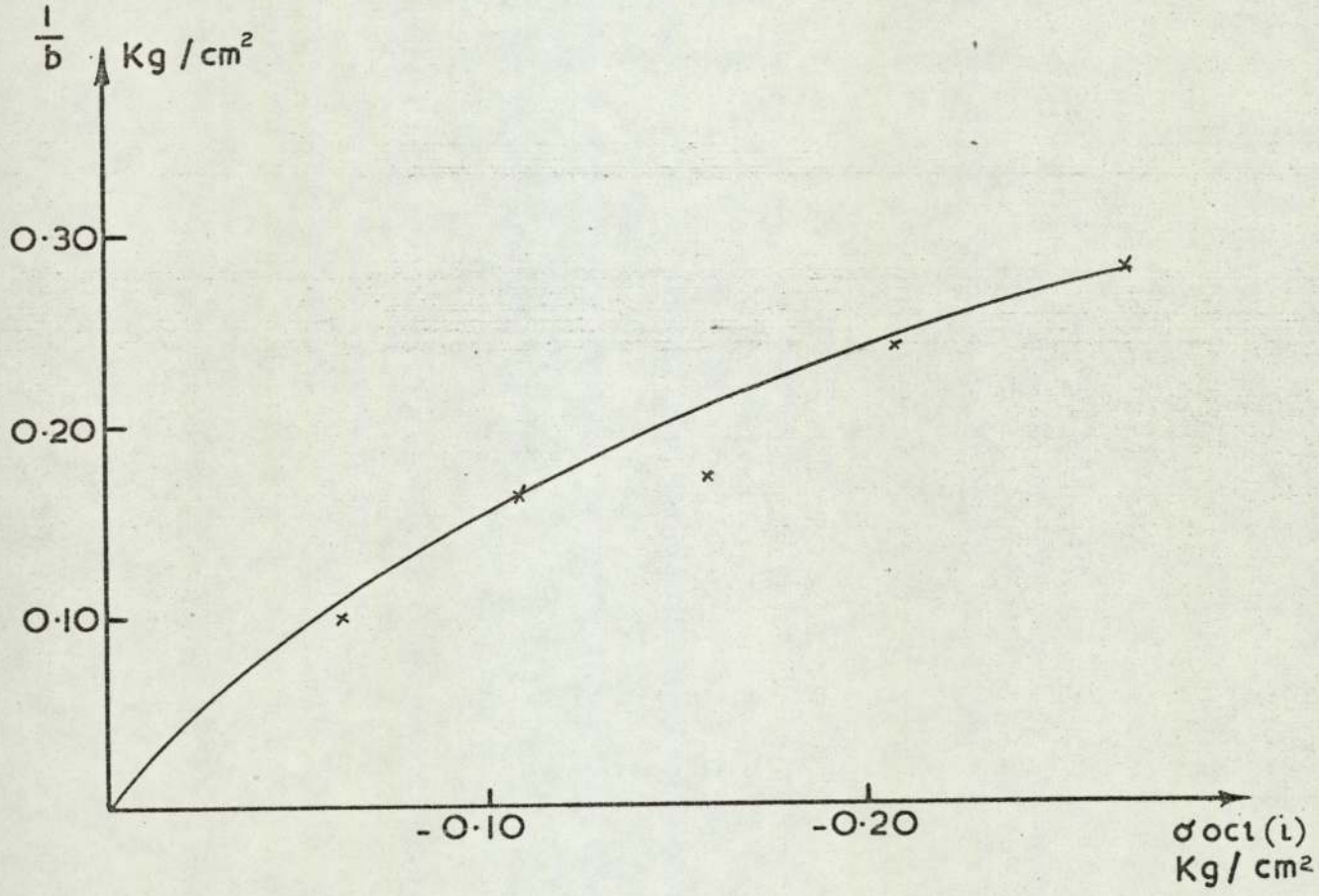

Figure 6.7 b

6.3.1) contd.

respectively. Both curves are drawn through the origin because without an initial octahedral stress the sand sample cannot exist. The linear relations proposed by Kondner and Zelasko[56,57] in equations (6.28) and (6.29) obviously do not hold at low stress levels. It is worth noting that Figure (6.7b) is a failure criteria for this sand, which is very similar to the generalised Mohr-Coulomb hypothesis proposed by Drucker and Prager[24].

The other pseudo-elastic modulus, K, the bulk modulus, was measured under conditions of hydrostatic stress, that is during the consolidation stage. For each of the five tests the volumetric strain resulting from consolidation is plotted against the consolidation pressure (equal to the initial octahedral normal stress) in Figure (6.8). Domaschuk and Wade[23] proposed an exponential relation but it can be seen from the figure that the relationship is reasonably linear over this range of pressure. A single value of bulk modulus was calculated using equations (6.17) and (6.21). The value obtained from Figure (6.8) is about 20×10^3 KN/m^2.

It is clear that this gives a much higher value of bulk modulus than shear modulus, from Table (6.2) that the initial value of shear modulus for test 1 is about 0.5×10^3 KN/m^2. Assuming isotropy the value of Poisson's ratio can be calculated from;

$$V = (3K-G)/(G+6K) \qquad (6.40)$$

and using the above values in this equation, a value of ν of about 0.42 is obtained. It can be seen from equation (6.40) that as the value of G, the shear modulus, decreases, Poisson's ratio becomes equal to 0.5. Values of Poisson's

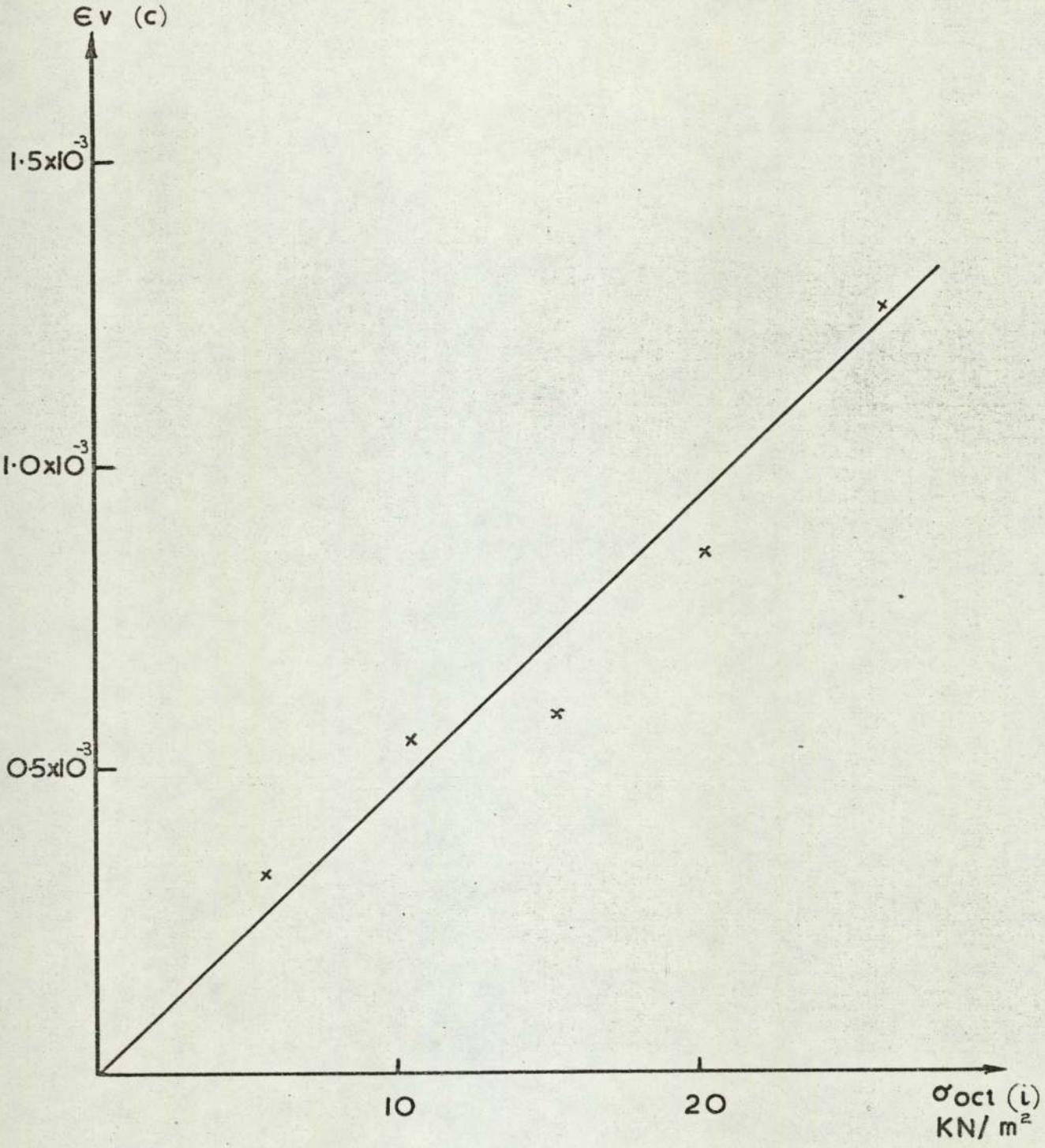

Figure 6.8 Graph of volumetric strain during consolidation against the consolidation pressure.

6.3.1) contd.

ratio near 0.5 gives rise to difficulties in the finite element method, because the bulk modulus becomes infinite, and for this reason it was decided to use a constant value of $\nu = 0.45$.

CHAPTER 7

THEORETICAL ANALYSIS OF COMPLETE THREE DIMENSIONAL STRUCTURES.

7.1) Introduction.

This chapter describes the procedure followed to analyse space frames together with their underlying foundation soils. Some detail is given of the main analysis program and of the mathematical model.

7.2) General Procedure.

The complete procedure that was followed in an analysis is shown in flowchart (7.1). It consisted of a number of steps, which wherever possible were automated.

As in any other problem the first step was to decide exactly what the problem was. This was followed by laboratory testing of the various materials both in the structure and the foundation. In the case of the latter this involved triaxial testing of the soil at the right porosity and confining pressure. These triaxial test results were then used to form an outline constitutive relationship. In this case, the two parameters a and b necessary to describe the Kondner hyperbola were derived from a statistical least squares fit from the transformed hyperbola of the experimental results. These two parameters were related to conditions of initial stress forming a comprehensive stress-strain relationship as described in Section (6.3).

The next step was to create the finite element data. In the large amount of data required for a three dimensional mesh there were bound to be errors and these were checked for using a program which collated the geometrical and topological data.

The corrected finite element data was used in a body force analysis program which computed the initial octahedral normal stresses at the centre of each hexahedral

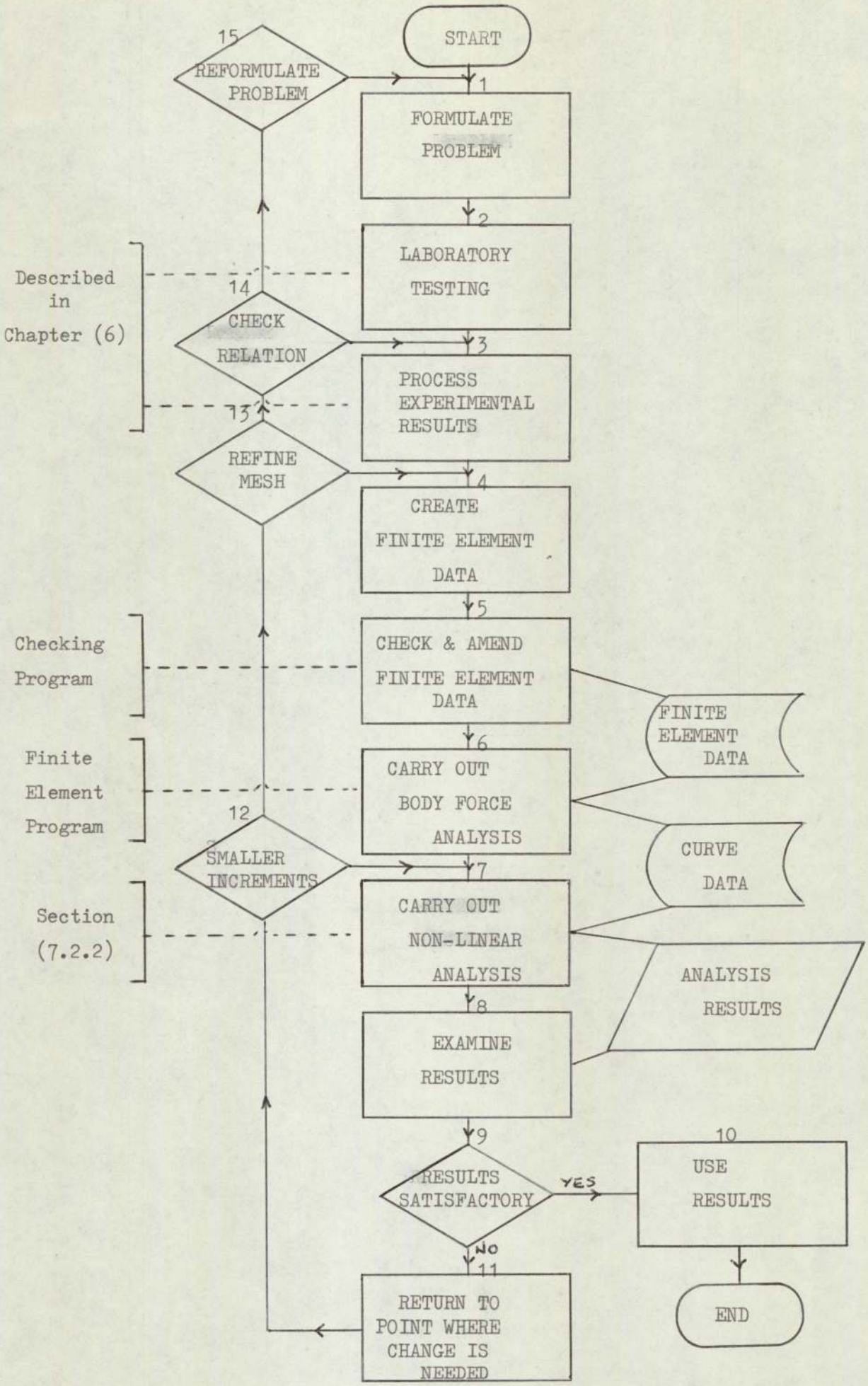
START
1
FORMULATE PROBLEM
2
LABORATORY TESTING
3
PROCESS EXPERIMENTAL RESULTS
4
CREATE FINITE ELEMENT DATA
5
CHECK & AMEND FINITE ELEMENT DATA
6
CARRY OUT BODY FORCE ANALYSIS
7
CARRY OUT NON-LINEAR ANALYSIS
8
EXAMINE RESULTS
9
RESULTS SATISFACTORY
YES
NO
10
USE RESULTS
END
11
RETURN TO POINT WHERE CHANGE IS NEEDED
12
SMALLER INCREMENTS
13
REFINE MESH
14
CHECK RELATION
15
REFORMULATE PROBLEM
FINITE ELEMENT DATA
CURVE DATA
ANALYSIS RESULTS
Described in Chapter (6)
Checking Program
Finite Element Program
Section (7.2.2)

7.2) contd.

element. The results of this analysis were used to calculate the values of the parameters a and b for each element from the curves illustrated in Figure (6.7). This body force analysis served another important purpose by establishing the accuracy of the mesh. This was possible because the vertical stress could be hand calculated at certain points and compared to the computed values.

The output from the body force analysis together with the finite element data file formed the complete input to the non-linear analysis program which was then run. The results of the non-linear finite element analysis program were checked by scrutinising the accuracy of known stresses and loads.

If the results were satisfactory then the analysis was complete, if not a decision would have to be made concerning what changes were necessary. If the tolerance of fit to the stress-strain relation were not good it could be simply a matter of changing the number and size of the applied load increments. Other possibilities could be refining or amending the finite element mesh, changing the stress-strain relation, or, in the extreme reformulating the problem.

7.2.1) Non-Linear Incremental Program.

This program in the main consisted of the following finite elements that are described in Appendix (2).

(i) Space member element, Section (A2.2.1)

(ii) Rectangular plate bending element, (Section (A2.2.2)

(iii) 8 noded, linear hexahedral isoparametric element, (Section (A2.2.3)

The linear hexahedral element was chosen instead of the

7.2.1) contd.

more desirable 20 noded quadratic element because of the problem involved in storing the stiffness matrix. From the results of Chapter (2) it is clear that for the same number of joints the quadratic element gives a more accurate result compared to that of the linear element. However, the connectivity in a 20 noded element is far greater than that in a linear element which gives rise to a much larger bandwidth for the same number of nodes. Another disadvantage of the 20 noded element is that distributed loads can only be applied around the edges of faces. This fault is not as serious with the linear element because the mesh is finer. This also leads onto the fact that the rectangular plate bending element, could not be matched to the twenty noded element without allowing a discontinuity in the mesh. The quadratic Lagrangian element would avoid these problems but the degree of connectivity with 27 nodes is even higher leading to a still larger bandwidth. From the results of the comparison of the various two dimensional elements in Chapter (2), it can be expected that, for a medium fine mesh, the stresses should be underestimated by not more than 5%. This is for the case of a mesh consisting of linear elements. When this accuracy is considered beside the various assumptions inherent in the constitutive relationship, it should prove adequate.

The model structure itself could be represented using the two structural elements in items (i) and (ii) above. The member elements idealising the frame and the plate bending element the pad footings.

The program was created by joining together the various subroutines of each of the elements in items (i),(ii)

7.2.1) contd.

and (iii) and the various ancillary operations required by the finite element method. The subroutines were, with one exception, unchanged. The exception was that the elasticity matrix in the subroutine forming the stiffness terms of the isoparametric element had to be changed. This was because the shear modulus G and Poisson's ratio ν had been chosen to represent the hypo-elastic behaviour in Chapter (6). The elastic matrix $\underline{D}$ became;

$$\underline{D} = \frac{2G}{(1-\nu)(1-2\nu)} \begin{bmatrix} (1-\nu) & \nu & \nu & 0 & 0 & 0 \\ \nu & (1-\nu) & \nu & 0 & 0 & 0 \\ \nu & \nu & (1-\nu) & 0 & 0 & 0 \\ 0 & 0 & 0 & \frac{1-2\nu}{2} & 0 & 0 \\ 0 & 0 & 0 & 0 & \frac{1-2\nu}{2} & 0 \\ 0 & 0 & 0 & 0 & 0 & \frac{1-2\nu}{2} \end{bmatrix}$$

The program required a new master segment to handle the various input/output facilities, assign initial values and initiate the incremental analysis. A further subroutine, called CONTROL, carried out the extra operations necessitated in following a non-linear incremental analysis. Further details of this routine are given later.

Initially the subroutine CONTROL had been written to control an iterative procedure identical to that used successfully in Chapter (3), where the relative merits of the incremental and iterative processes was discussed. Initial runs using the iterative process proved extremely lengthy with convergence taking place very slowly. This was particularly the case at the low stress levels. A tolerance level of 5% had been chosen and although almost all the elements were

7.2.1) contd.

near this accuracy after one iteration, a further 20 iterations were required to force all the elements within the 5% band. Examination of the various iterations revealed that this was due to the fact that the slope of the stress/strain curve was changing very gently, particularly near the origin where it was almost constant. It was therefore decided to adopt an incremental method as a reasonable alternative for operating on the relatively soft stress/strain curves used. The procedure followed by an incremental analysis was illustrated in Figure (3.1a). A value of the tangent modulus is calculated at the current strain level to represent the hypo-elastic modulus over the next increment of load. This means that the modulus is always too large, and the amount of error this leads to will depend upon the size of the load increment and the degree of curvature of the stress-strain curve. A check was kept upon the closeness of the calculated stresses to the stress/strain curve.

The procedure followed by the non-linear incremental analysis program is shown in flowchart (7.2). The corrected finite element data was read into the program and stored, as was the data containing the two curve parameters for each element. From the element topology the various control arrays, concerning positioning within the stiffness matrix and the division of the stiffness matrix for the solution procedure, were computed. These arrays were computed before the incremental applied loads were read in. The incremental load vector was thus formed at the same time as the data was read. At this stage the initial value of the shear modulus was also set from the inversion of the first curve parameters as;

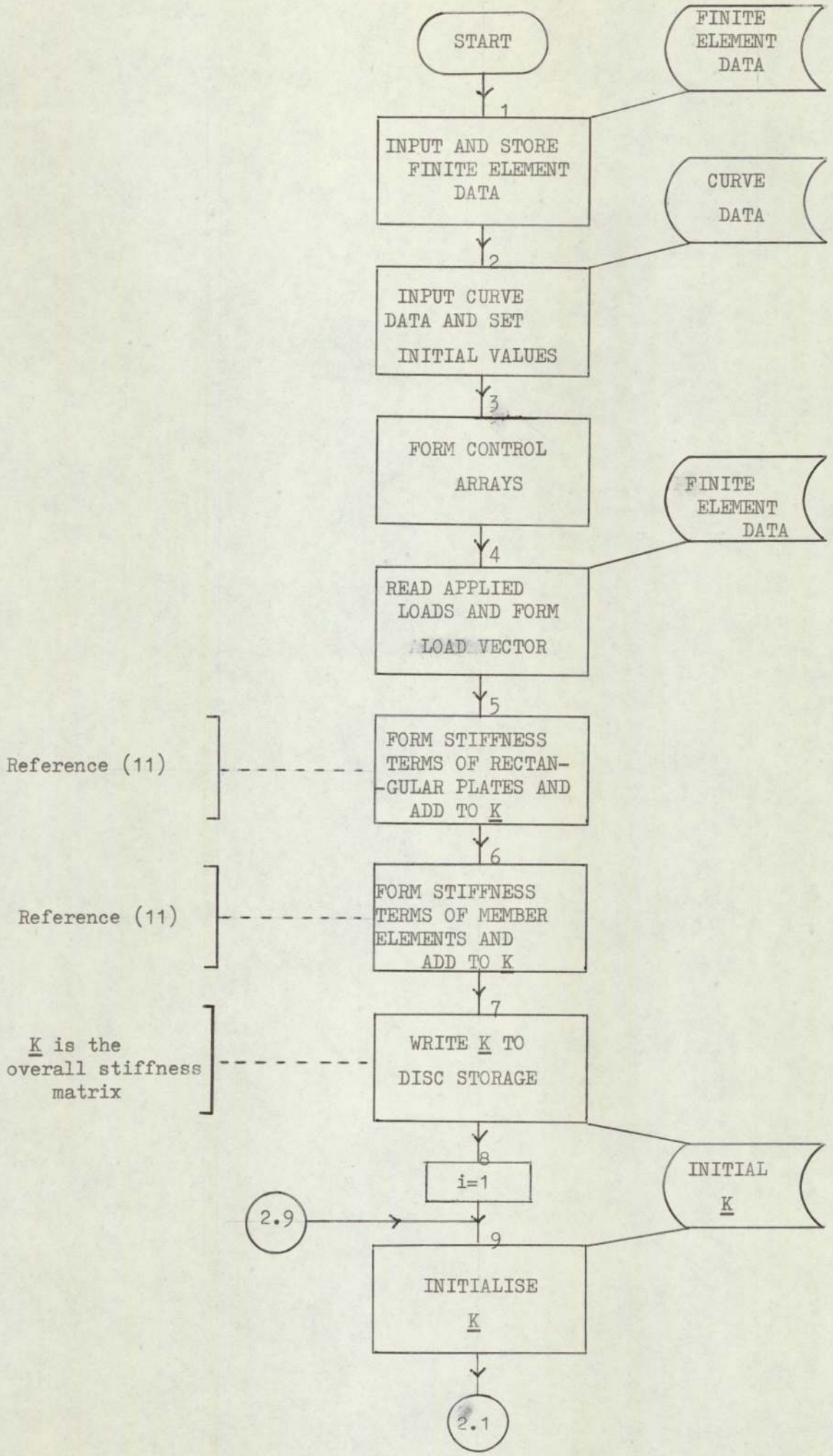
START
FINITE ELEMENT DATA
1
INPUT AND STORE FINITE ELEMENT DATA
CURVE DATA
2
INPUT CURVE DATA AND SET INITIAL VALUES
3
FORM CONTROL ARRAYS
FINITE ELEMENT DATA
4
READ APPLIED LOADS AND FORM LOAD VECTOR
5
Reference (11)
FORM STIFFNESS TERMS OF RECTANGULAR PLATES AND ADD TO K
6
Reference (11)
FORM STIFFNESS TERMS OF MEMBER ELEMENTS AND ADD TO K
7
K is the overall stiffness matrix
WRITE K TO DISC STORAGE
8
i=1
INITIAL K
2.9
9
INITIALISE K
2.1

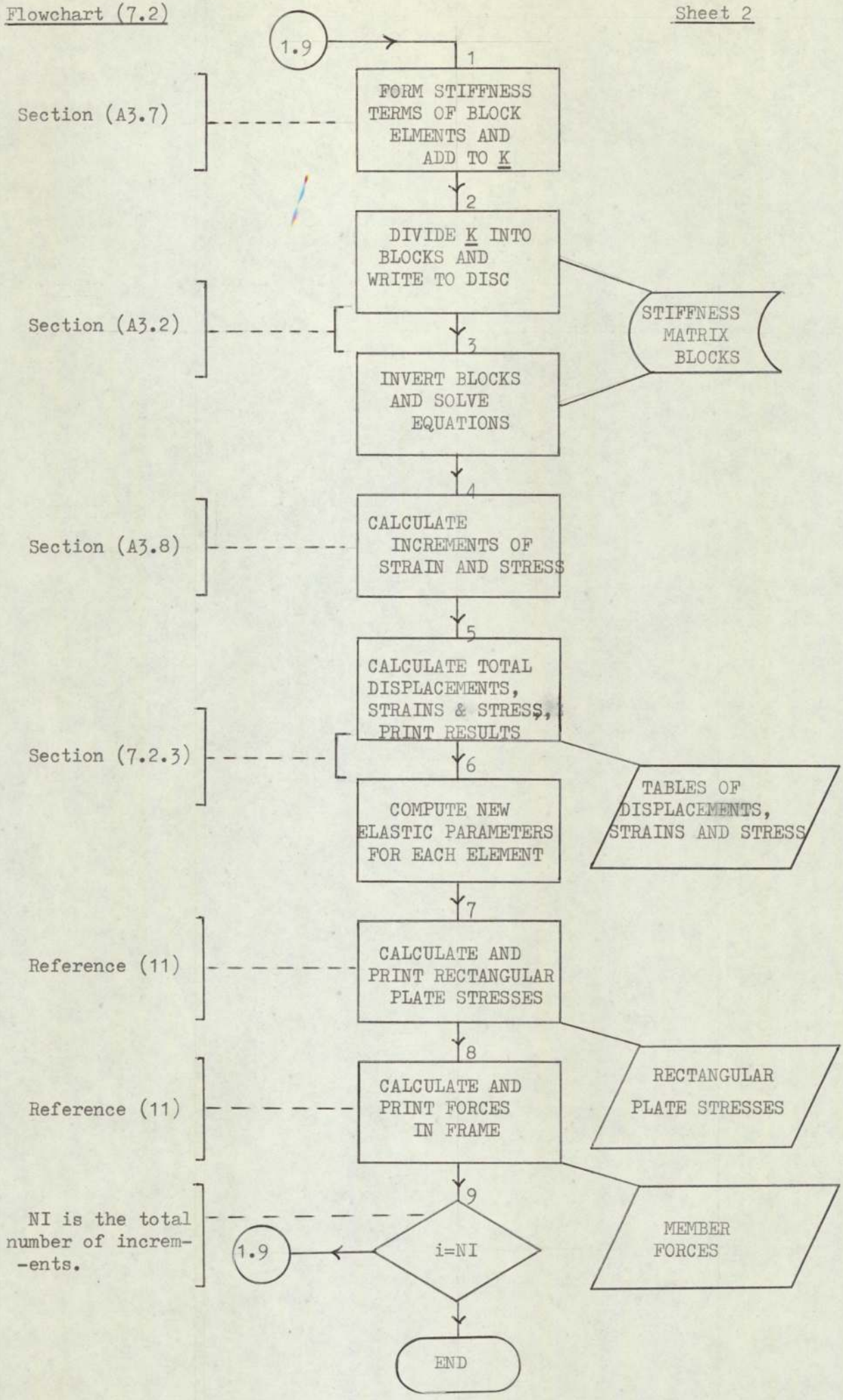
1.9
1
FORM STIFFNESS TERMS OF BLOCK ELMENTS AND ADD TO K
Section (A3.7)
2
DIVIDE K INTO BLOCKS AND WRITE TO DISC
STIFFNESS MATRIX BLOCKS
Section (A3.2)
3
INVERT BLOCKS AND SOLVE EQUATIONS
4
CALCULATE INCREMENTS OF STRAIN AND STRESS
Section (A3.8)
5
CALCULATE TOTAL DISPLACEMENTS, STRAINS & STRESS, PRINT RESULTS
Section (7.2.3)
6
TABLES OF DISPLACEMENTS, STRAINS AND STRESS
COMPUTE NEW ELASTIC PARAMETERS FOR EACH ELEMENT
7
CALCULATE AND PRINT RECTANGULAR PLATE STRESSES
Reference (11)
8
RECTANGULAR PLATE STRESSES
CALCULATE AND PRINT FORCES IN FRAME
Reference (11)
9
MEMBER FORCES
NI is the total number of increm--ents.
i=NI
1.9
END

7.2.1) contd.

$$G_i = \frac{1}{A_i}.$$

Here G_i is the initial value of the shear modulus and A_i the first curve parameter of element i.

The next step was to calculate the stiffness terms of the rectangular plate elements and to add them into the overall stiffness matrix. The same operations were then performed for the space member element. Because the structural elements remain in the elastic range their stiffness terms remain constant. These terms could be constructed once, written onto disc storage and then used repeatedly.

The first step in an increment was to initiate the stiffness matrix. The stiffness terms of the hexahedral elements were then computed using the current values of the pseudo-elastic parameters, and added into the stiffness matrix. The details of forming the stiffness matrix and solving the simultaneous equations are given in Appendix (3). The incremental displacements $\delta\{X\}$ were obtained from:

$$\delta\{X\} = \underline{K}^{-1} \delta\{L\} \quad , \qquad (7.1)$$

where $\underline{K}$ is the overall stiffness matrix and $\delta\{L\}$ the applied incremental load vector.

The incremental strains and stresses could then be calculated by the usual finite element procedures

$$\delta\{\epsilon\} = \underline{B}\,\delta\{X\} \qquad (7.2)$$

$$\delta\{\sigma\} = \underline{D}\,\delta\{\epsilon\} \qquad (7.3)$$

The subroutine CONTROL calculated the total components of displacement, strain and stress by keeping a running total. From these the octahedral shear components were

7.2.1) contd.

computed and used to calculate the new values of the shear modulus for each element. The final operation in this routine was to print the summed results. The last operation was to calculate and print the stresses and moments in the rectangular plate elements and the forces in the space member element.

If all the required increments had been computed then the analysis would finish, otherwise, the program would return for the next increment.

7.2.2) Subroutine Control.

This subroutine was written especially for the incremental analysis program and calculated the elastic parameters for each new increment. The input to the routine consisted of the incremental displacements, strains and stresses calculated earlier in the program and which were first summed to obtain the values of the total components.

$$\{X\}_i = \{X\}_{i-1} + \delta\{X\}_i \quad , \qquad (7.4)$$

$$\{\epsilon\}_i = \{\epsilon\}_{i-1} + \delta\{\epsilon\}_i \quad , \qquad (7.5)$$

and

$$\{\sigma\}_i = \{\sigma\}_{i-1} + \delta\{\sigma\}_i \quad . \qquad (7.6)$$

where $\{X\}_i$ and $\{X\}_{i-1}$ are total components of displacement respectively after and before the i^{th} increment of load and $\delta\{X\}_i$ is the incremental displacement due to the i^{th} load increment. $\{\epsilon\}$ and $\{\sigma\}$ are components of strain and stress.

From these Cartesian components of strain and stress the octahedral shear strain and stress components were calculated at the centre of each element. These are:

7.2.2) contd.

$$\gamma_{oct} = \frac{2}{3}\left\{ (\epsilon_x-\epsilon_y)^2 + (\epsilon_y-\epsilon_z)^2 + (\epsilon_z-\epsilon_x)^2 + \frac{3}{2}(\gamma_{xy}^2 + \gamma_{yz}^2 + \gamma_{zx}^2)\right\}^{1/2} \quad (7.7)$$

$$\tau_{oct} = \frac{1}{3}\left\{(\sigma_x - \sigma_y)^2 + (\sigma_y - \sigma_z)^2 + (\sigma_z - \sigma_x)^2 + 6(\tau_{xy}^2 + \tau_{yz}^2 + \tau_{zx}^2)\right\}^{1/2} \quad (7.8)$$

The accuracy with which the analysis was following the theoretical stress-strain curve could be assessed by comparing the value τ_{oct} calculated above with that value lying on the curve for the same value of γ_{oct}. The theoretical value can be calculated from the hyperbolic relation:

$$\tau'_{oct} = \frac{\gamma_{oct}}{a + b\,\gamma_{oct}} \quad (7.9)$$

where a and b are the two curve parameters. The accuracy can be calculated from

$$A_c = \frac{\tau'_{oct} - \tau_{oct}}{\tau'_{oct}} \quad (7.10)$$

The value of the shear modulus G for the next increment of load was calculated from;

$$G = \frac{a}{(a + b\,\gamma_{oct})^2} \,. \quad (7.11)$$

This equation is obtained by differentiating the hyperbolic relation with respect to γ_{oct} which gives the tangent modulus. The above procedures were carried out for all the block elements.

7.3) Finite Element Analysis of the Smaller Space Frame Model.

Details of the stress-strain relationship data have already been fully described in Chapter (6) and the previous sections. The model tests were all loaded at the mid-depth of the structure, and this symmetry was used to simplify the finite element data.

The finite element mesh used to represent the sand is shown in Figure (7.1). The mesh was symmetric about the centre line. For simplicity therefore only half of the actual mesh is shown. It can be seen from the figure that the mesh was refined close to the pad footings, where the greatest stresses could be expected. The representation of the model structure is illustrated in Figure (7.2). The complete mesh consisted of 205 nodes, 114 hexahedral elements, 8 rectangular plate bending elements, 9 space member elements, with a total of 527 degrees of freedom. All the outer boundaries, except the upper surface which was free, were assumed to be smooth and rigid. In the tests, sand paper had been glued to the underside of the pad footings. It was therefore assumed that the sand and footing remained in contact and no sandwich elements were required.

The four load cases corresponding to the four experimental positions of the applied load were analysed. The four cases were, X = 0, 0.33, 0.67 and 0.91. Each load case was achieved by changing the geometry of the loaded joint shown in Figure (7.2). The value of the applied load increment varied from 12 to 18.5 kg according to the load case. The number of increments was kept constant at 15. Tests revealed that increasing the number of increments beyond this figure had little or no effect on the results.

All the non-linear finite element analyses were performed on the ICL 1906A computer at the Atlas Computer

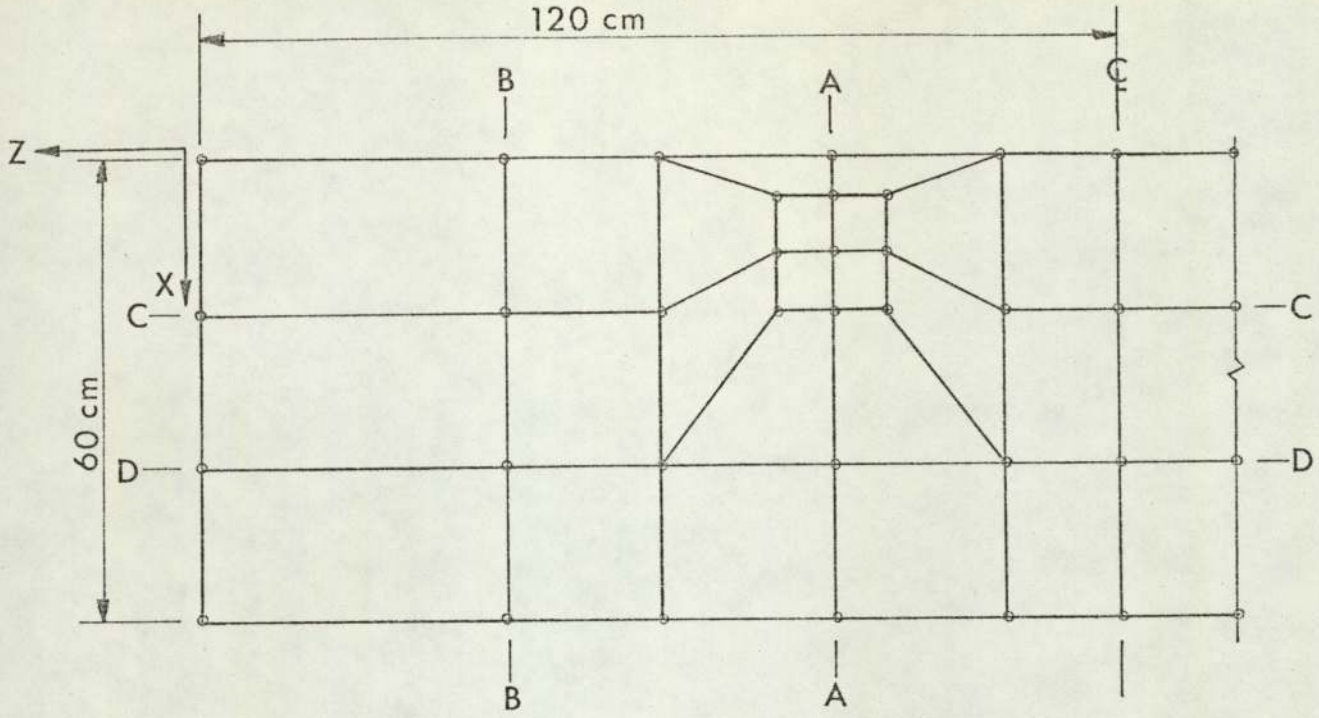

Plan View

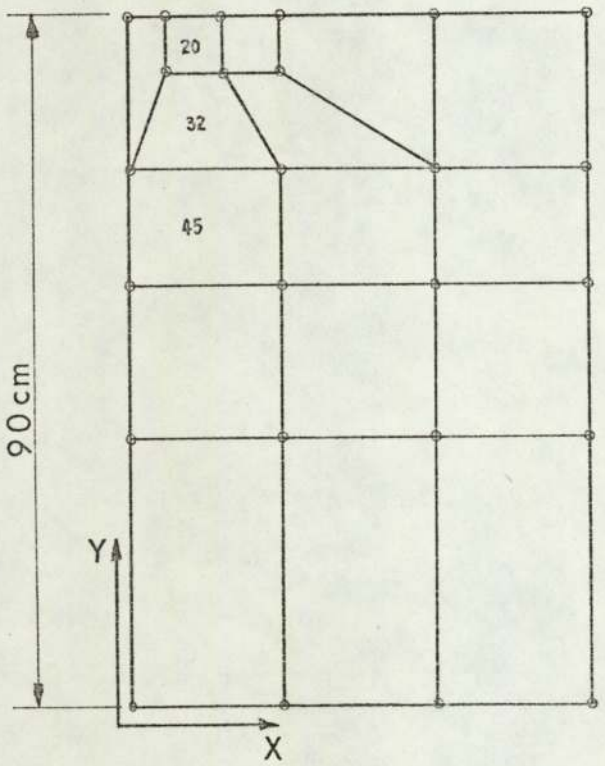

Section A–A

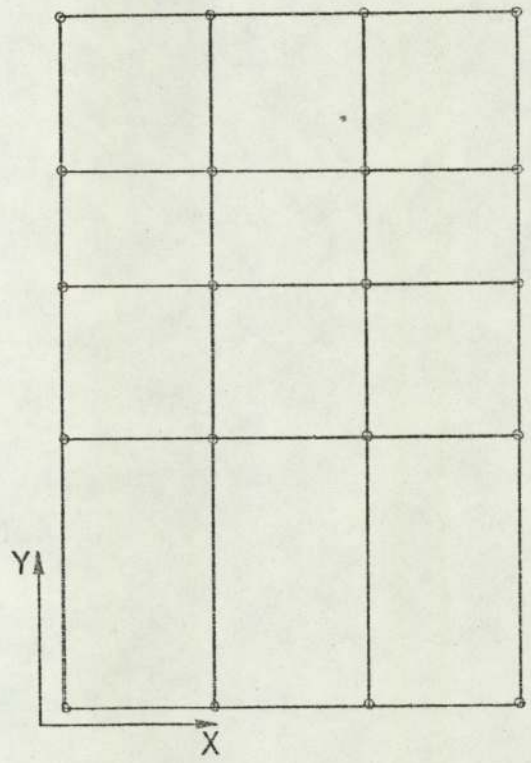

Section B–B

Figure 7.1 The Finite Element Mesh

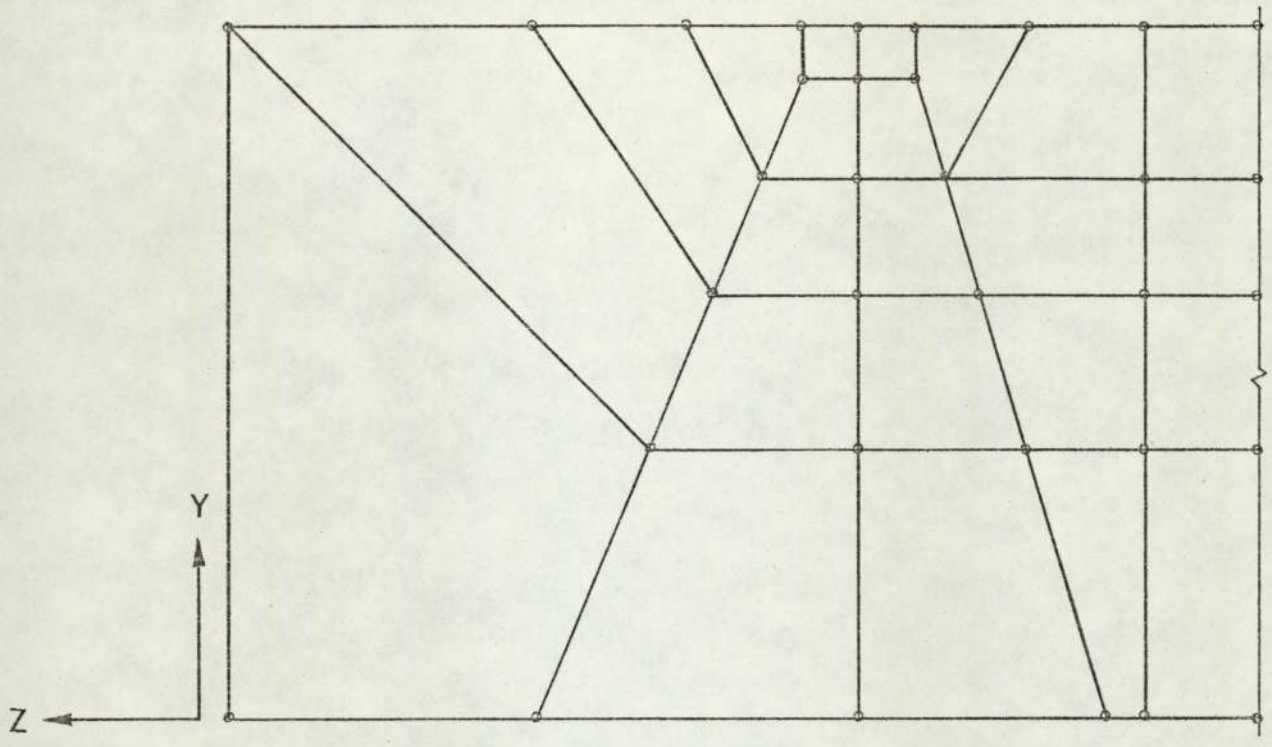

Section C-C

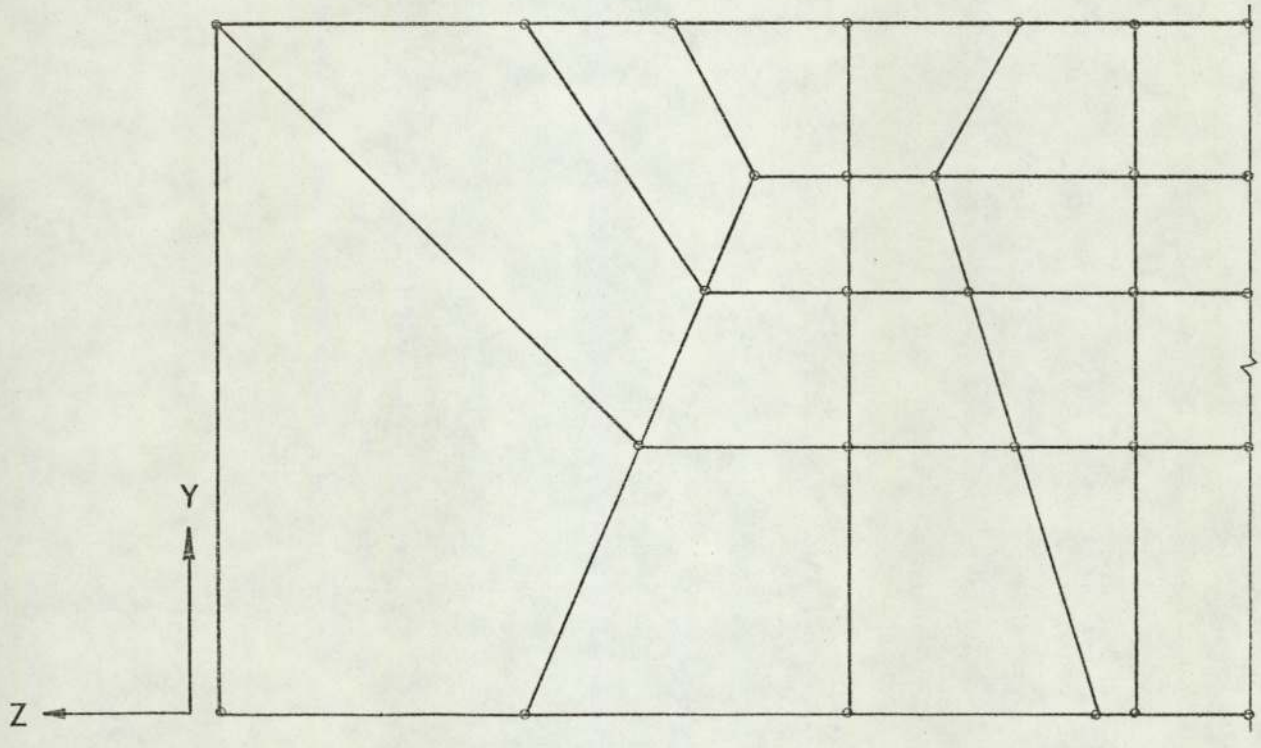

Section D-D

Figure 7.1 continued

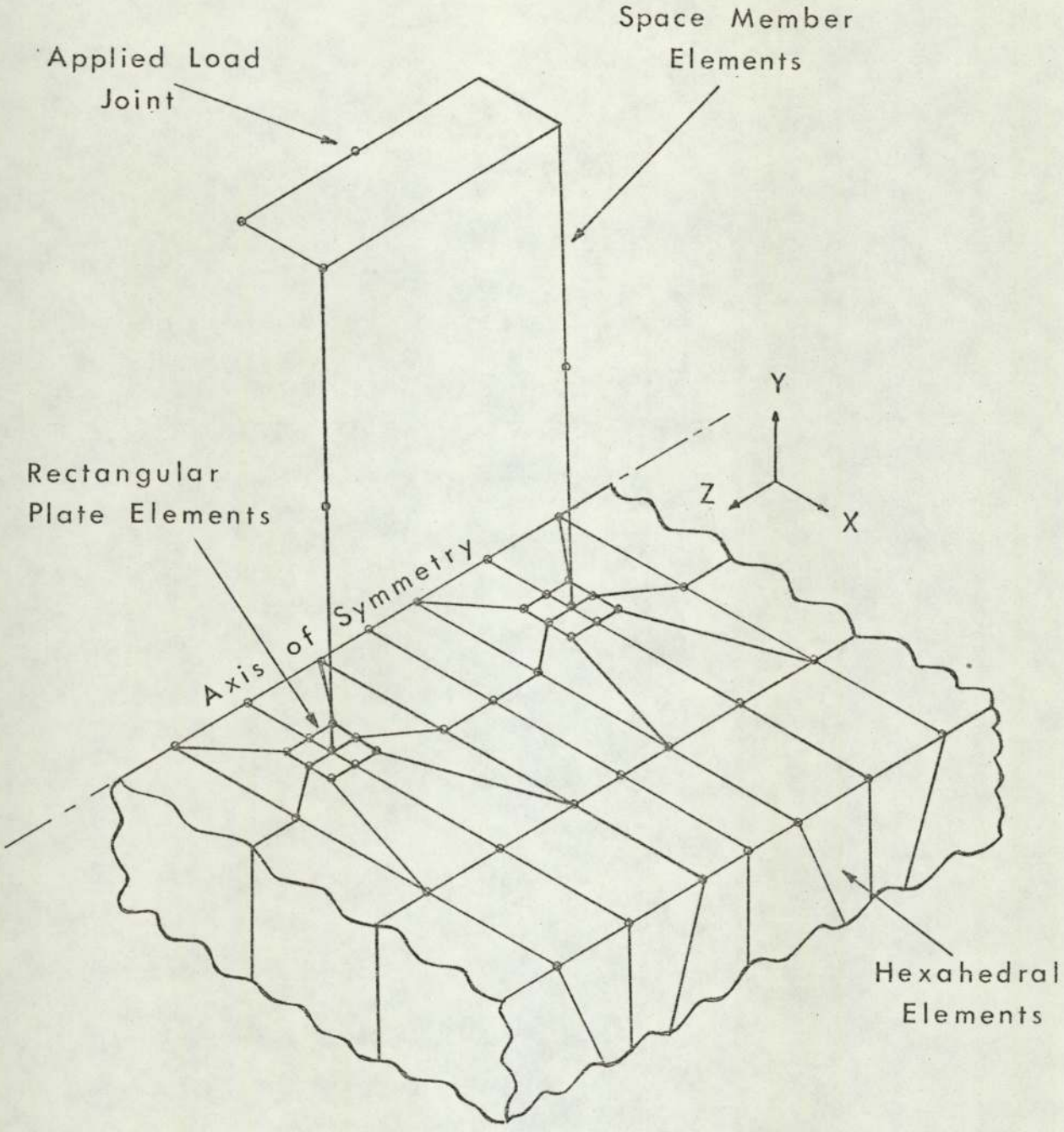

Figure 7.2 The Model Structure

(Dimensions and further details in figure 5.1)

7.3) contd.

Laboratory. Each analysis took 30 minutes of execution time, at a total cost of about £18.

CHAPTER 8.

ANALYSIS OF RESULTS.

8.1) Introduction.

In this Chapter the experimental results of three frames are presented and discussed. These are:

i) The plane frame described in Chapter (5), which will be referred to here as frame No.1.

ii) The larger space frame described in Chapter (5), which will be referred to here as frame No.2.

iii) The smaller space frame of the same chapter, which is referred to as frame No.3.

This is followed by a comparison of the theoretical and experimental results obtained for frame No.2. This frame was selected for the purpose of the comparison mainly because the results demonstrate the interaction between the foundations of the frame.

Each frame was loaded with four different types of loading. Each time the eccentricity of the loading was altered. A comparison between theoretical results obtained for frame 3 and those of a similar frame fixed to a rigid foundation are also presented. This reveals the manner in which the interaction between the foundation and the structure alters the distribution of the bending moments throughout the frame when differential settlement of the foundations occur. It also highlights the effect of non-linear behaviour of the materials of the foundation upon the redistribution of the bending moments in the members of the frame.

The results will demonstrate that when structures are resting on a flexible non-linear soil, two different kinds of bending moment redistribution take place. These are

i) That due to the relative settlement of the foundations, and

ii) That due to the non-linear behaviour of the actual soil,

8.1) contd.

ii) contd.

which aggrevates the bending moment redistribution.

8.2) Results of the Model Tests.

To save time, it was considered that the comparison of the experimental results should be limited to that of selected displacements of the foundations and the side sway of the frames. Once this has been ascertained, the bending moments throughout the frame can be calculated by an ordinary matrix method of structural analysis. The points where displacements were measured were:

1) Vertical displacement at:
   a) each of the pad footings, A,G,K and D shown in plate (5.1b),
   b) at the column heads B,C,H and J shown in the same plate,
   c) the displacement of the beam under the applied load, and
   d) at points E and F at either end of the beam to which the load is applied.
2) Horizontal displacements in the direction of the sway at:
   a) the column heads B,C,H and J,
   b) at the mid-height of each column.
3) The horizontal out of plane displacements of the frame, as stated in Chapter (5), were prevented by rollers. To check the efficiency of this, measurements were also taken at the column heads B and J.

As it is impossible to measure the vertical displacement of the footing at its centre, a dial gauge was placed along the centre line of each footing, 25 mm away from the columns,

8.2) contd.

as shown in plate (5.5c). In the same plate, it can be seen that the dial gauges for measuring the sway of the column heads are slightly below the top. These gauges were initially placed 30 mm below the beam level to ensure that they remain in contact with the columns as these settle during the loading process.

In order to obtain the correct vertical deflections of the footings at their centre, a linear interpolation of the gauge readings was performed in the manner shown in Figure (8.1). In this figure δ_A and δ_D are the gauge readings while $\delta_{A'}$ and $\delta_{D'}$ are the deflections at the centre of the footings. The results obtained in this manner were then averaged for the two columns on either side of the frame.

It was noticed that the sway deflections at the column heads were nearly equal. Hence the four gauge readings were averaged. The vertical displacements of the footings together with the horizontal sway at the top of the columns are considered to be the most significant when designing structures of the type presented here. These are therefore singled out in this chapter for detailed consideration. Figure (8.2) shows the notations adopted for presenting these results. In this figure x is the distance of the load from the centre line of the structure. The eccentricity ,e, of each load is calculated from

$$e = x/L, \qquad (8.1)$$

where 2L is the total span of each frame.

The differential settlement of the frame was calculated, using Figure (8.2), as δ_{DF} from:

$$\delta_{DF} = \delta_L - \delta_R \ , \qquad (8.2)$$

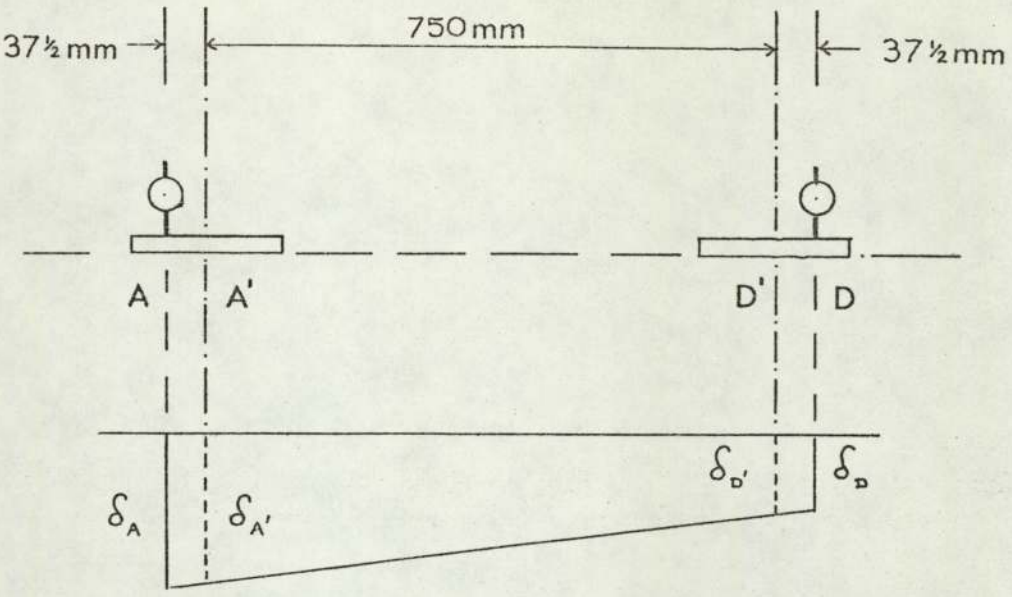

Figure 8.1 Interpolation of Gauge Readings.

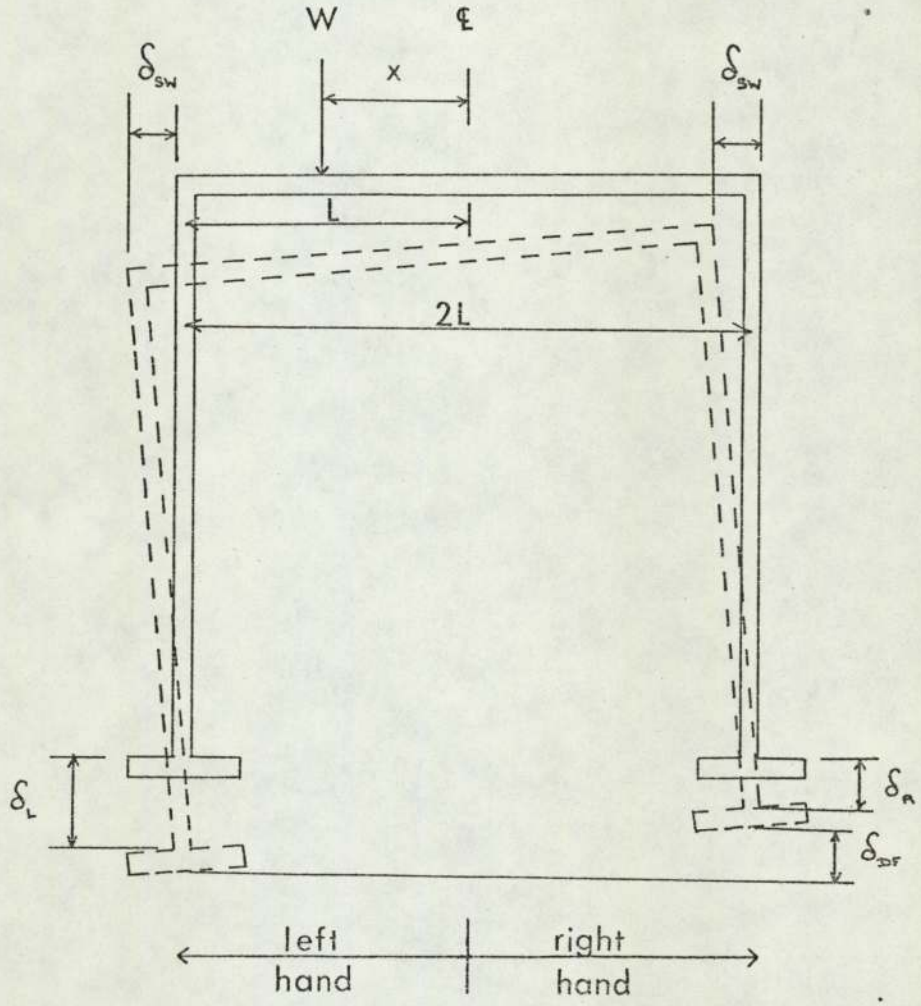

Figure 8.2 Displacement Notation

8.2) contd.

where δ_L and δ_R are the vertical displacements at the centre of the left and right footings respectively. Finally, δ_{SW} is the sway of the structure.

8.3) Analysis of the Experimental Results.

8.3.1) The Plane Frame No.1.

Figures (8.3a) and (8.3b) show the graphs of the vertical deflections δ_L and δ_R of frame No.1 against the applied load, for various eccentricities. Figure (8.4) gives the differential settlements δ_{DF} of the structure obtained from equation (8.2), and the graphs of figure (8.3). Finally Figure (8.5) gives the sway displacement δ_{SW} of the frame. These graphs indicate that the deflections under consideration are of a non-linear nature, each graph becoming flatter as the applied load increases. As expected, increasing the eccentricity of the load increases the settlement δ_L and reduces δ_R, thus aggrevating both the sway of the frame and differential settlement of the footings.

At the initial stage of loading, high stresses develop in the soil immediately under the footing, to the extent that the flat portion of the stress-strain diagram is reached. The stiffness of the soil here is therefore reduced considerably. Away from the footing however, the mass of the soil is subject to lower stresses and therefore exhibits non-linear behaviour. This indeed is the reason for the non-linearity of the graphs at the initial stages of the loading process. Later on, as the load is increased, the highly stressed zone spreads through the soil mass away from the footing. More and more soil therefore reaches the flat portion of the stress-strain relationship which forces the

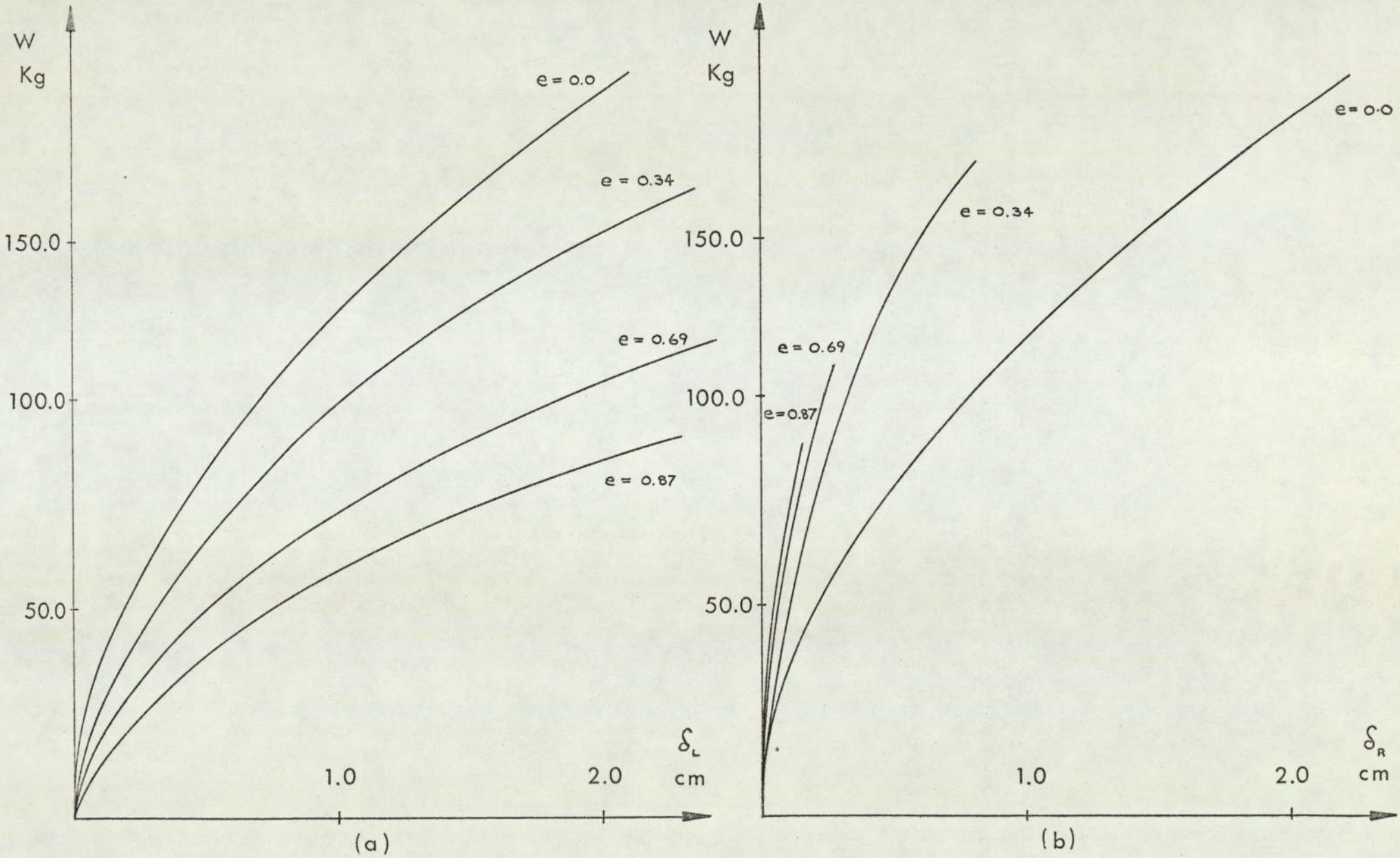

Figure 8.3 Vertical Deflection of the Footings of Frame No.1

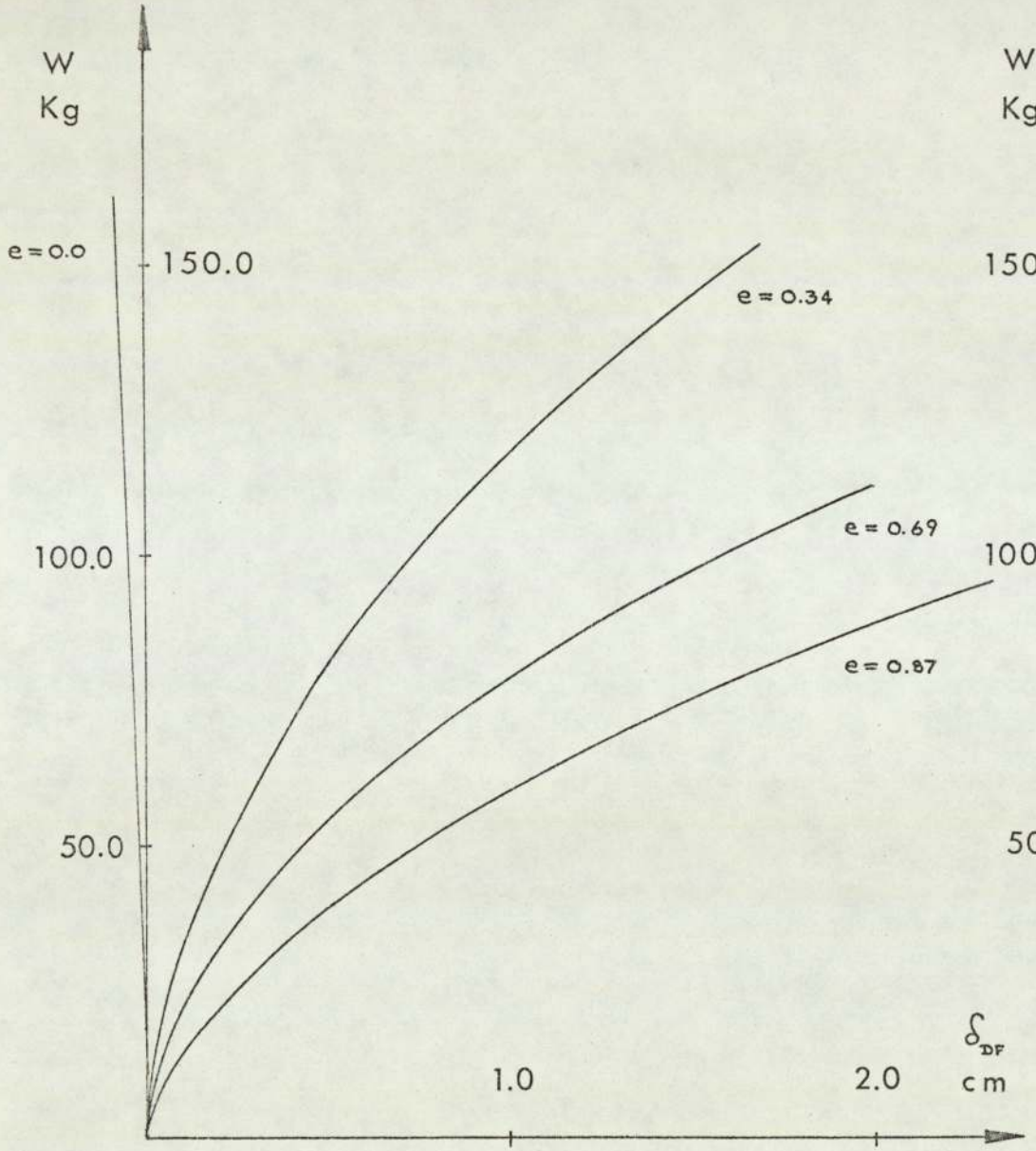

Figure 8.4

Differential Displacement of Frame No.1

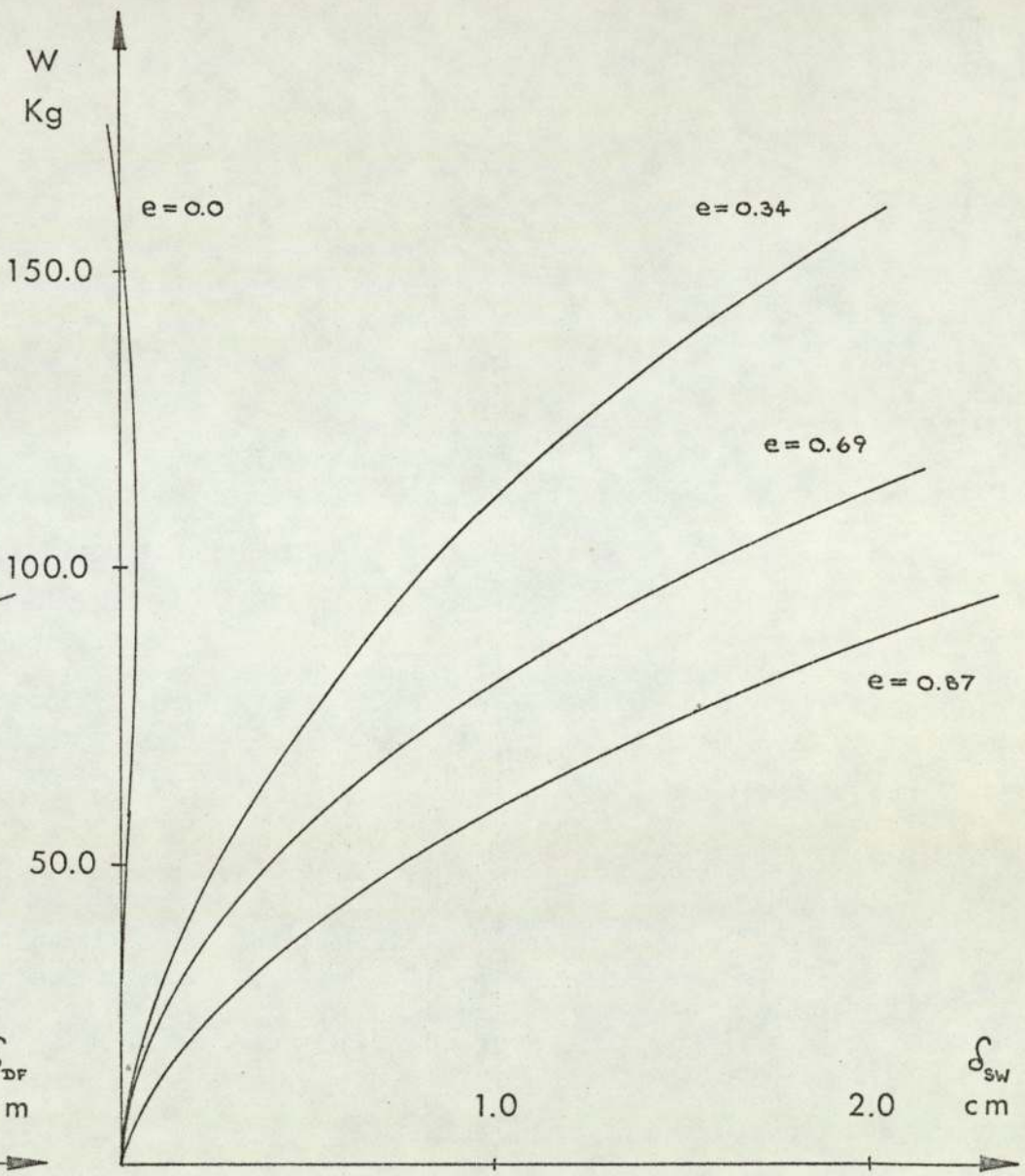

Figure 8.5

Sway of Frame No.1

8.3.1) contd.

settlement graphs to flatten out towards the horizontal.

The above observation was substantiated during the unloading process. When this was completed, no recovery in the settlement of the footings was observed, indicating the development of a failure zone in the soil. As explained above, the failure zone is gradual, spreading downwards from the footings. A rigid-plastic type of collapse, as proposed by Meyerhoff[105], did not occur during the process of loading of this or the other frames tested.

It can be seen from Figure (8.4) that there is a small imperfection in the loading system. This is the reason for recording negative deflections under the symmetrical load case. The order of this error is not only small but nearly the same for all three frames tested. In a later graph of the differential settlements of this and the other frames, this imperfection is rectified by a small shift of the origin of the graph.

8.3.2) <u>The Space Frame No.2.</u>

The deflections δ_L and δ_R, the differential settlement δ_{DF} and the sway δ_{SW} for this larger frame are plotted against the applied loads in Figures (8.6), (8.7) and (8.8) respectively. These graphs are similar to those obtained for the plane frame and warrant no further comment. Obviously, the load required to produce the same magnitude of displacements here is almost twice that required for the plane frame. The difference between the behaviour of the different frames will be discussed in detail later.

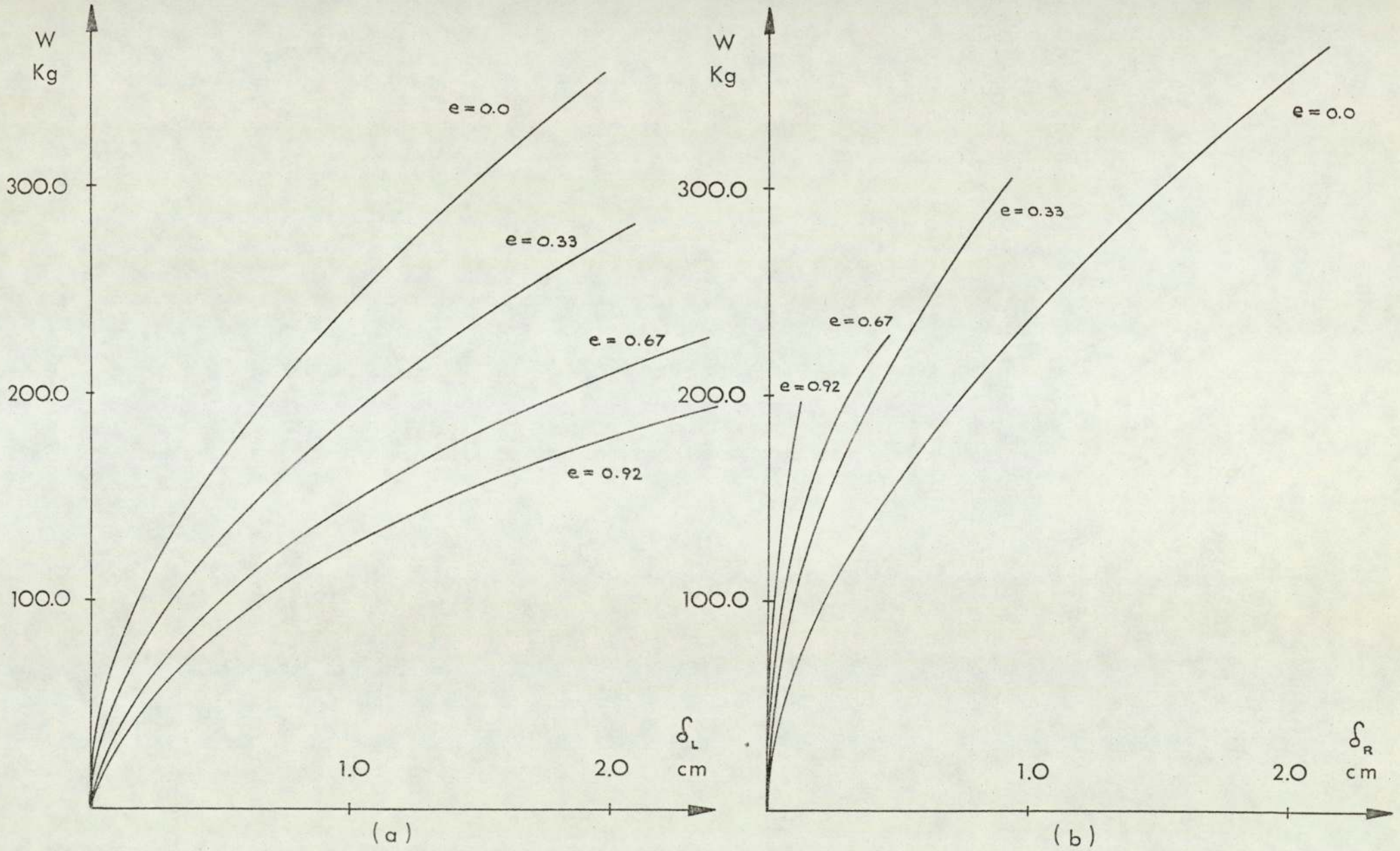

Figure 8.6 Vertical Deflection of the Footings of Frame No. 2

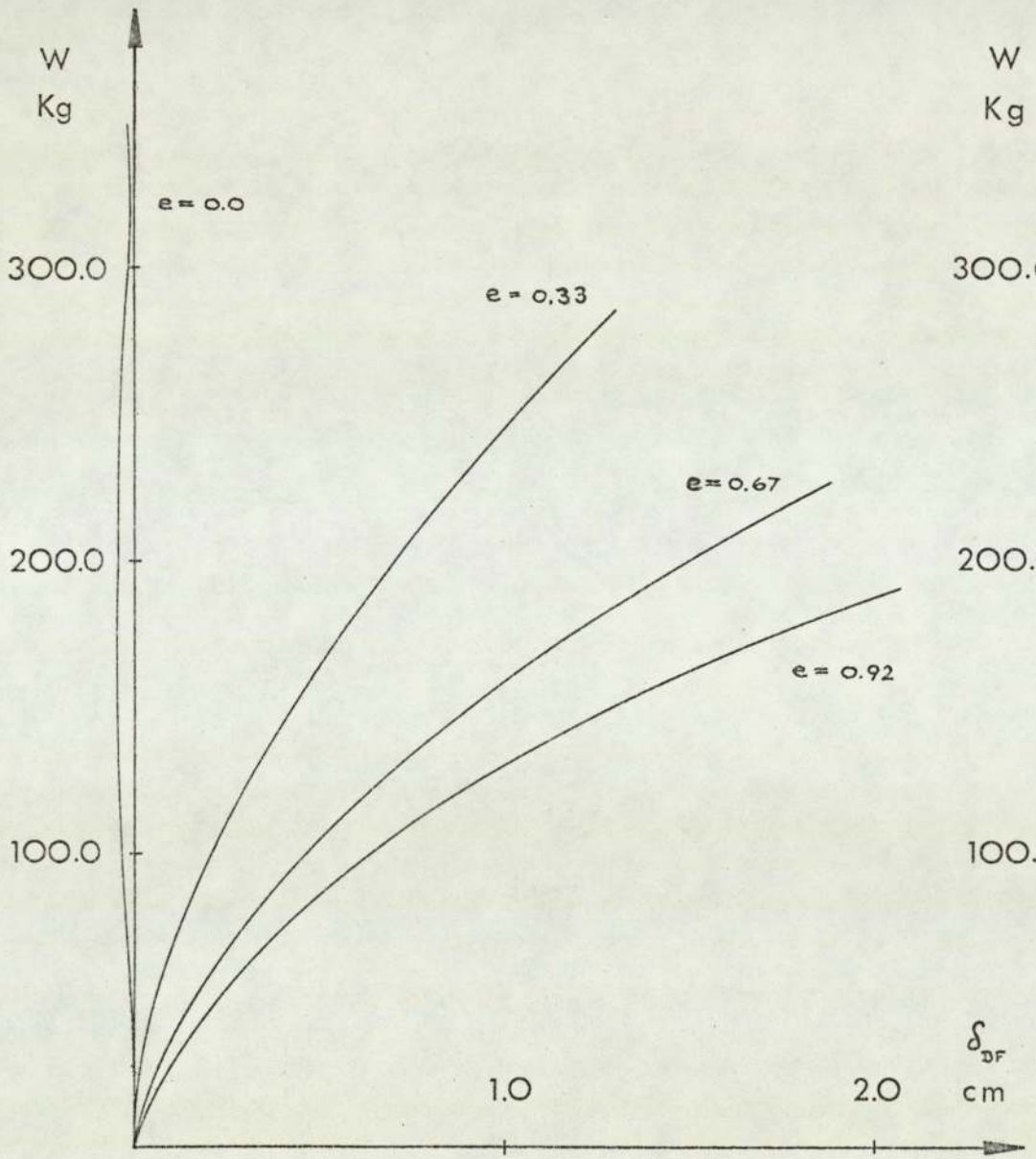

Figure 8.7
Differential Displacement of Frame No. 2

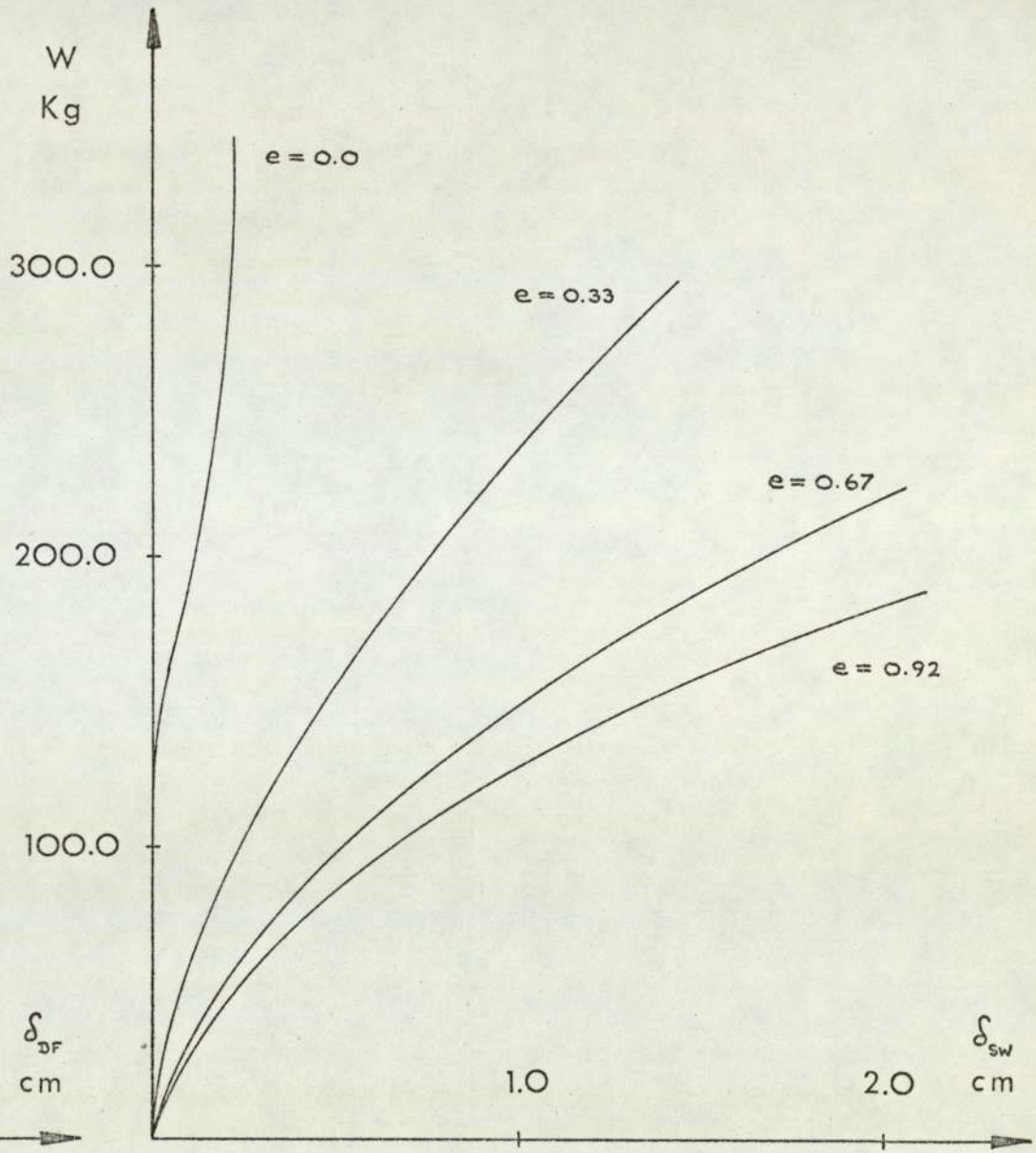

Figure 8.8
Sway of Frame No. 2

8.3.3) The Space Frame No.3.

Load displacement graphs for this smaller space frame are given in Figures (8.9), (8.10) and (8.11). A detailed comparison of the results obtained for the three frames are given in the next section.

8.3.4) Comparison of the Frames.

In Figure (8.12) the settlements δ_L and δ_R of the footings are plotted, for the frames, against the eccentricity of the loading e. This is carried out for the case when each space frame is subject to a load of 200 kg, while the plane frame is subject to 100 kg. The small defect in the loading system is here corrected for by an origin shift of the graphs. This resulted in moving the curve for δ_R of a given frame slightly to the left while the curve for δ_L moved to the right. The two graphs thus intersected on the δ axis at points A and B.

This figure reveals the nature of the interaction between the footings, the effect of the stiffnesses of the various structures on their individual behaviour and the manner in which the bending moments are redistributed in the frame, due to the differential settlements of the foundations on the one hand and the non-linear behaviour of the soil on the other. To begin with, when the applied load is symmetric, with e = 0, the settlement of the footings for the plane frame and larger space frame are almost equal - see point A on the δ axis of the graph. This indicates that the larger space frame behaves as two separate plane frames. On the other hand, point B on the graph gives the settlement of the footings for the smaller space frame 3. This shows that under symmetrical loading the settlement of this frame is 18.7% more than those of the other two frames. This can only be due to the inter-

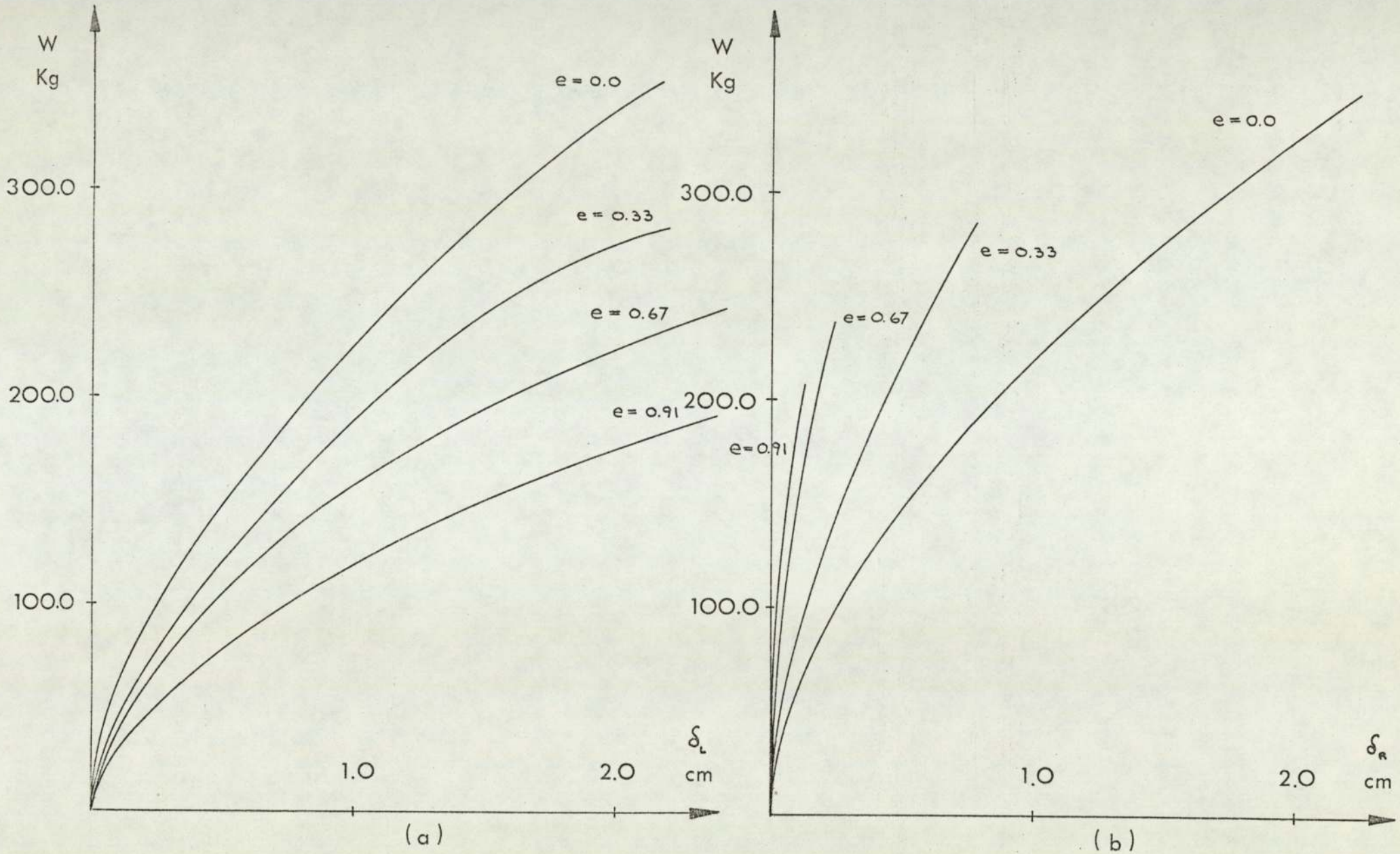

Figure 8.9 Vertical Deflection of the footings of the Frame No.3

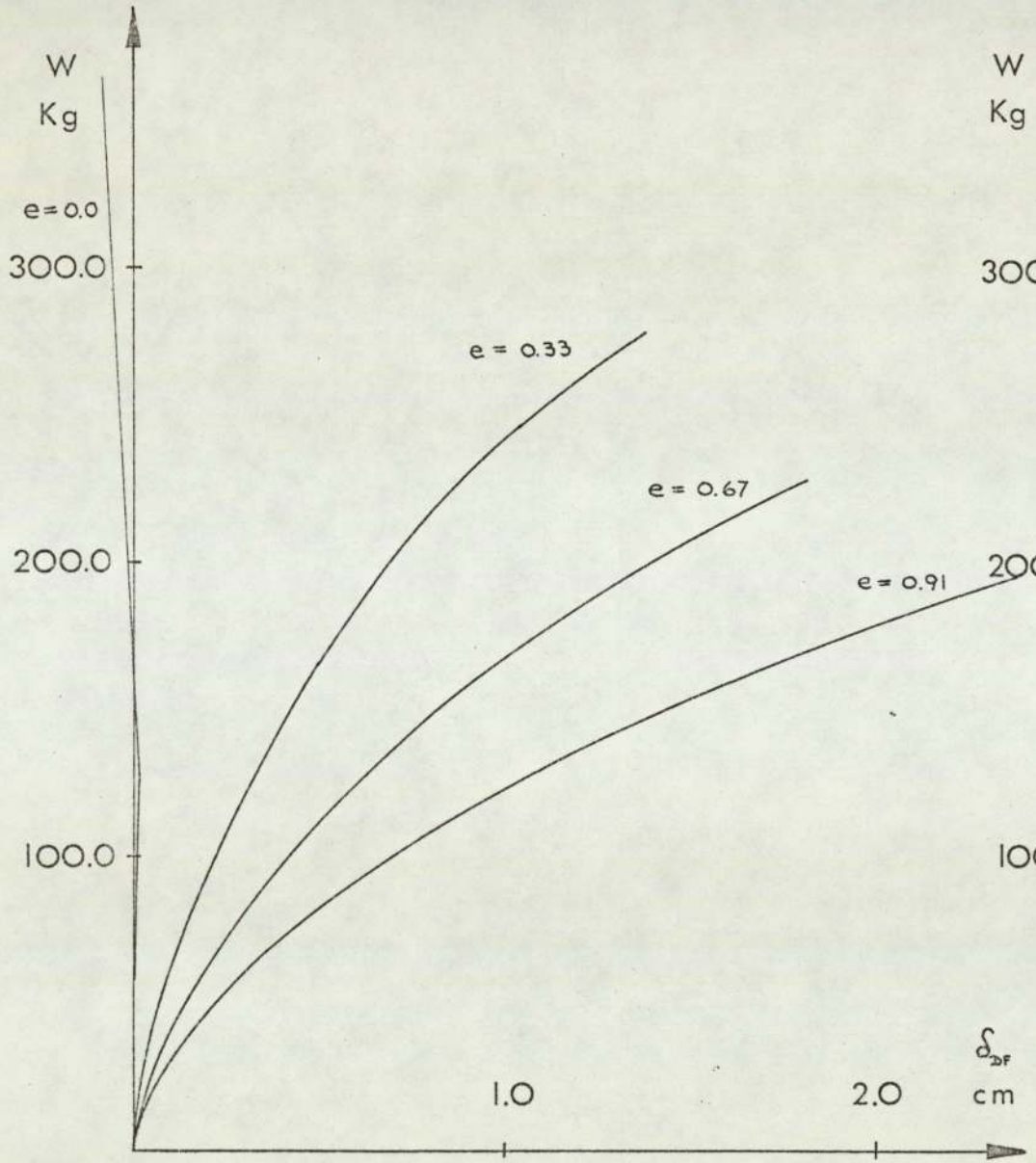

Figure 8.10
Differential Displacement of Frame No.3

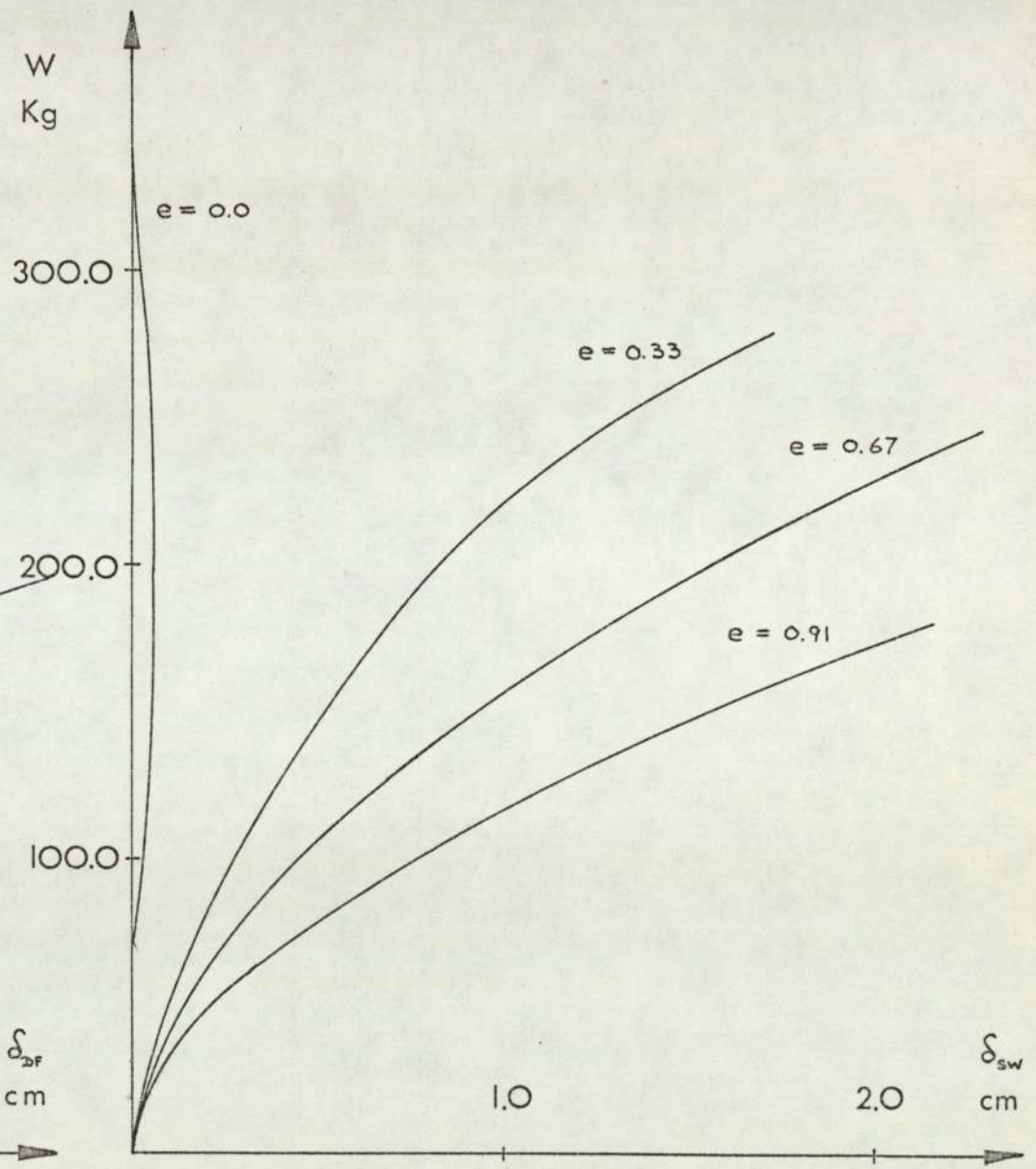

Figure 8.11
Sway of Frame No.3

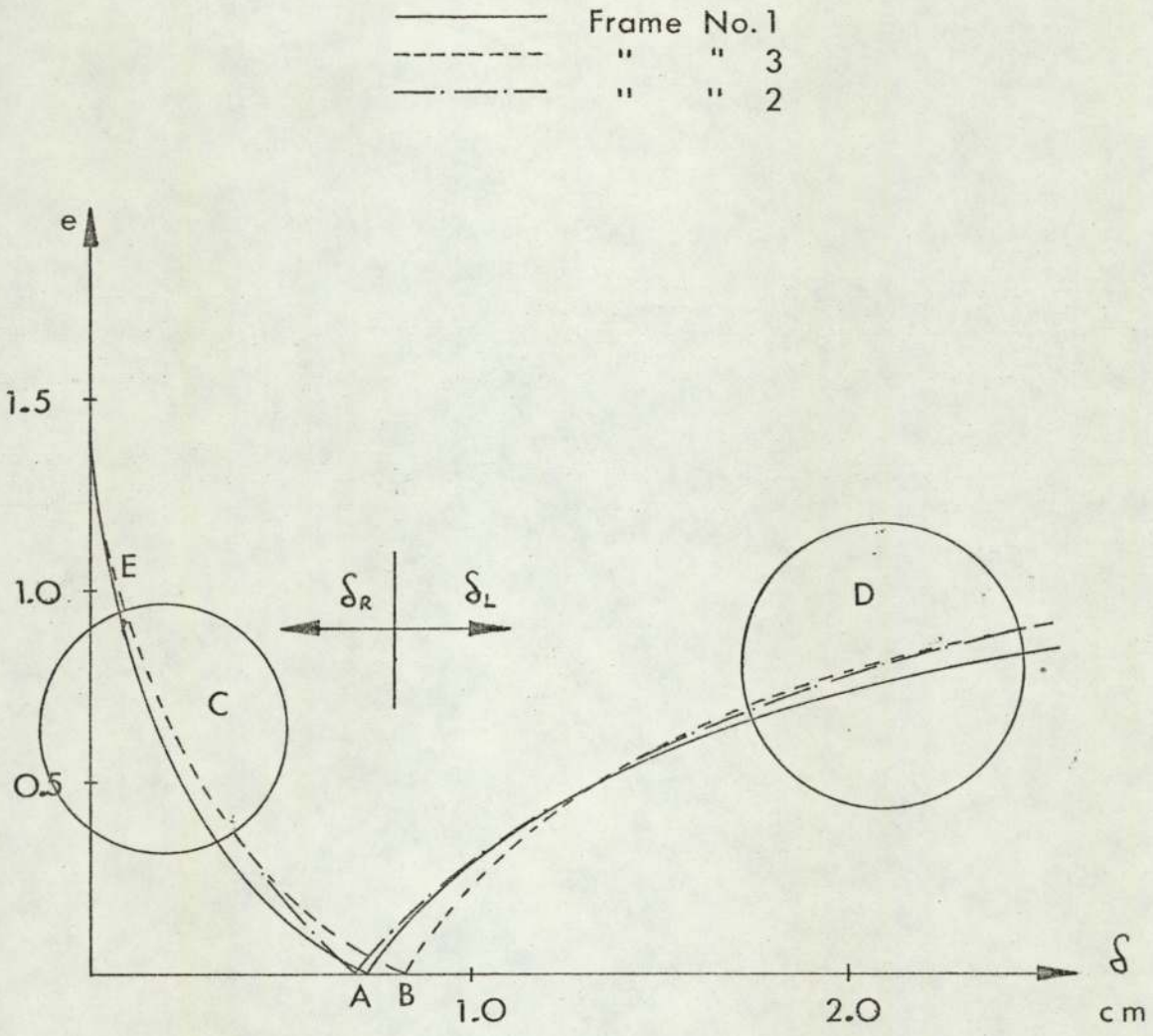

Figure 8.12 Comparison of δ_L and δ_R for the Frames at W = 200 Kg

8.3.4) contd.

action between the foundations of frame 3. The footings of this frame are so close together that the settlement of one of its footings is influenced by the loads acting on the adjacent footing.

In regions C and D of the graphs, it is noticed that the curves for the space frames coincide while the plane frame behaves differently. This is due to the fact that the stiffness of the space frames are nearly equal to each other, but both differ from that of the plane frame. Far more significant than this is the fact that graphs in the regions C and D reveal the interaction between the columns of the structures. Considering region D, for instance, the settlement δ_L at the left hand footing of a frame is retarded by the stiffness of the right hand portion of the structure. Since the space frames are stiffer than the plane frames, this retarding effect is more pronounced. This is why the settlement δ_L of the plane frame,for a given eccentricity, is larger than those of the space frames. On the other hand the reverse of this behaviour is evident in region C. Because the right hand side is holding up the left hand side, the settlement of this footing is aggrevated. This is naturally more so for the space frames. Obviously the interaction between the various parts of the structure does not play a part in the case of symmetrical loading.

At point E in the figure, the eccentricity of the load is unity. The applied load is thus acting vertically over the left hand column. Normally,therefore a settlement of the right hand footing is not expected, unless, of course, redistribution of bending moments takes place. The figure shows how, in fact, the right hand footing of all three frames

8.3.4) contd.

have suffered settlement. This is due to the enforced rotations in the joints in the right hand columns.

Figure (8.13) shows the graphs of the nett differential settlements δ_{DF} of the footings against the eccentricity of the load. Figure (8.14) shows the sway displacements of the frames against the eccentricity of the loads. Both these diagrams are for the case when the applied load is 200 kg for the space frame and 100 kg for the plane frame. In both these figures it is noticed that both δ_{DF} and δ_{SW} for the plane frame are larger than the corresponding values for the space frames. The difference is due to the fact that the plane frame No.1 is more flexible than the space frames.

The graphs also show a more significant fact than the mere relative stiffness of the frames. In the two space frames, it was pointed out that the smaller suffers from the interactions between the foundations. However, Figures (8.13) and (8.14) give the results for the two space frames. These show identical behaviour, which indicates that the interaction of the foundations of this frame is compensated for by the greater stiffening effect of the members. The nett result is that the interaction between the foundations is not as significant as it may appear. This fact is further substantiated by the identical behaviour of the space frames in regions C and D of Figure (8.12). It appears therefore that many analysts and experimentalists have over-emphasised the relative importance of the interaction of the foundations, at the expense of the interaction between the various connected parts of the superstructure.

Figures (8.12), (8.13) and (8.14) further indicate

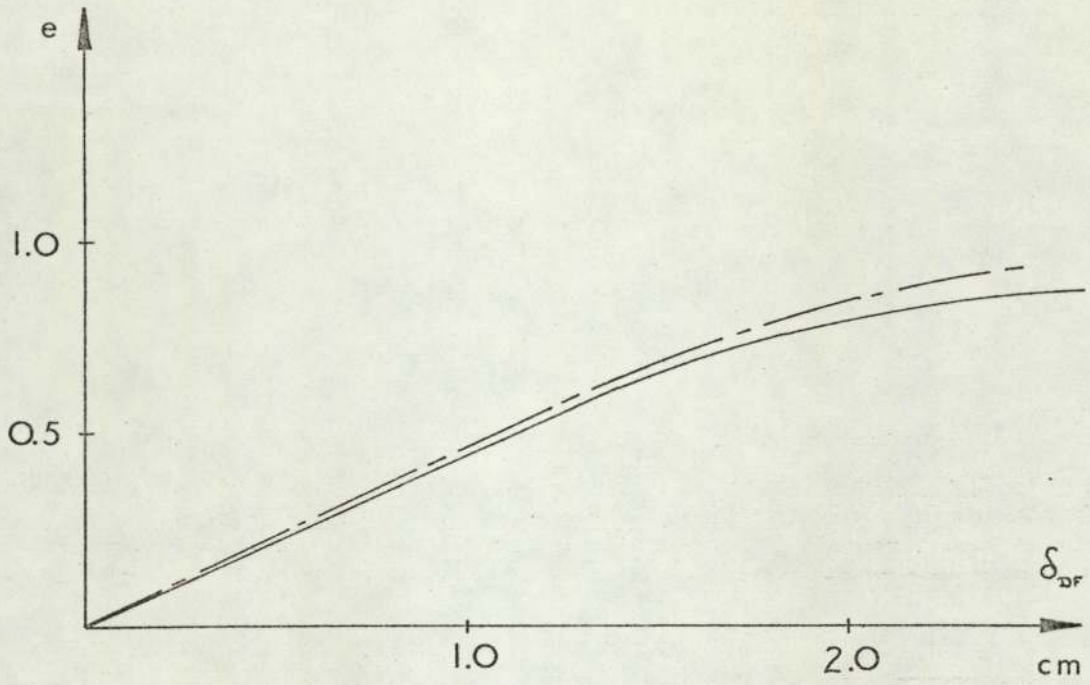

Figure 8.13 Differential Settlements

——— Space Frame
——— Plane Frame

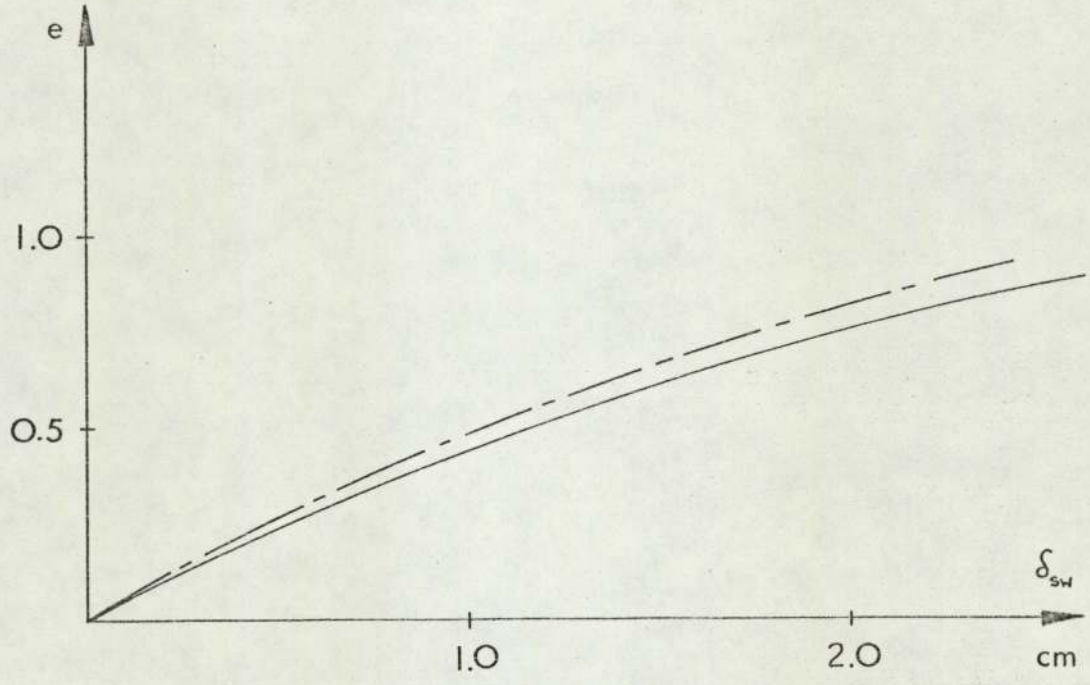

Figure 8.14 Sway Deflections

8.3.4) contd.

conclusively that to exclude the structure and treat each foundation as an unconnected body is indeed an over-simplification of the problem. Later in this chapter it will also be demonstrated that to exclude the foundation effects and concentrate on the behaviour of the superstructure alone is also an oversimplification.

8.4) Comparison of Theoretical and Experimental Results.

It was stated earlier that the smaller space frame No.3, exhibited some interaction between the foundations. This frame was therefore selected for theoretical non-linear analysis, using prismatic members to represent the structure and solid hexahedral isoparametric elements to represent the soil. In Figure (8.15) the theoretical graphs of the differential settlement of the footings are compared with those obtained experimentally. Figure (8.16) makes the same comparison for the sway of the structure. Figure (8.15) shows that as the eccentricity of the load increases, the agreement between the experimental and theoretical results improves. The effect of the adoption of a hyperbolic stress-strain response, as shown in Figure (6.5), is also noticed in Figures (8.15) and (8.16). Initially the theoretical analysis, for a given eccentricity, underestimates the sway and differential settlement. On the other hand at higher loads, the theoretical analysis over-estimates both δ_{DF} and δ_{SW}. A clearer presentation of the results is given in Figures (8.17) and (8.18), where the behaviour of the frame for various eccentricities under a vertical load of 200 kg has been singled out for inspection. The experimental results are those presented in Figures (8.13) and (8.14) which contained a correction for the experimental errors.

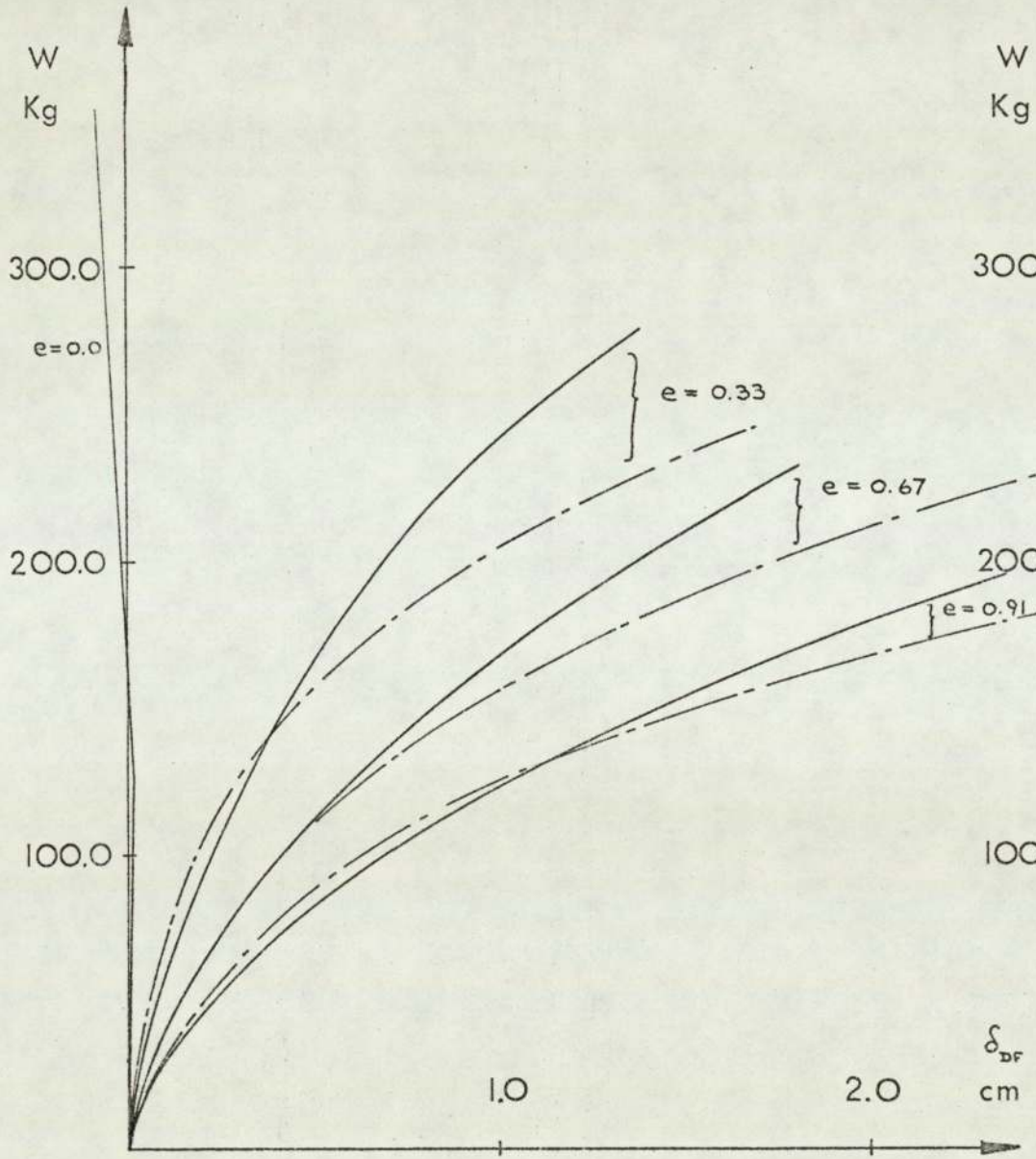

Figure 8.15 Comparison of Theoretical and Experimental Differential Settlements.

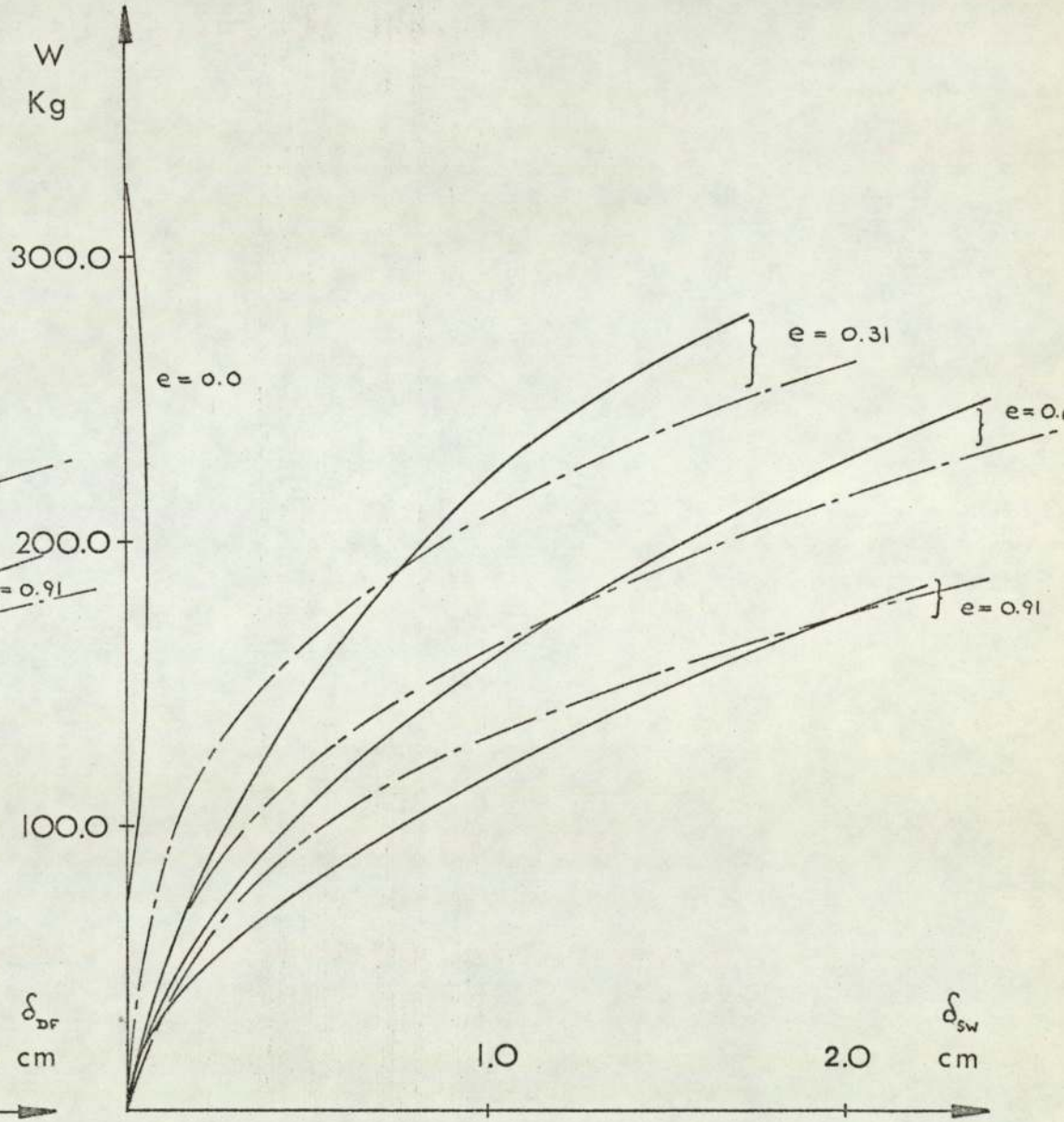

Figure 8.16 Comparison of Theoretical and Experimental Sways.

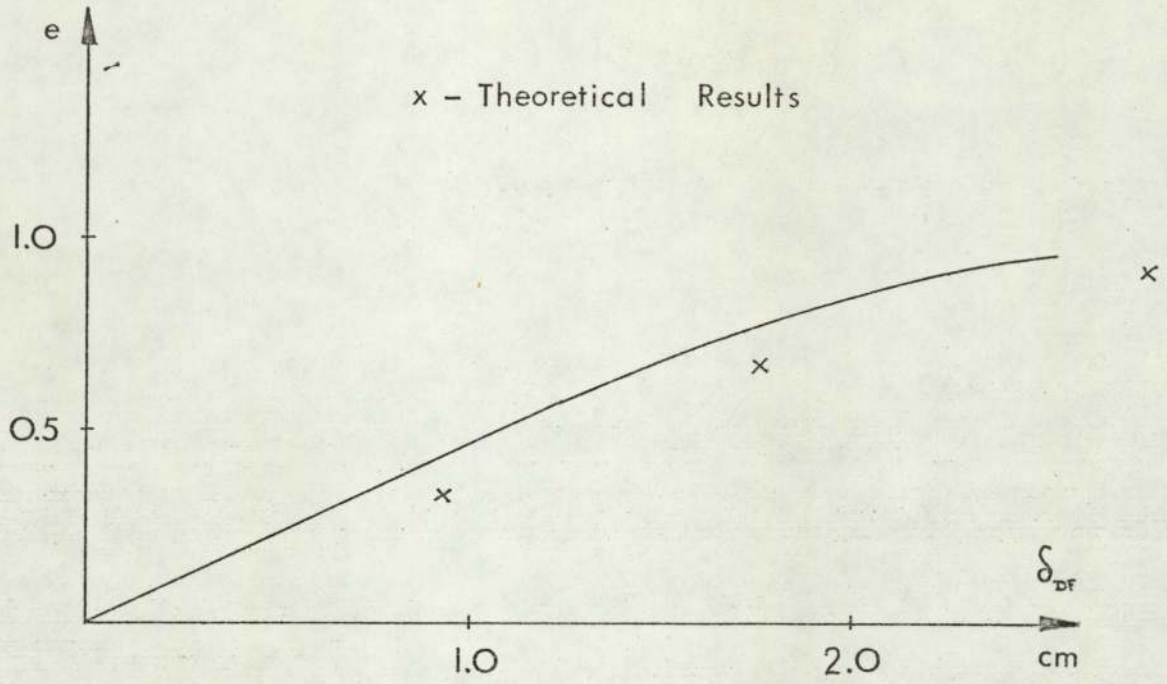

Figure 8.17 Comparison of Theoretical Results with Experimental Curve, Figure 8.13, W = 200 Kg

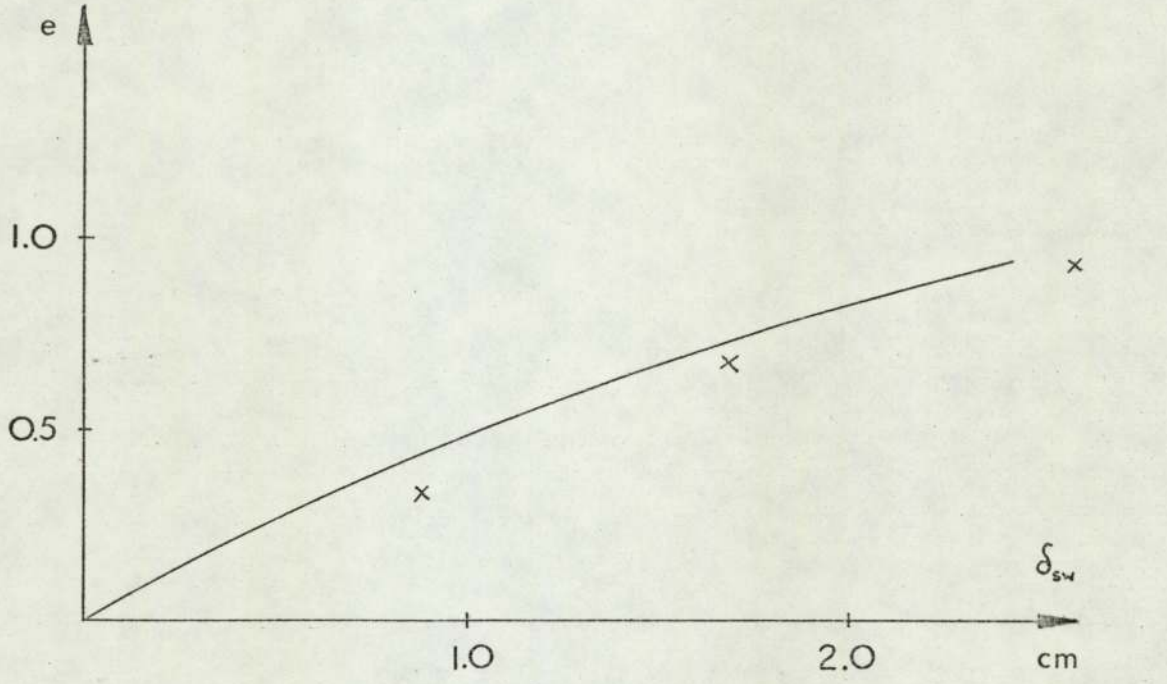

Figure 8.18 Comparison of Theoretical Results with Experimental Curve, Figure 8.14

8.3) contd.

While reasonable agreement exists between the two sets of results, the theoretical results, at the load level selected, consistently overestimate the values of δ_{DF} and δ_{SW}. This reflects that the theoretical results were on the safe side.

In the theoretical analysis, the tangent modulus method was adopted for following the hyperbolic stress-strain relationship. It is known that the errors in the tangent modulus approach accumulate and are dependent on the size of the load increment. To ensure an accurate analysis therefore, the loading increment was made as small as practicable for computer time. Altogether fifteen load increments were used and it was discovered that no significant gain is achieved by using smaller increments. To check the accuracy of the tangent approach, after each loading increment, the stresses computed in each element were compared to those given by the hyperbola. Figure (8.19) shows the percentage difference calculated in this manner for the most highly stressed elements. These are elements numbered 20, 32 and 45 which are immediately below the left hand footing, as shown in Figure (7.1). Element 20 is the most highly stressed and also the smallest. Figure (8.19) shows that the percentage error in this element is about 10% after ten loading increments, rising to 18% at the end of the analysis. The errors in elements 32 and 45 are noticed to be less than 10% throughout. Elsewhere the errors were insignificant and it was concluded that the theoretical approach was reasonable for the type of problem under consideration.

8.5) Redistribution of Bending Moments.

In this section the results obtained by the computer,

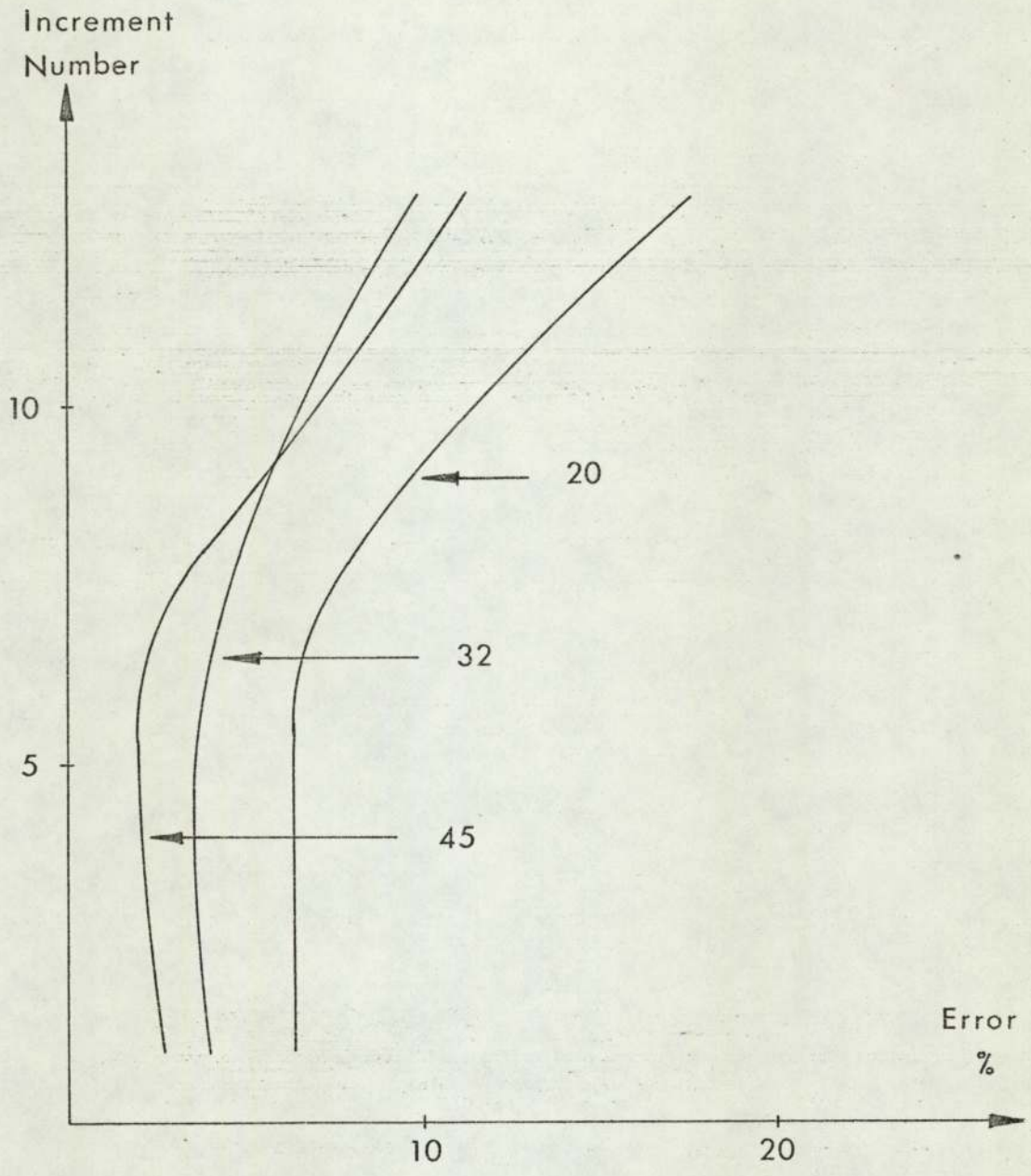

Figure 8.19 Percentage error of fit to the Hyperbolic Stress Strain Relation.

8.5) contd.

for the bending moments, for different values of eccentricity are presented for the smaller space frame No.3. The purpose here is to show the manner in which the bending moments are re-distributed throughout the frame due to the non-linear behaviour of the soil and the subsequent differential settlement of the footings. The results obtained are compared with an identical frame, but supported on a rigid foundation, known hereinafter as frame No.4.

Figure (8.20) shows the geometry and loading of both frames 3 and 4. The joints are lettered in the same manner as that shown in plate (5.1b). The figure also shows a set of Cartesian X-Y-Z axes. Because of symmetry in the Y-Z plane through EF, only half of each structure was analysed.

For both frames Figure (8.21) shows the bending moments about the X axis. Figure (8.22) gives the bending moments about the Z axis. Finally Figure (8.23) gives the bending moments in beams BH, CJ and EF about the X axis.

Considering Figure (8.21) first, figures a and a' are the bending moments for frames 3 and 4 respectively, for the symmetrical load case. These figures show how the magnitude of the bending moments in frame 3 is considerably different from that of frame 4. There is no differential settlements and the loading is symmetrical. The footings of frame 4 are rigidly fixed to their foundations. This produces considerable moments at the column ends A and D. Consequently a non-uniform stress distribution develops under each footing in the plane ABCD as shown in Figure (8.24a). On the other hand, frame 3 is supported on a flexible bed of sand. Any non-uniform stress distribution that may develop across a footing of this frame, causes these to tilt in the manner shown by N'P' and Q'R' in Figure (8.24b). This leads to a rotation of

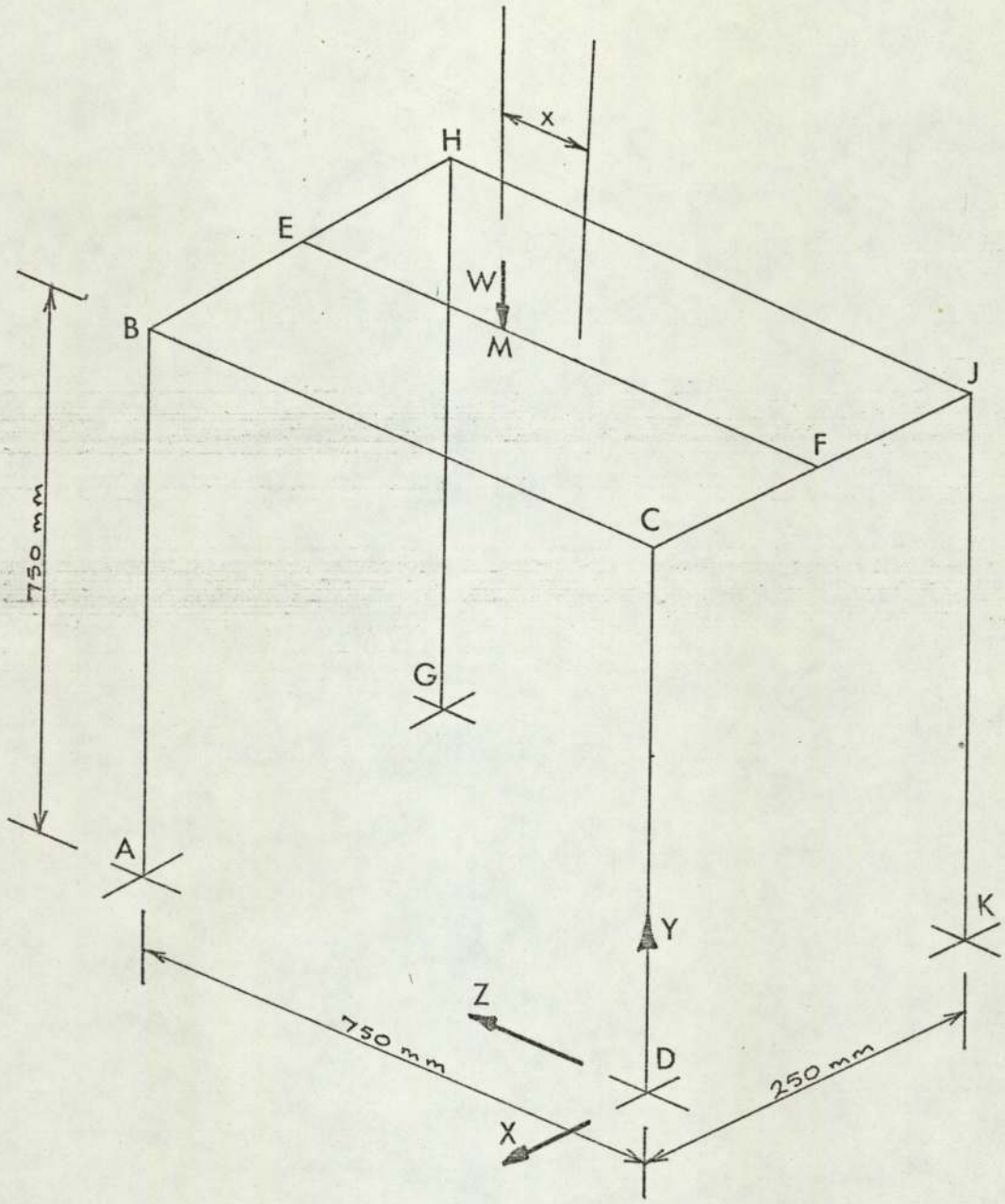

Figure 8.20 The Frame and Loading

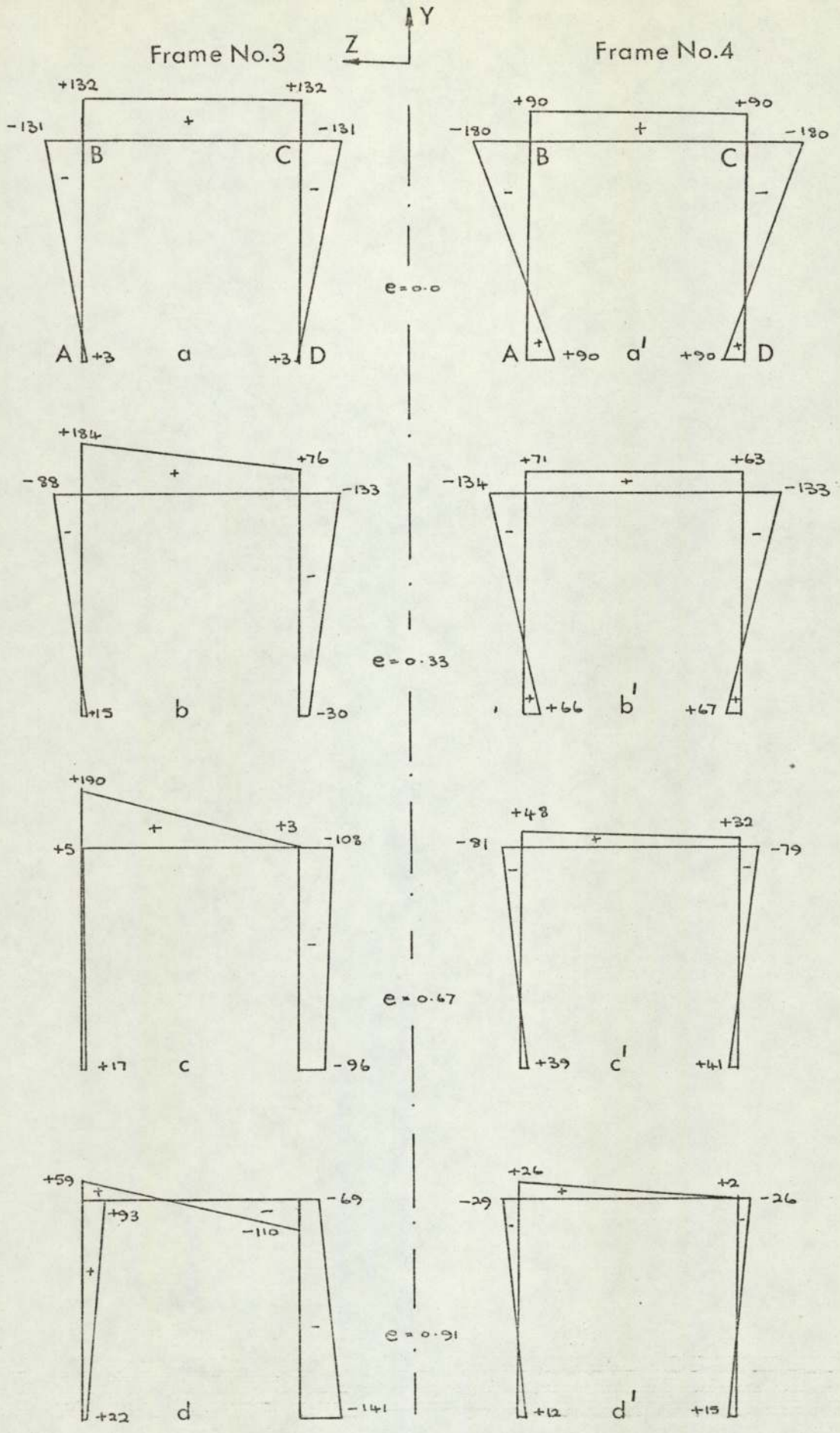

Figure 8.21 Bending Moments in Frame ABCD about X axis in Kg cm

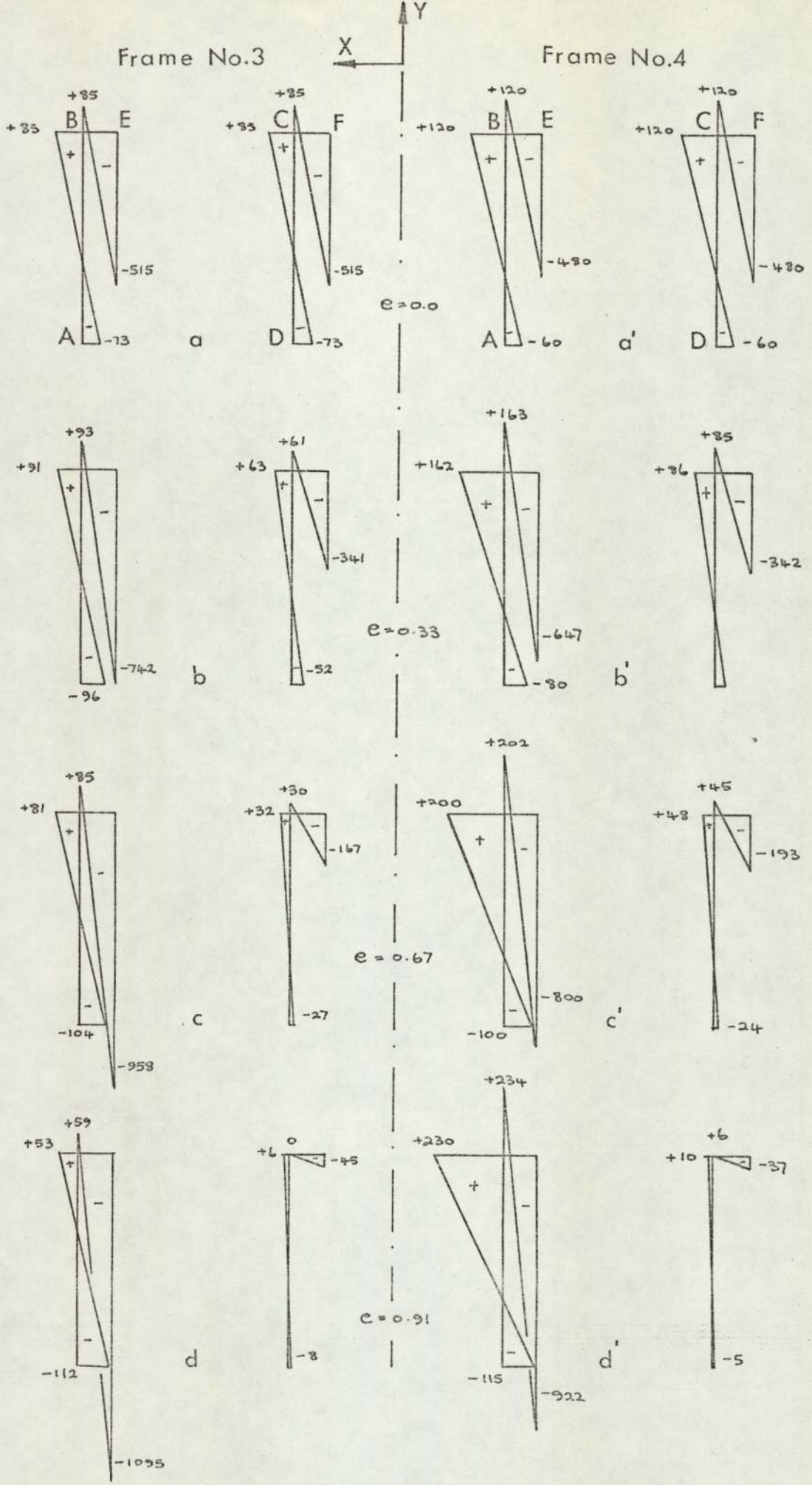

Figure 8.22 Bending Moments in Frames ABE and DCF about Z axis in Kg cm

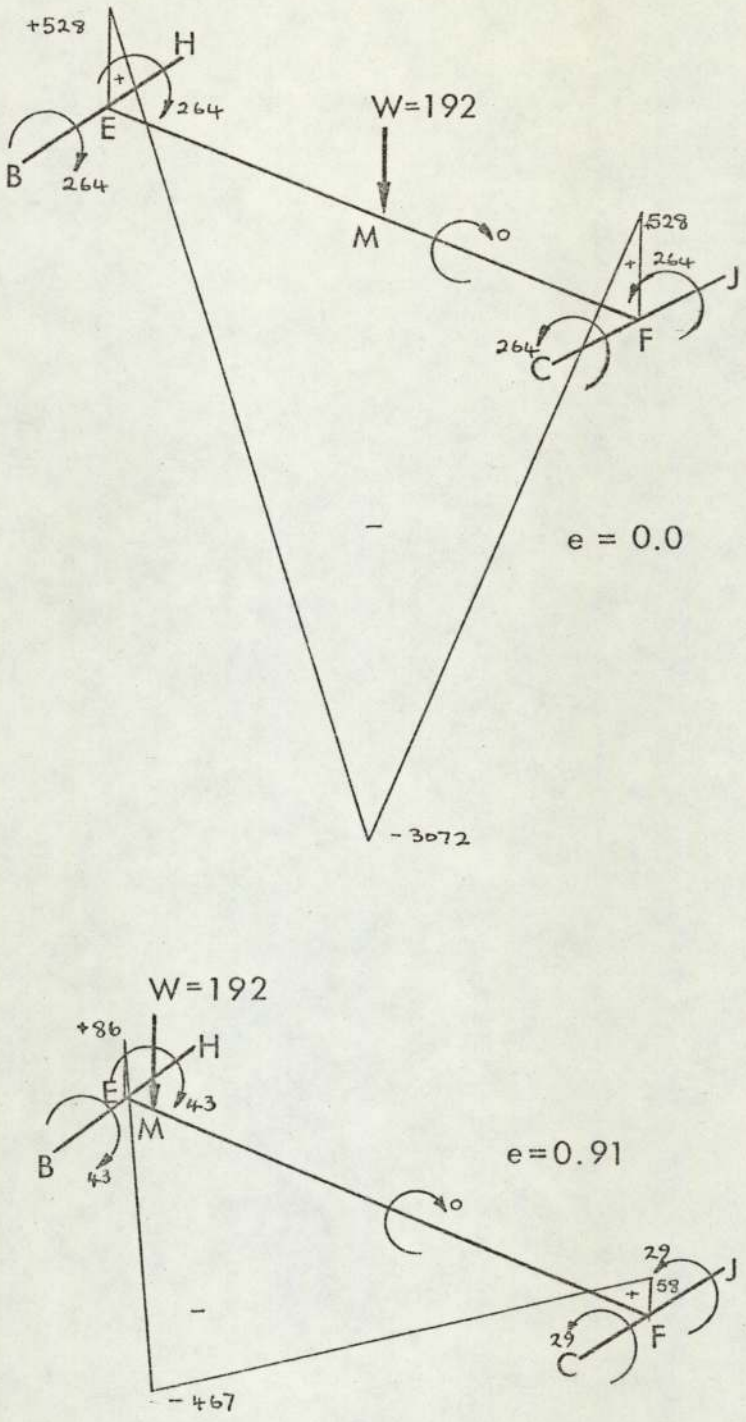

Figure 8.23 Bending Moments in BH, CJ and EF about X axis in Kgcm.

a – Distribution of Stress under the Pads of Frame 4

b – Tilting and Redistribution of Stress under the Pads of Frame 3

Figure 8.24

8.5) contd.

the column ends A and D which relieves the excess bending moments at these points. The values of the moments developed at A and D, in frame 3, are given in Figure (8.21a). Naturally this change in the rotation of the column ends gives rise to a redistribution of the moments throughout the members ABCD in the frame.

An inspection of Figures (8.21) a,b,c and d shows that as eccentricity of the load increases, leading to an increase in the differential settlement of the footings, the bending moments throughout frame 3 alters considerably. Most significant in these figures is the manner in which the bending moments at point D are changing. It is noticed that the bending moment here changes from a small positive value of +3 kg cm, for the symmetrical case to -141 kg cm for the case when e = 0.91. The stiffness of the column CD plays its part to retard the differential settlement of the frame. This forces the column to rotate about point D which gives rise to high negative bending moments there. In effect, therefore, column CD and indeed the entire right hand portion of the structure is contributing to reduce the development of high differential settlements - a fact that was substantiated experimentally and referred to earlier.

A comparison of the bending moments in frames 3 and 4 for a given eccentric loading indicates that the redistribution of bending moments alters due to the position of the load, but most significantly due to the development of differential settlements in frame 3.

It is noticed in Figure (8.22) that there is little difference in the bending moments about the Z axis, between frames 3 and 4. This is fully expected since these moments are not directly influenced by differential settlements to any great extent.

8.5) contd.

The effect of eccentric loading on the bending moments in beams BH, CJ and EF about the X axis are shown in Figure (8.23). No significant difference was recorded in the values of these moments between frames 3 and 4.

It is therefore concluded that differential settlement mainly affects the bending moments in the frames ABCD and GHJK about the X axis.

8.6) Stresses in the Soil.

Figures (8.25) and (8.26) show the distribution of the vertical stress σ_y, obtained by the analysis, below the left and right hand pad for various eccentricities when a vertical load of approximately 200 kg is acting on the frame. An attempt was made to check the vertical equilibrium of the forces to which each pad was subjected. For pad A, for instance, the vertical stresses at points a,b,c,d,e,f,g,h and A were averaged and multiplied by the area of the pad to give the average vertical reaction. The values of these reactions are also shown in the figures. The manner in which these forces were calculated eliminated the effect of bending stresses. Comparing these reactions with the vertical load in each column, which are also given in the figure, it is noticed for the left hand pad that the maximum difference is 9.2% for the symmetric load case, falling to 2.4% for the most highly loaded pad. For the right hand pads the difference is 9.2% for e = 0.0, 13.1% for e = 0.33, 12.8% for e = 0.67 and 35.0% for e = 0.91. The worst case is the last where it is noticed that tensile stresses have developed under the right hand pad. This was not allowed for in the computer finite element analysis and suggests that future development of the work should provide

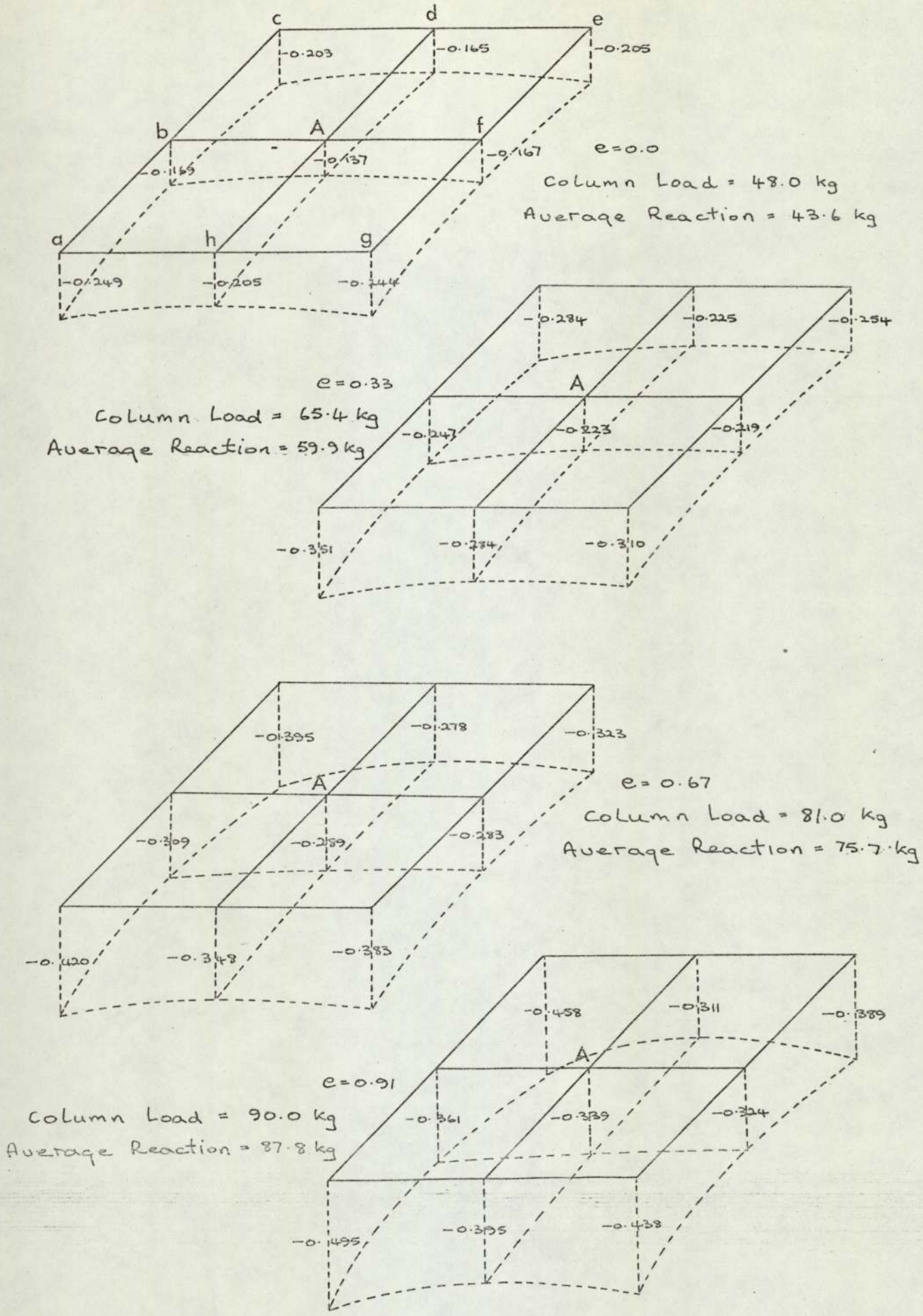

Figure 8.25 Vertical Stress Distribution Beneath the Left Hand Pad , W≑200Kg

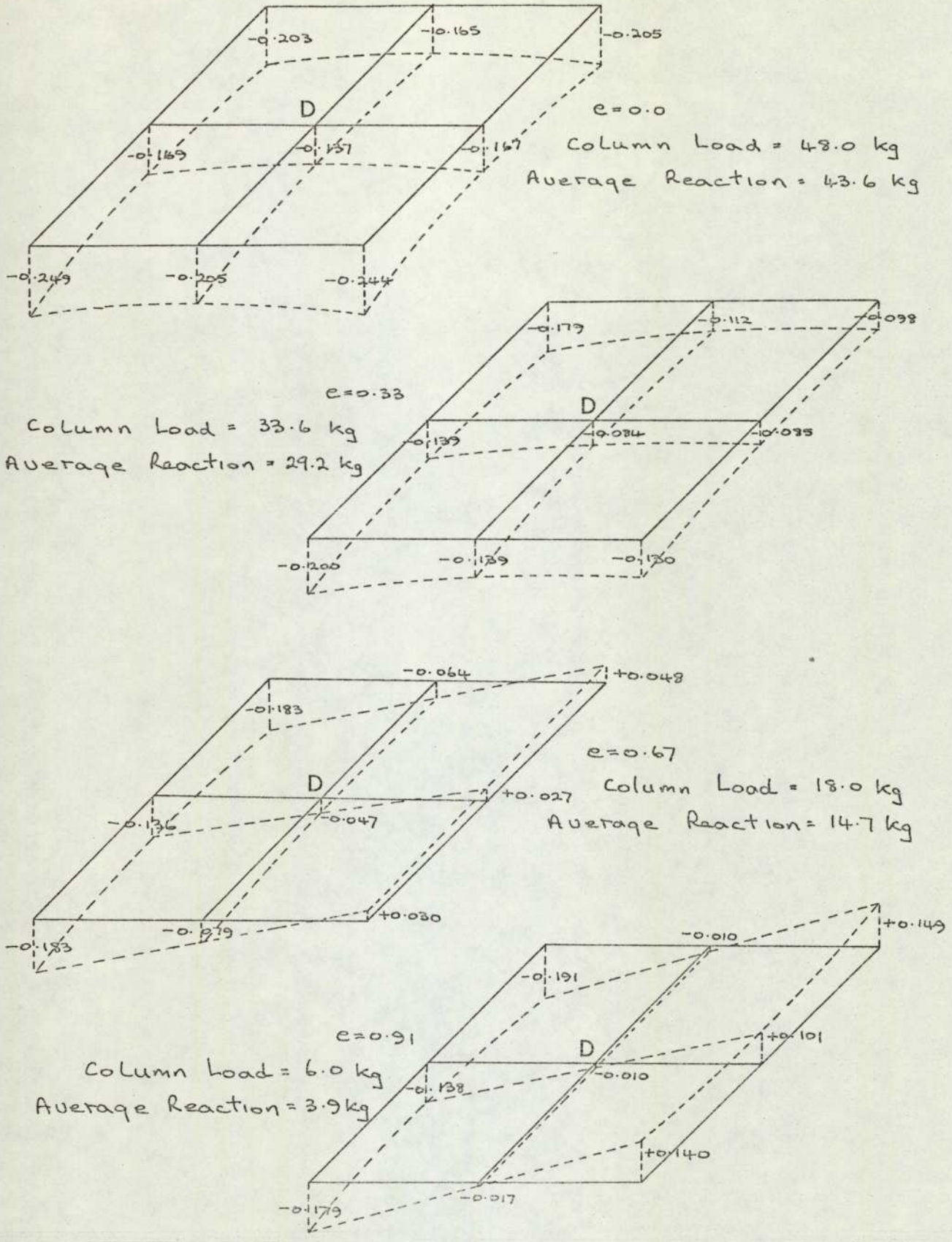

Figure 8.26 Vertical Stress Distribution Beneath the Right Hand Pad . W≐200Kg

8.6) contd.

facilities to allow for the separation of the footing and the soil. It should be pointed out that the stress level under the right hand pad is so low that averaging does not necessarily lead to realistic values. Furthermore, as can be seen in the figures, the distribution of stresses under a pad is non-linear and hence the above averaging process is approximate.

Figures (8.27) and (8.28) give the stress contours after σ_y and σ_x throughout the depth of the soil foundation in the plane YX through the centre of the left hand pad. It is evident that in most cases a distinct column of high stresses is developed under the footing. This was also observed by Majid and Craig[99] for the case of a two dimensional model.

It should be pointed out that the present model deals with a three dimensional frame supported by a deep bed of non-linear sand, in which the stiffness of the structure and the soil are both taken into consideration. The pad footings unlike the model of Majid and Craig are therefore subjected to both axial forces and bending moments. For these reasons, it is expected that the results obtained here could not have been achieved by the above workers. Indeed Figures (8.27) and (8.28) show how eccentric loading results in a complete redistribution of both σ_x and σ_y throughout the foundation. In particular the existence of bending moments has given rise to the development of high stresses under the footing in an unsymmetrical manner. On the other hand the results also suggest that the analysis should be altered to cope with tensile zones that develop in the sand. Noticed in the figure are small zones of zero stress which are developed away from the pad. Finally figures (8.29) and (8.30) show the distribution of σ_y in the plane Y-Z through the centre of the left and right hand pads. On the other hand

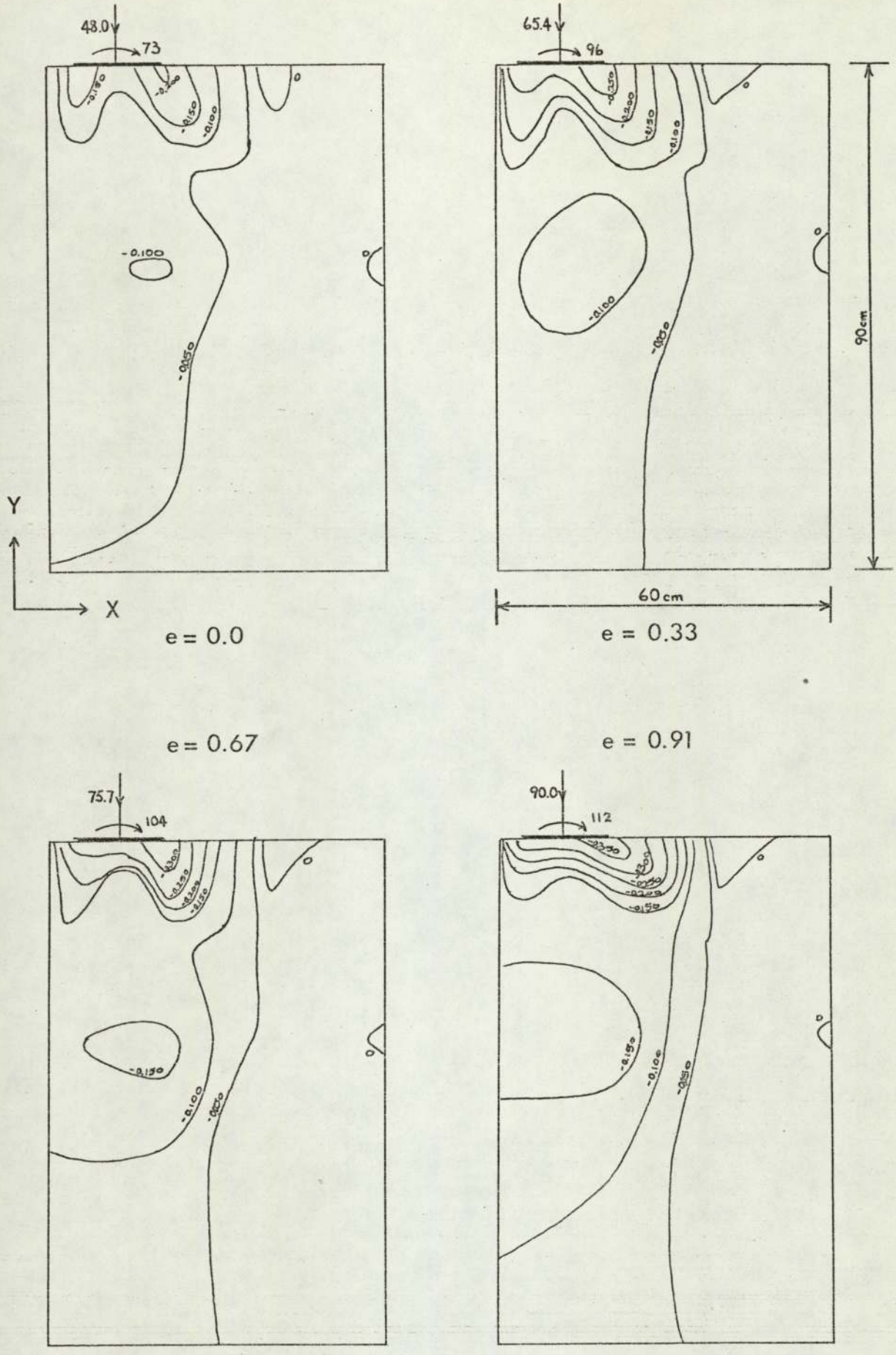

Figure 8.27 Contours of the Stress σ_y beneath the left hand pad

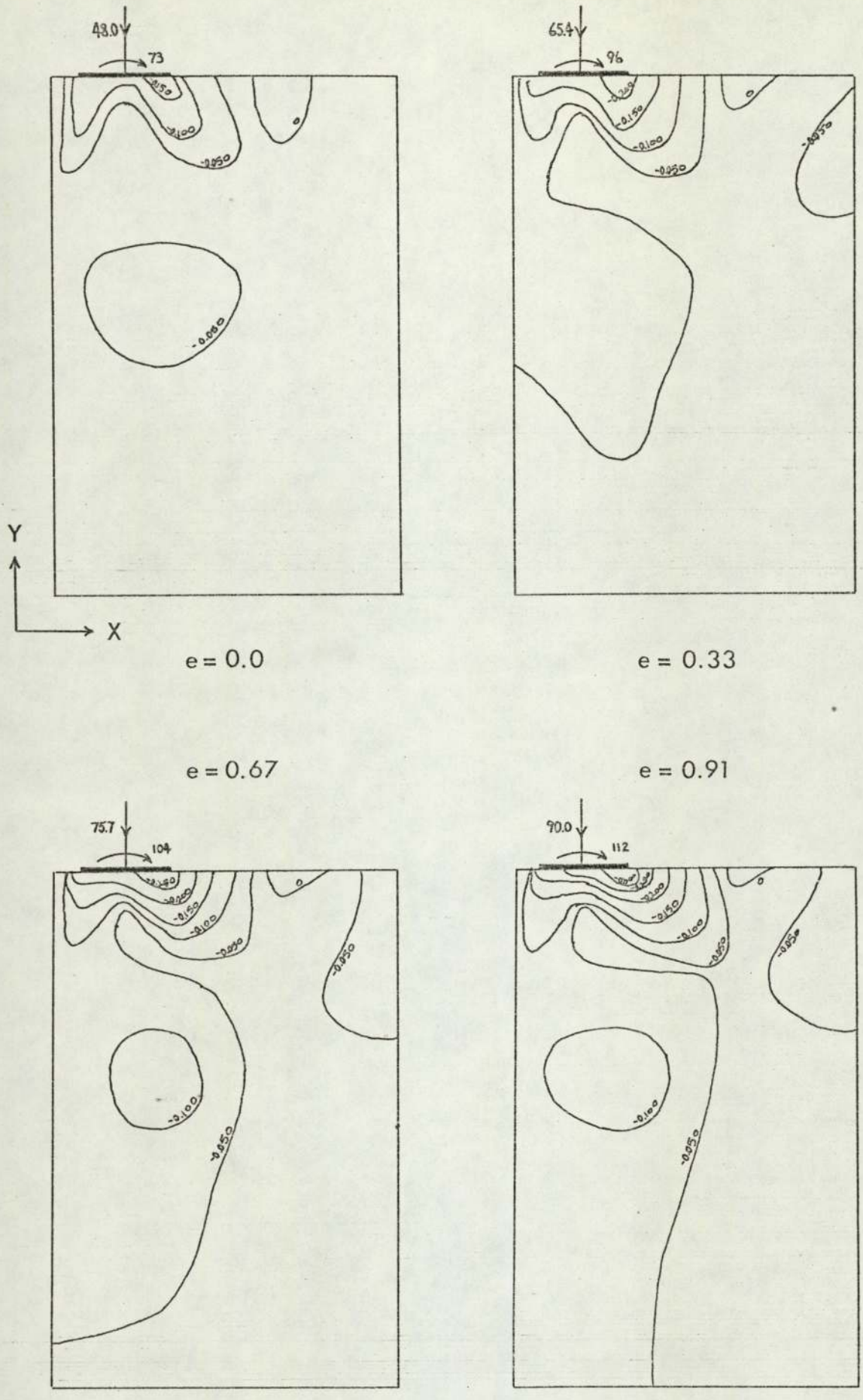

Figure 8.28 Distribution of the Stress σ_x beneath the left hand pad

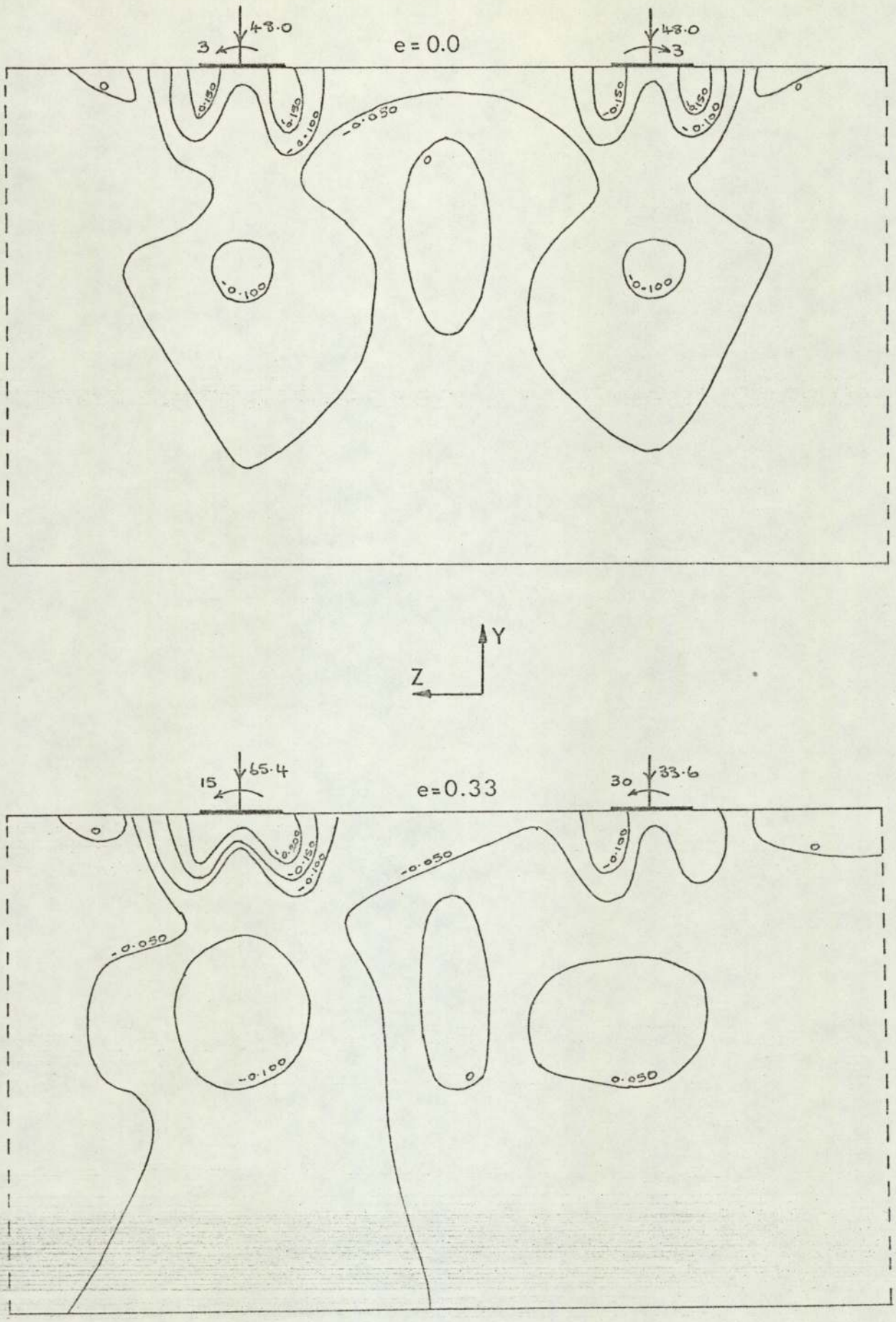

Figure 8.29 Contours of the Stress σ_y under both Pads, in Kg/cm².

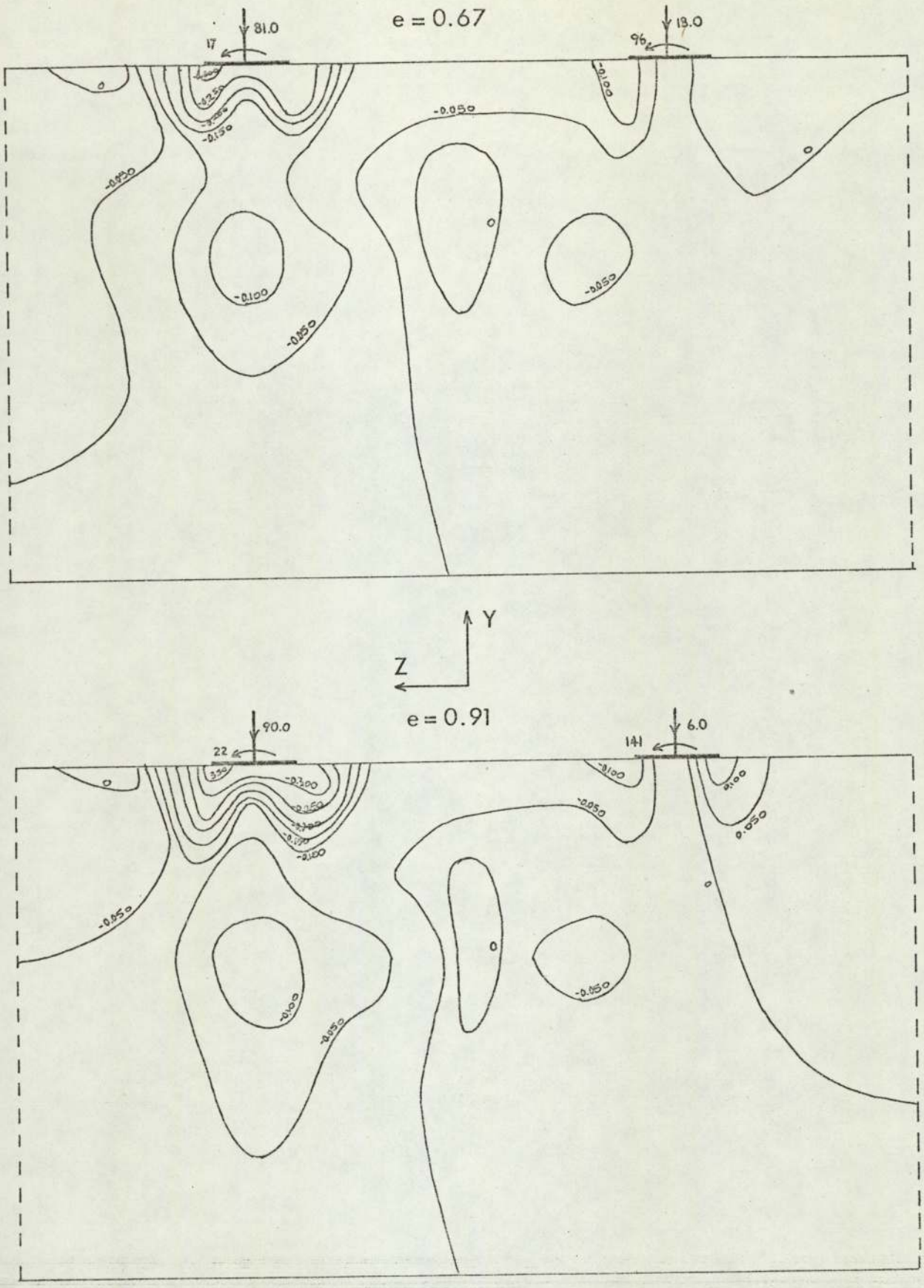

Figure 8.30 Contours of the Stress σ_y under both Pads, in Kg/cm^2.

8.6) contd.

figures (8.31) and (8.32) show σ_z in this plane. These figures lead to the same conclusions as those stated earlier.

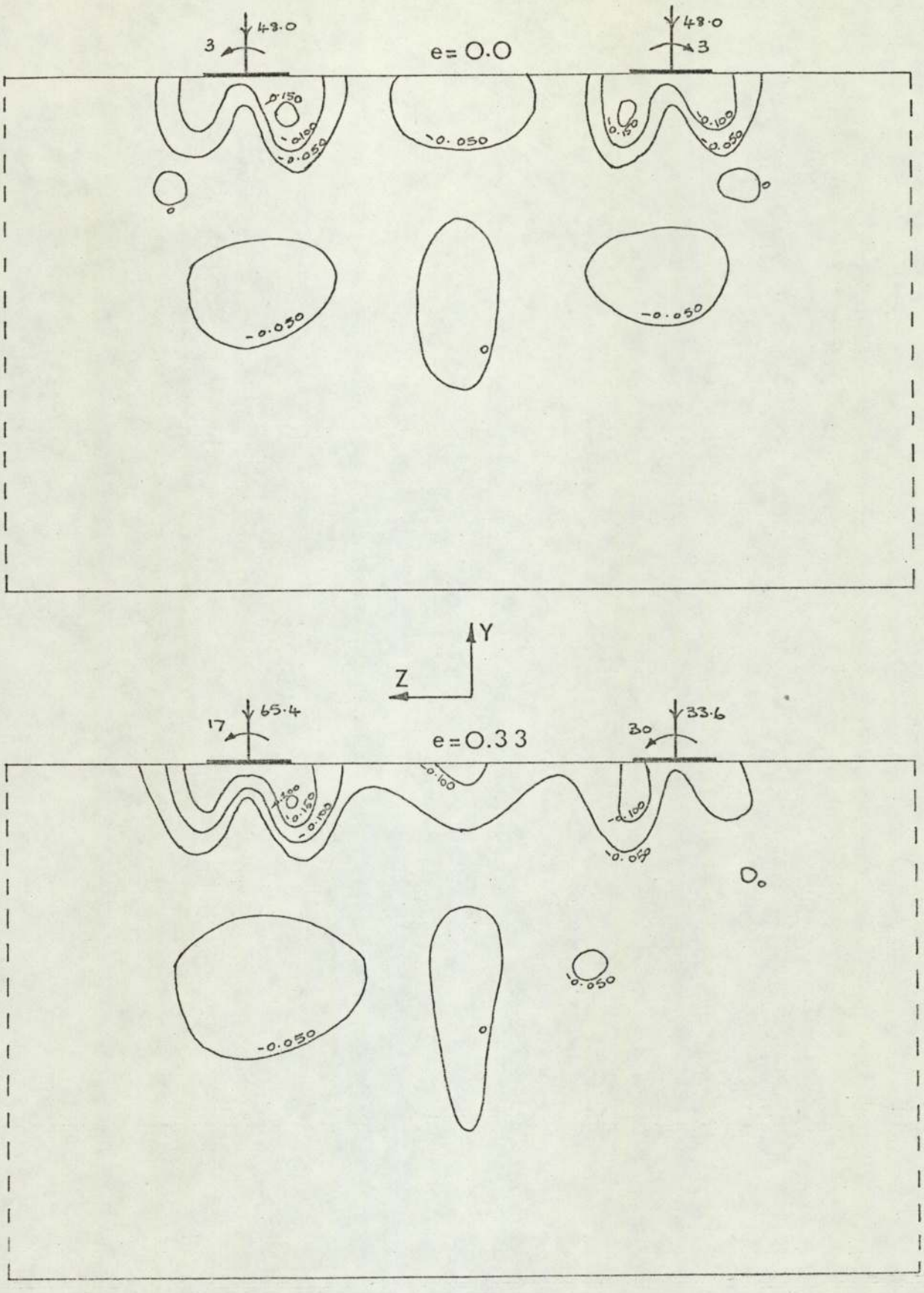

Figure 8.31 Contours of the Stress σ_{zz} under both Pads, in Kg/cm^2.

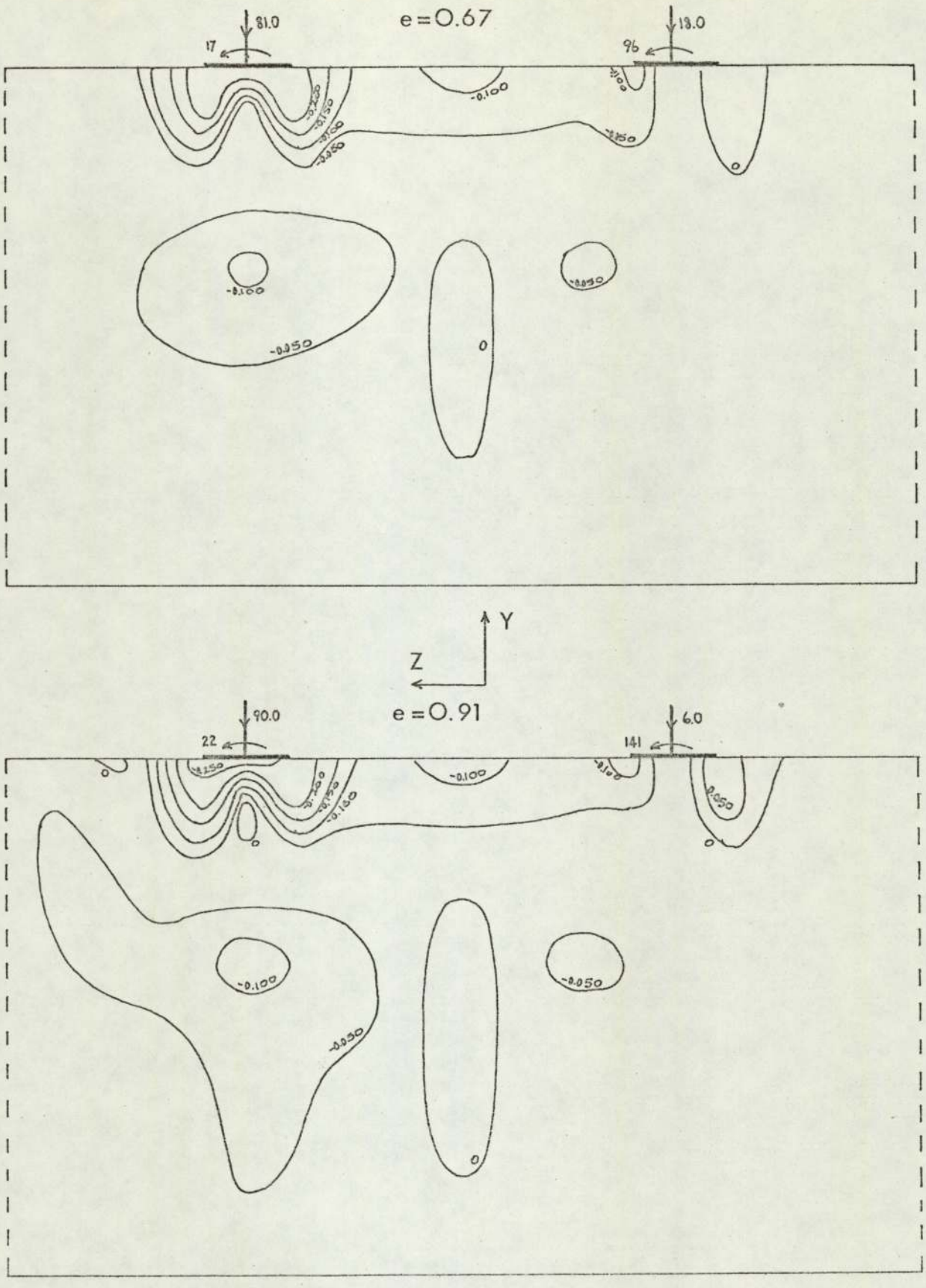

Figure 8.32 Contours of the Stress σ_z under both Pads, in Kg/cm^2.

CHAPTER 9

GENERAL CONCLUSIONS AND SUGGESTIONS FOR FUTURE WORK.

This thesis has investigated the use of the Finite Element technique in various problems in Civil Engineering. In all these problems the main considerations have been to obtain both a realistic structural idealisation and a realistic representation of the material behaviour.

To satisfy the first criterion, a major part of the work has involved producing a number of computer algorithms. These algorithms have been formed into various programs to carry out Finite Element stress analysis using the new families of two and three dimensional Isoparametric elements. It was essential that the techniques for forming the various stiffness matrices, should be both efficient and general. The former, because the Isoparametric elements require numerical integration, and the latter so that other elements could be added without major reprogramming.

From comparing the results obtained using the various two dimensional elements, several conclusions were drawn. Firstly, all the elements developed, were proved to be in good agreement with the analytical solution, showing that their development had been accurate. Secondly, the linear triangle gave much the worst results and they were also the most expensive to obtain. The eight noded Isoparametric quadrilateral was shown to give the best value for effort in terms of computer time, storage and data preparation.

It was noticed that the stresses near to the applied load were over or under estimated. The effect counted most against the cubic elements because of their larger size. The most significant effect of mesh refinement was that a better representation of the applied uniform pressure was achieved. From this point of view it would be worthwhile adding a special loading element to the element library. This element would have a large number of nodes on one face to which the pressure would be applied.

It was further noticed from these analyses that a large number of zeros were stored in the overall stiffness matrix. This was particularly apparent in the three dimensional elements, because of the large numbers of element nodes involved. This unnecessary storage could be saved by writing the element stiffness terms straight to the blocks required by the solution routine. Other possibilities are to revert to the traditional sparse matrix techniques, or, the frontal solution techniques.

The analysis of the plane strain compression test proved that the finite element method could be very useful in interpreting laboratory test results. It was concluded that, in agreement with experimental observations, the applied shear stresses caused by the friction on the surface of the loading platten led to zones of low stress under the centre of the platten. It was also demonstrated that it was possible to represent smooth surfaces, realistically and simply, by using sandwich elements of relatively low stiffness. It was noticed from the results that the vertical stress at every node under the platten was in exact agreement with the average applied pressure. In most Civil Engineering situations the load is applied through some body, so the errors involved in the Finite Element method, when using surface pressures, may not be as important as they first appeared.

The Finite Element technique was also used in Chapter (4) to follow the path of crack propagation. The method allowed separation to occur along element boundaries, and was shown to be in excellent agreement with an experiment result. In these analyses cracks were only allowed to develop in one direction. In reality cracks may go in any direction, thus the method could be improved by allowing separation along any element boundary. Automating the mesh changes necessitated by activating dummy nodes would considerably speed

up the procedure.

The major part of this thesis has been devoted to the model tests and their theoretical analysis. These proved to give very promising results, but clearly there was room for improvement and further research on both theoretical and experimental sides.

The sand deposition apparatus described in Chapter (5) was shown to be capable of forming large uniform beds of sand over almost the complete range of porosity. The model testing apparatus and technique proved reliable but a good deal could be gained from automating the test procedures. The twenty or so dial gauges could be replaced by displacement transducers, which could be automatically logged. This would avoid the need for the experimentor to clamber around the bed to read the dial gauges, with obvious danger to both himself and the test. The sand pouring technique could be improved by replacing the hand propulsion of the hopper by an electric motor, allowing exactly uniform speeds to be followed.

Extensions to the model testing should include the measurement of other quantities apart from displacements. Strain gauges on the model structure would allow bending moments to be calculated and stress transducers in the bases of the pads could measure contact stresses. Both the strain gauges and the stress transducers could be logged automatically, and would be a further valuable check on any proposed analysis method. All the model tests reported here were loaded symmetrically, founded on a uniform bed of sand and possessed members of the same section. Most structures are unsymmetrically loaded and most soils gain strength with depth. Both these conditions could be achieved, the first by applying the load on one of the side beams and the second by varying the apperture setting as the bed filled. It was shown that the stiffness of the structure played a very important part in determining the differential settlements. This

could be further confirmed by testing other frames of the same overall dimensions, but with different sections for the members.

It was seen from the theoretical analyses that the assumed hyperbolic relation for the sand behaviour, led to a reasonable agreement between the theoretical and experimental results. This hyperbola was chosen because of its simplicity and relation to physical parameters. However, recent work has shown that a single curve cannot adequately represent the stress-strain curve, and this was readily seen in the theoretical results. The use of spline functions would lead to a better representation of the stress-strain response.

However, a constant value of Poisson's ratio was assumed for the second hypo-elastic constant. In reality, sand could have a ratio greater than 0.5, because of dilatency under shear. Further, the stress-strain parameters were measured under conditions of axial symmetry, with a constant cell pressure and monotonically increasing vertical load. In the model, axi-symmetric conditions were only approximated to under the centre of the pads. The magnitude of the horizontal stresses in the test bed were dependent on the vertical stress. The actual stress path followed by the soil elements appears, from the results, to be nearer to a constant ratio of vertical to horizontal stress, rather than a constant horizontal stress.

It is from a truer representation of the material behaviour that the greatest benefit will be gained. This depends upon further research into the three points outlined above. However, whatever method is decided on, if it is to be used in practice then long laboratory programmes and complicated testing equipment must be avoided.

Improvements in the theoretical analysis can be derived

from three parts. First, the material model which has just been discussed, second, a higher order element and lastly a better method of following the non-linear stress-strain curve. The second point involves a change in the method of storing the overall stiffness matrix. It was shown from the results that the errors involved in the tangent modulus method accumulate. The problems that arose with convergence of the iterative secant modulus method were a function of the properties of sand at low pressure. At higher pressures, such as those in Chapter (3), no such problems would be encountered. The immediate problem of speeding convergence for model test analyses could be helped by some process such as overrelaxation. The non-linear procedure should also include a facility to allow the footings and sand to separate should tensile contact stresses arise. This could easily be achieved using dummy joints in a very similar manner to the crack propagation method.

It has been shown by both the theoretical and experimental results for the model space frame that the stiffness of a structure has an extremely important effect on differential and sway displacements. This effect is caused by a redistribution of bending moments in the superstructure and is so significant that it compensates for other effects such as interaction. Design approaches considering the superstructure alone, or the footings alone, severely oversimplify the problem. It is only by including both parts in the analysis that a realistic representation is achieved.

APPENDIX 1.

S. I. UNITS.

This report is based on the SI system of units. The name Système International d'Unités and the international abbreviation SI are used for the systematically organized system of units introduced by the General Conference of Weights and Measures in 1960 and later endorsed by the International Organization for Standardization. The SI system is constructed around six base units which are:

Quantity	Unit	Symbol
length	metre	m
mass	kilogramme	kg
time	second	s
electric current	ampere	A
thermodynamic temperature	kelvin	K
luminous intensity	candela	cd

All derived units are stated in terms of these six base units and for some of the derived units special names and symbols exist. The system provides a naturally coherent unit of force called the newton. This is defined as the force which, when applied to a body having a mass of one kilogramme, gives it an acceleration of one metre per second per second and is thus independent of gravitational acceleration. The more common SI derivatives and their equivalents in British values are listed below.

Quantity:	Unit:	Symbol:	Equivalent:
length	metre	m	39.3701 in
area	square metre	m^2	1 550 in^2
volume	cubic metre	m^3	61 023.7 in^3
volume	litre	l	0.22 UK gall
velocity	metre/second	m/s	3.280 84 ft/sec
acceleration	metre/second/second	m/s^2	3.230 84 ft/sec^2
mass	kilogramme	kg	2.204 62 lb
density	kilogramme/$metre^3$	kg/m^3	0.062 428 lb/ft^3
force	newton	N	0.224 809 lbf
torque	newton metre	N m	0.737 562 lbf ft
pressure	newton/square metre	N/m^2	0.000 145 038 lbf/in^2
dynamic viscosity	newton second/$metre^2$	$N\,s/m^2$	0.020 885 lbf s/ft^2
kinematic viscosity	metre squared/second	m^2/s	10.763 9 ft^2/sec
stress	newton/square metre	N/m^2	0.000 145 038 lbf/in^2
energy	joule	J	0.737 562 ft lbf
energy	joule	J	0.277 778 Wh
heat	joule	J	0.000 947 813 Btu
power	watt	W	0.001 341 hp
frequency	hertz	Hz	1/second

Multiples and submultiples of the units are formed by adding prefixes. A prefix added to any unit is subject to any power applied to the unit. For example 1 mm^3 means 1 $(mm)^3 = 10^{-9}\ m^3$ and <u>not</u> $10^{-3}\ m^3$. The standard prefixes are

T	tera	10^{12}	*da	deca	10	n	nano	10^{-9}
G	giga	10^{9}	*d	deci	10^{-1}	p	pico	10^{-12}
M	mega	10^{6}	*c	centi	10^{-2}	f	femto	10^{-15}
k	kilo	10^{3}	m	milli	10^{-3}	a	atto	10^{-18}
*h	hecto	10^{2}		micro	10^{-6}			

*(These are not preferred choice)

For further information readers should refer to:

THE USE OF SI UNITS. British Standards Institution publication PD 5686 1969
CHANGING TO THE METRIC SYSTEM. National Physical Laboratory. HMSO 1969.

APPENDIX 2.

DESCRIPTION OF ELEMENTS.

A2.1 Two Dimensional Elements

In order to analyse general two dimensional structures and the underlying foundation material it is necessary to include a member element in the library. It also means that no assumptions have to be made about the stress distribution beneath footings of various rigidity. It is also desirable to include the triangle since traditionally this has been the most popular element. Both these elements are well known so they are only dealt with briefly.

Any modern Finite Element analysis must make use of the new powerful families of Isoparametric curvilinear quadrilaterals. It is these elements which are being considered in detail in this thesis.

A2.1.1 Member Element

Figure(A2.1) shows a member situated in the plane XY and defined in this global system. For convenience of formulation the member is also defined in local axes pq such that the p-axis is in the direction end 1 to end 2 and the q-axis is perpendicular to it, as shown in the figure.

The stiffness matrix of an element is shown below. This is the one quoted by Majid (62) in his text.

$$\begin{bmatrix} H_i \\ V_i \\ M_i \\ H_j \\ V_j \\ M_j \end{bmatrix} = \begin{bmatrix} A & & & & & \\ B & F & & & & \\ -C & -T & e & & & \\ -A & -B & C & A & & \\ -B & -F & T & B & F & \\ -C & -T & f & C & T & e \end{bmatrix} \begin{bmatrix} u_i \\ v_i \\ \theta_i \\ u_j \\ v_j \\ \theta_j \end{bmatrix} \qquad (A2.1)$$

where $A = aL^2_p + bL^2_q$ $\qquad B = aL_p M_p + bL_q M_q$

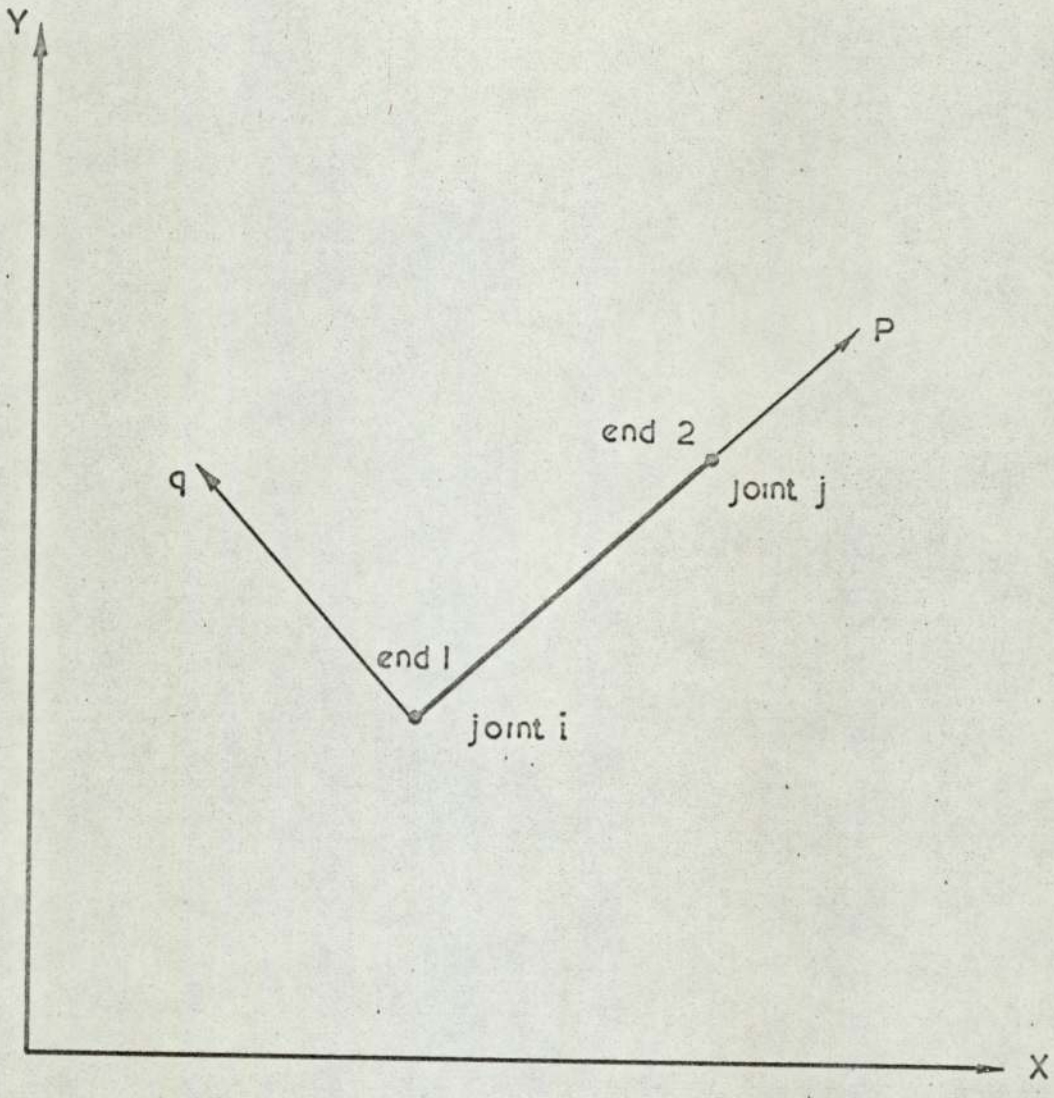

Figure A. 2.1. Plane member element

$$C = dL_q \qquad F = aM^2_p + bM^2_q \qquad T = dM_q$$

and $$a = \frac{EA}{L} \qquad b = \frac{12EI}{L^3} \qquad d = \frac{-6EI}{L^2}$$

$$e = \frac{4EI}{L} \qquad f = \frac{1}{2}e$$

where E is the modulus of elasticity

I the moment of inertia

A the cross sectional area

L the length of the member,

and L_p, L_q, M_p and M_q are direction cosines. Each end of the member is allowed three 'in plane' degrees of freedom, two translational and one rotation.

A 2.1.2 Triangular Element

This element was the first Finite Element and it is still popular today. It is very easy to formulate and has been proved ideal for mesh grading and refinement. The triangular shape is probably the most convenient one being a polygon with the least number of sides.

Figure(A2.2) shows a triangular element situated in the plane pq of its local axis. The p axis runs from node 1 to node 2 and the q axis is perpendicular to it in the direction of node 3. Each node of this element is allowed two translational degrees of freedom. As the element has only three nodes the displacement function is the simplest complete polynomial. The stiffness matrix of the triangular element can be represented by equation (A2.2).

$$\underline{K} = \begin{bmatrix} K_{11} & & \\ K_{21} & K_{22} & \\ K_{31} & K_{32} & K_{33} \end{bmatrix} \qquad (A2.2)$$

The on-diagonal terms K_{11}, K_{22} and K_{33} are defined by:

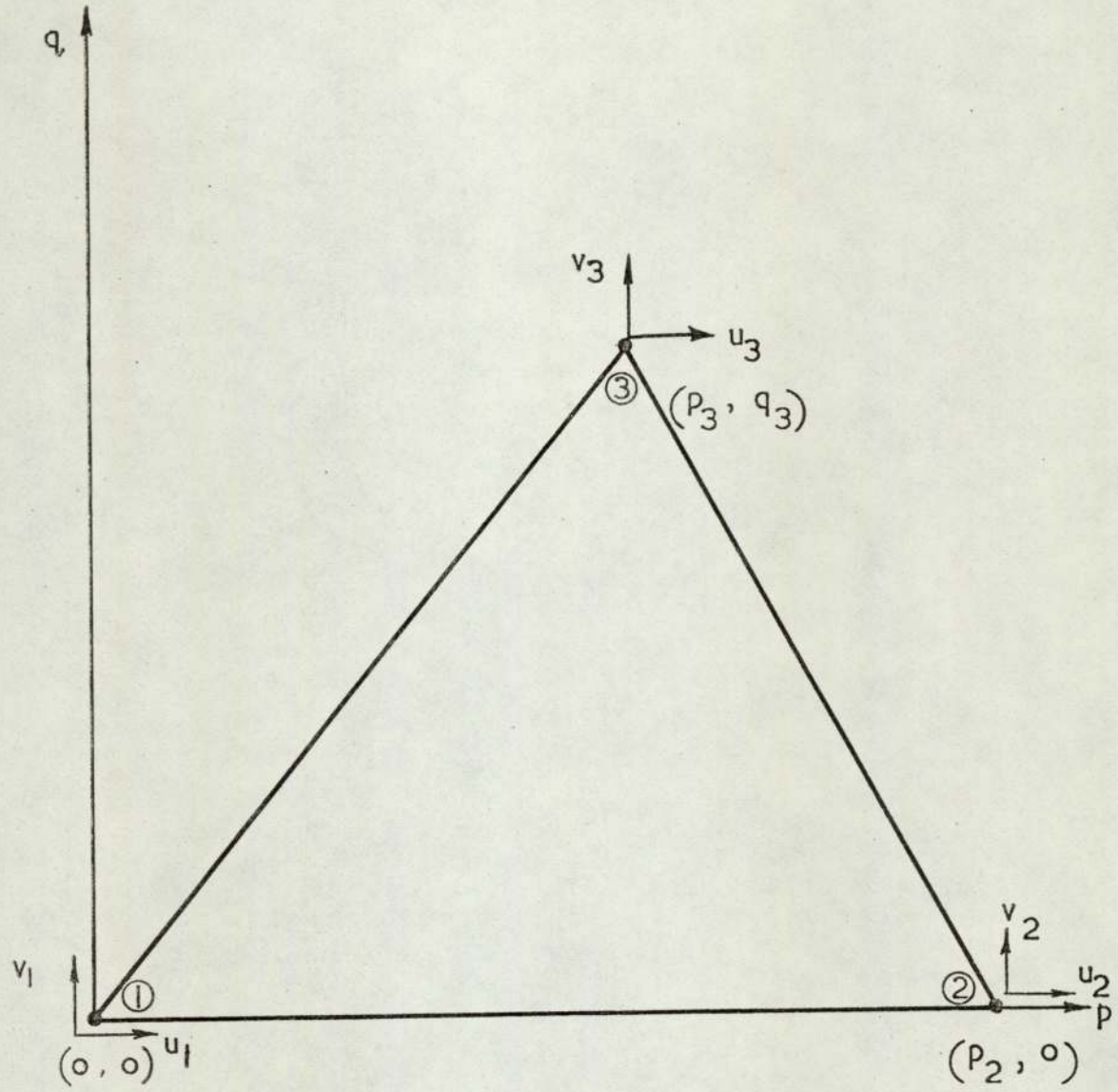

Figure A. 2.2. Triangular element.

$$\underline{K}_{ii} = \begin{bmatrix} L_p^2 k_{\ell\ell} + 2L_p L_q k_{m\ell} + L_q^2 k_{mn} & \text{SYMMETRIC} \\ L_p M_p k_{\ell\ell} + (M_q L_p + M_p L_q) k_{m\ell} + M_q L_q k_{mm} & M_p^2 k_{\ell\ell} + 2M_p M_q k_{m\ell} + M_q^2 k_{mn} \end{bmatrix} \qquad (A2.3)$$

where $k_{\ell\ell}$, k_{mn} and $k_{m\ell}$ are defined in equation (A2.5) and $m = 2i$, $\ell = m-1$.

The off-diagonal terms K_{21}, K_{31} and K_{32} are defined by:

$$\underline{K}_{jk} = \begin{bmatrix} L_p^2 k_{m\ell} + L_p L_q (k_{mp} + k_{o\ell}) + L_q^2 k_{op} & L_p M_p k_{m\ell} + M_p L_q k_{o\ell} + M_q L_p k_{mp} + M_q L_q k_{op} \\ L_p M_p k_{m\ell} + M_p L_q k_{mp} + M_q L_p k_{o\ell} + M_q L_q k_{op} & M_p^2 k_{m\ell} + M_p M_q (k_{mp} + k_{o\ell}) + m_q^2 k_{op} \end{bmatrix} \qquad (A2.4)$$

where $j > k$ and $0 = 2j$, $m = 0-1$, $p = 2k$ and $\ell = p-1$. The terms $k_{m\ell}$ etc are defined below and L_p, L_q, M_p and M_q are again direction cosines.

$$k = \frac{1}{2p_2q_3} \begin{bmatrix} q_3^2\alpha_1 + (p_3-p_2)^2\alpha_3 & & & & & \\ -q_3(p_3-p_2)\alpha_2 + -q_3(p_3-p_2)\alpha_3 & (p_3-p_2)^2\alpha_1 + q_3^2\alpha_3 & & \text{SYMMETRIC} & & \\ -q_3^2\alpha_1 + -q^3(p_3-p_2)\alpha_3 & q_3(p_3-p_2)\alpha_2 + p_3q_3\alpha_3 & q_3^2\alpha_1 + p_3^2\alpha_3 & & & \\ q_3^2\alpha_2 + q_3(p_3-p_2)\alpha_3 & -q_3(p_3-p_2)\alpha_1 + -q_3^2\alpha_3 & -q_3^2\alpha_2 + -p_3q_3\alpha_3 & q_3^2\alpha_1 + q_3^2\alpha_3 & & \\ p_2(p_3-p_2)\alpha_3 & -q_3p_2\alpha_3 & -p_3p_2\alpha_3 & p_2q_3\alpha_3 & p_2^2\alpha_3 & \\ -q_3p_2\alpha_2 & p_2(p_3-p_2)\alpha_1 & q_3p_2\alpha_2 & -q_3p_2\alpha_1 & 0 & p_2^2\alpha_1 \end{bmatrix} \qquad (A2.5)$$

where p_2, p_3 and q_3 were defined in the figure and α_1, α_2 and α_3 are defined below as the $\underline{D}$ matrix in $\{\sigma\} = \underline{D}\{\varepsilon\}$ as

$$\underline{D} = \begin{bmatrix} \alpha_1 & \alpha_2 & 0 \\ \alpha_2 & \alpha_1 & 0 \\ 0 & 0 & \alpha_3 \end{bmatrix} \qquad (A2.6)$$

A2.1.3 Higher Order Elements

The two previous elements are both constant strain elements, in that the strain, and hence the stress, is independent of position. Where large variations of stress occur in a continua many elements would be required to obtain an adequate solution. An increase in the number of nodes of an element adds extra terms into the polynomial and hence improves the accuracy of the solution. In the case of complex boundary shapes, often curved, methods other than Finite Element analysis are very difficult to apply. It is therefore necessary to have elements able to distort into arbitrary shapes.

A2.1.3.1 Rectangular Elements

Traditionally shape functions for rectangles possessing any number of nodes are formulated by writing a polynomial to define the unknown displacements. For example, for a rectangle having n nodes this polynomial is defined as:

$$u = a_1 + a_2x + a_3y + a_4xy + a_5x^2 + a_6y^2 \quad \ldots\ldots\ldots \quad (A2.7)$$

Substituting the known co-ordinates at each node into equation (A2.7) a set of equations is obtained:

$$\{\delta\} = \underline{C}\{a\} \quad (A2.8)$$

where $\{\delta\} = \{u_1\ u_2\ \ldots\ u_n\}$

$\{a\} = \{a_1\ a_2\ \ldots\ a_n\}$

and $\underline{C}$ contains coefficients depending upon the position of the nodes. To obtain the unknown constants this set of simultaneous equations are solved:

$$\{a\} = \underline{C}^{-1}\{\delta\} \quad (A2.9)$$

Back substituting these constants the interpolation formula is obtained

$$u = N_1u_1 + N_2u_2 + \ldots N_n\ u_n \quad (A2.10)$$

One property of the shape function is revealed by equation (A2.10) that is if $u = u_i$ then $N_i = 1$ and all other functions must be zero.

For rectangles having only four nodes considerable effort is involved in arriving at equation(A2.10) and the effort grows rapidly with increase in the number of nodes. The method does have the advantage that the right terms are visibly selected from a polynomial. The polynomials should be complete up to a certain degree.

Considerable savings can be made by obtaining equation(A2.10) directly. Displacement fields can be constructed satisfying the various criteria, in certain polynomials. These give rise to two basic families called Lagrangian and Serendipity by Zienkiewicz (98) in his text.

A2.1.3.1.1 Local Co-ordinates

Before going on to describe the families it is worth considering the role of the local co-ordinate system. In the triangle the origin of the system was chosen at corner one and its directions defined from there. For rectangles it seems more logical to have the origin at the centre, orientated parallel to the sides as shown in figure(A2.3a). Thus, the bottom left hand corner is defined as (-b,-a). It is more convenient if these co-ordinates are normalised such that $p = \frac{x}{b}$ and $q = \frac{y}{a}$ so the local co-ordinates p and q vary between the limits -1 and +1 as illustrated in figure(A2.3b).

A2.1.3.1.2 Lagrangian Family

A complete family of rectangular elements can be derived from the cross multiplication of one dimensional Lagrangian interpolation formulae of varying degrees. By having (n+1) nodes in the p direction and (m+1) nodes in the q direction, a total of (n+1)(m+1) nodes, the displacements can have up to an n^{th} degree of variation in the p direction and an m^{th} degree in the q direction.

In general the lagrangian polynomial at a point i can be expressed as:

$$L^n_i = \frac{(p-p_1)(p-p_2) \ldots (p-p_{i-1})(p-p_{i+1}) \ldots (p-p_n)}{(p_i-p_1)(p_i-p_2) \ldots (p_i-p_{i-1})(p_i-p_{i+1}) \ldots (p_i-p_n)} \quad (A2.11)$$

and hence the interpolation function for a two dimensional element is

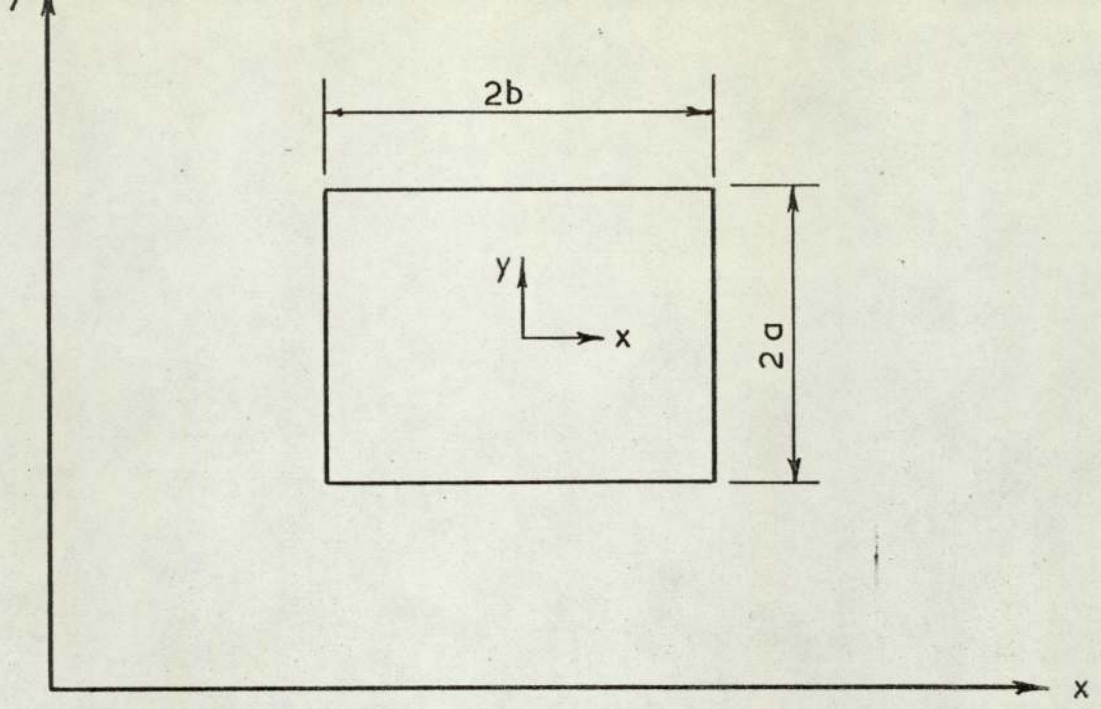

Figure A 2.3 a. Local co-ordinates

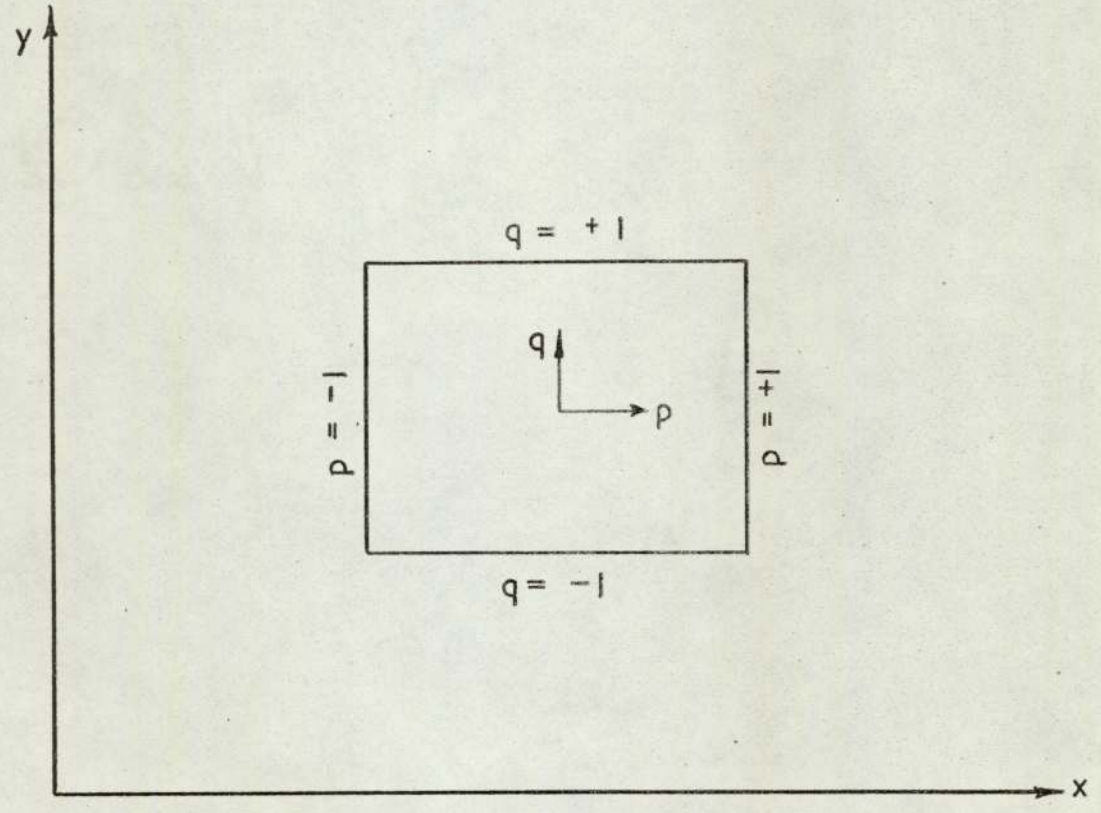

Figure A. 2.3.b Normalised local co-ordinates

$$N_{ij} = L^n_i(p)\, L^m_j(q) \qquad (A2.12)$$

where i and j define the node in a regular grid such as that in figure (A2.4b). The first three members of this family are shown in figure (A2.4). As an illustration of this family, consider the quadratic element shown in figure (A2.4b) and form the shape function at node 6 (i.e. i = 3, j = 2).

$$L^n_3 = \frac{(p-p_1)(p-p_2)}{(p_3-p_1)(p_3-p_2)} \qquad (A2.13.1)$$

$$L^m_2 = \frac{(q-q_1)(q-q_2)}{(q_2-q_1)(q_2-q_3)} \qquad (A2.13.2)$$

$$\therefore N_6 = \frac{(p-p_1)(p-p_2)(q-q_1)(q-q_3)}{(p_3-p_1)(p_3-p_2)(q_2-q_1)(q_2-q_3)} \qquad (A2.14)$$

and substituting in the values of the co-ordinates p_1, p_2 etc.

$$N_6 = \frac{1}{2}(p + p^2 - pq^2 - p^2q^2) \qquad (A2.15)$$

It is clear that the shape factors for the lagrangian elements can be generated automatically.

A 2.1.3.1.3 Serendipity Family

This other family of rectangles is where the nodes are concentrated on the boundaries of the element as much as is possible. The cartesian polynomials are complete with the addition of a few extra terms. The shape functions were derived intuitively using the property discovered in equation (A2.10) with the convergence criteria. The first three elements of this family are shown in figure (A2.5).

The shape functions quoted by Zienkiewicz (98) in his text are:-

(1) Linear Element (Fig.A2.5a)

$$N_i = \frac{1}{4}(1 + p_o)(1 + q_o) \qquad (A2.16)$$

where $p_o = pp_i$

$q_o = qq_i$

This is identical to the first member of the Lagrangian Family.

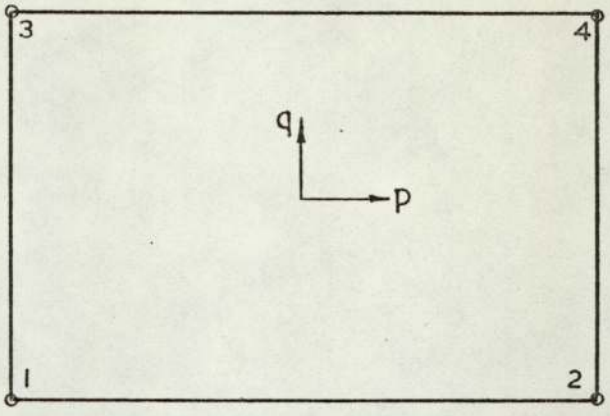

Figure A2.4. a. Linear element (4 nodes)

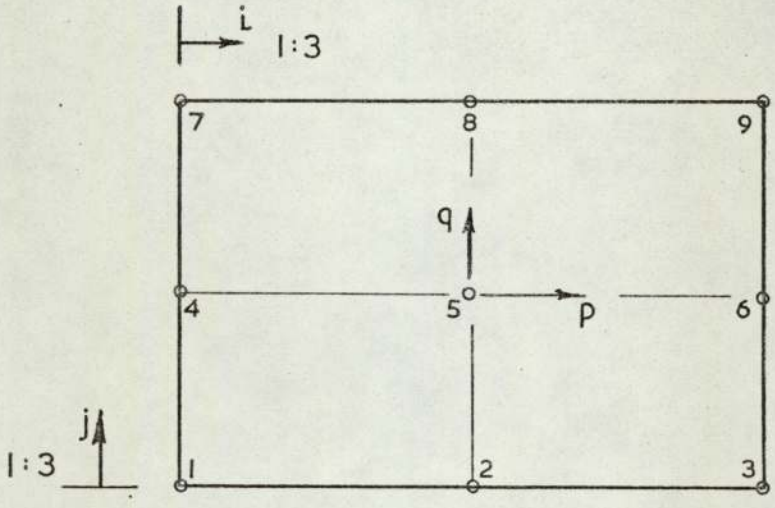

Figure A2.4. b. Quadratic element (9 nodes)

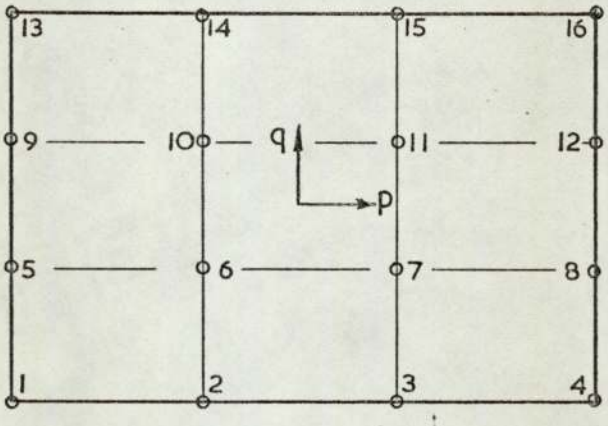

Figure A2.4.c. Cubic element (16 nodes)

Lagrangian family of rectangular elements

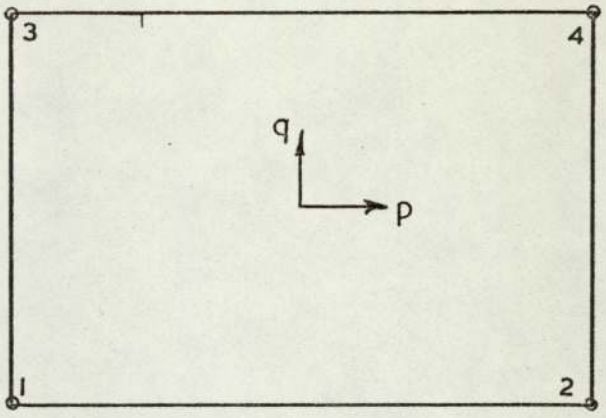

Figure A2. 5. a. Linear element (4 nodes)

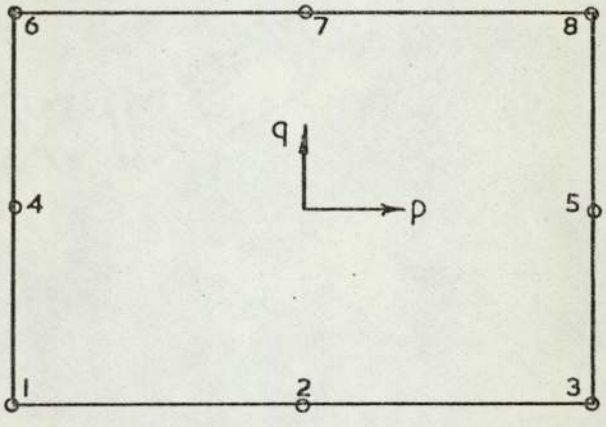

Figure A2. 5. b. Quadratic element (8 nodes)

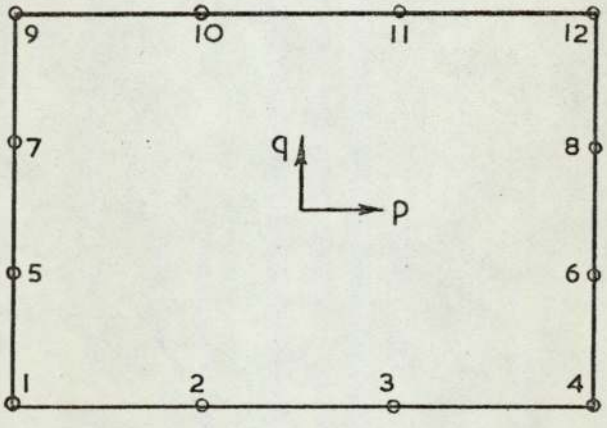

Figure A2. 5. c. Cubic element (12 nodes)

Serendipity family of rectangular elements.

(2) Quadratic Element (Fig.A2.5b)

Corner nodes $N_i = \frac{1}{4}(1 + p_o)(1 + q_o)(p_o + q_o - 1)$ (A2.17.1)

Mid-Side nodes $p_i = 0 \quad N_i = \frac{1}{2}(1 - p^2)(1 + q_o)$ (A2.17.2)

$q_i = 0 \quad N_i = \frac{1}{2}(1 + p_o)(1 - q^2)$ (A2.17.3)

(3) Cubic Element (Fig.A2.5c)

Corner nodes $N_i = \frac{1}{32}(1 + p_o)(1 + q_o)(-10 + 9)(p^2 + q^2))$ (A2.18.1)

Mid-Side nodes $p_i = \pm 1, \; q = \pm\frac{1}{3} \quad N_i = \frac{9}{32}(1 + p_o)(1 - q^2{}_2)(1 + 9q_o)$ (A2.18.2)

$p_i = \pm\frac{1}{3}, \; q_i = \pm 1 \quad N_i = \frac{9}{32}(1 + q_o)(1 - p^2)(1 + 9p_o)$ (A2.18.3)

A 2.1.3.2 Isoparametric Quadrilaterals

Quadrilateral elements cannot be formulated satisfactorily from cartesian polynomials, like those in the previous sections. They require the introduction of a curvilinear co-ordinate system having the same range, -1 to +1, as the normalised local cartesian system for the rectangles. Hence, precisely the same shape functions used for the rectangles can now be applied to these elements. It is for this reason that the rectangles are known as parent elements.

The 'Isoparametric' concept is to use the same interpolation function to transform the co-ordinates as that which defines the unknown displacements. This considerably facilitates the formulation of the curved elements. The isoparametric quadrilaterals born from the two families of parent rectangles are shown in figures (A2.6) and (A2.7). The element titles in figures (A2.4) and (A2.5), linear, quadratic, etc. describe the shape into which the element sides can be distributed.

A 2.1.3.3 Stiffness Formulation

This is shown most conveniently by means of an example. Consider the four noded quadrilateral in figure (A2.8) which is shown together with its parent element. The node numbers are shown circled and are particular to

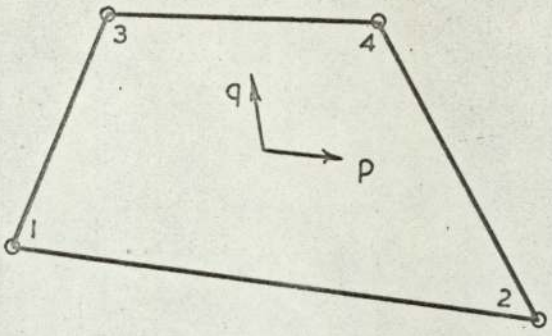

Figure A2.6. a. Linear quadrilateral

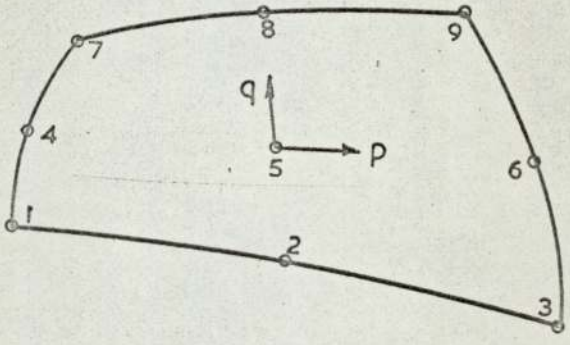

Figure A2.6. b. Quadratic quadrilateral

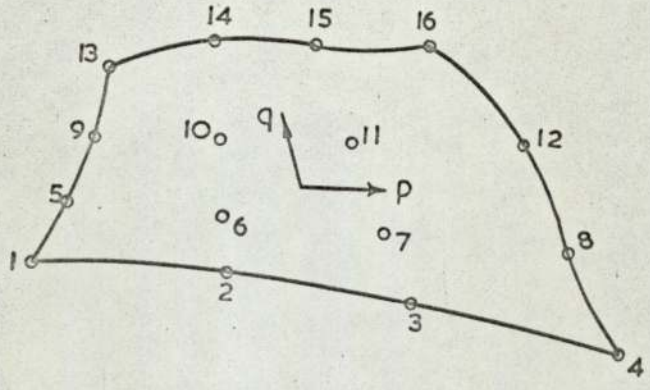

Figure A2.6.c. Cubic quadrilateral

Lagrangian family of isoparametric quadrilaterals

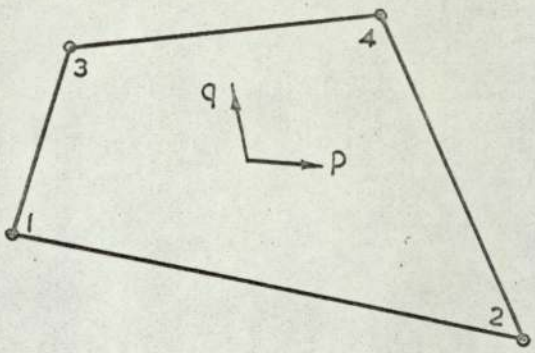

Figure A. 2.7.a. Linear quadrilateral

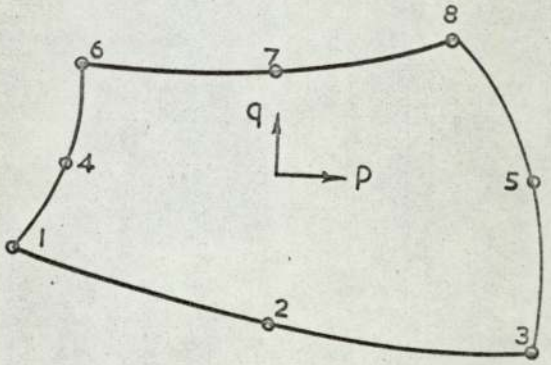

Figure A. 2.7. b Quadratic quadrilateral

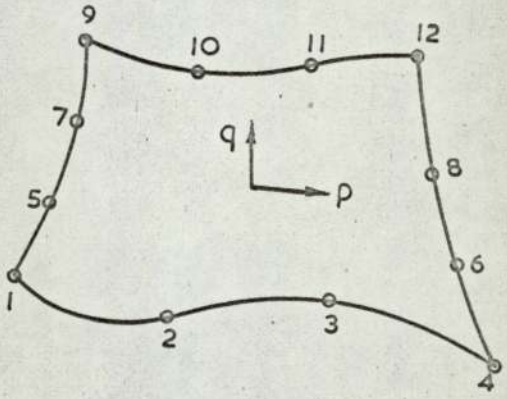

Figure A 2.7c Cubic quadrilateral

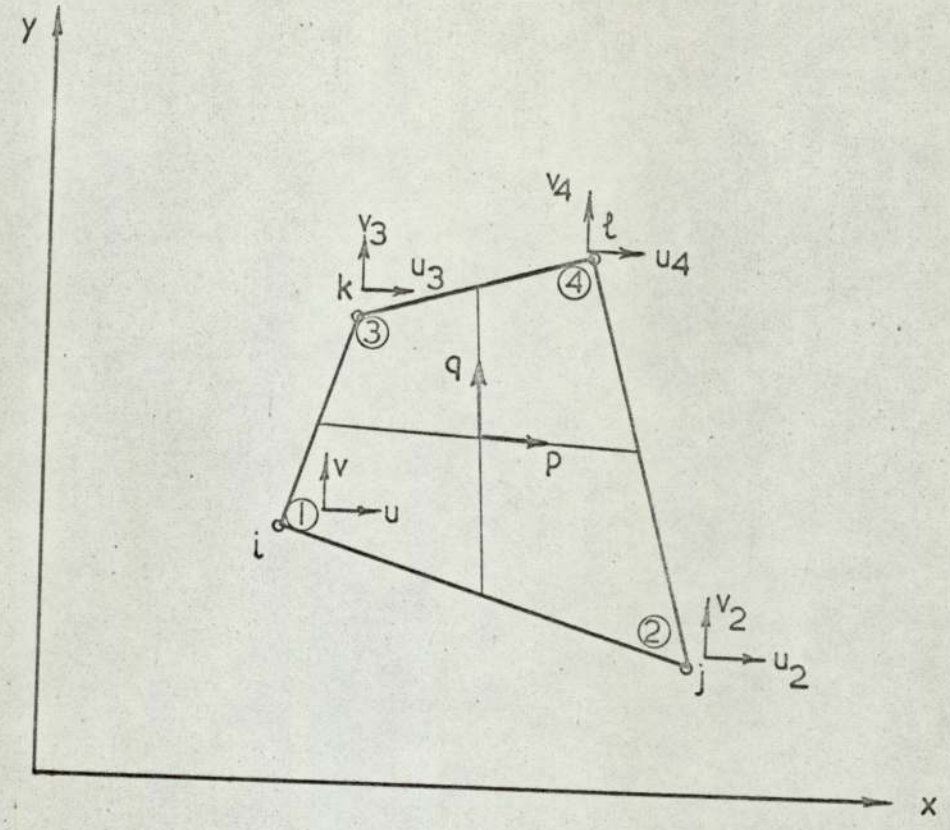

Isoparametric quadrilateral

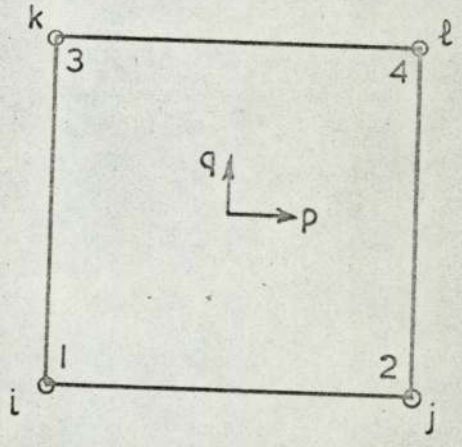

Parent rectangle

Figure A 2.8 Linear element

the element. The letters on the other hand are the joints to which the nodes are connected. Each node is allowed two translational degrees of freedom, defined here as u in the X direction and v in the Y direction, where X and Y are the global cartesian axes. Table(A2.1) below shows the local and global co-ordinates of nodes 1-4.

NODE	LOCAL AXES		GLOBAL AXES	
	p	q	X	Y
1	-1.0	-1.0	X_1	Y_1
2	1.0	-1.0	X_2	Y_2
3	-1.0	1.0	X_3	Y_3
4	1.0	1.0	X_4	Y_4

Table(A2.1)

The displacement interpolation functions will have the form:

$$u = N_1u_1 + N_2u_2 + N_3u_3 + N_4u_4 \qquad (A2.19.1)$$

$$v = N_1v_1 + N_2v_2 + N_3v_3 + N_4v_4 \qquad (A2.19.2)$$

where the shape functions are defined in equation(A2.16). After substituting in the values of p and q

$$\begin{aligned} N_1 &= \tfrac{1}{4}(1-p-q+pq) \\ N_2 &= \tfrac{1}{4}(1+p-q-pq) \\ N_3 &= \tfrac{1}{4}(1-p+q-pq) \\ N_4 &= \tfrac{1}{4}(1+p+q+pq) \end{aligned} \qquad (A2.20)$$

By invoking the isoparametric principle the transformed co-ordinates must obey the same interpolation function as the displacements, thus:

$$\begin{aligned} X &= N_1X_1 + N_2X_2 + N_3X_3 + N_4X_4 \\ Y &= N_1Y_1 + N_2Y_2 + N_3Y_3 + N_4Y_4 \end{aligned} \qquad (A2.21)$$

The first derivatives of equation(A2.19) become ;

$$\frac{\partial u}{\partial p} = \frac{\partial N_1}{\partial p} u_1 + \frac{\partial N_2}{\partial p} u_2 + \frac{\partial N_3}{\partial p} u_3 + \frac{\partial N_4}{\partial p} u_4 \qquad (A2.22)$$

and similarly for the other terms $\frac{\partial u}{\partial q}$, $\frac{\partial v}{\partial p}$ and $\frac{\partial v}{\partial q}$ and these can be expressed in matrix form as:

$$\begin{bmatrix} \frac{\partial u}{\partial p} \\ \frac{\partial v}{\partial p} \\ \frac{\partial u}{\partial q} \\ \frac{\partial v}{\partial q} \end{bmatrix} = \begin{bmatrix} \frac{\partial N_1}{\partial p} & 0 & \frac{\partial N_2}{\partial p} & 0 & \frac{\partial N_3}{\partial p} & 0 & \frac{\partial N_4}{\partial p} & 0 \\ 0 & \frac{\partial N_1}{\partial p} & 0 & \frac{\partial N_2}{\partial p} & 0 & \frac{\partial N_3}{\partial p} & 0 & \frac{\partial N_4}{\partial p} \\ \frac{\partial N_1}{\partial q} & 0 & \frac{\partial N_2}{\partial q} & 0 & \frac{\partial N_3}{\partial q} & 0 & \frac{\partial N_4}{\partial q} & 0 \\ 0 & \frac{\partial N_1}{\partial q} & 0 & \frac{\partial N_2}{\partial q} & 0 & \frac{\partial N_3}{\partial q} & 0 & \frac{\partial N_4}{\partial q} \end{bmatrix} \begin{bmatrix} u_1 \\ v_1 \\ u_2 \\ v_2 \\ u_3 \\ v_3 \\ u_4 \\ v_4 \end{bmatrix} \qquad (A2.23)$$

where differentiation of equations (A2.20) gives

$$\begin{aligned} \frac{\partial N_1}{\partial p} &= \frac{1}{4}(-1+q) & \frac{\partial N_1}{\partial q} &= \frac{1}{4}(-1+p) \\ \frac{\partial N_2}{\partial p} &= \frac{1}{4}(1-q) & \frac{\partial N_2}{\partial q} &= \frac{1}{4}(-1-p) \\ \frac{\partial N_3}{\partial p} &= \frac{1}{4}(-1-q) & \frac{\partial N_3}{\partial q} &= \frac{1}{4}(1-p) \\ \frac{\partial N_4}{\partial p} &= \frac{1}{4}(1+q) & \frac{\partial N_4}{\partial q} &= \frac{1}{4}(1+p) \end{aligned} \qquad (A2.24)$$

However, the derivatives $\frac{\partial u}{\partial p}$ etc are of little interest since strains are required with respect to the global axes. Since p and q are functions of x and y the derivatives in equation (A2.23) can be written as:

$$\frac{\partial u}{\partial p} = \frac{\partial u}{\partial x} \cdot \frac{\partial x}{\partial p} + \frac{\partial u}{\partial y} \cdot \frac{\partial y}{\partial p} \qquad (A2.25)$$

Similar operations for the other derivatives $\frac{\partial u}{\partial q}$, $\frac{\partial v}{\partial p}$ and $\frac{\partial v}{\partial q}$ yield other expressions which can be expressed in matrix form as:-

$$\begin{bmatrix} \frac{\partial u}{\partial p} \\ \frac{\partial v}{\partial p} \\ \frac{\partial u}{\partial q} \\ \frac{\partial v}{\partial q} \end{bmatrix} = \begin{bmatrix} \frac{\partial x}{\partial p} & 0 & \frac{\partial y}{\partial p} & 0 \\ 0 & \frac{\partial x}{\partial p} & 0 & \frac{\partial y}{\partial p} \\ \frac{\partial x}{\partial q} & 0 & \frac{\partial y}{\partial q} & 0 \\ 0 & \frac{\partial x}{\partial q} & 0 & \frac{\partial y}{\partial q} \end{bmatrix} \begin{bmatrix} \frac{\partial u}{\partial x} \\ \frac{\partial v}{\partial x} \\ \frac{\partial u}{\partial y} \\ \frac{\partial v}{\partial y} \end{bmatrix} \qquad (A2.26)$$

where the above square matrix is known as the Jacobian matrix [J]. The elements of this matrix are the first derivatives of equation(A2.21) which are formulated in a similar way to equation(A2.22), such that:

$$\frac{\partial x}{\partial p} = \frac{\partial N_1}{\partial p} x_1 + \frac{\partial N_2}{\partial p} x_2 + \frac{\partial N_3}{\partial p} x_3 + \frac{\partial N_4}{\partial p} x_4 \qquad (A2.27)$$

and so on for $\frac{\partial y}{\partial p}$, $\frac{\partial x}{\partial q}$ and $\frac{\partial y}{\partial q}$. The derivatives on the right hand side of equation (2.26) are required, so the Jacobian needs inverting, yielding:

$$\begin{bmatrix} \frac{\partial y}{\partial x} \\ \frac{\partial v}{\partial x} \\ \frac{\partial u}{\partial y} \\ \frac{\partial v}{\partial y} \end{bmatrix} = \frac{1}{\left(\frac{\partial x}{\partial p}\frac{\partial y}{\partial q} - \frac{\partial y}{\partial p}\frac{\partial x}{\partial q} \right)} \begin{bmatrix} \frac{\partial y}{\partial q} & 0 & -\frac{\partial y}{\partial p} & 0 \\ 0 & \frac{\partial y}{\partial q} & 0 & -\frac{\partial y}{\partial p} \\ -\frac{\partial x}{\partial q} & 0 & \frac{\partial x}{\partial p} & 0 \\ 0 & -\frac{\partial x}{\partial q} & 0 & \frac{\partial x}{\partial p} \end{bmatrix} \begin{bmatrix} \frac{\partial u}{\partial p} \\ \frac{\partial v}{\partial p} \\ \frac{\partial u}{\partial q} \\ \frac{\partial v}{\partial q} \end{bmatrix} \qquad (A2.28)$$

The right hand side of equation(A2.28) contains the terms of equation(A2.23), substituting equation(A2.23) into equation(A2.28) one obtains:

$$\begin{bmatrix} \frac{\partial u}{\partial x} \\ \frac{\partial v}{\partial x} \\ \frac{\partial u}{\partial y} \\ \frac{\partial v}{\partial y} \end{bmatrix} = \frac{1}{C} \begin{bmatrix} \frac{\partial y}{\partial q}\frac{\partial N_1}{\partial p} & 0 & \frac{\partial y}{\partial q}\frac{\partial N_2}{\partial p} & 0 & \frac{\partial y}{\partial q}\frac{\partial N_3}{\partial p} & 0 & \frac{\partial y}{\partial q}\frac{\partial N_4}{\partial p} & 0 \\ -\frac{\partial y}{\partial p}\frac{\partial N_1}{\partial q} & & -\frac{\partial y}{\partial p}\frac{\partial N_2}{\partial q} & & -\frac{\partial y}{\partial p}\frac{\partial N_3}{\partial q} & & -\frac{\partial y}{\partial p}\frac{\partial N_4}{\partial q} & \\ 0 & \frac{\partial y}{\partial q}\frac{\partial N_1}{\partial p} & 0 & \frac{\partial y}{\partial q}\frac{\partial N_2}{\partial p} & 0 & \frac{\partial y}{\partial q}\frac{\partial N_3}{\partial p} & 0 & \frac{\partial y}{\partial q}\frac{\partial N_4}{\partial p} \\ & -\frac{\partial y}{\partial p}\frac{\partial N_1}{\partial q} & & -\frac{\partial y}{\partial p}\frac{\partial N_2}{\partial q} & & -\frac{\partial y}{\partial p}\frac{\partial N_3}{\partial q} & & -\frac{\partial y}{\partial p}\frac{\partial N_4}{\partial q} \\ -\frac{\partial x}{\partial q}\frac{\partial N_1}{\partial p} & 0 & -\frac{\partial x}{\partial q}\frac{\partial N_2}{\partial p} & 0 & -\frac{\partial x}{\partial q}\frac{\partial N_3}{\partial p} & 0 & -\frac{\partial x}{\partial q}\frac{\partial N_4}{\partial p} & 0 \\ +\frac{\partial x}{\partial p}\frac{\partial N_1}{\partial q} & & +\frac{\partial x}{\partial p}\frac{\partial N_2}{\partial q} & & +\frac{\partial x}{\partial p}\frac{\partial N_3}{\partial q} & & +\frac{\partial u}{\partial p}\frac{\partial N_4}{\partial q} & \\ 0 & -\frac{\partial x}{\partial q}\frac{\partial N_1}{\partial p} & 0 & -\frac{\partial x}{\partial q}\frac{\partial N_2}{\partial p} & 0 & -\frac{\partial x}{\partial q}\frac{\partial N_3}{\partial p} & 0 & -\frac{\partial x}{\partial q}\frac{\partial N_4}{\partial p} \\ & +\frac{\partial x}{\partial p}\frac{\partial N_1}{\partial q} & & +\frac{\partial x}{\partial p}\frac{\partial N_2}{\partial q} & & +\frac{\partial x}{\partial p}\frac{\partial N_3}{\partial q} & & +\frac{\partial x}{\partial p}\frac{\partial N_4}{\partial q} \end{bmatrix} \begin{bmatrix} u_1 \\ v_1 \\ u_2 \\ v_2 \\ u_3 \\ v_3 \\ u_4 \\ v_4 \end{bmatrix} \qquad (A2.29)$$

where $C = \frac{\partial x}{\partial p}\frac{\partial y}{\partial q} - \frac{\partial y}{\partial p}\frac{\partial x}{\partial q}$ (A2.30)

From the Cauchy definition of strain using the usual small strain

approximation:

$$\varepsilon_x = \frac{\partial u}{\partial x} \qquad \varepsilon_y = \frac{\partial v}{\partial y} \qquad \gamma_{xy} = \frac{\partial u}{\partial y} + \frac{\partial v}{\partial x} \tag{A2.31}$$

Collecting together the terms of equation(A2.31)

$$\begin{bmatrix} \varepsilon_x \\ \varepsilon_y \\ \gamma_{xy} \end{bmatrix} = \frac{1}{C} \begin{bmatrix} \frac{\partial y}{\partial q}\frac{\partial N_1}{\partial p} & 0 & \frac{\partial y}{\partial q}\frac{\partial N_2}{\partial p} & 0 & \frac{\partial y}{\partial q}\frac{\partial N_3}{\partial p} & 0 & \frac{\partial y}{\partial q}\frac{\partial N_4}{\partial p} & 0 \\ -\frac{\partial y}{\partial p}\frac{\partial N_1}{\partial q} & & -\frac{\partial y}{\partial p}\frac{\partial N_2}{\partial q} & & -\frac{\partial y}{\partial p}\frac{\partial N_3}{\partial q} & & -\frac{\partial y}{\partial p}\frac{\partial N_4}{\partial q} & \\ 0 & -\frac{\partial x}{\partial q}\frac{\partial N_1}{\partial p} & 0 & -\frac{\partial x}{\partial q}\frac{\partial N_2}{\partial p} & 0 & -\frac{\partial x}{\partial q}\frac{\partial N_3}{\partial p} & 0 & -\frac{\partial x}{\partial q}\frac{\partial N_4}{\partial p} \\ & +\frac{\partial x}{\partial p}\frac{\partial N_1}{\partial q} & & +\frac{\partial x}{\partial p}\frac{\partial N_2}{\partial q} & & -\frac{\partial x}{\partial p}\frac{\partial N_3}{\partial q} & & +\frac{\partial x}{\partial p}\frac{\partial N_4}{\partial q} \\ -\frac{\partial x}{\partial q}\frac{\partial N_1}{\partial p} & \frac{\partial y}{\partial q}\frac{\partial N_1}{\partial p} & -\frac{\partial x}{\partial q}\frac{\partial N_2}{\partial p} & \frac{\partial y}{\partial q}\frac{\partial N_2}{\partial p} & -\frac{\partial x}{\partial q}\frac{\partial N_3}{\partial p} & \frac{\partial y}{\partial q}\frac{\partial N_3}{\partial p} & -\frac{\partial x}{\partial q}\frac{\partial N_4}{\partial p} & \frac{\partial y}{\partial q}\frac{\partial N_4}{\partial p} \\ +\frac{\partial x}{\partial p}\frac{\partial N_1}{\partial q} & -\frac{\partial y}{\partial p}\frac{\partial N_1}{\partial q} & +\frac{\partial x}{\partial p}\frac{\partial N_2}{\partial q} & -\frac{\partial y}{\partial p}\frac{\partial N_2}{\partial q} & +\frac{\partial x}{\partial p}\frac{\partial N_3}{\partial q} & -\frac{\partial y}{\partial p}\frac{\partial N_3}{\partial q} & +\frac{\partial x}{\partial p}\frac{\partial N_4}{\partial q} & -\frac{\partial y}{\partial p}\frac{\partial N_4}{\partial q} \end{bmatrix} \begin{bmatrix} u_1 \\ v_1 \\ u_2 \\ v_2 \\ u_3 \\ v_3 \\ u_4 \\ v_4 \end{bmatrix} \tag{A2.32}$$

where equation(A2.32) can be rewritten as:

$$\{\varepsilon\} = \underline{B}\{\delta\} \tag{A2.33}$$

From elastic theory stresses and strains are related by a $\underline{D}$ matrix, for a homogeneous material this will in general have the form:

$$\begin{bmatrix} \sigma_x \\ \sigma_y \\ \tau_{xy} \end{bmatrix} = \begin{bmatrix} E(1) & E(2) & 0 \\ E(2) & E(3) & 0 \\ 0 & 0 & E(4) \end{bmatrix} \begin{bmatrix} \varepsilon_x \\ \varepsilon_y \\ \gamma_{xy} \end{bmatrix} \tag{A2.34}$$

where, for example, an isotropically elastic material undergoing plane strain deformation would have:

$$E(1) = E(3) = \frac{E(1-\nu)}{(1+\nu)(1-2\nu)}$$

$$E(2) = \frac{E\nu}{(1+\nu)(1-2\nu)}$$

$$E(3) = \frac{E}{2(1+\nu)} \quad .$$

Where E is Young's modulus of elasticity and ν is poisson's ratio. In

shorthand form equation(A2.34) is rewritten as:

$$\{\sigma\} = \underline{D}\,\{\varepsilon\} \qquad (A2.35)$$

From chapter 1 it is known that by considering the principle of virtual work, the element stiffness matrix is:

$$K = \iint_{\text{area}} \underline{B}^T \underline{D}\, \underline{B}\, dx\, dy \qquad (A2.36)$$

It would be very difficult to determine the limits for the integration above, but it is known (33) that: $dx\,dy = \det[J]\,dp\,dq$ where $\det[J]$ is the determinant of the Jacobian matrix in equation(A2.26). Changing to the local co-ordinate system means that the limits are now straightforward.

$$\underline{K} = \int_{-1}^{+1}\int_{-1}^{+1} \underline{B}^T \underline{D}\, \underline{B}\, \det[J]\, dp\, dq \qquad (A2.37)$$

where $$\det[J] = \left\{\frac{\partial x}{\partial p}\frac{\partial y}{\partial q} - \frac{\partial y}{\partial p}\frac{\partial x}{\partial q}\right\} \qquad (A2.38)$$

defining $\underline{B}_*$ in $\underline{B} = \frac{1}{C}\underline{B}_*$ as in equation(A2.31) then

$$\underline{K} = \int_{-1}^{+1}\int_{-1}^{+1} \frac{1}{C}\underline{B}^T_*\, \underline{D}\, \underline{B}_*\, dp\, dq \qquad (A2.39)$$

where $\underline{K}$ is the stiffness matrix of one linear isoparametric quadrilateral element, in this example. As each node is allowed two degrees of freedom the $\underline{K}$ matrix will be of order 8×8. The stiffness matrix is square and symmetrical so only the lower triangle terms are considered. The element stiffness matrix can be divided into parts, called sub-blocks, as shown in figure(A2.9). There are two types of sub-blocks. Triangular sub-blocks (K_{11}, K_{22} etc.) which fall on the diagonal, and, rectangular sub-blocks (K_{21}, K_{32} etc.) which fall below the diagonal.

The only difference between sub-blocks is the node number (or numbers) that define it; it was therefore possible to formulate two general rectangular and triangular sub-blocks to represent all the others. By using the

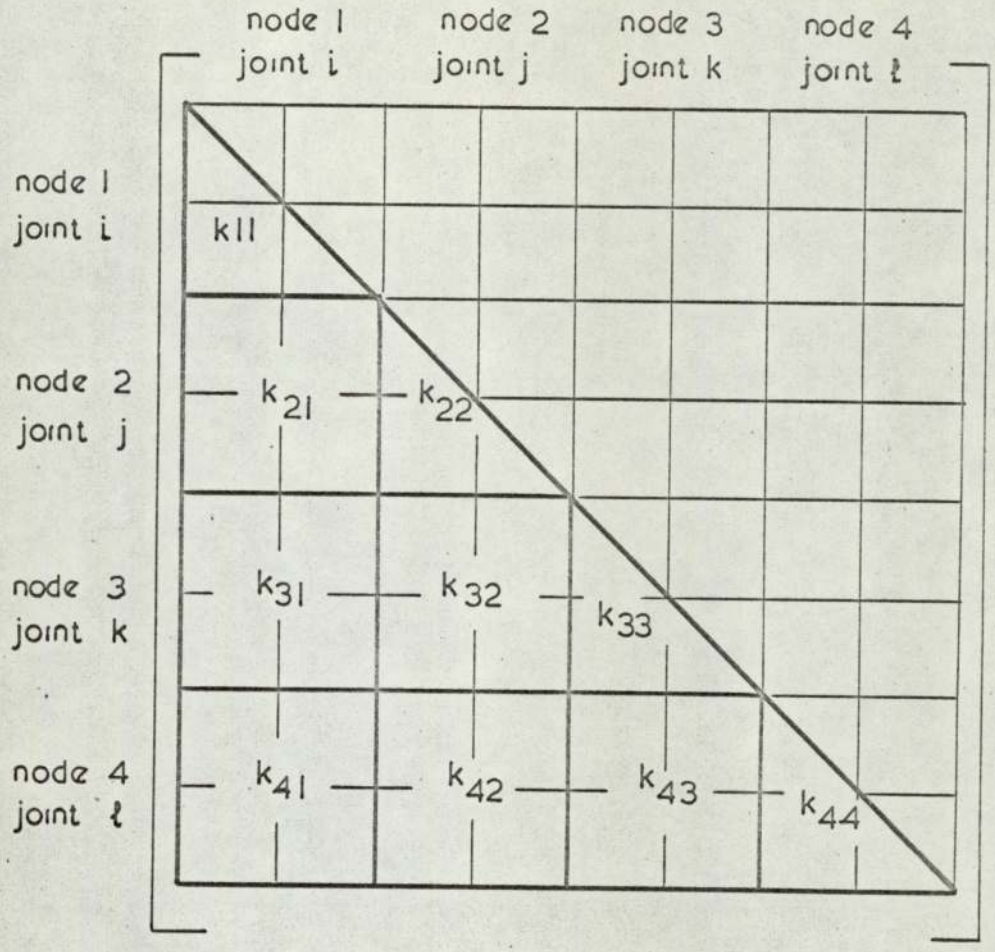

Figure A 2.9 Representation of element stiffness matrix

B_{11}	o	B_{13}	o	B_{15}	o	B_{17}	o
o	B_{22}	o	B_{24}	o	B_{26}	o	B_{28}
B_{31}	B_{32}	B_{33}	B_{34}	B_{35}	B_{36}	B_{37}	B_{38}

Figure A 2.10 Representation of B* matrix

$\underline{B}_*$ matrix represented in figure(A2.10) and carrying out the triple multiplication $\underline{B}^T_*\ \underline{D}\ \underline{B}_*$, where $\underline{D}$ was defined in equation(A2.34), these general sub-blocks were formed. The results are shown in figures(A2.11a) and (A2.11b).

It must be remembered that the equation(A2.39) has not been integrated yet, so these sub-blocks contain values of the integrand. The reasons for dividing the element stiffness matrix into parts will be made apparent in Appendix (3).

A2.1.3.4 Numerical Integration

In the last section the integrand in the equation:

$$\underline{K} = \int_{-1}^{+1}\int_{-1}^{+1} G(p,q)\ dp\ dq \qquad (A2.40)$$

where $G(p_1q)$ is itself very complex. It would be very difficult if not impossible to define $G(p_1q)$ explicitly, and then integrate it algebraicly. For these reasons, numerical integration has become a special feature of Isoparametric Quadrilaterals and has helped speed the formulation and programming of many elements.

The numerical integration technique used is Gaussian Quadrature, which is known to be some twice as efficient as an equivalent Simpson type rule. The method is exact when n sampling points are used to integrate a function of degree (2n-1).

Gauss quadrature replaces the definite integral $\int_{-1}^{+1} f(x)\ dx$ by the summation $\sum_{j=1}^{n} H_j\ f(a_j)$

where H_j is a weight coefficient, $f(a_j)$ is the value of the function at the specified point a_j and n is the number of gauss points used. Thus equation(A2.40) is replaced by the double summation:

$$\underline{K} = \sum_{j=1}^{n}\sum_{i=1}^{n} G(a_j, a_i)\ H_i\ H_j \qquad (A2.41)$$

end j

$E(1)_* B_{1k}^2 + E(4)_* B_{3k}^2$	
$E(2)_* B_2 B_{1k} + E(4)_* B_3 B_{3k}$	$E(3)_* B_2^2 + E(4)_* B_3^2$

end j

$m = 2 \times j$
$k = m-1$

Figure(A2.11a)

General Triangular Sub-Block End j (K_{jj})

end k

$E(1) \times B_1 \times B_1 + E(4) \times B_3 B_3$	$E(2) \times B_{2\ell} \times B_1 + E(4) \times B_3 \times B_{3\ell}$
$E(2)_* B_{2i} \times B_1 + E(4) \times B_{3i} \times B_3$	$E(3) \times B_{2i} \times B_{2\ell} + E(4) \times B_{3i} \times B_{3\ell}$

end j

$\ell = 2 \times k$
$i = 2 \times j$
$n = \ell - 1$
$m = i - 1$

Figure(A2.11b)

General Rectangular Sub-Block K_{jk}

A2.3.5 Stiffness Formulation of other Isoparametric Quadrilaterals

In section (A2.4.3) the element stiffness matrix of a linear quadrilateral was derived. The same procedure can be used for any Isoparametric element. In general, for higher order elements the various matrices (in equations (A2.32) for instance) will have more columns. The $\underline{B}$ matrix will be of order $3 \times 2n$ if the element has n nodes. The pattern of all the derived equations will be unchanged. Thus, the general sub-blocks derived and shown in figures (A2.11a) and (A2.11b) are applicable to all Isoparametric quadrilaterals. The essential difference between the various elements will be in the different shape functions (equation A2.20) and their first derivatives (equation A2.24).

A2.2 Three Dimensional Elements

To analyse general three dimensional structures and the foundation material it was necessary to include the space member and rectangular plate bending elements in the library of elements. These two elements are well known and are only mentioned briefly.

The three dimensional equivalent of the quadrilateral elements described in the previous section are called Hexahedral elements. It is these Isoparametric Hexahedrals which are mainly considered in this section.

A2.2.1 Space Member Element

The space member routines were obtained from the Prismatic Member Package of Bray (11). Figure (A2.12a) shows this element in which the local axis P, Q and R are orientated according to the right hand screw rule. Each end of the member is allowed six degrees of freedom as illustrated in figure (A2.12b). The eight resultant member forces are shown in figure (A2.13b).

To cope with the various irregularities that occur in structures at the joints, the member description included facilities to allow the representation of gusset plates and haunches as rigid portions, and, allow the centroid of the member section to be offset from the joint. These rigid portions and offsets are detailed in figure (A2.13a).

A2.2.2 Rectangular Plate Element

This plate bending element was also taken from a package by Bray (11). Each node of the element was allowed five degrees of freedom. Figure (A2.14a) shows the three in plane degrees of freedom and figure (A2.14b) the three out of plane ones. The in plane rotation ϕ_R is always suppressed.

A2.2.3 Higher Order Elements

The reasons for adopting the Isoparametric Quadrilateral equally apply to the three dimensional elements. The equivalent families of Hexahedral elements are described in this section.

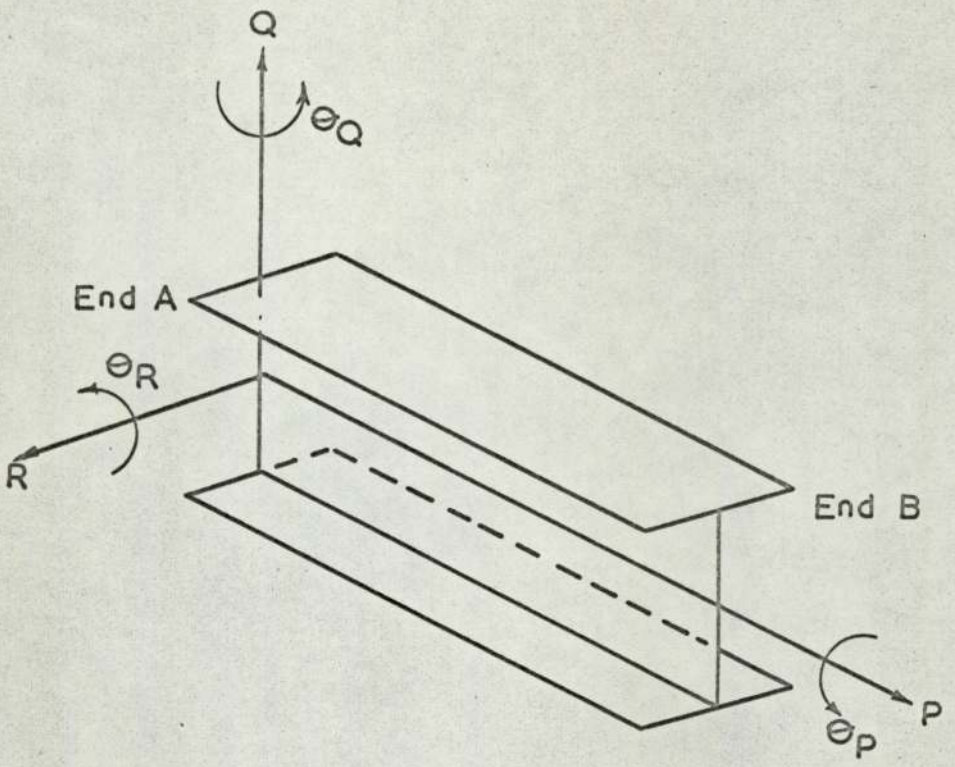

Figure A.2.12 a Member reference axes

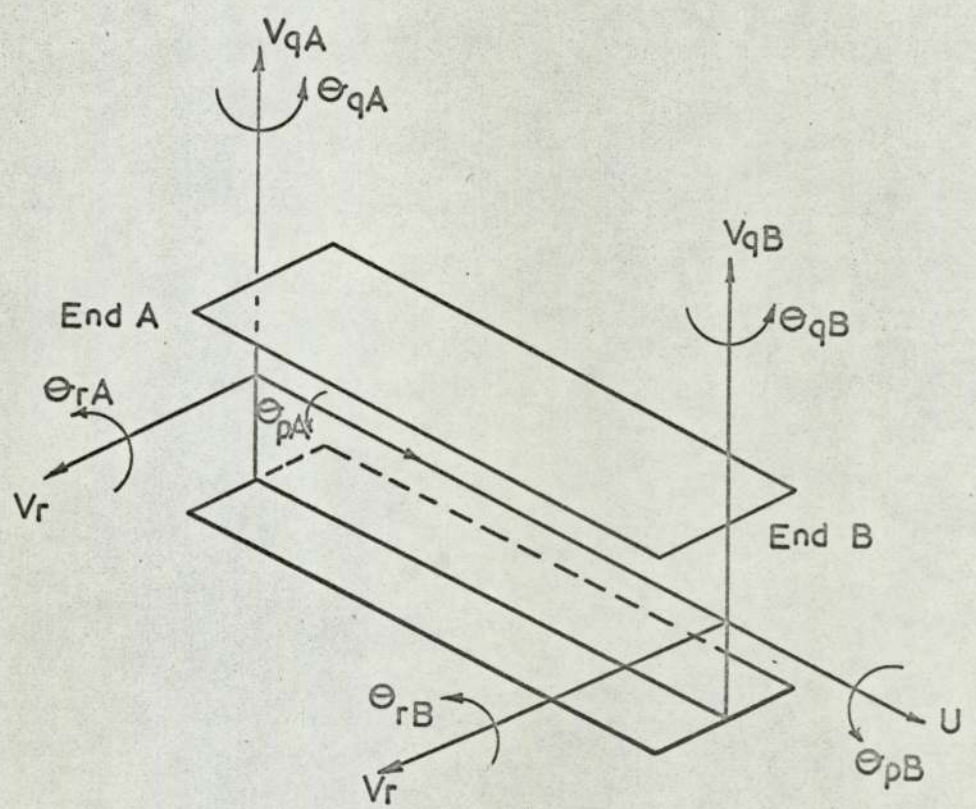

Figure . A 2.12 b Member deflections at each end

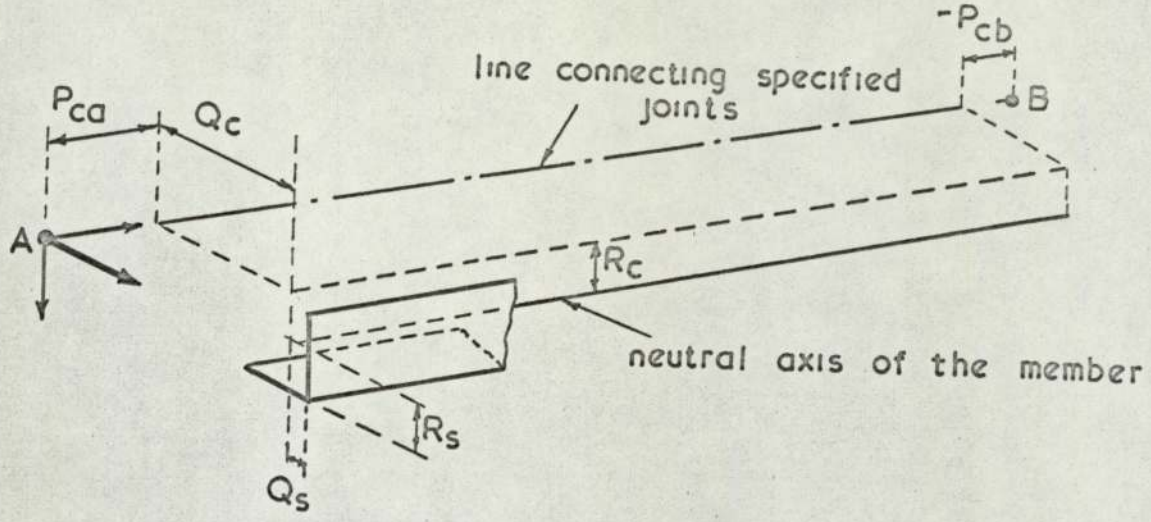

Figure A 2.13 a Rigid portions and offsets of a member's ends from the specified joints

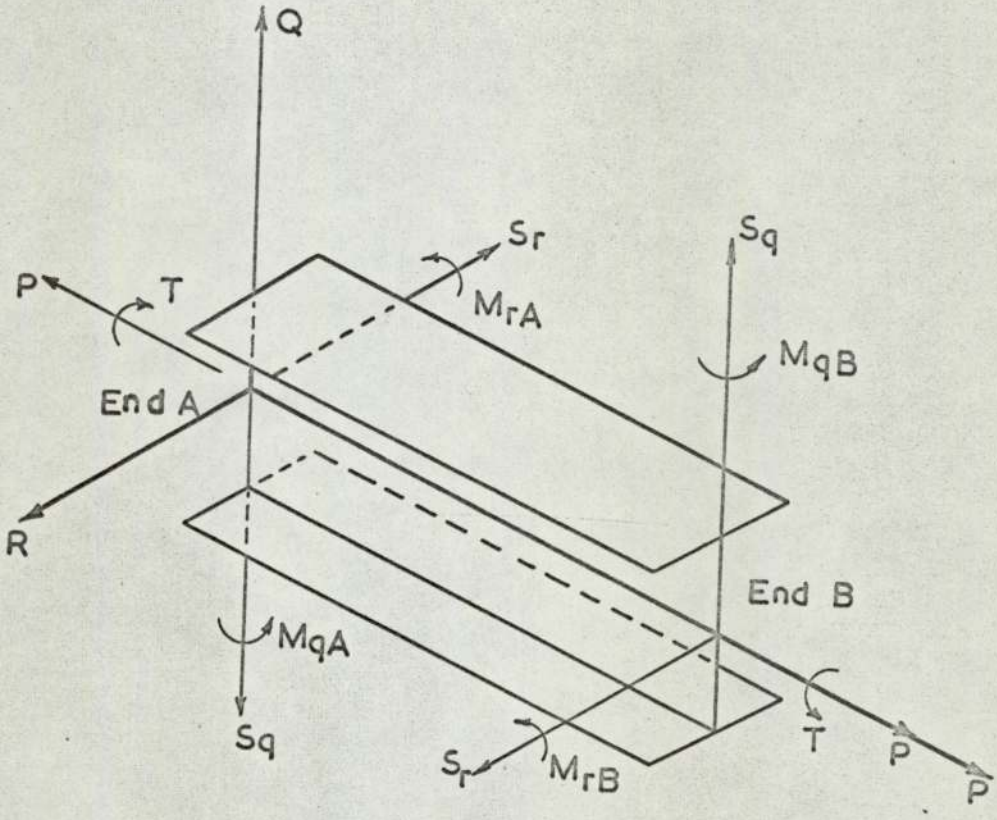

Figure A 2.13 b Member forces on each member.

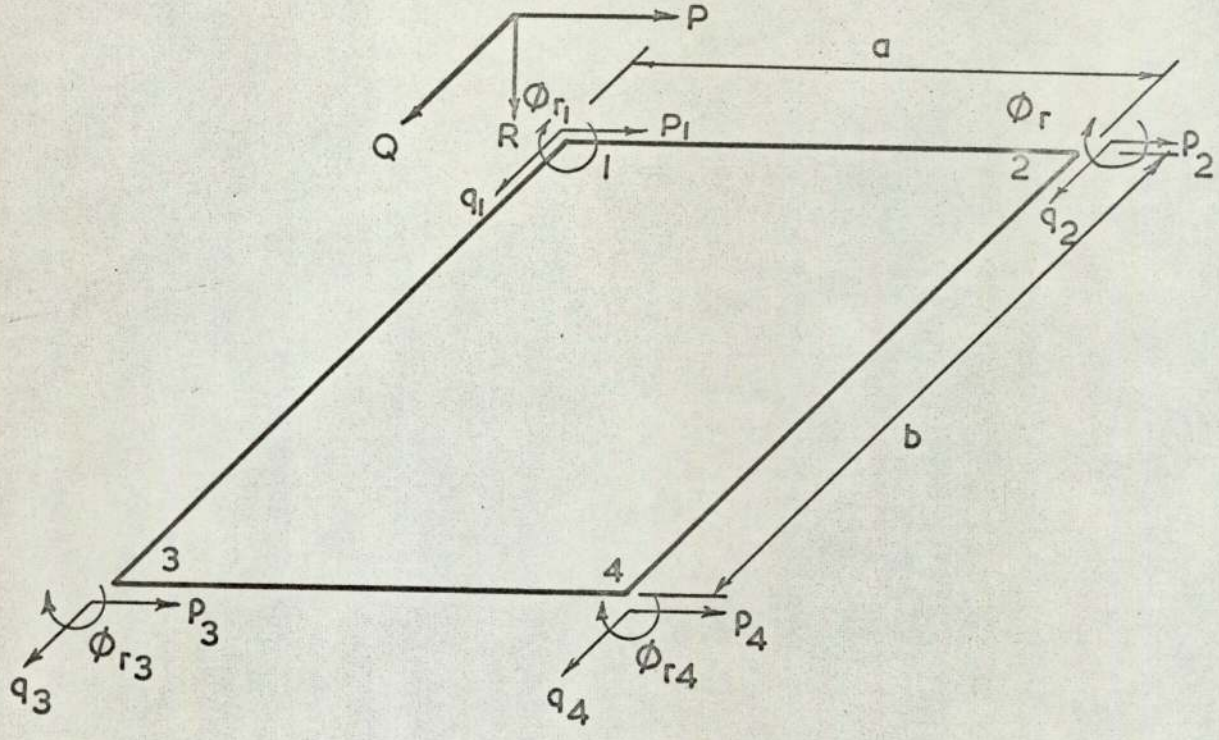

Figure. A 2.14a. In plane displacements

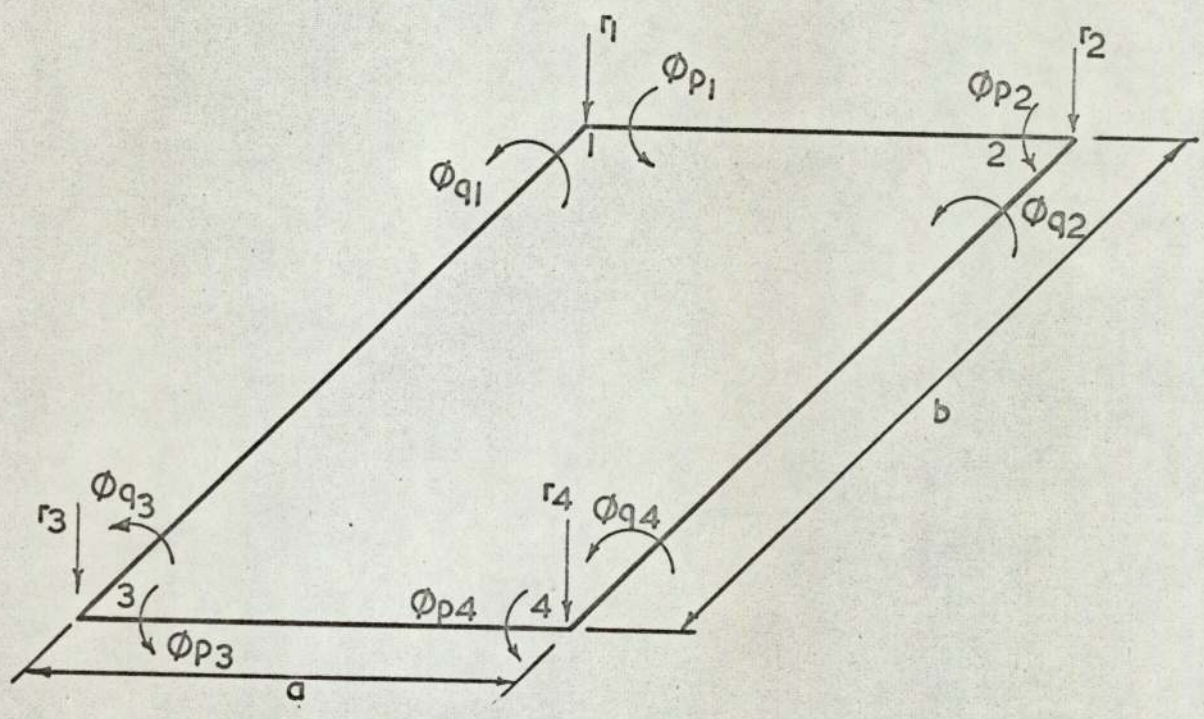

Figure. A 2.14 b Out of plane displacements

The derivation of the element stiffness matrix of an Isoparametric Quadrilateral was discussed in some detail in section(A2.1.3.3). As the formulation of the Hexahedral Element is basically similar, it is only dealt with briefly. Details are included in so far as they are necessary to define the terms in the general sub-blocks that are derived.

A2.2.3.1 Rectangular Prismoidal Elements

Each node of these elements is allowed three translational degrees of freedom, u, v and w parallel to the axes of the global cartesian system X, Y and Z. The role of the local co-ordinate was explained in section (A2.1.3.1.1). The addition of another dimension creates another axis r with usual range from -1 to +1. The direction of r is arbitrary except that the local axes and the global axes must obey the same sign convension.

These elements were again divided into two families by Zienkiewicz (98). The first element, with linear displacement along the edges, is common to both families.

A2.2.3.1.1 Lagrangian Family

The first two members of this family are shown in figure(A2.15). Their shape functions can be formed from:-

$$N_\ell = L_i^n(p)\, L_j^n(q)\, L_k^n(r) \qquad \ldots (A2.42)$$

where n is the number of nodes on any side, $L_i^n(p)$ is a lagrangian interpolation formula, defined in equation(A2.11), of degree n. The letters i, j and k define the node ℓ in a regular three dimensional grid.

A2.2.3.1.2 Serendipity Family

The first two members of this family are illustrated in figure(A2.16). Like the two dimensional family, the nodes are concentrated around the boundary, so that variation of displacement is achieved with a minimum number of nodes. The shape functions quoted by Zienkiewicz (98) for these elements are:-

(1) Linear Element (Figure A2.16a)

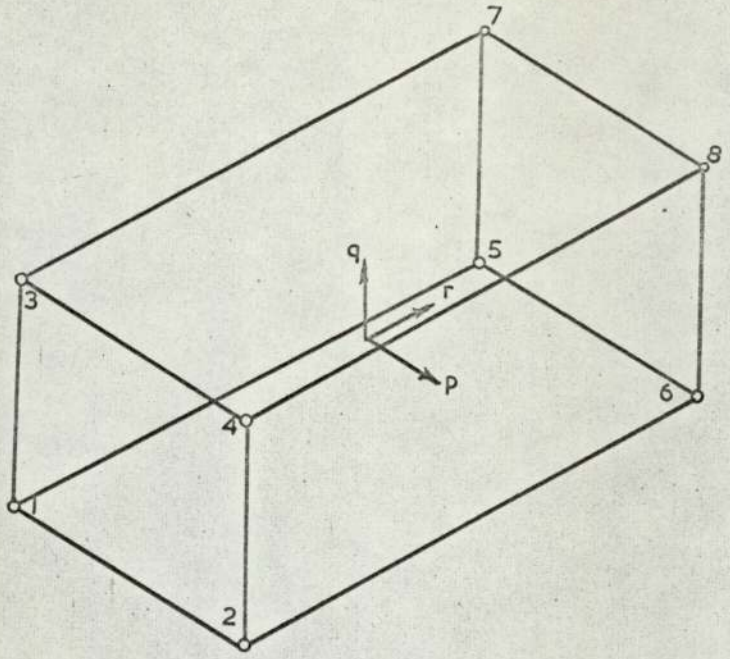

Figure . A 2.15. a Linear element (8 nodes)

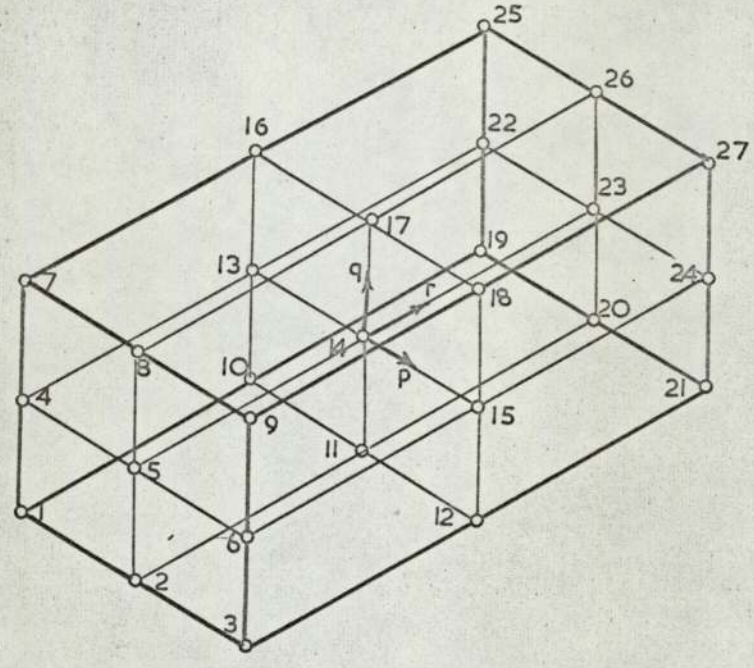

Figure A 2.15. b Quadratic element (27 nodes)

. Rectangular prisms - lagrange family

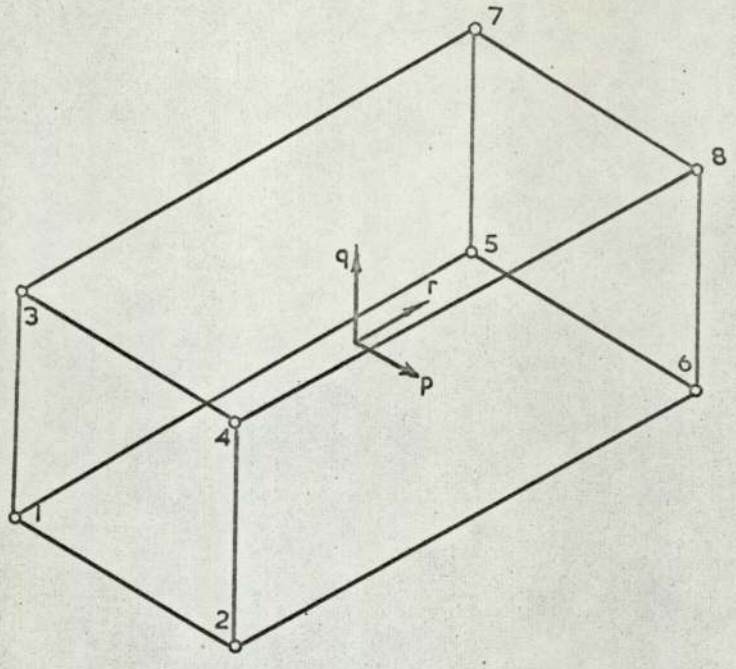

Figure A 2.16a Linear element (8 nodes)

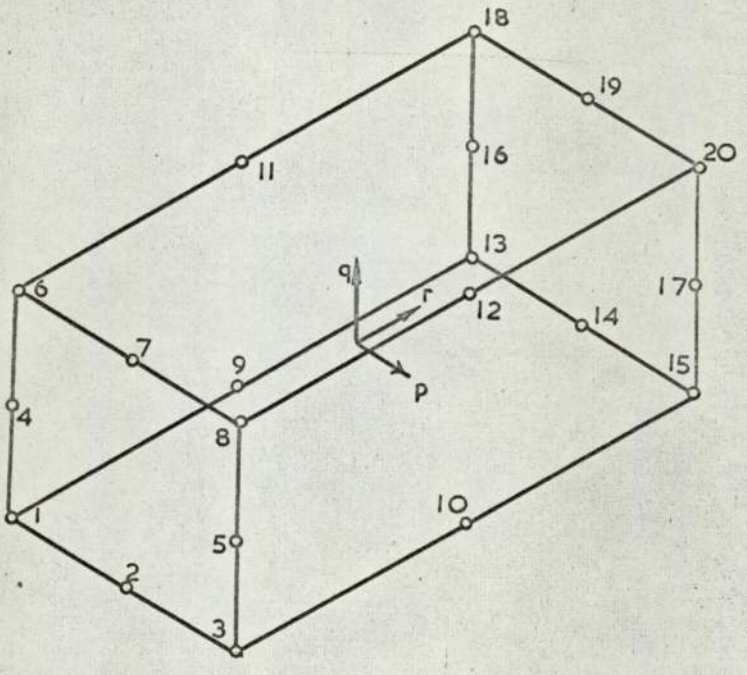

Figure A 2.16.b Quadratic element (20 nodes)

Rectangular prisms – serendipity family

$$N_i = \frac{1}{8}(1 + p_o)(1 + q_o)(1 + r_o) \quad \ldots (A2.43)$$

where $p_o = pp_i$, $q_o = qq_i$ and $r_o = rr_i$

(2) Quadratic Element (Figure A2.16b)

Corner nodes: $N_i = \frac{1}{8}(1 + p)(1 + q)(1 + r)$ ... (A2.44.1)

Mid-side nodes:

$$p_i = 0,\ q_i = \pm 1,\ r_i = \pm 1;\ N_i = \frac{1}{4}(1-p^2)(1+q_o)(1+r_o) \quad .. (A2.44.2)$$

$$p_i = \pm 1,\ q_i = 0,\ r_i = \pm 1;\ N_i = \frac{1}{4}(1+p_o)(1-q^2)(1-r_o) \quad .. (A2.44.3)$$

$$p_i = \pm 1,\ q_i = \pm 1,\ r_i = 0;\ N_i = \frac{1}{4}(1+p_o)(1+q_o)(1-r^2) \quad .. (A2.44.4)$$

A2.2.3.2 Isoparametric Hexahedrals

These elements were formulated in terms of the curvilinear co-ordinate system p, q, r. The Isoparametric concept is again invoked to facilitate the formulation of the element. The Isoparametric elements that are generated from the two parent families of rectangular prisms are illustrated in figures (A2.17) and (A2.18).

A2.2.3.3 Stiffness Formulation

Consider the linear hexahedral element in figure (A2.18a) and its parent element in figure (A2.16a). The shape functions for this element were defined in equation (A2.43). The three components of displacement anywhere within the element can be interpolated from:-

$$\begin{aligned} u &= N_1u_1 + N_2u_2 + N_3u_3 \ \ldots\ N_8u_8 \\ v &= N_1v_1 + N_2v_2 + N_3v_3 \ \ldots\ N_8v_8 \\ w &= N_1w_1 + N_2w_2 + N_3w_3 \ \ldots\ N_8w_8 \end{aligned} \quad \ldots (A2.45)$$

From the Isoparametric concept the coordinates are transformed by:-

$$\begin{aligned} X &= N_1X_1 + N_2X_2 + N_3X_3 \ \ldots\ N_8X_8 \\ Y &= N_1Y_1 + N_2Y_2 + N_3Y_3 \ \ldots\ N_8Y_8 \\ Z &= N_1Z_1 + N_2Z_2 + N_3Z_3 \ \ldots\ N_8Z_8 \end{aligned} \quad \ldots (A2.46)$$

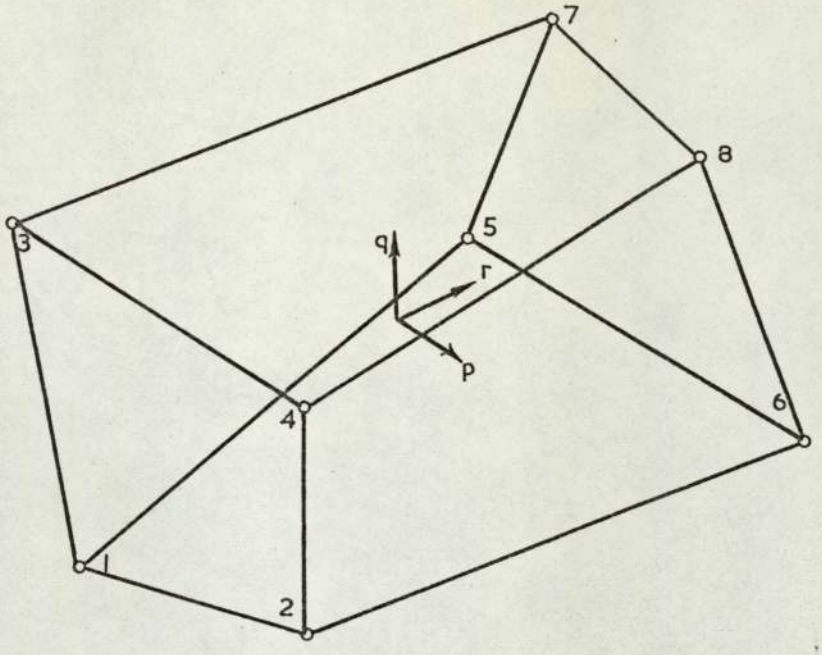

Figure A 2.17.a. Linear element

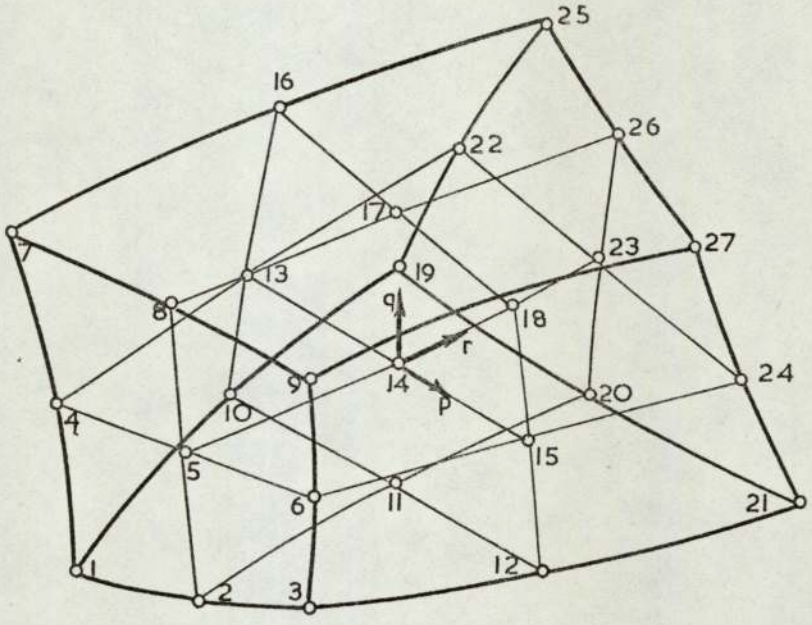

Figure A 2.17 b Quadratic element

Isoparametric hexahedral elements – lagrange family

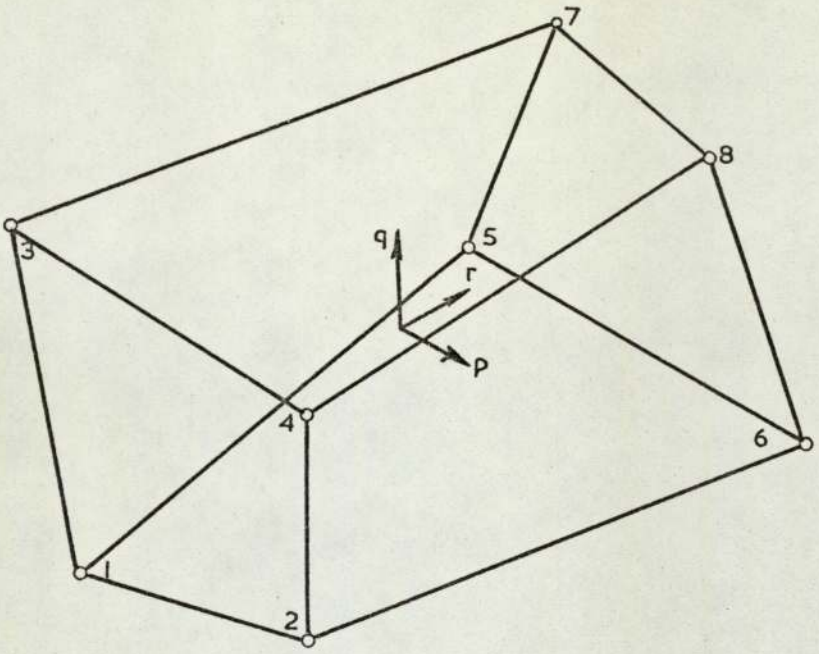

Figure .A 2.18. a. Linear element

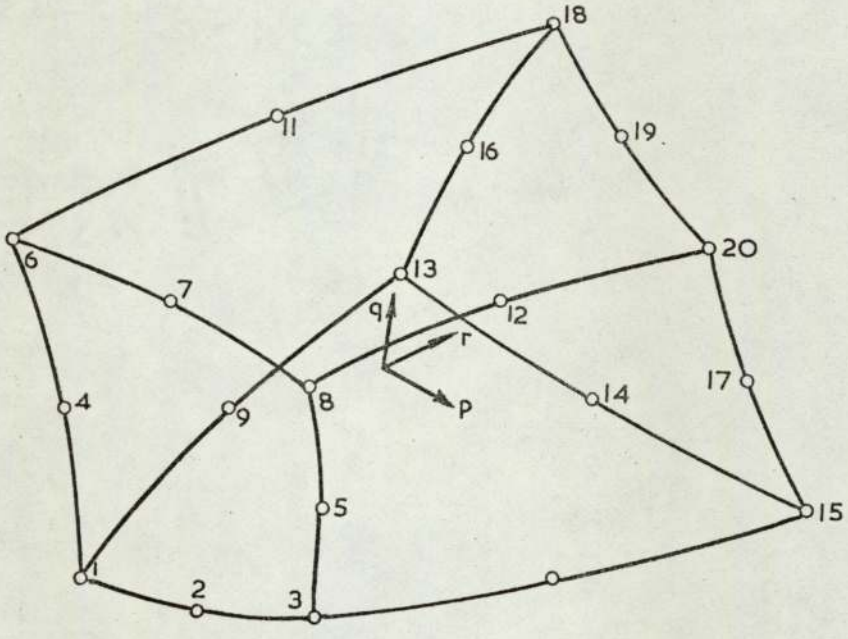

Figure. A 2.18 b. Quadratic element

Isoparametric hexahedral elements – serendipity family

Differentiation of equation(A2.45) with respect to p, q and r yields a set of equations which can be expressed in matrix form as:-

$$\begin{bmatrix} \frac{\partial u}{\partial p} \\ \frac{\partial u}{\partial q} \\ \frac{\partial u}{\partial r} \\ \frac{\partial v}{\partial p} \\ \frac{\partial v}{\partial q} \\ \frac{\partial v}{\partial r} \\ \frac{\partial w}{\partial p} \\ \frac{\partial w}{\partial q} \\ \frac{\partial w}{\partial r} \end{bmatrix} = \begin{bmatrix} \frac{\partial w_1}{\partial p} & 0 & 0 & \frac{\partial N_2}{\partial p} & 0 & 0 & \cdots\cdots & \frac{\partial N_8}{\partial p} & 0 & 0 \\ \frac{\partial N_1}{\partial q} & 0 & 0 & \frac{\partial N_2}{\partial q} & 0 & 0 & \cdots\cdots & \frac{\partial N_8}{\partial q} & 0 & 0 \\ \frac{\partial N_1}{\partial r} & 0 & 0 & \frac{\partial N_2}{\partial r} & 0 & 0 & \cdots\cdots & \frac{\partial N_8}{\partial r} & 0 & 0 \\ 0 & \frac{\partial N_1}{\partial p} & 0 & 0 & \frac{\partial N_2}{\partial p} & 0 & \cdots\cdots & 0 & \frac{\partial N_8}{\partial p} & 0 \\ 0 & \frac{\partial N_1}{\partial q} & 0 & 0 & \frac{\partial N_2}{\partial q} & 0 & \cdots\cdots & 0 & \frac{\partial N_8}{\partial q} & 0 \\ 0 & \frac{\partial N_1}{\partial r} & 0 & 0 & \frac{\partial N_2}{\partial r} & 0 & \cdots\cdots & 0 & \frac{\partial N_8}{\partial r} & 0 \\ 0 & 0 & \frac{\partial N_1}{\partial p} & 0 & 0 & \frac{\partial N_2}{\partial p} & \cdots\cdots & 0 & 0 & \frac{\partial N_8}{\partial p} \\ 0 & 0 & \frac{\partial N_1}{\partial q} & 0 & 0 & \frac{\partial N_2}{\partial q} & \cdots\cdots & 0 & 0 & \frac{\partial N_8}{\partial q} \\ 0 & 0 & \frac{\partial N_1}{\partial r} & 0 & 0 & \frac{\partial N_2}{\partial r} & \cdots\cdots & 0 & 0 & \frac{\partial N_8}{\partial r} \end{bmatrix} \begin{bmatrix} u_1 \\ v_1 \\ w_1 \\ u_2 \\ v_2 \\ w_3 \\ \cdot \\ \cdot \\ \cdot \\ \cdot \\ \cdot \\ u_8 \\ v_8 \\ w_8 \end{bmatrix} \quad \text{(A2.47)}$$

where the derivatives $\frac{\partial N_1}{\partial p}$ etc are obtained from the differentiation of equation (A2.43) containing the substituted values of the local co-ordinates for p_i etc. The derivatives $\frac{\partial u}{\partial p}$ etc. on the left hand side of equations (A2.47) are related to the derivatives $\frac{\partial u}{\partial x}$ etc. using the chain rule of differentiation, which can be expressed in matrix form as:-

$$\begin{bmatrix} \frac{\partial u}{\partial p} \\ \frac{\partial u}{\partial q} \\ \frac{\partial u}{\partial r} \\ \frac{\partial v}{\partial p} \\ \frac{\partial v}{\partial q} \\ \frac{\partial v}{\partial r} \\ \frac{\partial w}{\partial p} \\ \frac{\partial w}{\partial q} \\ \frac{\partial w}{\partial r} \end{bmatrix} = \begin{bmatrix} \frac{\partial X}{\partial p} & \frac{\partial Y}{\partial p} & \frac{\partial Z}{\partial p} & 0 & 0 & 0 & 0 & 0 & 0 \\ \frac{\partial X}{\partial q} & \frac{\partial Y}{\partial q} & \frac{\partial Z}{\partial q} & 0 & 0 & 0 & 0 & 0 & 0 \\ \frac{\partial X}{\partial r} & \frac{\partial Y}{\partial r} & \frac{\partial Z}{\partial r} & 0 & 0 & 0 & 0 & 0 & 0 \\ 0 & 0 & 0 & \frac{\partial X}{\partial p} & \frac{\partial Y}{\partial p} & \frac{\partial Z}{\partial p} & 0 & 0 & 0 \\ 0 & 0 & 0 & \frac{\partial X}{\partial q} & \frac{\partial Y}{\partial q} & \frac{\partial Z}{\partial q} & 0 & 0 & 0 \\ 0 & 0 & 0 & \frac{\partial X}{\partial r} & \frac{\partial Y}{\partial r} & \frac{\partial Z}{\partial r} & 0 & 0 & 0 \\ 0 & 0 & 0 & 0 & 0 & 0 & \frac{\partial X}{\partial p} & \frac{\partial Y}{\partial p} & \frac{\partial Z}{\partial p} \\ 0 & 0 & 0 & 0 & 0 & 0 & \frac{\partial X}{\partial q} & \frac{\partial Y}{\partial q} & \frac{\partial Z}{\partial q} \\ 0 & 0 & 0 & 0 & 0 & 0 & \frac{\partial X}{\partial r} & \frac{\partial Y}{\partial r} & \frac{\partial Z}{\partial r} \end{bmatrix} \begin{bmatrix} \frac{\partial u}{\partial X} \\ \frac{\partial u}{\partial Y} \\ \frac{\partial u}{\partial Z} \\ \frac{\partial v}{\partial X} \\ \frac{\partial v}{\partial Y} \\ \frac{\partial v}{\partial Z} \\ \frac{\partial w}{\partial X} \\ \frac{\partial w}{\partial Y} \\ \frac{\partial w}{\partial Z} \end{bmatrix} \quad \ldots \quad (A2.48)$$

Inversion of the equations (A2.48) gives:-

$$\begin{bmatrix} \frac{\partial u}{\partial X} \\ \frac{\partial u}{\partial Y} \\ \frac{\partial u}{\partial Z} \\ \frac{\partial v}{\partial X} \\ \frac{\partial v}{\partial Y} \\ \frac{\partial v}{\partial Z} \\ \frac{\partial w}{\partial X} \\ \frac{\partial w}{\partial Y} \\ \frac{\partial w}{\partial Z} \end{bmatrix} = \frac{1}{C} \begin{bmatrix} A & B & D & 0 & 0 & 0 & 0 & 0 & 0 \\ E & F & G & 0 & 0 & 0 & 0 & 0 & 0 \\ H & K & L & 0 & 0 & 0 & 0 & 0 & 0 \\ 0 & 0 & 0 & A & B & D & 0 & 0 & 0 \\ 0 & 0 & 0 & E & F & G & 0 & 0 & 0 \\ 0 & 0 & 0 & H & K & L & 0 & 0 & 0 \\ 0 & 0 & 0 & 0 & 0 & 0 & A & B & D \\ 0 & 0 & 0 & 0 & 0 & 0 & E & F & G \\ 0 & 0 & 0 & 0 & 0 & 0 & H & K & L \end{bmatrix} \begin{bmatrix} \frac{\partial u}{\partial p} \\ \frac{\partial u}{\partial q} \\ \frac{\partial u}{\partial r} \\ \frac{\partial v}{\partial p} \\ \frac{\partial v}{\partial q} \\ \frac{\partial v}{\partial r} \\ \frac{\partial w}{\partial p} \\ \frac{\partial w}{\partial q} \\ \frac{\partial w}{\partial r} \end{bmatrix} \quad \ldots \quad (A2.49)$$

Where $C = \frac{\partial XA}{\partial P} + \frac{\partial YE}{\partial P} + \frac{\partial ZH}{\partial P} = \det [J]$, ... (A2.50)

det [J] is the determinant of the Jacobian matrix in equation (A2.48),

and $A = \frac{\partial Y}{\partial q}\frac{\partial Z}{\partial r} - \frac{\partial Z}{\partial q}\frac{\partial Y}{\partial r}$, $B = \frac{\partial Z}{\partial p}\frac{\partial Y}{\partial r} - \frac{\partial Y}{\partial p}\frac{\partial Z}{\partial r}$,

$D = \frac{\partial Y}{\partial p}\frac{\partial Z}{\partial r} - \frac{\partial Z}{\partial p}\frac{\partial Y}{\partial r}$, $E = \frac{\partial Z}{\partial q}\frac{\partial X}{\partial r} - \frac{\partial X}{\partial q}\frac{\partial Z}{\partial r}$,

$F = \frac{\partial X}{\partial p}\frac{\partial Z}{\partial r} - \frac{\partial Z}{\partial p}\frac{\partial X}{\partial r}$, $G = \frac{\partial Z}{\partial p}\frac{\partial X}{\partial q} - \frac{\partial X}{\partial p}\frac{\partial Z}{\partial q}$, ... (A2.51)

$H = \frac{\partial X}{\partial q}\frac{\partial Y}{\partial r} - \frac{\partial Y}{\partial q}\frac{\partial X}{\partial r}$, $K = \frac{\partial Y}{\partial p}\frac{\partial X}{\partial r} - \frac{\partial X}{\partial p}\frac{\partial Y}{\partial r}$,

and $L = \frac{\partial X}{\partial p}\frac{\partial Y}{\partial q} - \frac{\partial Y}{\partial p}\frac{\partial X}{\partial q}$.

From the Cauchy definition of strain using the usual small strain approximation the six components are defined as:-

$$\varepsilon x = \frac{\partial u}{\partial x}, \quad \varepsilon y = \frac{\partial v}{\partial y}, \quad \varepsilon z = \frac{\partial w}{\partial z}, \qquad \text{... (A2.52)}$$

$$\gamma xy = \frac{\partial u}{\partial y} + \frac{\partial v}{\partial x}, \quad \gamma xz = \frac{\partial u}{\partial z} + \frac{\partial w}{\partial x}, \quad \gamma yz = \frac{\partial v}{\partial z} + \frac{\partial w}{\partial y}$$

By placing the right hand side of equation (A2.49) with equation (A2.43) and then collecting the terms on the left hand side to form the required components of strain in equations (A2.52) the $\underline{B}$ matrix in $\{\underline{\varepsilon}\} = \underline{B}\{\partial\}$ is obtained as; (see fig. (A2.53) over page).

Where the terms in the matrix can be formed from:-

$$B1,j = A\frac{\partial Nn}{\partial p} + B\frac{\partial Nm}{\partial q} + D\frac{\partial Nm}{\partial r},$$

$$B2,k = E\frac{\partial Nm}{\partial p} + F\frac{\partial Nm}{\partial q} + G\frac{\partial Nm}{\partial r}, \qquad \text{... (A2.54)}$$

$$B3,l = H\frac{\partial Nm}{\partial p} + K\frac{\partial Nm}{\partial q} + L\frac{\partial Nm}{\partial r},$$

and $B4,j = B2,k$, $B4,k = B1,j$,

$B5,j = B3,l$, $B5,l = B1,j$,

$B6,k = B3,l$, $B6,l = B2,k$.

Where m is the node number and $l = 2m$, $k = l-1$, $j = l-2$. The stresses are related to the strain by the elasticity matrix in;

$$
\begin{array}{cccccccccccccc}
 & & & m=1 & & & & m=2 & & & & & m=8 & \\
\begin{bmatrix} \epsilon_x \\ \epsilon_y \\ \epsilon_z \\ \gamma_{xy} \\ \gamma_{xz} \\ \gamma_{yz} \end{bmatrix} & = \frac{1}{c} & \begin{bmatrix} B1,1 & 0 & 0 & B1,4 & 0 & 0 & - & -- & - & B1,22 & 0 & 0 \\ 0 & B2,2 & 0 & 0 & B2,5 & 0 & - & -- & - & 0 & B2,23 & 0 \\ 0 & 0 & B3,3 & 0 & 0 & B3,5 & - & -- & - & 0 & 0 & B3,24 \\ B4,1 & B4,2 & 0 & B4,4 & B4,5 & 0 & - & -- & - & B4,22 & B4,23 & 0 \\ B5,1 & 0 & B5,3 & B5,4 & 0 & B5,6 & - & -- & - & B5,22 & 0 & B5,24 \\ 0 & B6,2 & B6,3 & 0 & B6,5 & B6,6 & - & -- & - & 0 & B6,23 & B6,24 \end{bmatrix} & \begin{bmatrix} u_1 \\ v_1 \\ w_1 \\ u_2 \\ v_2 \\ w_2 \\ ' \\ ' \\ ' \\ ' \\ u_8 \\ v_8 \\ w_8 \end{bmatrix} &
\end{array}
$$

Equation. A2.53)

$$[\sigma] = \underline{D}\ [\varepsilon]$$

Where $\underline{D}$ =

$$\begin{bmatrix} E(1) & E(2) & E(3) & 0 & 0 & 0 \\ E(2) & E(4) & E(5) & 0 & 0 & 0 \\ E(3) & E(5) & E(6) & 0 & 0 & 0 \\ 0 & 0 & 0 & E(7) & 0 & 0 \\ 0 & 0 & 0 & 0 & E(8) & 0 \\ 0 & 0 & 0 & 0 & 0 & E(9) \end{bmatrix} \quad \ldots \quad (A2.55)$$

For a isotropic, homogeneous material for example;

$$E(1) = E(4) = E(6) = \frac{E\,(1-v)}{(1+v)\,(1-2v)},$$

$$E(2) = E(3) = E(5) = \frac{Ev}{(1+v)\,(1-2v)}, \quad \ldots \quad (A2.56)$$

and $$E(7) = E(8) = E(9) = \frac{E}{2(1+v)}.$$

By considering the principle of virtual work the element stiffness matrix is calculated from:

$$\underline{K} = \int^{vol} \underline{B}^{t}\ \underline{D}\ \underline{B}\ d\,(vol) \quad \ldots \quad (A2.57)$$

The integration in equation (A2.57) is most easily carried out with respect to the local axies whose limits are known, thus

$$\underline{K} = \int_{-1}^{+1}\int_{-1}^{+1}\int_{-1}^{+1} \underline{B}^{t}\ \underline{D}\ \underline{B}\ \det[J]\ dp\ dq\ dr \quad \ldots \quad (A2.58)$$

The $\underline{B}_*$ matrix is defined in equation (6.13) as $\underline{B} = \frac{1}{c}\ \underline{B}_*$, thus

$$\underline{K} = \int_{-1}^{+1}\int_{-1}^{+1}\int_{-1}^{+1} \frac{1}{c}\,\underline{B}_*^{\,t}\ \underline{D}\ \underline{B}_*\ dp\ dq\ dr. \quad \ldots \quad (A2.59)$$

The triple multiplication in the equation above yields a matrix of order 24 x 24 for the linear (8 nodal) element. This matrix which represents the integrand of the element stiffness matrix can as usual be divided into sub-blocks. The two general sub-blocks derived from this product are shown in figure (A2.19).

NODE 'a'

$B^2(1,k)\ E(1) + B^2(4,k)\ E(7) + B^2(5,k)\ E(8)$		
$B(2,j)\ B(1,k)\ E(2) + B(4,j)\ B(4,k)\ E(7)$	$B^2(2,j)\ E(4) + B^2(4,j)\ E(7) + B^2(6,j)\ E(9)$	
$B(3,i)\ B(1,k)\ E(3) + B(5,i)\ B(5,k)\ E(8)$	$B(3,i)\ B(2,j)\ E(5) + B(6,i)\ B(6,j)\ E(9)$	$B^2(3,i)\ E(6) + B^2(5,i)\ E(8) + B(6,i)^2\ E(9)$

Where i = 3a j = i - 1 k = i - 2

GENERAL TRIANGULAR SUB-BLOCK Kaa

FIGURE (A2.19a)

NODE 'b'

$B(1,k)\ B(1,n)\ E(1) + B(4,k)\ B(4,m)\ E(7) + B(5,k)\ B(5,n)\ E(8)$	$B(1,k)\ B(2,m)\ E2 + B(4,k)\ B(4,m)\ E(7)$	$B(1,k)\ B(3,1)\ E(3) + B(5,k)\ B(5,1)\ E(8)$
$B(2,j)\ B(1,n)\ E(2)\ B(4,j)\ B(4,n)\ E(7)$	$B(2,j)\ B(2,m)\ E(4) + B(4,j)\ B(4,m)\ E(7) + B(6,j)\ B(6,m)\ E(9)$	$B(2,j)\ B3,1)\ E(5) + B(6,j)\ B(6,1)\ E(9)$
$B(3,i)\ B(1,n)\ E(3) + B(5,i)\ B(5,n)\ E(8)$	$B(3,i)\ B(2,m)\ E(5) + B(6,i)\ B(6,m)\ E(9)$	$B(3,i)\ B(3,1)\ E(6) + B(5,i)\ B(5,1)\ E(8) + B(6,i)\ B(6,1)\ E(9)$

NODE 'a'

Where i = 3a j = i - 1 k = i - 2 and 1 = 3b m = 1-1 n = 1 - 2

GENERAL RECTANGULAR SUB-BLOCK Kab

FIGURE (A2.19b)

A2.2.3.4 Numerical Integration

Gaussion quadrature was used to carry out the triple integration in equation (A2.59). The equation was replaced by the triple summation;

$$\underline{k} = \sum_{i=1}^{n} \sum_{j=1}^{n} \sum_{k=1}^{n} G(ai, aj, ak)\, Hi\, Hj\, Hk \qquad \ldots (A2.60)$$

Where G(ai, aj, ak) is the value of the integrand at the various sampling points ai, aj, and ak, Hi etc. is the weight coefficients and n is the number of gauss sampling points.

A.2.2.3.5 Stiffness Formulation of other Isoparametric Hexahedrals

Like the general sub-blocks derived for the quadrilateral elements (figure A.2.11) the sub-blocks in figure (A2.19) apply to any hexahedral element. The only difference is formulating the stiffness items for other elements is in the choice of the shape functions and the number of columns in the various matrices.

A2.3 Convergence Criteria

To ensure convergence to the correct solution by finer sub-division of the mesh, the assumed displacement function must satisfy the convergence criteria which were discussed in Chapter (1). The three main criteria are:-

(1) Displacements must be continuous over element boundaries.

(2) Rigid body movements should be possible without straining.

(3) A state of constant strain should be reproducible.

The arguments used by Ergatoudis (50) to show that the Isoparametric elements conformed to these convergence criteria are outlined here for completeness.

To satisfy criterior (1) the displacements must be uniquely defined over the face of the element, by the displacements of the nodes on that face only. The shape functions for nodes not on the face are zero, therefore the variation of displacements on that face is identical for both elements.

Criteria (2) and (3) are closely related and both are associated with a displacement function of the form ;

$$U = a + bx + cy + dz \qquad (A2.61)$$

This is because the first derivatives of the above equation contain only the arbitrary constants a, b, c and d. The displacements anywhere within an Isoparametric element can be interpolated from ;

$$U = N_1U_1 + N_2U_2 + N_3U_3 + \ldots\ldots \qquad (A2.62)$$

Substituting equation (A2.61) into equation (A2.62) for each node of the element gives ;

$$U = N_1(a + bx_1 + cy_1 + dz_1) + N_2(a + bx_2 + cy_2 + dz_2) + \ldots \qquad (A2.63)$$

or,
$$U = a(N_1 + N_2 + \ldots) + b(N_1x_1 + N_2x_2 + \ldots) + c(N_1y_1 + N_2y_2 + \ldots) + d(N_1z_1 + N_2z_2 + \ldots) \qquad (A2.64)$$

From the definition of x, y and z in equation (A2.46) , and the property of the shape functions that , $\sum_{i=1}^{n} N_i = 1$ that was discussed in section (A2.1.3.1) , it can be seen that equation (A2.64) is an identity with equation (A2.61) as the element size decreases to zero and $x_1 \to x_2 \to x$. Further , as the shape functions are functions only of p,q and r , the local axes, and since any change in the origin of the global axes does not alter the position of any point (p,q,r) relative to the nodes no straining can be incurred .

APPENDIX 3.

ELASTIC ANALYSIS PROGRAM.

A 3.1 Introduction

In problems concerning the analysis of continua it is difficult to determine initial strain conditions, while it is common practice to ignore body forces as their effect is usually small compared to an applied load. The analysis of slope and embankments, where body forces are important, was dealt with as a special case. Conditions such as non-homogeneity and orthotropy are common and were allowed for. The input data had to be prepared by hand and punched on to cards. Careful thought was given to this and the effort was kept to a minimum.

It is advisable to check the performance of the various elements against an explicit solution. To ensure that the results are indicative of the element efficiency, a series of programs were written, one for each of the elements outlined in Appendix(2). The routines in these programs formed the basis of all the future programs.

A 3.2 Solution of the Equations and Storage of the Overall Stiffness Matrix

The method of storage and solution of the equations adopted by the author was that due to Jennings and Tuff (50). This method stored the equations using a variable band width technique using Choleski triangular factorisation method for their solution.

During the reduction of a set of sparse equations by any variant of Gaussian elimination, the zeros before the first non-zero term remain zero if there is no row or column interchange. A variable band storage scheme makes use of this property by storing for each row only those coefficients between the first non-zero term and the leading diagonal. The rows are stored consecutively in a uni-dimensional array (W), while another uni-dimensional array (DAS) is used to store the locations of the diagonal terms within the array . For example, the matrix:

Row						
1	1.5					
2	0.2	1.2				
3	-1.1	0	2.2			
4	0	0	5.1	10.6		
5	0	0	0	0	2.6	
6	0	0	-1.2	0	0	6.1

would be stored as:-

Location	1	2	3	4	5	6	7	8	9	10	11	12	13
W	1.5	0.2	1.2	-1.1	0	2.2	5.1	10.6	2.6	-1.2	0	0	6.1

and the address sequence becomes:

row no. + 1	1	2	3	4	5	6	7
DAS	0	1	3	6	8	9	13

Some zero terms however will be stored, the number of these depends upon the least joint number, which in turn depends upon the efficiency of the overall joint numbering scheme.

Jennings and Tuff further improved their method by using backing store facilities. This is achieved by the division of the storage array into a number of segments, each segment containing an integral number of rows. The segment size can be chosen to match the core store available. When the address sequence is known it is relatively easy to obtain the maximum number of rows that can fit into each segment.

Choleski factorisation of the equations $\underline{L} = \underline{K}\,\underline{X}$ yields a matrix of the form

$$\underline{G}\,\underline{G}^{T} = \underline{K} \qquad (A\,3.1)$$

where $\underline{G}$ is the lower triangle matrix with positive diagonal terms. Substituting equation (A3.1) into $\underline{L} = \underline{K}\,\underline{X}$ gives:

$$\underline{G}\,\underline{G}^{T}\{X\} = \{L\} \qquad (A3.2)$$

$$\text{or} \quad \underline{G}\,\underline{Y} = \{L\} \qquad (A3.3)$$

where $\underline{Y} = \underline{G}^{T}\{\underline{X}\}$.

The variables in $\underline{Y}$ are the modified right hand side coefficients after elimination. The back substitution process to complete the solution is the determination of $\{X\}$ from:

$$\underline{G}^{T}\{X\} = \underline{Y} \qquad (A3.4)$$

The matrix $\underline{G}$ overwrites $\underline{K}$ in the store by use of the recursive relations

$$g_{ii} = \left\{ K_{ii} - \sum_{k=1}^{i-1} g^{2}_{ik} \right\}^{1/2} \quad \text{for diagonal terms, and}$$

$$g_{ij} = \left\{ k_{ij} - \sum_{k=1}^{j-1} g_{ik}\, g_{jk} \right\} \div g_{jj} \quad \text{for off-diagonal terms.}$$

These relations show that to form any coefficient g_{ij} only rows i and j of the stiffness matrix are required to be stored. The segment containing row j is known as the passive segment and that containing row i the active segment.

Adoption of the variable band width storage scheme makes it unnecessary to call all the passive units up to the area to be reduced if this area lies entirely to the left of the stored elements. To determine the first passive unit required by an active unit it is necessary to inspect the column numbers of the first element in each row of the active segment. If the least of these is cq it is possible to determine in which segment the corresponding row occurs, and this will be the first passive segment to be called. Figure (A3.1) shows the area in which elements g_{ij} will be determined for a given active segment q and passive segment p.

As the matrix $\{L\}$ is kept in the core during the reduction of $\underline{K}$, the reduction of $\{L\}$ to form $[Y]$ is carried out simultaneously with the

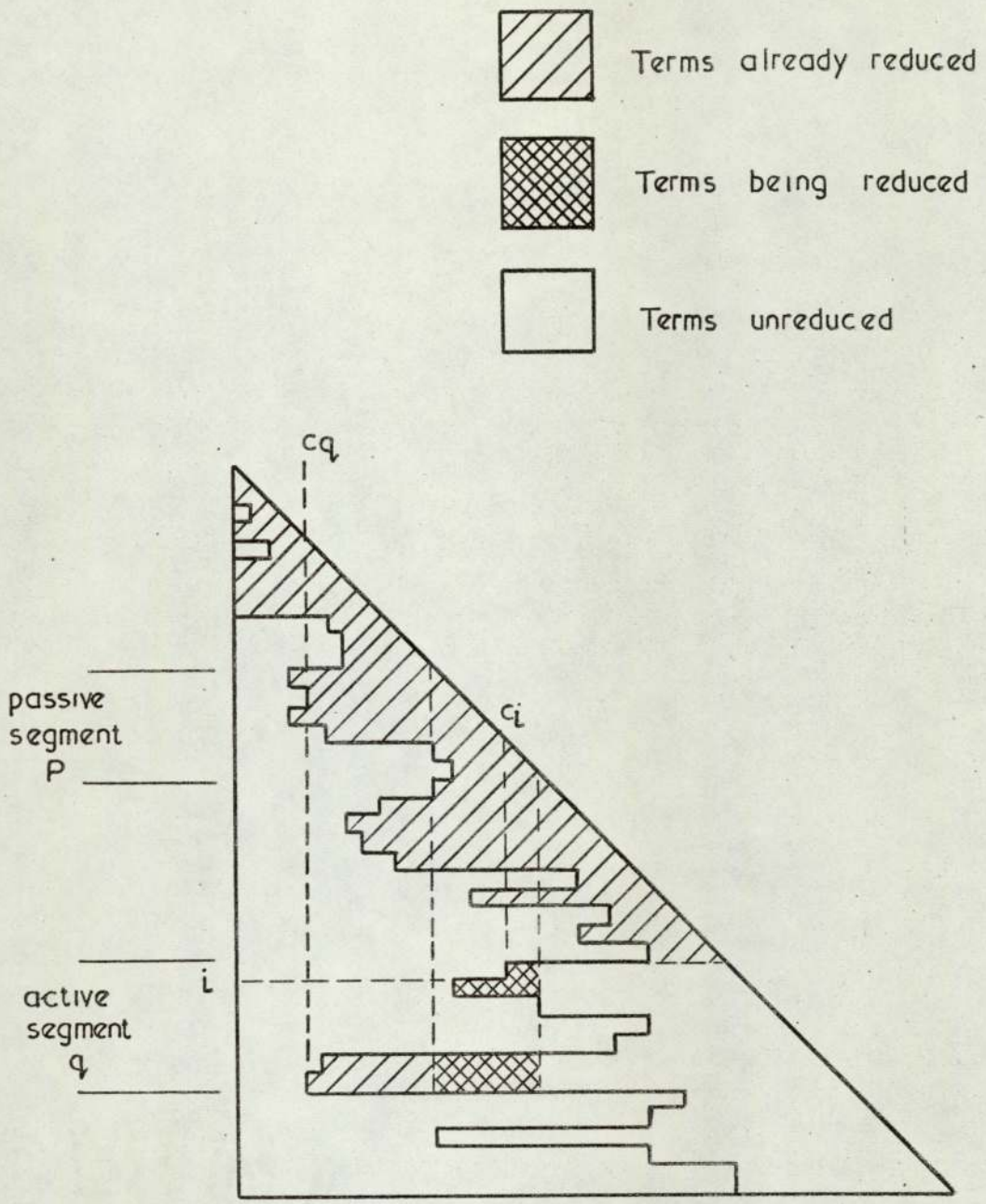
Terms already reduced
Terms being reduced
Terms unreduced
cq
ci
passive
segment
P
i
active
segment
q

Figure A 3.1.

determination of G. When reduction is completed the segments of G are called in the reverse order to perform the back substitution to obtain {X}, which overwrites {L}.

Jennings and Tuff also showed that random access disc facilities were the most efficient method of handling the segments provided that their size corresponds to a multiple of a bucket size. The maximum bucket size is 512 variables (1024 words) on I.C.L. 1900 series facilities and this was therefore chosen as a convenient segment size.

A 3.3 Formation of the Overall Stiffness Matrix, Two Dimensional Elements

It was seen in Appendix (2) that the stiffness matrix of one linear quadrilateral is of order 8 x 8, each row or column represents one of the two possible degrees of freedom at each node. The finite element mesh shown in figure(A 3.2a) has only one element (number 3) which is allowed two degrees of freedom at each node. The other elements are connected to joints with some degree of freedom suppressed.

The lower triangle of the stiffness matrix for this mesh is shown in figure(A 3.2b), where the shaded area represents stiffness coefficients. The limits of the band are shown by double lines and only those terms between it and the diagonal will be stored. The band width depends upon the lowest numbered joint attached to any particular joint. Thus, the overall joint numbering system must keep the degree of connectivity to a minimum otherwise a great number of zeros may be unnecessarily stored. The DAS array is calculated by inspecting the least joint numbers, and the result for this mesh is shown below the figure(A 3.2b).

The problem in forming the overall stiffness matrix was to select the right terms from the general sub-blocks of the element stiffness matrix and then insert them into the correct position in the overall stiffness array; to do this the author followed a method proposed by Bray (11) for structural elements.

The degrees of freedom were input in the familiar structural notation, in which the digit 1 indicates an allowed degree of freedom

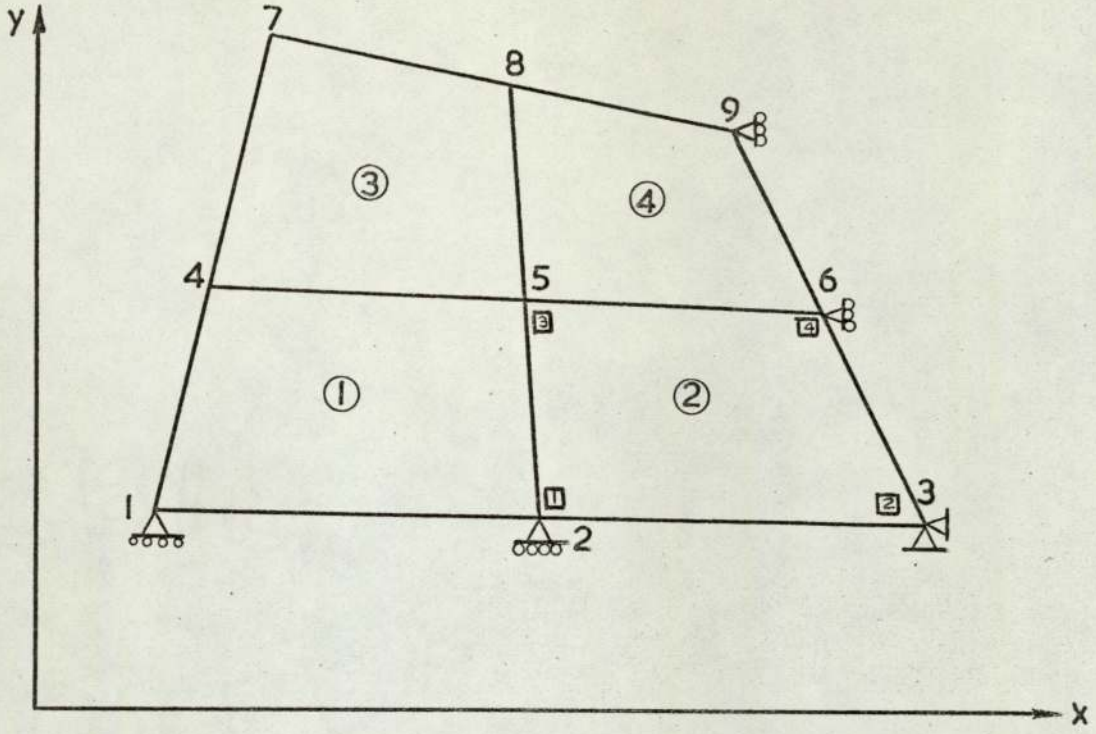

Figure A3.2.a

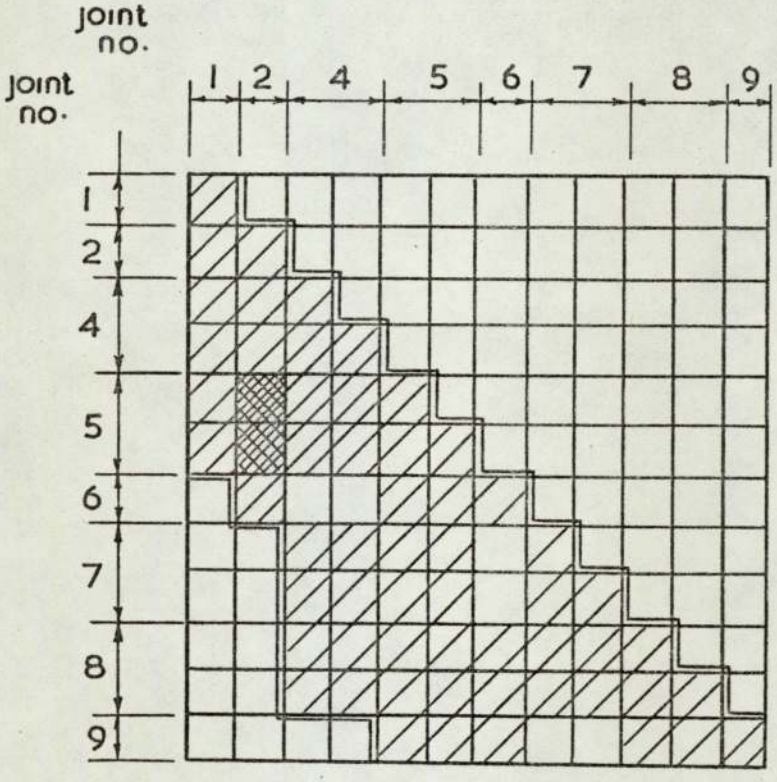

Figure A3.2.b

DAS – (0, 1, 3, 6, 10, 15, 21, 27, 33, 40, 48, 57, 65,)

DF – (1, 2, 2, 4, 6, 7, 9, 11, 12,)

and the digit 0 indicates a suppressed one. In two dimensions, three degrees of freedom are possible as shown in figure(A 3.3a). Figure(A 3.3b) shows how the joints in figure(A 3.2a) would be represented in structural notation. Figure(A 3.3c) shows another way of representing the degrees of freedom in what was called indicator form. These values are stored in the IR array in a left justified fashion. This is called indicator form because the digit 1 actually indicates the existence of a degree of freedom in the X-direction, the digit 2 indicates a degree in the Y direction and 3 indicates a rotation.

Consider the general rectangular sub-block, which was derived in section(A2.1.33), illustrated in figure(A 3.4a). This sub-block represents the combined contribution of nodes i and j of an element e. If either of these nodes are connected at joints with some degree of freedom suppressed then the sub-block will not be the same shape. Each row or column exists for one particular degree of freedom. If either of the joints has no degrees of freedom then the sub-block will not exist. Consider the sub-block [3,1] of element 2 in the mesh shown in figure(A 3.2a). These nodes are connected at joints 5 and 2 respectively. The position of this sub-block in the overall stiffness matrix is shown by the heavily shaded area in figure(A 3.2b). This sub-block is not the only contribution to this area because the sub-block [4,2] of element 1 will also add into the space. The sub-block allowed by the degrees of freedom of joints 5 and 2 is shown in figure (A 3.4b). The subscripts for the terms are those allowed by the combination of the two rows of the indicator array (figure(A3.3c)) for joints 5 and 2. Joint 5, the larger joint number, determines the number of rows, while joint 2 determines the number of columns. The two dimensional array known as the code array (IAA) is shown in figure(A3.4c).

It was also necessary to introduce another array (DF), containing, for each joint, the summated degrees of freedom up to and including that joint. The result for this example is shown below figure(A 3.2b). The

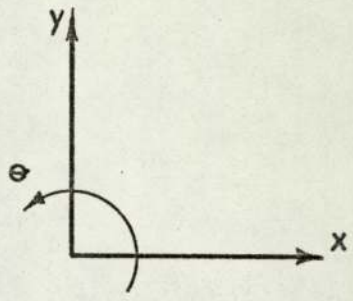

Figure A3.3. a

joint	x	y	o
1	1	0	0
2	1	0	0
3	0	0	0
4	1	1	0
5	1	1	0
6	0	1	0
7	1	1	0
8	1	1	0
9	0	1	0

Figure A3.3. b

joint	IR		
1	1		
2	1		
3			
4	1	2	
5	1	2	
6	2		
7	1	2	
8	1	2	
9	2		

Figure A3.3. c.

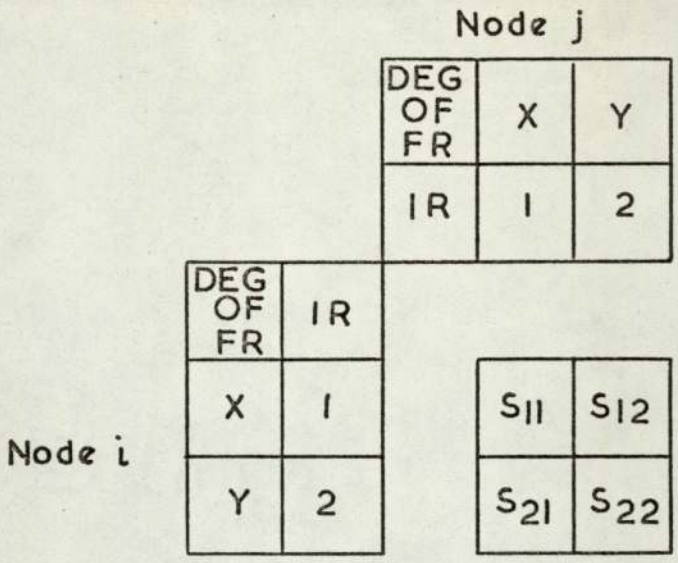

Figure A3.4.a. General rectangular sub block i, j

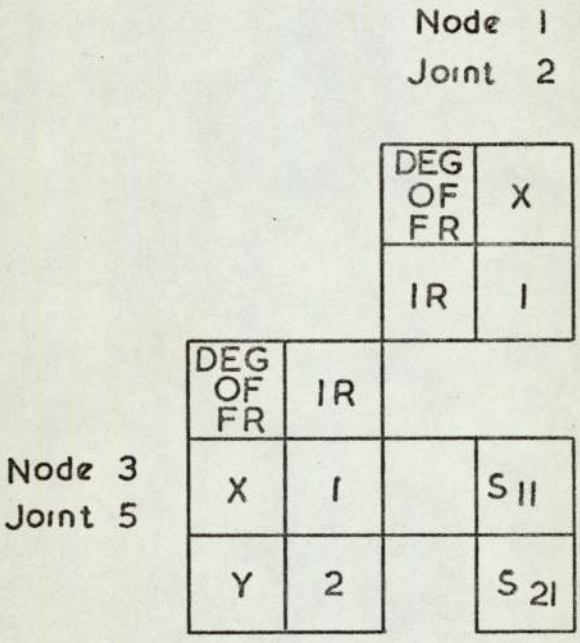

Figure. A3.4.b. Rectangular sub block (3.1)

	1	2	3
1	1	4	9
2	2	3	8
3	5	6	7

Figure A3.4.c. Code array IAB

degree of freedom of any joint a $\neq$ 1 is DF(a)-DF(a-1). The code array contains labels for the terms in a general sub-block, three degrees of freedom being allowed. The combinations of the IR array terms of the two joints defining the sub-block gives the desired terms. For the example of sub-block[3,1] in figure(A3.4b) this would be labels 1 and 2.

Only one problem remained and that was to put these terms into the right place in the stiffness array. Only the lower triangle of the stiffness matrix is stored and thus only those sub-blocks that fall below the diagonal are required. Any sub-block[i,j],where nodes i and j are connected to joints A and B respectively, will be constructed and written away only when joint number A is greater than that of B.

The position of the sub-block in the overall stiffness matrix is defined by its row number and its distance from the diagonal. The first row of the sub-block[m,n](attached to A and B, A > B) will be DF(A-1)+1 and the distance, from the diagonal to the first term, is DF(A-1)-DF(B-1)+1. In general, for the i^{th} degree of freedom at joint A and the j^{th} degree of freedom at joint B, the location in the W array is given by:-

$$L = DAS\{DF(A-1)+i+1\} - \{DF(A-1)-DF(B-1)\}+i-j \qquad (A3.5)$$

The procedure shown in the flowchart(A3.1) shows how the terms for rectangular sub-block[m,n]were selected and written away into the stiffness array. Nodes m and n are connected to joints A and B, where A is greater than B. It can be readily seen that the process can be applied to any two dimensional element. The method was also independent of the order of the quadrilateral. The only difference between the treatment of the linear quadrilateral and say the cubic lagrangian element is that the latter has many more sub-blocks.

Triangular sub-blocks were treated as a special case of the rectangular sub-block. Here only one joint decides the shape and position. An element having n nodes will contribute a maximum of n triangular sub-blocks and

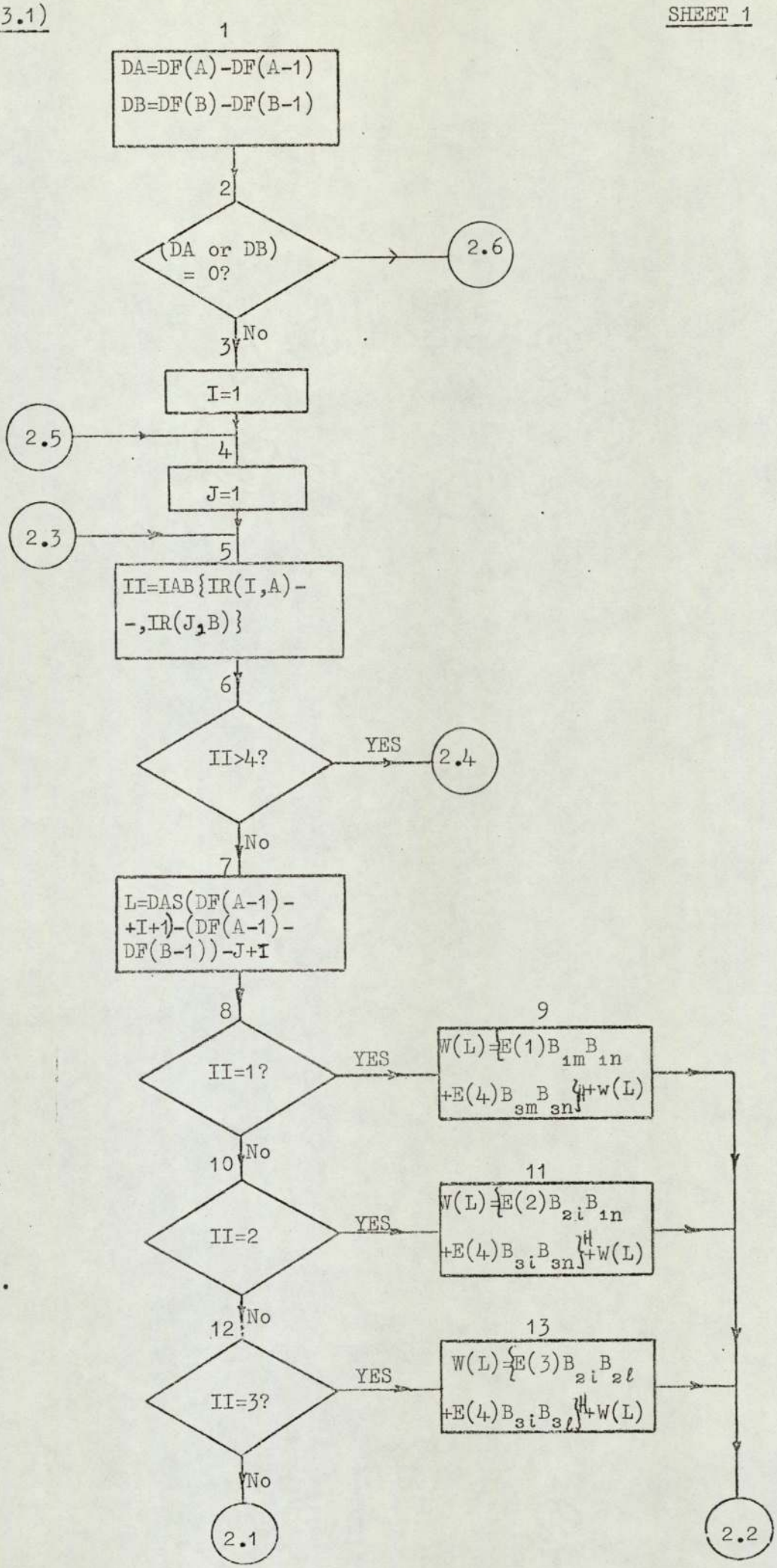

The terms were defined in figure(A2.11b). H is the weight coefficient product $H_p H_q$.

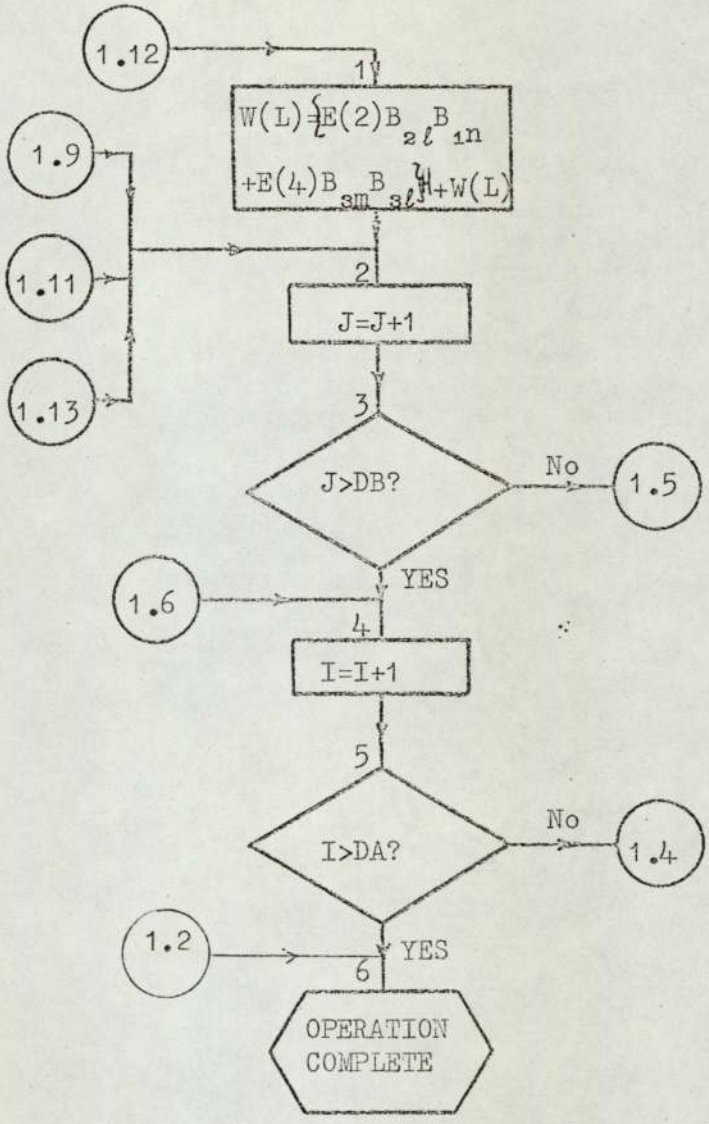
1.12
1
W(L)=Σ{E(2)B2ℓB1n
+E(4)B3mB3ℓ}+W(L)
1.9
1.11
1.13
2
J=J+1
3
J>DB?
No
1.5
YES
1.6
4
I=I+1
5
I>DA?
No
1.4
1.2
YES
6
OPERATION
COMPLETE

$0.5 \times (n-1)n$ rectangular sub-blocks. The required rectangular sub-blocks, those below the diagonal, are selected by inspecting every possible permuation of node numbers, ignoring diagonal terms and those permutations where the joint number attached to the first node is less than that at the second.

A3.4.1 Numerical Integration

It was shown in section(A2.1.3.4) that the complexity of the stiffness matrix of an Isoparametric quadrilateral element required the use of numerical integration. This was achieved by the double summation:

$$\underline{K} = \sum_{j=1}^{n} \sum_{i=1}^{n} G(a_j, a_i) H_j H_i \qquad (A3.6)$$

where a is the position of the gauss point and H its associated weight coefficient. Thus, if an n point Gauss rule is used, the operations discussed in the previous section have to be repeated n^2 times. The $\underline{B}$ matrix will have to be calculated for each value of p and q associated with the rule, formed into sub-blocks, multiplied by the weight coefficient, and written into the stiffness array. The final coefficients are thus summed up in the stiffness array.

This operation required the use of a table of values for a and H, from which the various values of p and q together with their weights were selected. These values were stored, in a BLOCK DATA segment, as two two-dimensional arrays. The values for up to a six point rule were only included as these were judged to be adequate. These values were taken from Kopal (58) and are illustrated in figure(A3.5). The equation(A3.6) was modified to become:

$$\underline{K} = \sum_{j=1}^{n} \sum_{i=1}^{n} G\{AB(n-i,i), AB(n-1,j)\}\, H(n-1,i) H(n-1,j) \qquad (A3.7)$$

The complete process of forming the overall stiffness matrix, including numerical integration is shown in flowchart(A3.2).

ORDER OF RULE n	1	2	3	4	5
2	+0.57735027	-0.57735027			
3	+0.77459667	-0.77459667	0.00000000		
4	+0.86113631	-0.86113631	+0.33998104	-0.33998104	
5	+0.90617985	-0.90617985	+0.53846931	-0.53846931	0.00000000

The abscissae are held in the array AB

ORDER OF RULE n	1	2	3	4	5
2	1.00000000	1.00000000			
3	0.55555556	0.55555556	0.88888889		
4	0.34785485	0.34785485	0.65214515	0.65214515	
5	0.23692689	0.23692689	0.47862867	0.47862867	0.56888889

The weight coefficients are held in the array H

The arrays that make up the Block Data segment containing the values for Gauss Quadrature

Fig.A3.5

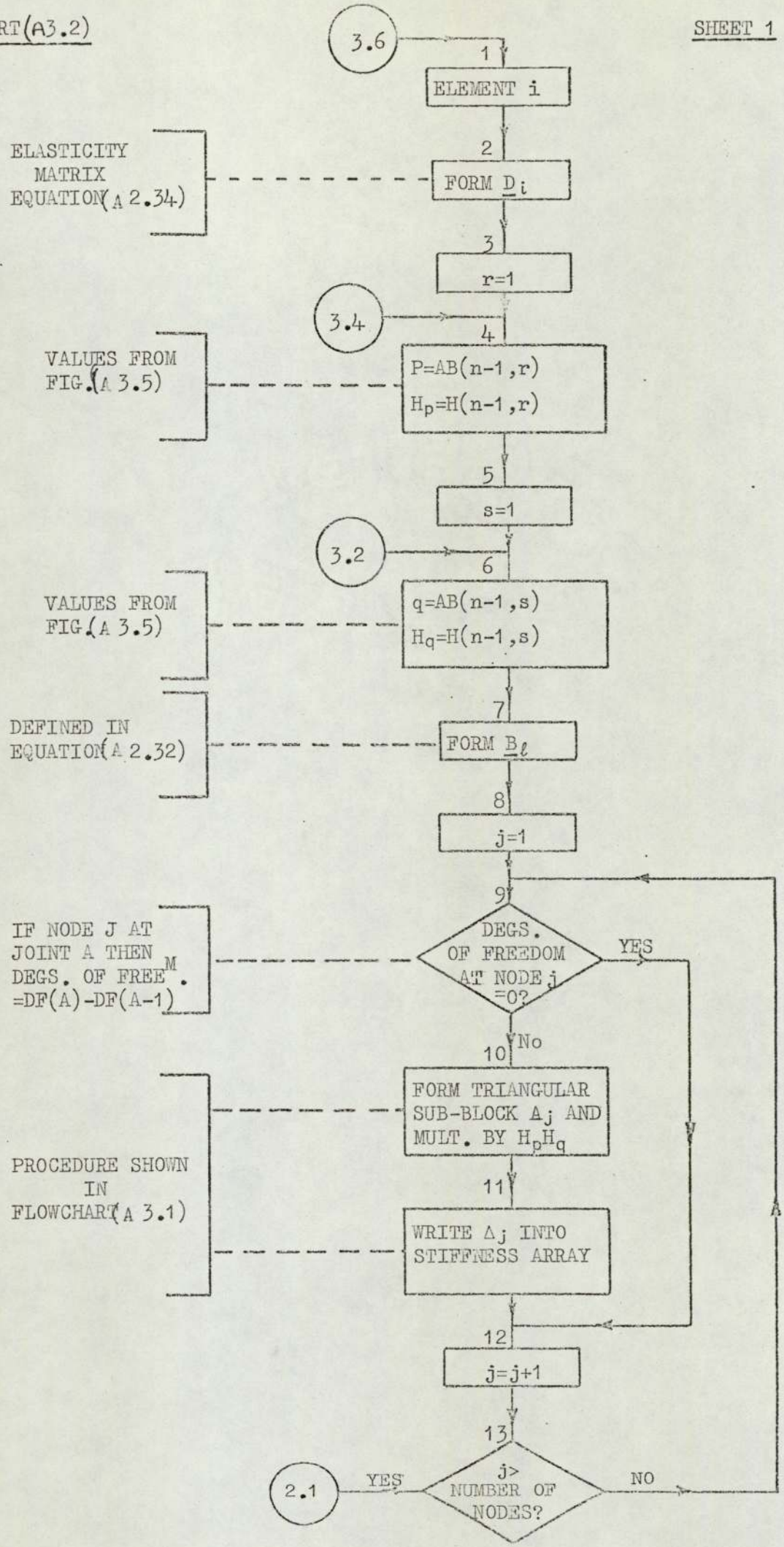
3.6
1
ELEMENT i
ELASTICITY MATRIX EQUATION (A 2.34)
2
FORM $\underline{D}_i$
3
r=1
3.4
4
VALUES FROM FIG. (A 3.5)
P=AB(n-1,r)
H_p=H(n-1,r)
5
s=1
3.2
6
VALUES FROM FIG. (A 3.5)
q=AB(n-1,s)
H_q=H(n-1,s)
7
DEFINED IN EQUATION (A 2.32)
FORM $\underline{B}_\ell$
8
j=1
9
IF NODE J AT JOINT A THEN DEGS. OF FREEM. =DF(A)-DF(A-1)
DEGS. OF FREEDOM AT NODE j =0?
YES
No
10
PROCEDURE SHOWN IN FLOWCHART (A 3.1)
FORM TRIANGULAR SUB-BLOCK A_j AND MULT. BY H_pH_q
11
WRITE Δ_j INTO STIFFNESS ARRAY
12
j=j+1
13
2.1
YES
j> NUMBER OF NODES?
NO
A

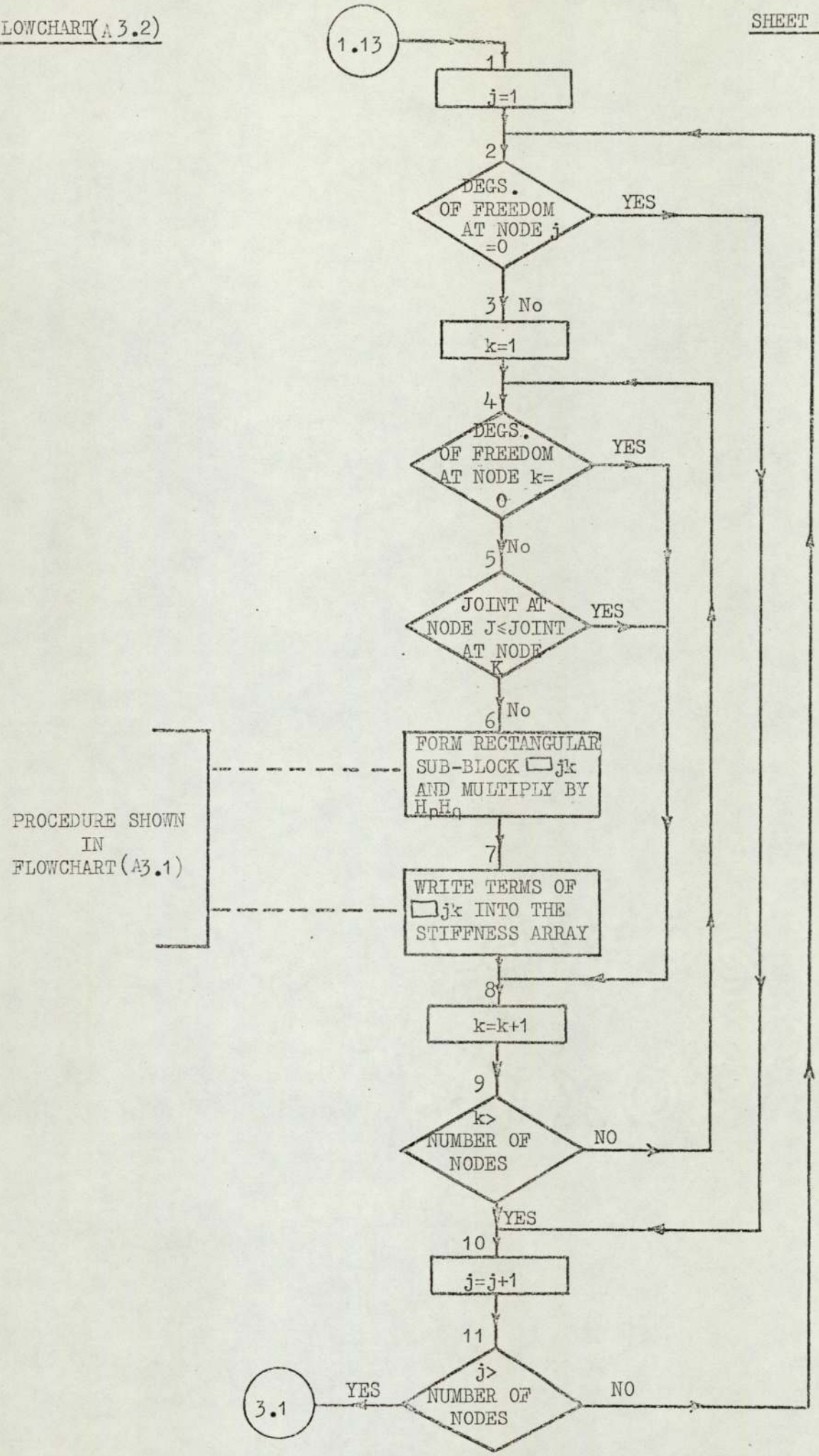
1.13
1
j=1
2
DEGS. OF FREEDOM AT NODE j =0
YES
3
No
k=1
4
DEGS. OF FREEDOM AT NODE k= 0
YES
No
5
JOINT AT NODE J≤JOINT AT NODE K
YES
No
6
FORM RECTANGULAR SUB-BLOCK □jk AND MULTIPLY BY HnHn
PROCEDURE SHOWN IN FLOWCHART(A3.1)
7
WRITE TERMS OF □jk INTO THE STIFFNESS ARRAY
8
k=k+1
9
k> NUMBER OF NODES
NO
YES
10
j=j+1
11
j> NUMBER OF NODES
YES
NO
3.1

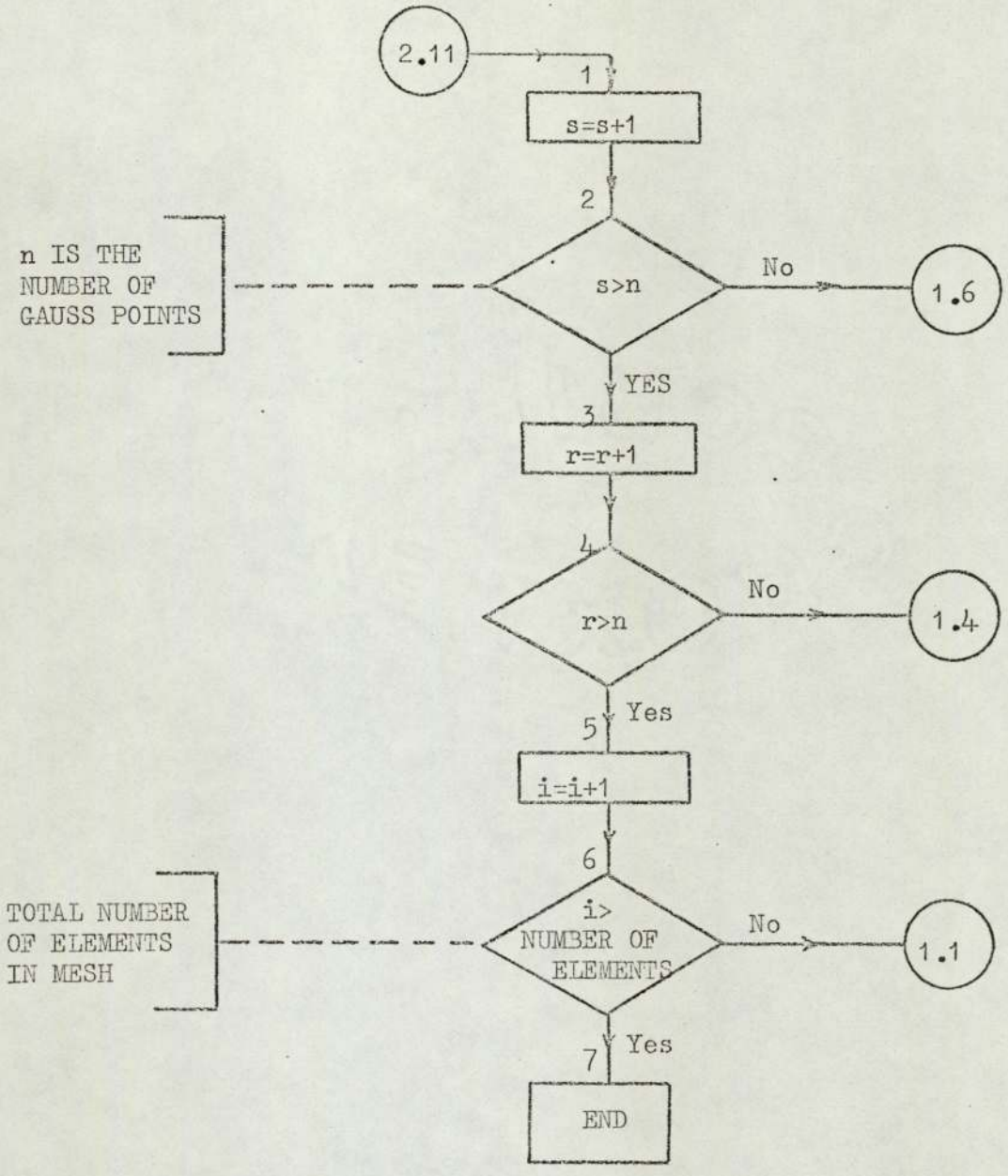
2.11
1
s=s+1
2
n IS THE NUMBER OF GAUSS POINTS
s>n
No
1.6
YES
3
r=r+1
4
r>n
No
1.4
Yes
5
i=i+1
6
TOTAL NUMBER OF ELEMENTS IN MESH
i> NUMBER OF ELEMENTS
No
1.1
Yes
7
END

A 3.4 Calculation of Stresses, Two Dimensional Elements

In general, engineers are interested in the stress distribution throughout a media. The stresses should therefore be calculated at as many points as it is convenient. It seemed logical therefore to treat the stresses in a similar manner to the displacements calculated at each point. In Appendix (2) it was shown that strains are calculated from the displacements

$$\{\varepsilon\} = \underline{B}\,\{\delta\} \qquad (A\,3.8)$$

and the stresses are then calculated from

$$\{\sigma\} = \underline{D}\,\{\varepsilon\} \qquad (A\,3.9)$$

For any element the strain can be calculated at a node by forming the $\underline{B}$ matrix, using the local co-ordinates of that node, and then multiplying it by the displacement vector associated with the element. Four nodes are connected to joint 5 in figure (A3.2a) so the calculation of strain at one of these nodes would seem adequate. However, the convergence criteria for the Finite Element method, with the displacement model, ensures displacement continuity throughout the mesh. Approximate slope continuity is achieved by careful mesh design. The strain at joint 5 (figure A 3.2a) is best expressed as the average of the strain at each of the appropriate nodes of the elements surrounding it. When the average strain was known at each joint the average stress could be calculated using equation (A 3.9). Soils usually gain strength with depth thus to make the procedure general it is advantageous to calculate the average stress at each node in a similar way to that used for the strains.

The routine to calculate strains and stresses uses an array (CD) to hold the local co-ordinates of each node. The final average stresses and strains were stored in another array (SQ) which has seven rows and a column for each joint. Six of the rows hold strains and stresses while the seventh row holds a counter.

For each element the routine is calculated the stress and strain at

each node. These values were added into the array SQ at the joint the node is attached to. Each time SQ is entered at a joint the count at that joint is increased by one. When all the elements are finished the average strains and stresses are calculated by dividing the sums, now stored in the SQ array, by the counts. The procedure is shown in the flow chart (A 3.3).

A 3.5 Other Two Dimensional Elements

The procedures described in the two previous sections are applicable to any elements. The method of formation of the overall stiffness matrix only requires the construction of the two general sub-blocks. In the case of triangular and member elements, numerical integration is not required and the process is only carried out once.

The strains in a triangular element were relative to the local co-ordinate system, which was not very convenient. This element is a constant strain element not requiring strain calculation at each of its three nodes. For these reasons the strain was calculated at the centre of the element and then transformed to the global axes using the transformation:

$$\begin{bmatrix} \varepsilon_x \\ \varepsilon_y \\ \gamma_{xy} \end{bmatrix} = \begin{bmatrix} L_p^2 & L_q^2 & L_p L_q \\ M_p^2 & M_q^2 & M_p M_q \\ 2M_p L_p & 2M_q L_q & M_q L_p + M_p L_q \end{bmatrix} \begin{bmatrix} \varepsilon_p \\ \varepsilon_q \\ \gamma_{pq} \end{bmatrix} \qquad (A\ 3.10)$$

where L_p, L_q, M_p and M_q are direction cosines of the element.

The stresses are then calculated using the transformed strains and the results added into the SQ array for each of the three joints attached to the triangle. Average strains and stresses are again calculated when all the elements have been processed.

A 3.6 Plane Strain Linear Elastic Analysis Programs

Initially six programs were written. One for the triangular element and one for each of the Isoparametric elements dealt with in Appendix(2) All these programs were very similar. Indeed, one program could have been

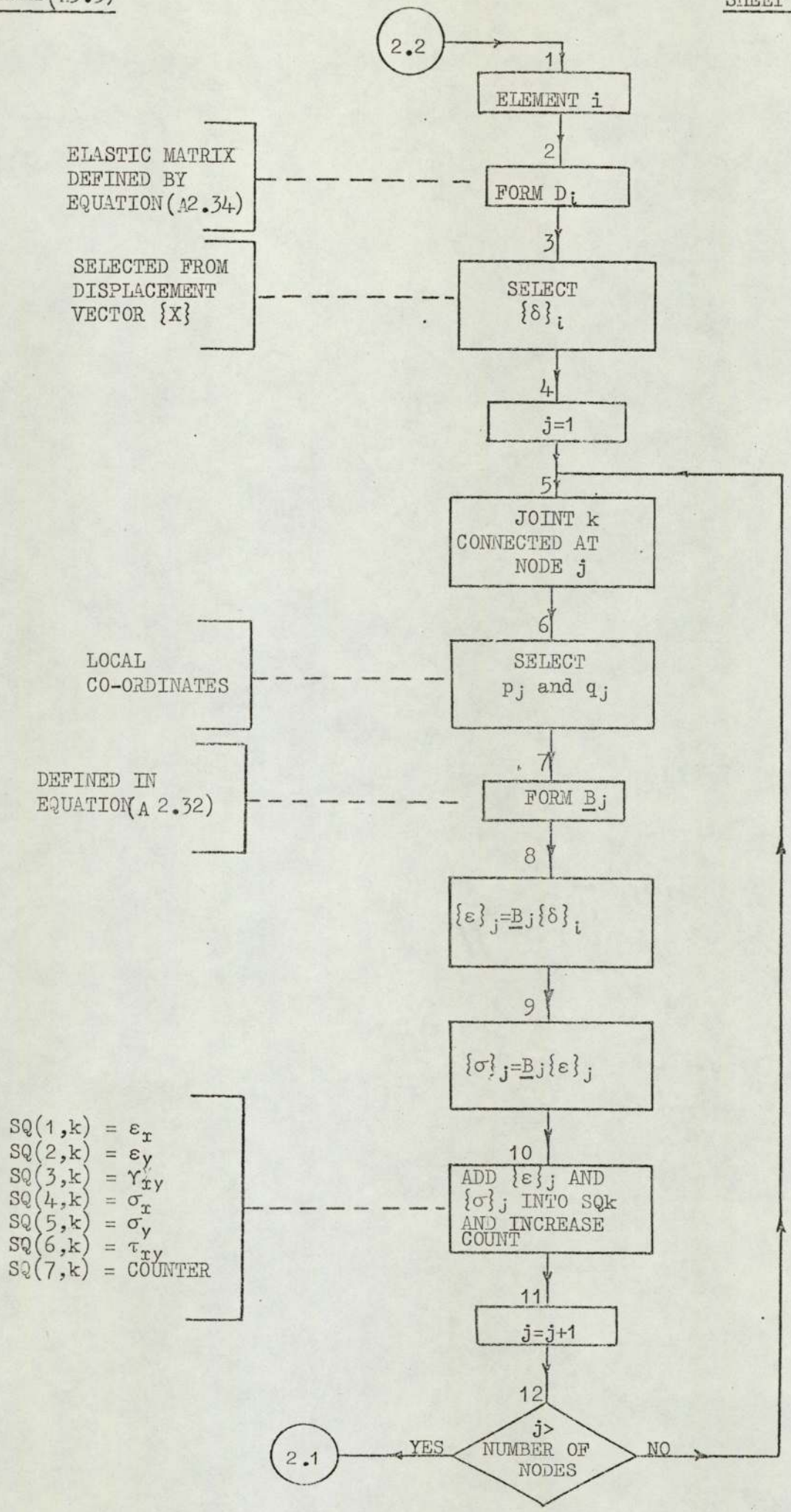
2.2
1
ELEMENT i
2
FORM D_i
ELASTIC MATRIX DEFINED BY EQUATION (A2.34)
3
SELECT $\{\delta\}_i$
SELECTED FROM DISPLACEMENT VECTOR {X}
4
j=1
5
JOINT k CONNECTED AT NODE j
6
SELECT p_j and q_j
LOCAL CO-ORDINATES
7
FORM $\underline{B}_j$
DEFINED IN EQUATION (A 2.32)
8
$\{\varepsilon\}_j = \underline{B}_j \{\delta\}_i$
9
$\{\sigma\}_j = \underline{B}_j \{\varepsilon\}_j$
SQ(1,k) = ε_x
SQ(2,k) = ε_y
SQ(3,k) = γ_{xy}
SQ(4,k) = σ_x
SQ(5,k) = σ_y
SQ(6,k) = τ_{xy}
SQ(7,k) = COUNTER
10
ADD $\{\varepsilon\}_j$ AND $\{\sigma\}_j$ INTO SQk AND INCREASE COUNT
11
j=j+1
12
j> NUMBER OF NODES
YES
NO
2.1

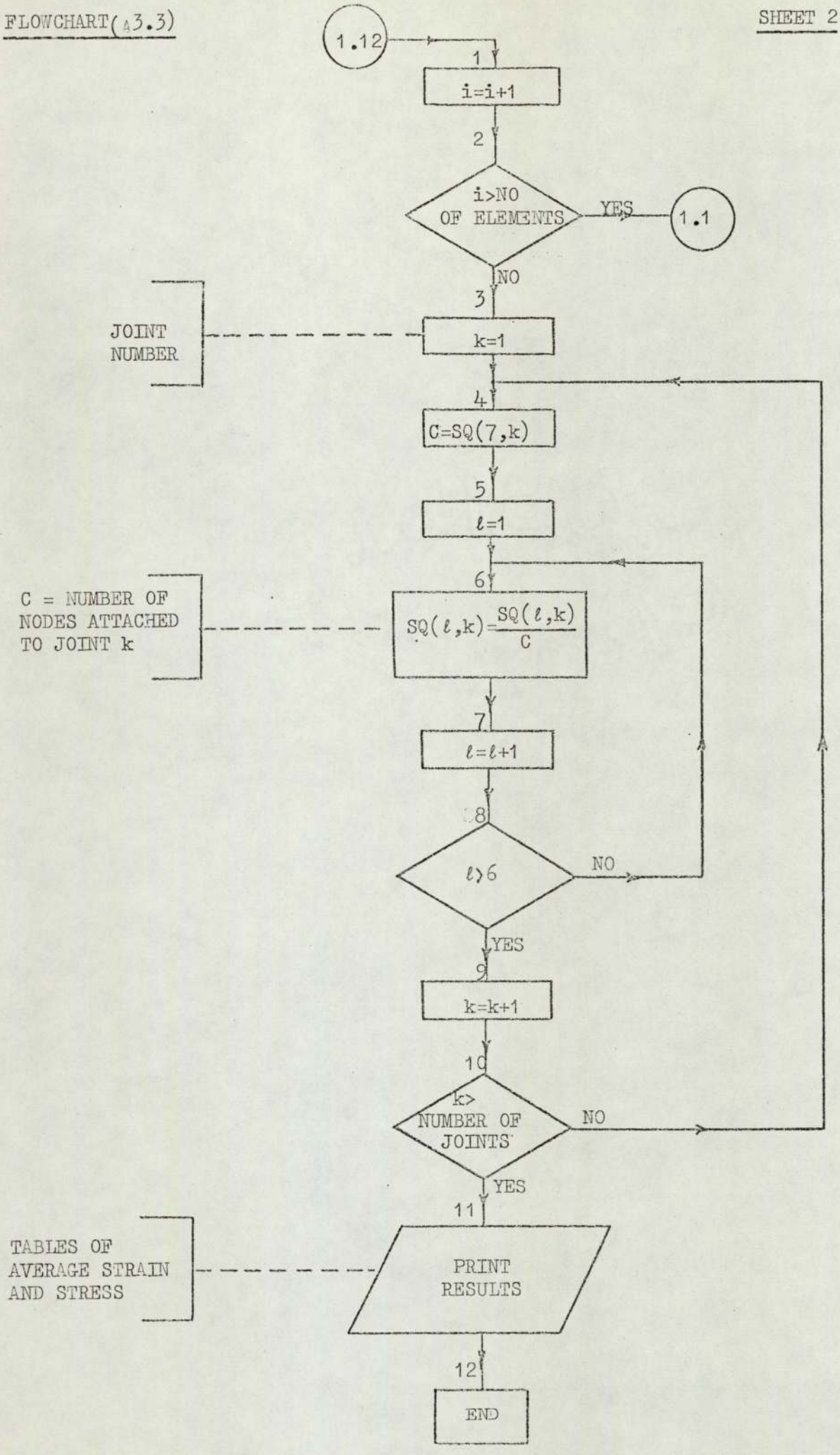
1.12
1
i=i+1
2
i>NO OF ELEMENTS
YES
1.1
NO
3
JOINT NUMBER
k=1
4
C=SQ(7,k)
5
ℓ=1
6
C = NUMBER OF NODES ATTACHED TO JOINT k
SQ(ℓ,k)=SQ(ℓ,k)/C
7
ℓ=ℓ+1
8
ℓ>6
NO
YES
9
k=k+1
10
k> NUMBER OF JOINTS
NO
YES
11
TABLES OF AVERAGE STRAIN AND STRESS
PRINT RESULTS
12
END

written containing all the element sub-routines. However, this would have been very innefficient for the series of analyses carried out in Chapter(2), where meshes were composed of only one type of element. The ease with which files are handled under the I.C.L. GeorgeIV operating system meant that new programs, and even new suites of programs, could be assembled from the various available sub-routines without much difficulty. These programs all carried out linear elastic analysis of an isotropic homogeneous continuum subject to surface loading. The procedure followed by each of the programs is shown in flowchart (A3.4).

Several of the routines, like those involved in reading the load vector and solving the equations, are exactly the same for all elements. These were stored as library routines. Hence, a program like the one in flowchart (A3.4) would be formed by a Master segment, the two routines ISOQUADn and ISQnSAS, for the formation of the overall stiffness matrix and calcutation of stresses, plus the standard routines in the library.

Once a routine has been called and used it may not be needed again. To make the most efficient use of the core store these routines were kept on disc and called as required. This technique is usually called overlaying and was performed under the I.C.L. system by selecting areas of core, the routines are put into these areas as they are called, overwriting the routines called previously. The overlay scheme is shown in figure(A3.6).

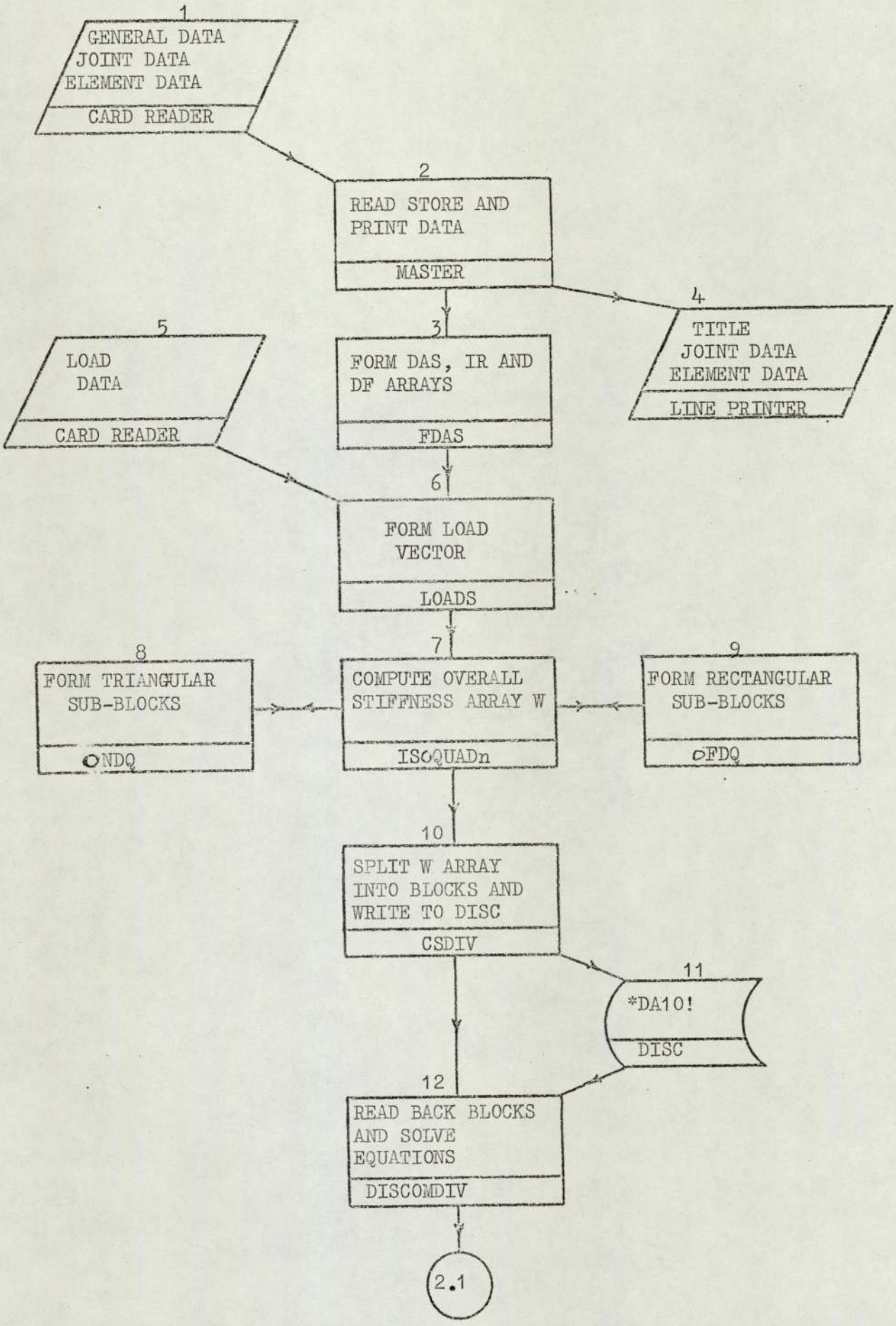
1
GENERAL DATA
JOINT DATA
ELEMENT DATA
CARD READER
2
READ STORE AND PRINT DATA
MASTER
4
TITLE
JOINT DATA
ELEMENT DATA
LINE PRINTER
5
LOAD DATA
CARD READER
3
FORM DAS, IR AND DF ARRAYS
FDAS
6
FORM LOAD VECTOR
LOADS
7
8
FORM TRIANGULAR SUB-BLOCKS
ONDQ
COMPUTE OVERALL STIFFNESS ARRAY W
ISOQUADn
9
FORM RECTANGULAR SUB-BLOCKS
OFDQ
10
SPLIT W ARRAY INTO BLOCKS AND WRITE TO DISC
CSDIV
11
*DA10!
DISC
12
READ BACK BLOCKS AND SOLVE EQUATIONS
DISCOMDIV
2.1

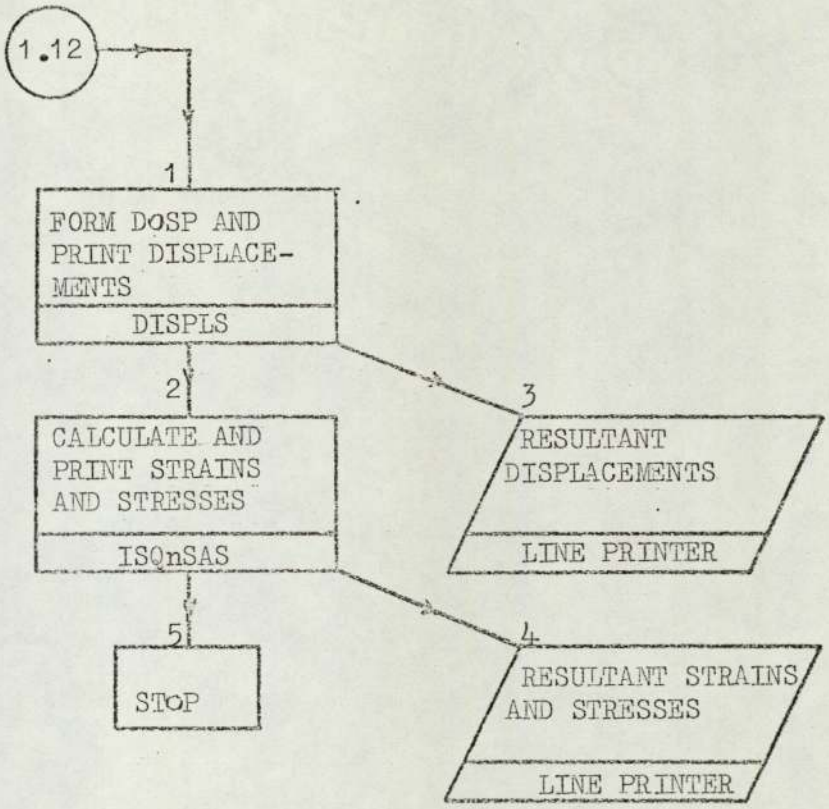
1.12
1
FORM DOSP AND PRINT DISPLACE-MENTS
DISPLS
2
CALCULATE AND PRINT STRAINS AND STRESSES
ISQnSAS
3
RESULTANT DISPLACEMENTS
LINE PRINTER
4
RESULTANT STRAINS AND STRESSES
LINE PRINTER
5
STOP

GENERAL AREA	MASTER SEGMENT BLOCK DATA SEGMENT	
AREA 1	1	SUBROUTINE FDAS
	2	SUBROUTINE ISOQUADn
	3	SUBROUTINE CSDIV
	4	SUBROUTINE DISCOMDIV
	5	SUBROUTINE ISQnSAS
AREA 2	1	SUBROUTINE LOADS
	2	SUBROUTINE ONDQ
	3	SUBROUTINE OFDQ
	4	SUBROUTINE DISPLS

SEGMENT OVERLAY SCHEME

FIG.(A3.6)

A3.7 Formation of Overall Stiffness Matrix, Hexahedral Elements

All the points discussed in the previous sections can in general be extended to three dimensional elements. The method adopted for storing and solving the equations applies to all elements. The differences arise, in that a joint is in general allowed six degrees of freedom as shown in figure(A3.7a).

The method of forming the overall stiffness matrix, as it applies to three dimensional elements, is again most conveniantly illustrated by means of an example. Consider the four linear Hexahedral Elements representing a material enclosed in a smooth sided box shown in figure(A3.7b). The degrees of freedom in structural notation and in the indicator form are shown in figures(A3.8a) and (A3.8b) respictively, for the joints numbered 1 to 12.

The general rectangular sub-block derived for the Isoparametric Hexahedral element in Appendix(2), figure(A2.19b) is represented in figure(3.9a). The code array (IAC) for three dimensional elements is shown in figure(A3.9b).. This array contains labels identifying the terms in the general sub-blocks. Consider the formation of the sub-block (5,3), of element 2 (figure(A3.7b)), the nodes of which are connected to joints 8 and 5 respectively. Figure(A3.9c) shows the sub-block (5,3) formed from the combination of the degrees of freedom in figure(A3.8b). In the program this would mean selecting the terms labelled, 1 , 4, 8 , and 5 as shown beside the sub-block, would be selected and calculated. The process of forming the sub-block (I,J) of an element is shown in flowchart(A3.5). Triangular sub-blocks were again treated as a special case, since they are dependant upon one joint only.

The complete process followed in forming the overall stiffness matrix of a mesh of Hexahedral Elements, including numerical integration, is shown in flowchart(A3.6).

A3.8 Stress Calculations , Hexahedral Elements

The method discussed in section(A3.4) is applicable to these elements. The only modification necessary is that since there are six components of

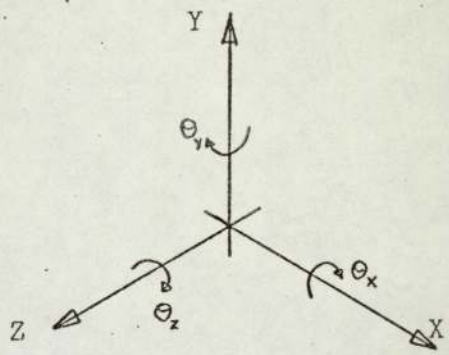

Degrees of Freedom

Figure (A3.7a)

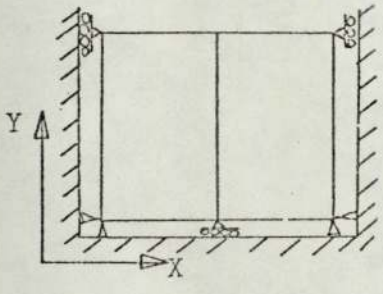

Section A-A

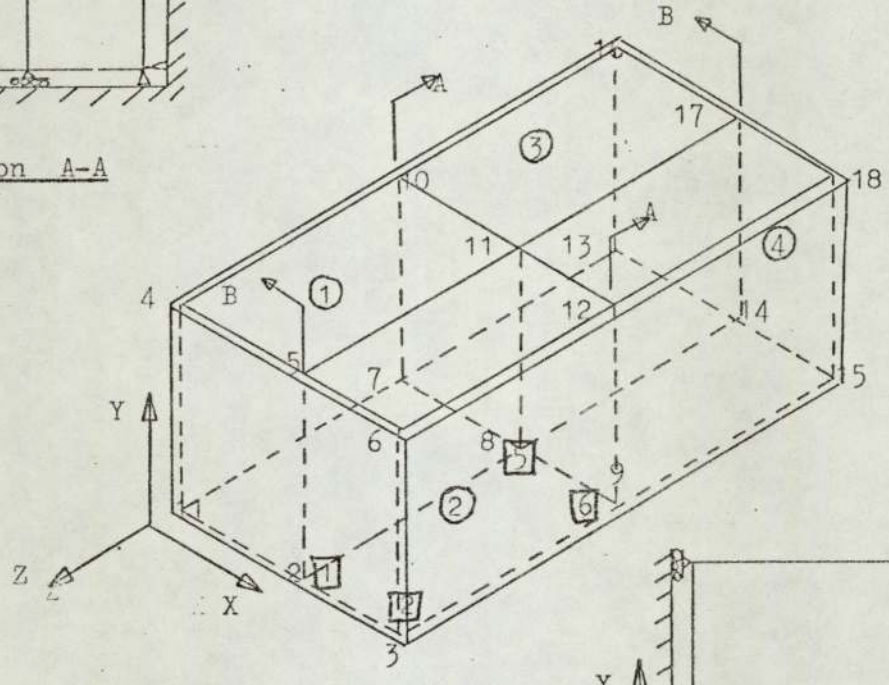

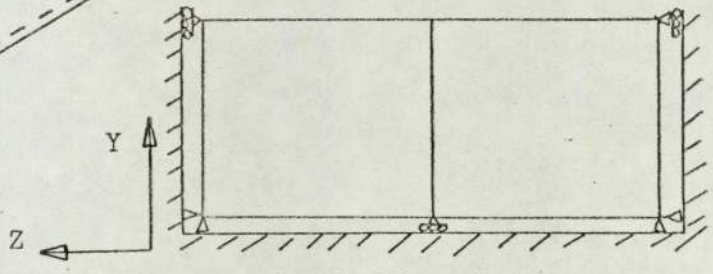

Section B-B

Example of Mesh of Hexahedral Elements

Figure (A3.7b)

	X	Y	Z			
1	0	0	0	0	0	0
2	1	0	0	0	0	0
3	0	0	0	0	0	0
4	0	1	0	0	0	0
5	1	1	0	0	0	0
6	0	1	0	0	0	0
7	0	0	1	0	0	0
8	1	0	1	0	0	0
9	0	0	1	0	0	0
10	0	1	1	0	0	0
11	1	1	1	0	0	0
12	0	1	1	0	0	0

Degrees of Freedom of Joints 1-12 in Figure(A3.7b) in Structural Notation

Figure (A3.8a)

	IR array					
1						
2	1					
3						
4	2					
5	1	2				
6	2					
7	3					
8	1	3				
9	3					
10	2	3				
11	1	2	3			
12	2	3				

Degrees of Freedom of Joints 1-12 in Figure(A3.7b) in Indicator Form

Figure (A3.8b)

Node J

Deg of Fr.		X	Y	Z
	IR	1	2	3
X	1	S_{11}	S_{12}	S_{13}
Y	2	S_{21}	S_{22}	S_{23}
Z	3	S_{31}	S_{32}	S_{33}

Node I

Representation of General Rectangular Sub-Block (I,J)

Figure (A3.9a)

IR_i \ IR_j	1	2	3	4	5	6
1	1	8	9	34	35	36
2	2	3	7	31	32	33
3	4	5	6	28	29	30
4	10	11	12	13	26	27
5	14	15	16	17	18	25
6	19	20	21	22	23	24

Code Array (IAC)

Figure (A3.9b)

Node 3

Deg of Fr.		X	Y
	IR	1	2
X	1	S_{11}	S_{12}
Z	3	S_{31}	S_{32}

Node 5

IR_5 \ IR_3	1	2
1	1	8
3	4	5

The Sub-Block (5,3) in Figure (A3.7b) and its associated labels

Figure (A3.9c)

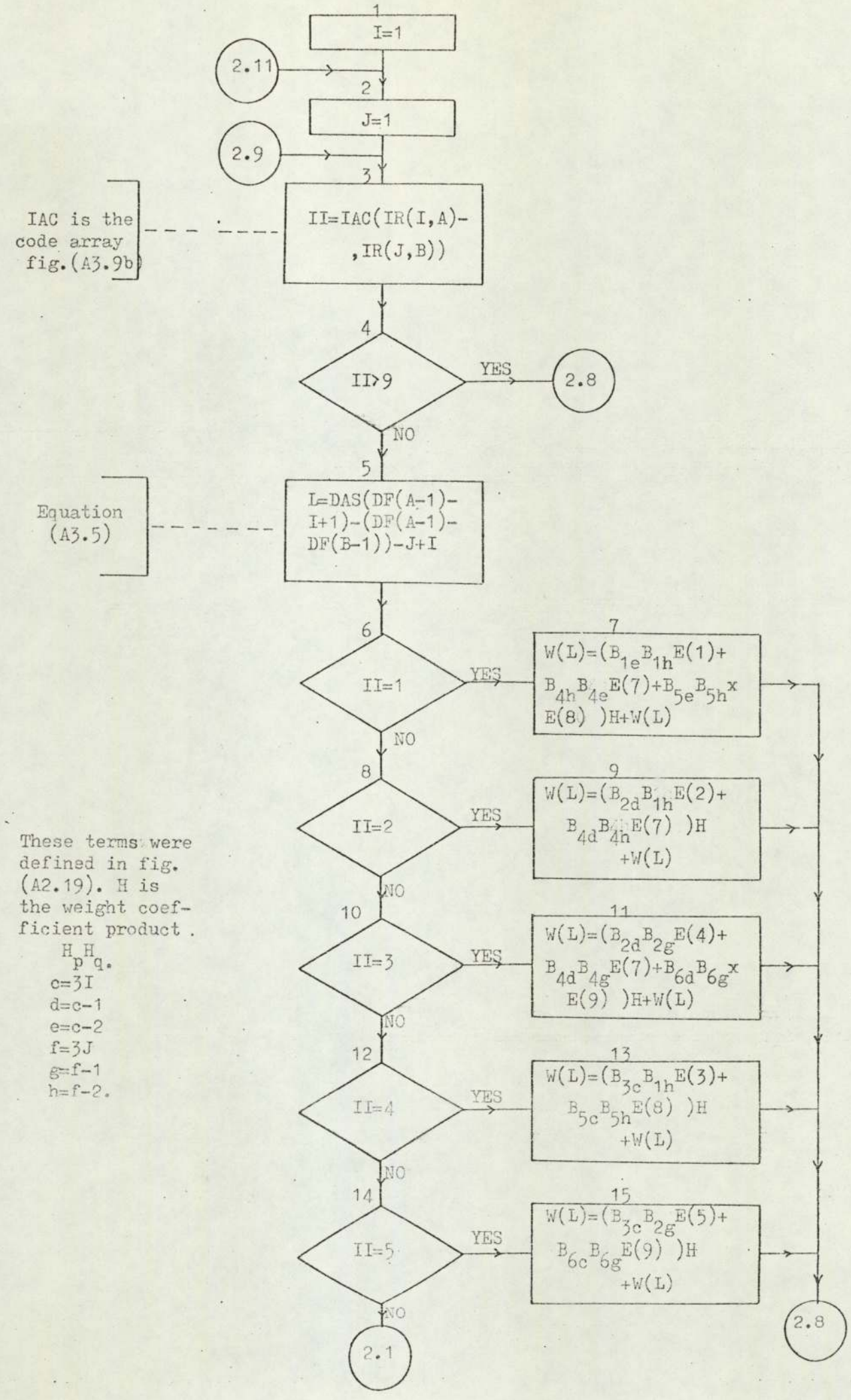

These terms were defined in fig. (A2.19). H is the weight coefficient product. $H_p H_q$.

c=3I
d=c-1
e=c-2
f=3J
g=f-1
h=f-2.

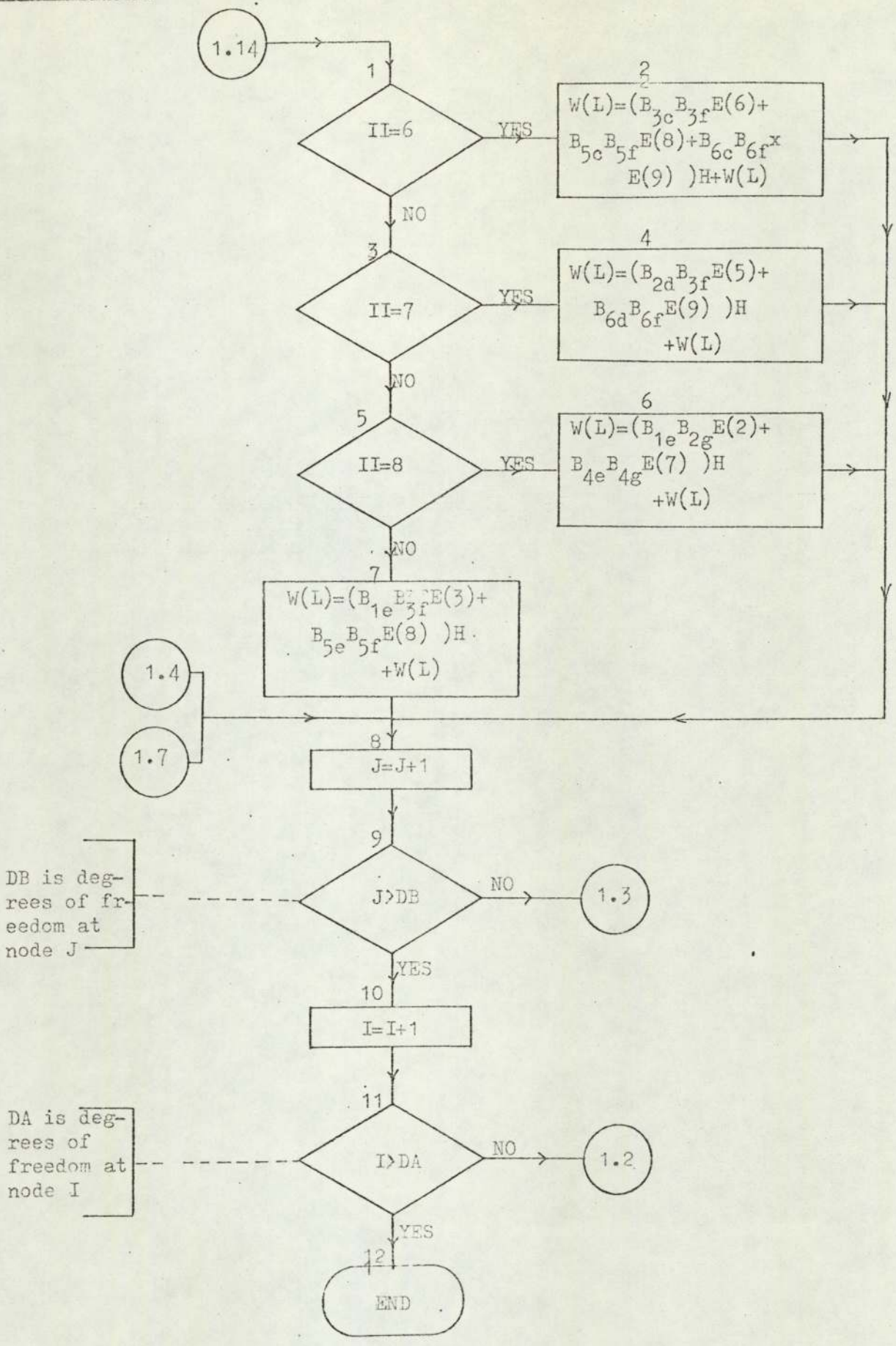
1.14
1
II=6
YES
2
W(L)=(B3cB3fE(6)+ B5cB5fE(8)+B6cB6fx E(9))H+W(L)
NO
3
II=7
YES
4
W(L)=(B2dB3fE(5)+ B6dB6fE(9))H +W(L)
NO
5
II=8
YES
6
W(L)=(B1eB2gE(2)+ B4eB4gE(7))H +W(L)
NO
7
W(L)=(B1eB3fE(3)+ B5eB5fE(8))H +W(L)
1.4
1.7
8
J=J+1
9
DB is degrees of freedom at node J
J>DB
NO
1.3
YES
10
I=I+1
11
DA is degrees of freedom at node I
I>DA
NO
1.2
YES
12
END

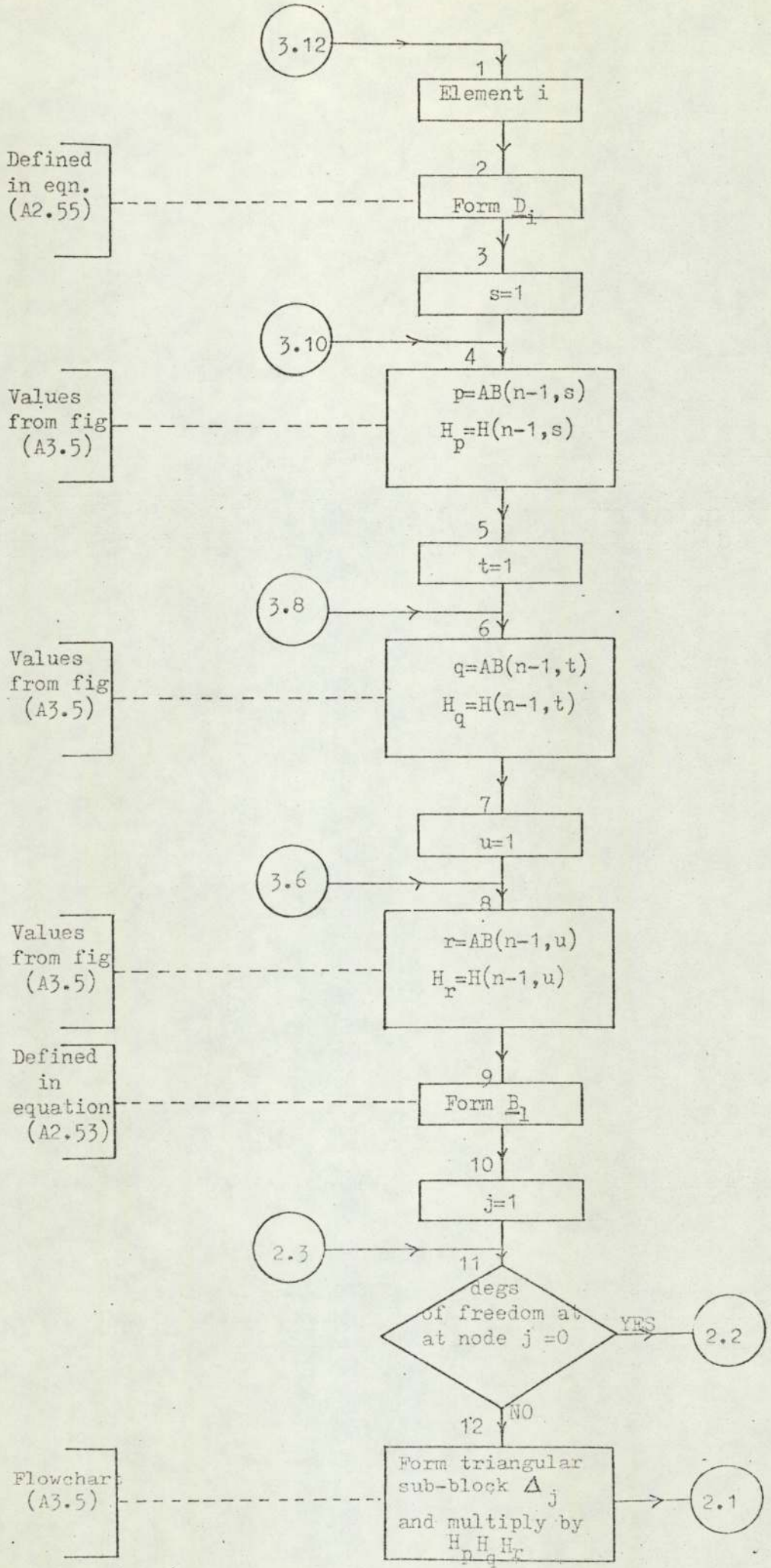
3.12
1
Element i
Defined in eqn. (A2.55)
2
Form $\underline{D}_i$
3
s=1
3.10
4
p=AB(n-1,s)
H_p=H(n-1,s)
Values from fig (A3.5)
5
t=1
3.8
6
q=AB(n-1,t)
H_q=H(n-1,t)
Values from fig (A3.5)
7
u=1
3.6
8
r=AB(n-1,u)
H_r=H(n-1,u)
Values from fig (A3.5)
Defined in equation (A2.53)
9
Form $\underline{B}_1$
10
j=1
2.3
11
degs of freedom at at node j =0
YES
2.2
NO
12
Form triangular sub-block Δ_j and multiply by $H_p H_q H_r$
Flowchart (A3.5)
2.1

FLOWCHART (A3.6)

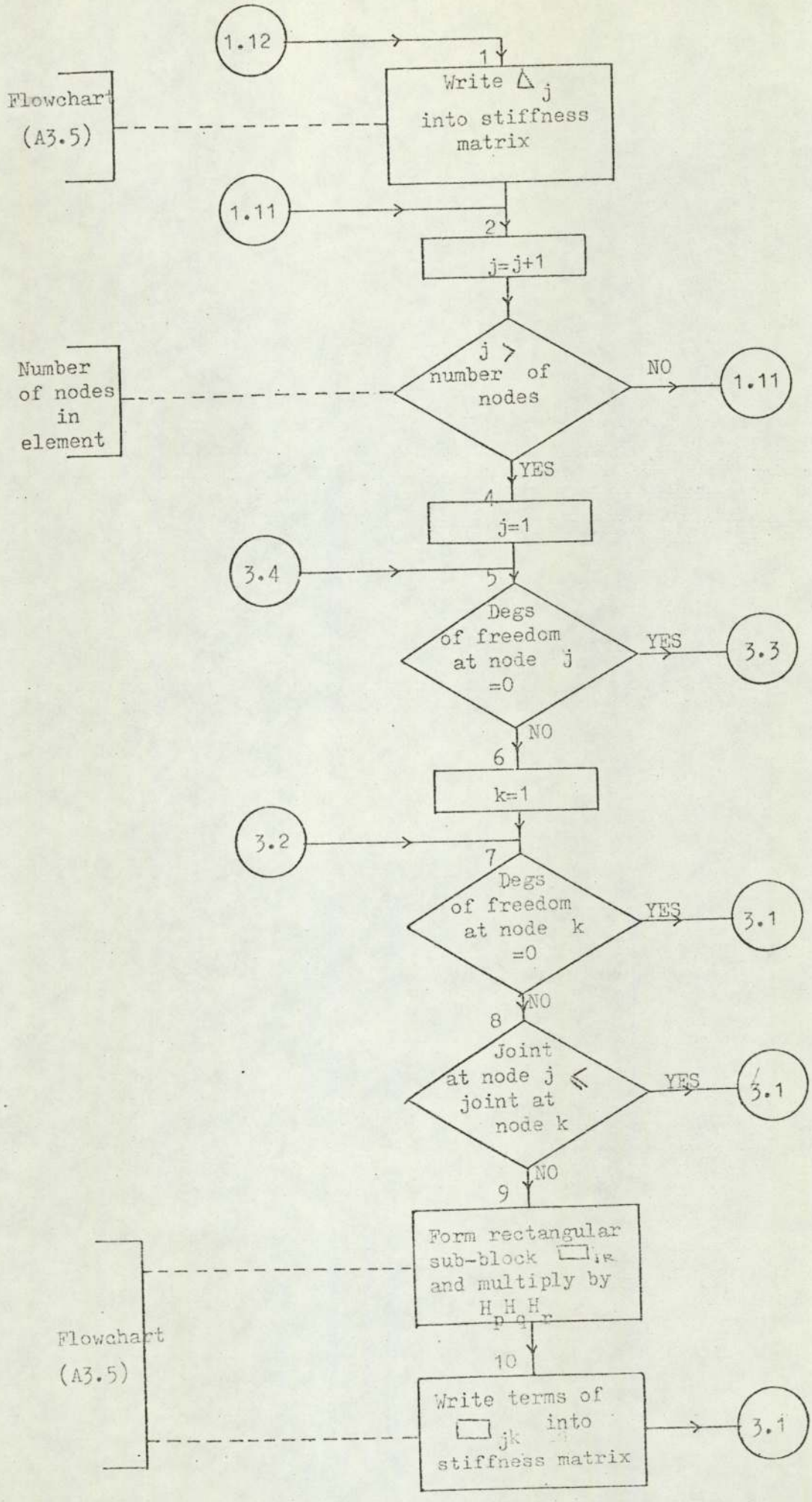

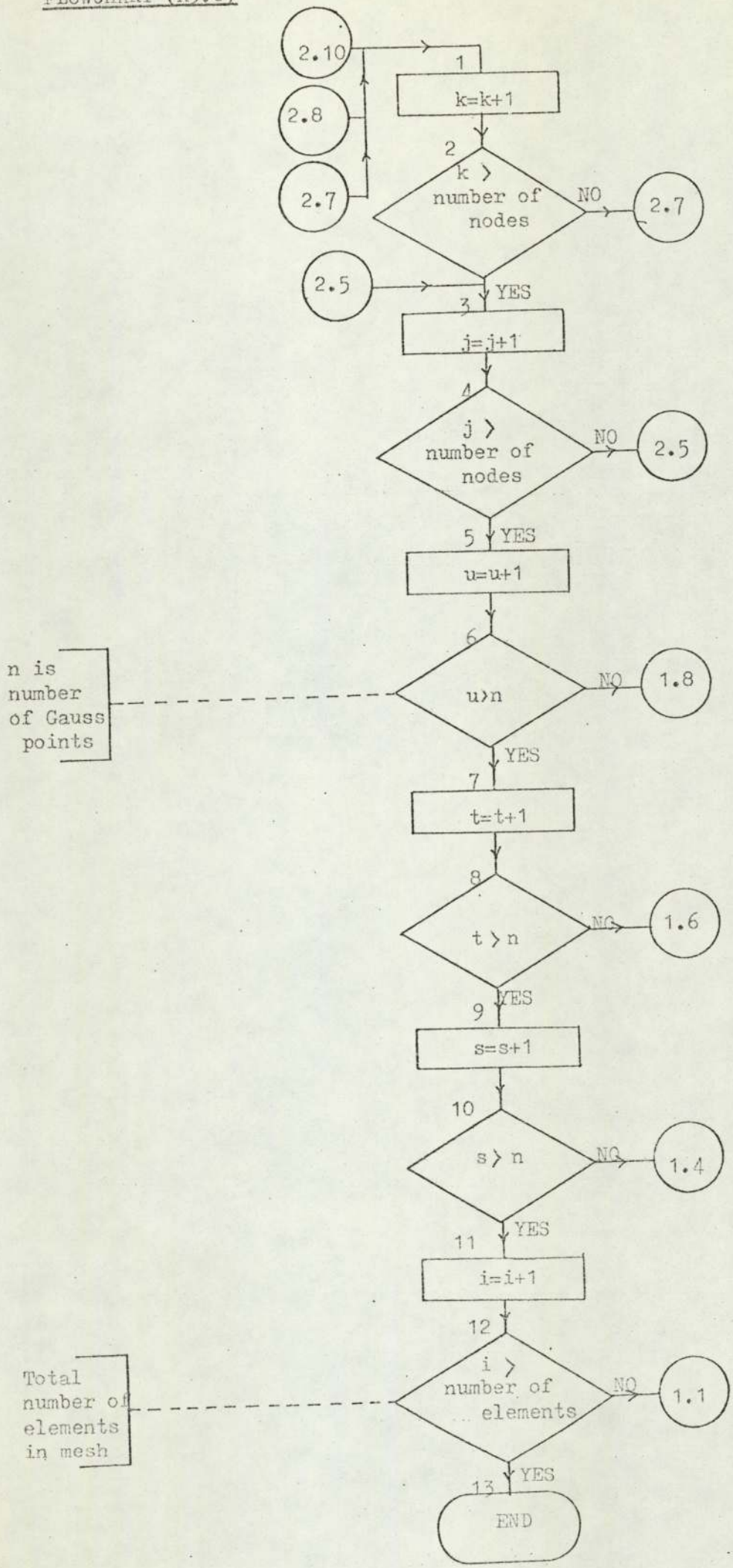
2.10
1
k=k+1
2.8
2
k > number of nodes
NO
2.7
2.7
2.5
YES
3
j=j+1
4
j > number of nodes
NO
2.5
5
YES
u=u+1
6
u>n
NO
1.8
n is number of Gauss points
YES
7
t=t+1
8
t > n
NO
1.6
YES
9
s=s+1
10
s > n
NO
1.4
YES
11
i=i+1
12
i > number of elements
NO
1.1
Total number of elements in mesh
YES
13
END

stress and strain, the SQ array must have thirteen columns.

A3.9 Three Dimensional Linear Elastic Analysis Programs

Initially three programs were written, one for each of the elements described in section (A2.2). These programs were all intended to analyse linear elastic homogeneous isotropic materials subject to surface loading, thus enabling accurate checks to be made. However, all the routines were written bearing in mind the fact that their future use would be in less ideal conditions. The procedure followed by the program is shown in flowchart(A3.7).

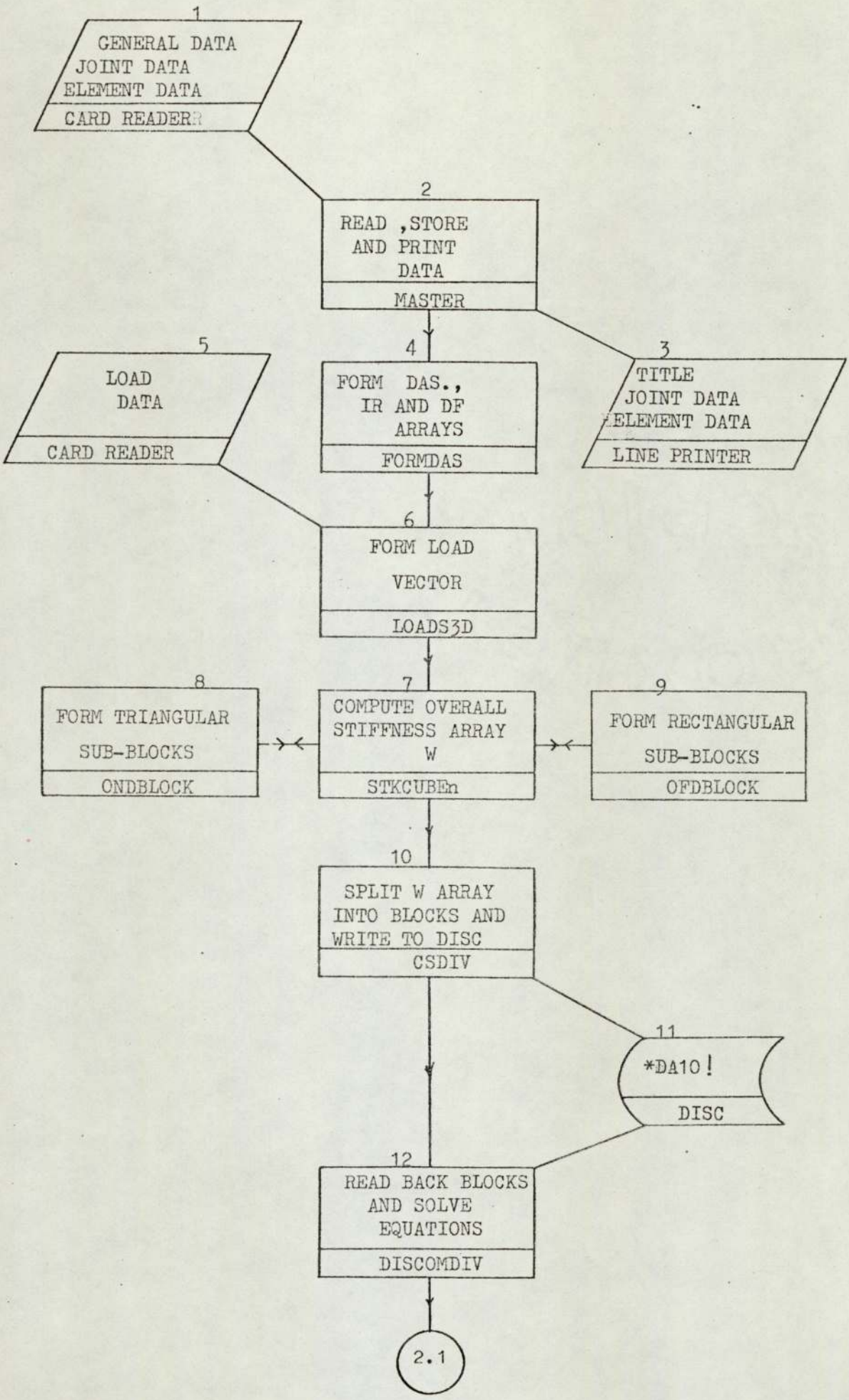
1
GENERAL DATA
JOINT DATA
ELEMENT DATA
CARD READER
2
READ ,STORE
AND PRINT
DATA
MASTER
3
TITLE
JOINT DATA
ELEMENT DATA
LINE PRINTER
4
FORM DAS.,
IR AND DF
ARRAYS
FORMDAS
5
LOAD
DATA
CARD READER
6
FORM LOAD
VECTOR
LOADS3D
7
COMPUTE OVERALL
STIFFNESS ARRAY
W
STKCUBEn
8
FORM TRIANGULAR
SUB-BLOCKS
ONDBLOCK
9
FORM RECTANGULAR
SUB-BLOCKS
OFDBLOCK
10
SPLIT W ARRAY
INTO BLOCKS AND
WRITE TO DISC
CSDIV
11
*DA10!
DISC
12
READ BACK BLOCKS
AND SOLVE
EQUATIONS
DISCOMDIV
2.1

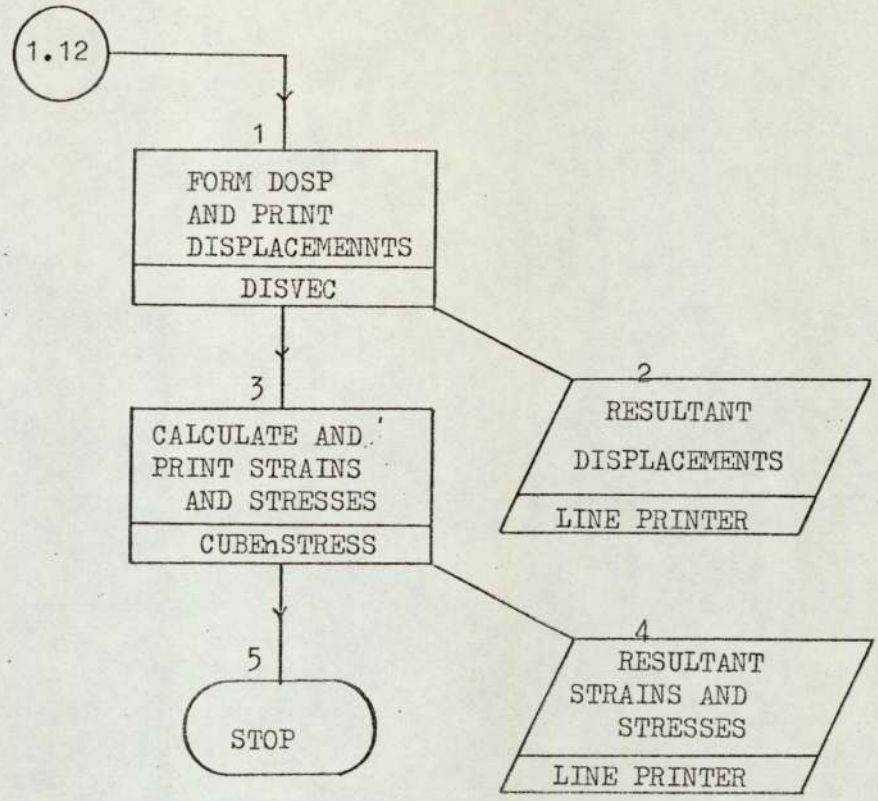
1.12
1
FORM DOSP
AND PRINT
DISPLACEMENNTS
DISVEC
2
RESULTANT
DISPLACEMENTS
LINE PRINTER
3
CALCULATE AND
PRINT STRAINS
AND STRESSES
CUBEnSTRESS
4
RESULTANT
STRAINS AND
STRESSES
LINE PRINTER
5
STOP

REFERENCES.

1) Ahmad,S.,Irons,B.M., and Zienkiewicz,O.C. 1970. 'Analysis of Thick and Thin Shells by Curved Elements'. Int.J.Num. Meth Eng.2.

2) Al-Hashimi,K. 1972, Ph.D.Thesis. The University of Birmingham.

3) Argyris,J.H. 1960. 'Energy Theorems and Structural Analysis'. Butterworth Scientific Publications.

4) Argyris,J.H. 1965. 'Continua and Discontinua'. Proc.Conf.Matrix Meths.Struct.Mech., Wright-Patterson AF Base, Ohio.

5) Argyris,J.H. 1968 'Elastic-Plastic Matrix Displacement Analysis of Three Dimensional Continua'. J.Roy.Aero.Soc., 69.

6) Balla,A., 1960. 'Stress Conditions in Triaxial Compression'. Proc A.S.C.E.,J.S.M.F.Div. 86, SM6.

7) Barden,L. and McDermott,J.W., 1965. 'Use of Free Ends in Triaxial Testing of Clays'. Proc.A.S.C.E.,J.S.M.F.Div. 91, SM6.

8) Bishop,A.W. and Green,G.E., 1965. 'The Influence of End Restraint on the Compression Strength of a Cohesionless Soil'. Geotechnique 15.

9) Bishop,A.W. and Henkel,D.J., 1957. 'The Measurement of Soil Properties in the Triaxial Test'. Edward Arnold.

10) Blake,W., 1966. 'Application of the Finite Element Method of Analysis in Solving Boundary Value Problems in Rock Mechanics'. Int J,Rock Mech 3.

11) Bray,K.H.M., 1973. Ph.D.Thesis, The University of Aston in Birmingham.

12) Butterfield,K. and Andrawes,K.Z., 1970. 'An Air Activated Spreader for Forming Uniform Beds of Sand'. Geotechnique 20.

13) Cheung,Y.K. and Zienbiewicz,O.C., 1965. 'Plates and Tanks on Elastic Foundations, an Application of the Finite Element Method'. Int.J.Sol.Struct,1.

14) Cheung,Y.K.and Nag,D.K. 1968. 'Plates and Beams on Elastic Foundations - Linear and Non-linear Behaviour'. Geotechnique 18.

15) Clough,R.W., 1960. 'The Finite Element Method in Plane Stress Analysis'. Proc.2nd Conf.Electronic Computation, A.S.C.E.

16) Clough,R.W. and Chopra,A.K. 1965 'Earthquake Stress Analysis in Earth Dams'. Res.Rep.Univ. of California,Berkeley.

17) Clough,R.W. and Woodward,R.J., 1967. 'Analysis of Embankment Stresses and Deformations'. Proc.A.S.C.E., J.S.M.F.Div. 93, SM4.

18) Christian,J.T. and Boehmer,J.W., 1970.'Plane Strain Consolidation by Finite Elements'. Proc.A.S.C.E, J.S.M.F.Div.96,SM.4.

19) Cornforth,D.H., 1964. 'Some Experiments on the Influence of Strain Conditions on the Strength of Sand'. Geotechnique 14.

20) Craig,J.S., 1971. Ph.D.Thesis, The University of Aston in Birmingham.

21) Desai,C.S., 1971. 'Non-Linear Analysis Using Spline Functions'. Proc.A.S.C.E, J.S.M.F.Div. 97.

22) Desai,C.S. and Reese,L.C., 1970. 'Analysis of Circular Footings in Layered Soils' Proc.A.S.C.E.,J.S.M.F.Div. 96, SM.4.

23) Domaschuk,L. and Wade,N.H., 1969 'A Study of Bulk and Shear Modulii of a Sand'. Proc.A.S.C.E.,J.S.M.F.Div 95, SM.2.

24) Drucker,D.C. and Prager,W., 1952. 'Soil Mechanics and Plastic Analysis or Limit Design'. Q.Appl.Maths 10,2.

25) Duncan,J.M. and Chang,C-Y., 1970. 'Non-Linear Analysis of Stress and Strains in Soil'. Proc.A.S.C.E., J.S.M.F.Div. 96, SM.5.

26) Duncan,J.M. and Clough,G.W., 1971. 'Finite Element Analysis of Port Allen Lock'. Proc.A.S.C.E.,J.S.M.F.Div.97, SM8.

27) Duncan,J.M. and Dunlop,P. 1968. 'The Significance of Cap and Base Restraint'. Proc.A.S.C.E.,J.S.M.F.Div. 94, SM3.

28) Duncan,J.M.,Monosmith C.L. and Wilson,C.L., 1968 'Finite Element Analysis of Pavements'. Proc.Annual Meeting H.R.B.

29) Dunlop,P. and Duncan,J.M., 1969. 'Development of Failure Around Excavated Slopes'. 95, SM.2.

30) Ergatoudis,J.G., 1968. Ph.D.Thesis, The University of Wales, Swansea.

31) Ergatoudis,J., Irons,B.M. and Zienkiewicz, O.C., 1968. 'Curved Isoparametric Elements for Finite Element Analysis'. Int.J.Sol.Struct.,4.

32) Feda,J., 1961. 'Research on the Bearing Capacity of Loose Soil'. Proc.5th Int.Conf.Soil Mech, Paris, Vol.1.

33) Ferrar,W.L., 1958. 'Integral Calculus'. Oxford Press, p.205

34) Fraeijs De Veubeke,B.M., 1964, 'Upper and Lower Bounds in Matrix Structural Analysis'. Matrix Meth. in Struct. An. Agardograph 72.

35) Fraeijs De Veubeke,B.M., 1965. 'Displacement and Equilibrium Models in the Finite Element Method'. Stress Analysis, Wiley.

36) Gallagher,R.H., Padlog,G. and Bylaard,P.P., 1962. 'Stress Analysis of Heated Complex Shapes'. J.Am.Roc. Soc, 32.

37) Gallagher,R.H., 1963. 'Techniques for the Derivation of Element Stiffness Matrices'. J.A.I.A.A., 1.

38) Girijavallabhan,C.U. and Reese,L.C., 1968. 'Finite Element Method for Problems in Soil Mechanics'. Proc.A.S.C.E.,J.S.M.F.Div. 94, SM.2.

39) Gisbourne,R., 1970. Ph.D.Thesis, The University of Aston in Birmingham.

40) Gradshteyn,I.S. and Ryzhik,I.M., 1965. 'Tables of Integrals Series and Products'. Academic Press.

41) Green,G.E., 1966. Ph.D.Thesis, Imperial College of Science and Technology, University of London.

42) Hansen,J.B., 1963. Discussion of a paper by Kondner and Zelasko (56). Proc.A.S.C.E., J.S.M.F.Div., 89, SM.4.

43) Haythornthwait ,R.M., 1960. 'Mechanics of the Triaxial Test for Soils'. Proc.A.S.C.E.,J.S.M.F.Div.,86, SM.5.

44) Hoëg,K., 1972. ' Finite Element Analysis of Strain Softening Clays'. Proc.A.S.C.E.,J.S.M.F.Div.,98, SM1.

45) International Computer and Tabulators Ltd., Scientific Subroutines, Technical Publication 4096.

46) Irons,B.M. and Draper,K.J., 1965. 'Inadequacy of Nodal Connections in a Stiffness Solution for Plate Bending '. J.A.I.A.A.,5.

47) Irons,B.M., 1966. 'Numerical Integration Applied to Finite Element Methods'. Conf. on use Digital Computers in Struct. Eng., University of Newcastle.

48) Irons,B.M., 1966. 'Engineering Applications of Numerical Integration in Stiffness Methods'. J.A.I.A.A., 4.

49) Irons,B.M. and Zienkiewicz,O.C., 1968. 'The Isoparametric Finite Element System - A New Concept in Finite Element Analysis'. Conf. on Recent Advances in Stress Analysis Roy.Aero.Soc. London.

50) Jennings,A. and Tuff,A.D., 1970.' A Direct Method for the Solution of Large Sparse Symmetric Simultaneous Equations'. Int. Conf. on Large Sparse Sets of Linear Equations, Oxford.

51) Kay,S., 1970. M.Sc.Thesis, The University of Manchester.

52) Kirkpatrick,W.M. and Belshaw,D.J., 1968. 'On the Interpretation of the Triaxial Test'. Geotechnique 18.

53) Kolbuszewski ,J., 1965. 'Sand Particles and their Density'. Lecture to the Mat.Sci. Club Sump. on Densification of Particulate Materials, London.

54) Kolbuszewski,J. and Jones,R.H., 1961, 'The Preparation of Sand Samples for Triaxial Testing'. Proc.Midland S.M.F.E.Soc.,4.

55) Kondner,R.L., 1963. 'Hyperbolic Stress/Strain Response, Cohesive Soils'. Proc.A.S.C.E.,J.S.M.F.Div., 89, SM.1.

56) Kondner,R.L. and Zelasko,J.S., 1963. 'A Hyperbolic Stress-Strain Formulation for Sands' 2nd Pan American Conf.on Soil Mechs., Vol.1, Brazil.

57) Kondner,R.L. and Zelasko,S., 1963. 'Voids Ratio Effects on the Hyperbolic Stress-Strain Response of Sand'. Laboratory Shear Testing of Soils, A.S.T.M., STP. 361.

58) Kopal,Z., 1961. 'Numerical Analysis'. Chapman and Hall.

59) Kraft,L.M. and Krishnamurthy,N.,1971. 'Analytical Model for Evaluating Stress-Strain Response of Soils'. J.of Materials, 6,4.

60) Livesley,R.K., 1964. 'Analysis of Rigid Frames by an Electronic Digital Computer'. Engineering, 76.

61) Livesley,R.K., 1954. 'Matrix Methods of Structural Analysis'. Pergammon Press.

62) Majid,K.I., 1972. 'Non-Linear Structures'. Butterworths.

63) Mareal,P.V., 1965. 'A Stiffness Method for Elastic-Plastic Problems'. Int.J.Mech.Sci.7.

64) Martin,H.C.,1965. 'On the Derivation of Stiffness Matrices for the Analysis of Large Deflection and Stability Problems'. Proc. Conf. on Matrix Meths. in Struct.Mechs., Wright-Patterson A.F.Base,Ohio.

65) Melosh,R.J., 1961. 'A Stiffness Matrix for the Analysis of Thin Plates in Bending'. Roy.Aero.Soc., 28.

66) Melosh,R.J., 1963. 'Basis of Derivation for the Direct Stiffness Method'. J.A.I.A.A.,1.

67) Naylor,D.J. and Zienkiewicz,O.C., 1971. 'Settlement Analysis of a Strip Footing Using a Critical State Model in Conjunction with Finite Elements'. Conf.Midland S.M.F.Soc.

68) Penman,A.D.M., Burland,J.B. and Charles,J.A., 1971. 'Observed and Predicted Deformations in a Large Embankment Dam during Construction'. Proc.I.C.E.

69) Perloff,W.H., and Pombo,L.E., 1969. 'End Restraint Effects in the Triaxial Test'. Proc. 7th Int.Conf. on S.M. and F.Eng. Vol.1, Mexico.

70) Ponce,U.M. and Bell,J.M., 1971. 'Shear Strength of Sand at Extremely Low Pressures'. Proc.A.S.C.E.,J.S.M.F.Div., 98.

71) Pope,G.G.,1965. 'A Discrete Element Method for Analysis of Plane Elasto-plastic Stress Problems." R.A.E.Farnborough, TR65028.

72) Roscoe,K.H. and Burland,J.B., 1968. 'The Generalised Stress-Strain Behaviour of Wet Clay'. Eng.Plasticity Conf. at Cambridge.

73) Rowe,P.W., 1971. 'Theoretical Meaning and Observed Values of Deformation Parameters for Soil.' Roscoe Memorial Symp., Cambridge.

74) Rowe,P.W. and Barden,L., 1964, 'Importance of Free Ends in Triaxial Testing'. Proc.A.S.C.E., J.S.M.F.Div.,90,SM1.

75) Schofield,A. and Wroth,P., 1968. 'Critical State Soil Mechanics'. McGraw Hill.

76) Severn,R.T., 1966. 'The Solution of Foundation Mat Problems by Finite Element Methods'. The Structural Engineering;44,6.

77) Smith,I.M., 1970. 'A Finite Element Approach to Elastic Soil-Structure Interaction'. Canadian Geotech.,7,2.

78) Smith,I.M., 1970. 'Incremental Numerical Solution of a Simple Deformation Problem in Soil Mechanics'. Geotechnique 20,4.

79) Smith,I.M., 1971. 'Plane Plastic Deformation of Soil'. Roscoe Memorial Symp., Cambridge.

80) Smith,I.M. and Kay,S.,1971. 'Stress Analysis of Contractive or Dilative Soil'. Proc.A.S.C.E.,J.S.M.F.Div.,97.

81) Sneddon,I.N.,1945. 'Elastic Stresses Produced in a Thick Plate by the Application of Pressure to its Free Surfaces'. Proc. Cambridge Phil.Soc.,42, 260.

82) Sneddon,I.N.,1951. 'Fourier Transforms'. McGraw-Hill.

83) Terzaghi,K., 1948. 'Theoretical Soil Mechanics'. John Wiley and Sons.

85) Trikha,D.N. and Edwards,A.D., 1972. 'Analysis of Concrete Girders before and after Cracking'. Proc.ICE, 53.

88) Turner,M.J.,Clough,R.W.,Martin,H.C. and Topp,L.J., 1956. 'Stiffness and Deflection Analysis of Complex Structures'. J.Aero.Sci.,23.

89) Valliapan,S., 1968. Ph.D.Thesis, The University of Wales, Swansea.

90) Walker,B.P. and Whittaker,T., 1967. 'Apparatus for Forming Uniform Beds of Sand for Model Foundation Tests'. Geotechnique 17.

91) Watson,R.,1967. M.Sc.Thesis, The University of Wales, Swansea.

92) Watwood,V.B., 1969. 'The Finite Element Method for Prediction of Crack Behaviour'. Nucl.Eng.Des.

93) Zienkiewicz,O.C.,Irons,B.M., and Nath,B. 1965. 'Natural Frequencies of Complex Free or Submerged Structures By the Finite Element Method'. Sym.Vibrations in Civil Eng.I.C.E, London.

94) Zienkiewicz,O.C.,Valliapan,S. and King,I.P., 1968. 'The Stress Analysis of Rock as a No-Tension Material'. Geotechnique 18.

95) Zienkiewicz,O.C., and Naylor,D.J., 1971. 'The Adaption of the Critical State Soil Mechanics Theory for use in Finite Elements'. Roscoe Mem.Symp.,Cambridge.

96) Zienkiewicz,O.C.,Valliapan,S. and King,I.P. 1969, 'Elasto-Plastic Solutions in Engineering Problems Initial Stress, Finite Element Approach'. Int.J.Num.Meths.Engg.,1

97) Zienkiewicz,O.C.,Irons,B.M., Ergatoudis,J.,Ahmad,S., and Scott,F.C., 1969. 'Isoparametric and associated Element Families for 2 and 3 Dimensional Analysis'. Proc.Conf. on F.E. methods in Stress Analysis, Trondheim Univ., Norway.

98) Zienkiewicz,O.C., 1971. 'The Finite Element Method in Engineering Science', McGraw-Hill.

99) Majid,K.I. and Craig,J.S., 1971. 'An Incremental Finite Element Analysis of Structural Interaction with Soil of Non-Linear Properties'. Mid.S.M.F.Soc Conf, Birmingham.

100) Kolbuxzewski,J., 1948. 'An Experimental Study of the Maximum and Minimum Porosities of Sands'. Proc.2nd Int.Conf. on S.M.& F.Eng., Vol.1.

103) Kulhawy,F.H. and Duncan,J.M., 1972. 'Stresses and Movements in Oroville Dam'. Proc.A.S.C.E.,J.S.M.F.E.,SM7, 98.

105) Meyerhoff,G.G., 1963. 'Some Recent Research on the Bearing Capacity of Foundations'. Canadian Geotech.,1.No.1.

106) Nelson,I. and Baron,M.C., 1971. 'Application of Variable Modulii Models to Soil Behaviour'. Int.J.Sols. and Structs.,7.